Controlling the Reactivity of Mononuclear Palladium(II) Complexes. Substitution Kinetics and Mechanisms

By

Daniel Omondi Onunga

BSc. (Hons) KU; MSc. (MMUST), Kenya

Submitted in Partial fulfilment of the academic requirements for the degree of

Doctor of Philosophy

In the College of Agriculture, Engineering and Science

School of Chemistry and Physics

University of KwaZulu-Natal, Pietermaritzburg

South Africa

2019

UNIVERSITY OF KWAZULU-NATAL

INYUVESI YAKWAZULU-NATALI

Declaration

I hereby declare that the experimental work and results presented in this thesis are the original work of my study carried out in the discipline of chemistry in the School of Chemistry and Physics, University of KwaZulu-Natal, Pietermaritzburg campus and has never been submitted for the fulfillment of any degree at any university and, except where the work of others is acknowledged in the text, the results reported are due to investigations by the candidate.

…… ……

Daniel Omondi Onunga

We as supervisors hereby certify that this is correct.

…… …….. … …

Dr. A. Mambanda **Prof. D. Jaganyi**

University of KwaZulu-Natal

School of Chemistry and Physics

Pietermaritzburg

March 2019

Dedications

This work is dedicated to my wife, Rosebellah, my son, Zabdi, and daughters; Shelomith and Hadassah, who gave me their love, peace of mind, encouragement and strength to accomplish my desire. I hope to be with each one of them as they face their own challenges and difficulties to pursue their life's dreams as long as God grants me life.

Epigraph

Only one life, 'twill soon be past,

Only what's done for Christ will last.

Charles Thomas Studd (1860 – 1931)

Acknowledgements

My appreciation goes to acknowledging the contributions of various people and parties who participated directly or indirectly during the process of carrying out this research and putting up this monumental work. First and foremost, I am indeed very grateful to the Lord God Almighty, my creator, savior and redeemer, under whose breath, guidance, gift of abundance life and strength has made me accomplish this enormous task.

I am very grateful to my supervisors Prof. Deogratius Jaganyi and Dr. Allen Mambanda for their continual guidance, advices, valuable suggestions, support, trust in me and granting me the opportunity to model this work as well as their patience throughout the study period. May God richly reward you all. Many thanks to Dr. Isaac Wekesa through whom this great journey began.

I am deeply grateful to the University of KwaZulu-Natal, South Africa for financial support. In addition, I express my gratitude to all the academic and technical staff in the School of Chemistry and Physics. In particular, I sincerely thank Prof. Ojwach for providing conducive working environment in the chemistry cluster, Dr. Reddy, Dr. Xulu, Prof. Owaga and Mr. Muvhango for their encouragements. Technically, I am indebted to Mr. Craig Grimmer who tirelessly acquiring the NMR spectral data of the synthesized compounds and ran the kinetic experiments as well as his wise counsel and insights on to the data. In the same spirit, I am thankful to Leigh Hunter and Sizwe Zamisa for the X-ray crystallographic analysis and Caryl Janse van Rensburg for assisting with MS and CHN spectroscopic analysis. Very grateful to Prudence Lubanyana, Mr. Hashim for providing the needed technical assistance and Shawn for the procurements.

Thanks to my fellow Deo group members Dr. Rajesh, Meshack, Gershom, Tshesphiso and Moses whose presence and critiques brought great encouragements towards completing the task.

More appreciation to Andrew, Ebenezer, Abimbola, Grace, Nandipha for their constant inspirations and to all the postgraduate students in Chemistry under ChemBurg. Am thankful to the Kenya Community in Pietermaritzburg (KCP) for providing a home for me far from home. You are a bunch of great and wonderful people.

Finally, I express my deepest gratitude to my wife, Rosebellah as backed by my children for their unwavering and indefatigable stand with me all along and in times of need. Your continual presence, emotional support, love, patience and motivation gave me additional strength to work towards achieving this dream. May God grant you peace and fulfill all your life's desires.

Table of Contents

Declaration ii

Dedications iii

Acknowledgements v

Table of Contents vii

List of Figures.....xiv

List of Tables xviii

List of Schemes xx

List of Abbreviations xxi

Publications and Conferences Contributions.....xxii

Abstract..... xxiii

CHAPTER 1 1

Platinum and Palladium Anticancer Drugs 1

1.0 Introduction.....1

1.1 Cancer: A global Killer Disease 1

1.2 Platinum-based Anticancer Drugs 2

1.2.1 Mechanism of Action of Pt-based Drugs 4

1.2.2 Side Effects of Pt-based Drugs and the Need for Alternatives 7

1.3 Palladium Anticancer Chemistry 8

1.3.1 Mononuclear Palladium(II) Complexes 9

1.3.1.1 Trans-palladium(II) Complexes 10

1.3.1.2 Bidentated Pd(II) Complexes 13

1.3.1.3 Terdentate Palladium(II) Complexes 15

1.4 Kinetic and Mechanistic Studies.....20

1.5 Aims of the Study 21

1.6 References 25

CHAPTER 2 33

Ligand Substitution Reactions of Square Planar Complexes 33

2.0 Introduction 33

2.1 Substitution Kinetics of Square Planar d^8 Complexes 34

2.2 Substitution Mechanisms of Square Planar Complexes 34

2.2.1 Associative Mechanism (A) 36

2.2.2 Dissociative Mechanism (D) 37

2.2.3 Interchange Mechanism (I) 39

2.3 Kinetic Parameters 40

2.3.1 Reversible Second-order Reactions 40

2.3.2 Activation Parameters 44

2.3.2.1 Determination of Activation Enthalpy ($\Delta H^{\neq}$) and Entropy ($\Delta S^{\neq}$) Changes 44

2.3.2.2 Determination of Activation Volume ($\Delta V^{\#}$) 47

2.4 Instrumentation Techniques Used for Measuring the Rate of Substitution Reactions 49

2.4.1 UV-Visible Spectrophotometry 50

2.4.2 Flow Methods 54

2.4.2.1 Stopped-flow Methods 55

2.5 Factors Affecting the Rate of Substitution of Square Planar Complexes 56

2.5.1 The Effect on Rate of the Incoming Ligand 56

2.5.2 Solvent Effects 60

2.5.3 The Effect of the Leaving Group 61

2.5.4 The Effects of Spectator Ligands 62

2.5.4.1 Steric Effects 62

2.5.4.2 The Trans Effects 63

2.5.4.3 The Cis Effects 65

2.6 References 68

CHAPTER 3 75

Tuning the Reactivity of Palladium(II) Complexes of Pyrazolyl-based Terpyridyl Type of Ligands through Electronic and Steric effects. Crystal Structures 75

3.0 Abstract 75

3.1 Introduction 76

3.2 Experimental Section 79

3.2.1 Materials and Methods 79

3.2.2 Syntheses of the Ligands 79

3.2.3 Synthesis of the Pd(II) Complexes 81

3.2.4 Physical Measurements and Instrumentation 84

3.2.5 Kinetic Measurements 84

3.2.6 Computational Modelling 85

3.2.7 X-ray Crystallography 86

3.3 Results 86

3.3.1 Computational Details 86

3.3.2 X-ray Crystal Determination of the Complexes 89

3.3.3 Kinetic and Mechanistic Studies 95

3.4 Discussion 100

3.5 Conclusions 105

3.6 References 106

3.7 Supporting Information (ESI‡) 111

CHAPTER 4 129

The Role of 8-quinolinyl Moieties in Tuning the Reactivity Palladium(II) Complexes: A Kinetic and Mechanistic Study 129

4.0 Abstract 129

4.1 Introduction 130

4.2 Experimental Section 133

4.2.1 Materials and Methods 133
4.2.2 Synthesis of Ligands 133
4.2.3 Synthesis of Palladium(II) Complexes 135
4.2.4 Physical Measurements and Instrumentation 137
4.2.5 Preparations of Kinetic Solutions 138
4.2.6 Kinetic Analysis 138
4.2.7 Computational Modelling 139
4.3 Results 139
4.3.1 Computational Analysis 139
4.3.2 Kinetic Measurements 142
4.4 Discussion 145
4.5 Conclusions 150
4.6 References 152
4.7 Supporting Information (ESI‡) 156
CHAPTER 5 171
Controlling the Reactivity of Pd(II) Complexes of 1,3-Bis(2-pyridylimino)isoindoline Ligands through Alkylation and Benzannulation: X-ray structure, Kinetics, Mechanistic and DFT Study 171
5.0 Abstract 171
5.1 Introduction 173
5.2 Experimental Section 176
5.2.1 Materials and Methods 176
5.2.2 Syntheses of Ligands 177
5.2.3 Syntheses of Complexes 179
5.2.4 Physical Measurements and Instrumentation 181
5.2.5 X-ray Crystallography 181
5.2.6 Computational Modelling 182
5.2.7 Kinetic Solutions 182
5.2.8 Kinetic Analysis 183

5.3 Results 183
5.3.1 X-ray Crystal Structure 183
5.3.2 DFT-Calculated Optimized Structures 187
5.3.3 Kinetic Analysis 190
5.4 Discussion 199
5.5 Conclusions 205
5.6 References 206
5.7 Supporting Information (ESI‡) 211
CHAPTER 6 235
The Reactivity of Pd(II) Complexes with C^N^N Cyclometalated Polypyridylphenyl Ligands: Crystal Structures, Kinetics and Computational studies 235
6.0 Abstract 235
6.1 Introduction 236
6.2 Experimental Section 238
6.2.1 Materials and Methods 238
6.2.2 Syntheses of Precursors and C^N^N Ligands 239
6.2.3 Syntheses of Ligands 241
6.2.4 Syntheses of Cyclometalated Pd(II) Complexes 243
6.2.5 Physical Measurements and Instrumentation 245
6.2.6 X-ray Crystallography 245
6.2.7 Computational Modelling 246
6.2.8 Preparation of Kinetic Solutions and Measurements 246
6.3 Results 247
6.3.1 X-ray Crystal Structures 247
6.3.2 Computational Details 252
6.3.3 Kinetic Analysis 255
6.4 Discussion 259
6.5 Conclusions 263

6.6 References 264

6.7 Supporting Information (ESI‡) 269

CHAPTER 7 287

Controlling the Reactivity of Palladium(II) Complexes Using 2,6-Bis-N-heterocyclic Carbene Ligands: Kinetic and Computational Study 287

7.0 Abstract 287

7.1 Introduction 289

7.2 Experimental Section 292

7.2.1 Materials and Methods 292

7.2.2 Syntheses of Azolium Ligand Salts 293

7.2.3 Syntheses of Palladium Carbene Complexes 295

7.2.4 Physical Measurements and Instrumentation 297

7.2.5 Preparations of the Kinetic Solutions 298

7.2.6 Kinetic Analysis 298

7.2.7 Computational Modelling 298

7.3 Results 299

7.3.1 Computational Analysis 299

7.3.2 Kinetic and Mechanistic Studies 303

7.4 Discussion 307

7.5 Conclusions 310

7.6 References 312

7.7 Supporting Information (ESI‡) 318

CHAPTER 8 337

Summary and Future Prospects 337

8.1 Introduction 337

8.2 Summary 337

8.3 Future Prospects.....342

8.4 References.....345

List of Figures

Figure 1. 1 Process of cancerous cell development process [5] 1

Figure 1. 2 Commercial platinum-based anticancer drugs 3

Figure 1. 3 Hydrolysis of *cisplatin* and its interaction with DNA.[40] 4

Figure 1. 4 Different ways of interaction of *cisplatin* with DNA showing 1,2-intrastrand cross-links.[26] 5

Figure 1. 5 Schematic pathways of *cisplatin* in the cell showing the biological processes involving sulfur compounds thought to act as potential drug agents in chemotherapy.[49] 7

Figure 1. 6 Some of the palladium(II) complexes anticancer agents.[38, 84, 91] 11

Figure 1. 7 Palladium complexes bearing N-heterocyclic carbene ligands which have shown potential antitumor activity.[97, 98] 13

Figure 1. 8 Some of the N^N bidentate Pd(II) complexes as antitumor agents.[54, 92, 101, 102] ... 14

Figure 1. 9 Schematic structures of N^N^S, C^N^N and N^N^N terdentate Pd(II) complexes that have been tested for anticancer activity.[28, 86, 90, 104-107, 110] 17

Figure 2. 1 Potential energy profiles of different mechanisms occurring at a square planar metal centre as proposed by Langford-Gray.[40, 44] 36

Figure 2. 2 A representative linear plot of k_{obs} against nucleophile concentration ([Nu]) for the *pseudo* first-order substitution reaction. 43

Figure 2. 3 A typical representation of the UV/Visible spectrophotometer components.[66] 51

Figure 2. 4 UV-visible spectra for the second step reaction of Pd(II) complex with thiourea nucleophile. Inset; single exponential kinetic trace at 360 nm at 298 K. (**Chapter 5**) 54

Figure 2. 5 A typical schematic diagram of the stopped-flow apparatus. The direction of the movement of the syringes are shown by the blue arrows.[72] 55

Figure 2. 6 Stopped-flow kinetic trace at 388 nm for the substitution reaction between a Pd(II) complex and **Dmtu** at 298 K. (**Chapter 7**). 56

Figure 2. 7 An illustration of π-back donation of electrons from the filled d orbital of the metal (Pt) to the vacant orbitals of the *trans* ligand of *trans*-PtA_2LX.[9, 97] 65

Figure 3. 1 Structures of the studied Pd(II) complexes (counter ions omitted to enable clarity).79

Figure 3. 2 Molecular structures of a) **PdL2** and b) **PdL3** with atom numbering scheme**.** The displacement ellipsoids of atoms are shown at the 50% probability level. The counter anion, chloride, is hydrogen bonded to the solvent molecule as shown by the blue dash.....91

Figure 3. 3 Molecular structure of **PdL4** with atom numbering scheme**.** The displacement ellipsoids of atoms are shown at the 50% probability level. The counter ion and the solvent for crystallization is omitted for clarity. 92

Figure 3. 4 A portion of the crystal packing of **PdL2** showing an inversion dimer, Pd–Pd interactions and Cl1⋯H interaction between the molecules (shown in blue dashed line). The chloride counter ion and the solvent water molecules are omitted for clarity. 94

Figure 3. 5 Crystal packing of **PdL3** showing an inversion dimer having Pd-Pd interactions. The chloride counter ion and methanol solvent molecule omitted for clarity. 95

Figure 3. 6 UV-Visible absorption spectra scans of **PdL3** (3.0×10^{-4} M) and **Tmtu** (0.015M).96

Figure 3. 7 Stopped-flow kinetic trace at 380 nm of **PdL2** and **Dmtu** at 298 K 97

Figure 3. 8 Dependence of k_{obs} on the nucleophile concentration for chloride substitution from **PdL4** at T = 298 K. 98

Figure 3. 9 Eyring plots for tne **PdL3** complex 100

Figure 4. 1 Structures of the Pd(II) complexes under study (where necessary, counter ions omitted for clarity) 133

Figure 4. 2 Stopped-flow kinetic trace at 330 nm for the reaction of **Pd3** (2.0×10^{-4} M) with **Dmtu** (4.0×10^{-3} M) solutions in methanol at 298 K. 142

Figure 4. 3 The dependence of k_{obs} on the nucleophile concentrations for the chloride substitution from **Pd1** at T = 298 K. 143

Figure 4. 4 Eyring plots for the reactions of **Pd4** with the nucleophiles.....145

Figure 4. 5 A pictorial illustration of nature of change in the trans-effect indicating flow of electron density in **Pd2** and **Pd3** complexes. 149

Figure 5. 1 Structures of the investigated Pd(II) complexes in this study 176

Figure 5. 2 Molecular structure of **Pd(4-Me-PBI)Cl** with atom numbering scheme. The displacement ellipsoids of atoms are shown at the 50% probability level. 185

Figure 5. 3 Stopped flow kinetic trace at 360 nm for the first step reaction of **Pd(BPI)Cl** (1.0×10^{-4} M) with **Tu** (3.0×10^{-3} M) at 308 K.....191

Figure 5. 4 UV-visible spectra for the second step reaction of **Pd(BPI)Cl** (1.0×10^{-4} M) with Tu (3.0×10^{-3} M). Inset; single exponential kinetic trace at 360 nm at 298 K..192

Figure 5. 5 Dependence of $k_{obs(1\ or\ 2)}$ on the nucleophile concentrations reactions with **Pd(BBPI)Cl** in ethanol solvent, I = 0.01 M CF_3SO_3H, T = 298 K (**a**) First step (chloride substitution) (**b**) Second step (dechelation). 193

Figure 5. 6 Eyring plots of the reactions of **Pd(BII)Cl** with the nucleophiles 195

Figure 5. 7 **(a)** Time-dependent changes in the ^{1}H NMR chemical shifts of the $H_\beta/H_{\beta'}$ and N–H protons for the reaction between **Pd(4-Me-BPI)Cl** and **Tu** (6 equivalents) in tetrahydrofuran-d_8. (**b**) ^{1}H NMR of the free ligand showing only the $H_{\beta'}$ proton and N-H chemical shifts.....197

Figure 6. 1 Structures of the investigated Pd(II) complexes 238

Figure 6. 2 Molecular structure of [**a**] **PdL^2** and [**b**] **PdL^3** with atom numbering scheme. The displacement ellipsoids of atoms are shown at 50% probability. Solvent of crystallization is omitted for clarity in the case of **PdL^2**. 248

Figure 6. 3 Part of the crystal packing of **PdL^2** showing asymmetric unit of inversion dimer with C···C interactions (shown in blue dashed lines) and π···π interactions (shown in purple lines) between the aromatic rings of the molecules.....251

Figure 6. 4 A section of the crystal packing diagram of **PdL^3** showing an inversion dimer with C···C interactions (shown in blue dashed lines) and π···π interactions (shown in purple lines) between the aromatic rings of the molecules.....252

Figure 6. 5 Stopped-flow kinetic trace at 388 nm of **PdL^4** (1.0×10^{-4} M) and **Dmtu** (4.0×10^{-3} M) at 298 K.....256

Figure 6. 6 Dependence of k_{obs} on the concentration of the nucleophiles for the reactions with from **PdL^2** at T = 298 K.....257

Figure 6. 7 Eyring plots of **PdL^3** with the nucleophiles.....259

Figure 7. 1 Structures of the investigated complexes (counter ion tetrafluoroborate omitted for clarity) 292

Figure 7. 2 DFT optimized structure of **(NHC)Pd4** showing the deviation of the twisted angle between the *cis*-fragment plane and the main plane and the H⋯Cl length 303

Figure 7. 3 Stopped-flow kinetic trace at 320 nm of **(NHC)Pd3** (4.0 x 10^{-4} M) and **Dmtu** (1.6 x 10^{-2} M) at 298 K. 304

Figure 7. 4 Dependence of k_{obs} (s^{-1}) on the concentration of nucleophiles for the reactions with **(NHC)Pd2** in water I = 20 mM LiCl, T = 298 K. 305

Figure 7. 5 Eyring plots for the reactions of **(NHC)Pd4** with the nucleophiles 307

Figure 8. 1 Structures of the nucleophiles suggested for the substitution from the Pd(II) aqua complexes.....343

Figure 8. 2 Proposed polypyridyl Pd(II) complexes to further the work in this study. 344

List of Tables

Table 2. 1 The entering group effects on the rate of substitution of $Pd(acac)_2$.....59

Table 2. 2 Effect of solvent on the rate of chloride exchange from the *trans*-$[Pt(py)_2Cl_2]$[101]...60

Table 2. 3 The effects of leaving group on the observed *pseudo* first order rate, k_{obs}, of $[Pt(dien)X]^+$ and $[Pt(dien)X]^+$ complexes in water at 25 °C.[104, 105].....62

Table 2. 4 The rate constants and activation parameters for the substitution of chloride ligand from $[Pd(R_n dien)Cl]^+$ by iodine in water at 25 ºC.[112].....63

Table 3. 1 DFT optimized HOMO, LUMO frontier molecular orbitals and planarity structures of the Pd(II) complexes at B3LYP/LANL2DZ theory level (iso value = 0.02).....87

Table 3. 2 Summary of calculated parameters for complexes studied 88

Table 3. 3 Crystal data and structure refinement for the complexes 90

Table 3. 4 Selected bond distances (Å) and angles (º).....93

Table 3.5 k_2 values and thermodynamic parameter data for the reactions of the Pd(II) complexes with the nucleophiles in methanol, I= 30mmol, LiCl. 99

Table 4. 1 The DFT optimized HOMO, LUMO frontier molecular orbitals and the planarity structures of the complexes at B3LYP/LANL2DZ theory level (Iso value = 0.02). 140

Table 4. 2 Calculated parameters for the Pd(II) complexes 141

Table 4. 3 k_2 values and thermodynamic parameter data for the reactions of Pd(II) complexes with thiourea ligands in methanol, I = 20 mM, LiCl.....144

Table 5. 1 Crystal data and structure refinement parameters 184

Table 5. 2 Selected bond angles and bond lengths for X-ray and DFT for **Pd(4-Me-PBI)Cl**. 185

Table 5. 3 The DFT optimized HOMO, LUMO frontier molecular orbitals and planarity for the complexes at B3LYP/LANL2DZ theory level (Iso value = 0.02).....188

Table 5. 4 Summary of the calculated parameters for complexes studied 189

Table 5. 5 k_1 and k_2 data for the reactions of the Pd(II) complexes with the nucleophiles in ethanol, I = 0.01M CF_3SO_3H, T = 298 K.....194

Table 5. 6 Thermodynamic parameters 196

Table 6. 1 Crystal data and structure refinement parameters for **PdL^2** and **PdL^3** 249
Table 6. 2 Selected bond lengths and bond angles 250
Table 6. 3 DFT optimized HOMO and LUMO frontier molecular orbitals and the planarity for the complexes at B3LYP/LANL2DZ theory level (Iso value = 0.02). 253
Table 6. 4 Calculated parameters of the Pd(II) complexes 254
Table 6. 5 Values k_2 at 298 K, $\Delta H^{\#}$ and $\Delta S^{\#}$ for the reactions of Pd(II) complexes with the nucleophiles. 258

Table 7. 1 DFT optimized HOMO, LUMO molecular orbitals and planarity of Pd(II) complexes at B3LYP/LANL2DZ theory level (Iso value = 0.02). 300
Table 7. 2 Summary of calculated parameters for complexes studied 301
Table 7. 3 The values of k_2 and thermodynamic parameter data of the reactions Pd(II) complexes with thiourea ligands in water, I = 20 mM LiCl. 306

List of Schemes

Scheme 2. 1 Associative substitution mechanism[45] 37

Scheme 2. 2 Proposed direct nucleophilic attack and solvotic pathways of associative substitution reaction of square planar complexes 44

Scheme 4. 1 Proposed reaction mechanism 144

Scheme 5. 1 Possible proposed mechanism for the reaction between Pd(II) complexes with thiourea nucleophiles in ethanol, I = 0.01M CF_3SO_3H. 199

List of Abbreviations

Å	Angstrom (10^{-10} m)
T	Temperature
K	Kelvin
C	Celsius
kJ	Kilojoules
g	Gram
mg	Milligram
mL	Milliliter
M	Molar, (mol L^{-1}) or metal
k_1, k_2, k_{-2}, k_{-1}	Rate constants
I	Ionic strength
DFT	Density functional theory
s, m, h, d (time)	Seconds, minutes, hours, days
NMR	Nuclear magnetic resonance
s, d, t, m, br (NMR)	Singlet, doublet, triplet, multiplet, broad
δ	Chemical shift
ppm (NMR)	Parts per million
MS	mass spectrometry
LC-MS	Liquid chromatography-mass spectrometry
TOF-MS	Time-of-flight mass spectrometry
ESI	Electrospray ionization
HOMO	Highest occupied molecular orbital
LUMO	Lowest unoccupied molecular orbital
MLCT	Metal to ligand charge transition
NBO	Natural bond orbital
nm	Nanometre(s)

Publications and Conferences Contributions

Publications

Tuning the reactivity of Pd(II) complexes through electronic and steric effects (**Submitted to New Journal of Chemistry, Manuscript ID NJ-ART-08-2018-003952**)

The role of 8-quinolinyl moieties in tuning the reactivity of Pd(II) complexes: A kinetic and mechanistic study. (**J Coord Chem, DOI: 10.1080/00958972.2019.1573994**)

Controlling the reactivity of Pd(II) complexes of 1,3-bis(2-pyridylimino)isoindoline ligands through alkylation and benzannulation: X-ray structure, kinetics, mechanistic and DFT study (**manuscript prepared and ready for submission**)

The Reactivity of Pd(II) complexes with C^N^N cyclometalated polypyridylphenyl Ligands: X-ray structures, kinetics and computational studies. (**manuscript prepared and ready for submission**)

Controlling the reactivity of Pd(II) complexes using 2,6-bis-N-heterocyclic carbene ligands: Kinetic and computational study (**manuscript prepared and ready for submission**)

Conferences Attended: Oral presentations

The 9th International Conference of the Kenya Chemical Society, United States University, Kenya 9th – 15th May 2017. *Controlling the reactivity of Pd(II) complexes using N-donor ligands: Crystal structures Kinetics and computational study.*

The 43rd SACI National Convention 2018 CSIR-ICC, Pretoria, South Africa, 2nd to 7th December 2018. *Controlling the reactivity of Pd(II) complexes through alkylation and benzannulation of 1,3-bis(2-arylimino)isoindoline ligands: Kinetics, mechanistic and computational study.*

Abstract

The influence of electronic and structural characteristics of the tridentate ligand systems of the type; N^N^N, C^N^N and C^N^N on the rate of substitution of the chloride ligand from mononuclear palladium(II) complexes were investigated. In this respect, five sets of modelled palladium(II) complexes were tailor-synthesised. Their characterization was done by NMR and mass spectroscopic techniques, while their purity was confirmed by the elemental analysis. The rate of the substitution of coordinated chloride from the complexes using bio-relevant thiourea nucleophiles of varied steric orientations was studied in solutions of methanol, water, ethanol, or dichloromethane under *pseudo*-first order conditions. The rate of substitution was measured as a function of concentration and temperature using stopped-flow and UV-visible spectrophotometer. Kinetic and mechanistic studies performed on the palladium(II) complexes with the stated nucleophiles would be helpful in predicting their possible interaction with the DNA. This has become part of the basic and prolonged search for alternative non-platinum based therapeutic drugs of better efficacy. Second-order kinetics with large negative activation entropies fully support the fact that mode of activation is associative.

The first set of complexes (in chapter 3) compared the effects of pyrazole and pyridine having different *cis*-positioned structural derivatives in the palladium complexes of chlorido-(2,2′:6′,2″-terpyridine)palladium(II) chloride (**PdL1**), chlorido-(2,6-bis(N-pyrazolyl)pyridine)palladium(II) chloride (**PdL2**), chlorido-(2,6-bis(3,5-dimethyl-N-pyrazolyl)pyridine)palladium(II) chloride (**PdL3**) and chlorido-(2,6-bis(3,5-dimethyl-N-pyrazolylmethyl)pyridine)palladium(II) tetrafluor-oborate (**PdL4**). The pyridine-based complex had higher rates of substitution due to its effective π-acceptor character than the pyrazole-based. The lower rate of substitution in the pyrazole based complexes is because of the poor π-acceptor ability and the strong σ-donor effect caused by the pyrazolic *N*-atom present in the chelate ring. Complexes with substituted methyl groups attached

to the pyrazole ring showed a deceleration in reactivity possibly due to the electron rich pyrollic-*N*, accumulating excess electron density around the palladium(II) metal centre. This makes it less electrophilic and lower the rate of reaction. A remarkable decrease in the reactivity was shown when a methylene spacer group was introduced between the *trans*-pyridyl and the *cis*-pyrazolyl rings, further lowering the electrophilicity due to reduction of π-acceptability of the ligand as well as causing flexibility into the complex framework which introduces steric hinderance further dampening the reactivity. X-ray quality crystal structures of the pyrazolyl-based complexes were isolated.

The second batch of Pd(II) complexes (in chapter 4) were those of N^N^N chelated framework, in which the π-extension was systematically increased by either introducing 8-quinolinyl moiety in place of 2-pyridylmethyl moiety or imine bond in the bis(2-pyridylmethyl)amine ligand framework. This was evidently done in the complexes of chloro-bis-(2-pyridylmethyl)amine)palladium(II), **Pd1**, chloro-8-[(2-pyridylmethyl)amino]quinolone)palladium(II), **Pd2**, chloro-N-(2-pyridinylmethylene)-8-quinolinamine)palladium(II), **Pd3** and chloro-bis(8-quinolinyl)amine)palladium(II), **Pd4**. The results showed that the introduction of the 8-quinolinyl moiety increases the π-conjugation but decreases the π-acceptability of the entire ligand leading to lower rates of substitution. Bis(8-quinolinyl)amine complex exhibited the slowest rate of substitution due to the stronger σ-donor effect of the coordinated 8-quinolinyl moiety, which make the Pd metal centre more electron-rich. This slows down the nucleophilic attack by the incoming nucleophiles.

The third series (in Chapter 5) inspected the influence of alkylation and π extension through benzannulation on the chlorido(1,3-bis(2-pyridylimino)isoindoline)palladium(II) complexes; chlorido-(1,3-bis(2-pyridylimino)isoindoline)palladium(II), **Pd(BPI)Cl**, chlorido-(1,3-bis(4-methyl-2-pyridylimino)isoindoline)palladium(II), **Pd(4-Me-PBI)Cl**, chlorido-(1,3-bis(2-pyridyl-

imino)benz(*f*)isoindoline)palladium(II), **Pd(BBPI)Cl** and chlorido-(1,3-bis(1-isoquinolylimino)isoindo-line)palladium(II), **Pd(BII)Cl**. The rate of substitution decreased through benzannulation in both the *cis* and *trans*-positions as well as by the *cis*-alkylation. This reiterated the electron richness caused by the *cis*-alkylation and *trans*-benzannulation on the complexes. *Trans*-benzannulation and *cis*-benzannulation causes electronic and steric influences respectively, while the *cis*-methylation influences the reactivity through both factors. ^{1}H NMR confirmed the detachment of the ligand from the Pd metal centres of all the complexes except that of the *cis*-benzannulated complex. The reactivity trend is contrary to the increasing extended π-conjugation. X-ray crystal structure of the *cis*-alkylated complex was elucidated.

The fourth set of complexes (in chapter 6) deals with understanding the role of *cis*-π-extension and the strong *cis*-carbon σ-bond on the rate and mechanism of substitution of the labile chloride ligand from the cyclometalated Pd(II) complexes coordinated to C^N^N polypyridylphenyl ligands; chloro-4-(3,5-di-tert-butylphenyl)-6-phenyl-2,2'-bipyridine)palladium(II), **PdL1**, chloro-3-(4-(3,5-di-tert-butylphenyl)-6-phenylpyridin-2-ylisoquinoline)palladium(II), **PdL2**, chloro-(4-(3,5-di-tert-butylphenyl)-6-(naphthalen-2-yl)-2,2'-bipyridine)palladium(II), **PdL3** and chloro-3-(4-(3,5-di-tert-butylphenyl)-6-(naphthalen-2-yl)pyridin-2-ylisoquinoline)palladium(II), **PdL4**. The *cis*-coordinated naphthyl group behaves in anomalous way in the complexes and reduces the reactivity of the Pd metal centre more than the *cis*-isoquinolyl group in a similar coordination position. A combination of both isoquinoline and naphthalene moieties in the *cis*-position of the ligand structure further decelerates the rate of reaction due to strong σ-donation of electrons around the metal centre. The solid-state crystal structures of the complexes bearing isoquinoline and naphthalene moieties are reported. The DFT descriptor electronic chemical potential (μ) supports the reactivity trend of the complexes.

The fifth system of a series of 2,6-bis(NHC) Pd(II) complexes (in chapter 7) sought to investigate the effects of strong σ-donor properties caused by the two *cis*-carbon of the bis(NHC) carbene ligand as well as steric properties forced on their coordinated Pd metal centre through methylene spacer group and size of N-substituent. The complexes under investigation were, chloro-2,6-bis(3-methylimidazolium-1-yl)pyridine)palladium(II) tetrafluoroborate, **Pd1**, chloro-2,6-bis[(3-methylimidazolium-1-yl)methyl]pyridine)palladium(II) tetrafluoroborate, **Pd2**, chloro-2,6-bis[(3-butylimidazolium-1-yl)methyl]pyridine)palladium(II) tetrafluoroborate, **Pd3**, and chloro-2,6-bis[(3-methylbenzimidazol-1-yl)methyl]pyridine)palladium(II) tetrafluoroborate, **Pd4.** The reactivity of pyridine-bridged complex is higher than those of lutidine-bridged complexes due to π-backbonding of the in-plane aromatic rings. The reactivity of the lutidine-bridged type of complexes is influenced by both electronic and steric factors with the least reactive being that of the N-butyl substituent due to strong σ-donation into the coordination centre. In addition, the net σ-donation of the ligands to the metal centre plays a role in determining the reactivity trend of the complexes. This is seen in the successive increase in HOMO energy levels going from the most reactive to the least reactive complex reflected in the DFT calculations which supports the reactivity trend.

CHAPTER 1

Platinum and Palladium Anticancer Drugs

1.0 Introduction

This chapter reviews the chemistry of active antitumor platinum(II), Pt(II), and palladium(II), Pd(II) metal complexes some of which are already in use for the chemotherapeutic treatment of cancer. Pd(II) complexes, especially those coordinated by N-donor ligands have been explored for their antitumour cytotoxic activity against several cancer cell lines and some of them have demonstrated good antiproliferation activity. The review will conclude by outlining the aim and objectives of the work which will be reported in chapters 3 – 7.

1.1 Cancer: A global Killer Disease

Cancer is one of the world's leading debilitating disease and killer to the humanity.[1] It is caused mainly by abnormally rapid and uncontrolled genetic cell transformation.[2, 3] Cancer is triggered by irreparable mutation of normal cells in the human body [4] and their abnormally rapid replication. Due to their uncontrollable rate of multiplication, masses of tissues known as tumours are formed as illustrated in Figure 1.1.

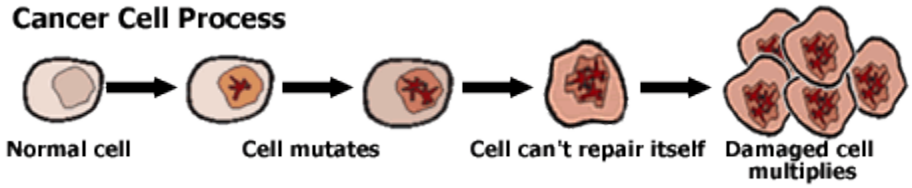

Figure 1. 1 Process of cancerous cell development process [5]

In humans, genetic mutations and abnormalities are caused mainly by environmental factors such as exposure to carcinogens (such as from car exhaust fumes), toxic chemicals (such as asbestos, arsenic, tobacco smoke) and sensitising and ionising radiations (such as gamma and X- and γ-rays, ultraviolet B) which directly damage DNA.[6-9] Internal factors such as compromised

immune systems and inherited mutations also cause cancer.[10] Aging has been linked to more risk to cancer triggering environmental factors [11]

The common types of cancer affecting humans are cancer of the oesophagus, lung, liver, stomach, cervical, colorectal, breast, and prostate. A 2018 report by the World Health Organization (WHO) revealed that an estimated 9.6 million people died of various cancer. Of these deaths the most common were caused by lung (2.09 million), skin (non-melanoma 1.04 million), prostrate (1.28 million), colorectal (1.80 million), stomach (1.03 million) and breast (2.09 million) cancer cases.[12] In most cases cancer is treated by chemotherapy, immunotherapy, surgery and radiotherapy methods.[13-20] Each of these methods can be used alone or as a combination, depending on the location, stage and type of cancer as well as patient's health status.[20-23] Despite the treatment methods and anti-proliferation medicinal agents, curing of cancer still remains a mammoth task due to resistance which may develop after initial response to the drugs.[24] Besides, there is no broad spectrum chemical drug that is active in all cancer cells. Also, some cancer metastates to other tissues and parts of the body. Because of this, efforts geared towards finding new drugs, particularly metallodrugs, with improved cytotoxic efficacy towards the cancerous cells have been given priority.

1.2 Platinum-based Anticancer Drugs

The discovery of *cisplatin* as an anticancer drug[25] and its subsequent approval for clinical use in 1978,[26] made it one of the most widely used metallodrug for cancer chemotherapy globally.[27] To date, it has been used with good success for the treatment of testicular, small cell lung, ovarian, bladder, cervical, head, neck and esophageal cancers [28-35] among others. Tailor designed synthesis and activity evaluation of analogues of *cisplatin* such as *carboplatin* (*cis*-diammine(1,1-cyclobutanedicarboxylato) platinum(II)), *oxaliplatin* (*trans*-R,R-cyclohexane-(1,2-diamine)oxalatoplatinum(II)) led to their clinical approval in some countries for use, in

combinations or as complementary anticancer drugs.[26, 27, 36, 37] In addition, *lobaplatin*, *nedaplatin* and *heptaplatin* have also received clinical approvals in china, Japan and North Korea respectively,[27] while others including *satraplatin* and *picoplatin* are still in the development stages.[38] The structures of *cisplatin* and its analogues are shown in Figure 1.2. However, some of the Pt-based anticancer lead drug candidates have since been terminated from further clinical trials due to either their acute toxicity or their lack of superiority over *cisplatin*.[39] These include drugs such as enloplatin, cycloplatam, TRK-710, sebriplatin, BBR3464, miboplatin, iproplatin, spiroplatin, SPI-077, zeniplatin, NSC 170898, ormaplatin JM 11 and aroplatin.[39]

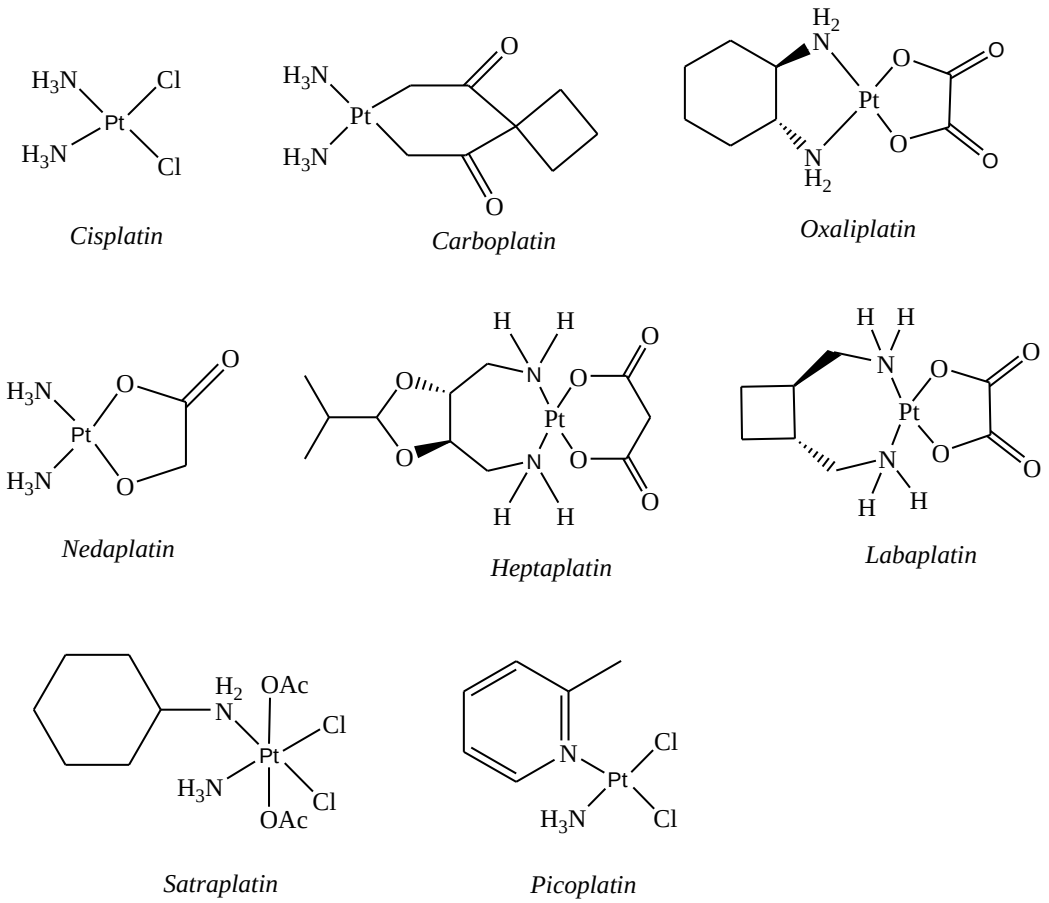

Figure 1. 2 Commercial platinum-based anticancer drugs

1.2.1 Mechanism of Action of Pt-based Drugs

The mode of action of *cis*-Pt-based anticancer drug candidates follows the same mechanism as that of *cisplatin* which is shown in Figure 1.3.[40] Due to poor solubility, c*isplatin*, is administered through the vein into the blood stream to protect it from premature hydrolysis in the acidic medium of the digestive track.[41] The high concentration of the chloride ion (100 mM) in the blood stream prevents the premature hydrolysis of the drug before reaching the nuclei of the cells.[26, 36] Diffusion into the cell takes place through passive or active transport mechanisms [42] depending on the charge of the Pt complex, and the lipophilic or hydrophobic characteristics of the ligand.[43] Once *cisplatin* enters inside the cell, the lower chloride ion concentration (4–20 mM) aids its hydrolysis to form a positively charged complex, $[Pt(NH_3)_2Cl(H_2O)]^+$.[36] The positively charged species bind with the most nucleophilic sites of the DNA which have the least hinderance, *viz.* the N7 atoms of purine residues of guanine or to some extent those of adenosine. This leads to the formation of monofunctional DNA adducts.[26, 44] The remaining chloride ligand is subsequently hydrolysed also, and the aqua ligand is then substituted by the second guanine-base resulting into the formation of the DNA cross-link.[26]

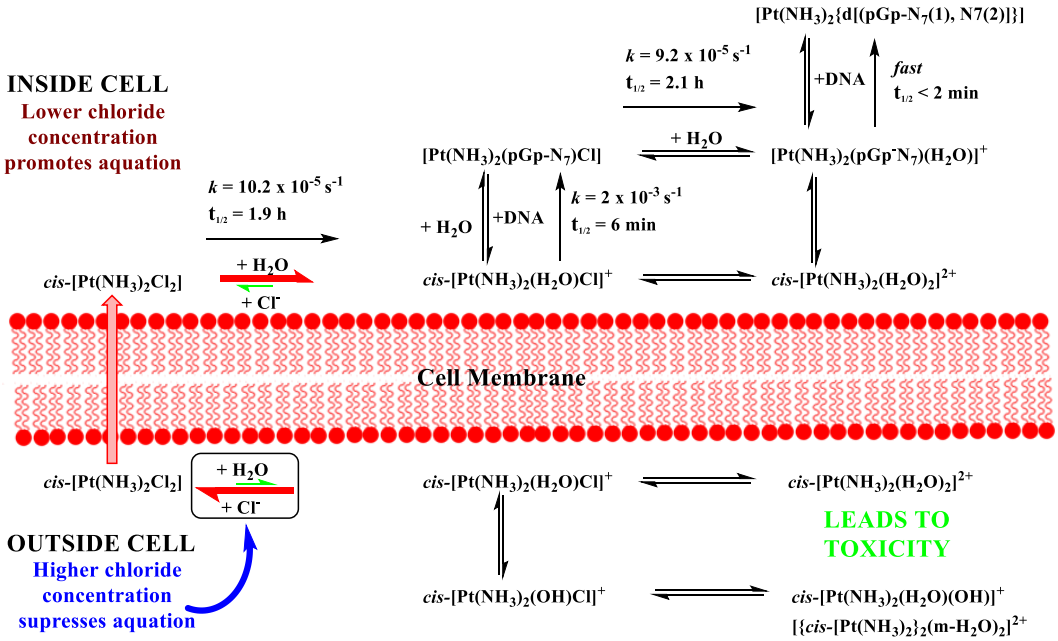

Figure 1. 3 Hydrolysis of *cisplatin* and its interaction with DNA.[40]

The DNA cross-link can either occur between deoxyguanosines of the same strand or on different strands yielding intrastrand and interstrand DNA cross-links, respectively (Figure 1.4). However, the most prevalent form is the intrastrand cross-links, 1,2-d(GpG) (65-70 %), 1,2-(ApG) (25%) and 1,3-d(GpTpG) (5 - 10 %), which are the major cytotoxic DNA adducts,[45] along with small amounts of GG cross-links which also form.[26, 46, 47] Figure 1.4 illustrates the different binding possibilities between the Pt(II) drug and the DNA.[26] The GG intrastand platination deforms the helical structure of the DNA through bending and this illicit the binding of high mobility group (HMG) proteins into such impairments. The binding of the HMG protein shields the impairments against cellular machinery repair resulting in some cases to apoptosis ("programmed cell death").[48] If the Pt-DNA adducts are repaired and the cell survives death, then drug resistance may ensue.

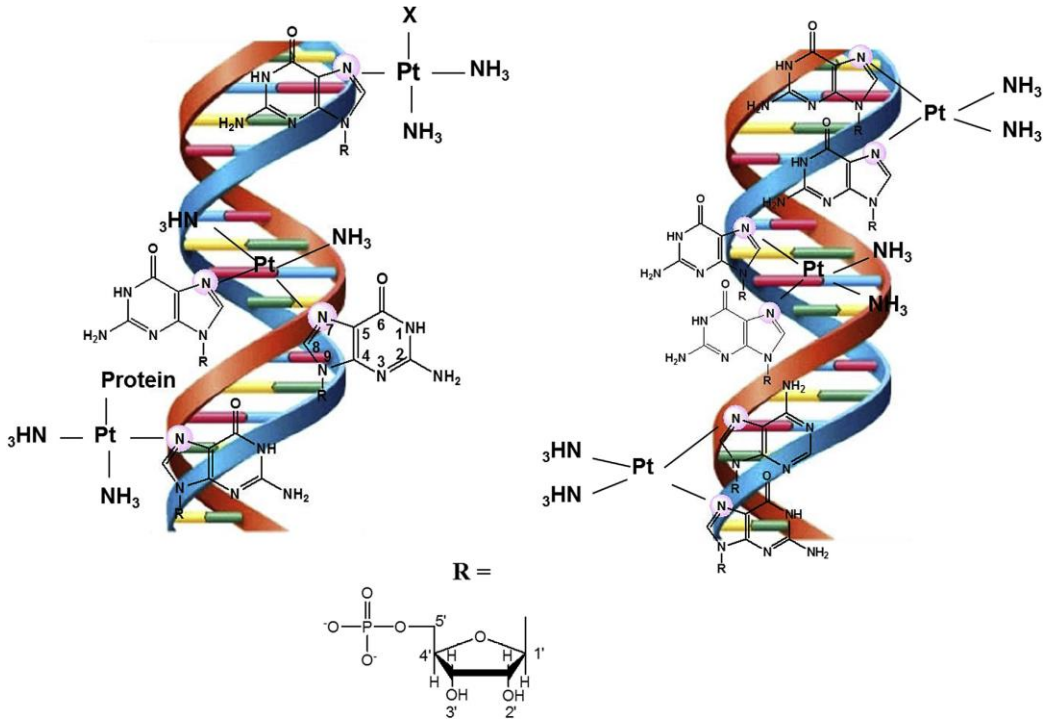

Figure 1. 4 Different ways of interaction of *cisplatin* with DNA showing 1,2-intrastrand cross-links.[26]

Along the way to the targets, Pt complexes can also react with other S-containing biomolecules present inside the cell such as thioethers and thiols as depicted in Figure 1.5.[49] This is because the S-containing biomolecules have a strong affinity for Pt complexes resulting into stable Pt–S compounds. Most of the Pt drugs is thought to priory bind to sulfur before reaching DNA given the relatively high concentration (about 10 mM) of glutathione(GSH) and L-cysteine within the cell system.[49, 50] The ligand exchange reactions of S-nucleophiles with Pt(II) complexes is kinetically favoured. However, competition studies have demonstrated that the Pt–S(thioether) bond can then be substituted by DNA purine bases to form N7 kinetic substituted products. Because of this some Pt–S compounds has been mixed with Pt drugs as Pt-reservoirs and as chemoprotectors. [49, 51] However, Pt(II) complexes can also bind to sulfur atoms of thiols forming a much more stable Pt–S(thiol) bond which is substitutionally inert. The Pt–S(thiol) compounds are deactivated forms of the metal drug and onsets development of resistance. Their inertness has been largely considered as the one responsible for severe/acute toxic side effects if the Pt(II) complexes' drug is to bound to a thiol of an amino residue of proteins. To minimize the side effects, Pt(II) drugs are normally administered along with chemoprotecting (rescue) agents which are exclusively S-containing compounds.[26, 49, 52]

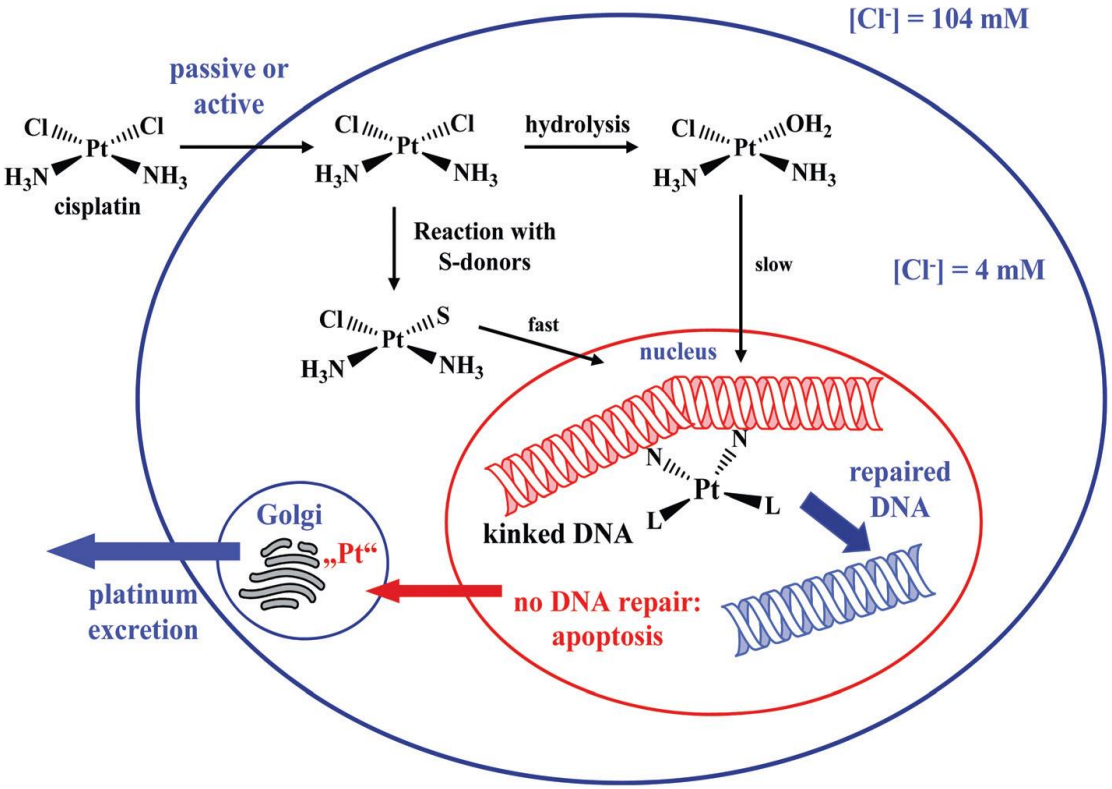

Figure 1. 5 Schematic pathways of *cisplatin* in the cell showing the biological processes involving sulfur compounds thought to act as potential drug agents in chemotherapy.[49]

1.2.2 Side Effects of Pt-based Drugs and the Need for Alternatives

Chemotherapy of Pt-based anticancer drugs is shrouded with nephrotoxicity, gastrointestinal toxicity, ototoxicity, cardiotoxicity, nausea vomiting, acquired or intrinsic resistance, bone marrow suppression, and neurotoxicity.[26, 45, 53] These limitations have challenged researchers to look for alternative transition metal-based drugs with better efficacy, reduced toxicity and increased spectrum of activity as well as limited solubility.[54, 55] Some metal complexes of copper, iridium, tin, ruthenium, gallium, rhodium, gold, palladium and rhenium have shown antitumour activity.[56-63] Of these, Pd(II) complexes are the closest structural analogues of Pt-based drugs and as a result, some of the Pd(II) complexes have emerged as promising attractive alternative drugs because they have shown good activity against tumours which are resistant to *cisplatin* or in which *cisplatin* is inactive.[64] In addition, some of these Pd(II) complexes have

shown good cytotoxicity towards several cancer cell lines,[65] less side effects[66-68] and better aqueous solubility[26, 69-71] compared to *cisplatin* as well as other Pt-based drugs. Furthermore, Pd derivatives permeate easily between the membranes in the body as well as exhibiting good interactions with DNA[72] resulting in better anticancer activity and lower toxic side effects[54, 66, 73] as well as less kidney toxicity (nephrotoxicity)[74, 75] than some of the clinically used metallodrugs.[26] Therefore, some of the Pd(II) complexes which have been synthesized and shown antitumor activity over the years are reviewed in the subsequent section, their activity will be compared with the classical Pt(II)-based antitumor drugs currently in use.

1.3 Palladium Anticancer Chemistry

Even though the synthesis of Pd complexes with antibacterial, antifungal, anticancer and antiviral activities dates back to 40 years ago,[76] the anticancer activity of Pd complexes has attracted enormous interest from various researchers within the last 20 years and as such, they have advocated for the use of Pd(II) complexes as possible anticancer agents.[38] This has been made more applicable due to the similarity between its structural and coordination chemistry with Pt(II) complexes as well as exhibiting promising cytotoxicity.[65] As much as the structural similarities exists, designing Pd anticancer drugs has posed great challenges since they are about 10^3 – 10^5 times more reactive than their Pt(II) analogues.[26, 77-79] As a result, Pd compounds should theoretically show lower antitumor activity because of their fast hydrolysis of the leaving groups that would readily dissociates in solution. The highly reactive species which form would limit the complexes from reaching their pharmacological targets (DNA) to perform their therapeutic function.[65, 80, 81] In addition, some of the Pd complexes, particularly those with non-cyclometalated ligands, undergo rapid *cis-trans* isomerism kinetics. [81-83] Because of the high rate of isomeric interconversion, Pd(II) complexes that are antitumour active can be stabilised by a strongly coordinated nitrogen multidentate non-leaving ligand and a suitable leaving group. A

reasonably non-labile group would enable the drug to maintain its form *in vivo* for a long time.[81, 84]

On the contrary, researchers have made strides worldwide in looking for Pd(II) complexes which are coordinated with strategic spectator ligand and are antitumor active. These compounds have displayed promising activity against several tumour cell lines. [28, 54, 55, 71, 77, 85-91] In general, the synthetic design of these Pd(II) antitumor agents have followed the same strategies that have been used to design potential Pt antitumor drugs,[84] and their cytotoxicity are normally compared to the standard Pt-based drugs (e.g. *cisplatin*, *carboplatin* and o*xaliplatin*). The mode of action of Pd(II) complexes are noticeably similar to that of Pt(II) reference standard drugs with less side effects in comparison to other heavy metal anticancer compounds.[73, 77]

1.3.1 Mononuclear Palladium(II) Complexes

Mononuclear Pd(II) complexes are simple compounds in which a single central Pd atom is coordinated with other monodentate or multidentate (bidentate or tridentate) ligands.[38] These ligands, particularly the multidentate, easily affects the stability of the coordinated Pd metal centre through electronic and steric influences. In addition, the flexibility of their structures due to a variety of properties influences reaction pathways that makes them suitable for biological studies. For purposes of anticancer studies, nitrogen donor ligands are known to strongly coordinate to Pd metal centre, making it stable and hence maintain its structural integrity long enough in biological systems which allows it to reach its *in vivo* target and perform its therapeutic action. Several Pd(II) complexes with such coordination have raised hopes towards finding antitumor Pd drugs because their cytotoxicity against some cancer cell lines have shown either comparable or superior activity relative to the known standard clinically used Pt-based anticancer drugs (*vide infra*).

1.3.1.1 Trans-palladium(II) Complexes

Some *trans*-Pd(II) complexes have shown higher cytotoxicity values than their *cis*-isomers.[38, 84] In addition, they have also been shown to have equal, better and for some cases superior antitumor activity than their *cis*-Pt analogues as well as some Pt anticancer drugs already in clinical use (*cisplatin*, *carboplatin* and *oxaliplatin) in vitro* studies.[71, 84] For instance, compared to *cisplatin*, the corresponding Pd(II) complex, **1,** *cis*-[$PdCl_2(NH_3)_2$] (Figure 1.6) as well as a related complex, *cis*-[Pd(DACH[a])Cl_2] do not show any activity against tumour cells.[84] This is because they rapidly isomerize to their inactive *trans*-isomers which in turn rapidly hydrolyses leading to *in vivo* interactions with many other biomolecules such as proteins. This prevents them from reaching their pharmacological target, DNA. [71, 92] This significantly compromises their antitumor activity and is in sharp contrast to their Pt analogues which are active. Because the reactivity of Pd complexes is high, spectator ligands with favourable attributes as well as bulky monodentate chelates should be utilised so as to slow down the rate of their hydrolysis in biopic media to ensure kinetic inertness of the complex and hence better antitumor activity of the Pd compound. [71, 83, 84] These attributes can be electronic or steric derived. For example, steric hindrance due to coordinated bulky spectator ligands have been exploited to curtail the rate of hydrolysis and also the rate of *cis-trans* isomerism as illustrated in Figure 1.6. In the shown examples, the *trans*-palladium isomer is more inert towards hydrolysis and the subsequent rapid reactions with deactivating bionucleophiles such as sulfur containing molecules.[71, 93]

[a] 1R,2R)-(-)-1,2-diaminocyclohexane

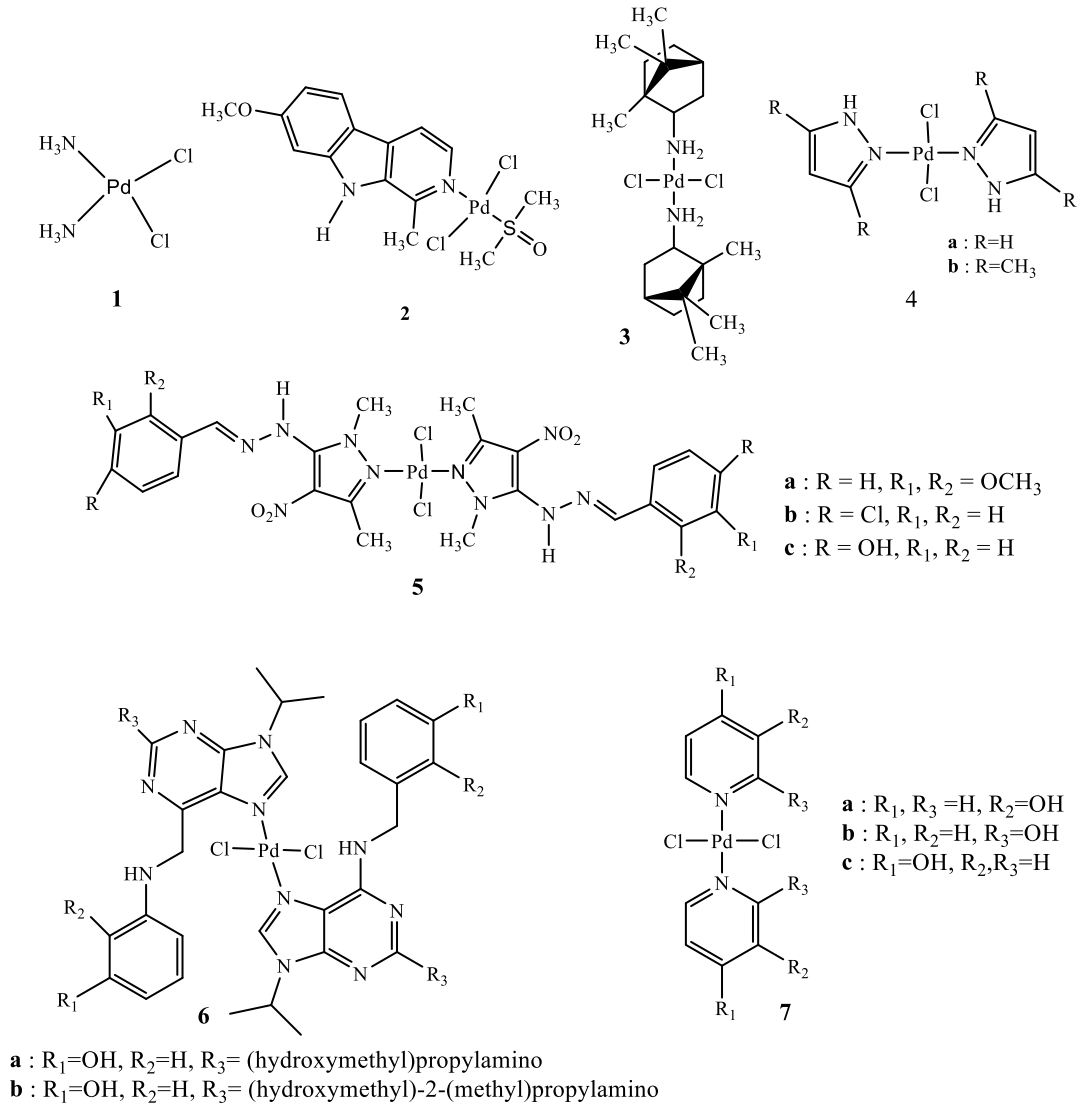

Figure 1. 6 Some of the palladium(II) complexes anticancer agents.[38, 84, 91]

One way of making *trans*-Pd(II) complex was achieved by the use of naturally occurring spectator ligands, such as that used in **2** [94] (Figure 1.6). This complex was tested for antitumor activity and found to exhibit higher cytotoxicity against a series of leukaemia (P388, L1210 and K562) cell lines than the reference anticancer drugs; *cisplatin*, *carboplatin* and *5-fluorouracil*. [94] The earlier study [93] on complex **3,** the bornylamine-coordinated complex showed a similar and high cytotoxic activity against HeLa cell lines when compared with the activity of *cisplatin*, *carboplatin* and *oxaliplatin*.[93]

Several trans-Pd(II) complexes coordinated with pyrazole or its derivatives have been evaluated for their antitumor activity. For example, Keter[95] synthesized Pd(II) complexes **4a** and **b** containing pyrazole and 3,5-dimethylpyrazole ligands, respectively. *In vitro* evaluation confirmed that these complexes caused apoptosis on human cancer cells (of cervical epithelial carcinoma and T-cell leukemia) and ovarian fibroma of hamster.[91] Abu-Surrah et al.[71] synthesized complexes, **5a**, **b** and **c**, bearing pyrazole-based Schiff bases. The cytotoxic effect of these complexes against the head and neck squamous carcinoma cells (SQ20B and SCC-25) was found to be dose dependent and varied between cell type. The complexes **5a**, **b** and **c**, had higher clonogenic cytotoxic effects than *cisplatin* when tested on SQ20B cell line. In addition, further modification of the pyrazole ligand, in complexes **6a** and **b** presented better anticancer activities towards breast cancer and leukaemia cell lines compared to *oxaliplatin* and *cisplatin*.[88]

Apart from the Pd complexes of the *trans*-5-membered ring system, pyrazole, antitumor studies were extended to complexes **7a-c**. In these complexes, the *trans*-6-membered ring, pyridine was used as spectator ligands of complexes of the form: *trans*-$PdCl_2L_2$, where L = 4-hydroxypyridine, 3-hydroxypyridine and 2-hydroxypyridine, for **7a,** 7**b** and 7**c,** respectively. They were tested for antitumor activity against three ovarian cancer cell lines (A2780, $A2780^{cisR}$ and $A2780^{ZD0473R}$) by Huq *et al.*[96] All these compounds were less active than *cisplatin.* However, they were found to be more active against the resistant cell lines than the parent cell lines. The 2-hydroxypyridine based complex was found to be the most active against the three cell lines.[96]

Strong σ-donor N-heterocyclic carbene (NHC) ligands have been coordinated to Pd(II) complexes and their *trans*-complexes have also been shown to have some promising anticancer activities.[38] Ghosh and his co-workers synthesized Pd(II)(NHC) complexes **8** – **9** (Figure 1.7) and evaluated their activity.[97] The moieties on the ligands assumed a *trans* orientation to each

other to minimize steric repulsions of the bulky substituents in the NHC ligand. These complexes showed good antitumor activity against three human tumour cells *viz*: breast cancer (MCF-7), cervical cancer (HeLa) and colon adenocarcinoma (HCT 116). Antiproliferative activity of **9** was significantly stronger than that of *cisplatin*. Mechanistically this complex's antitumor activity was thought to be based on its prevention of the progression of the cell cycle at the G-2 stage and P-53 pathway followed by a programmed cell death. Another example of Pd(NHC) complex **10** (Figure 1.7) which is an isomer to complex **9**, was later presented by Haque and his co-workers. [98] This complex was synthesized through a transmetallation reaction between Ag(I)-NHC and a Pd(II) precursor. Using MTT assay method, the antitumor activity of **10** against human colorectal cancer cell lines (HCT 116) showed higher cytotoxicity at very low IC_{50} value making it a potential anticancer agent.

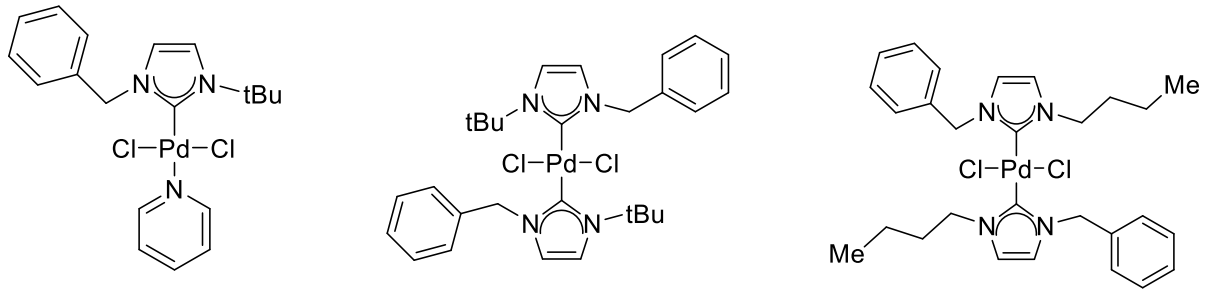

8 **9** **10**

Figure 1. 7 Palladium complexes bearing N-heterocyclic carbene ligands which have shown potential antitumor activity.[97, 98]

1.3.1.2 Bidentated Pd(II) Complexes

Bidentate N^N ligands coordinated to Pd(II) complexes have been shown to decrease the challenging effects of *cis-trans* isomerism[83, 99, 100] and improve their anticancer activity. For instance, **11** (Figure 1.8), a complex with a bidentate N^N coordination derived from a modification of ethylenediamine-spermine as well as putrescine (tetramethyldiamine) were found to have good antiproliferation of plasmid DNA conformational changes.[101] The spermine

complex gave similar antitumor activity to that of *cisplatin* towards breast (MDA- MB 468) and human leukaemia cancer (HL-60) cell lines, while the putrescine anticancer activity was encouragingly better because of lower IC_{50} values than *cisplatin*. A series of cationic complexes with ethylenediamine-based and pyridine and its derivatives as spectator ligands [92] one of which is **12**, (Figure 1.8) were evaluated for their cytotoxicity. These complexes showed significant increase in the cytotoxicity due to the increase in the electron donation properties of the substituents, leading to the improved donor strength of the coordinated pyridine ligand.[84] The family of these complexes further demonstrated *in vitro* cytotoxic activity against human leukaemia cell lines (HL-60) similar to that of *cisplatin*.[72]

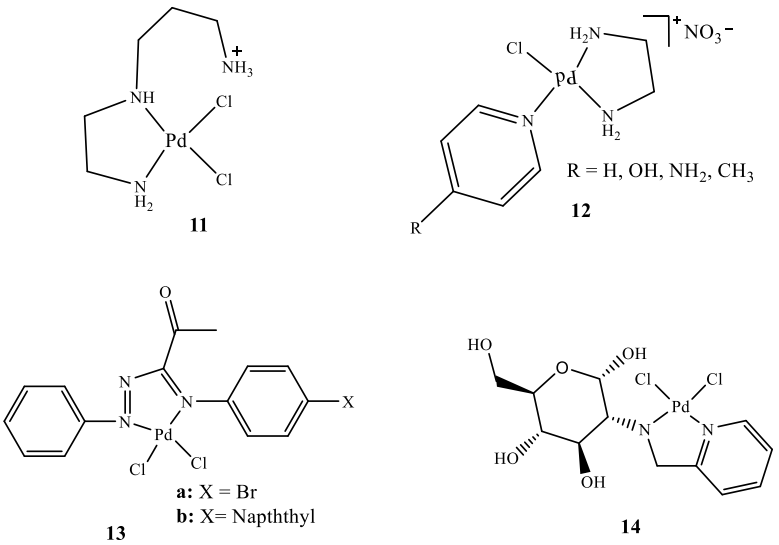

Figure 1. 8 Some of the N^N bidentate Pd(II) complexes as antitumor agents.[54, 92, 101, 102]

Pd(II) complexes **13a** and **b** (Figure 1.8) which have common phenylazo arylmethine bidentate ligand were also evaluated for antitumor activity against human ductal carcinoma (T47D) and murine mammary adenocarcinoma (MTLn3).[54] Higher cytotoxicity was shown against T47D breast cancer cell lines by these complexes than in the case of *cisplatin*, while their activity against MTLn3 was comparable. The enhancement of cytotoxicity was attributed to the electronegativity of the substituent attached on the azoimine ligand that is; the more the

electronegative the substituent is, the more the cytotoxicity against the cancer cell lines.[54] This meant that complex **13a** was more active than **13b**.

A glycoconjugated Pd(II) complex, [$PdCl_2(L^b)$], **14** (Figure 1.8) was synthesized by Tanaka *et al*.[102] The complex was tested for its cytotoxicity, ability to induce apoptosis as well as its ability to cause double-strand breaks in the DNA of the *cisplatin*-resistant gastric as well as the *cisplatin*-sensitive cancer cell lines *in vitro* and *in vivo*. Significant antitumor activity of **14** was reported in *cisplatin*-sensitive gastric cancer and the ability to overcome the *cisplatin*-resistant gastric cancer cells. Moreover, it also induced considerable apoptosis effects. This led to a conclusion that **14** is likely to show less toxicity to the kidney compared to *cisplatin*. In addition, this complex would present a better-quality anticancer drug because of its glucose conjugation component that may improve drug solubility and the tumour selectivity.

1.3.1.3 Terdentate Palladium(II) Complexes

Earlier structure – activity relationship of Pt(II) anticancer drugs had stipulated the *cis*-geometry as a necessary structural requirement for anticancer activity. One of the class of the complexes that defied this was the monofunctional terdentate complexes of Pd(II). This is so because only the chloride or aqua acts as the potential leaving group, yet they were found to be quite active. The differences in the lability of the leaving chloride group in different types of the Pd complexes changes the biochemical properties of the complexes since the bond breaking ability of Pd–Cl is a very critical step in the reaction of the complex with DNA strands.[55, 103] In addition, Pd metal centre benefits a lot from the terdentate coordination by gaining its stability and hence improving its antitumor activity. Figure 1.9 depicts some of the terdentate monofunctional Pd(II) complexes that have shown antitumor activity. Complexes **15**–**22** have demonstrated high cytotoxicity against several cancer cell lines. Complexes **15** and **16** (Figure 1.9) derived from 8-

[b] 2-deoxy-2-[(2-pyridinylmethylene) amino]-α-D-glucopyranose

aminoquinoline were tested on three cell lines, that is, human cervical cancer cell line (HeLa), human mammary cancer cell line (MCF-7) and human lung cancer cell line (A-549). Complex **15** exhibits a cytotoxicity comparable to that of *cisplatin* against A-549 and MCF-7 cell lines, and a higher antitumor activity against HeLa cell line while complex **16** is much less active than *cisplatin* in all the three cell lines.[104]

Various Pd(II) complexes bearing a terpyridine ligand system have been tested for their toxicity against several cell lines. Ulukaya *et al.* tested **17** (Figure 1.9) ([PdCl(terpy[c])](sac[d])·$2H_2O$, for its cytotoxicity against six prostate cancer cell lines, cancer stem cells, and primary culture. They found that the complex caused DNA damage, cell death, and autophagy,[105 28] because it binds strongly to the DNA as a metal intercalator and interacts with it *via* insertion of the planar terpyridine ring between the DNA base pairs followed by covalent binding.[106, 107] The complex also showed activity against breast cancer and antigrowth effect on a dose dependant marrow *in vitro* and *in vivo*[107] as well as small lung cancer cells,[108] prostate cancer cells[105] and fibrosarcoma[77] among others.[109] Further cytotoxicity studies were undertaken on a structurally similar complex to **17,** [Pd(sac)(terpy)](sac).$4H_2O$ **18** (Figure 1.9) against human breast cancer.[86] This complex emerged as a novel active drug for the treatment of breast cancer cell lines (MCF-7 and MDA-MB-231) with excellent antiproliferative properties observed *in vivo* on the Balb/c mice.[86] The mechanism of antitumor activity of the complex *in vitro* experiments was through induction of apoptosis by means of cell death receptors.

[c] 2,2' : 6',2''-terpyridine
[d] saccharinate

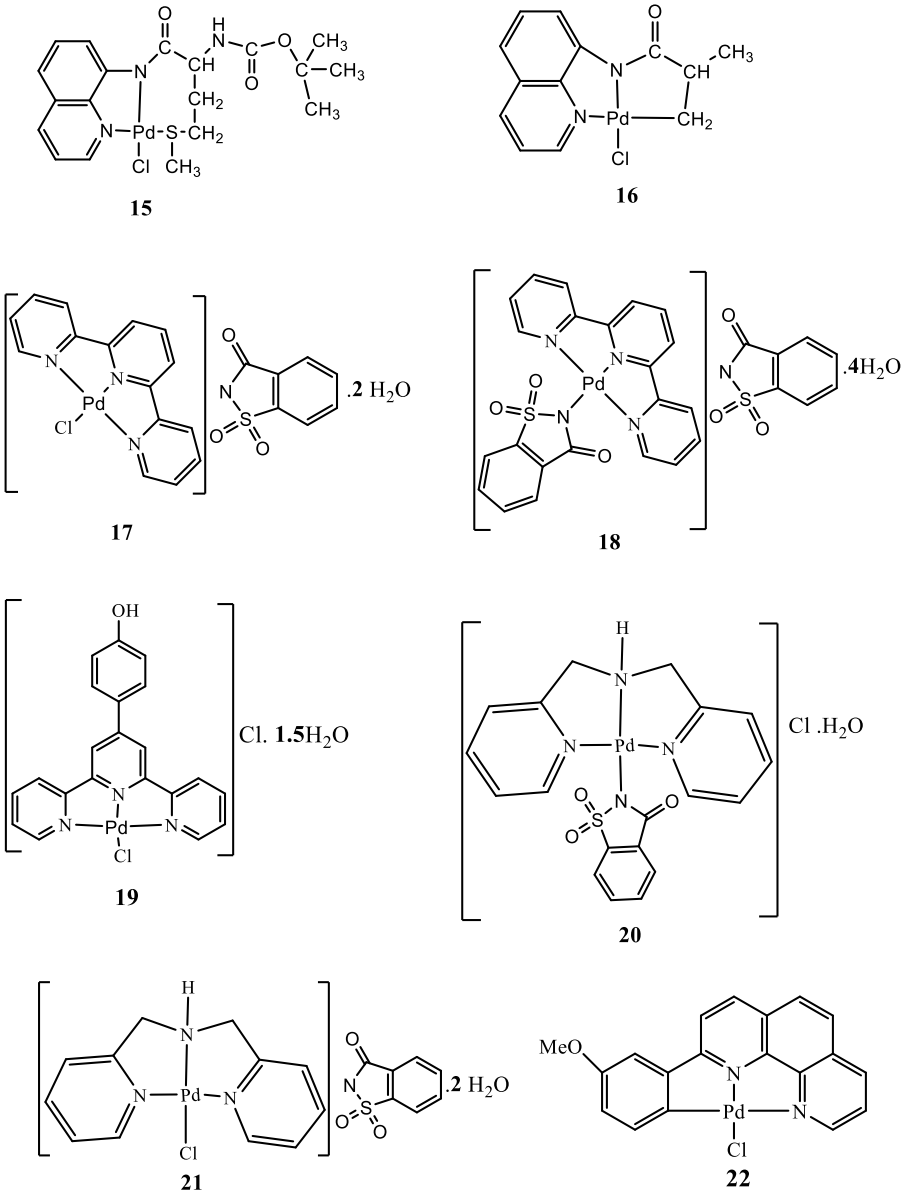

Figure 1. 9 Schematic structures of N^N^S, C^N^N and N^N^N terdentate Pd(II) complexes that have been tested for anticancer activity.[28, 86, 90, 104-107, 110]

Recently, Darabi *et al.* extended anticancer studies from complexes **17** and **18**, to their derivative [Pd(4-OHPh-terpy[e])Cl] **19 (**Figure 1.9**).** [110] The binding properties of this complex was shown to interact through a combination of effects such as intercalation, hydrogen bonding and covalent interactions with calf-thymus DNA (CT-DNA). The complex was tested for cytotoxic activity against five human tumour cell lines namely; breast cancer (MCF-7), erythroleukemic (K562),

[e] 4'-(4-hydroxyphenyl)-2,2',6',2''-terpyridine

small lung cancer (A549), hepatocellular carcinorma (Hep-G2) and colorectal adenocarcinoma (HT29).[110] The results illustrated that this complex is more effective against A549, HT29, MCF-7 and K562 by virtue of their lower IC_{50} values when compared to that of *cisplatin*.

Attractive lipophilic Pd-based complexes **20** and **21** bearing a bis(2-pyridylmethyl) amine (bpma) ligand and a saccharinate (sac), respectively, were tested for their anticancer activity in search for a better cytotoxicity. The cytotoxicity of these complexes were found to be active against Chinese hamster ovary (CHO), human lung carcinoma cancer (A549) and glioma cancer (C6) cell lines.[90] Compared to their Pt counterparts, Pd complexes were found to be more active against these cancer cell lines with complex **21** having close cytotoxicity to *cisplatin*.[90] The cytotoxicity of **21** against A549 was found to be comparable to those of earlier studied complexes [Pd(dmnp[f])$_2$Cl$_2$] and [Pd$_2$(dmnp)$_2$Cl$_4$]. [111] In addition, its cytotoxicity towards C6 cell lines was higher than those reported for [Pd(C2-dmba[g])(N$_3$[h])(dppp[i]) and [Pd(C2-N-dmba)(*cis*-dppet[j])][N$_3$].[112] Later, utilising MTT and ATP assays, complex **20** and **21** were examined against human breast cancer cell lines (MDA-MB-231 and MCF-7).[113] In the same study, these complexes were found to be more active against the breast cancer cell lines than their Pt counterparts as they could sufficiently induce apoptosis. Moreover, complex **20** was found to be the most active against the cell lines and was further subjected to *in vivo* studies against mouse and rat embryonic fibroblast NIH/3T3 and 5RP7, respectively.[113] The results revealed that the cytotoxicity was remarkable and the cell death process was induced by apoptosis.

Cyclopalladated complexes containing strong C – M σ-bond are promising anticancer agents since they can lead to lower rates of hydrolysis[38] and hence improved antitumor property of the

[f] 2,6-dimethyl-4-nitro-pyridine
[g] N,N-dimethylbenzylamine
[h] azide
[i] 1,3-bis(diphenylphosphino)propane
[j] 1,2-bis(diphenylphosphino)ethane

metal complexes. Because of this, complex **22** (Figure 1.9) was synthesized *via* cyclopalladation of 2-arylphenanthroline[38, 114] among several other related cyclopalladated complexes for cytotoxicity studies. Cytotoxicity screening was performed against a variety of human cancer cell lines namely; colon carcinoma (SW403, SW620 and SW1116), bladder carcinoma (HT1376), colorectal carcinoma (HT29/129) and breast carcinoma (ZR75-1). The *in vitro* cytotoxicity results demonstrated a good activity of the complexes including **22** against the cancer cells lines. With the understanding of the cytotoxicity of the complexes, an extrapolation of these complexes to *in vivo* antitumor activity of the cell lines that showed a differential cytotoxic response to *cisplatin* [38, 115] could easily be achieved.

Many Pd complexes have been shown to have anticancer activity comparable to *cisplatin* or even better. However, to date, despite the encouragingly promising efficacy of Pd metallodrugs for anticancer treatment, none of its compounds have been proven to be effective in patients[28] or subjected for clinical trials. This continues to impose great need for continued enthusiasm for research towards finding Pd complexes with efficacy towards a wider spectrum of action on tumours, higher cytotoxicity potential, high tumour selectivity, better solubility and further elimination of side effects in clinical use.[55] Also, key to developing novel Pd antitumor drugs is the continued search for good choice of ligands that are able to stabilize the Pd metal centre through appropriate ligand-metal interactions. In achieving this, there is need to underscore on the thermodynamic and kinetic stability of tailor-made Pd complexes with good antitumor activity. There remains limited data on kinetic and mechanistic studies on Pd-based complexes even though they are continuously being fronted as alternative antitumor drugs to Pt-based complexes.

1.4 Kinetic and Mechanistic Studies

The challenge to the inorganic and medicinal chemists to date, is to find ligands that would stabilize Pd-center to design kinetically inert and thermodynamically stable complexes that greatly increases its potential as antitumor agent. These type of ligands would confer varied structural orientation, electronic and steric, aqueous solubility and lipophilicity, ligand exchange behaviour and lability of the complex which finally enhances its capacity to interact with DNA and/or proteins.[55] Structural changes on the carrier ligand can significantly alter the physical and chemical properties of a complex, that is σ-donicity, π-acceptability, steric properties, solubility and hence improving their biological activities, particularly cytotoxicity towards cancer cells.[36, 41, 116-119] In addition, metal–ligand interactions always produces exceptional complexes whose properties are different from their individual ligands or metals. This metal-ligand interactions can influence ligand substitution reactions [120] which may provide several advantages towards metal interactions and coordinating with biological molecules.[39, 121] It is therefore important to elucidate the distinctive effects and roles played by varying spectator ligands on the kinetic properties of the complexes. This would predict the structure-activity relationship which is an important aspect in designing new metallodrugs.

To develop a good and efficient Pd anticancer drug, a comprehensive kinetic and mechanistic studies towards cellular targets is thus required. This will aid in understanding the mechanism of interactions between the palladium complexes and sulphur containing biomolecules as well as with DNA.[122] In addition, the stability of the final substituted product resulting from this interaction under different experimental conditions would provide basic foundation for further *in vivo* studies of the promising pharmacological agents and finding an alternative drug.[49]

In this thesis, the kinetic and mechanistic investigation of the substitution behaviour of modelled Pd(II) complexes of varied ligands were undertaken using appropriate sulfur containing

nucleophiles of varied steric influences. The reactions mimics possible interactions of Pd(II) complexes in biological systems, and the reactivity data forms part of essential information source in the protracted search of alternative Pd therapeutic drug with improved efficiency over the commonly used standard drugs.[123-125] Furthermore, the role of the ligand in making the highly reactive Pd centre inert with an aim of controlling the reactivity at the metal so as to put forward possible alternative candidate complexes with improved antitumor activity is exemplified.

1.5 Aims of the Study

It has been postulated that the better antitumor activity of Pd complexes is due to the easier detachment of the chloride ligand from the Pd centre, nevertheless this notion has not been substantiated.[38] In addition, multidentate nitrogen donor ligands are known to be good chelates and are able to strongly coordinate and cause inertness at the Pd metal center.[26] They have many distinctive advantages such as readily available and relevance in industrial applications as intermediates.[38] This aspect of nitrogen donor ligands allows numerous modifications resulting into ligands with distinct physicochemical properties relevant for anticancer studies.

Therefore, this work measured the rates of substitution from five sets of mononuclear Pd complexes having N^N^N, C^N^N and C^N^C chelates. Sulfur-based thiourea nucleophiles with varied steric influences *viz;* thiourea, N,N'-dimethylthiourea and N,N,N'N'-tetramethylthiourea were used as incoming or substituting ligands. These nucleophiles were chosen on the basis of their biological significance, good nucleophilicity, high solubility and appropriate model compounds representing thioether (σ-donor, π-acceptor) and thiolate (σ-donor) groups in the human cell.[126] Moreover, thiourea has been used as a protective agent to minimize nephrotoxicity caused by *cisplatin* administration.[52, 127, 128] Similarly, N,N'-

dimethylthiourea has been used in cytoprotection of kidney and liver against mitochondrial oxidative damage caused by *cisplatin*.[129, 130]

The main aim of this project was to use a variety of multidentate ligands to synthesize chelated Pd(II) complexes and to establish the substitution reactivity trends within each set. The rate of substitution of the chloride ligand from these complexes by biologically relevant thiourea nucleophiles were measured in solutions using stopped-flow and UV-Visible under *pseudo*-first order conditions. The trends in the rate of substitution would be insightful in understanding to what extent the spectator ligand would be influential in controlling the reactivity of the Pd metal. Density function theory (DFT) calculations were employed on the complexes using Gaussian 09 program suite[131] at the B3LYP (Becke 3-Lee-Yang-Parr) functional level in the basis set LANL2DZ (Los Alamos National Laboratory 2 Double ζ).[132] The data obtained was used to explain the observed experimental trends in the reactivity between the complexes. The specific objectives of this study were;

1. To investigate the role of pyrazole-based ligands in controlling the reactivity of the complexes from the well-known labilizing terpyridine-based ligands by measuring the rates of substitution from synthesized Pd(II) complexes chelated with bis(pyrazolyl)pyridine ligands with different substituents on the azole rings. The details of the findings, results and discussions are presented in **chapter 3**.

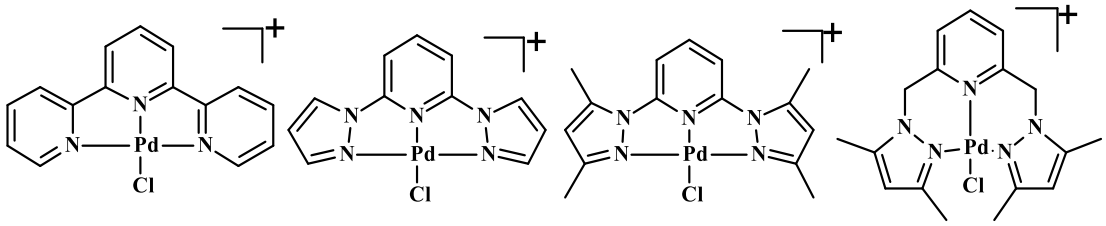

PdL1 **PdL2** **PdL3** **PdL4**

2. To measure the rates of substitution from tailor-made Pd(N^N^N) complexes (**Pd1** – **4**) having pyridine and quinoline moieties so as to understand the role of quinoline in tuning the reactivity of Pd(II) complexes. The details of the results will be reported and discussed in **chapter 4**.

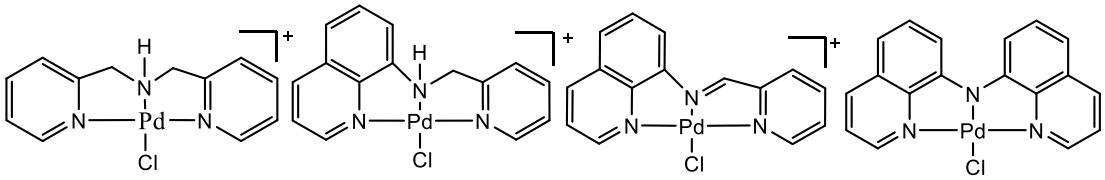

Pd1 **Pd2** **Pd3** **Pd4**

3. To measure the rates of substitution from the synthesized Pd(II) complexes coordinated with bis(2-pyridylimino)isoindolines so as to understand how the terdentates would control the reactivity of the complexes through *cis*-alkylation and *cis* and *trans* benzannulation of the Pd(II) coordinated to 1,3-bis(2-arylimino)isoindoline ligand as the reference complex. X-ray diffraction method was also used to characterize **Pd(4-Me-BPI)Cl**. The details of the results are presented in **chapter 5**.

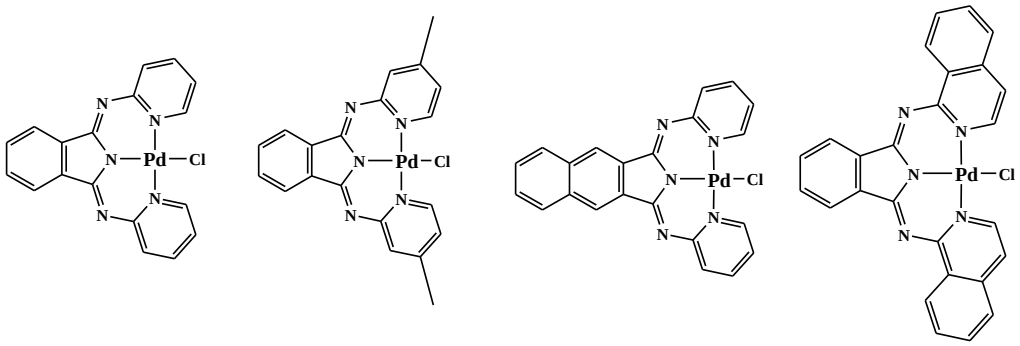

Pd(BPI)Cl **Pd(4-Me-BPI)Cl** **Pd(BBPI)Cl** **Pd(BII)Cl**

4. To measure the rates of substitution from Pd(C^N^N) complexes (**PdL^1 – L^4**) using stopped flow methods in order to quantify the role played by the σ-donation on the *cis*-

positioned groups on the ligand and also π-conjugation. The results and details are reported in **chapter 6**.

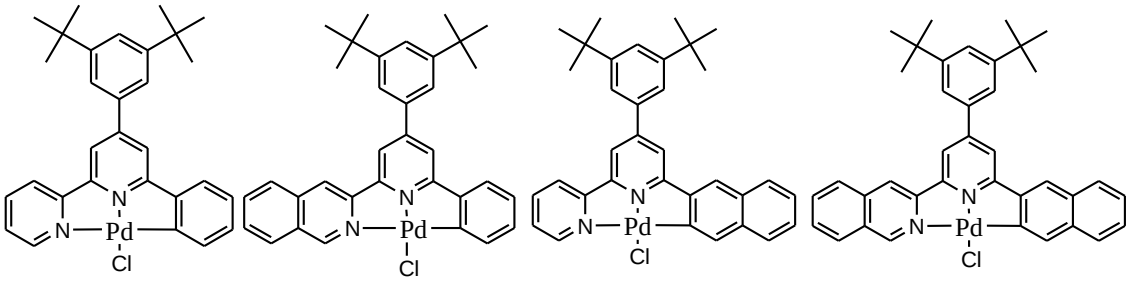

PdL[1] **PdL[2]** **PdL[3]** **PdL[4]**

5. To synthesize Pd(C^N^C) complexes [**(NHC)Pd1 – 4**] and measure the rates of their chloride substitution so as to explore the extent to which the σ-donation and steric effects of the tridentate C^N^C ligands of 2,6-bis-N-heterocyclic carbenes (bis(NHC)) would control the reactivity of the Pd(II) complexes. The results and the details of the findings are presented in **chapter 7**.

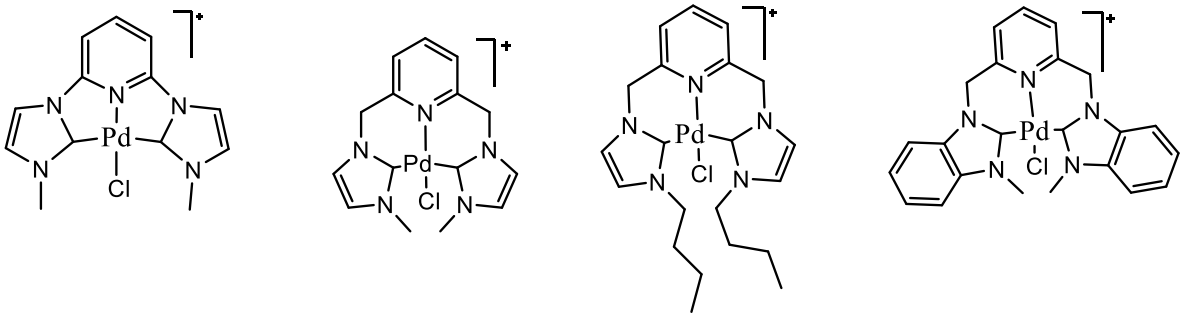

(NHC)Pd1 **(NHC)Pd2** **(NHC) Pd3** **(NHC)Pd4**

In conclusion, these objectives (in **Chapters 3** to **7**) are summarized in **Chapter 8** of this thesis with particular interest to propose future aspects in the areas of research interest to be further pursued in keeping with this study.

1.6 References

1. M. Shaharyar, M. Abdullah, M. Bakht and J. Majeed, *European Journal of Medicinal Chemistry*, 2010, **45**, 114-119.
2. M.-H. Pan and C.-T. Ho, *Chemical Society Reviews*, 2008, **37**, 2558-2574.
3. R. Baskar, J. Dai, N. Wenlong, R. Yeo and K.-W. Yeoh, *Frontiers in Molecular Biosciences*, 2014, **1**, 24.
4. C. Net, Types of Cancer, https://www.cancer.net/cancer-types, (accessed 12th September, 2017).
5. P. N. T. Collaborative., Introduction to Chronic Disease, Module 3: Cancer, http://www.patientnavigatortraining.org/chronic_disease/module3/1_index.htm, (accessed 11th September, 2018).
6. D. Parkin, L. Boyd and L. Walker, *British Journal of Cancer*, 2011, **105**, S77.
7. P. Vineis and B. W. Stewart, *International Journal of Cancer*, 2016, **138**, 2309-2311.
8. T. Revenco, G. Lapouge, V. Moers, S. Brohée and P. A. Sotiropoulou, *Stem Cells*, 2017, **35**, 1355-1364.
9. D. T. Silverman, *Occupational and Environmental Medicine*, 2017, oemed-2016-104197.
10. P. Anand, A. B. Kunnumakara, C. Sundaram, K. B. Harikumar, S. T. Tharakan, O. S. Lai, B. Sung and B. B. Aggarwal, *Pharmaceutical Research*, 2008, **25**, 2097-2116.
11. S. Sattar, S. M. Alibhai, M. Fitch, M. Krzyzanowska, N. Leighl and M. T. Puts, *Journal of Geriatric Oncology*, 2018, **9**, 47-52.
12. W. H. Organization, *Cancer fact sheet updated September, 12, 2018*, 2018.
13. N. Colombo, E. Preti, F. Landoni, S. Carinelli, A. Colombo, C. Marini, C. Sessa and E. G. W. Group, *Annals of Oncology*, 2013, **24**, vi33-vi38.
14. M. Bañobre-López, A. Teijeiro and J. Rivas, *Reports of Practical Oncology & Radiotherapy*, 2013, **18**, 397-400.
15. M. Li, Q. Zhao, X. Yi, X. Zhong, G. Song, Z. Chai, Z. Liu and K. Yang, *ACS Applied Materials & Interfaces*, 2016, **8**, 9557-9564.
16. Y. Monnier and C. Simon, *Current Treatment Options in Oncology*, 2015, **16**, 42.
17. I. Kareva, D. J. Waxman and G. L. Klement, *Cancer Letters*, 2015, **358**, 100-106.
18. P. M. Bruno, Y. Liu, G. Y. Park, J. Murai, C. E. Koch, T. J. Eisen, J. R. Pritchard, Y. Pommier, S. J. Lippard and M. T. Hemann, *Nature Medicine*, 2017, **23**, 461.

19. P. M. Bruno, Y. Liu, G. Y. Park, J. Murai, C. E. Koch, T. J. Eisen, J. R. Pritchard, Y. Pommier, S. J. Lippard and M. T. Hemann, *Nature Medicine*, 2017, **23**, 461.
20. C. E. DeSantis, C. C. Lin, A. B. Mariotto, R. L. Siegel, K. D. Stein, J. L. Kramer, R. Alteri, A. S. Robbins and A. Jemal, *CA: A Cancer Journal for Clinicians*, 2014, **64**, 252-271.
21. J. N. Blattman and P. D. Greenberg, *Science*, 2004, **305**, 200-205.
22. M. Galanski, M. A. Jakupec and B. K. Keppler, *Current Medicinal Chemistry*, 2005, **12**, 2075-2094.
23. A. Recht, S. E. Come, I. C. Henderson, R. S. Gelman, B. Silver, D. F. Hayes, L. N. Shulman and J. R. Harris, *New England Journal of Medicine*, 1996, **334**, 1356-1361.
24. V. Panda, P. Khambat and S. Patil, *International Journal of Clinical Medicine*, 2011, **2**, 515.
25. B. Rosenberg, L. Vancamp, J. E. Trosko and V. H. Mansour, *Nature*, 1969, **222**, 385-386.
26. T. Lazarević, A. Rilak and Ž. D. Bugarčić, *European Journal of Medicinal Chemistry*, 2017, **142**, 8-31.
27. N. J. Wheate, S. Walker, G. E. Craig and R. Oun, *Dalton Transactions*, 2010, **39**, 8113-8127.
28. S. Hadizadeh, N. Najafzadeh, M. Mazani, M. Amani, H. Mansouri-Torshizi and A. Niapour, *Biochemistry Research International*, 2014, **2014**, 1-9.
29. A. Burger, J. Double and D. Newell, *European Journal of Cancer*, 1997, **33**, 638-644.
30. D. K. Armstrong, B. Bundy, L. Wenzel, H. Q. Huang, R. Baergen, S. Lele, L. J. Copeland, J. L. Walker and R. A. Burger, *New England Journal of Medicine*, 2006, **354**, 34-43.
31. E. G. Konstantakou, G. E. Voutsinas, P. K. Karkoulis, G. Aravantinos, L. H. Margaritis and D. J. Stravopodis, *International Journal of Oncology*, 2009, **35**, 401-416.
32. P. G. Rose, B. N. Bundy, E. B. Watkins, J. T. Thigpen, G. Deppe, M. A. Maiman, D. L. Clarke-Pearson and S. Insalaco, *New England Journal of Medicine*, 1999, **340**, 1144-1153.
33. M. R. Posner, D. M. Hershock, C. R. Blajman, E. Mickiewicz, E. Winquist, V. Gorbounova, S. Tjulandin, D. M. Shin, K. Cullen and T. J. Ervin, *New England Journal of Medicine*, 2007, **357**, 1705-1715.

34. M. S. Kies, S. T. Rosen, T. K. Tsang, R. Shetty, P. A. Schneider, C. B. Wallemark and T. W. Shields, *Cancer*, 1987, **60**, 2156-2160.
35. G. Giaccone, R. S. Herbst, C. Manegold, G. Scagliotti, R. Rosell, V. Miller, R. B. Natale, J. H. Schiller, J. von Pawel and A. Pluzanska, *Journal of Clinical Oncology*, 2004, **22**, 777-784.
36. D. Wang and S. J. Lippard, *Nature Reviews Drug Discovery*, 2005, **4**, 307-320.
37. P. J. Dyson and G. Sava, *Dalton Transactions*, 2006, 1929-1933.
38. A. R. Kapdi and I. J. Fairlamb, *Chemical Society Reviews*, 2014, **43**, 4751-4777.
39. U. Ndagi, N. Mhlongo and M. E. Soliman, *Drug Design, Development and Therapy*, 2017, **11**, 599.
40. C. J. Jones and J. R. Thornback, *Medicinal applications of coordination chemistry*, Royal Society of Chemistry, Cambrigde, 2007.
41. B. Lippert, *Cisplatin: chemistry and biochemistry of a leading anticancer drug*, John Wiley & Sons, New York, 1999.
42. C. A. Puckett, R. J. Ernst and J. K. Barton, *Dalton Transactions*, 2010, **39**, 1159-1170.
43. P. O. Ongoma, PhD Thesis, University of KwaZulu-Natal, 2012.
44. D. P. Bancroft, C. A. Lepre and S. J. Lippard, *Journal of the American Chemical Society*, 1990, **112**, 6860-6871.
45. T. Soldatović, S. Jovanović, Ž. D. Bugarčić and R. van Eldik, *Dalton Transactions*, 2012, **41**, 876-884.
46. A. M. J. Fichtinger-Schepman, J. L. Van der Veer, J. H. Den Hartog, P. H. Lohman and J. Reedijk, *Biochemistry*, 1985, **24**, 707-713.
47. M. Kartalou and J. M. Essigmann, *Mutation Research/Fundamental and Molecular Mechanisms of Mutagenesis*, 2001, **478**, 1-21.
48. U.-M. Ohndorf, M. A. Rould, Q. He, C. O. Pabo and S. J. Lippard, *Nature*, 1999, **399**, 708.
49. Ž. D. Bugarčić, J. Bogojeski, B. Petrović, S. Hochreuther and R. van Eldik, *Dalton Transactions*, 2012, **41**, 12329-12345.
50. J. Reedijk, *European Journal of Inorganic Chemistry*, 2009, **2009**, 1303-1312.
51. T. Soldatović and Ž. D. Bugarčić, *Journal of Inorganic Biochemistry*, 2005, **99**, 1472-1479.
52. L. Ronconi and P. J. Sadler, *Coordination Chemistry Reviews*, 2007, **251**, 1633-1648.

53. B. Petrović, Ž. D. Bugarčić, A. Dees, I. Ivanović-Burmazović, F. W. Heinemann, R. Puchta, S. N. Steinmann, C. Corminboeuf and R. Van Eldik, *Inorganic Chemistry*, 2012, **51**, 1516-1529.
54. M. Al-Noaimi, A. S. Abu-Surrah and L. Tahtamouni, *Arabian Journal of Chemistry*, 2012, **9**, S1503-S1509.
55. E. Z. Jahromi, A. Divsalar, A. A. Saboury, S. Khaleghizadeh, H. Mansouri-Torshizi and I. Kostova, *Journal of the Iranian Chemical Society*, 2016, **13**, 967-989.
56. M. E. Alberto, C. Cosentino and N. Russo, *Structural Chemistry*, 2012, **23**, 831-839.
57. Z. Guo and P. J. Sadler, *Angewandte Chemie International Edition*, 1999, **38**, 1512-1531.
58. N. J. Farrer, L. Salassa and P. J. Sadler, *Dalton Transactions*, 2009, **0**, 10690-10701.
59. P. Blower, *Dalton Transactions*, 2006, 1705-1711.
60. X. Wang and Z. Guo, *Dalton Transactions*, 2008, 1521-1532.
61. S. P. Fricker, *Dalton Transactions*, 2007, 4903-4917.
62. S. P. Fricker, *Metallomics*, 2010, **2**, 366-377.
63. J. Reedijk, Medicinal applications of metal complexes binding to biological macromolecules. In *Macromolecular symposia* Weinheim: WILEY-VCH Verlag. August, 2008, Vol. 270, No. 1, pp. 193-201.
64. M. Galanski, V. Arion, M. Jakupec and B. Keppler, *Current Pharmaceutical Design*, 2003, **9**, 2078-2089.
65. N. Sharma, R. Ameta and M. Singh, *Journal of Cancer Science and Research*, 2016, **1**, 1-7.
66. E. Gao, C. Liu, M. Zhu, H. Lin, Q. Wu and L. Liu, *Anti-Cancer Agents in Medicinal Chemistry (Formerly Current Medicinal Chemistry-Anti-Cancer Agents)*, 2009, **9**, 356-368.
67. K. S. Prasad, L. S. Kumar, S. Chandan, R. N. Kumar and H. D. Revanasiddappa, *Spectrochimica Acta Part A: Molecular and Biomolecular Spectroscopy*, 2013, **107**, 108-116.
68. A. Divsalar, A. A. Saboury, H. Mansoori-Torshizi and F. Ahmad, *The Journal of Physical Chemistry B*, 2010, **114**, 3639-3647.
69. L. Tušek-Božić, A. Furlani, V. Scarcia, E. De Clercq and J. Balzarini, *Journal of Inorganic Biochemistry*, 1998, **72**, 201-210.

70. N. A. Al-Masoudi, B. H. Abdullah, A. H. Essa, R. Loddo and P. LaColla, *Archiv der Pharmazie: An International Journal Pharmaceutical and Medicinal Chemistry*, 2010, **343**, 222-227.

71. A. S. Abu-Surrah, K. A. A. Safieh, I. M. Ahmad, M. Y. Abdalla, M. T. Ayoub, A. K. Qaroush and A. M. Abu-Mahtheieh, *European Journal of Medicinal Chemistry*, 2010, **45**, 471-475.

72. J. Pranczk, D. Jacewicz, D. Wyrzykowski and L. Chmurzynski, *Current Pharmaceutical Analysis*, 2014, **10**, 2-9.

73. E. Budzisz, U. Krajewska, M. Rozalski, A. Szulawska, M. Czyz and B. Nawrot, *European Journal of Pharmacology*, 2004, **502**, 59-65.

74. A. Trevisan, C. Marzano, P. Cristofori, M. B. Venturini, L. Giovagnini and D. Fregona, *Archives of Toxicology*, 2002, **76**, 262-268.

75. A. Divsalar, M. J. Bagheri, A. A. Saboury, H. Mansoori-Torshizi and M. Amani, *The Journal of Physical Chemistry B*, 2009, **113**, 14035-14042.

76. R. D. Graham and D. R. Williams, *Journal of Inorganic and Nuclear Chemistry*, 1979, **41**, 1245-1249.

77. M. D. Coskun, F. Ari, A. Y. Oral, M. Sarimahmut, H. M. Kutlu, V. T. Yilmaz and E. Ulukaya, *Bioorganic & Medicinal Chemistry*, 2013, **21**, 4698-4705.

78. H. Khan, A. Badshah, G. Murtaz, M. Said, C. Neuhausen, M. Todorova, B. J. Jean-Claude and I. S. Butler, *European Journal of Medicinal Chemistry*, 2011, **46**, 4071-4077.

79. H. A. Ewais, M. Taha and H. N. Salm, *Journal of Chemical & Engineering Data*, 2010, **55**, 754-758.

80. J. Cao, X. Xia, X. Chen, J. Xiao and Q. Wang, *Food and Chemical Toxicology*, 2013, **51**, 242-250.

81. M. Marques, *ISRN Spectroscopy*, 2013, **2013**, 1 - 29.

82. M. González, J. Tercero, A. Matilla, J. Niclós-Gutiérrez, M. Fernández, M. López, C. Alonso and S. González, *Inorganic Chemistry*, 1997, **36**, 1806-1812.

83. H. Mansuri-Torshizi, T. Srivastava, H. Parekh and M. Chitnis, *Journal of Inorganic Biochemistry*, 1992, **45**, 135-148.

84. A. S. Abu-Surrah, H. H. Al-Sa'doni and M. Y. Abdalla, *Cancer Therapy*, 2008, **6**, 1-10.

85. S. Nadeem, M. Bolte, S. Ahmad, T. Fazeelat, S. A. Tirmizi, M. K. Rauf, S. A. Sattar, S. Siddiq, A. Hameed and S. Z. Haider, *Inorganica Chimica Acta*, 2010, **363**, 3261-3269.

86. E. Ulukaya, F. Ari, K. Dimas, E. I. Ikitimur, E. Guney and V. T. Yilmaz, *European Journal of Medicinal Chemistry*, 2011, **46**, 4957-4963.

87. K. S. Ferraz, L. Ferandes, D. Carrilho, M. C. Pinto, M. de Fátima Leite, E. M. Souza–Fagundes, N. L. Speziali, I. C. Mendes and H. Beraldo, *Bioorganic & Medicinal Chemistry*, 2009, **17**, 7138-7144.

88. L. Szűčová, Z. Trávníček, M. Zatloukal and I. Popa, *Bioorganic & Medicinal Chemistry*, 2006, **14**, 479-491.

89. H. Mansouri-Torshizi, I. Mahboube, A. Divsalar and A.-A. Saboury, *Bioorganic & Medicinal Chemistry*, 2008, **16**, 9616-9625.

90. E. Guney, V. T. Yilmaz, F. Ari, O. Buyukgungor and E. Ulukaya, *Polyhedron*, 2011, **30**, 114-122.

91. F. K. Keter, S. Kanyanda, S. S. Lyantagaye, J. Darkwa, D. J. G. Rees and M. Meyer, *Cancer Chemotherapy and Pharmacology*, 2008, **63**, 127-138.

92. G. Zhao, H. Lin, Y. Ping, H. Sun, S. Zhu, S. Xuncheng and Y. Chen, *Journal of Inorganic Biochemistry*, 1999, **73**, 145-149.

93. A. S. Abu-Surrah, T. A. Al-Allaf, L. J. Rashan, M. Klinga and M. Leskelä, *European Journal of Medicinal Chemistry*, 2002, **37**, 919-922.

94. T. A. Al-Allaf and L. J. Rashan, *European Journal of Medicinal Chemistry*, 1998, **33**, 817-820.

95. F. K. Keter, Masters in Science Thesis, University of the Western Cape, 2004.

96. F. Huq, H. Tayyem, P. Beale and J. Q. Yu, *Journal of Inorganic Biochemistry*, 2007, **101**, 30-35.

97. S. Ray, R. Mohan, J. K. Singh, M. K. Samantaray, M. M. Shaikh, D. Panda and P. Ghosh, *Journal of the American Chemical Society*, 2007, **129**, 15042-15053.

98. R. A. Haque, A. W. Salman, S. Budagumpi, A. A.-A. Abdullah and A. M. A. Majid, *Metallomics*, 2013, **5**, 760-769.

99. A. S. Abu-Surrah and M. Kettunen, *Current Medicinal Chemistry*, 2006, **13**, 1337-1357.

100. M. Gonzalez, J. Tercero, A. Matilla, J. Niclós-Gutiérrez, M. Fernández, M. López, C. Alonso and S. González, *Inorganic Chemistry*, 1997, **36**, 1806-1812.

101. C. Navarro-Ranninger, F. Zamora, J. Masaguer, J. Pérez, V. González and C. Alonso, *Journal of Inorganic Biochemistry*, 1993, **52**, 37-49.

102. M. Tanaka, H. Kataoka, S. Yano, H. Ohi, K. Kawamoto, T. Shibahara, T. Mizoshita, Y. Mori, S. Tanida and T. Kamiya, *BMC Cancer*, 2013, **13**, 237

103. M. Juribašić, K. Molčanov, B. Kojić-Prodić, L. Bellotto, M. Kralj, F. Zani and L. Tušek-Božić, *Journal of Inorganic Biochemistry*, 2011, **105**, 867-879.

104. L. Yan, X. Wang, Y. Wang, Y. Zhang, Y. Li and Z. Guo, *Journal of Inorganic Biochemistry*, 2012, **106**, 46-51.

105. E. Ulukaya, F. M. Frame, B. Cevatemre, D. Pellacani, H. Walker, V. M. Mann, M. S. Simms, M. J. Stower, V. T. Yilmaz and N. J. Maitland, *PloS one*, 2013, **8**, e64278-e64278.

106. C. Icsel and V. T. Yilmaz, *DNA and Cell Biology*, 2013, **32**, 165-172.

107. F. Ari, B. Cevatemre, E. I. I. Armutak, N. Aztopal, V. T. Yilmaz and E. Ulukaya, *Bioorganic & Medicinal Chemistry*, 2014, **22**, 4948-4954.

108. E. Ulukaya, F. Ari, K. Dimas, M. Sarimahmut, E. Guney, N. Sakellaridis and V. T. Yilmaz, *Journal of Cancer Research and Clinical Oncology*, 2011, **137**, 1425-1424.

109. O. Kacar, Z. Adiguzel, V. T. Yilmaz, Y. Cetin, B. Cevatemre, N. Arda, A. T. Baykal, E. Ulukaya and C. Acilan, *Anti-Cancer Drugs*, 2014, **25**, 17-29.

110. F. Darabi, H. Hadadzadeh, J. Simpson and A. Shahpiri, *New Journal of Chemistry*, 2016, **40**, 9081-9097.

111. J. Kuduk-Jaworska, A. Puszko, M. Kubiak and M. Pełczyńska, *Journal of Inorganic Biochemistry*, 2004, **98**, 1447-1456.

112. A. C. F. Caires, E. T. Almeida, A. E. Mauro, J. P. Hemerly and S. R. Valentini, *Quimica Nova*, 1999, **22**, 329-334.

113. F. Ari, E. Ulukaya, M. Sarimahmut and V. T. Yilmaz, *Bioorganic & Medicinal chemistry*, 2013, **21**, 3016-3021.

114. J. D. Higgins III, L. Neely, S. Fricker and J. Matthey, *Journal of Inorganic Biochemistry*, 1993, **49**, 149-156.

115. B. S. Kalirai, J.-D. Foulon, T. A. Hamor, C. J. Jones, P. D. Beer and S. P. Fricker, *Polyhedron*, 1991, **10**, 1847-1856.

116. J. Bogojeski, J. Volbeda, M. Freytag, M. Tamm and Ž. D. Bugarčić, *Dalton Transactions*, 2015, **44**, 17346-17359.

117. N. P. Barry and P. J. Sadler, *Chemical Communications*, 2013, **49**, 5106-5131.

118. S. van Zutphen and J. Reedijk, *Coordination Chemistry Reviews*, 2005, **249**, 2845-2853.

119. H. Zorbas and B. K. Keppler, *ChemBioChem*, 2005, **6**, 1157-1166.
120. K. L. Haas and K. J. Franz, *Chemical Reviews*, 2009, **109**, 4921-4960.
121. M. Frezza, S. Hindo, D. Chen, A. Davenport, S. Schmitt, D. Tomco and Q. Ping Dou, *Current Pharmaceutical Design*, 2010, **16**, 1813-1825.
122. Ž. D. Bugarčić, G. Liehr and R. van Eldik, *Journal of the Chemical Society, Dalton Transactions*, 2002, 951-956.
123. D. Jaganyi, K. L. D. Boer, J. Gertenbach and J. Perils, *International Journal of Chemical Kinetics*, 2008, **40**, 808-818.
124. A. Mambanda and D. Jaganyi, *Dalton Transactions*, 2012, **41**, 908-920.
125. P. O. Ongoma and D. Jaganyi, *Dalton Transactions*, 2013, **42**, 2724-2734.
126. W. C. Schiessl, N. K. Summa, C. F. Weber, S. Gubo, C. Dücker-Benfer, R. Puchta, N. J. van Eikema Hommes and R. van Eldik, *Zeitschrift für Anorganische und Allgemeine Chemie*, 2005, **631**, 2812-2819.
127. J. Reedijk, *Chemical Reviews*, 1999, **99**, 2499-2510.
128. M. Jakupec, M. Galanski and B. Keppler, in *Reviews of Physiology, Biochemistry and Pharmacology*, Springer, 2003, pp. 1-53.
129. N. A. G. dos Santos, N. M. Martins, C. Curti, M. d. L. P. Bianchi and A. C. dos Santos, *Chemico-Biological Interactions*, 2007, **170**, 177-186.
130. N. Santos, C. C. Bezerra, N. Martins, C. Curti, M. Bianchi and A. Santos, *Cancer Chemotherapy and Pharmacology*, 2008, **61**, 145-155.
131. M. Frisch, G. Trucks, H. Schlegel, G. Scuseria, M. Robb, J. Cheeseman, G. Scalmani, V. Barone, B. Mennucci, G. Petersson, Gaussian 09, revision D. 01, Gaussian, Inc., Wallingford CT (2009).
132. P. J. Hay and W. R. Wadt, *The Journal of Chemical Physics*, 1985, **82**, 299-310.

CHAPTER 2

Ligand Substitution Reactions of Square Planar Complexes

2.0 Introduction

The designing of new and improved metal-based anticancer agents and studying their rates and mechanism of substitution with modelled nucleophile simulating their interactions with nucleophilic targets such as DNA as well as S-donor ligands is important in understanding their antitumour activity.[1, 2] The antitumour mechanism of action by most of the transition metal complexes is through their covalent binding to bionucleophilic targets such as DNA after a substitution reaction. The rate of substitution of their labile ligands with such bionucleophiles and potential interference is important in optimising the cytotoxic activity of the drugs. This has been achieved through a kinetic process of measuring the rates and mechanisms of ligand exchange reactions of modelled complexes *in vivo* or *in vitro*.

Chemical kinetics is the study of the rate of reaction and factors affecting the rate of a reaction in order to come up with a plausible reaction mechanism. The reaction mechanism is a profile of elementary steps defining the reaction pathway leading to the final products while the rate of a reaction is the speed at which the products are formed, or reactants are consumed. In a given substitution chemical reaction, intermediate products are normally formed which requires a thorough examination of their structural, equilibrium, kinetic properties and other factors that may influence the rate of substitution reaction and mechanism.[3, 4] These investigations usually involve experimental determination of the rate as well as employing theoretical procedures such as density function theory (DFT) calculations to help in interpreting the trends in the rate and mechanism of substitution of a given set of complexes. This remains the sole focus of this chapter.

2.1 Substitution Kinetics of Square Planar d^8 Complexes

The biochemical transformations are dominated by nucleophilic substitution reactions, some of which are of chemotherapeutic value. The rate of these reactions determines how fast or slow such chemotherapeutic events happen. Data acquired from studying the kinetics of these reactions can be used in drug design. The substitution reaction from square planar d^8 complexes, [5, 6] especially those of Pt(II) [7, 8] have been useful in understanding the biochemical transformation that leads to chemotherapeutic value of metal based anticancer drugs. Other metals such as Rh(I), Ir(I), Pd(II), Ni(II) and Au(III), also form square planar complexes. [7]

Square planar complexes are the most well studied and well understood in terms of the kinetics of their substitution reactions. Most of the complexes have a good low-moderate reactivity and redox stability. [9-15] This has enabled the synthesis of tailor-made Pt(II) complexes, whose rate and mechanisms can be systematically studied. [5-7, 10] Hitherto, several researchers have reported on the rate and mechanisms of the substitution reactions of Pt(II) complexes.[16-31] The mechanism of substitution from Pt(II) complexes is known to be similar to those of the other square planar d^8 metal complexes. Because of this, the reactivity trends observed in Pt(II) complexes can be observed in other square planar complexes. For instance, the substitution behaviour of Pd(II) is very similar to that of Pt(II), except that it is $10^3 – 10^5$ times faster.[32, 33] It is well known that majority of the substitution reactions of Pt(II) complexes proceed by an associative mechanism *via* a 5-coordinate eighteen-valence electrons trigonal bipyramidal intermediate.[34] However, a dissociative mechanism have also been reported in some square planar Pt(II) complexes.[13, 14, 35-37]

2.2 Substitution Mechanisms of Square Planar Complexes

A reaction mechanism is a sequence of elementary reaction steps resulting into the observed overall reaction.[38, 39] Langford and Gray[40] classified the mechanism of ligand substitution

reactions into three categories namely; associative (*A*), dissociative (*D*) and Interchange (*I*) mechanisms.[40-42] The interchange mechanism is further divided into two, *viz* associatively activated (I_A) and dissociatively activated (I_D). In a simple consecutive reaction schemes, the slowest reaction step dominates over the overall rate and rate law of the reaction, and hence is called the rate determining step.[40, 43]

For a typical substitution reaction where L, M, Y and X represents the spectator ligand, metal centre, incoming group and leaving group respectively, the three categories of mechanism are presented in *Equations 2.1–2.3*.

$$\text{A: } [L_nMX] \underset{-Y}{\overset{+Y}{\rightleftharpoons}} [L_nMXY] \underset{+X}{\overset{-X}{\rightleftharpoons}} [L_nMY] \tag{2.1}$$

$$\text{D: } [L_nMX] \underset{+X}{\overset{-X}{\rightleftharpoons}} [L_nM] \underset{-Y}{\overset{+Y}{\rightleftharpoons}} [L_nMY] \tag{2.2}$$

$$\text{I: } [L_nMX] + Y \longrightarrow [L_nMX]\text{---}Y \longrightarrow [L_nMY]\text{---}X \longrightarrow [L_nMY] + X \tag{2.3}$$

The profiles of the reaction pathways represented by *Equations 2.1–2.3* are depicted in Figure 2.1 with the interchange mechanism illustrated in its associatively (I_A) and dissociatively (I_D) activated profiles. On one hand, the associative substitution mechanism is bimolecular and hence the rate limiting step, depends on the formation of the metal – entering ligand bond. On the other hand, the dissociative mechanism is a unimolecular and the rate limiting step is dependent on the energy required to activate the dissociation of the bond between the metal and the leaving group. In between the two, there is an interchange mechanism which can be associatively (I_A) or dissociatively (I_D) activated.

Reaction Profile →

Potential Energy →

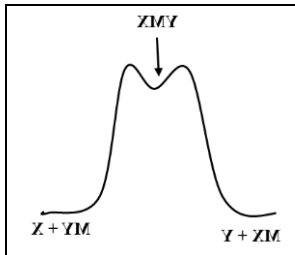	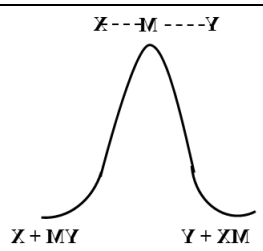	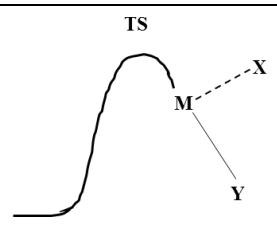	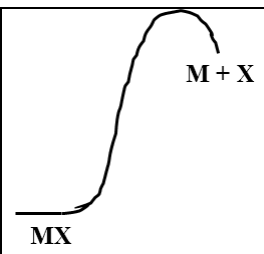
2 transition states and 1 intermediate	1 transition state	1 transition state within a preformed aggregate	1 transition state
Associative Mechanism		Dissociative Mechanism	
A	I_A	I_D	D

Figure 2. 1 Potential energy profiles of different mechanisms occurring at a square planar metal centre as proposed by Langford-Gray.[40, 44]

2.2.1 Associative Mechanism (*A*)

An associative mechanism for a substitution reaction defines a pathway that involves the formation of an intermediate whose coordination number is always higher than that of the original complex. In a square planar geometry, the incoming nucleophile forms a new bond on the metal centre (M---Y) while facilitating the breaking of the metal – leaving group bond (M---X). In the process, a trigonal bipyramidal intermediate forms as shown in scheme 2.1.[45] The final product is formed from the intermediate with stereo retention in the square planar geometry. The formation of the new bond is the rate determining step and thus the rate of substitution depends on the nature and the concentration of the incoming ligand.

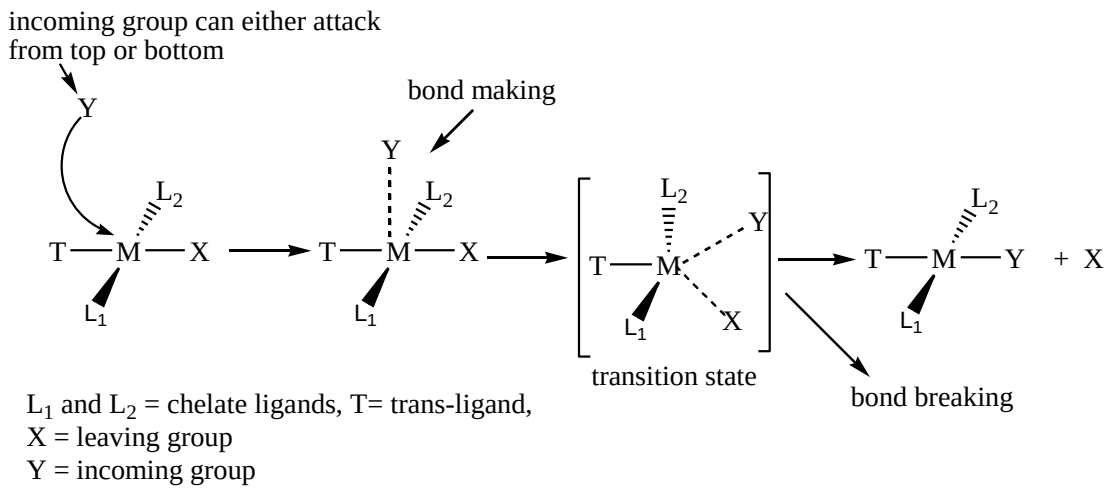

Scheme 2. 1 Associative substitution mechanism[45]

In cases where the incoming group (Y**)** and the leaving group (X**)** are similar in their chemical characteristics such as nucleophilicity, the bond formation and the bond breaking transition states would have equal energy. On the other hand, in a non-coordinating medium and in the presence of excess of the concentration of the incoming group (Y) over the metal complex, the rate of substitution reaction strongly depends on the nature of the incoming group.[40] This is because the incoming group (Y) gets involved in the early stages of the transition state which ends up retaining the stereochemistry of the complex at the five-coordinated associated intermediate.[7, 46, 47]

In an associative substitution process, the incoming group (Y), the non-living ligands (L_1/L_2) or the leaving group (X) can affect the inertness (kinetic) stability and the activation energy of the reaction. Any of these can be used to experimentally verify or corroborates if the substitution proceeds by an associative mechanism.[12]

2.2.2 Dissociative Mechanism (D)

As shown in *Equation 2.2*, a dissociative substitution mechanism is characterized by a pathway that proceeds *via* the formation of an intermediate with a reduced coordination number than that

of the complex. In this mechanism, the reactant is activated unimolecularly to a single transition state forming a 14-electron (three-coordinate) intermediate, stable enough to swiftly equilibrate with its environment before reacting with the incoming group, Y, to form the desired product. The bond between the leaving group and the metal ion is broken first to form an intermediate before that of the incoming ligand is formed. Therefore, the rate of breaking the bond to form the intermediate is not influenced by ligands within its secondary shell assemblage. As a result, the rate of substitution depends solely on the nature of the leaving group**,** X, (and hence the strength of the M – X bond) and is independent of the nature and steric constraints of the incoming ligand, Y. [6] The transition state has a more microstates than the reactants and is thus more disordered. Hence, the change in entropy due to the activation of the reactant's entropy ($\Delta S^{\#}$) is positive for dissociatively activated.

Theoretically, substitution proceeds dissociatively in complexes coordinated with bulky and electron rich donor ligands around the metal centre. This destabilizes the ground state properties (weaken M – X bond) by reducing the electrophilicity or blocking the axial approach of the incoming group from either above or below the metal centre.[40, 44] In a square planar geometry, a strong *trans*-σ donor ligand can significantly weaken the M–X bond *trans* to it, thereby favouring the formation of the 14-electron transition state. The same can be said for square planar complexes with a strong *cis*-σ donor ligands such as *cis*-$[PtR_2L_2]$, where R = C-donor ligand e.g. alkyl or aryl and L= DMSO, thioethers (neutral ligands). [13, 15, 48, 49] The substitution proceeds dissociatively and are entirely independent of the nature (electronic and steric properties) of the incoming nucleophiles. The *cis* and strong σ-donors accumulates electron density at the metal centre leading to a facile dissociation of the M–X bond.

2.2.3 Interchange Mechanism (I)

An Interchange (**I**) mechanism involves a concerted path in which the M–X bond elongates into the outer coordination sphere while at the same time the entering group, Y, form a bond which shorten into inner coordination sphere as shown in *Equation 2.3* and depicted in Figure 2.1. The interchange mechanism is divided into two; associatively activated interchange mechanism (I_A) and dissociatively activated interchange mechanism (I_D). Depending on the geometry and the spectator ligands, the character of the transition state (activated complex) can be dissociatively I_D (breaking of M–X is the rate-limiting step) or associatively activated I_A (where the formation of the new bond is the rate-limiting step). In either case, the mechanism is characterised by a single activated complex where the bond formation and the bond breaking between the metal centre, the entering ligand, and the leaving ligand, takes place simultaneously. The activation parameters for interchange mechanism are characterized by $\Delta S^{\#}$, $\Delta H^{\#}$ and $\Delta V^{\#}$ values that are closer to zero.

From an I_A mechanism, the rate of the substitution is weakly dependent on the nature of the incoming group since the rate limiting step involves, to a minor extent, the formation of a bond between the entering group and the metal centre in the transition state. The rate is less affected by bond breaking process in as much as the two steps co-exist leading to a single activated complex.[6] On the other hand, for an I_D, the breaking of the bond between the leaving group and the metal limits the rate of substitution as it break away from the inner to the outer coordination sphere, while the entering ligand moves from the outer to the inner coordination sphere. In a case where the bond between the leaving group and the metal is weakened before the incoming group is tightly held to the metal in the coordination sphere, then the probability of solvolytic pathway would be high (since the solvent is present in excess). This minimizes the discrimination between the entering group and the solvent molecules.

2.3 Kinetic Parameters

2.3.1 Reversible Second-order Reactions

Ligand substitution reactions in a square planar complex normally have a tendency of not going to completion but attains a state of equilibrium which can be shown in *Equation 2.4*.

$$\mathbf{A} + \mathbf{B} \underset{k_{-2}}{\overset{k_2}{\rightleftharpoons}} \mathbf{C}$$

or

$$\mathbf{ML_3X} + \mathbf{Y} \underset{k_{-2}}{\overset{k_2}{\rightleftharpoons}} \mathbf{ML_3Y} + \mathbf{X} \qquad (2.4)$$

Where, **A** = Metal complex (**ML_3X**), **X** is the leaving group

B = incoming nucleophile, **Y**

C = Product **ML_3Y**

k_2 = second-order rate constant

k_{-2} = first-order rate constant for the reverse reaction

From *Equation 2.4*, the forward reaction is second order while the reverse reaction is first-order, which results into a mixed order dependence system. This overall mixed order system complicates the study and therefore to practically follow the reaction, *pseudo*-first order conditions[50] is employed to simplify the study. This is basically achieved by making the concentration of the incoming nucleophile higher by at least ten-fold excess of the complex, such that $[B]_0 >> [A]_0$. The reaction therefore assumes a reversible process and the rate of formation of the product C can be expressed as;

$$-\frac{d[A]}{dt} = -\frac{d[B]}{dt} = \frac{d[C]}{dt} = k_2[A]_t[B]_t - k_{-2}[C]_t \qquad 2.5$$

By applying a mass balance for a given stoichiometry of unit equivalents, at time, t = 0 and t = t

$$[A]_t = [A]_0 - [C]_t \text{ and } [B]_t = [B]_0 - [C]_t \quad 2.6$$

And at equilibrium,

$$[A]_{eq} = [A]_0 - [C]_{eq} \text{ and } [B]_{eq} = [B]_0 - [C]_{eq} \quad 2.7$$

In addition, at equilibrium the rates of the forward and reverse reactions are equal, and the net reaction equals to zero, thus

$$-\frac{d[A]}{dt} = k_2[A]_{eq}[B]_{eq} - k_{-2}[C]_{eq} = 0 \quad 2.8$$

Hence, $k_2[A]_{eq}[B]_{eq} = k_{-2}[C]_{eq}$ 2.9

Making $[C]_{eq}$ the subject of the formula from *Equation 2.7* and substituting it in *Equation 2.9*, the following equation can be obtained

$$k_2[A]_{eq}[B]_{eq} = k_{-2}([A]_0 - [A]_{eq}) \quad 2.10$$

And rearranging *Equation 2.10* by making $k_{-2}[A]_0$ the subject of the formula gives

$$k_{-2}[A]_0 = k_2[A]_{eq}[B]_{eq} + k_{-2}[A]_{eq} \quad 2.11$$

Again, making $[C]_t$ the subject in *Equation 2.6* and substituting it into *Equation 2.5* gives

$$-\frac{d[A]}{dt} = k_2[A]_t[B]_t - k_{-2}([A]_0 - [A]_t)$$

$$k_2[A]_t[B]_t - k_{-2}[A]_0 = k_{-2}[A]_t \quad 2.12$$

Combining *Equation 2.11* and *Equation 2.12* yields

$$-\frac{d[A]}{dt} = k_2[A]_t[B]_t - k_{-2}[A]_{eq}[B]_{eq} - k_{-2}[A]_{eq} - k_{-2}[A]_t \quad 2.13$$

Considering that under *pseudo* first-order conditions, $[B]_0 >> [A]_0$ and substitution $[B]_t$ and $[B]_{eq}$ according to *Equations 2.6* and *2.7* and approximating that $k_2[A]_t[A]_0 \approx k_2[A]_{eq}[A]_0$ and $k_2[A]_t^2 \approx k_2[A]_{eq}^2$ leads to

$$-\frac{d[A]}{dt} = k_2[A]_t[B]_0 - k_2[A]_{eq}[B]_0 + k_{-2}[A]_t - k_{-2}[A]_{eq}$$

$$= (k_2[B]_0 + k_{-2})([A]_t - [A]_{eq}) \qquad 2.14$$

Rearranging *Equation 2.14* and introducing the integrals gives

$$\int_{[A]_0}^{[A]_t} \frac{dt}{[A]_t + [A]_{eq}} = -(k_2[B]_0 + k_{-2}) \int_0^t dt \qquad 2.15$$

This results to

$$\ln\left(\frac{[A]_t - [A]_{eq}}{[A]_0 - [A]_{eq}}\right) = -(k_2[B]_0 + k_{-2})t$$

$$= -k_{obs}t \qquad 2.16$$

Where, $k_{obs} = k_2[B]_0 + k_{-2}$

k_{obs} = observed *pseudo*-first order rate constant

k_2 = second order rate constant

k_{-2} = first-order rate constant for the reverse reaction

$[B]_0$ = initial concentration of the incoming nucleophile [Nu]

Equation 2.16 can therefore be rewritten as

$$k_{obs} = k_2[Nu] + k_{-2} \qquad 2.17$$

Therefore, in ligand substitution reactions, the second-order rate constants are experimentally determined by measuring the dependence of the observed *pseudo* first-order rate constant, k_{obs} on the initial concentration of the nucleophile, [Nu] using *Equation 2.17*. The mathematical treatment of a set of data by plotting k_{obs} against [Nu] gives a straight-line graph with the second order rate constant as the slope of the graph and y-intercept as first-order rate constant, k_{-2}. A representative plot of a substitution reaction under *pseudo* first-order condition is shown in Figure 2. 2.

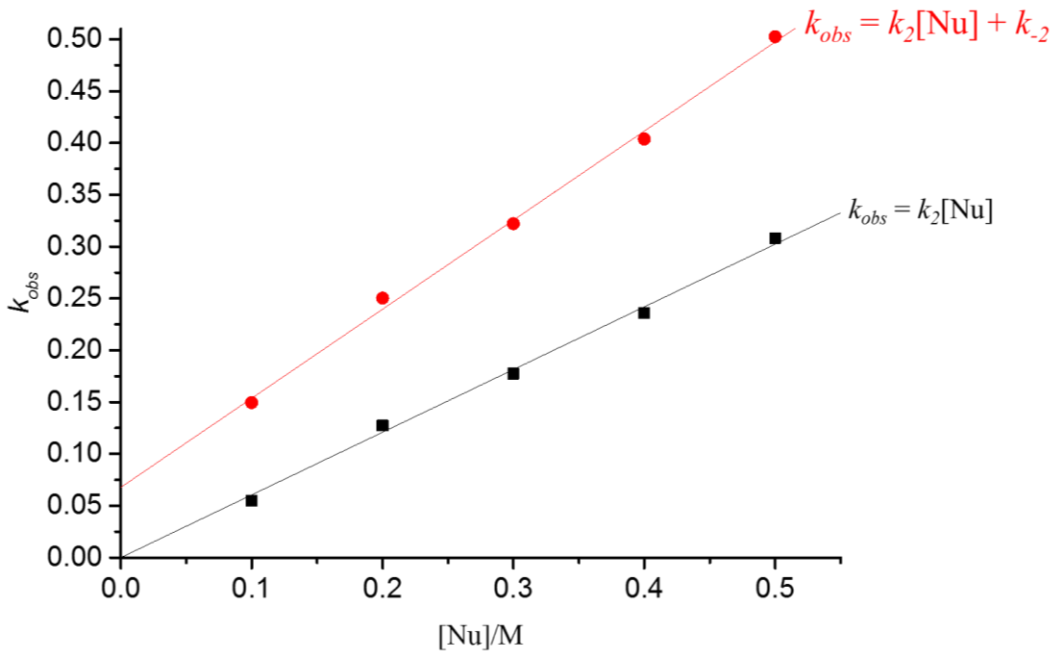

Figure 2. 2 A representative linear plot of k_{obs} against nucleophile concentration ([Nu]) for the *pseudo* first-order substitution reaction.

From the graph in Figure 2.2, the plot that passes through the origin is an indication that the substitution reaction proceeds to completion in an irreversible manner, while the plots with a y-intercept shows that the reaction proceeds in a reversible manner or through coordination of a solvent molecule (solvolytic pathway). Therefore, a *pseudo* first-order substitution reaction of square planar complexes can proceed in two possible pathways as illustrated in scheme 2.2.

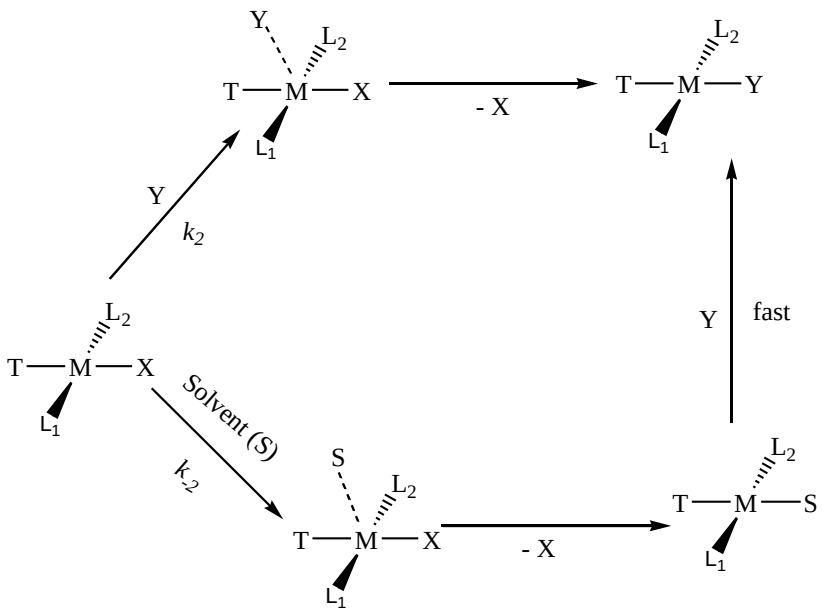

Scheme 2. 2 Proposed direct nucleophilic attack and solvotic pathways of associative substitution reaction of square planar complexes

2.3.2 Activation Parameters

Measuring the dependence of the rate constant on the concentration and nature of the nucleophile of a given substitution reaction of square planar complex, is not conclusive enough for assigning the mechanism of the reaction. The dependence of the rate on temperature or pressure leads to the deduction of activation parameters, thermal activation ($\Delta H^{\#}$, $\Delta S^{\#}$) and pressure activation, $\Delta V^{\#}$, whose sign and relative magnitudes are more useful in deducing the nature of the substitution mechanism. These parameters are experimentally arrived at by measuring the dependence of the *pseudo* first-order rate constant of a reaction on chemical and physical variables such as temperature, pressure, pH, among others.[7, 51, 52]

2.3.2.1 Determination of Activation Enthalpy ($\Delta H^{\neq}$) and Entropy ($\Delta S^{\neq}$) Changes

The rate of a reaction depends on the thermal energy that is injected to drive the reactant beyond the thermal activation complex. The relationship between the rate, the activation barrier is as stipulated in the transition state theory.[53, 54] In accordance to this theory, a reaction between M (the metal complex) and B (the nucleophile) reaches a pre-equilibrium[55] with the activated

complex $[M^{\cdots}B]^{\neq}$ at the transition state before forming C (the substituted product) as illustrated in the reaction *Equation 2.18*.

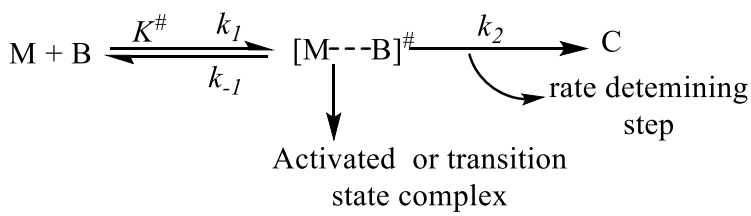

2.18

The rate of the reaction can be written as

$$\frac{d[M]}{dt} = k_2[M \cdots B]^{\#} = \frac{k_b T}{h}[M \cdots B]^{\#} \qquad 2.19$$

From pre-equilibrium $K^{\#} = \frac{[M \cdots B]^{\#}_{eq}}{[M]_{eq}[B]_{eq}}$ implying

$$[M \cdots B]^{\#}_{eq} = [M]_{eq}[B]_{eq} K^{\#} \qquad 2.20$$

Substituting for $[M \cdots B]^{\#}_{eq}$ (from *Equation 2.20*) in *Equation 2.19* gives

$$-\frac{d[M]}{dt} = \frac{k_b T}{h} K^{\#}[M]_{eq}[B]_{eq} \qquad 2.21$$

Where, k_b = Boltzmann's constant (1.38 x 10^{-23} JK^{-1})

h = Plank's constant (6.626 x 10^{-34} Js^{-1})

Assuming first-order kinetics

$$-\frac{d[M]}{dt} = k_2[M]_t[B]_t \qquad 2.22$$

And equating *Equation 2.21* and *Equation 2.22* gives

$$k_2 = \frac{k_b T}{h} K^{\#} \qquad 2.23$$

But $K^{\#}$ is related to the Gibb's free energy of activation $\Delta G^{\#}$ by the equation

$$RTlnK^{\#} = \Delta G^{\#} = \Delta H^{\#} - T\Delta S^{\#}$$

This implies $K^{\#} = e^{-\left(\frac{\Delta G^{\#}}{RT}\right)}$

$$\text{Therefore} \quad K^{\#} = e^{\left(\frac{\Delta S^{\#}}{R}\right)} e^{-\left(\frac{\Delta H^{\#}}{RT}\right)} \qquad 2.24$$

Substituting for $K^{\#}$ (as expressed in *Equation 2.24*) in *Equation 2.23* results

$$k_2 = \frac{K_b T}{h} e^{\left(\frac{\Delta G^{\#}}{RT}\right)} = \frac{K_b T}{h} e^{\left(\frac{\Delta S^{\#}}{R}\right)} e^{-\left(\frac{\Delta H^{\#}}{RT}\right)} \qquad 2.25$$

Rearranging *Equation 2.25* and introducing natural logarithms on both sides

$$ln\left(\frac{k_2}{T}\right) = -\frac{\Delta H^{\#}}{RT} + \left(23.8 + \frac{\Delta S^{\#}}{R}\right)$$

This equation can as well be written as

$$ln\left(\frac{k_2}{T}\right) = -\frac{\Delta H^{\#}}{R}.\frac{1}{T} + \left(23.8 + \frac{\Delta S^{\#}}{R}\right) \qquad 2.26$$

Thus, from *Equation 2.26*, a plot of $ln\left(\frac{k_2}{T}\right)$ against $\frac{1}{T}$ gives a straight-line graph with a slope of $-\frac{\Delta H^{\#}}{R}$ and y-intercept of $\left(23.8 + \frac{\Delta S^{\#}}{R}\right)$ from which the values of $\Delta H^{\#}$ and $\Delta S^{\#}$ can therefore be computed, respectively. This plot is commonly known as an Eyring plot. [4, 55, 56] The magnitude of these two activation parameters ($\Delta H^{\#}$ and $\Delta S^{\#}$) can therefore be used to verify the mode of substitution mechanism. For an associative substitution mechanism, the magnitude of $\Delta H^{\#}$ should generally be small while that of $\Delta S^{\#}$ are usually negative in comparison to those of dissociative mechanism which usually have large and positive values of $\Delta H^{\#}$ and $\Delta S^{\#}$. [44]

However, when mechanism is assigned only on the basis of these activation parameters, then measuring rate constants of the reaction using different nucleophiles is necessary to draw valid conclusions on the type of mechanism for the substitution reaction. For an associative substitution process, the rate depends on the steric and nucleophilicity of the entering ligand, while for the dissociative pathway the rate is independent of the nature and properties of the nucleophile. The values of $\Delta H^{\#}$ obtained from the slope tend to be reasonably reliable compared to those of $\Delta S^{\#}$ which usually have large relative errors since they are computed from values that are extrapolated to infinite temperatures.[46] This error is normally three times higher than that of $\Delta H^{\#}$.[57]

2.3.2.2 Determination of Activation Volume ($\Delta V^{\#}$)

This is a more dependable and a better parameter in determining the mechanism of a substitution reaction. It is usually determined by a series of experiments involving measuring the rate constants, k_2, while varying the pressure on the reaction mixture.[44, 58] Nevertheless, in order to make a conclusive and authentic assignment of the substitution mechanism, it is still very important to include the values of activation enthalpy ($\Delta H^{\neq}$) and activation entropy ($\Delta S^{\neq}$) parameters. The activation volume, $\Delta V^{\neq}$ is related to the change in the molar volume of the activated complex relative to that of the reactants. This parameter can be derived from the thermodynamic equation,

$$dG = VdP - SdT \qquad 2.27$$

If there is no variation in temperature (isothermal conditions), the partial derivative of the free energy change (ΔG) of a given reaction, in relation to the pressure applied, can be expressed as,

$$\left(\frac{\partial(\Delta G)}{\partial P}\right)_T^0 = \Delta V^0 \qquad 2.28$$

where ΔV^0 is the difference in the partial molar volumes between the products and the reactants.

Given that $\Delta G = -RTlnK$, thus *Equation 2.28* can be rewritten as

$$\left(\frac{\partial(-RTlnK)}{\partial P}\right)_T^0 = \Delta V^0 \qquad 2.29$$

and can be rearranged as,

$$\left(\frac{\partial(lnK)}{\partial P}\right)_T^0 = -\frac{\Delta V^0}{RT} \qquad 2.30$$

considering that the equilibrium constant is $K = {k_2}/{k_{-2}}$ and replacing it in *Equation 2.30* results in;

$$\left(\frac{\partial\left(\ln\left({k_2}/{k_{-2}}\right)\right)}{\partial P}\right)_T^0 = -\frac{\Delta V^0}{RT} \qquad 2.31$$

which implies that

$$\left(\frac{\partial \ln k_2}{\partial P}\right) = \left(\frac{-\Delta V^0}{RT} + \frac{\partial\, ln\, k_{-2}}{\partial P}\right) = \frac{-\Delta V^{\#}}{RT} \qquad 2.32$$

where $\Delta V^{\#}$ is the volume of activation, which is equal to the difference in the partial molar volumes between the intermediate complex and the reactants which are usually considered to be independent of the applied pressure. Taking integrals of both sides within the applied pressure range of P = 0 to P = P and $k_2 = (k_2)_0$ gives;

$$lnk_2 = ln(k_2)_0 - \frac{\Delta V^{\#}}{RT}P \qquad 2.33$$

Thus, from *Equation 2.33*, a plot of lnk_2 versus applied pressure, P, gives a linear graph with a gradient of $-\frac{\Delta V^{\#}}{RT}$ from which the activation volume, $\Delta V^{\#}$, can be arrived at. The value of $\Delta V^{\#}$ combines two terms namely; intrinsic activation volumes $\left(\Delta V_{int}^{\#}\right)$ and electrostriction activation volumes $\left(\Delta V_{elec}^{\#}\right)$ which are due to changes in internuclear distances within the reactants in forming the intermediate and electrostrictive changes of the solvent, respectively.[59, 60] In most cases for solvent exchange reactions the $\Delta V^{\#} \approx \Delta V_{int}^{\#}$, $\Delta V_{elec}^{\#}$ contribution is normally absent in most cases except when the reactions proceed without changes in the overall charge between the reactants and the products, and $\Delta V^{\#}$ is as a result of the activation step for bond making.[60] Therefore a positive value of $\Delta V^{\#}$ is an indication of dissociative, while a negative value confirms associative mechanistic pathway. [46, 47]

2.4 Instrumentation Techniques Used for Measuring the Rate of Substitution Reactions

Kinetic studies have often been done by measuring the dependence of a known physical parameter such as pH, pressure, absorbance, density, temperature, optical rotation and electrical conductivity[61] on the concentration of the reactants or products as a function of time. A number of experimental techniques have been developed to measure the rate of substitution reactions depending on the duration for the reactions which can be from days to femtoseconds (1 fs = 10^{-15} s).[57] Slow reactions are usually simpler to monitor even using manual means while fast reactions requires more specialised techniques. To measure the rates, the reactants are quickly mixed together and the timing of the progress of the reaction should be initiated immediately to collect as much data with the time scale of the reaction. At the same time the concentration or an indirect variable dependent on concentration of the reactant or the product should be monitored as a function of time. Where an instrument is used, its design should monitor the progression of a reaction through measuring the analytical signal of a physical parameter related to concentration

with time. The acquired data is fitted to appropriate standard equations from which the rate constant can be determined. However, the choice of the instrumentation technique for monitoring the kinetics is determined by the nature as well as the speed of the reaction.[62] Instrumental techniques that have been used for monitoring chemical kinetics of substitution reactions includes nuclear magnetic resonance (NMR) , infrared (IR), stopped-flow spectrophotometry, UV/Visible spectrophotometry and pulse methods.[63] Fast reactions are mainly measured using stopped-flow methods and pulse methods while the other methods monitor slow reactions.[63] Among the methods used, only UV/Visible spectrophotometry and stopped-flow spectrophotometry are reviewed in this thesis.

2.4.1 UV-Visible Spectrophotometry

The rate of substitution reactions which proceed at moderate rate to slow pace and which normally takes more than about 1000 s (16 minutes) are conveniently monitored using UV-visible spectrophotometry. This technique is sensitive[10] and can reliably detect analytes of concentrations as low as between 10^{-4} – 10^{-6} M. [64] This instrument is characterized by absorption of light radiation within a visible region (800 nm – 400 nm) and ultra-violet region (400 nm – 200 nm). Absorption of light energy within the two regions by a chromophore causes electronic excitations of compounds which have π-electrons and/ or non-bonding pair, from the highest occupied molecular orbital (HOMO) to the lowest unoccupied molecular orbital (LUMO). This is recorded as absorption bands in the acquired spectrum. The portion of a molecule which is UV-Visible active and hence responsible for its colour is known as a chromophore.[65]

A typical UV-Visible instrument comprises of sources of radiation (deuterium and tungsten lamps) beam splitter compartment, sample and reference holding compartment with a temperature control unit, wavelength selector (monochromator), data processing (detector) as well as output-readout system (data readout) as schematically presented in Figure 2.3.[66] The

reactants are pre-equilibrated in a two compartment tandem cuvettes (usually made of quartz or silica glass) before they get mixed manually and throughout kinetic data acquisition.

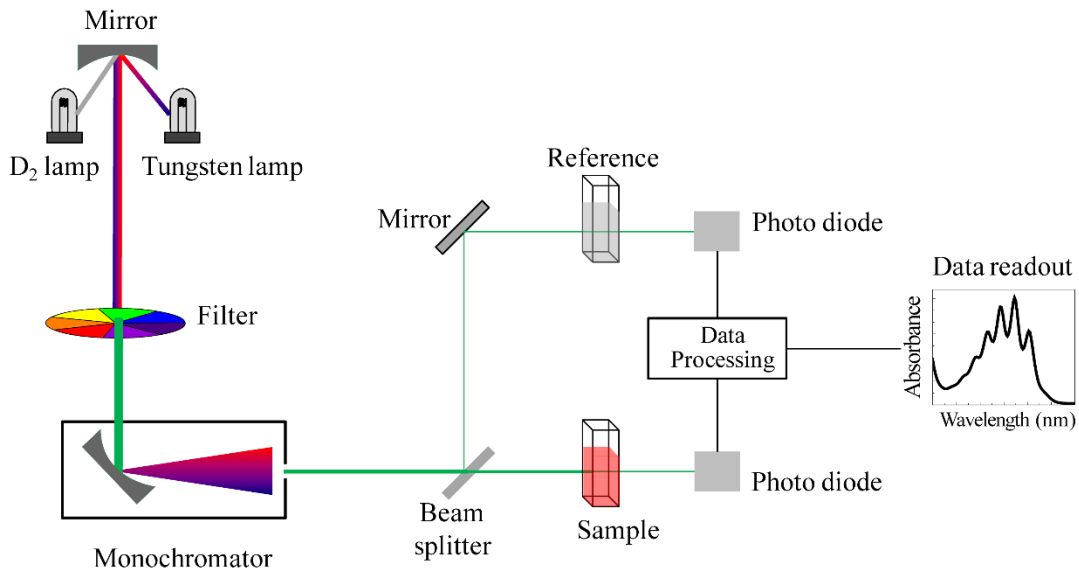

Figure 2. 3 A typical representation of the UV/Visible spectrophotometer components.[66]

The extent of interactions between the light radiation (transmittance or absorbance) and the analyte is determined by measuring the intensity of the incident radiation, I_0 and the transmitted intensity, I. The light transmitted T from the sample can be given as follows.

$$T = \frac{I_0}{I} \qquad 2.34$$

Where I_0 = intensity of the incident light obtained from the solvent reference cell

I = intensity of the transmitted light from the power source after passing through the analyte cell

Thus, the absorbance can then be written as

$$A = -\log T \qquad 2.35$$

By measuring the absorbance of the reaction mixture at specific time intervals or continuously, the concentration-time resolved spectrum of the mixture is determined from Beer-Lambert's law [62, 67] given as on *Equation 2.36*.

$$A = \varepsilon c l \qquad 2.36$$

where, A = optical absorbance (dimensionless)

ε = molar absorptivity (L $mol^{-1}cm^{-1}$)

c = concentration (mol dm^{-3})

l = path length (cm)

UV-Visible absorption spectra normally have broad absorptions overlapping with those from other species in the solution, which pauses more demanding task on the product analysis. Despite this, kinetic analysis can still be done on the overlapping absorption spectra. [68]

For a given first-order reaction,

$$X \xrightarrow{k_1} Y \qquad 2.37$$

From *Equation 2.37*, the rate equation can be arrived at as

$$Rate = -\frac{d[X]}{dt} = k_1[X] \qquad 2.38$$

At any time, *t*, the absorbance is given by

$$A_t = \varepsilon_X[X] + \varepsilon_Y[Y] = \varepsilon_X[X] + \varepsilon_X(Y_0 - X) \qquad 2.39$$

where, A_t = the absorbance at any time, t.

ε_X , ε_Y = molar absorptivities of X and Y, respectively.

At the end of the reaction, the absorption is given by;

$$A_\infty = \varepsilon_X[X]_0 + \varepsilon_Y[Y]_0 \qquad 2.40$$

where $A_\infty =$ absorbance upon completion of the reaction

and $[X]_0$ and $[Y]_0$ being the initial concentration of X and Y, respectively

The Beer-Lambert's law *Equation 2.36* which relates kinetic analysis to absorbance allows for substitution of *Equation 2.39* into *Equation 2.40* and integrating to yield the first-order kinetics integrated rate-law as follows;

$$ln\frac{[X]_0}{[X]_t} = ln\left(\frac{A_0 + A_\infty}{A_t - A_\infty}\right) = k_1 t \qquad 2.41$$

where A_0 , A_∞ and A_t are the initial, final and at any time, *t*, absorbances, respectively.

Therefore, the absorbance-time resolved data can be used to directly determine the observed *pseudo* first-order rate constant, k_{obs} using *Equation 2.41*. By measuring the observed rate constants at different concentrations and plotting the data against the concentration gives a straight-line graph of slope k_2 (the nucleophilic rate constant for forward reaction) and an intercept k_{-2} (rate constant for reverse reaction) as was discussed in section 2.3.1. The spectra evolving from a substitution reaction and the accompanying focussed kinetic trace are presented in Figure 2.4. The observed rate constants are calculated by fitting the induction time of the growth or decay of the absorbance data to standard *Equation 2.41*.

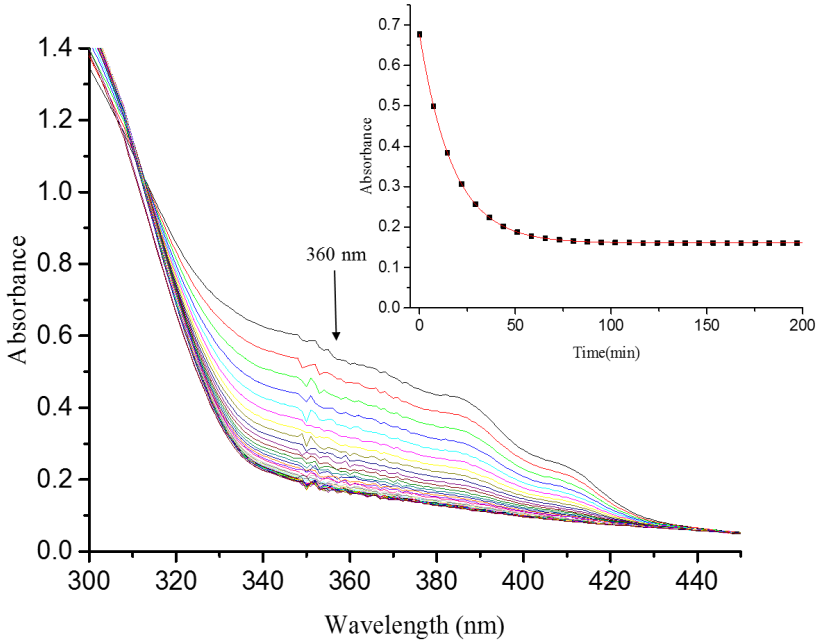

Figure 2. 4 UV-visible spectra for the second step reaction of Pd(II) complex with thiourea nucleophile. Inset; single exponential kinetic trace at 360 nm at 298 K. (**Chapter 5**)

UV/Visible spectrophotometry technique is also very useful in spectrophotometric titrations, particularly to determine the pK_a of aquated complex derivatives. The pK_a values are important thermodynamic data which gives an indication of the π-acidity and hence electrophilicity of the metal ion to which the aqua ligand is coordinated.[69, 70]

2.4.2 Flow Methods

Flow techniques are used to monitor the kinetics of rapid reactions whose half-lives are about 10^{-2} seconds or less.[62, 71] Flow methods are divided into two, namely; continuous flow and stopped-flow. The former techniques have a limitation because it requires large amounts of the reactants and high flow velocities to effectively monitor the reactions. The drawbacks is successfully avoided by using alternative or complementary method known as stopped-flow method.[62] In this work, the stopped-flow technique was widely used for monitoring the kinetics of the substitution reactions and its instrumentation is further discussed.

2.4.2.1 Stopped-flow Methods

Stopped-flow techniques have been successfully employed in measuring the rates of reactions whose half-lives ranges between 1 – 1000 seconds.[62] The schematic diagram of a stopped-flow instrument is as shown in Figure 2.5.[72]

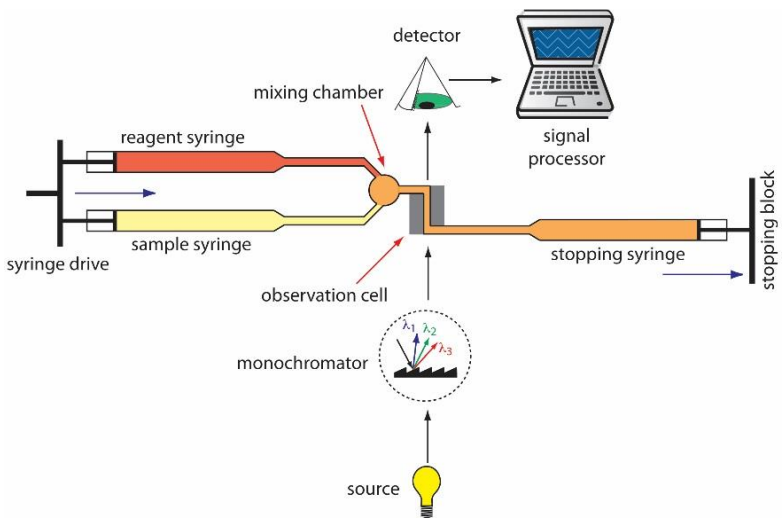

Figure 2. 5 A typical schematic diagram of the stopped-flow apparatus. The direction of the movement of the syringes are shown by the blue arrows.[72]

As depicted in Figure 2.5, the apparatus consists of two drive syringes, a reagent syringe and a sample syringe. The syringes are independently filled with individual solutions of the reactants which are then rapidly charged (in small volumes) into the mixing chamber by a compressed gas-driven (usually nitrogen) piston at a pressure not less than 800 kPa. This allows the two reactants to quickly mix within milliseconds. The reaction mixture flows into the stop syringe which triggers the striking of the stop block causing cessation of the flow of the reacting solution mixture in the observation cell.[10, 62, 63] This also triggers the data acquisition device to promptly record the absorbance-time resolved kinetic trace at a set wavelength during which the reacting species are static (stopped-flow).[10] The kinetic traces are then processed and the observed *pseudo* first-order rate constants evaluated by an online computer program. The commonly used primary detector is UV/visible spectrophotometry in the reaction analyzer. An example of a single

exponential kinetic trace that gives the observed rate constant, k_{obs}, from the stopped-flow reaction analyser is shown in Figure 2.6.

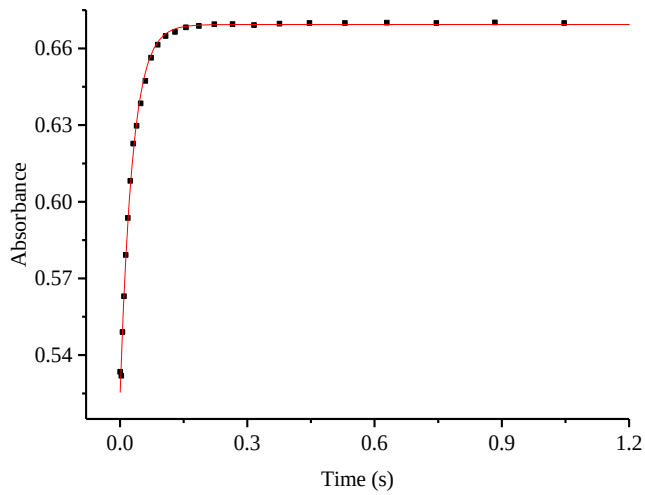

Figure 2. 6 Stopped-flow kinetic trace at 388 nm for the substitution reaction between a Pd(II) complex and **Dmtu** at 298 K. (**Chapter 7**).

2.5 Factors Affecting the Rate of Substitution of Square Planar Complexes

Square planar complexes of Pd share the same mechanism of substitution with Pt complexes. Therefore, they are all influenced in the same way by the same factors that affect the rate of substitution.[7] The only significant difference is that Pd(II) complexes undergoes substitution at rates which are 10^2 - 10^5 times higher than Pt(II) complexes.[20, 32, 73, 74] Thus, a review on the factors that affect the rate of substitution at the Pt(II) metal centre will be given since the same factors also affect the substitution kinetics at the Pd(II) centre in the same way. Common factors that are known to affect the rate of substitution are;- the nature of the incoming group, leaving group, solvent and spectator ligands will be reviewed briefly.

2.5.1 The Effect on Rate of the Incoming Ligand

The second order rate constant, k_2, of associative substitution mechanism is dependent on the nucleophilicity of the incoming ligand (nucleophile). Nucleophilicity is a measure of how readily the nucleophile attacks an electron-deficient metal centre such as Pd. Stronger nucleophiles

exhibit higher rates of substitution at the metal centre than weak nucleophiles.[40, 44] Several factors that influences the strength of nucleophilicity;[7, 42, 55]

i. *Basicity:* Basicity is the capacity of an electron-rich species to share its electrons with the proton[75, 76] The basicity of the incoming nucleophile is characterised by its p*K*a which also correlates well with the nucleophilicity of the nucleophile towards the metal centre.[77, 78] For reversible substitution reaction, the reverse reaction is largely dependent on the basicity of the nucleophile than for the forward reaction.[79, 80]

ii. *Polarisability*: Polarisability of the nucleophile is an important consideration for the rates rather than for equilibria of chemical reactions.[9] Polarizability of a ligand can be explained by using Peasons's "Hard Soft Acid Base" (HSAB)[a]† theory.[42, 81-83] In ligand substitution reactions, high nucleophilicity values at the Pt(II) substrates are normally known for highly polarizable incoming ligands such as the sulfur containing nucleophiles and iodide.[28, 29, 84, 85] Increasing the polarizability improves the electron donor ability of the incoming nucleophile.

iii. *Oxidizability:* Ligands that can easily lose their electrons, such as strong reducing agents are normally good nucleophiles. The ability to lose electrons are usually as a result of the values of their electrode reduction potentials (electrochemical data).[55]

iv. *Solvation energy:* Strongly solvated ligands are weak nucleophiles due to the requirement of high energy to free the nucleophile from the bonded solvent, prior to the ligand's attempt to coordinate to the metal centre.

---

[a]† The theory states that hard acids, i.e. small metal ions have a high charge and possess a valence electron shell which is not easily distorted and hence prefer hard bases, e.g. Li^{+}, Mg^{2+} and F^{-}. Similarly, soft acids, i.e. large metal ions have a low charge with a valence electron shell which can easily be distorted or removed hence would prefer soft bases, e.g. Pt^{2+} and SCN^{-}.

v. *Metal centre*: The nature of the metal centre influences nucleophilicity of the incoming ligand since reaction show dependence on the nature of the metal center. In transition state, the lighter elements are less polarised than the heavier ones. This can be seen when isovalent metal ions are compared.[86] Thus, the rate of substitution of d^8 complexes, Ni(II), Pd(II), Pt(II) follows the trend Ni > Pd > Pt in the ratio of 5 x 10^6: 10^5: 1.[87-89]

Comprehensive studies were performed to rank the nucleophiles at a prototype Pt(II) complex, *trans*-[Pt(py[b])$_2$Cl$_2$] as the standard substrate in methanol at 30 ºC.[7, 9] The nucleophilicity constant of the entering ligand, n^o_{Pt} was measured for the rate of the chloro substitution from the standard Pt(II) according to the equation;

$$\textbf{\textit{trans}-[Pt(py)}_2\textbf{Cl}_2\textbf{]} + \textbf{Y}^{\textbf{n}} \longrightarrow \textbf{\textit{trans}-[Pt(py)}_2\textbf{ClY]}^{(\textbf{n+1})} + \textbf{Cl}^- \qquad 2.42$$

A set of nucleophilic reactivity constants,[44, 90] n_{Pt} for an entering nucleophiles (**Y**), was initially defined as:

$$log\left(\frac{k_Y}{k_s}\right) = n_{Pt} \qquad 2.43$$

where, k_Y = the measured rate constant for the entering nucleophile, Y

k_s= rate constant for the solvent attack (methanol)

The above equation was found to be inadequate in taking care of the existing solvolytic pathway because k_Y and k_s differ in their dimensions. Therefore, k_s was substituted by the second-order rate since solvolytic pathway was associative in nature to give an expression;

$$log\left(\frac{k_Y}{k_s^0}\right) = n_{Pt}^0 \text{ , but } \quad k_s^0 = k_s[MeOH] \qquad 2.44$$

[b] Pyridine

Given that the concentration of pure methanol is 24.3 mol dm^{-3} at 30 °C, *Equation 2.44* can further be simplified in *Equation 2.45*

$$n_{Pt}^{0} = n_{Pt} + 1.39 \qquad 2.45$$

By definition, n_{Pt}^{0} for the methanol as the entering group is zero, being that it is the standard, while the highest value recorded was for triphenylphosiphine, Ph_3P being 8.99. Nucleophilicity constants from several studies[91-97] using the *trans*-[Pt(II)$(py)_2Cl_2$] was shown to follow the trend,

Ph_3P > Et_3As ~ $S_2O_3^{2-}$ > CN^- ~ Ph_3As, SO_3^{2-} > SCN^-~ Me_2Se > I^- > N_3^- > thiourea ~ $(Et_2N)_3P$ ~ Et_2S > PhSH ~ Br^- > NH_2OH ~ NH_2NH_2 > $Ph(CH_2)_2S_2$ ~ imidazole > Ph_2S ~ $PhNH_2$ ~ C_5H_5N ~ NO_2^- > Me_2SO ~ NH_3 ~ Cl^- ~ OH^- > H_2O > F^- > methanol.

Interestingly, the effect of the incoming group on Pd(acac[c])$_2$ demonstrated the same trend with the few incoming groups studied[98] as shown in Table 2.1.

Table 2. 1 The entering group effects on the rate of substitution of $Pd(acac)_2$.

X	k_2 (x 10^2 s^{-1})
H_2O	3.2
OH^-	3.2
Cl^-	8.9
Br^-	32
I^-	Fast
SCN^-	Very fast

The increasing rates of substitution following the order; $H_2O \approx OH^- < C1^- < Br^- < I^- < SCN^-$ for $Pd(acac)_2$ was an indication that the polarizability is a crucial factor in determining nucleophilic reactivity which corroborated with that of the Pt(II) complexes.[99]

[c] Acetylacetonate

2.5.2 Solvent Effects

The substitution reactions are carried out in the solvent medium which can swiftly substitute the leaving ligand making the rate to be independent of the incoming ligand due to the solvotic pathway (as shown in *Equation 2.17* and scheme 2.2) as have been reported in Pd(II) and Pt(II) complexes.[73, 77, 78, 100] The coordinating ability of the solvent proportionally determines the overall rate of the reaction.[9, 10, 44] A solvent that have electron rich-donor atoms as well as lone pairs of electrons exhibits acceleration in their coordinating tendency.

An example which have been used to quantify the effect of solvent was demonstrated in the reactions involving the substitution of chloride from *trans*-$[Pt(py)_2Cl_2]$ by the radio-labelled chloride ($^{36}Cl^-$) depicted in *Equation 2.46* and the data shown in Table 2.2.

$$\textbf{\textit{trans}-[Pt(py)}_2\textbf{Cl}_2\textbf{]} + {}^{36}\textbf{Cl}^- \longrightarrow \textbf{\textit{trans}-[Pt(py)}_2\textbf{Cl(}^{36}\textbf{Cl)]} + \textbf{Cl}^- \qquad (2.46)$$

Table 2. 2 Effect of solvent on the rate of chloride exchange from the *trans*-$[Pt(py)_2Cl_2]$[101]

Coordinating Solvents	$k_{-2}/(10^{-5}\ s^{-1})$	Non-/weakly Coordinating solvents	$k_2/M^{-1}\ s^{-1}$
DMSO	380	CCl_4	10^4
H_2O	3.5	C_6H_6	10^2
EtOH	1.4	*i*-BuOH	10^{-1}
PrOH	0.4	Me_2CO	10^{-2}
		DMF	10^{-3}

From Table 2.2, a highly coordinating solvent medium leads to the reaction proceeding predominantly *via* the direct solvent attack which is independent of the concentration of the entering nucleophile. The k_2, (second order rate constant) for direct nucleophilic substitution is therefore much less than k_{-2} of the solvolytic pathway. The rate of substitution by the solvent follows the trend, ROH < $H_2O \approx CH_3NO_2$ < DMSO in agreement with the nucleophilicity of the solvents. This indicates that the Pt–S bond making process in the reaction of DMSO takes pre-

eminence over the bond breaking process in the transition state. For example, if the solvent solvates the Cl^-, then DMSO should be less efficient solvent than H_2O. DMSO coordinates to Pt(II) *via* its high polarizable S atom and hence has high nucleophilicity at Pt(II) centre.[102] As a result, rate of exchange is higher for DMSO than for H_2O. On the other hand, weakly coordinating solvents such as CCl_4, C_6H_6 and sterically hindered alcohols are dominated by direct nucleophilic attack towards the complex since their k_2 is significantly larger than k_{-2}. In addition, higher rates are observed in non-polar solvents such as CCl_4, which prevents solvation by the Cl^- unlike in the polar and highly solvating solvents like DMF or H_2O.

2.5.3 The Effect of the Leaving Group

The leaving group effect on the rate is normally less important for the associative mechanism of square planar complexes as compared to the entering group. However, it is connected to the nature of the incoming group since leaving group ability (nucleofugacity) of a given ligand is a combination of its intrinsic lability and labilizing effects in it caused by other ligands.[44] For a dissociative substitution mechanism the nature of the leaving group plays a role since the bond breaking process in the transition state is highly dependent on it. On the other hand, in an associative reaction process, the leaving group effect is determined by the extent of the bond breaking process in the intermediate state.[7, 44] The effect of the leaving group have been extensively studied on $[Pd(dien)X]^+$ and $[Pt(dien)X]^+$ complexes[103, 104] as represented by *Equation 2.47* and the obtained data is tabulated in Table 2.4.

$$\mathbf{[M(dien)X]^{2-n} + py \longrightarrow [M(dien)py]^{2+} + X^n}\text{, } \mathbf{M = Pd \text{ or } Pt} \qquad 2.47$$

Table 2. 3 The effects of leaving group on the observed *pseudo* first order rate, k_{obs}, of $[Pt(dien)X]^+$ and $[Pt(dien)X]^+$ complexes in water at 25 °C.[103, 104]

Leaving group (X)	k_{obs} (s^{-1}) at 25 °C	
	$[Pt(dien)X]^+$	**$[Pd(dien)X]^+$**
NO_3^-	Very fast	-
H_2O	1900	-
Cl^-	35	Very fast
Br^-	23	Very fast
I^-	10	Very fast
N_3^-	0.83	-
SCN^-	0.30	4.47×10^4
NO_2^-	0.050	3.30×10^4
CN^-	0.017	-

As always the case, Pd(II) complexes are faster than their analogous Pt complexes. The rate of substitution of the leaving group X from the complexes by pyridine decreased in the order; NO_3^- > H_2O > Cl^- > Br^- > I^- > N_3^- > SCN^- > NO_2^- > CN^-

2.5.4 The Effects of Spectator Ligands

2.5.4.1 Steric Effects

For the substitution reactions involving associative mechanism steric effects plays a role in the transition state since at this state the formation of a new bond and dissociation of the labile ligand results in a 5-coordinate shell where steric effects can be experienced more easily. The steric effect is divided into two namely, steric bulk, which arises from the spectator ligands or incoming ligands and steric hinderance due to slowing down of the incoming nucleophile. Sterically bulky complex experiences slower rates of associative substitution due to destabilization of the transition state without necessarily altering the nature of substitution mechanism. This suggests that the effects due to electronic factors are less important in comparison to steric effects.[28, 29, 55, 78, 105-108] However, steric effect may also favour mechanistic change over to dissociative[6] especially when the bulky spectator ligand groups are in the *cis*-

position to the leaving group due to ground state destabilization.[55] In addition, the substituents with steric imparting properties in the *cis*-position to the leaving group induces retardation of the rate of substitution.

Studies by van Eldik and his coworkers,[109-113] to uncover the effects of bulky spectator ligand on the rate and mechanism of substitution reactions was performed from a series of Pd(II) complexes. This was achieved by systematically introducing methyl and ethyl substituent in the ligand of $[Pd(R_n dien)Cl]^+$ complex (R = ethyl or methyl and n = 0, 3 – 5). It emerged that increasing the steric hinderance reduced the rate of substitution from the Pd metal complexes by factors of up to six orders of magnitude compared to that of the sterically unhindered complex without change in the mode of mechanism.[32] The data is presented in Table 2.5.

Table 2. 4 The rate constants and activation parameters for the substitution of chloride ligand from $[Pd(R_n dien)Cl]^+$ by iodine in water at 25 ºC.[111]

$R_n$dien	k_2, s^{-1}	$\Delta H^{\#}$ (kJ mol^{-1})	$\Delta S^{\#}$ ($JK^{-1}mol^{-1}$)	$\Delta V^{\#}$ (cm^3 mol^{-1})
dien	44	43	-69	-10
1,4,7-Me_3dien	25	38	-87	-9.2
1,4,7-Et_3dien	10	41	-86	-10.8
1,1,7,7-Me_4dien	0.99	49	-79	-13.4
1,1,4-Et_3dien	0.77	51	-76	-14.5
1,1,4,7,7-Me_5dien	0.28	50	-88	-10.9
1,1,7,7-Et_4dien	2.2×10^{-3}	66	-74	-14.9
1,1,4,7,7-Et_5dien	7.2×10^{-4}	59	-106	-12.8

2.5.4.2 The *Trans* Effects

The rate of substitution of the labile group from the square planar as well as octahedral complexes is determined by the spectator ligand group *trans* to it.[114] The *trans* effect which has been explained from many kinetic reactions, is the effect caused by *trans*-coordinated ligand on the rate of substitution of the leaving ligand opposite it. [69, 114-118] The strong *trans* ligands can labilise exchangeable ligands by factors of between 10^5 – 10^6. [119] Thus, the greater *trans*

labilization effect, the higher the rate of substitution. Studies have established that the general order of labilization through *trans*-directing ligands follows: [7, 9, 10, 44]

CN^-, C_2H_4, CO, NO > R_3P ≈ H^- ≈ $SC(NH_2)_2$ > CH_3^- > $C_6H_5^-$ > SCN^- > NO_2^- > I^- > Br^- > Cl^- > NH_3 > OH^- > H_2O

A ligand that has a higher *trans*-effect in the series causes a weakening of the *trans* ligand bond or stabilises the transition state which ends up affecting both the transition and the ground state.[5, 7]

A special form of the *trans*-effect is the *trans*-influence, which affect ground state property of square planar complex structures. It is the propensity of a ligand to weaken the bond *trans* to itself and observed effect is elongated bond lengths and lower frequency of vibration. [40, 44, 120] Therefore, the *trans*-influence is a property that effects ground state characteristics of a metal complex, making it purely a thermodynamic effect while *trans*-effect is purely a kinetic factor affecting the stabilities of both the ground state and the activated intermediate states of the reactants in the process of the substitution reaction. This is caused by the increased crowding around the metal centre by the bulky ligands which is *cis* to the leaving group, causing steric hindrance.[44, 121, 122]

The order of *trans*-directing abilities of the ligand shows that π-acceptor and σ-donor ligands are stronger *trans* labilisers. A good π-acceptor ligand *trans* to the leaving group coordinated to the square planar metal, destabilises the ground state while it enhances stabilisation of the transition state by accepting electron density from the metal centre's d-orbitals into its empty π* p-orbitals through π-backbonding.[9, 123] This makes the metal centre more electrophilic,[84, 85] lowering the activation energy resulting in increase in the rate of substitution. This explains the high *trans*-directing abilities of ligands such as CO, C_2H_4 which are strong π-acceptors. An illustration of π-

bonding stabilizing the transition intermediate complex, *trans*-PtA_2LX as proposed in literature [123, 124] is shown in Figure 2.7.

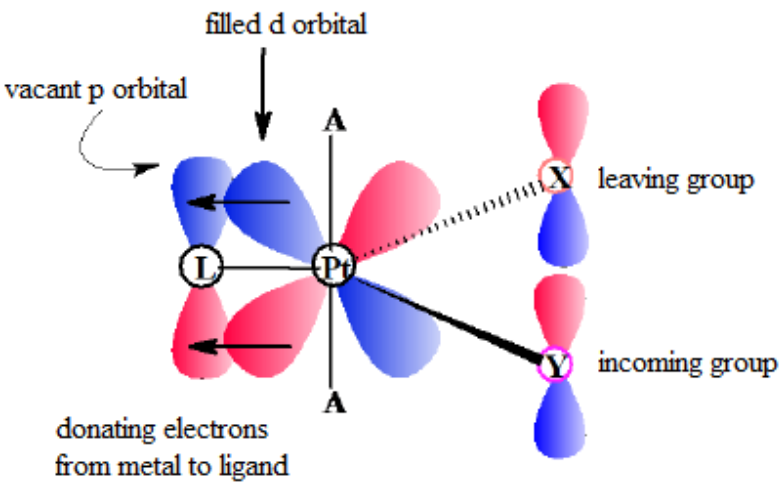

Figure 2. 7 An illustration of π-back donation of electrons from the filled d orbital of the metal (Pt) to the vacant orbitals of the *trans* ligand of *trans*-PtA_2LX.[9, 97]

Also, a stronger σ-donor *trans*-ligand (L) leads to the shortening of a square planar Pt–L bond while elongating and weakening the Pt–X bond resulting into less electron density available for this bond.[69] This leads to faster cleavage of the weakened bond (Pt–X), *trans* to strong σ-donors throughout the substitution process and resulting into a significant reduction of the electrophilicity of the metal centre. Therefore, the rate of substitution of the leaving group is faster when the *trans*-ligand is a good π-acceptor or a strong σ-donor and vice versa due to *trans*-effect.[124]

2.5.4.3 The *Cis* Effects

In terms of the electronic effects, the σ-*cis*-effect presents an opposite effects on the rate of substitution to that of the σ-*trans*-effect.[125, 126] For example, a strong *cis*-σ-donor carbon in a square planar Pt(II)(terpy) complexes reduces the rate of substitution. The Pt–C bond in the *cis*-position retards the rate of substitution of the leaving chloride group from Pt(II) complex coordinated to a terpyridine spectator ligand.[23, 127] The reduction in the associative rate of

substitution is due to the accumulation of electron density around the metal centre which stabilizes the transition state and destabilizes the ground state, thus making the complex less electrophilic and hence repels the incoming nucleophiles.[14, 23, 127] However, a mechanistic change over from associative to dissociative have been reported for complexes where the Pt–C was located in the *cis*-positions. [13, 15, 48, 49] The complexes were of the type *cis*-[PtR_2L_2] where R = alkyl or Aryl and L= DMSO, thioethers (neutral ligands). The two *cis*-Pt–C bonds accumulated electron density at the metal centre and also stabilized the 14-valence electron (three-coordinate) intermediate. Another notable *cis* effect on the rate has been reported in Pt(II) coordinated with multidentate ligands having quinoline or isoquinoline moiety at the *cis*-position to the leaving group. The complexes showed lower rates due to effectiveness in decreased electrophilicity of the Pt(II) metal centre caused by the accumulation of electron density to the metal centre by the *cis* N–Pt bonds.[25, 26, 29] On the contrary, the *cis*-π-acceptor ligands to the leaving group presents an opposite effects to the *cis*-σ-donor effect, thus accelerating the rate of substitution.[23, 128, 129]

Apart from lowering the rates, the *cis*-σ-donor ligands such as pyrazolyl moiety has also been shown to reduce the rate of substitution. The retardation in the substitution rate is due to the presence of the pyrrolic-N-*π*-donor within the chelate ring [31, 86] which accumulated electron density in the Pt–N bond from the π-electron rich pyrazole ring due to the extra pyrollic-N π-electrons within the chelate ring.[130, 131] This results into lower rates of nucleophilic attack.

While most of the factors controlling the rates of substitution of square planar complexes have extensively been studied for Pt(II) complexes, those of other square planar complexes such as Pd(II) are still not well understood. Given that Pd(II) complexes reacts faster than Pt(II) complexes, finding ligands with good σ/π-donor and π-acceptor properties and with good structural motifs that can control the reactivity of Pd(II) complexes to levels comparable to Pt(II)

complexes remains a challenge. In the next chapters, the influence of some of the ligands with viable factors that can control the rate of substitution at the Pd(II) metal centre is reported based on experimental findings whose objectives are outlined in chapter one.

2.6 References

1. J. Reedijk, *European Journal of Inorganic Chemistry*, 2009, **2009**, 1303-1312.
2. J. Reedijk, *Proceedings of the National Academy of Sciences*, 2003, **100**, 3611-3616.
3. K. A. Connors, *Chemical kinetics: the study of reaction rates in solution*, John Wiley & Sons, 1990.
4. S. R. Logan, *Fundamentals of chemical kinetics*, Longman, Essex, 1996.
5. R. A. Henderson, *The Mechanism of Reactions at Transition Metal Sites*, Oxford University Press, Oxford, 1993.
6. R. A. Henderson, *The Mechanism of Reactions at Transition Metal Sites*, Oxford University Press, 2003.
7. J. D. Atwood, *Inorganic and organometallic reaction mechanisms*, Wiley-VCH Publishers, New York, 2nd edn., 1997.
8. R. K. Murmann, R. T. Frazer and J. Bauman, *Mechanisms of Inorganic Reactions*, American Chemical Society, Washington D. C., 1965.
9. F. Basolo and R. G. Pearson, *Mechanisms in Inorganic Reactions*, Wiley, New York, 2nd edn., 1967.
10. R. G. Wilkins, *Kinetics and mechanisms of reactions of transition metal complexes*, VCH Publishers, Weinheim, 2nd edn., 1991.
11. D. Banerjea, F. Basolo and R. G. Pearson, *Journal of the American Chemical Society*, 1957, **79**, 4055-4062.
12. L. Cattalini, in *Inorganic Reaction Mechanisms: SJ Lippard, Progress In Inorganic Chemistry*, ed. J. O. Edwards, John Wiley & Sons, Inc., USA, 1970, vol. 13, pp. 263-327.
13. M. Rashidi, S. M. Nabavizadeh, A. Zare, S. Jamali and R. J. Puddephatt, *Inorganic Chemistry*, 2010, **49**, 8435-8443.
14. R. Romeo, M. R. Plutino, L. Monsù Scolaro, S. Stoccoro and G. Minghetti, *Inorganic Chemistry*, 2000, **39**, 4749-4755.
15. M. R. Plutino, L. Monsù Scolaro, R. Romeo and A. Grassi, *Inorganic Chemistry*, 2000, **39**, 2712-2720.
16. J. Bogojeski and Ž. D. Bugarčić, *Transition Metal Chemistry*, 2011, **36**, 73-78.
17. P. W. Asman, *Journal of Coordination Chemistry*, 2017, 1-20.
18. P. W. Asman, *Inorganica Chimica Acta*, 2018, **469**, 341-352.

19. R. Bellam, D. Jaganyi, A. Mambanda and R. Robinson, *New Journal of Chemistry*, 2018, **42**, 12557-12569.
20. Ž. D. Bugarčić, J. Bogojeski, B. Petrović, S. Hochreuther and R. van Eldik, *Dalton Transactions*, 2012, **41**, 12329-12345.
21. Ž. D. Bugarčič, G. Liehr and R. van Eldik, *Journal of the Chemical Society, Dalton Transactions*, 2002, 2825-2830.
22. M. Đurović, J. Bogojeski, B. Petrović, D. Petrović, F. W. Heinemann and Ž. D. Bugarčić, *Polyhedron*, 2012, **41**, 70-76.
23. A. Hofmann, L. Dahlenburg and R. van Eldik, *Inorganic Chemistry*, 2003, **42**, 6528-6538.
24. D. Jaganyi, K. L. D. Boer, J. Gertenbach and J. Perils, *International Journal of Chemical Kinetics*, 2008, **40**, 808-818.
25. B. B. Khusi, A. Mambanda and D. Jaganyi, *Journal of Coordination Chemistry*, 2016, **69**, 2121-2135.
26. G. Kinunda and D. Jaganyi, *Transition Metal Chemistry*, 2014, **39**, 451-459.
27. A. Mambanda and D. Jaganyi, in *Advances in Inorganic Chemistry*, Elsevier, 2017, vol. 70, pp. 243-276.
28. A. Mambanda, D. Jaganyi, S. Hochreuther and R. van Eldik, *Dalton Transactions*, 2010, **39**, 3595-3608.
29. P. Ongoma and D. Jaganyi, *Dalton Transactions*, 2012, **41**, 10724-10730.
30. A. Shaira and D. Jaganyi, *Journal of Coordination Chemistry*, 2014, **67**, 2843-2857.
31. I. M. Wekesa and D. Jaganyi, *Journal of Coordination Chemistry*, 2016, **69**, 389-403.
32. B. Petrović, Ž. D. Bugarčić, A. Dees, I. Ivanović-Burmazović, F. W. Heinemann, R. Puchta, S. N. Steinmann, C. Corminboeuf and R. Van Eldik, *Inorganic Chemistry*, 2012, **51**, 1516-1529.
33. Ž. D. Bugarčić, J. Bogojeski and R. van Eldik, *Coordination Chemistry Reviews*, 2015, **292**, 91-106.
34. L. Helm and A. E. Merbach, *Chemical Reviews*, 2005, **105**, 1923-1960.
35. S. Lanza, D. Minniti, P. Moore, J. Sachinidis, R. Romeo and M. L. Tobe, *Inorganic Chemistry*, 1984, **23**, 4428-4433.
36. R. Romeo, *Comments on Inorganic Chemistry*, 1990, **11**, 21-57.

37. R. Romeo, L. M. Scolaro, M. R. Plutino, F. F. de Biani, G. Bottari and A. Romeo, *Inorganica Chimica Acta*, 2003, **350**, 143-151.
38. D. O. Cooke, *Inorganic reaction mechanisms*, Chemical Society, London, 1979.
39. M. B. Smith and J. March, *March's advanced organic chemistry: reactions, mechanisms, and structure*, John Wiley & Sons, Hoboken, New Jersey, Sixth edn., 2007.
40. C. H. Langford and H. B. Gray, *Ligand Substitution Processes*, WA Benjamin Inc., New York, 1965.
41. P. J. Fischer and D. A. Tarr, *Inorganic Chemistry*, Pearson Education, Inc. , Upper Saddle River, New Jersey, Fifth edn., 2014.
42. S. Asperger, *Chemical Kinetics and Inorganic Reaction Mechanisms* Kluwer Academic / Plenum New York, 2nd edn., 2003.
43. P. W. Atkins, T. L. Overton, M. T. Weller, F. A. Armstrong and M. Hagerman, *Shriver and Atkins' inorganic chemistry*, Oxford University Press, USA, Fifth edn., 2010.
44. M. Tobe and J. Burgess, *Inorganic Reaction Mechanisms* Addison Wesley Longman Inc, Essex, 1999.
45. J. Cooper and T. Ziegler, *Inorganic Chemistry*, 2002, **41**, 6614-6622.
46. L. Helm and A. E. Merbach, *Journal of the Chemical Society, Dalton Transactions*, 2002, 633-641.
47. R. Van Eldik, W. Gaede, S. Wieland, J. Kraft, M. Spitzer and D. Palmer, *Review of Scientific Instruments*, 1993, **64**, 1355-1357.
48. R. Romeo, A. Grassi and L. Monsu Scolaro, *Inorganic Chemistry*, 1992, **31**, 4383-4390.
49. M. Schmüling and R. van Eldik, *Chemische Berichte*, 1997, **130**, 1791-1799.
50. H. Krüger and R. van Eldik, *Journal of the Chemical Society, Chemical Communications*, 1990, DOI: 10.1039/C39900000330, 330-331.
51. R. Van Eldik, in *High Pressure Molecular Science*, eds. R. Winter and J. Jonas, Springer Netherlands, Dordrecht, 1999, vol. 358, pp. 267-289.
52. D. T. Richens, *Chemical Reviews*, 2005, **105**, 1961-2002.
53. M. G. Evans and M. Polanyi, *Transactions of the Faraday Society*, 1935, **31**, 875-894.
54. K. Laidler and J. Meiser, *Physical Chemistry*, Houghton Mifflin, New York, 3rd edn., 1999.
55. R. B. Jordan, *Reaction mechanisms of inorganic and organometallic systems*, Oxford University Press Inc., New York, 3rd edn., 2007.

56. H. Eyring, *The Journal of Chemical Physics*, 1935, **3**, 107-115.
57. J. H. Espenson, *Chemical kinetics and reaction mechanisms*, McGraw-Hill, New York, 2nd edn., 1995.
58. M. Kotowski, D. Palmer and H. Kelm, *Inorganic Chemistry*, 1979, **18**, 2555-2560.
59. F. P. Rotzinger, *Chemical Reviews*, 2005, **105**, 2003-2038.
60. A. E. Merbach, *Pure and Applied Chemistry*, 1987, **59**, 161-172.
61. F. Wilkinson, *Chemical kinetics and reaction mechanism*, Van Nostrand Reinhold Company, 1980.
62. D. A. Skoog, D. M. West, F. J. Holler and S. Crouch, *Fundamentals of analytical chemistry*, Nelson Education, 9th edn., 2013.
63. K. Laidler, J. meiser and B. Sanctuary, *Physical Chemistry*, Houghton Mifflin Company New York, 4th edn., 2003.
64. D. Reddy, PhD Thesis, University of KwaZulu-Natal, 2009.
65. R. Shukla, A. Dubey, V. Pandey, D. Golhani and A. P. Jain, *Inventi Rapid: Pharm Analysis & Quality Assurance*, 2012, **2012**, 1 - 4.
66. W. C. contributors, File:Schematic of UV- visible spectrophotometer.png, https://commons.wikimedia.org/w/index.php?title=File:Schematic_of_UV-_visible_spectrophotometer.png&oldid=218744938, (accessed 20th October, 2018).
67. P. Glaister, *Journal of Chemical Education*, 1997, **74**, 744.
68. B. G. Cox, *Modern liquid phase kinetics*, Oxford University Press, 1994.
69. A. Mambanda and D. Jaganyi, *Dalton Transactions*, 2011, **40**, 79-91.
70. P. O. Ongoma and D. Jaganyi, *Dalton Transactions*, 2013, **42**, 2724-2734.
71. J. W. Moore and R. G. Pearson, *Kinetics and mechanism*, John Wiley & Sons, New York, 3rd edn., 1981.
72. D. Harvey, Chemistry LibreTexts: 13.2: Chemical Kinetics, https://chem.libretexts.org/Textbook_Maps/Analytical_Chemistry/Book%3A_Analytical_Chemistry_2.0_(Harvey)/13_Kinetic_Methods/13.2%3A_Chemical_Kinetics, (accessed 20th October, 2018).
73. Ž. D. Bugarčić, D. M. Jančić, A. A. Shoukry and M. M. Shoukry, *Monatshefte für Chemie/Chemical Monthly*, 2004, **135**, 151-160.
74. P. Illner, S. Kern, S. Begel and R. van Eldik, *Chemical Communications*, 2007, **0**, 4803-4805.

75. P. Bruice, *Organic Chemistry*, Prentice-Hall, Upper Saddle River, New Jersey, 2nd edn., 1998.
76. J. Harris and S. McManus, *Nucleophilicity Advances in Chemistry Series*, , American Chemical Society, Washington, DC, 1987.
77. A. Shaira, D. Reddy and D. Jaganyi, *Dalton Transactions*, 2013, **42**, 8426-8436.
78. D. Reddy, K. J. Akerman, M. P. Akerman and D. Jaganyi, *Transition Metal Chemistry*, 2011, **36**, 593-602.
79. M. Bellicini, L. Cattalini, G. Marangoni and B. Pitteri, *Journal of the Chemical Society, Dalton Transactions*, 1994, **0**, 1805-1811.
80. B. Pitteri, G. Marangoni and L. Cattalini, *Journal of the Chemical Society, Dalton Transactions*, 1994, **0**, 3539-3543.
81. R. G. Pearson, *Journal of the American Chemical Society*, 1963, **85**, 3533-3539.
82. R. G. Pearson, *Journal of Chemical Education*, 1968, **45**, 581-587.
83. R. G. Pearson, *Journal of Chemical Education*, 1968, **45**, 643-648.
84. K. Purcell and J. Kotz, *Inorganic Chemistry* WB Saunders Company, Philadelphia, 1977.
85. S. M. Owen, *A guide to modern inorganic chemistry*, Addison-Wesley Longman Limited, England, 1991.
86. I. M. Wekesa, PhD Thesis, University of KwaZulu-Natal, South Africa, 2014.
87. J. J. Pesek and W. R. Mason, *Inorganic Chemistry*, 1983, **22**, 2958-2959.
88. F. Basolo, J. Chatt, H. B. Gray, R. G. Pearson and B. L. Shaw, *Journal of the Chemical Society (Resumed)*, 1961, DOI: 10.1039/JR9610002207, 2207-2215.
89. D. Benson, *Mechanisms of inorganic reactions in solution*, McGraw-Hill, England, 1968.
90. D. K. Lin and C. S. Garner, *Journal of the American Chemical Society*, 1969, **91**, 6637-6643.
91. R. G. Pearson, *Journal of Chemical Education*, 1987, **64**, 561 - 568.
92. R. G. Pearson, *Inorganic Chemistry*, 1988, **27**, 734-740.
93. R. G. Pearson, H. R. Sobel and J. Songstad, *Journal of the American Chemical Society*, 1968, **90**, 319-326.
94. L. Cattalini, M. Bonivento, G. Michelon, M. Tobe and A. Treadgold, *Gazzetta Chimica Italiana*, 1988, **118**, 725-728.
95. T. Hoover and A. P. Zipp, *Inorganica Chimica Acta*, 1982, **63**, 9-11.
96. J. Gaylor and C. Senoff, *Canadian Journal of Chemistry*, 1971, **49**, 2390-2393.

97. U. Belluco, M. Martelli and A. Orio, *Inorganic Chemistry*, 1966, **5**, 582-586.

98. R. G. Pearson and D. A. Johnson, *Journal of the American Chemical Society*, 1964, **86**, 3983-3989.

99. J. O. Edwards and R. G. Pearson, *Journal of the American Chemical Society*, 1962, **84**, 16-24.

100. J. Bogojeski, R. Jelić, D. Petrović, E. Herdtweck, P. G. Jones, M. Tamm and Ž. D. Bugarčić, *Dalton Transactions*, 2011, **40**, 6515-6523.

101. R. G. Pearson, H. B. Gray and F. Basolo, *Journal of the American Chemical Society*, 1960, **82**, 787-792.

102. F. A. Cotton and R. Francis, *Journal of the American Chemical Society*, 1960, **82**, 2986-2991.

103. F. Basolo, H. B. Gray and R. G. Pearson, *Journal of the American Chemical Society*, 1960, **82**, 4200-4203.

104. H. B. Gray and R. J. Olcott, *Inorganic Chemistry*, 1962, **1**, 481-485.

105. G. L. Miessler and D. A. Tarr, *Upper Saddle River, NJ*, 2004, 397, 415 - 446.

106. J. Bogojeski, Ž. D. Bugarčić, R. Puchta and R. van Eldik, *European Journal of Inorganic Chemistry*, 2010, **2010**, 5439-5445.

107. T. Soldatović, S. Jovanović, Ž. D. Bugarčić and R. van Eldik, *Dalton Transactions*, 2012, **41**, 876-884.

108. A. Mijatović, J. Bogojeski, B. Petrović and Ž. D. Bugarčić, *Inorganica Chimica Acta*, 2012, **383**, 300-304.

109. E. Breet and R. Van Eldik, *Inorganic Chemistry*, 1984, **23**, 1865-1869.

110. M. Kotowski and R. Van Eldik, *Inorganic Chemistry*, 1984, **23**, 3310-3312.

111. M. Kotowski and R. Van Eldik, *Inorganic Chemistry*, 1986, **25**, 3896-3899.

112. J. Pienaar, M. Kotowski and R. Van Eldik, *Inorganic Chemistry*, 1989, **28**, 373-375.

113. J. Berger, M. Kotowski, R. Van Eldik, U. Frey, L. Helm and A. Merbach, *Inorganic Chemistry*, 1989, **28**, 3759-3765.

114. F. Basolo and R. G. Pearson, *Progress in Inorgarnic Chemistry*, 1962, **4**, 381-453.

115. I. Chernyaev, *Ann Inst Platine (USSR)*, 1926, **4**, 243-275.

116. A. S. Fleischhacker and R. G. Matthews, *Biochemistry*, 2007, **46**, 12382-12392.

117. A. C. Albéniz, P. Espinet and B. Martín-Ruiz, *Dalton Transactions*, 2007, DOI: 10.1039/B706817D, 3710-3714.

118. S. Hochreuther, R. Puchta and R. van Eldik, *Inorganic Chemistry*, 2011, **50**, 12747-12761.

119. J. R. Gispert, *Coordination chemistry*, Wiley-VCH Weinheim, Weinheim, 2008.

120. A. Pidcock, R. E. Richards and L. M. Venanzi, *Journal of the Chemical Society A: Inorganic, Physical, Theoretical*, 1966, DOI: 10.1039/J19660001707, 1707-1710.

121. R. Romeo, D. Minniti and M. Trozzi, *Inorganic Chemistry*, 1976, **15**, 1134-1138.

122. G. Faraone, V. Ricevuto, R. Romeo and M. Trozzi, *Journal of the Chemical Society, Dalton Transactions*, 1974, DOI: 10.1039/DT9740001377, 1377-1380.

123. J. Chatt, L. A. Duncanson and L. M. Venanzi, *Journal of the Chemical Society (Resumed)*, 1955, DOI: 10.1039/JR9550004456, 4456-4460.

124. L. Orgel, *Journal of Inorganic and Nuclear Chemistry*, 1956, **2**, 137-140.

125. J. K. Burdett, *Inorganic Chemistry*, 1977, **16**, 3013-3025.

126. S. Okeya, K. Wakamatsu, T. Shibahara, H. Yamakado and K. Nishimoto, *Journal of Computer Chemistry, Japan*, 2002, **1**, 97-102.

127. D. Jaganyi, D. Reddy, J. Gertenbach, A. Hofmann and R. van Eldik, *Dalton Transactions*, 2004, 299-304.

128. A. Hofmann, D. Jaganyi, O. Q. Munro, G. Liehr and R. van Eldik, *Inorganic Chemistry*, 2003, **42**, 1688-1700.

129. D. Jaganyi, A. Hofmann and R. van Eldik, *Angewandte Chemie International Edition*, 2001, **40**, 1680-1683.

130. J. M. Holland, J. A. McAllister, C. A. Kilner, M. Thornton-Pett, A. J. Bridgeman and M. A. Halcrow, *Journal of the Chemical Society, Dalton Transactions*, 2002, 548-554.

131. T. Astley, A. J. Canty, M. A. Hitchman, G. L. Rowbottom, B. W. Skelton and A. H. White, *Journal of the Chemical Society, Dalton Transactions*, 1991, 1981-1990.

CHAPTER 3

Tuning the Reactivity of Palladium(II) Complexes of Pyrazolyl-based Terpyridyl Type of Ligands through Electronic and Steric effects. Crystal Structures

3.0 Abstract

The rate and mechanism of substitution of the labile chloride ligand from the Pd(II) complexes namely: chlorido-(2,2′:6′,2″-terpyridine)palladium(II) chloride (**PdL1**), chlorido-(2,6-bis(N-pyrazolyl)pyridine)palladium(II) chloride (**PdL2**), chlorido-(2,6-bis(3,5-dimethyl-N-pyrazolyl)pyridine)palladium(II) chloride (**PdL3**) and chlorido-(2,6-bis(3,5-dimethyl-N-pyrazolylmethyl)pyridine)palladium(II) tetrafluoroborate (**PdL4**) were investigated in methanolic solution using thiourea nucleophiles *viz*; thiourea (**Tu**), N,N'-dimethylthiourea (**Dmtu**) and N,N,N',N'-tetramethylthiou-rea (**Tmtu**). The substitution reactions of the chloride ligand from the complexes by the thiourea nucleophiles were done under *pseudo*-first-order conditions using stopped-flow spectrometric techniques. The reactions appreciably followed the facile rate law $k_{obs} = k_2$[Nu] in the order **PdL1** > **PdL2** > **PdL3 >> PdL4**. The negative values of entropy suggest that the substitution mechanism is associatively activated. The study showed that the presence of pyrollic-N π-donor in the chelate ring decelerates the liability of the chloro leaving group. In addition, the introduction of the six-membered ring in **PdL4** introduces steric hinderance which highly decelerates the lability. The DFT calculations performed supported the reactivity trend. X-ray structures of **PdL2** and **PdL3** belonging to monoclinic space group P21/c, while **PdL4** belonging to triclinic space group *P*ī are also reported. These results could be helpful in finding Pd(II) complexes with good pharmacological action.

Keywords: Pd(II) complexes, anticancer, pyrollic-N π-donor, kinetics, thiourea

3.1 Introduction

Palladium is one of the metals belonging to the platinum group of metals, whose members include ruthenium, rhodium, osmium, iridium, and platinum which are characteristically square planar d^8 complexes.[1] Platinum group metal complexes have increasingly shown great potential for anti-tumour activity making them useful in chemotherapy.[2-7] For example, Pt(II) complexes such as carboplatin, oxaliplatin and *cisplatin* have been used in chemotherapy for the treatment of ovarian and testicular cancer.[2, 8-13] Some of these drugs have shown serious side effects such as nausea, vomiting, nephrotoxicity, neurotoxicity and ototoxicity among others[11, 14-16] creating a continuous need for the search for alternative non-platinum drugs with high efficacy, less side effects and easy administration.

Pd(II) among other transition metals[17-24] are promising alternatives as some of them showed activity on tumours which had developed resistance to *cisplatin* or in which *cisplatin* was inactive.[25] Pd(II) complexes having antitumor activity have been demonstrated.[26-29] In general, the synthetic design of these Pd(II) antitumor agents follows the same strategies that have been used to design potential Pt(II) antitumor drugs.[30] Pt(II) and Pd(II) complexes are very similar in their chemical equilibrium and structural activities, their mechanistic and kinetic studies have so far indicated that Pd(II) complexes are 10^3 –10^5 more labile than Pt(II). [1, 31-34]

The use of Pd(II) complexes as an antitumour agent has been neglected because of the serious effects caused by rapid hydrolysis of the leaving groups (e.g., Cl^-) in the cell medium, producing highly reactive species which hinders them from reaching their targeted DNA[17, 35] This implies that Pd(II) complexes will undergo side reactions with biomolecules other than DNA and dissociate before reaching the DNA target. Another draw-back is that some of them undergo rapid *cis–trans* isomerism kinetics.[35-37] For instance, cispalladium complex (*cis*-$[Pd(NH_3)_2Cl_2]$), an analogue of *cisplatin* complex (*cis*-$[Pt(NH_3)_2Cl_2]$) do not show any antitumour activity, which

is also similar for *cis*-[Pd(DACH)Cl_2]; (DACH: (1R,2R)-(–)-1,2-diamine-cyclohexane). This is because the former undergoes *cis-trans* isomerization to form an inactive *trans*-conformer whose hydrolysis is very fast,[30, 38] leading to *in vivo* interactions with other non-targeted biomolecules thus compromising their antitumor activity. Therefore, a good antitumor active Pd(II) complexes, should be stabilised by a strongly coordinated N-donor multidentate spectator ligands and a reasonably non-leaving group is required to enable the drug maintain its structure *in vivo* long enough so as to reach its DNA target and perform its therapeutic function.[35, 39] Furthermore, the Pd(II) complexes can also be stabilized and side reactions prevented by introducing inert sterically hindered ligands into the Pd(II) complex coordination sphere. These structural modifications on the ligand framework can offer a thermodynamically stable and kinetically inert Pd(II) complexes with improved cytotoxic ability towards the cancer cells.[2-5, 40, 41]

It has been shown that the terpy ligand and its derivatives coordinated to Pd(II) and Pt(II) complexes affects the lability of their leaving group through electronic and steric effects as well as influence their interaction with bio-relevant nucleophiles and DNA fragments.[42] The $[Pt(terpy)Cl]^+$ and $[Pd(terpy)Cl]^+$ complexes are known to be highly labile.[43-46] The high lability is attributed to the ability of terpy ligand to accept electrons from the metal leading to the stabilization of the five coordinate intermediate compared to ground state.[47, 48] The lability was doubled when the ligand was modified to 2-(2'-pyridyl)-1,10-phenanthroline[49, 50] due to extended π-conjugation as a result of the fused ring enhancing π-back bonding making the metal centre more electrophilic. However, the presence of substituents at the 4'-position of the terpyridyl system[49, 51] and electron donating groups at 4, 4' and 4" positions lowers the rate of lability by diminishing the π-back bonding ability of the ligand.[52, 53]

Substitution reactions of Pd(II) complexes with tridentate N-donor ligands such as terpy, bpma [(2-pyridylmethyl)-amine], dien (diethylenetriamine), Me_4-dien and Et_4-dien, having varied steric and electronic effects, have provided good basic substrates for ligand exchange studies of square-planar d^8 complexes[13, 33, 34, 43-45, 49, 54-56] and DNA interaction.[57] For instance, van Eldik and his coworkers showed that the introduction of substituents such as ethyl and methyl on a tridentate R_5dien chelate decreased the substitution rate of a series of $[Pd(R_5dien)Cl]^+$ complexes by several orders of magnitude without the steric hindrance introduced affecting the associative mechanistic nature across the series of the complexes.[58-62]

The rate of substitution from Pt(II) complexes coordinated with tridentate N^N^N and N^C^N of a terpyridine ligand framework was decelerated when the *cis*-pyridyl rings were replacement with pyrazolyl and its derivatives due to the presence of the pyrrolic-*N* π-donor within the chelate ring.[63, 64] The effect of the pyrazole ligand coordinated to Pd(II) complex, particularly on the *cis*-position to the leaving group remains unknown. Given the good π/σ-donor properties of pyrazole and in anticipation to control the highly reactive Pd metal from the already known labile $[Pd(terp)Cl]^+$ complex as a reference, the role of *cis*-pyrazole is investigated. Therefore, the rate of substitution of the chloride ligand from the complexes in Figure 3.1 by bio-relevant thiourea nucleophiles, **Tu**, **Dmtu** and **Tmtu,** was measured using stopped-flow methods. The thiourea nucleophiles was used because of their high solubility, good nucleophilicity and appropriate model compounds representing thioether (σ-donor, π-acceptor) and thiolate (σ-donor) groups[65-67] in the human cell. Density function theory (DFT) calculations was performed to give insights into understanding the experimental reactivity trends. The X-ray crystal structures of **PdL2**, **PdL3** and **PdL4** are also reported.

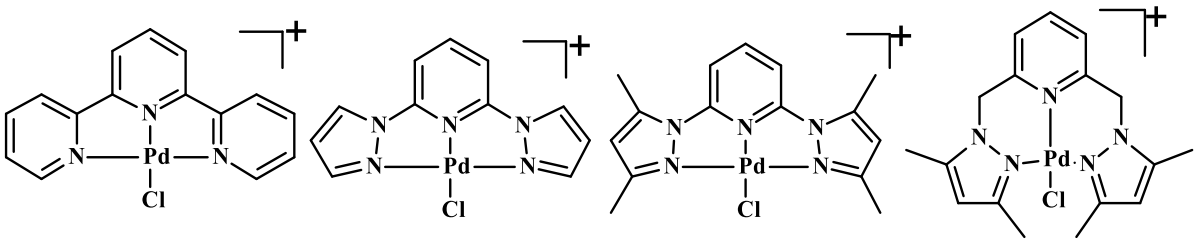

PdL1 **PdL2** **PdL3** **PdL4**

Figure 3. 1 Structures of the studied Pd(II) complexes (counter ions omitted to enable clarity)

3.2 Experimental Section

3.2.1 Materials and Methods

All syntheses were conducted under inert atmosphere of nitrogen employing standard Schlenk line techniques fitted with vacuum-line systems. Palladium tetrachloropalladate(II) (K_2PdCl_4, 98%), bis(acetonitrile)dichloropalladium(II) ($Pd(NCMe)_2Cl_2$, 99.99%), 2,6-bis(bromomethyl)pyridine, 2,6-dichloropyridine, magnesium sulphate, pyrazole, 3,5-dimethylpyrazole and potassium metal were purchased from Sigma-Aldrich and used as supplied.

Lithium chloride (96%) and the nucleophiles: thiourea (Tu, 99%), N,N'-dimethylthiourea (Dmtu, 99%), N,N,N',N'-tetramethylthiourea (Tmtu, 98%) were used as received from Aldrich. The solvents, anhydrous benzene and diglyme were of analytical grade purchased from Aldrich while methanol was purchased from Merck and was used as received without further purification. The ligand 2,6-Bis(2-pyridyl)pyridine (2,2′:6′,2″-Terpyridine, 98%) was obtained from Sigma-Aldrich and used as supplied.

3.2.2 Syntheses of the Ligands

The ligands 2,6-bis(N-pyrazolyl) pyridine[68], 2,6-bis (3,5-dmethyl- N-pyrazolyl)pyridine[68, 69] and 2,6-Bis(3,5-dimethyl-N-pyrazolylmethyl)pyridine[68, 70] were synthesized according to the standard literature methods and including slight modifications.

2,6-Bis(N-pyrazolyl)pyridine, L2: A mixture of pyrazole (4.49 g, 66 mmol), 120 mL anhydrous diglyme (diethylene glycol dimethyl ether) and potassium metal (2.4 g, 61.3 mmol), was stirred at 75 ºC until the metal completely dissolved. 2,6-dichloropyridine (3.0 g, 20 mmol) was then added to the reaction mixture and stirred at 115 ºC for 5 days. The solvent was removed under reduced pressure resulting into oil. The final traces of the solvent were removed from the oily product by adding water and reducing the volume under vacuum. Water was added, and the resultant white solid collected by filtration. Purification of the compound was the achieved by dissolving it in equal amounts of methanol and dichloromethane and reducing the volume was reduced under *vacuo* to obtain a white solid product (3.22 g, 76%) and analysed. ^{1}H NMR (400 MHz $CDCl_3$**)** δ = 6.47 (dd, 2H) 7.74 (dd, 2H) 7.80-7.93 (m, 3 H), 8.54 (dd, 2 H) ^{13}C NMR (100 MHz CDC13) δ = 108.095, 109.525, 127.138, 141.534, 142.511, 150.188. MS-ES^{+}, *m/z* = 234 (M + Na) $^{+}$ *Anal. Calc. for* $C_{11}H_9N_5$: C, 62.55; H, 4.29; N, 33.16 *Found*: C, 62.06; H, 4.02; N, 33.62%.

2,6-Bis(3,5-dimethyl-N-pyrazolyl)pyridine, L3: This ligand was prepared employing the same procedure used for the synthesis of 2,6-bis(N-pyrazolyl)pyridine. A solution of 3,5-dimethylpyrazole (1.62 g, 16.85mmol) in 20 mL of anhydrous diglyme (diethylene glycol dimethyl ether) was stirred with potassium metal (0.67 g, 16.85mmol) at 120 °C until complete dissolution of metal was achieved. To this solution mixture, 2,6-dichloropyridine (1.24 g, 8.44mmol) was added and mixture stirred for 5 days. The solvent was removed in vacuo, and water was added resulting in the formation of light brown precipitate which was obtained by suction filtration. The crude product was purified on silica gel on chromatography column using hexane: ethyl acetate (8:2, R_f = 0.4) (1.29 g, 57 %) and analysed. ^{1}H NMR (400 MHz $CDCl_3$) δ = 2.33 (s, 6H), 2.62 (s, 6H), 6.04 (s, 2H), 7.72 – 7.93 (m, 3H). ^{13}C NMR (100MHz, $CDCl_3$, ppm) δ

= 13.6, 14.3, 109.2, 113.9, 140.6, 141.3, 150.1, 151.4. MS-ES$^+$, *m/z* = 290 (M + Na) $^+$ *Anal. Calc for* $C_{15}H_{17}N_5$: C, 67.39; H, 6.41; N, 26.20. *Found:* C, 67.27; H, 6.55; N, 26.63 %.

2,6-Bis(3,5-dimethyl-N-pyrazolylmethyl)pyridine, L4: To a solution of 3,5-dimethyl-pyrazole (1.9226 g, 20mmol) in anhydrous benzene (30 mL), potassium metal (0.782 g, 20 mmol) was added and the mixture stirred under nitrogen at 80 ºC until complete dissolution of the potassium metal was achieved. 2,6-bis(bromomethyl)pyridine (2.65 g, 20 mmol) was then added to the reaction solution and the mixture stirred at 80 ºC for 24 hours. The solvent was removed to dryness using rotary-vapor and water added to the residue. The product was then extracted with chloroform (3 × 20 mL) and combined organic portions dried over $MgSO_4$. The volume was reduced under pressure yielding an offwhite solid (2.55 g, 86.5%). This was then analysed. ^{1}H NMR (400 MHz $CDCl_3$**)** δ = 2.18 (s, 6H) 2.26 (s, 6H) 5.32 (s, 4H), 5.88 (s, 2 H), 6.67 (d, 2H), 7.53 (t, 1H). ^{13}C NMR (100 MHz CDC13) δ = 157.03, 148.05, 139.85, 138.13, 119.60, 105.70, 54.25, 13.49, 11.07. TOF MS-ES$^+$, *m/z* = 296.1711 (M + H) $^+$ *Anal. Calc. for* $C_{17}H_{21}N_5$. ½$H_2$0 C, 67.08; H, 7.28; N, 23.01 *Found*: C, 67.47; H, 6.95; N, 22.96%.

3.2.3 Synthesis of the Pd(II) Complexes

The complexes chloride-(2,2′:6′,2″-terpyridine)palladium(II) chloride, [71] **PdL1**, chlorido(2,6-Bis(N-pyrazolyl)pyridine)palladium(II) chloride**,**[72] **PdL2**, chlorido(2,6-Bis(3,5-dimethyl-N-pyrazolyl)pyridine)palladium(II) chloride,[72] **PdL3**, and chlorido(2,6-Bis(3,5-dimethyl-N-pyrazolylmethyl)pyridine palladium(II) tetrafluoroborate,[73] **PdL4** were synthesized according to the standard literature procedures.

chlorido-(2,2′:6′,2″-terpyridine)palladium(II) chloride, PdL1. Potassium tetrachloropalladate(II), K_2PdCl_4, (0.163g, 0.5mmol) was dissolved in 30 mL of deionized water in a beaker. In another beaker, (0.1165g, 0.5mmol) of 2,2′:6′,2″-Terpyridine (terpy) was dissolved in 20 mL of

methanol. To a stirring aqueous solution of K_2PdCl_4, methanolic solution of terpy was gradually added. A light orange precipitate formed immediately. The mixture was heated on a hot plate (≈50°C) to evaporate methanol and to concentrate the solution to 10 mL. After filtration on a Buchner funnel, light orange crystals were obtained. The crystals were washed with diethyl ether (3×20mL) and dried at 50º C in a vacuum. Yield 0.1925g, 86.2%). ^{1}H NMR 400MHz (CD_3OD, ppm): δ = 7.77(dd, 2H), 8.48–8.44 (m, 4H), 8.37(td, 2H), 7.89(s, 1H), 7.78(d, 2H). ^{13}C NMR (100MHz CD_3OD, ppm): δ = 78.01, 124.06, 124.80, 128.34, 142.22, 142.66, 152.33, 155.21. TOF MS-ES$^+$, *m/z* = 375.9579 [M – Cl] $^+$. *Anal. Calc for* $C_{15}H_{11}N_3PdCl_2.2H_2O$: C, 40.34; H, 3.39; N, 9.41. *Found:* C, 40.32; H, 3.30; N, 9.20 %.

Chlorido-(2,6-bis(N-pyrazolyl)pyridine)palladium(II) chloride, **PdL2**. Was prepared according to the procedure of Willison and co-workers [72] with modification. K_2PdCl_4 (0.1959g, 0.60 mmol) was dissolved in 30 mL of water in a flask. In a separate beaker, 2,6-bis(N-pyrazolyl) pyridine (0.15g, 0.71mmol) was dissolved in 20 mL of methanol. The solution of 2,6-bis(N-pyrazolyl) pyridine in methanol was gradually added to a stirring a solution of aqueous K_2PdCl_4. Yellowish orange precipitate formed immediately. The mixture was then refluxed for 48 hours at 70 °C, the yellow-tan mixture cooled to room temperature and then filtered. The filtrate was evaporated to dryness under reduced pressure and the resultant yellow product solid washed with cold water, methanol, chloroform, diethyl ether and hexanes. (0.1436 g, 56.4 %), ^{1}H NMR (400 MHz, CD_3OD, ppm): δ = 9.05 (d, 2H), 8.64 (t, 1H), 8.13 (d, 2H), 8.92 (dd, 2H), 6.96 (d, 2H). ^{13}C NMR (100 MHz, CD_3OD, ppm): δ = 109.0, 110.6, 133.2, 145.8, 146.5. MS-ES$^+$, *m/z* = 353 [M – Cl] $^+$ *Anal Calc* for $C_{11}H_9N_5PdCl_2.2H_2O$: C, 31.12; H, 3.09; N, 16.49 *Found:* C, 31.02; H, 3.00; N, 16.22%. X-ray quality crystals were grown from slow evaporation of a mixture of methanol and water.

Chlorido-(2,6-Bis(3,5-dimethyl-N-pyrazolyl)pyridine)palladium(II) chloride, **PdL3**. This complex was synthesized by employing the same procedure used for **PdL2.** K_2PdCl_4 (0.0984g, 0.301mmol) and 2,6-bis(N-pyrazolyl)pyridine (0.096g, 0.366 mmol). The yellow solid was washed thoroughly with diethyl ether and hexanes. (0.142g, 96.3%). ^{1}HNMR (400MHz, CD_3OD, ppm): δ = 2.63 (s, 6H), 2.86 (s, 6H), 6.52 (s, 2H), 7.88 (t, 2H), 8.49 (t, 1H). ^{13}CNMR (125 MHz, CD_3OD, ppm): δ = 12.9, 78.4, 108.5, 113.2, 145.4, 146.6, 147.5, 160.4. MS ES^+ *m/z* = 410 [M – Cl] $^+$. *Anal Calc for* $C_{15}H_{17}N_5PdCl_2.2.5H_2O$: C, 36.79; H, 4.53; N, 14.30 *Found:* C, 36.78; H, 4.26; N, 14.05 %. X -ray quality crystals were grown from slow diffusion of diethyl ether into methanol.

Chlorido-(2,6-Bis(3,5-dimethyl-N-pyrazolylmethyl)pyridine)palladium(II) tetrafluoroborate, PdL4. To a solution of 2,6-Bis(3,5-dimethyl-N-pyrazolylmethyl)pyridine (0.1152 g, 0.39 mmol) in CH_2Cl_2 (20 mL) was added $[Pd(NCMe)_2Cl_2]$ (0.1011 g, 0.39 mmol). The pink solution was stirred for 12 hours and the product precipitated by addition of hexane (20 mL) to give a pink solid (0.1546 g, 0.3275 mmol). The solid was then suspended in CH_2Cl_2 (10 mL) and a solution of $NaBF_4$ (0.036 g, 0.3275 mmol) in CH_2Cl_2 (10 mL) added and stirred for 10 min. The resultant mixture containing Pd black was filtered over Celite to give a clear solution. Hexane (20 mL) was added to the filtrate and kept at -4ºC to afford colourless single crystals suitable for X-ray analysis. (0.0441 g, 25.7%). ^{1}H NMR (400MHz CD_3OD, ppm): δ = 8.20 (t, 1H), 7.90 (d, 2H), 6.13(m, 4H), 5.78 (d, 2H), 2.56 (s, 6H), 2.47 (s, 6H). ^{13}CNMR (100 MHz, CD_3OD, ppm): δ = 12.9, 78.4, 108.5, 113.2, 145.4, 146.6, 147.5, 160.4. MS ES^+. *m/z* = 438 [M – BF_4] $^+$. *Anal Calc for* $C_{15}H_{17}N_5PdClBF_4$: C, 38.96; H, 4.04; N, 13.36 *Found:* C, 38.64; H, 3.66; N, 12.97 %

3.2.4 Physical Measurements and Instrumentation

H^1-NMR and ^{13}C-NMR were performed using Bruker Avance DPX 400 NMR or DPX 500 with a 5 mm BBOZ probe at 30º C to characterize the ligands and complexes. Low-resolution electron-spray ionization (ESI^+) detector mass spectral data were recorded on Shimadzu LC-MS 2020 or on a Waters TOF Micro-mass LCT Premier spectrometer fitted with a positive ion mode. A selection of NMR and mass spectra data for the synthesized ligands and complexes shown in Figures SI 3.1– 3.19, Supporting Information (ESI‡). Elemental compositions of the ligands and complexes were determined using a Thermo Scientific Flash 2000 and a Carlo Erba Elemental Analyzer 1106. Cary 100 Bio UV–visible spectrophotometer was used to determine a suitable wavelength for monitoring the substitution reaction. The wavelengths selected for kinetic analysis are reported is Table SI 3.1, Supporting Information (ESI‡). Applied Photophysics SX 20 stopped-flow reaction analyzer coupled to an online data acquisition system was used for kinetic and thermodynamic of the substitution reactions. The instrument was thermo-controlled within ± 0.1 °C. The X-ray data was collected on a Bruker Apex Duo fitted with an Incoatec microsource operating at 30 W power and Oxford Instruments Cryojet operating at 100(2) K.

3.2.5 Kinetic Measurements

All palladium complexes used in this study were prepared by dissolving 3.0 x 10^{-4} M in methanol solution containing 30 mmol lithium chloride (LiCl). The LiCl was used to prevent any possibility of spontaneous solvolysis of the chloro complexes. The complex concentration was kept constant while the ligand concentration was varied through five values, 50, 40, 30, 20, and 10-fold excess of the complex concentration. The substitution reactions were performed under *pseudo*-first-order conditions using at least a 10-fold excess of the nucleophile concentration over that of the metal complexes. All reactions were initiated by mixing equal volumes of ligand and complex solutions directly in the stopped-flow instrument. The kinetic traces for

concentration and temperature dependence were of excellent fit to a single-exponential decay function. All concentration dependence substitution reactions of the complexes were carried out at 298 K except for **PdL1** and **Tu** nucleophile which was carried out at 293 K. This was due to high reactivity of the **PdL1** complex and the said nucleophile which could not be monitored by stopped-flow instrument at 298 K. To determine activation parameters $\Delta H^{\neq}$ and $\Delta S^{\neq}$, temperature dependence reactions were carried out within a range of 20 °C to 40 °C with 5 °C intervals for all the substitution reactions except for **PdL1** and **Tu** where a range of 10 °C to 20 °C with an interval of 2.5 °C was used. The *pseudo*-first-order rate observed, k_{obs}, were obtained as the average value of 6–10 independent runs. The rate constant, k_2, for the reaction of every metal complex with a specific nucleophile concentration was got from the slope of the plot of k_{obs} against the concentration of the nucleophile using OriginPro 9.1® software.[74]

3.2.6 Computational Modelling

To understand the structure, steric and electronic factors of the complexes contributing to the kinetic and thermodynamic results, ground state electronic structures of **PdL1**, **PdL2**, **PdL3** and **PdL4** were optimized using the density functional theory (DFT) calculations. The DFT calculations were performed with the Gaussian 09 program suite[75] using the B3LYP (Becke 3-Lee-Yang-Parr) functional method, utilizing LANL2DZ (Los Alamos National Laboratory 2 Double ζ)[76] as the basis set. The influence caused by the bulk solvent was evaluated *via* single-point computations using the C-PCM (conductor-like polarizable continuum model) [77, 78] formalism in methanol solvent. All the complexes were modelled with a formal charge of +1 and at singlet state.

3.2.7 X-ray Crystallography

The X-ray data for the palladium complexes were obtained from a Bruker Apex Duo fitted with an Incoatec microsource operating at 30 W power and Oxford Instruments Cryojet operating at 100(2) K. The data were collected with MoKα (λ = 0.71073 Å) radiation at a crystal-to-detector distance of 50 mm. The structures were solved by direct methods SHELX-2014[79] and WinGX[80] and refined with full-matrix least-squares technique on F^2 using SHELX-2014[79]. All hydrogen atoms were included as idealised contributors in the least squares process.

3.3 Results

3.3.1 Computational Details

DFT calculations was performed on the modelled palladium complexes to complement the experimental results. The geometry the optimized frontier molecular orbitals and the planarity structures of the complexes are presented in Table 3.1, whereas the extracts of calculated data are depicted in Table 3.2.

The frontier orbital mappings from Table 3.1 reveal that the HOMO electron densities are from the contributions of 4d orbitals of the palladium and 3p orbitals of the chloride atoms as well as from the ligand moieties. While in **PdL1** and **PdL2** the pyridyl ligand moiety contributes to the HOMOs, pyrazolyl ligand moieties' contribution is evident on **PdL3** and majorly in **PdL4**. On the other hand, the LUMOs are entirely distributed in all the complexes except in **PdL4** where the distribution is largely seen in the pyridyl fragment as well as around the palladium metal centre.

Table 3. 1 DFT optimized HOMO, LUMO frontier molecular orbitals and planarity structures of the Pd(II) complexes at B3LYP/LANL2DZ theory level (iso value = 0.02).

Complex structure	HOMO	LUMO	Planarity
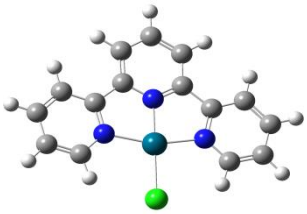 **PdL1**	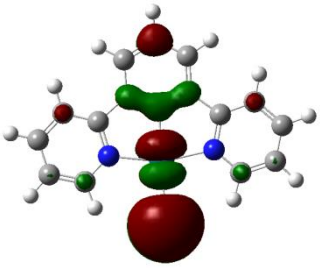	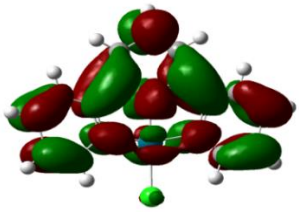	
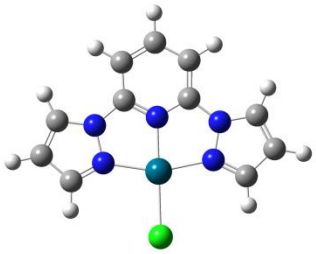 **PdL2**	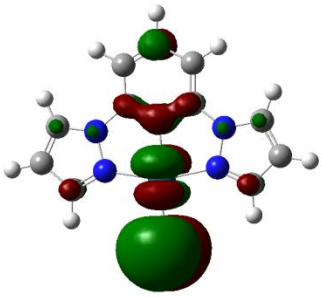	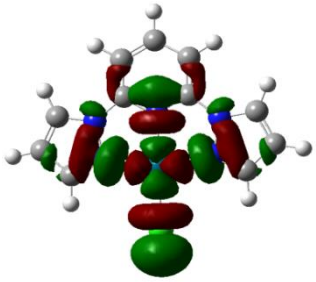	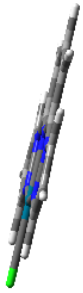
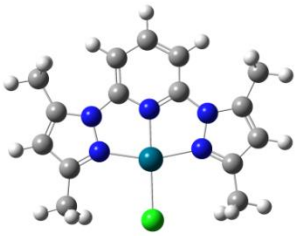 **PdL3**	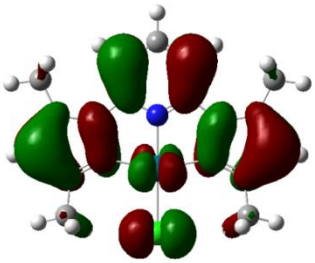	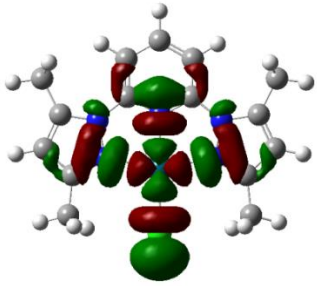	
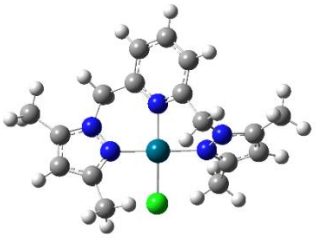 **PdL4**	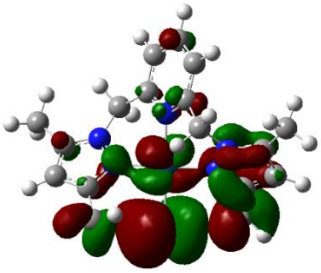	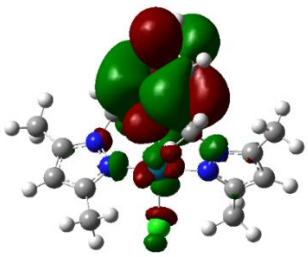	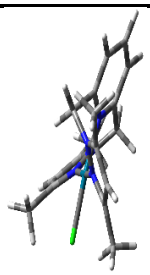

Table 3. 2 Summary of calculated parameters for complexes studied

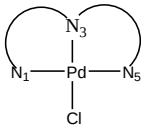 **Property**	**PdL1**	**PdL2**	**PdL3**	**PdL4**
NBO Charges				
Pd^{2+}	0.582	0.582	0.567	0.433
N_1	-0.483	-0.313	-0.332	-0.297
N_3	-0.422	-0.463	-0.488	-0.486
N_5	-0.483	-0.313	-0.332	-0.305
Cl	-0.522	0.489	-0.498	-0.424
Electrophilicity index (ω)	7.046	6.451	6.090	4.572
Bond lengths (Å)				
N_1 – Pd	2.062	2.044	2.058	1.962
N_3 – Pd	1.970	1.984	1.983	1.991
N_5 – Pd	2.063	2.044	2.058	1.989
Pd – Cl	2.415	2.397	2.408	2.270
Energy gap (eV)				
LUMO (eV)	-3.307	-3.114	-2.969	-2.286
HOMO (eV)	-7.296	-7.388	-7.286	-6.806
$\Delta E_{LUMO-HOMO}$	3.989	4.274	4.317	4.520
Bond angles (º)				
N_1 – Pd – Cl	99.328	100.193	100.068	91.148
N_3 – Pd – Cl	179.998	179.968	179.338	175.072
N_5 – Pd – Cl	99.339	100.128	100.069	91.310
Dipole moment (Debye)	13.163	15.353	14.815	14.200

The LUMO electron density in **PdL1** is entirely delocalized on the pyridyl rings and little amounts on the metal with essentially no distribution on the chloride atom. This is consistent with the fact that terpyridine ligand system is a better π-acceptor than the pyrazolyl ligand

systems as supported by the lowest ΔE value (Table 3.2) than the rest of the complexes. The more delocalization of electrons in **PdL1**'s ligand system than rest of the complexes results into a favourable overlap of the metal's dπ orbitals and π* orbitals of the ligands.

The data in Table 3.2 illustrates that the complexes adopts slightly distorted square planar geometry with N5–Pd–N1 deviating from the ideal 180º by angles between 5.5º – 14.5º. On the other hand, the optimized planarity structures of **PdL1**, **PdL2** and **PdL3** shows the ligand structures are in plane with the metal centre, while in **PdL4**, the pyrazole ligand fragments are twisted out of plane at 56.53º away from N3–Pd–Cl main axis. This is due to the methylene spacer group causing flexibility within the ligand system hence steric hinderance which agrees with the X-ray crystal structure (Figure 3.3).

The trend in the HOMO-LUMO energy differences of the complexes increases in the order **PdL1**< **PdL2** < **PdL3**< **PdL4** which agrees with the reactivity trend. In addition, the successive increase in the HOMO energy level going from **PdL1** to **PdL4** is an indication that the electron donation density around the metal increases, while the successive increase on the LUMO energy in the same manner shows a reduction in π-acceptability of the ligand system in the complexes.[81, 82]

3.3.2 X-ray Crystal Determination of the Complexes

The molecular structures of the complexes **PdL2** **(**$C_{11}H_9N_5PdCl_2.2H_2O$), **PdL3** **(**$C_{15}H_{17}N_5PdCl_2.CH_3OH$) and **PdL4** ($C_{17}H_{21}N_5PdClBF_4.CH_2Cl_2$) were confirmed by X-ray crystal structure determination. The crystal structures were deposited at Cambridge Crystallographic Data Centre (deposition numbers; CCDC 1587601, 1587602 and 1829126 for **PdL2, PdL3** and **PdL4,** respectively) which can be obtained free of charge *via* https://www.ccdc.cam.ac.uk/structures/. The crystallographic data and refinement structure

parameters for **PdL2, PdL3** and **PdL4** are summarized in Table 3.3, while the molecular structures are shown in Figure 3.2 for **PdL2** and **PdL3** and Figure 3.3 for **PdL4**.

Table 3. 3 Crystal data and structure refinement for the complexes

	PdL2	**PdL3**	**PdL4**
Molecular formula	$C_{11}H_9N_5PdCl_2.2H_2O$	$C_{15}H_{17}N_5PdCl_2.$ CH_3OH	$C_{17}H_{21}N_5PdClBF_4.$ CH_2Cl_2
M_r	424.56	476.68	608.97
Crystal size/ mm^3	0.210×0.190× 0.140	0.180×0.140×0.110	0.36×0.19×0.11
T/K	100(2)	100(2)	100(2)
λ/ Å	0.71073	0.71073	0.71073
Crystal system	Monoclinic	Monoclinic	Triclinic
Space group	P21/c	P 21/c	P-1
a/Å	11.2092(7)	10.2667(4)	7.7353(3)
b/Å	6.7184(4)	11.0524(5)	12.3436(9)
c/Å	20.5656(12)	16.0338(7)	13.4839(9)
α/º	90	90	115.036(3)
β/º	105.340(3)	95.028(2)	90.896(3)
γ/º	90	90	92.142(4)
V/ $Å^3$	1493.57(16)	1812.38(13)	1164.98(14)
Z	4	4	2
D_c /Mg m^{-3}	1.888	1.747	1.736
μ/ mm^{-1}	1.611	1.334	1.189
F(000)	840	960	608
θ range/º	1.884 - 27.168	2.241 - 28.263	1.668 – 27.075
Reflections collected (independent)	12629 (3292)	16424 (4460)	18239(4962)
R_{int}	0.0252	0.0279	0.0587
No. of parameters (restraints)	205 (6)	232 (0)	330(unknown)
R indices (all data)	R_1=0.0386, wR_2=0.0772	R_1=0.0269, wR_2=0.0562	R_1=0.0807, wR_2=0.1518
Goodness-of-fit on F^2	1.054	1.072	1.034
Max, Min Δρ/e $Å^{-3}$	1.742, - 0.898	0.846, - 0.606	1.564, -2.183

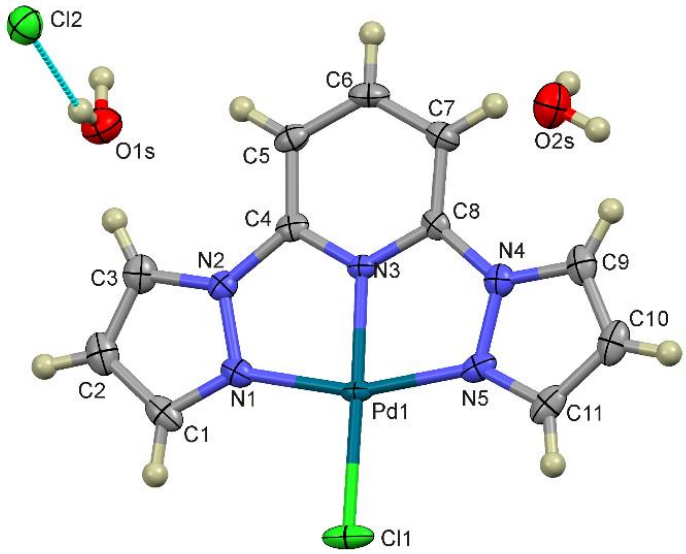

[a]

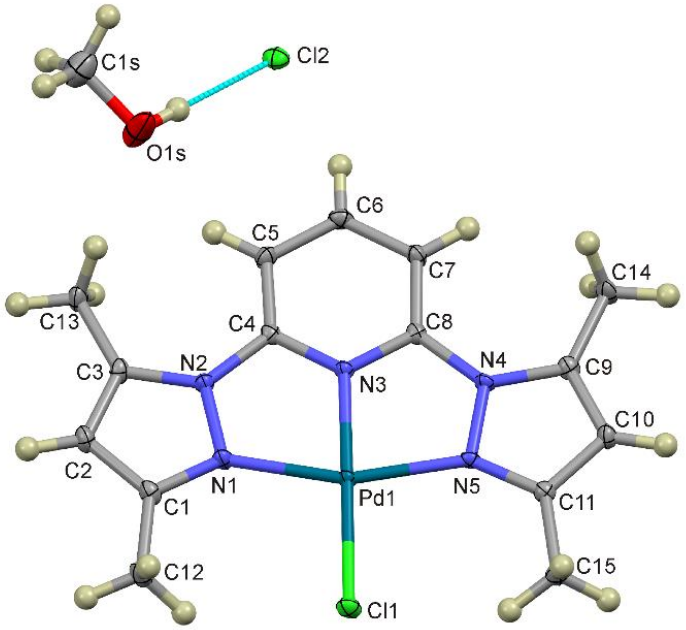

[b]

Figure 3. 2 Molecular structures of a) **PdL2** and b) **PdL3** with atom numbering scheme**.** The displacement ellipsoids of atoms are shown at the 50% probability level. The counter anion, chloride, is hydrogen bonded to the solvent molecule as shown by the blue dash.

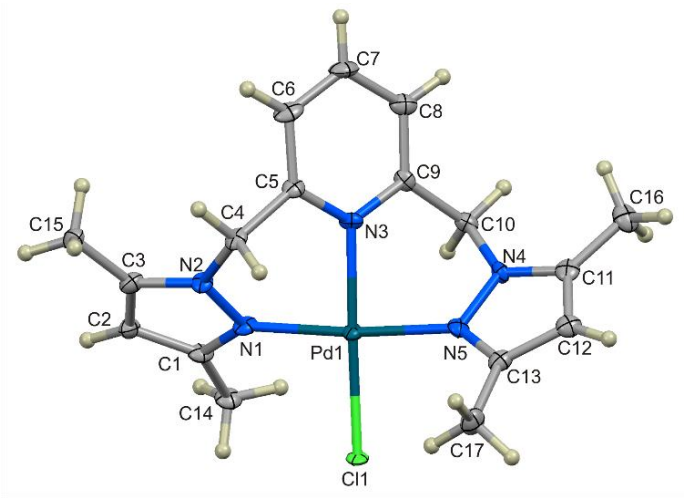

Figure 3. 3 Molecular structure of **PdL4** with atom numbering scheme**.** The displacement ellipsoids of atoms are shown at the 50% probability level. The counter ion and the solvent for crystallization is omitted for clarity.

The complexes crystallise with chloride counter ion, for both **PdL2** and **PdL3** and tetrafluoroborate for **PdL4**. In addition, the crystallization proceeds with two water, methanol, and dichloromethane solvent molecules for **PdL2**, **PdL3** and **PdL4,** respectively. Tridentate ligands coordinate to the Pd-centre by the nitrogen of the *trans*-positioned pyridyl ring and the nitrogen of the *cis*-positioned pyrazolyl rings while the fourth position is covalently bonded to chloride ligand in all the complexes (Figure 3.2 and 3.3). The other non-coordinated chloride atom for **PdL2** and **PdL3** and tetrafluoroborate for **PdL4** are held by unconventional hydrogen bonding contacts within the unit cell and are (indicated by the blue dash in Figure 3.2) between the hydrogen of one water molecule and methanol molecule for **PdL2** and **PdL3**, respectively. Selected bond lengths and angles of the X-ray structures of **PdL1, PdL2** and **PdL4** are tabulated in Table 3.4.

Table 3. 4 Selected bond distances (Å) and angles (º)

	PdL2	**PdL3**	**PdL4**
Bond lengths (Å)			
Pd1 – N1	2.001(3)	2.027(1)	2.019(4)
Pd1 – N3	1.938(2)	1.941(1)	2.204(4)
Pd1– N5	2.001(3)	2.027(1)	2.008(4)
Pd1 – Cl1	2.273(1)	2.297 (1)	2.311(1)
Angles (º)			
N1 – Pd1 – Cl1	98.46(8)	99.32(5)	93.7(1)
N3 – Pd1 – Cl1	178.74(8)	179.17(5)	177.3(1)
N5 – Pd1 – Cl1	100.77(8)	100.35(4)	92.3(1)
N1 – Pd1 – N3	80.34(11)	80.28(6)	87.5(2)
N1 – Pd1 – N5	160.77(11)	160.33(6)	174.1(2)
N3 – Pd1 – N5	80.43(11)	80.05(6)	86.3(2)

The complexes adopt a distorted square planar coordination geometry around the metal centre given that the the angles N1–Pd1–N3, N5–Pd–N3, N3–Pd–Cl1 and N5–Pd–Cl1 deviaviates approximately by angles between 2˚ – 10˚ from the ideal square planar angle 90˚. This is slight distortion is further confirmed by the bite angle N5–Pd1–N1 deviates significantly from linearity (180º) to 160.77(11)º 160.33(6)º and 174.1(2)º for **PdL2 PdL3** and **PdL4**, respectively. In addition, N3–Pd1–Cl1 bite angles 178.74(8) º, 179.17(5) º and 177.3(1) º for **PdL2**, **PdL3**, and **PdL4** respectively, also shows slight deviation from the linearity. All these bite angles are comparable to the DFT calculated values (Table 3.2). The bond angle N3–Pd1–Cl1 for **PdL2** is in agreement with that of a X-ray related structure of analogous Pt(II) (178.91(13)˚)[72] complex, while that of **PdL4** (177.3(1)º) is almost equal to that of a similar X-ray structure (177.63(12)º).[73] The bond distances N3 – Pd1 (**PdL2** 1.938(2) Å **PdL3** 1.9406(15) Å) are well below 2.0 Å and interestingly shorter than Pd1–N1 and Pd1–N5 distances while that of **PdL4** 2.204(4) Å is slightly above 2.0 Å. These bond lengths are within the range of values reported for other X-ray related structures. [72, 73, 83] The Pd1–N3 bond distances are noticeably shorter than

the Pd1–Cl1 (2.273(1) Å, 2.297(1) Å and 2.311(1) Å for **PdL2, PdL3**, and **PdL4**, respectively) due to strong interactions between the *trans*-N-pyridyl ring and the Pd(II) metal centre.

The crystal packing for the complexes evidences an inversion dimer fashion (Figures 3.4 and 3.5). The Pd – Pd distances between the dimers (**PdL2,** 3.3622(3) Å and **PdL3,** 3.4697(3) Å) being less than 4 Å clearly indicates that there is an intermolecular metal – metal interactions as was observed in similar X-ray structure of Pt(II) complex.[72] However, there is no metal-metal interactions in **PdL4** (10.1507(9) Å) since Pd–Pd distances > 4 Å. In **PdL2**, there is C6–H⋯Cl1 bonding linkage indicating intermolecular interaction as shown in Figure 3.4, which is not the case with **PdL3** and **PdL4** complexes.

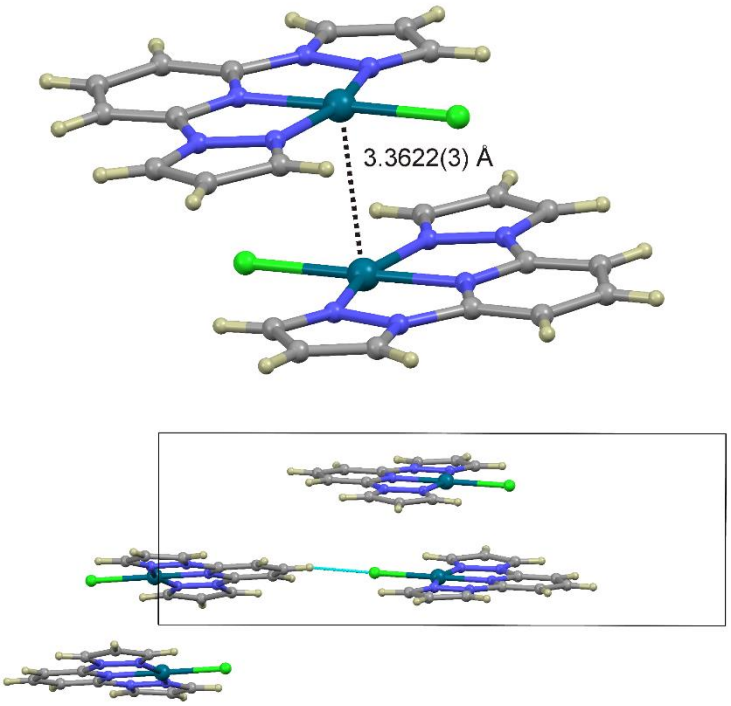

Figure 3. 4 A portion of the crystal packing of **PdL2** showing an inversion dimer, Pd–Pd interactions and Cl1⋯H interaction between the molecules (shown in blue dashed line). The chloride counter ion and the solvent water molecules are omitted for clarity.

The dihydrate crystals of **PdL2** and the solvent molecule of methanol of **PdL3** results in hydrogen bonding system between the water, methanol subunits and the chlorine anion. This bonding type is inferred because of the short inter-molecular interaction distances between the water O atoms and the chloride anion (Cl2), Cl2 – O1 (3.182(4) Å) for **PdL2** and the methanol O, Cl2 – O1 (3.044 (2) Å) for **PdL3**.

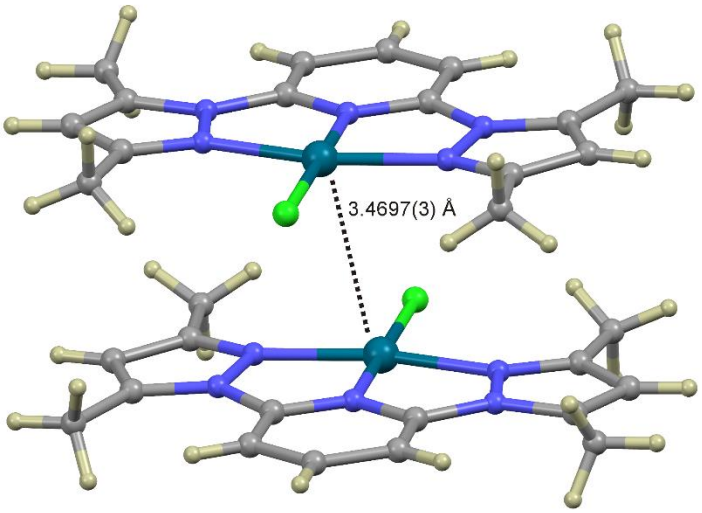

Figure 3. 5 Crystal packing of **PdL3** showing an inversion dimer having Pd-Pd interactions. The chloride counter ion and methanol solvent molecule omitted for clarity.

3.3.3 Kinetic and Mechanistic Studies

Substitution of chloride ligands from the square planar Pd(II) complexes was studied with thiourea based nucleophiles under *pseudo* first-order conditions, employing the stopped-flow spectrophotometric technique, as a function of the nucleophile concentration and temperature. The best wavelengths at which the reaction could be monitored were determined spectrophotometrically by recording the UV/Vis-spectral changes before and after mixing the complex and the nucleophile. Typical spectral changes accompanying the reaction and the predetermined wavelength at which the reaction between **PdL3** and **Tmtu** was undertaken is shown in Figure 3.6. The wavelengths suitable for stopped-flow detection ranged between 380

nm and 435 nm depending on the Pd(II) complex and the nucleophile used are presented in Table SI 3.1 in the supporting information (ESI‡).

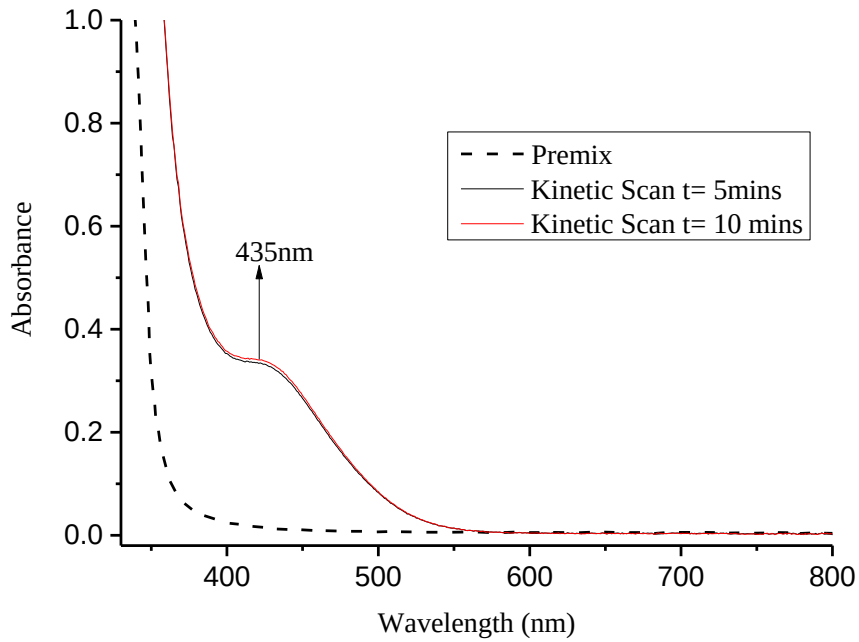

Figure 3. 6 UV-Visible absorption spectra scans of **PdL3** (3.0×10^{-4} M) and **Tmtu** (0.015M).

All the kinetic traces were of excellent fit to a single-exponential decay function which generated observed *pseudo*-first-order rate constant (k_{obs}) using *Equation 3.1*[84], suggesting that the substitution reactions are first-order in both the thiourea nucleophiles and Pd(II) complexes.

$$A_t = A_0 + (A_0 - A_\infty)exp(-k_{obs}\, t) \tag{3.1}$$

where A_t , A_0 and A_∞ represent the absorbance of initial reaction mixture, at time t, and at the end of the reaction respectively. Dependence of the rate constant on the concentration of the entering nucleophiles of different concentrations were analysed in the same manner at 298 K. A typical example of stopped-flow kinetic trace at 380 nm recorded by mixing methanolic solutions of **PdL2** and **Dmtu** at 298 K is shown in Figure 3.7.

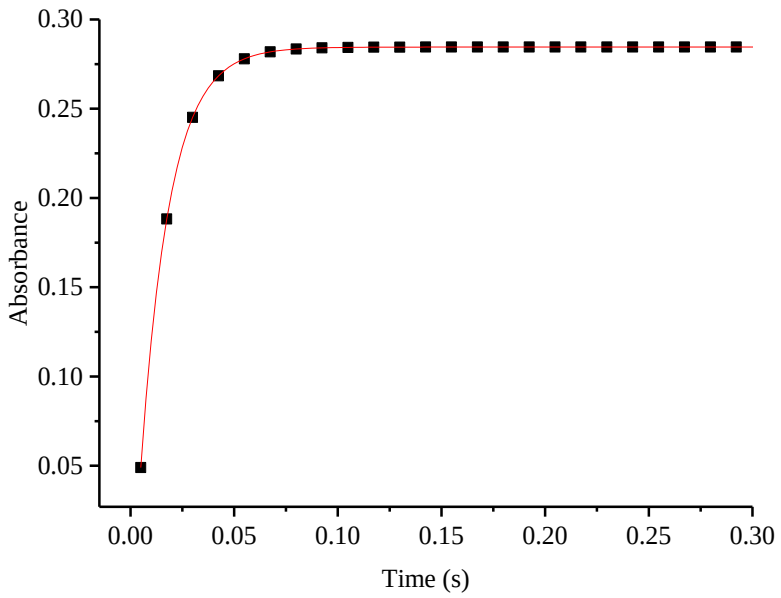

Figure 3. 7 Stopped-flow kinetic trace at 380 nm of **PdL2** and **Dmtu** at 298 K

The average observed rate constant, $k_{obs,}$ from the kinetic traces was plotted against the concentration of the entering nucleophiles using OriginPro 9.1® [74]. The k_{obs} from the stopped-flow plotted against the concentration of each of the entering nucleophiles gave straight lines with zero intercept. The zero-intercept indicated that the reverse or solvotic pathway was insignificant or absent. A representative plot of k_{obs} versus concentration of the nucleophiles of **PdL4** is shown in Figure 3.8; similar plots for the other complexes are shown in Figures SI 3.20 – 3.22 while the values of k_{obs} with their respective nucleophile concentrations are tabulated in Tables SI 3.2 – 3.5 in the supporting information (ESI‡). These results imply that the *pseudo*-first-order rate constant is related to the incoming nucleophile concentration [Nu] by the *Equation 3.2*, in which the entering thiourea nucleophiles systematically displace the chloride ligand from the metal complexes in an irreversible manner.

$$k_{obs} = k_2 [Nu] \tag{3.2}$$

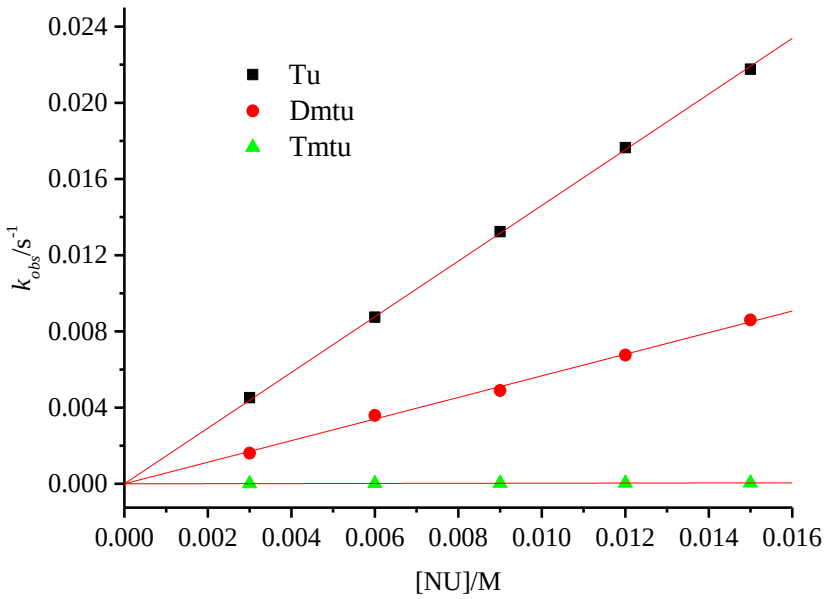

Figure 3. 8 Dependence of k_{obs} on the nucleophile concentration for chloride substitution from **PdL4** at T = 298 K.

The rate constant values for the forward reactions, k_2 obtained from the gradient of the linear plots of k_{obs} against nucleophile concentration, along with the thermodynamic parameters, enthalpies ($\Delta H^{\neq}$) and entropies ($\Delta S^{\neq}$) calculated from the temperature dependence of the rate constants using Eyring equation are summarized in Table 3.5. Also included in Table 3.5, are the k_2 values in literature[64] for analogous platinum(II) complexes for comparison purposes of the reactivities of Pd(II) and Pt(II) complexes of the same ligand framework. The rate of chloride substitution by **Tu** from **PdL1** was too fast to be followed at 298 K, therefore it was monitored at 293 K, and Eyring plots linear equation [$\ln(k_2/T) = m(1/T) + c$] for the range of temperatures 283 K–293 K, was used to extrapolate the kinetic at 298 K as shown in Figures SI 3.23 – 3.24 in the supporting information (ESI‡), for comparison purposes with the rest of the complexes, the true value was **(1.09 ± 0.013) × 10^5 M^{-1}s^{-1}** at 293 K. A representative Eyring plots for **PdL3** with the thiourea nucleophiles at different temperatures is shown in Figure 3.9; similar plots for the reactions of other complexes are shown in Figures SI 3.25 – 3.27, while the values $\frac{1}{T}$ and their respective $ln\left(\frac{k_2}{T}\right)$ are tabulated in Tables SI 3.6 – 3.9 in the supporting information (ESI‡).

Table 3.5 k_2 values and thermodynamic parameter data for the reactions of the Pd(II) complexes with the nucleophiles in methanol, I= 30mmol, LiCl.

Complex	Nucleophile	k_2/M^{-1} s^{-1}	$\Delta H^{\neq}$/kJ mol^{-1}	$\Delta S^{\neq}$/JK^{-1} mol^{-1}	Pt(II) k_2 /M^{-1} s^{-1}
PdL1	Tu*	(1.18± 0.002) × 10^5	18 ± 1	-88 ± 4	1494 ± 10[a]
	Dmtu	(4.07± 0.29) × 10^4	23 ± 2	-80 ± 6	448 ± 10[a]
	Tmtu	(4.66 ± 0.02) × 10^3	49 ± 1	-11 ± 3	82 ± 4[a]
PdL2	Tu	(1.26 ± 0.003) × 10^4	24 ± 1	-85 ± 3	0.86 ± 0.01[b]
	Dmtu	(4.99 ± 0.03) × 10^3	32 ± 1	-68 ± 3	0.37 ± 0.01[b]
	Tmtu	(3.04 ± 0.09) × 10^2	44 ± 1	-86 ± 3	0.17 ± 0.03[b]
PdL3	Tu	(1.01 ± 0.01) × 10^4	24 ± 1	-87 ± 3	0.31 ± 0.02[b]
	Dmtu	(4.33 ± 0.03) × 10^3	24 ± 1	-95 ± 5	0.13 ± 0.01[b]
	Tmtu	(1.13 ± 0.02) × 10^2	63 ± 1	-36 ± 3	0.014 ± 0.001[b]
PdL4	Tu	1.461 ± 0.014	52 ± 2	-67 ± 6	-
	Dmtu	(5.67 ± 0.07) × 10^{-1}	39 ± 1	-119 ± 4	-
	Tmtu	(3.28 ± 0.012) ×10^{-3}	61 ± 2	-85 ± 7	-

* Represent extrapolated value. **PdL1** k_2 for **Tu** at 293 K= (1.09 ± 0.013) × 10^5 M^{-1}s^{-1}

[a] Extracted from reference, [45] and [b] from reference [64]

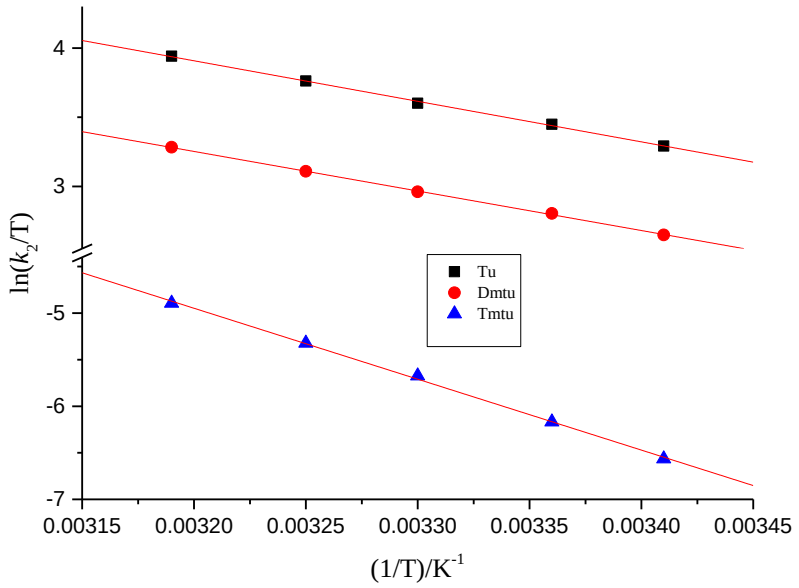

Figure 3. 9 Eyring plots for tne **PdL3** complex

3.4 Discussion

Based on the results as tabulated in Table 3.5, the activation enthalpies ($\Delta H^{\neq}$) are positive while the entropy ($\Delta S^{\neq}$) values are largely negative. The trend in the values of the thermodynamic parameters clearly indicates that the substitution mechanism is associatively activated, which is well in agreement with square-planar d^8 metal complexes.[85, 86] The thermodynamic parameter values therefore suggests that the process of activation is highly dominated by bond-making process leading to formation of an intermediate with trigonal bipyramidal structure. On the other hand, the second order-rate constants, k_2, of the nucleophilic substitution of the chloride ligand of the complexes by the thiourea nucleophiles follows the order **Tu** > **Dmtu** > **Tmtu** for all the complexes. This order agrees with the different steric demands of the thiourea-based nucleophiles with less sterically hindered **Tu** reacting faster while **Tmtu,** being most sterically hindered, reacting much slower.

Comparing the rates of the substitution of the chloride ligands from the complexes by the thiourea nucleophiles in Table 3.5, the obtained second-order rate constants, k_2, unsurprisingly indicates that **PdL1** is the most reactive of all the complexes under the current study. **PdL1** has a

terpy ligand system framework, whose high liability of the chloro and aqua complexes of Pd(II) and Pt(II) have been well reported in literature with different solvents, including ionic media, with various nucleophiles,[43-46, 87, 88] with the highest recorded substitution rate being (7.8 ± 0.2) × 10^5 $M^{-1}s^{-1}$ at 25° C for the chloro Pd(II) complex and **Tu** as the entering nucleophile in water solvent.[43] This high lability of the terpy complexes of Pd(II) and Pt(II) have been attributed to their terpy ligand having stronger π-acceptor properties ascribed to effective π-back donation of electrons from the filled d-orbital of the metal into the empty nonbonding or antibonding (π*) orbitals of the in-plane aromatic ligand pyridyl rings.[87, 89, 90] The electrophilicity of the metal centre is thus increased making it more positive, hence easily attracts the incoming nucleophile. This phenomenon was observed in the **PdL1** of the current study which is supported by DFT calculations showing high electrophilicity index of 7.046 (Table 3.2) compared to 6.451, 6.090 and 4.572 for **PdL2**, **PdL3** and **PdL4,** respectively.

Using the reaction of **PdL1** with **Tu** as a reference for comparison with the other complexes in this study, it was observed that the trend of the reactivity decreases in the order of **PdL1 > PdL2 > PdL3 >> PdL4**. This same trend was also observed for all the nucleophiles investigated in this study (Table 3.5). A close examination of the structures of **PdL1** and **PdL2** shows that the only difference between the complexes is the replacement of the *cis*-pyridyl rings in **PdL1** with N-pyrazolyl ring in **PdL2**. This replacement surprisingly, reduced the reactivity of the coordinated palladium metal centre by approximately 10 times with the **Tu** nucleophiles going from **PdL1** to **PdL2**. It is therefore important to understand the underlying factors that is responsible for controlling this reactivity in as much as these complexes are characterized by delocalized π-system that simply allows electron transfer from the metal to ligand. Studies on absorption of terpy, (**L1)** and 2,6-bis(N-pyrazolyl)pyridine, (**L2**) based complexes of ruthenium and platinum showed higher energetic metal ligand charge transfer bands (MLCT) in complexes having **L2**

ligands than those having **L1** ligands.[64, 91, 92] The higher MLCT of **L2** relative to **L1** based complexes was due to the high electron density making **L2** a weaker π-acceptor and a stronger σ-donor than **L1**.

Moreover, the π-bonding properties of pyridine rings in **PdL1** readily accepts π-back donation from the metal, as already mentioned, as opposed to pyrazole ring that is π-electron rich because of extra pyrollic-N within the chelate ring making it a better π-donor[93, 94] in **PdL2**. Therefore, the *cis*-pyrazolyl ring in **PdL2** introduces pyrollic-N π-donor into the chelate rings as opposed to stronger π-acceptability of the *cis*-pyridyl ring in **PdL1**. The presence of pyrollic-N π-donor in the chelate ring of **PdL2** together with a strong σ-donation plays a major role in lowering its substitution rate than that of **PdL1**. The pyrollic-N π-donor in the chelate ring of **PdL2** acts by building up electron density around the palladium metal centre through π-resonance[63, 95] creating poor π-acceptability and promoting good π/σ-donor character of the pyrazolyl ligand than the pyridyl ligand. The build-up of electron density around the palladium metal centre in **PdL2** lowers the electrophilicity of the complex thereby making it less attractive to nucleophilic attack than **PdL1**. This is supported by the electrophilicity indices 7.046 and 6.451 (Table 3.2) for **PdL1** and **PdL2**, respectively. As a result, the LUMO energy in **PdL2** is raised to -3.114 eV than in **PdL1** -3.307 eV which eventually widens the HOMO-LUMO gap of **PdL2** (4.274eV) compared to that of **PdL1** (3.989 eV). The effect is enhanced in **PdL3** whose reactivity is further lowered due to the presence of electron-rich ancilliary methyl groups which builds more electron density into the chelate ring through σ-donation which eventually increases accumulation of electron density at the metal centre making it less electrophilic. The NBO charges at the palladium metal centre supports the reactivity trend (Table 3.2). In addition, it is worth noting that in **PdL2** and **PdL3** the π-backbonding on the *trans*-pyridyl ring competes with the π/σ-

donation ability of the *cis*-pyrazolyl rings for the palladium metal centre. The stronger π/σ-donation of the pyrazole reduces the π-backbonding.

The observed reactivity of **PdL4** is greatly reduced by approximately 5 and 4 orders of magnitude with respect to the entering **Tu** nucleophile when compared with **PdL1** and **PdL2**/**PdL3**, respectively. In this case, the structural differences between the complexes plays a major role in their reactivity differences. The structural differences between the complexes is that in **PdL4**, the *trans*-pyridyl ring is bridged with methylene to the *cis*-pyrazolyl derivative. The introduction of the methylene group in **PdL4** introduces a six-membered ring into the coordination sphere of the palladium metal centre destroying the aromaticity of the ligand. This destruction results into the reduction of π-backbonding. This is confirmed by the shorter DFT calculated values of Pd–N1 and Pd–N5 bond distances in **PdL4** (1.962 Å and 1.989Å) compared to the other complexes (Table 3.2). This is also supported by the NBO charges and electrophilicity index indicating that **PdL4** has poor interaction between the orbitals of d_{xz} and d_{yz} with the empty anti-bonding or non-bonding ligand orbitals in comparison to the other complexes.

Secondly, **PdL4** complex is more flexible than the other complexes due to the introduction of a six-membered ring in the system. Such a phenomenon was observed in a related structure $[Pd(tpdm)Cl]^+$ complex (where tpdm = tripyridinedimethane) in which the methylene group bridged the *cis*-pyridine rings.[13, 96] The tetrahedral arrangement of the methylene groups forces the pyrazolyl derivative ligands to be out of plane with the metal centre which significantly introduces steric effects and eventually retards the rate of chloride substitution in **PdL4**. The observed planarity in the DFT optimized structures in Table 3.1 confirms this argument in which

PdL4 has a distorted planar (non-planar) while the other complexes have a planar geometry. The same was observed in their crystal structures in Figures 3.2 and 3.3.

The reactivity of Pd(II) complexes (**PdL1**, **PdL2**, **PdL3**) in this study was compared with their analogous Pt(II) complexes [45, 64] (Table 3.5). The chloride substitution with the thiourea nucleophiles of Pd(II) complexes have higher reactivity than their corresponding Pt(II) complexes. The reactivity difference of chloro complexes can be accounted for by the fact that Pd(II) metal center have a higher electrophilicity than Pt(II)-metal center. A similar trend have been reported for closely related complexes by van Eldik and co-workers which is well in agreement with the results of this study.[6, 13, 33, 44] The data in this study show that the reactivity of Pd(II) complexes is 10^2 - 10^5 times faster than their Pt(II) analogues. The reactivity differences between the complexes of Pd(II) and Pt(II) is attributed to the differences in the degree of softness between the metals. Pt(II) is a softer metal center than Pd(II) and therefore more sensitive to electronic communication with the spectator ligand than Pd(II) metal center.[34, 87, 88] This is observed when one looks at the k_2 values, with respect to **Tu**, between the **PdL1** and **PdL2** from a terpy to a pyrazole system where the value decreases by a factor of 10 in Pd(II) but by 10^4 in Pt(II) metal. In principle, electronic effects have been used to increase the reactivity of Pt(II) complexes to reach their closely related Pd(II) complexes whereas steric hinderance have been helpful in tuning the lability of Pd(II) complexes to reach their closely related Pt(II) complexes.[13, 34, 55] In this study, a combination of electronic and steric factors decreased the reactivity of Pd(II) metal center to a level comparable to Pt(II) complexes.

3.5 Conclusions

In general, the reactivity of the designed complexes under this study is controlled by both electronic and steric factors with electronic factors largely controlling **PdL1**, **PdL2** and **PdL3**, while steric factors dominantly control the reactivity of **PdL4**. The study shows that the reactivity of palladium metal can be tuned by use of pyrollic-N-π-donor which decreases the ability of π-back bonding resulting in accumulation of electrons around the metal centre. The removal of the aromatic property around the metal centre through the introduction of a six-membered ring introduces steric hinderance and destroys the electronic communication through π-back bonding resulting in a less nucleophilic centre. This magically reduces the rate of substitution from **PdL4** by 4 – 6 orders of magnitude relative to most labile **PdL1** for all the nucleophiles in keeping with their steric demands. These findings are important since ligands that can reduce the reactivity of Pd(II) metal centre could lead to Pd(II) complexes with increased antitumour potential that might possibly be useful for biological application. The values of thermodynamic parameters show that the ligand exchange mechanism is associative in nature.

3.6 References

1. Ž. D. Bugarčić, J. Bogojeski and R. van Eldik, *Coordination Chemistry Reviews*, 2015, **292**, 91-106.
2. B. Lippert, *Cisplatin: chemistry and biochemistry of a leading anticancer drug*, John Wiley & Sons, 1999.
3. D. Wang and S. J. Lippard, *Nature Reviews Drug Discovery*, 2005, **4**, 307-320.
4. S. van Zutphen and J. Reedijk, *Coordination Chemistry Reviews*, 2005, **249**, 2845-2853.
5. H. Zorbas and B. K. Keppler, *ChemBioChem*, 2005, **6**, 1157-1166.
6. Ž. D. Bugarčić, J. Bogojeski, B. Petrović, S. Hochreuther and R. van Eldik, *Dalton Transactions*, 2012, **41**, 12329-12345.
7. E. Alessio, *Bioinorganic medicinal chemistry*, John Wiley & Sons, 2011.
8. Ž. D. Bugarčič, G. Liehr and R. van Eldik, *Journal of the Chemical Society, Dalton Transactions*, 2002, 2825-2830.
9. T. Rau, M. Shoukry and R. van Eldik, *Inorganic Chemistry*, 1997, **36**, 1454-1463.
10. B. Lippert, *Chemistry and biochemistry of a leading anticancer drug*, Verlag Helvetica Chimica Acta, Zürich; Weinheim : Wiley-VCH, Zürich, Switzerland, 1999.
11. J. Reedijk, *Chemical Reviews*, 1999, **99**, 2499-2510.
12. E. R. Jamieson and S. J. Lippard, *Chemical Reviews*, 1999, **99**, 2467-2498.
13. B. Petrović, Ž. D. Bugarčić, A. Dees, I. Ivanović-Burmazović, F. W. Heinemann, R. Puchta, S. N. Steinmann, C. Corminboeuf and R. Van Eldik, *Inorganic Chemistry*, 2012, **51**, 1516-1529.
14. E. Wong and C. M. Giandomenico, *Chemical Reviews*, 1999, **99**, 2451-2466.
15. J. Lokich, *Cancer Investigation*, 2001, **19**, 756-760.
16. S. Shibata, *Neurologia Medico-Chirurgica*, 1990, **30**, 242-245.
17. M. E. Alberto, C. Cosentino and N. Russo, *Structural Chemistry*, 2012, **23**, 831-839.
18. Z. Guo and P. J. Sadler, *Angewandte Chemie International Edition*, 1999, **38**, 1512-1531.
19. N. J. Farrer, L. Salassa and P. J. Sadler, *Dalton Transactions*, 2009, 10690-10701.
20. P. Blower, *Dalton Transactions*, 2006, 1705-1711.
21. X. Wang and Z. Guo, *Dalton Transactions*, 2008, 1521-1532.
22. S. P. Fricker, *Dalton Transactions*, 2007, 4903-4917.
23. S. P. Fricker, *Metallomics*, 2010, **2**, 366-377.

24. J. Reedijk, Medicinal applications of metal complexes binding to biological macromolecules. In *Macromolecular symposia* Weinheim: WILEY-VCH Verlag. August, 2008, Vol. 270, No. 1, pp. 193-201.
25. M. Galanski, V. Arion, M. Jakupec and B. Keppler, *Current Pharmaceutical Design*, 2003, **9**, 2078-2089.
26. M. Tanaka, H. Kataoka, S. Yano, H. Ohi, K. Kawamoto, T. Shibahara, T. Mizoshita, Y. Mori, S. Tanida and T. Kamiya, *BMC Cancer*, 2013, **13**, 237
27. A. S. Abu-Surrah, M. Kettunen, K. Lappalainen, U. Piironen, M. Klinga and M. Leskelä, *Polyhedron*, 2002, **21**, 27-31.
28. M. Al-Noaimi, A. S. Abu-Surrah and L. Tahtamouni, *Arabian Journal of Chemistry*, 2012, **9**, S1503-S1509.
29. A. R. Kapdi and I. J. Fairlamb, *Chemical Society Reviews*, 2014, **43**, 4751-4777.
30. A. S. Abu-Surrah, H. H. Al-Sa'doni and M. Y. Abdalla, *Cancer Therapy*, 2008, **6**, 1-10.
31. T. Rau and R. van Eldik, *Metal Ions in Biological Systems*, 1996, **32**, 339 - 378.
32. J. Bogojeski, R. Jelić, D. Petrović, E. Herdtweck, P. G. Jones, M. Tamm and Ž. D. Bugarčić, *Dalton Transactions*, 2011, **40**, 6515-6523.
33. Ž. D. Bugarčić, G. Liehr and R. van Eldik, *Journal of the Chemical Society, Dalton Transactions*, 2002, 951-956.
34. Z. D. Bugarcic, B. Petrovic and E. Zangrando, *Inorganica chimica acta*, 2004, **357**, 2650-2656.
35. M. Marques, *ISRN Spectroscopy*, 2013, **2013**, 1 - 29.
36. M. González, J. Tercero, A. Matilla, J. Niclós-Gutiérrez, M. Fernández, M. López, C. Alonso and S. González, *Inorganic Chemistry*, 1997, **36**, 1806-1812.
37. H. Mansuri-Torshizi, T. Srivastava, H. Parekh and M. Chitnis, *Journal of Inorganic Biochemistry*, 1992, **45**, 135-148.
38. J. Butoura, S. Wimmerb, F. Wimmerb and P. Castanc, *Chemico-Biological Interactions*, 1997, **104**, 165-178.
39. A. S. Abu-Surrah and M. Kettunen, *Current Medicinal Chemistry*, 2006, **13**, 1337-1357.
40. J. Bogojeski, J. Volbeda, M. Freytag, M. Tamm and Ž. D. Bugarčić, *Dalton Transactions*, 2015, **44**, 17346-17359.
41. N. P. Barry and P. J. Sadler, *Chemical Communications*, 2013, **49**, 5106-5131.
42. T. Al-Allaf and L. Rashan, *Bollettino Chimico Farmaceutico*, 2000, **140**, 205-210.

43. S. Kern, P. Illner, S. Begel and R. van Eldik, *European Journal of Inorganic Chemistry*, 2010, **2010**, 4658-4666.
44. P. Illner, S. Kern, S. Begel and R. van Eldik, *Chemical Communications*, 2007, **0**, 4803-4805.
45. D. Jaganyi, D. Reddy, J. Gertenbach, A. Hofmann and R. van Eldik, *Dalton Transactions*, 2004, 299-304.
46. A. Hofmann, L. Dahlenburg and R. van Eldik, *Inorganic Chemistry*, 2003, **42**, 6528-6538.
47. D. Jaganyi, K. L. D. Boer, J. Gertenbach and J. Perils, *International Journal of Chemical Kinetics*, 2008, **40**, 808-818.
48. B. Pitteri, G. Marangoni, L. Cattalini, F. Visentin, V. Bertolasi and P. Gilli, *Polyhedron*, 2001, **20**, 869-880.
49. P. Ongoma and D. Jaganyi, *Dalton Transactions*, 2012, **41**, 10724-10730.
50. A. Shaira, D. Reddy and D. Jaganyi, *Dalton Transactions*, 2013, **42**, 8426-8436.
51. A. Shaira, D. Reddy and D. Jaganyi, *Dalton Transactions*, 2013, **42**, 8426-8436.
52. D. Reddy and D. Jaganyi, *Dalton Transactions*, 2008, 6724–6731.
53. D. Reddy, K. J. Akerman, M. P. Akerman and D. Jaganyi, *Transition Metal Chemistry*, 2011, **36**, 593-602.
54. Ž. D. Bugarčić, D. M. Jančić, A. A. Shoukry and M. M. Shoukry, *Monatshefte für Chemie/Chemical Monthly*, 2004, **135**, 151-160.
55. D. Jaganyi, F. Tiba, O. Q. Munro, B. Petrović and Ž. D. Bugarčić, *Dalton Transactions*, 2006, 2943-2949.
56. M. Kosović, Ž. Jaćimović, Ž. D. Bugarčić and B. Petrović, *Journal of Coordination Chemistry*, 2015, **68**, 3003-3012.
57. C. S. Peyratout, T. K. Aldridge, D. K. Crites and D. R. McMillin, *Inorganic Chemistry*, 1995, **34**, 4484-4489.
58. E. Breet and R. Van Eldik, *Inorganic Chemistry*, 1984, **23**, 1865-1869.
59. M. Kotowski and R. Van Eldik, *Inorganic Chemistry*, 1984, **23**, 3310-3312.
60. M. Kotowski and R. Van Eldik, *Inorganic Chemistry*, 1986, **25**, 3896-3899.
61. J. Pienaar, M. Kotowski and R. Van Eldik, *Inorganic Chemistry*, 1989, **28**, 373-375.
62. J. Berger, M. Kotowski, R. Van Eldik, U. Frey, L. Helm and A. Merbach, *Inorganic Chemistry*, 1989, **28**, 3759-3765.

63. I. M. Wekesa and D. Jaganyi, *Journal of Coordination Chemistry*, 2016, **69**, 389-403.
64. I. M. Wekesa, PhD Thesis, University of KwaZulu-Natal, South Africa, 2014.
65. W. C. Schiessl, N. K. Summa, C. F. Weber, S. Gubo, C. Dücker-Benfer, R. Puchta, N. J. van Eikema Hommes and R. van Eldik, *Zeitschrift für Anorganische und Allgemeine Chemie*, 2005, **631**, 2812-2819.
66. M. T. Ashby, *Comments on Inorganic Chemistry*, 1990, **10**, 297-313.
67. S. G. Murray and F. R. Hartley, *Chemical Reviews*, 1981, **81**, 365-414.
68. D. L. Jameson and K. A. Goldsby, *The Journal of Organic Chemistry*, 1990, **55**, 4992-4994.
69. G. S. Nyamato, M. G. Alam, S. O. Ojwach and M. P. Akerman, *Applied Organometallic Chemistry*, 2016, **30**, 89-94.
70. A. A. Watson, D. A. House and P. J. Steel, *Inorganica Chimica Acta*, 1987, **130**, 167-176.
71. T. V. Dalrymple and T. U. o. T. a. S. A. Chemistry, *Synthesis and Characterization of Palladium(II) Complexes as Potential Antitumor Agents*, University of Texas at San Antonio, 2007.
72. S. A. Willison, H. Jude, R. M. Antonelli, J. M. Rennekamp, N. A. Eckert, J. A. Krause Bauer and W. B. Connick, *Inorganic Chemistry*, 2004, **43**, 2548-2555.
73. S. O. Ojwach, I. A. Guzei, J. Darkwa and S. F. Mapolie, *Polyhedron*, 2007, **26**, 851-861.
74. OriginPro 9.1. OriginLab Corporation, One Roundhouse Plaza, Suite 303, Northampton, MA 01060, United States. 1800-969-7720
75. M. Frisch, G. Trucks, H. Schlegel, G. Scuseria, M. Robb, J. Cheeseman, G. Scalmani, V. Barone, B. Mennucci, G. Petersson, Gaussian 09, revision D. 01, Gaussian, Inc., Wallingford CT (2009).
76. P. J. Hay and W. R. Wadt, *The Journal of Chemical Physics*, 1985, **82**, 299-310.
77. V. Barone and M. Cossi, *The Journal of Physical Chemistry A*, 1998, **102**, 1995-2001.
78. M. Cossi, N. Rega, G. Scalmani and V. Barone, *Journal of Computational Chemistry*, 2003, **24**, 669-681.
79. G. Sheldrick, *University of Göttingen, Göttingen*, 2014.
80. L. J. Farrugia, *Journal of Applied Crystallography*, 2012, **45**, 849-854.
81. G. L. Eakins, J. S. Alford, B. J. Tiegs, B. E. Breyfogle and C. J. Stearman, *Journal of Physical Organic Chemistry*, 2011, **24**, 1119-1128.

82. A. Mambanda and D. Jaganyi, *Dalton Transactions*, 2011, **40**, 79-91.

83. G. Intille, C. Pfluger and W. Baker, *Journal of Crystal and Molecular Structure*, 1973, **3**, 47-54.

84. J. D. Atwood, *Inorganic and organometallic reaction mechanisms*, Wiley-VCH Publishers, New York, 2nd edn., 1997.

85. R. Van Eldik, T. Asano and W. Le Noble, *Chemical Reviews*, 1989, **89**, 549-688.

86. M. Tobe and J. Burgess, *Inorganic Reaction Mechanisms* Addison Wesley Longman Inc, Essex, 1999.

87. D. Jaganyi, A. Hofmann and R. van Eldik, *Angewandte Chemie International Edition*, 2001, **40**, 1680-1683.

88. A. Hofmann, D. Jaganyi, O. Q. Munro, G. Liehr and R. van Eldik, *Inorganic Chemistry*, 2003, **42**, 1688-1700.

89. J. K. Burdett, *Inorganic Chemistry*, 1975, **14**, 931-934.

90. J. K. Burdett, *Inorganic Chemistry*, 1977, **16**, 3013-3025.

91. F. Schramm, R. Chandrasekar, Thomas A. Zevaco, Manfred Rudolph, Helmar Görls, Wolfgang Poppitz and M. Rube, *European Journal of Inorganic Chemistry*, 2009, 53–61.

92. D. L. Jameson, J. K. Blaho, K. T. Kruger and K. A. Goldsby, *Inorganic Chemistry*, 1989, **28**, 4312-4314.

93. J. M. Holland, J. A. McAllister, C. A. Kilner, M. Thornton-Pett, A. J. Bridgeman and M. A. Halcrow, *Journal of the Chemical Society, Dalton Transactions*, 2002, 548-554.

94. T. Astley, A. J. Canty, M. A. Hitchman, G. L. Rowbottom, B. W. Skelton and A. H. White, *Journal of the Chemical Society, Dalton Transactions*, 1991, 1981-1990.

95. K. L. Garner, L. F. Parkes, J. D. Piper and J. G. Williams, *Inorganic Chemistry*, 2009, **49**, 476-487.

96. A. Mijatović, J. Bogojeski, B. Petrović and Ž. D. Bugarčić, *Inorganica Chimica Acta*, 2012, **383**, 300-304.

3.7 Supporting Information (ESI‡)

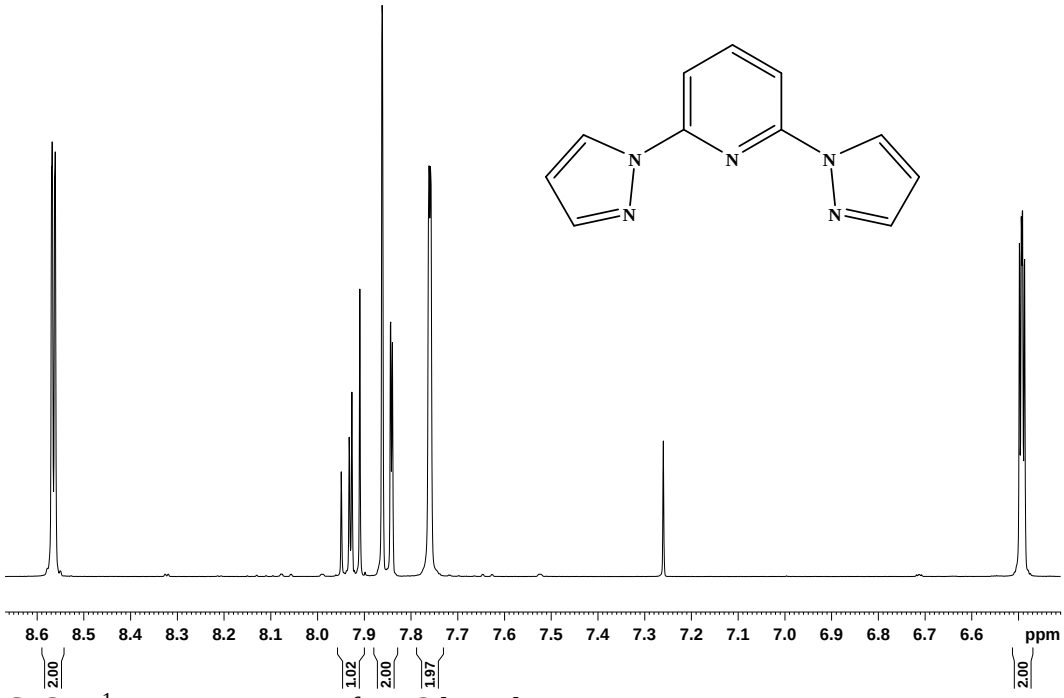

Figure SI 3. 1 ^{1}H NMR spectrum for **L2** ligand

Figure SI 3.2 ^{13}C NMR spectrum for **L2** ligand

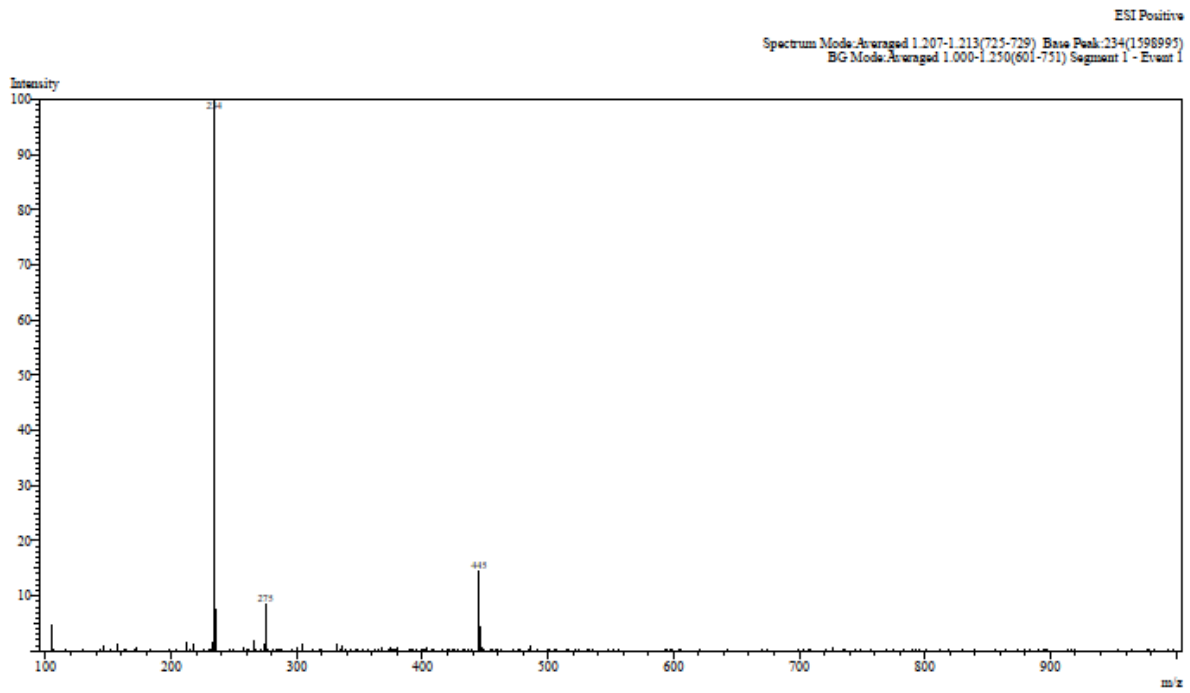

Figure SI 3. 3 LC-MS mass spectrum **L2** ligand

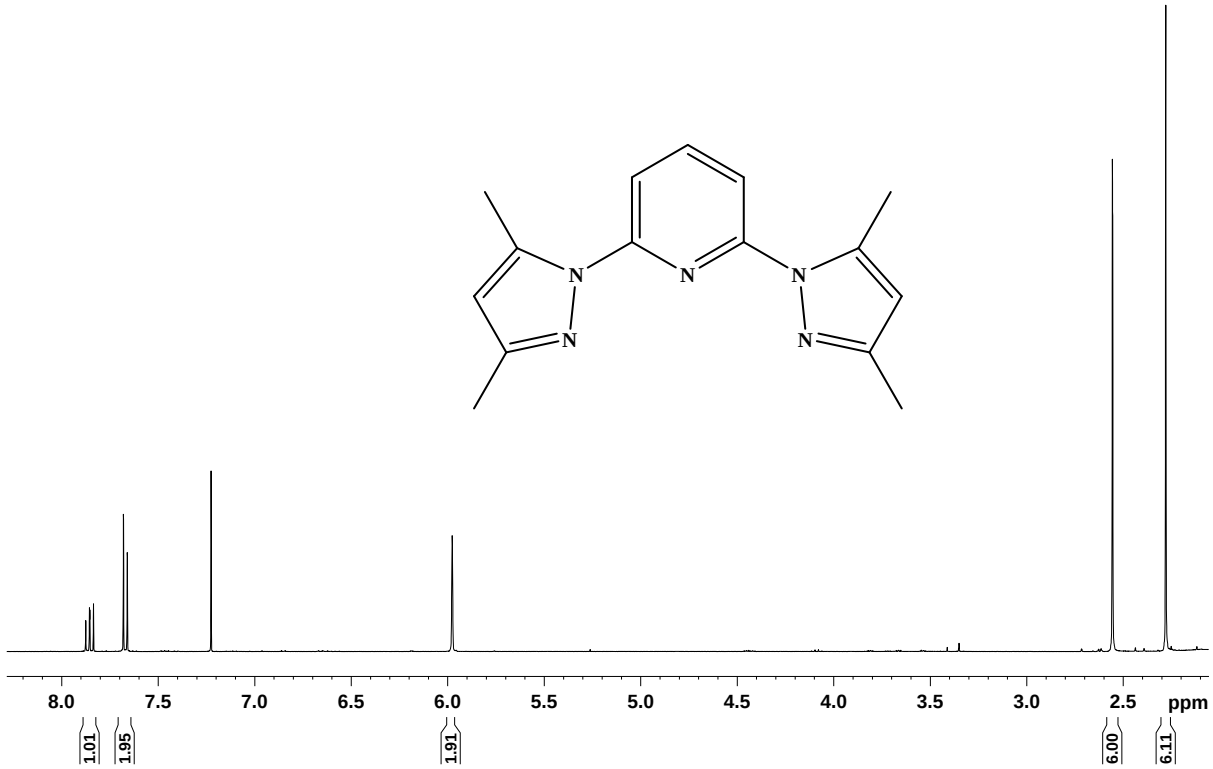

Figure SI 3. 4 ^{1}H NMR spectra for **L3** ligand

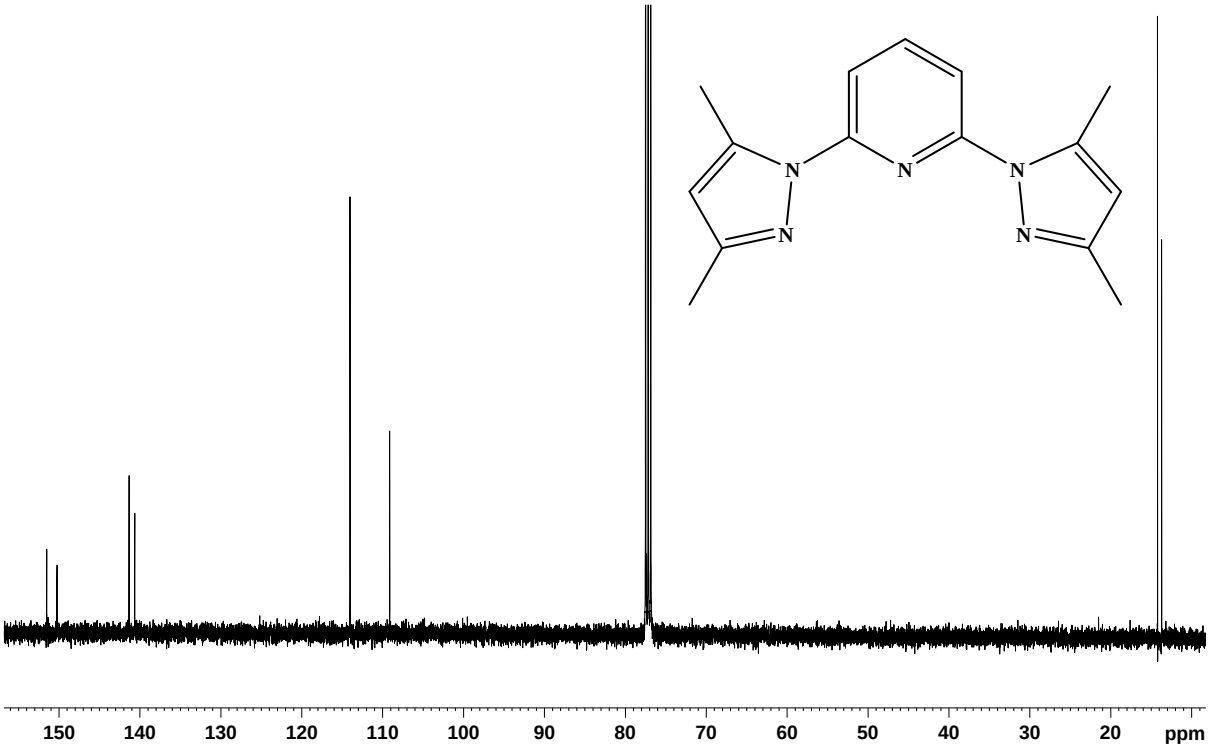

Figure SI 3. 5 ^{13}C NMR spectra for **L3** ligand

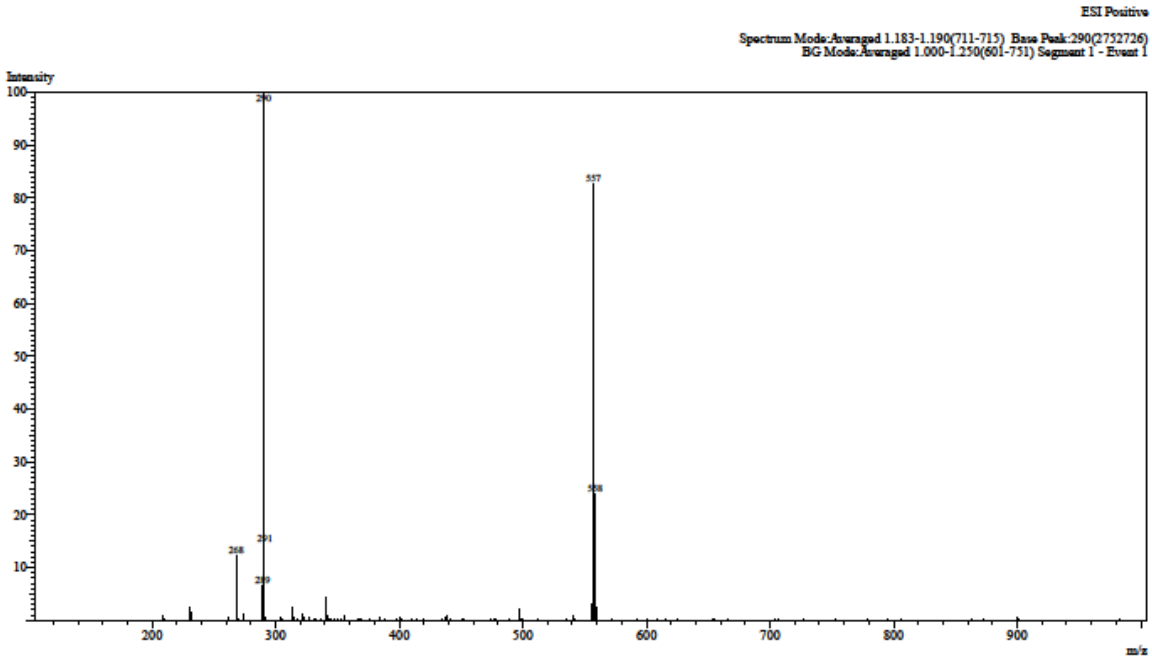

Figure SI 3. 6 LC MS mass spectrum of **L3**

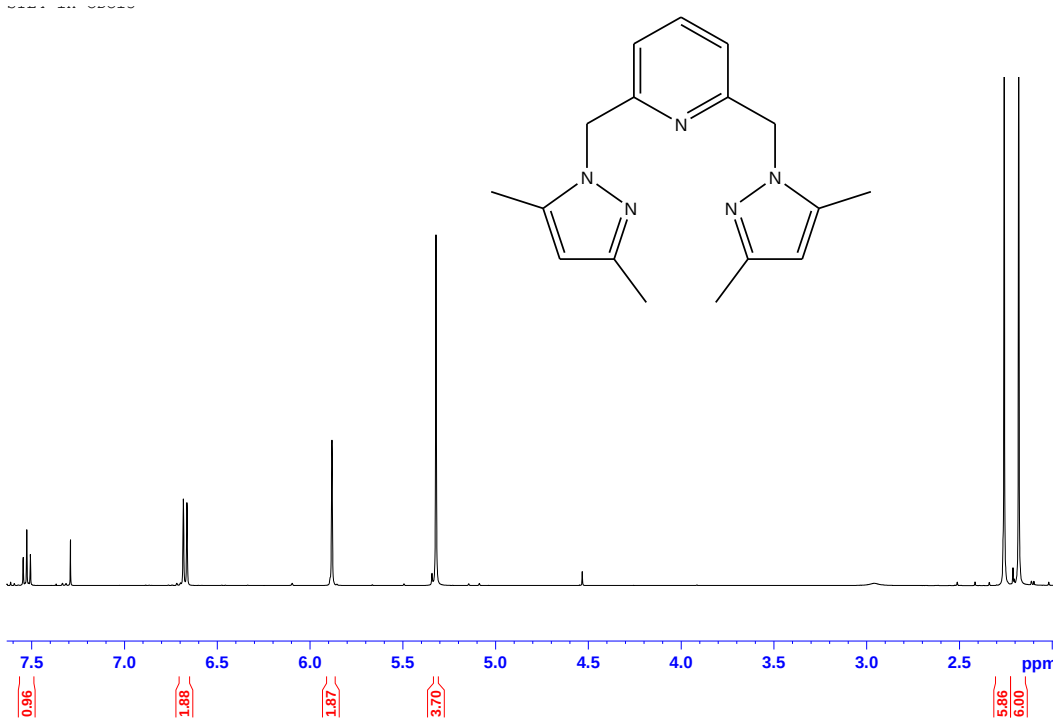

Figure SI 3. 7 ^{1}H NMR spectrum for **L4** ligand

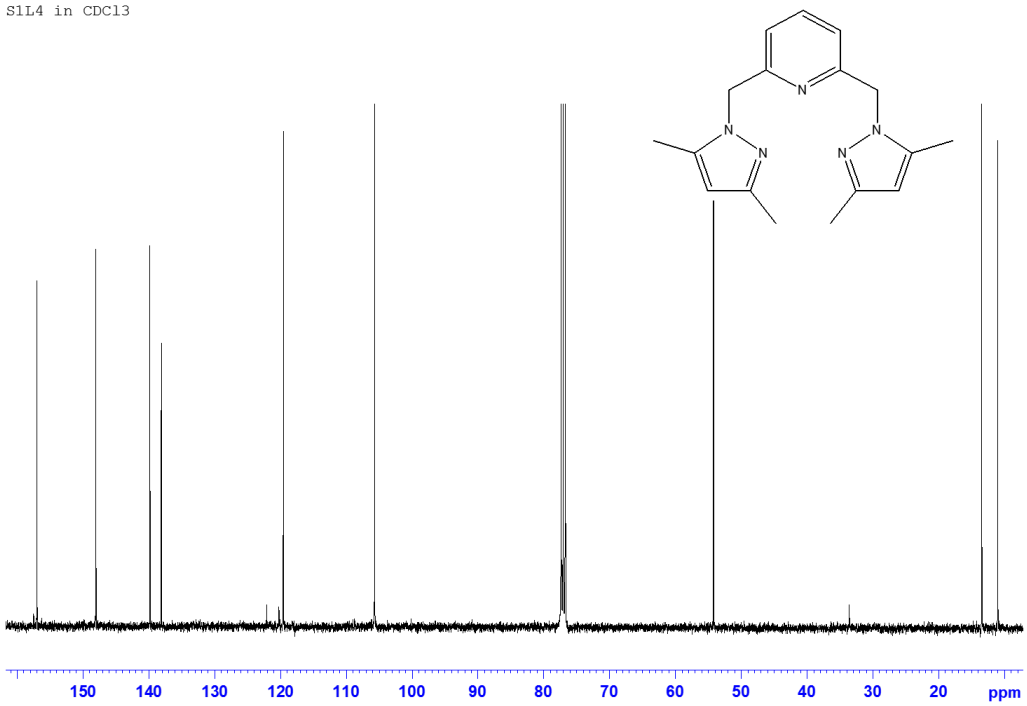

Figure 3. 8 ^{13}C NMR spectrum for **L4** ligand

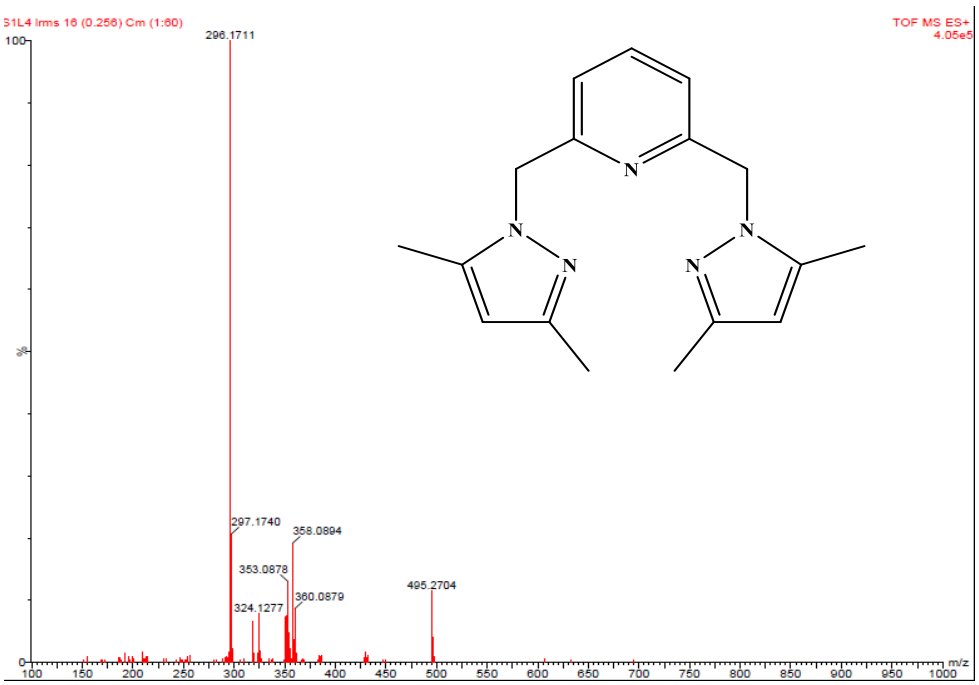

Figures SI 3. 9 TOF-MS mass spectrum for **L4** ligand

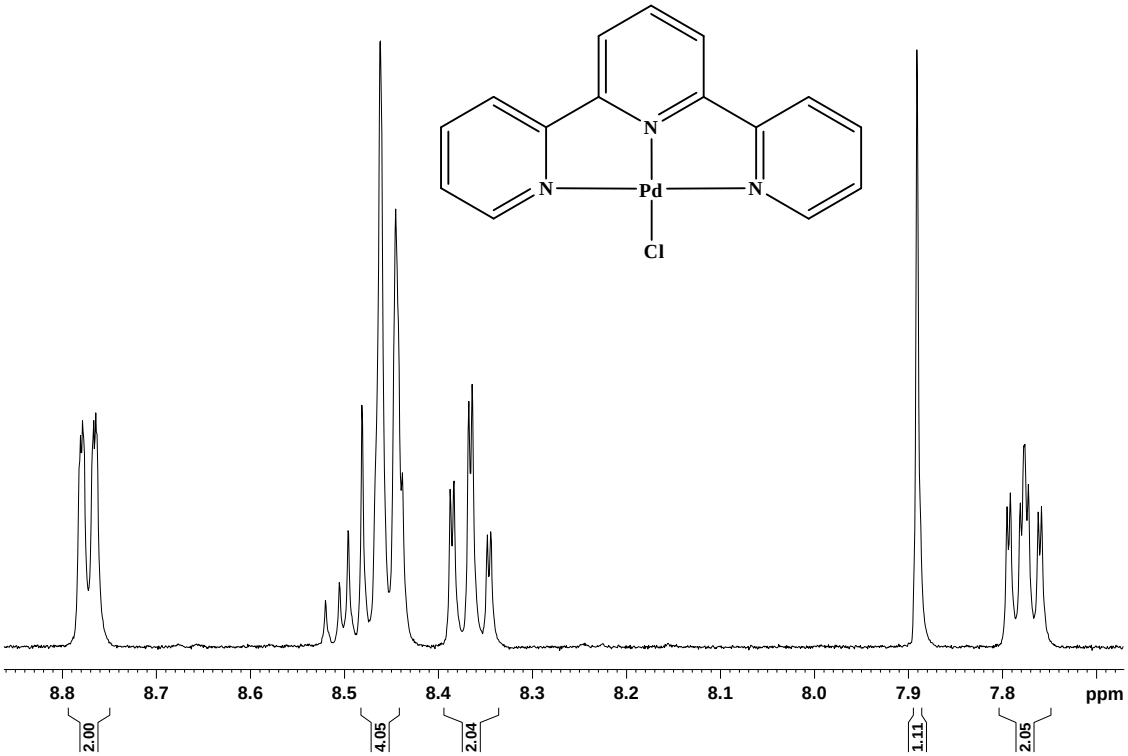

Figure SI 3. 10 ^{1}H NMR spectrum for **PdL1** complex

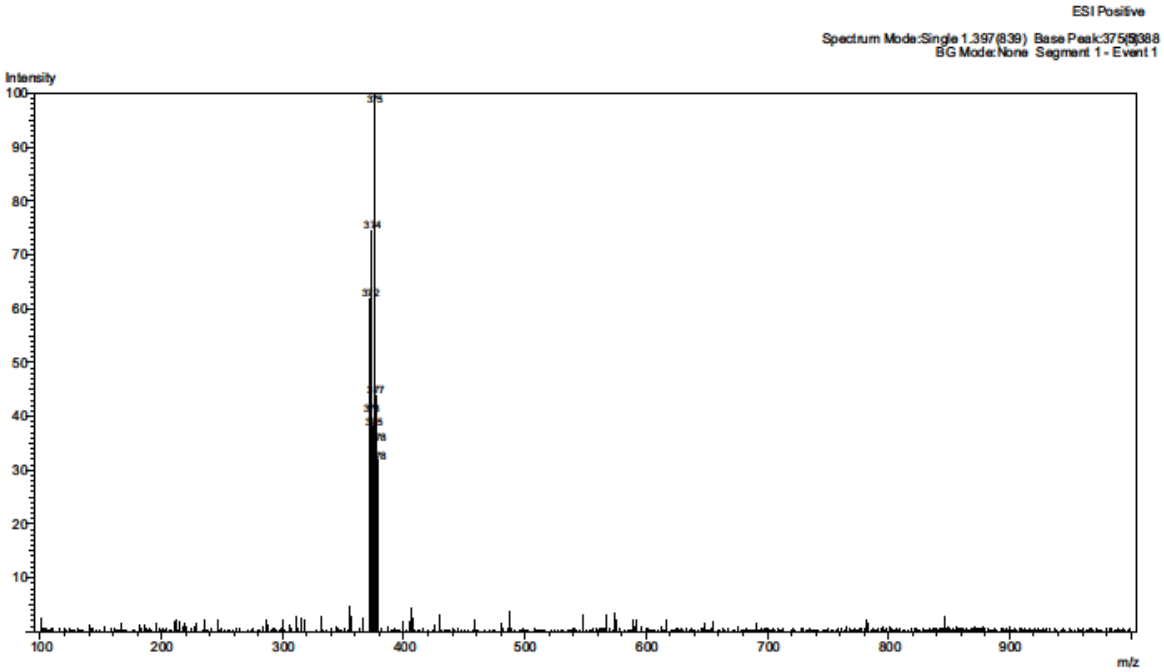

Figure SI 3. 11 LC-MS mass spectra of **PdL1** complex

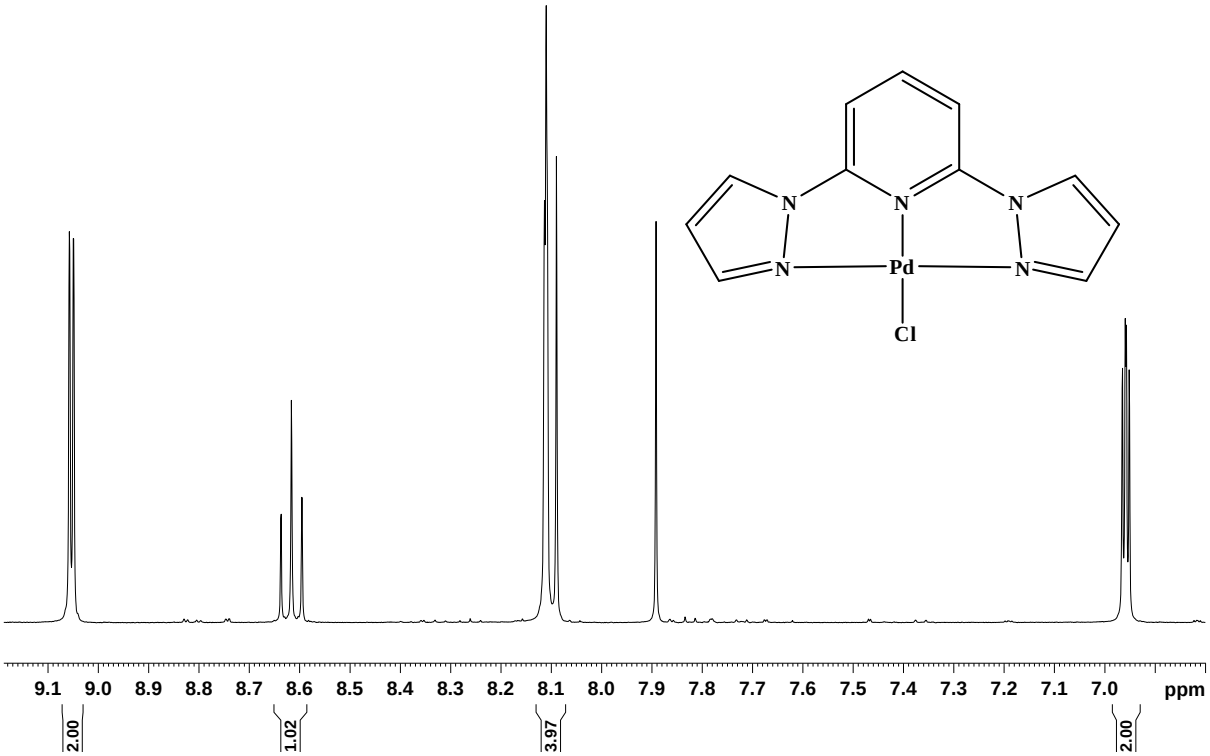

Figure SI 3. 12 ^{1}H NMR spectrum **PdL2** complex

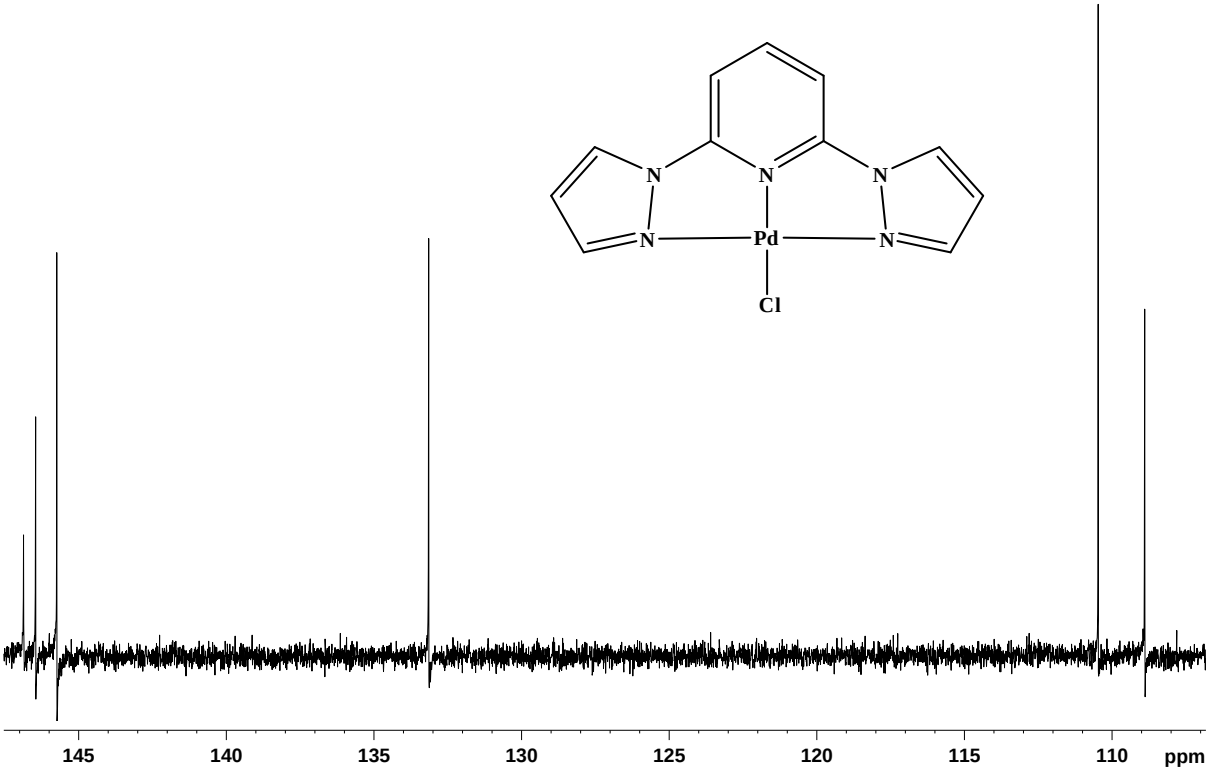

Figure SI 3. 13 ^{13}C NMR spectrum for **PdL2** complex

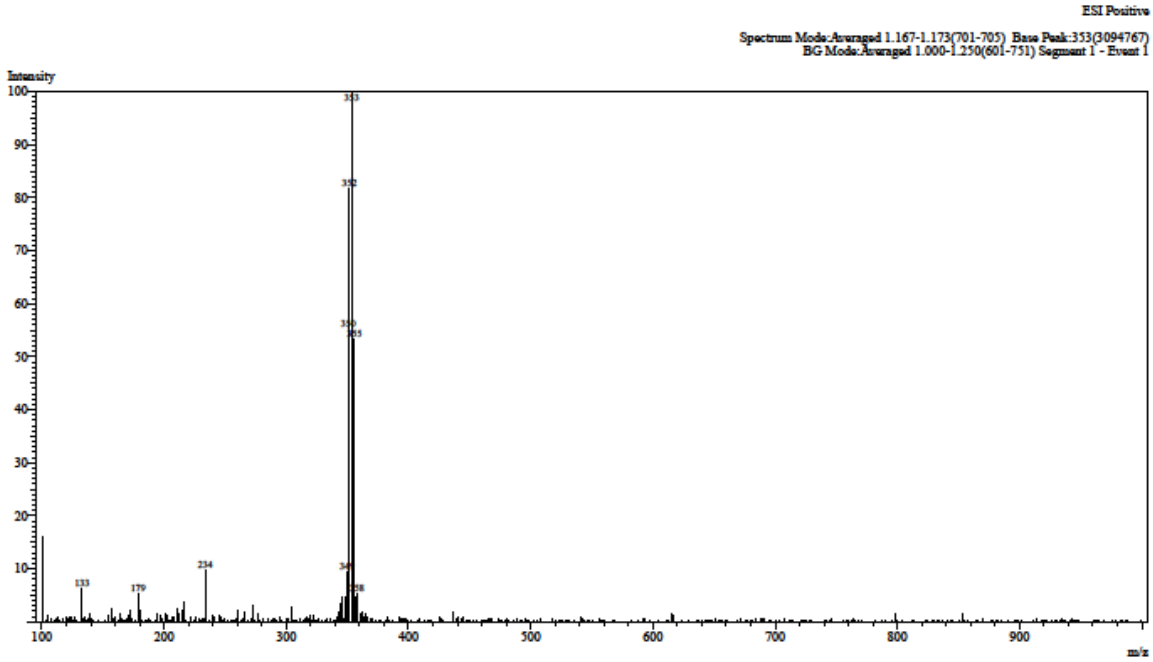

Figure SI 3. 14 LC-MS mass spectrum for **PdL2** complex

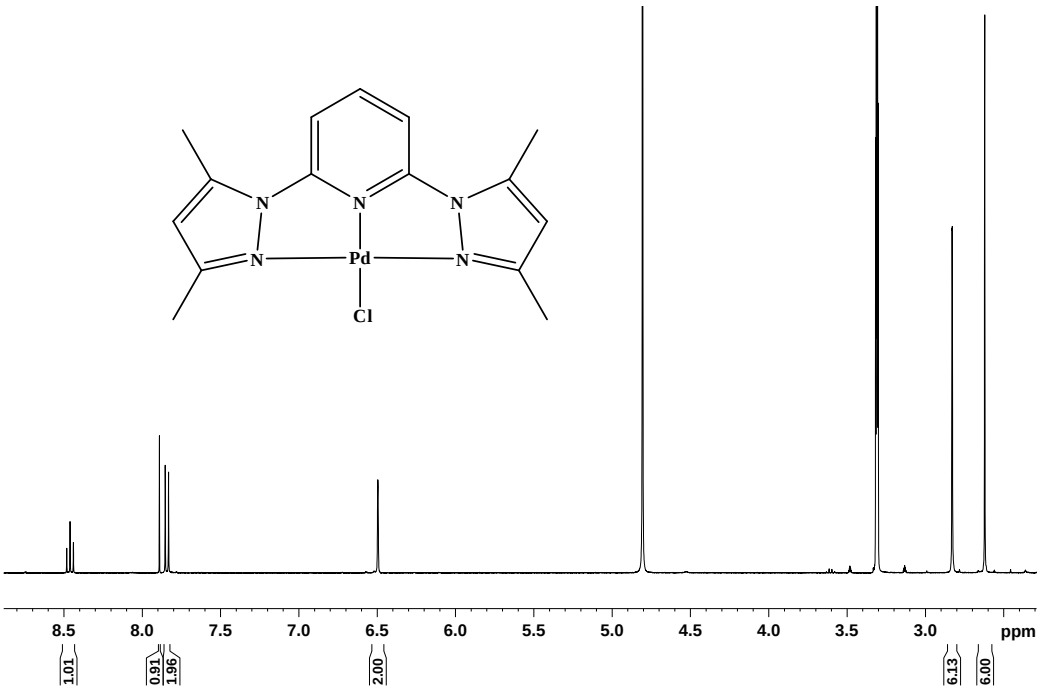

Figure SI 3. 15 ^{1}H NMR spectrum for **PdL3** complex

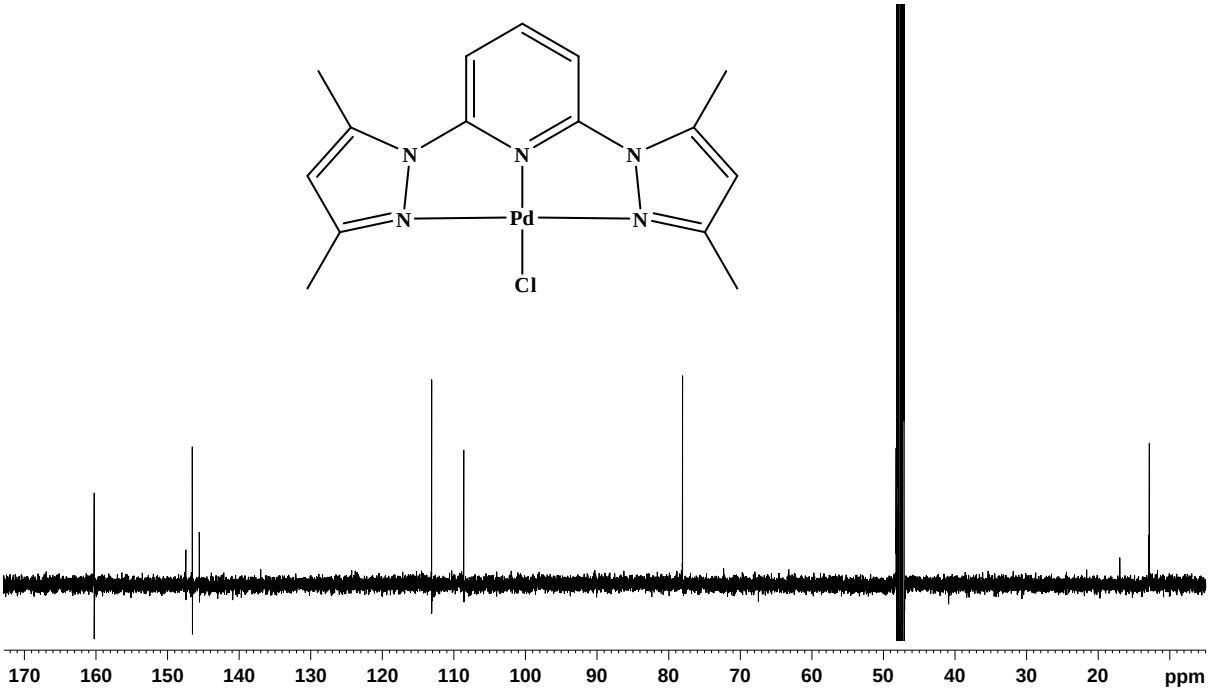

Figure SI 3. 16 ^{13}C NMR spectrum **PdL3** complex

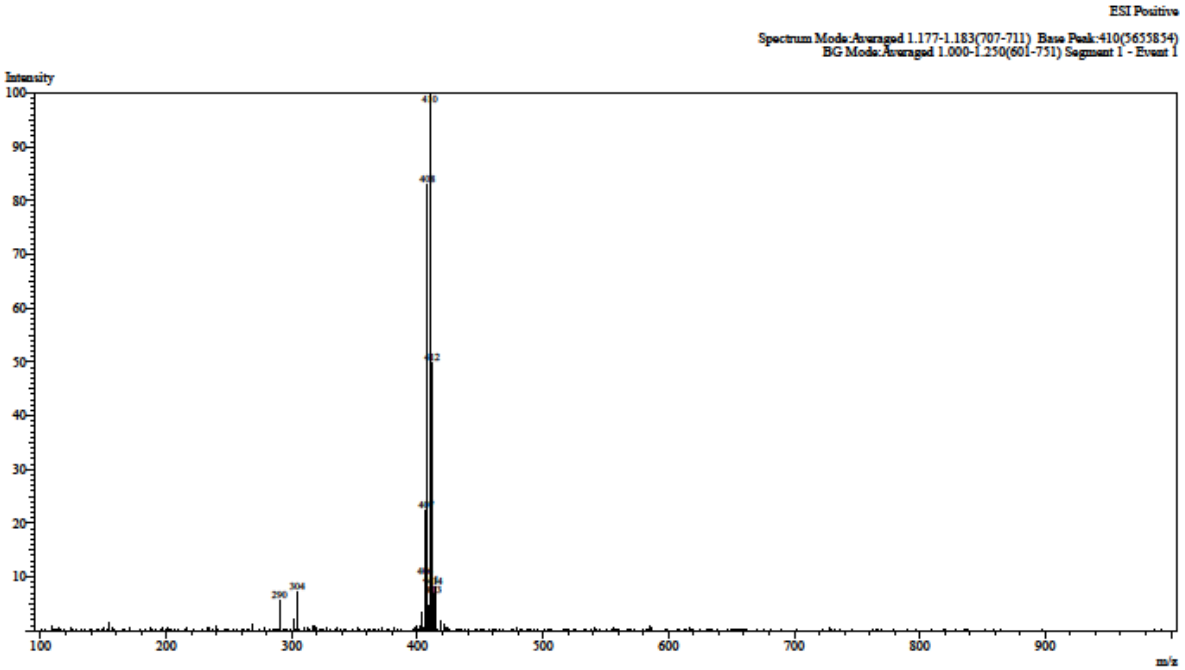

Figure SI 3. 17 LC-MS mass spectrum for **PdL3** complex.

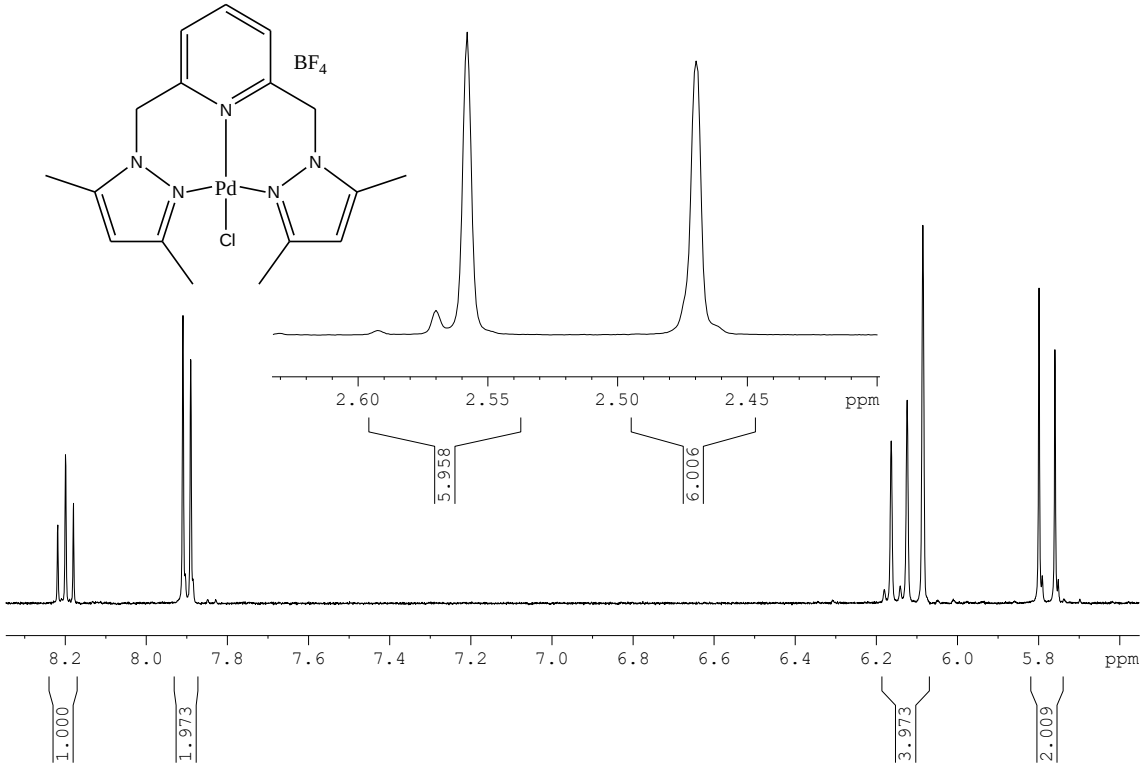

Figure SI 3. 18 ^{1}H NMR spectrum for **PdL4** complex

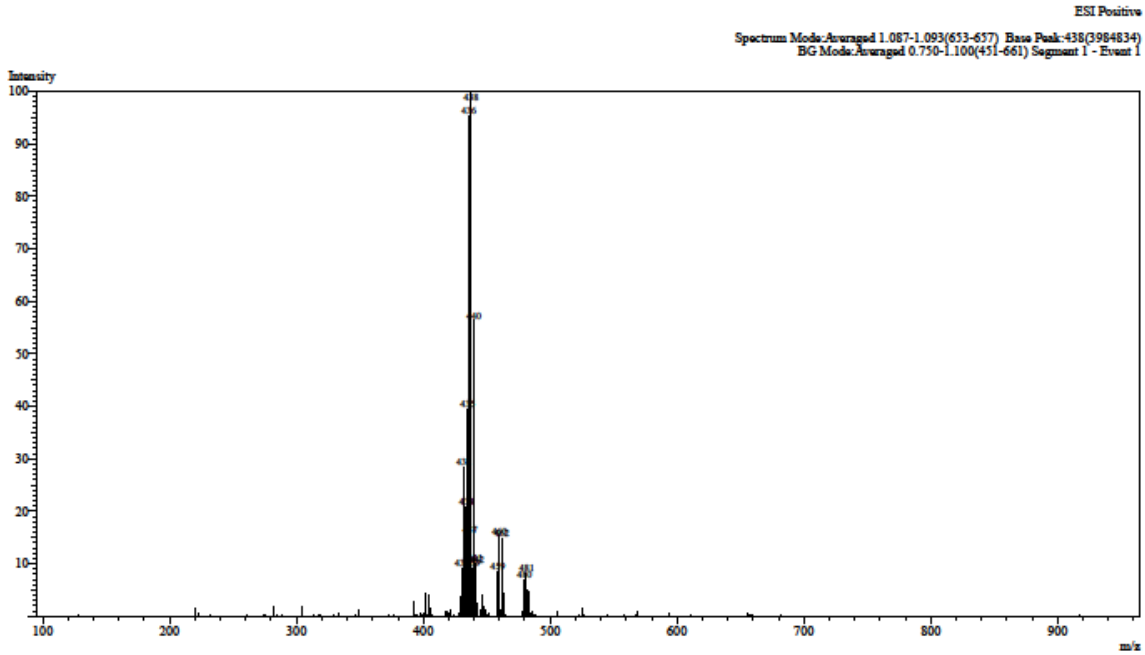

Figure SI 3. 19 LC-MS mass spectra for **PdL4** complex

Table SI 3. 1 Wavelengths (nm) used for monitoring the kinetic reactions of Pd(II) complexes with the nucleophiles

Complex	Nucleophiles	Wavelength, λ (nm)
	Tu	385
PdL1	Dmtu	385
	Tmtu	386
	Tu	380
PdL2	Dmtu	380
	Tmtu	430
	Tu	384
PdL3	Dmtu	390
	Tmtu	435
	Tu	375
PdL4	Dmtu	375
	Tmtu	420

Table SI 3. 2 Average k_{obs}, (s^{-1}) for the reactions of **PdL1** with the nucleophiles in methanol, I= 30 mmol LiCl, T = 293 K for **Tu** and T = 298 K for **Dmtu** and **Tmtu**

	k_{obs} /s^{-1}		
[NU]/M	**Tu***	**Dmtu**	**Tmtu**
0.003	380.3361	128.5068	13.98540
0.006	654.1735	248.1915	27.54009
0.009	957.2714	375.4589	42.07268
0.012	1299.9981	485.4682	55.34254
0.015	1635.43375	605.8242	70.28800

* Tu was done at 293 K

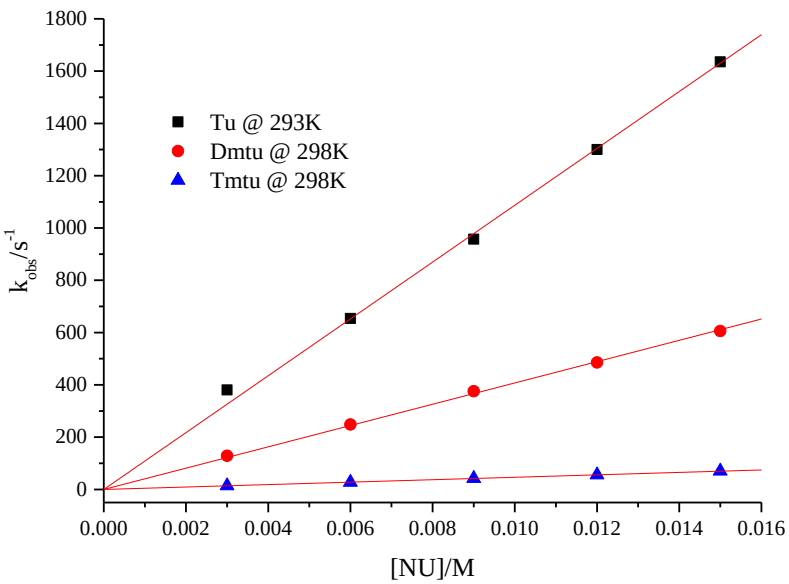

Figure SI 3. 20 The dependence of k_{obs})(s^{-1}) on the nucleophile concentrations for the chloride substitution from **PdL1** in methanol, I= 30 mmol (LiCl), T = 293 K (**Tu**) and T=298 K (**Dmtu** and **Tmtu**)

Table SI 3. 3 Average k_{obs}, (s^{-1}) for the reactions of **PdL2** and the nucleophiles in methanol, I = 30 mmol (LiCl), T = 298 K

	k_{obs} /s^{-1}		
[NU]/M	**Tu**	**Dmtu**	**Tmtu**
0.003	37.6797	15.06665	1.05866
0.006	75.11498	30.39905	2.13978
0.009	112.04	44.9674	2.77405
0.012	150.8426	60.71738	3.67145
0.015	189.135	73.99393	4.36871

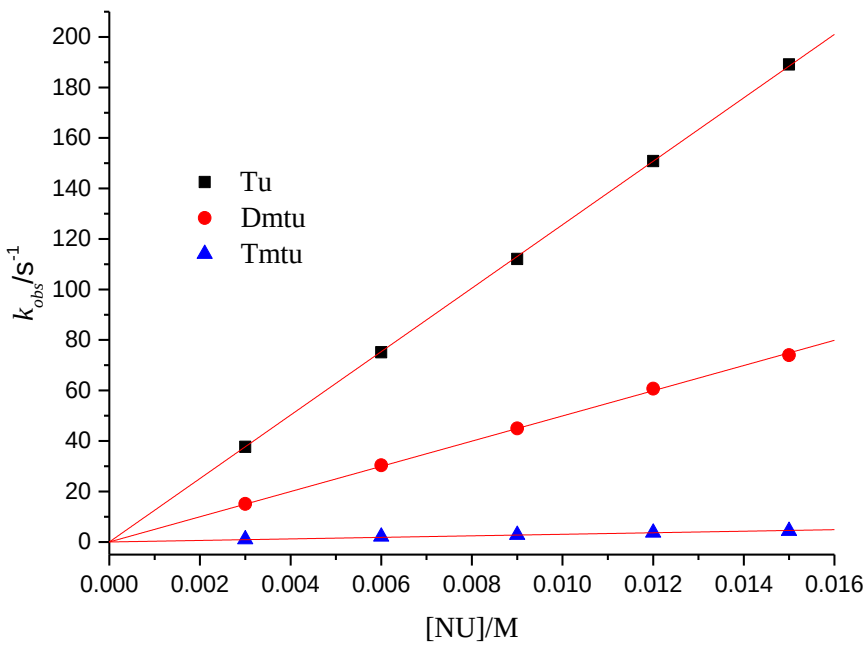

Figure SI 3. 21 The dependence of k_{obs} on the nucleophile concentrations for reactions with **PdL2** in methanol, I = 30 mmol (LiCl), T = 298 K.

Table SI 3. 4 Average k_{obs}, (s^{-1}) for the reactions of **PdL3** with the nucleophiles in methanol, I = 30 mmol (LiCl), T = 298 K

[NU]/M	k_{obs} /s^{-1}		
	Tu	**Dmtu**	**Tmtu**
0.003	29.8715	11.9696	0.38691
0.006	59.4996	25.2052	0.66911
0.009	89.586	38.9918	0.98994
0.012	119.082	52.1357	1.34168
0.015	153.8946	65.2012	1.73086

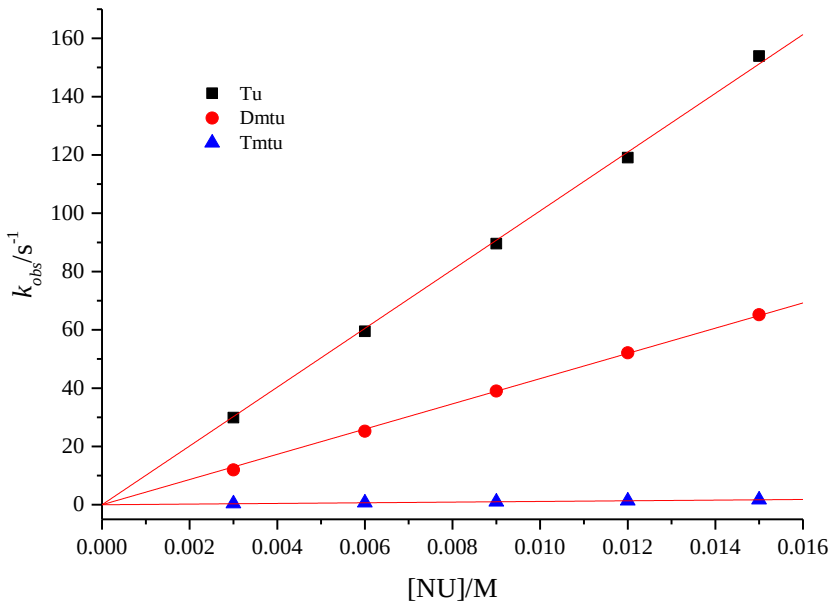

Figure SI 3. 22 Dependence of the *pseudo*-first-order rate constants (k_{obs}) on the concentration of thiourea nucleophiles for chloride substitution on **PdL3** in methanol, 30 mmol LiCl, T = 298 K.

Table SI 3. 5 Average k_{obs}, (s^{-1}) for the reactions of **PdL4** with the nucleophiles in methanol, I = 30 mmol (LiCl), T = 298 K

[NU]/M	k_{obs} /s^{-1}		
	Tu	**Dmtu**	**Tmtu**
0.003	0.00452	0.00161	9.65654E-6
0.006	0.00875	0.00359	1.99800E-5
0.009	0.01324	0.00490	2.98121E-5
0.012	0.01765	0.00676	3.91112E-5
0.015	0.02176	0.00860	4.91153E-5

Table SI 3. 6 Temperature dependence of k_2, M^{-1} s^{-1}, for the reactions of **PdL1** with the nucleophiles at 30-fold excess [metal complex], I = 30 mmol (LiCl).

Tu			ln(k_2/T)	
(1/T) K^{-1}	ln(k_2/T)	(1/T) K^{-1}	**Dmtu**	**Tmtu**
0.00353	5.6032	0.00341	4.8847	2.2858
0.0035	5.6645	0.00336	5.018	2.6555
0.00347	5.7341	0.0033	5.1789	2.9914
0.00344	5.7952	0.00325	5.3086	3.27265
0.00341	5.8631	0.00319	5.4881	3.6033

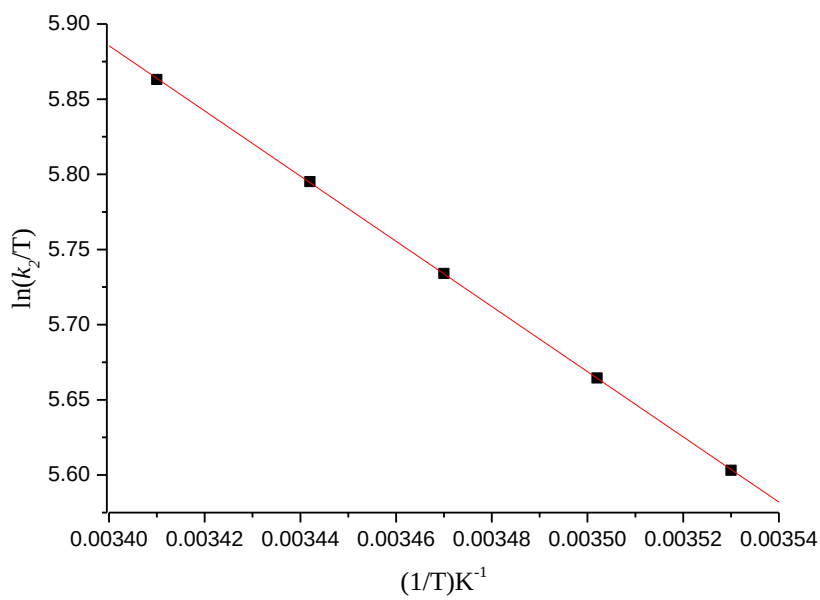

Figure SI 3. 23 Eyring plot of **PdL1** with **Tu** nucleophiles at different temperatures

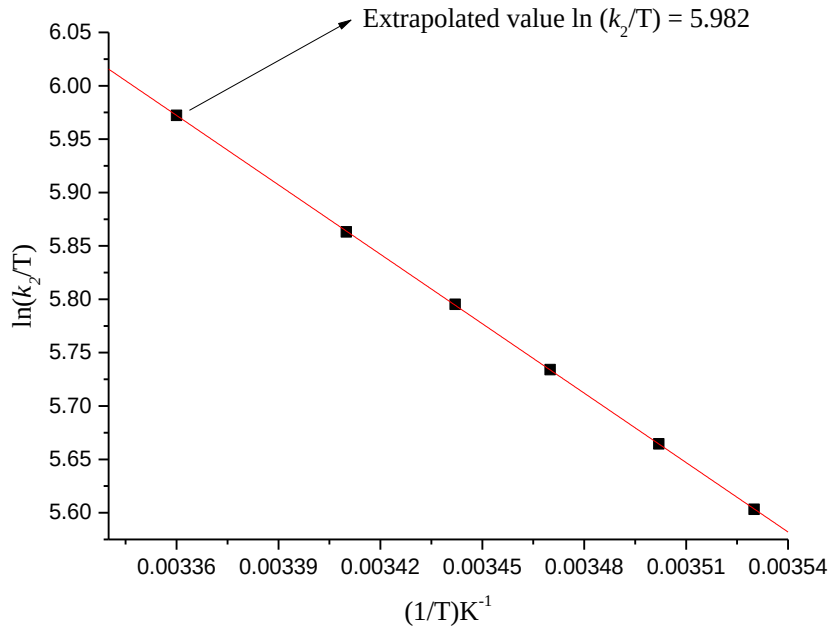

Figure SI 3. 24 Eyring plot of **PdL1** with **Tu** showing how the extrapolated value at 25 ºC arrived at from the linear graph and k_2 was calculated from the value ln(k_2/T) = 5.982

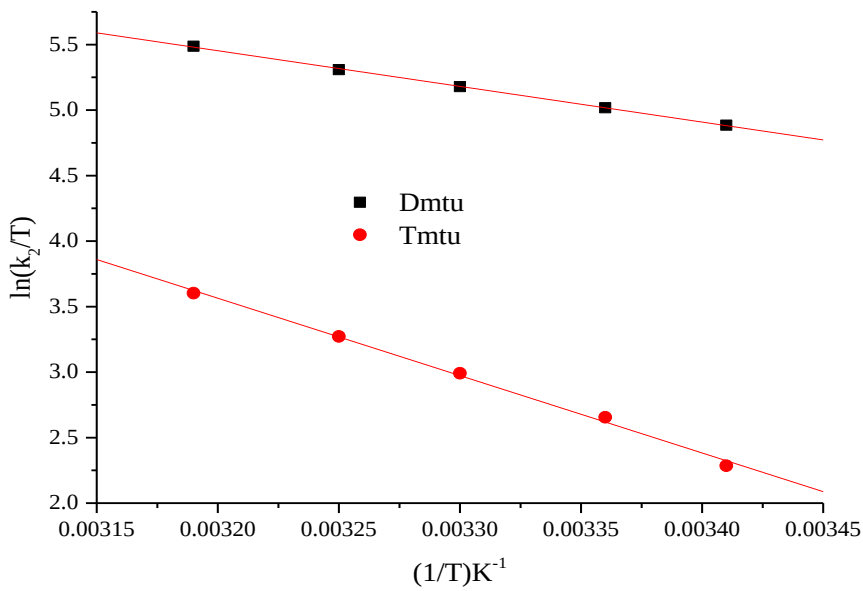

Figure SI 3. 25 Eyring plots of **PdL1** with **Dmtu** and **Tmtu**

Table SI 3. 7 Temperature dependence of k_2, M^{-1} s^{-1}, for the reactions of **PdL2** with the nucleophiles at 30-fold excess [metal complex], I = 30 mmol (LiCl).

(1/T) K^{-1}	ln(k_2/T)		
	Tu	**Dmtu**	**Tmtu**
0.00341	3.58921	2.54753	-4.54019
0.00336	3.73219	2.73346	-4.2952
0.0033	3.91984	2.98412	-4.0228
0.00325	4.05697	3.14599	-3.6648
0.00319	4.23046	3.39886	-3.40072

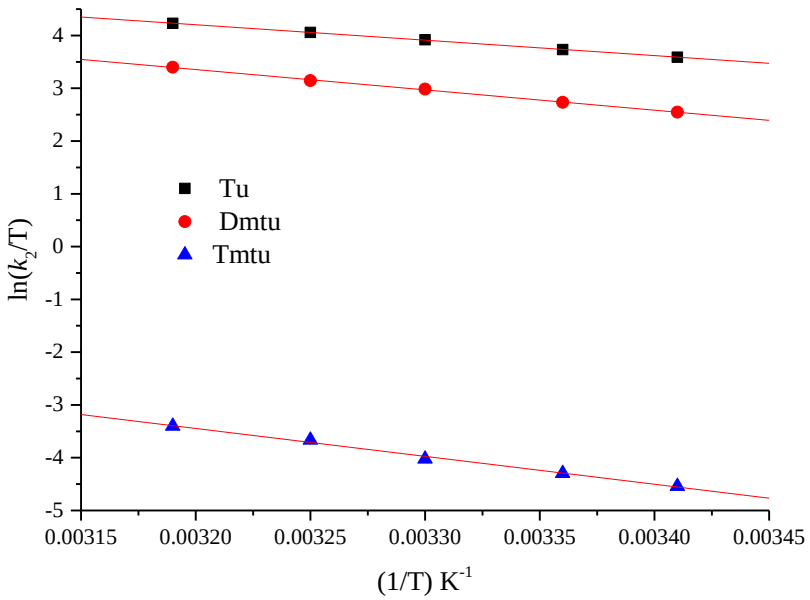

Figure SI 3. 26 Eyring plots of **PdL2** with thiourea nucleophiles at different temperatures

Table SI 3. 8 Temperature dependence of k_2, M^{-1} s^{-1}, for the reactions of **PdL3** with the nucleophiles at 30-fold excess [metal complex], I = 30 mmol (LiCl).

(1/T) K^{-1}	ln(k_2/T)		
	Tu	**Dmtu**	**Tmtu**
0.00341	3.2915	2.6491	-6.56455
0.00336	3.4496	2.8045	-6.16856
0.0033	3.6012	2.9607	-5.67413
0.00325	3.7619	3.1087	-5.32295
0.00319	3.9417	3.2833	-4.89275

Table SI 3. 9 Temperature dependence of k_2, M^{-1} s^{-1}, for the reactions of **PdL4** with the nucleophiles at 30-fold excess [metal complex], I = 30 mmol (LiCl).

(1/T) K^{-1}	ln(k_2/T)		
	Tu	**Dmtu**	**Tmtu**
0.00341	-5.65717	-6.52581	-11.45214
0.00336	-5.31134	-6.3055	-11.0932
0.0033	-4.9457	-5.99044	-10.68476
0.00325	-4.58774	-5.74473	-10.22055
0.00319	-4.29118	-5.51597	-9.86691

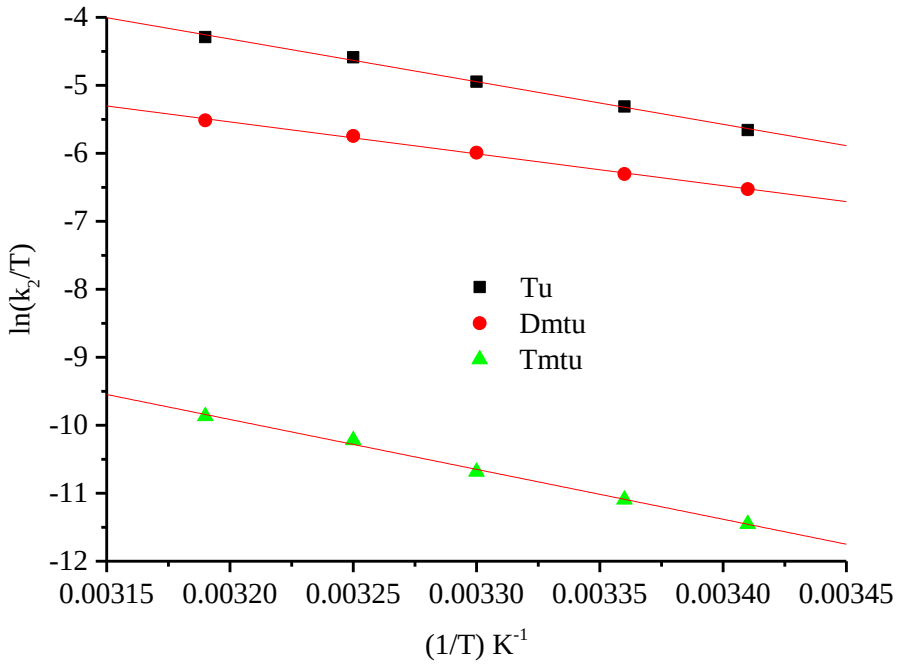

Figure SI 3. 27 Eyring plots for **PdL4** complex with the nucleophiles

CHAPTER 4

The Role of 8-quinolinyl Moieties in Tuning the Reactivity Palladium(II) Complexes: A Kinetic and Mechanistic Study

4.0 Abstract

The rate and mechanism of chloride substitution from Pd(II) complexes, namely: chlorobis-(2-pyridylmethyl)amine)palladium(II), **Pd1**, chloro-8-[(2-pyridylmethyl)amino]quinolinepalladium-(II), **Pd2**, chloro-N-(2-pyridinylmethylene)-8-quinolinamine)palladium(II), **Pd3** and chlorobis(8-quinolinyl)aminepalladium(II), **Pd4** are reported. The labile chloride was substituted from the complexes by thiourea nucleophiles *viz*, thiourea (**Tu**), N,N'-dimethylthiourea (**Dmtu**) and N,N,N',N'-tetramethylthiourea (**Tmtu**). The reactions were monitored under *pseudo*-first-order conditions in methanol using stopped flow spectrophotometry as a function of concentration and temperature. All the substitution reactions obeyed the equation $k_{obs} = k_2$[Nu] following the order **Pd1** > **Pd3** > **Pd2** > **Pd4**. **Pd4** exhibited the slowest rate of substitution due to the stronger σ-donor effect of 8-quinolinyl moiety of the coordinated ligand, which make the Pd metal centre more electron-rich. This slows down the nucleophilic attack by the incoming nucleophiles. The values of the thermodynamic parameters ($\Delta H^{\#}$ and $\Delta S^{\#}$) support an associative substitution mechanism. The trends in the DFT calculated data supports the experimental observed order of the reactivity of the complexes.

Keywords: π-conjugation, electronic effects, quinoline, σ-donation

4.1 Introduction

Substitution reactions of square planar Pd(II) and Pt(II) complexes with tridentate N^N^N ligands have attracted immense attention for over four decades from various investigators.[1-5] The focus has been to tune the reactivity of Pt(II) or Pd(II) complexes with the intention of optimizing it to ensure future complexes with improved antitumor efficacy. Despite a common square planar geometry and similar mechanism of substitution, Pd(II) complexes are 10^2 - 10^5 more reactive than Pt(II) complexes[3, 6-8] leading to lower antitumour activity of the former complexes. As a result, efforts have been made to design new Pd(II) complexes with reactivity that can be compared to those of Pt(II) complexes so as to minimize their deactivation by serum bio-nucleophiles and thus ultimately improving their anti-tumor activity. The approach is to use carefully designed spectator ligands with favourable electronic and steric influences to slow down the intrinsic reactivity of the Pd(II) complexes.[9-12]

The interactions of Pt(II) and Pd(II) complexes with sulfur-based biomolecules is very significant. For example, such interactions led to the discovery of the antitumor activity of *cis*-$[PtCl_2(NH_3)_2]$[13] which can be tracked back to its substitution reaction with nucleophilic biomolecules, and have been used for the treatment of several tumors.[6, 14, 15] However, most Pt(II)-based drugs are acutely toxic and some tumour cells develop resistance to their activity.[16, 17] This has prompted interest into designing alternative complexes of other d^8 metal ions such as Pd(II) with lower toxicity and improved cytotoxicity.[17] One of the ways to achieve this is to use a strongly coordinated N-donor and sterically hindered ligands.[10, 11] This ensures stable Pd(II) drugs towards deactivation by biological nucleophiles and thus is able to reach the targeted DNA for their therapeutic action. Given the significant similarity in the coordination chemistry of Pd(II) and Pt(II) complexes, the design of Pd antitumour drugs have followed the same procedures used in developing Pt antitumor drugs.[17] Thus the first step towards tuning the

antitumour activity of the Pd(II) complexes is to have a good understanding of the critical factors that influence their reactivity.[18]

The rate of the substitution of the leaving chloride or aqua ligand of Pt(II) complexes has been shown to be influenced by π/σ-donor and π-acceptor of the spectator ligands.[6, 19-26] For instance, a σ-donating ligand which is coordinated *trans* to the leaving group increases the rate of substitution through its *trans*-influence[25, 27, 28] on the ground state properties of the complex. Strong *cis*- and /or *trans*- π-acceptor ligands, especially those with extended aromatic rings, withdraw electrons from the metal centre through π-backbonding as well as π-resonance thereby stabilizing the transition state. [20, 21] As a result, the rate of substitution of the coligand is increased. Moreover, it has been reported that the *trans* π-acceptability is weaker than the *cis* π-acceptability while for polypyridyl and related tridentate ligands, the π-acceptability exhibits a multiplicative affect when the ligand is a conjugated system.[20, 21, 24, 29] However, if the ligand is *cis* coordinated and a strong π/σ-donor, the rate of substitution is decelerated due to increased electron density donated around the metal centre which repels the incoming nucleophiles.[25, 27] This is known as the *cis*-effect.[20, 24, 25] However, ligands with both *cis*-π-acceptor and σ-donating properties can potentially accelerate or decelerate depending on whichever has a dominant control on the reactivity since the former increases while the latter decreases the reactivity of the metal centre.

Non-antitumor active monofunctional coordination compounds of chloro and aqua Pd(II) and Pt(II) complexes of the N^N^N tridentate ligands such as 2,2':6',2"-terpyridine (terpy), bis(2-pyridylmethyl)amine (bpma), and diethylenetriamine (dien) [8, 20, 23, 30-34] have provided useful model substrates for studying the kinetics and mechanisms of ligand exchange reactions of square-planar complexes.[30] For example, it was shown that the reactivity of these complexes

could reduce by a factor of upto 5 orders of magnitude going from terpy spectator ligand to dien system. This was because of stepwise reduction of π-back bonding by replacing pyridine donor groups by amine ligands hence reducing electrophilicity of the metal center in that order. Moreover, a systematic increase in the π-conjugation around the metal center of terpy framework results in either increase or decrease in the rate of substitution depending on the relative position of the π-extension. The acceleration of the reactivity is due to increase in π-back bonding character caused by the favorable overlap of the dπ-orbitals of the metal and the ligands' π*-orbitals [20, 22, 24, 35] while the dampening of reactivity is as a result of net σ-donor effect on the metal center.[18, 22, 36]

Given that any slight structural modification of polypyridyl spectator ligands can produce significant changes on the reactivity of Pd(II) complexes,[37-39] derivatives of non-leaving ligands such as bpma can have their lateral pyridines replaced with strong σ-donor quinolinyl rings. This can then be used to slow down the high reactivity of the Pd(II) complexes which is necessary to their antitumour activity.

The rate of substitution from Pt(II) complexes with quinolinyl moiety have been reported to be lower than that from analogous complexes with terpyridyl moiety.[18, 22, 36, 40] However, there is no similar literature on kinetic and mechanistic data aimed at controlling the reactivity of Pd(II) complexes particularly with quinolinyl moieties. With this in mind the rate and mechanism of substitution from Pd(II) complexes with benzopyridine spectator ligands shown in Figure 4.1 was investigated. **Pd1,** an analogue with a pyridine moiety was included for comparative purpose so as unravel the distinctive role of quinolinyl moiety in the ligand framework on reactivity. The substitution reactions were studied using bio-relevant thiourea nucleophiles having varied steric

influences. The density function theory (DFT) calculations were performed to provide an insight into the observed reactivity trends of the complexes.

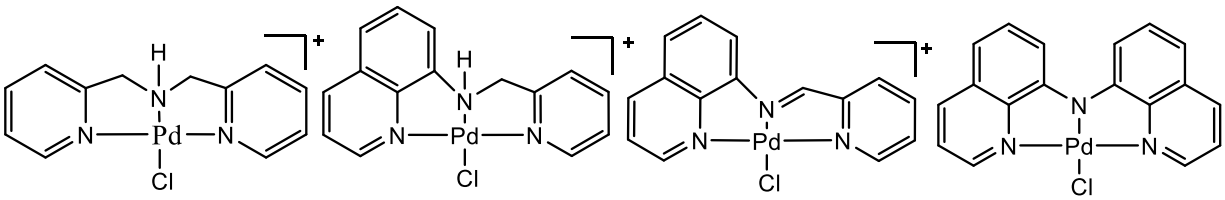

Pd1 **Pd2** **Pd3** **Pd4**

Figure 4. 1 Structures of the Pd(II) complexes under study (where necessary, counter ions omitted for clarity)

4.2 Experimental Section

4.2.1 Materials and Methods

All Syntheses were done under nitrogen atmosphere. *RAC*-2,2'-bis(diphenylphosphino)-1,10-binaphthyl (97 %), 8-aminoquinoline (98 %), 8-bromoquinoline (98 %), NaO^tBu (97 %), 2-picolylchloride hydrochloride (98 %), pyridine-2-carboxyaldehyde (99 %), Tris(dibenzylideneacetone)dipalladium(0) (97 %), lithium perchlorate (98 %), Potassium tetrachloropalladate (K_2PdCl_4 99.99 %), Dichloro-1,5-cyclooctadiene palladium(II) ($Pd(COD)Cl_2$, 99%), thiourea nucleophiles, and the ligand, di-(2-picolyl)amine were all purchased from Aldrich and used as received. Solvents were distilled before use and dried through standard procedures.[41]

4.2.2 Synthesis of Ligands

The ligands 8-[(2-pyridylmethyl)amino]quinoline and Bis(8-quinolinyl)amine (BQA) were synthesized according to the standard published methods.[42, 43]

8-[(2-pyridylmethyl)amino]quinoline

To a stirring solution of 2-picolylchloride hydrochloride (820 mg, 5 mmol) in water (15 mL) was added aqueous solution (4 mL) of sodium hydroxide (0.01 M) dropwise. Ten minutes later, ethanolic solution (10 mL) of 8-aminoquinoline (288 mg, 2 mmol) was added in portions. To the

reaction mixture, 0.01 M aqueous solution of sodium hydroxide (6 mL) was added dropwise under nitrogen and the mixture left to stir for 5 days at room temperature. The crude product was then extracted with chloroform (3 × 25 mL) and the organic extracts were combined and dried over sodium sulfate. The solvent was removed under reduced pressure to obtain a brown oily gum which was purified by short column chromatography on silica gel using a 4:1 hexane/ethyl acetate. A pure brownish-yellow oil was concentrated from a second elution fraction. Yield (161.0 mg, 34.3 %) ^{1}H NMR ($CDCl_3$, 400 MHz, ppm): δ = 8.78 (td, 1H), 8.63 (d, 2H), 8.09 (ddd, 1H), 7.63 (td, 1H), 7.44-7.30 (m, 2H), 7.18 (dd, 1H), 7.08 (dd, 1H), 6.62 (d, 1H), 4.74 (s, 2H). ^{13}C NMR ($CDCl_3$, 100 MHz): δ /ppm = 159.3, 149.3, 147.6, 136.7, 136.3, 127.7, 127.4, 122.0, 121.4, 121.3, 116.3, 114.5, 110.2, 105.6, 49.3. MS ESI$^+$, *m/z* = $[M + H]^+$ = 236.

Bis(8-quinolinyl)amine (BQA)

Tris(dibenzylideneacetone)dipalladium(0) (22 mg, 0.024 mmol), RAC-2,2'-bis(diphenyl-phosphino)-1,10-binaphthyl (29.87 mg, 0.048 mmol) and dry toluene (10 mL) were added into a two-necked round bottomed flask under inert flow of nitrogen. After allowing the reactants to stir for 5 minutes, 8-bromoquinoline (0.16 mL, 1.2 mmol), 8-aminoquinoline (0.1737 g, 1.2 mmol) and additional dry toluene (20 mL) were added. Subsequently, NaO^{t}Bu (0.1387 g, 1.44 mmol) was added, resulting into a red solution. The reaction mixture was further stirred vigorously for 3 days at 110 ºC. The solution was then allowed to cool to room temperature, filtered through a silica plug and extracted with dichloromethane to ensure complete removal of the desired product. Removal of the solvent under reduced pressure yielded a crude red solid. The solid was purified on a short column of silica gel using 4:1 toluene/ethyl acetate as an eluent. An orange solid was formed upon evaporation of the solvent. Yield: (293 mg, 89.9 %) ^{1}H NMR ($CDCl_3$, 400 MHz, ppm): δ = 10.64 (s, 2H), 8.97 (dd, 2H), 8.23(ddd, 2H), 8.17 (dd, 2H), 7.90 (d, 2H), 7.54-7.46 (m, 4H), 7.34 (d, 2H). ^{13}C NMR ($CDCl_3$, 100 MHz, ppm): δ = 147.96, 139.73,

138.81, 136.93, 129.3, 127.49, 121.70, 118.28, 111.12. *Anal. Calcd. for* $C_{18}H_{13}N_3$: C, 79.68; H, 4.83; N, 15.49. *Found:* C, 79.87; H, 4.83; N, 15.21. MS ESI^+, *m/z* = $[M + H]^+$ = 272.

4.2.3 Synthesis of Palladium(II) Complexes

The precursor, *trans*-dichlorobis(dimethylsulfide)palladium(II), [44] **Pd1**,[45] **Pd2**,[40] **Pd3**[46, 47] and **Pd4**[43] complexes were all synthesized according to literature procedures.

***Trans*-dichlorobis(dimethylsulfide)palladium(II)**

In a three-necked round-bottomed flask K_2PdCl_4 (1279.2 mg, 4.12mmol) was stirred in 100 mL of water until complete dissolution. To the stirring solution dimethyl sulphide (2.25 mL, 0.0615 mol) was added under nitrogen. A pink/yellow precipitate formed immediately. The mixture was refluxed for 1 hour during which time all the precipitate dissolved. Microcrystalline orange crystals were formed upon cooling the solution to room temperature and were collected by filtration, washed with cold water and dried under vacuo. NMR analysis confirmed the formation of the complex. Yield (819.8 mg, 66.0 %). ^{1}H NMR ($CDCl_3$, 400MHz) δ /ppm = 2.40 (s, SMe_2) ^{13}C NMR ($CDCl_3$, 100 MHz, ppm) δ = 22.77 (s, SMe_2). This complex was used as a precursor for the synthesis of **Pd2** and **Pd3** complexes.

Chlorobis(2-pyridylmethyl)aminepalladium(II), Pd1

To a solution of $Pd(COD)Cl_2$ (156.7 mg, 0.48 mmol) in methanol (20 mL), di-(2-picolyl)amine (0.1 mL) was added and refluxed at 50 ºC for 1 day. The solution mixture was then filtered and the filtrate evaporated to dryness under reduced pressure to give a yellow solid which was washed with tetrahydrofuran (THF), diethyl ether and dried under vacuum yielding a yellow powder solid. Yield: (165.30 mg, 86.3 %). ^{1}H NMR (DMSO-d_6, 400 MHz, ppm): δ = 8.82 (dd, 2H), 8.60 (br s, 1H), 8.23(ddd, 2H), 7.76 (d, 2H), 7.63 (t, 2H), 4.92(m, 2H), 4.51 (dd, 2H). ^{13}C NMR (DMSO-d_6, 400 MHz, ppm): δ = 167.4, 149.4, 141.4, 125.7, 123.4, 59.4. *Anal. Calcd. for*

$C_{12}H_{13}N_3PdCl_2.1.25H_2O$: C, 36.11; H, 3.91; N, 10.53. *Found:* C, 36.51; H, 3.80; N, 10.16. TOF MS ESI$^+$, *m/z* = [M – Cl]$^+$ = 342.0280.

Chloro-8-[(2-pyridylmethyl)amino]quinolinepalladium(II), Pd2

A solution of 8-[(2-pyridylmethyl)amino]quinoline (155.0 mg, 0.66 mmol) in methanol (5 mL) was added to a refluxing solution of *trans*-[$PdCl_2(SMe_2)_2$] (199.05 mg, 0.66 mmol) in methanol (15 mL) and allowed to reflux for 12 h. The solution was cooled to room temperature, evaporated to dryness under reduced pressure and washed with acetonitrile, chloroform, diethyl ether and dried under vacuum. Yield: (109.4 mg, 40.2 %). ^{1}H NMR (400 MHz, DMSO-d_6, ppm,): δ = 9.66 (s, 1H), 8.98(d, 1H), 8.76 (dd, 1H), 8.65 (dd, 1H), 8.41 (td, 1H), 8.29 (ddd, 1H), 8.04–7.95 (m, 1H), 7.91 (m, 1H), 7.78 (m, 2H), 7.69 (m, 1H), 7.63 (m, 2H). ^{13}C NMR (DMSO-d_6, 100 MHz, ppm): δ = 159.8, 148.7, 147.6, 135.7, 135.3, 128.7, 128.4, 125.0, 122.4, 121.7, 115.3, 113.5, 109.2, 106.6, 51.1. *Anal. Calcd.* for $C_{15}H_{13}N_3PdCl_2$: C, 43.66; H, 3.18; N, 10.18. *Found:* C, 43.77; H, 3.35; N 9.79. TOF MS ES$^+$, *m/z* = [M – Cl]$^+$ = 375.9905.

Chloro-N-(2-pyridinylmethylene)-8-quinolinamine)palladium(II), Pd3

A suspension of *trans*-$PdCl_2(SMe_2)_2$ (171.9 mg, 0.57 mmol) in methanol (20 mL) was heated to 50 ºC until the complex was completely dissolved. To the solution, a mixture of 8-aminoquinoline (0.082 g, 0.57 mmol) and pyridine-2-carboxyaldehyde (0.05 mL, 0.57 mmol) in methanol (10 mL) was added dropwise. The resulting solution was stirred at room temperature for 3 h and excess lithium perchlorate (0.35 g, 2.85 mmol) added. A brown solid precipitated from the solution and the reaction mixture was then kept at -10 ºC for 1 hour. The precipitated product was filtered off, washed with methanol, ethanol and diethyl ether. Yield: (240.9 mg, 89.1 %). ^{1}H NMR (400 MHz, DMSO-d_6, ppm): δ = 9.62(s, 1H), 8.94 (dd, 1H), 8.76 (d, 1H), 8.71 (dd, 1H), 8.61 (d, 1H), 8.45 (td, 1H), 8.19 (dd, 1H), 7.99 (d, 1H), 7.62 (ddd, 1H), 7.50 (t, 1H), 7.42 (d, 1H). ^{13}C NMR (100 MHz, DMSO-d_6, ppm): δ = 166.9, 156.9, 149.0, 150.8, 149.6, 148.8,

147.5, 144.5, 141.4, 140.1, 129.6, 129.1, 126.8, 122.9, 122.1, 120.3. *Anal. Calcd. for* $C_{15}H_{11}N_3PdCl_2O_4$: C, 37.96; H, 2.34; N 8.85. *Found:* C, 38.28; H, 2.41; N, 9.19. TOF MS ES^+, *m/z* = $[M – ClO_4]^+$ = 375.9718.

Chlorobis(8-quinolinyl)amine)palladium(II), Pd4

To a reaction flask containing $(COD)PdCl_2$ (85.37 mg, 0.3 mmol) dissolved in THF (20 mL) was added a THF solution of 8-[(2-pyridylmethyl)amino]quinoline **(**81 mg, 0.3 mmol) and triethylamine (70 µL, 0.5 mmol). The vessel was sealed and heated at 95 °C for 48 h. Thereafter the mixture was cooled to room temperature and the excess solvent removed in vacuo, affording a red solid. The solid was dissolved in CH_2Cl_2 (50 mL), filtered through Celite on a sintered-glass frit, and washed with dilute brine solution (3 x 20 mL). The volume was reduced in vacuo, and the product precipitated from the solution using hexane. The resulting red microcrystalline solid was washed with petroleum ether (3x15 mL) and dried to afford spectroscopically pure product. Yield: (78.5 mg, 63.6 %). ^1H NMR (400 MHz, $CDCl_3$, ppm): δ = 8.99 (d, 2H), 8.22 (d, 2H), 7.67 (d, 2H), 7.49 (m, 2H), 7.40 (m, 2H), 7.09 (d, 2H). ^{13}C NMR (400 MHz, $CDCl_3$, ppm): δ = 149.70, 149.14, 148.55, 138.97, 131.48, 129.6, 121.48, 115.24, 112.56. *Anal. Calcd. for* $C_{18}H_{12}N_3PdCl$: C, 52.45; H, 2.93; N, 10.19. *Found*: C, 52.17; H, 2.92; N, 9.85. TOF MS ES^+, *m/z* = $[2M+Na]^+$ = 846.9298.

4.2.4 Physical Measurements and Instrumentation

NMR spectra were acquired using either Bruker Avance DPX 400 NMR or DPX 500 with a 5 mm BBOZ probe at 30 ºC. mass spectra data was recorded on Shimadzu LC-MS 2020 or on a Waters TOF Micro-mass LCT Premier mass spectrometer with electrospray ionization source operated on the positive ion mode. A selection of NMR and mass spectra data for the synthesized ligands and complexes shown in Figures SI 4.1– 3.15, Supporting Information (ESI‡). The purity of the compounds was confirmed by elemental analysis using Carlo Erba Elemental Analyzer

1106. Cary 100 Bio UV–visible spectrophotometer was used to determine a suitable wavelength for monitoring the substitution reaction. An Applied Photophysics SX 20 stopped-flow reaction analyzer coupled to an online data acquisition system was used to measure observed rate constant of the substitution reactions as a function of concentration and temperature. The instrument was thermo-controlled within ± 0.1 °C.

4.2.5 Preparations of Kinetic Solutions

Palladium(II) complex solutions whose concentration was 2.0 x 10^{-4} M were prepared in 4 % DMF to enhance solubility and topped up with 96 % methanolic solvent system containing 20 mM LiCl.[48] Nucleophiles solutions were freshly prepared just before use by dissolving a measured quantity in 20 mM LiCl methanolic solution. LiCl was used to suppress possibility of any solvolysis.[49, 50] The stock solution of the nucleophiles approximately 50-fold excess of the concentration of the complex was serially diluted with the methanolic solution to afford 40- 30- 20- and 10-fold in excess of the complex concentrations to maintain *pseudo*-first-order conditions.

4.2.6 Kinetic Analysis

To determine the wavelength at which the kinetic measurements would be monitored, the reaction between the solutions of the complexes and the nucleophiles were followed spectrophotometrically by recording the spectral changes over a range of wavelengths between 800 nm – 200 nm. All reactions were initiated by mixing equal volumes of ligand and complex solutions directly in the stopped-flow instrument. The rate of the chloride substitution from the complexes by the entering nucleophiles were monitored as a function of concentration at 298 K. To determine activation parameters $\Delta H^{\neq}$ and $\Delta S^{\neq}$, the rates of substitution reactions were measured within a range of 20 °C to 40 °C with 5 °C intervals for all the substitution reactions.

All the *pseudo*-first-order rate observed, k_{obs}, were average values computed from 4 – 8 independent runs.

4.2.7 Computational Modelling

To understand how the structural and electronic factors affect the kinetics of the substitution reactions. Ground state electronic structures of the complexes were optimized using the density functional theory (DFT). The DFT calculations were performed with the Gaussian 09 program suite[51] using the B3LYP (Becke 3-Lee-Yang-Parr) functional method, utilizing LANL2DZ (Los Alamos National Laboratory 2 Double ζ)[52] as the basis set. The influence caused by the bulk solvent was evaluated *via* single-point computations using the C-PCM (conductor-like polarizable continuum model) [53, 54] in methanol solvent. All the complexes were modelled at a charge of +1 except **Pd4** complex which was done at 0 charge in accordance to its neutrality [43, 55] and singlet state. Global electrophilicity index (ω) of the complexes were calculated using literature methods.[18, 56, 57]

4.3 Results

4.3.1 Computational Analysis

DFT calculations were performed to gain more insights into structural and electronic factors influencing the reactivity of the modelled Pd(II) complexes. The geometry of the optimized molecular frontier orbitals and the planarity structures for the complexes are presented in Table 4.1, while the geometric data extracted from the DFT calculations are presented in Table 4.2.

The DFT optimised structures reveal that the HOMO orbital of **Pd1** are contributed by the orbitals of ligand's *trans*-nitrogen, Pd and chloride atoms while those of **Pd2** are mostly centred on the Pd and chloride atoms as well as on the quinoline moiety. However, for **Pd3** and **Pd4**, the HOMOs are entirely distributed in the whole complex. The LUMOs of all the complexes are mainly centred on the ligand's aromatic rings with small contribution from the Pd atom's d-

orbitals. In addition, the planarity of the complexes also increases with increasing π-conjugation compares well with their analogous Pt(II) complexes.[40]

Table 4. 1 The DFT optimized HOMO, LUMO frontier molecular orbitals and the planarity structures of the complexes at B3LYP/LANL2DZ theory level (Iso value = 0.02).

Complex structure	HOMO	LUMO	Planarity
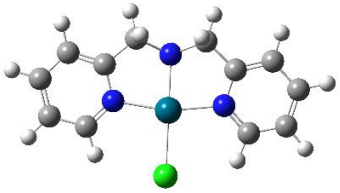 **Pd1**	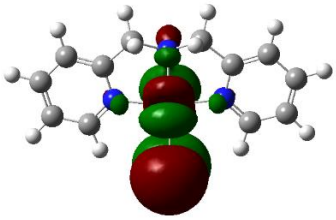	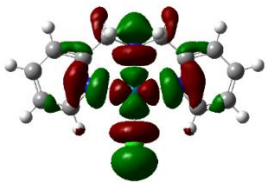	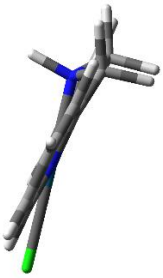
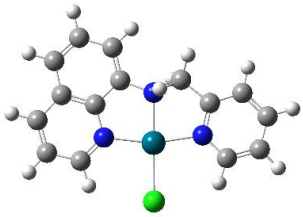 **Pd2**	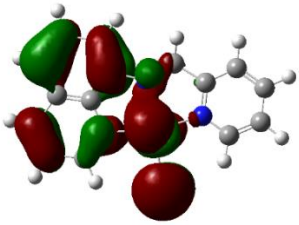	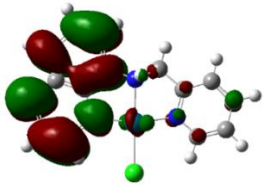	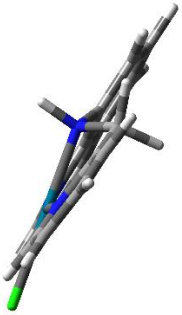
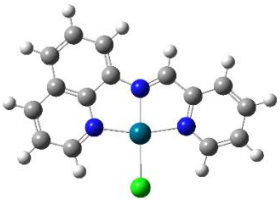 **Pd3**	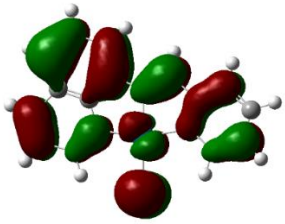	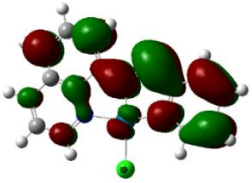	
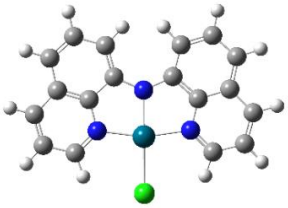 **Pd4**	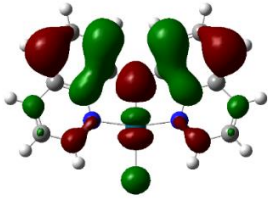	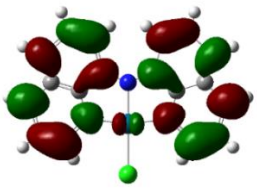	

Table 4. 2 Calculated parameters for the Pd(II) complexes

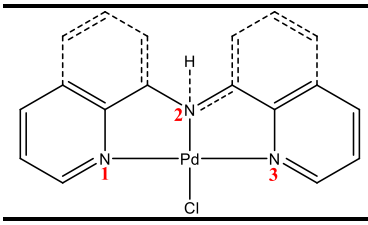

Property	Pd1	Pd2	Pd3	Pd4
NBO Charges				
Pd	0.555	0.563	0.577	0.509
N2	-0.632	-0.649	-0.437	-0.570
Cl	-0.518	-0.510	-0.508	-0.566
Electrophilicity index (ω)	6.077	5.696	8.902	4.764
Bond lengths (Å)				
N1 – Pd	2.050	2.045	2.046	2.038
N2 – Pd	2.059	2.070	2.006	2.003
N3 – Pd	2.050	2.049	2.060	2.039
Pd – Cl	2.415	2.411	2.405	2.449
Bond angles (º)				
N2 – Pd – Cl	179.77	179.28	179.58	179.98
N1 – Pd – N3	165.60	165.49	163.57	165.17
HOMO-LUMO Energy (eV)				
LUMO (eV)	-2.984	-2.809	-3.782	-2.276
HOMO (eV)	-7.545	-7.251	-7.120	-5.241
$\Delta E_{LUMO-HOMO}$ (eV)	4.561	4.442	3.338	2.965
Dipole moment (D)	13.640	12.452	12.789	7.019

The data from Table 4.2 shows that the complexes adopts a slightly distorted square planar geometry with N2 – Pd – N3 deviating from 180º by 14.4º – 15.5º. The HOMO-LUMO energy gap decreases in the order **Pd1 > Pd2 > Pd3 > Pd4** which is in accordance with their increasing

π-conjugation. On stepwise extension of the π-conjugation, the energy levels of the HOMO orbitals are successively raised. This suggests that the σ-donation of electron density towards the Pd(II) metal centres[28] subsequently increases in the same order.

4.3.2 Kinetic Measurements

The chloride substitution reactions of the Pd(II) complexes with the nucleophiles was investigated as a function of nucleophile concentration and temperature. The reactions were monitored using stopped flow techniques with a specified wavelength that had been predetermined from the UV-visible spectra of the reaction between the complex and the nucleophile. The wavelengths used for the substitution reactions ranged between 320 nm to 396 nm depending on the respective complexes and the nucleophiles used as shown in Table SI 4.1, supporting information (ESI‡). A representative stopped-flow kinetic trace for **Pd3** and **Dmtu** is shown in Figure 4.2.

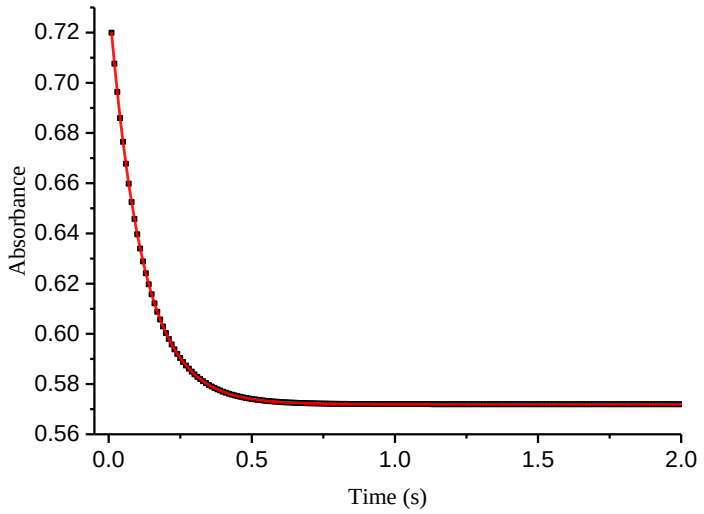

Figure 4. 2 Stopped-flow kinetic trace at 330 nm for the reaction of **Pd3** (2.0×10^{-4} M) with **Dmtu** (4.0×10^{-3} M) solutions in methanol at 298 K.

All the kinetic traces from the stopped flow were of excellent fit to a single-exponential decay function suggesting that all the substitution reactions were first-order in both the thiourea

nucleophiles and Pd(II) complexes. The observed *pseudo*-first-order rate constant, k_{obs}, was generated from the plots. The second-order rate constants, k_2, for the reactions was obtained from the gradient of a plot of k_{obs} versus nucleophile concentration using OriginPro 9.1® software.[58] Straight line plots with zero intercepts were obtained which indicated that the reverse or solvotic pathway was absent or insignificant. A representative plot of k_{obs} versus concentration of the nucleophiles of **Pd1** is shown in Figure 4.3, other similar plots are shown in Figures SI 4.16 – 4.18 while the values of k_{obs} with their respective nucleophile concentrations are tabulated in Tables SI 4.2 – 4.5 in the supporting information (ESI‡). From these results, it can be stated that the *pseudo*-first-order rate constant, k_{obs}, is related to the nucleophile concentration by the *Equation 1*, where the entering thiourea nucleophiles irreversibly displace the leaving chloride ligand from the metal complexes.

$$k_{obs} = k_2 [Nu] \tag{1}$$

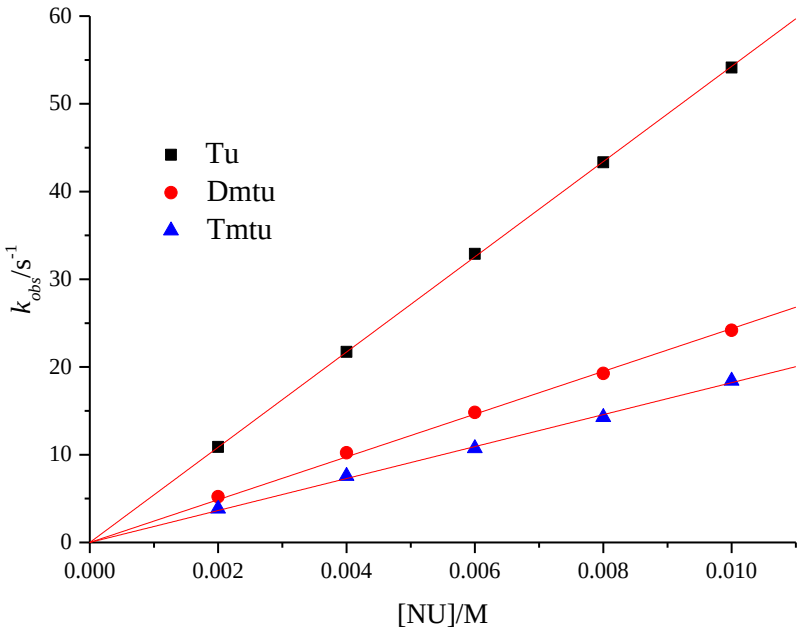

Figure 4. 3 The dependence of k_{obs} on the nucleophile concentrations for the chloride substitution from **Pd1** at T = 298 K.

The values of the second order rate constants, k_2, obtained from the reactions of the complexes are presented in Table 4.3. Based on the results, the reaction mechanism can therefore be proposed as illustrated in scheme 4.1.

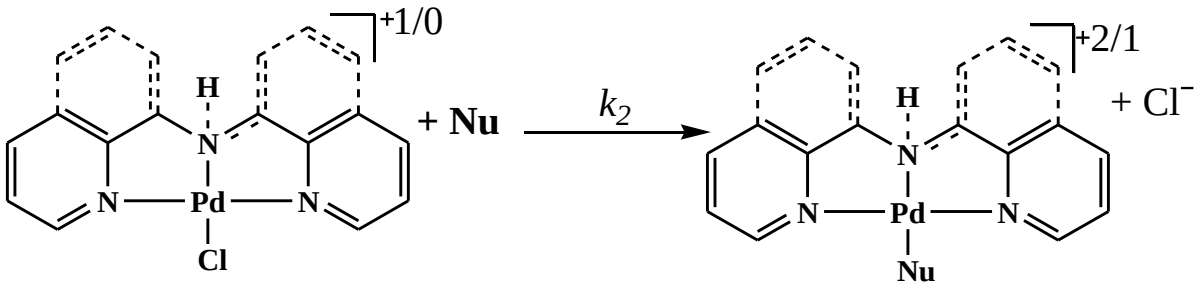

Scheme 4. 1 Proposed reaction mechanism

Table 4. 3 k_2 values and thermodynamic parameter data for the reactions of Pd(II) complexes with thiourea ligands in methanol, I = 20 mM, LiCl.

Complexes	Nucleo-philes	k_2 (M^{-1} s^{-1})	$\Delta H^{\neq}$ (kJ mol^{-1})	$\Delta S^{\neq}$ ($JK^{-1}mol^{-1}$)
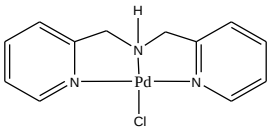 **Pd1**	**Tu**	5427 ± 13	31 ± 1	-70 ± 2
	Dmtu	2438 ± 23	41 ± 1	-43 ± 2
	Tmtu	1822 ± 18	40 ± 1	-43 ± 5
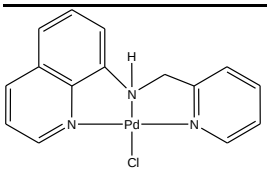 **Pd2**	**Tu**	730 ±12	36 ± 2	-69 ± 7
	Dmtu	473 ± 13	43 ± 2	-49 ± 7
	Tmtu	332 ± 3	50 ± 2	-28 ± 6
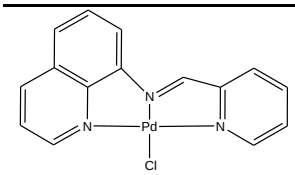 **Pd3**	**Tu**	849 ± 6	45 ± 2	-52 ± 5
	Dmtu	532 ± 9	48 ± 2	-46 ± 6
	Tmtu	351 ± 4	38 ± 1	-93 ± 4
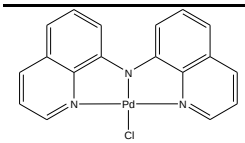 **Pd4**	**Tu**	181 ± 3	42 ± 1	-57 ± 2
	Dmtu	100 ± 2	38± 1	-73 ± 3
	Tmtu	74 ± 10	37 ± 2	-76 ± 6

From the temperature dependence of k_2, Eyring plots of ln $\left(\frac{k_2}{T}\right)$ versus $\frac{1}{T}$ were constructed. The enthalpy of activation **(**$\Delta H^{\neq}$) and entropy of activation ($\Delta S^{\neq}$) were calculated from the slopes and y-intercepts, respectively from the plots according to Eyring *Equation 4.2.* [59]

$$\ln\left(\frac{k_2}{T}\right) = -\frac{\Delta H^{\neq}}{RT} + \left(23.8 + \frac{\Delta S^{\neq}}{R}\right) \tag{4.2}$$

where T and R represent temperature and gas constant, respectively. Representative Eyring plots for the reactions of **Pd4** is presented in Figure 4.4; plots for reactions of other complexes are shown in Figures SI 4.19 – 4.21 and the values $\frac{1}{T}$ and their respective $ln\left(\frac{k_2}{T}\right)$ are tabulated in Tables SI 4.6 – 4.9 in the supporting information (ESI‡). The calculated activation parameter values are summarized in Table 4.3.

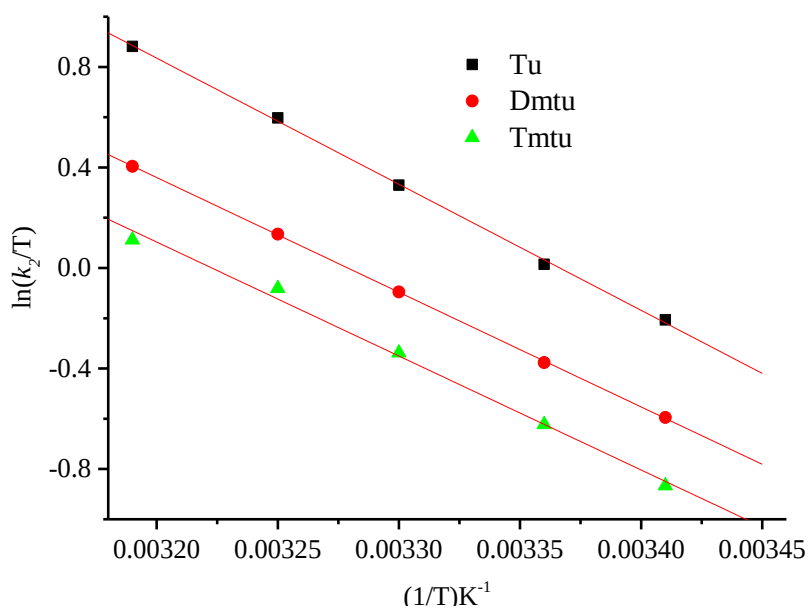

Figure 4. 4 Eyring plots for the reactions of **Pd4** with the nucleophiles

4.4 Discussion

In this study, the reactivity of Pd(II) complexes with varied degrees of π-conjugation was investigated. This was achieved by systematically and appropriately replacing 2-pyridylmethyl

groups of the bis(2-pyridylmethyl)amine (bpma) ligand in **Pd1** with 8-quinolinyl groups resulting in other complexes. The quinolinyl moiety, known to have both π-acceptor/donor phenyl and an electron deficient pyridine ring,[60] would offer π-extension as well as σ-donation. The intention was to try to understand how the competing effect of the net σ-donation of the quinolinyl moiety and the increasing π-conjugation of the complexes will control the reactivity of Pd(II) metal.

In **Pd2** one of the 2-pyridylmethyl group in bpma of **Pd1** is replaced with 8-quinolinyl group while both rings are replaced in **Pd4**. In **Pd3**, an imine bond replaces amino methyl bond in the ligand of **Pd2**. In doing so, the rate of substitution of the labile chloride ligand from the complexes decreased in the order **Pd1** > **Pd3** > **Pd2** > **Pd4** for all the nucleophiles. All the measured rate constants and activation parameters ($\Delta H^{\#}$ and $\Delta S^{\#}$) are given in Table 4.3. The reactivity trend observed in the Pd(II) complexes can be explained majorly in terms of the electronic effects of the quinolinyl moiety in their ligands' framework.

Quinoline having a net σ-donor effect is expected to be less acidic than pyridine since more resonance structures can be drawn to delocalize the positive charge on the conjugate acid.[61] Furthermore, inductive effects of quinoline also play a role in stabilizing the conjugate acid. The less acidic nature of the quinoline ligand in a complex implies increase in σ-inductive effects in the complex which reduces the ligand's π-acceptability. Quinoline is known to form several charge transfer complexes by means of acting as a good σ-donor.[62] This effect usually leads to destabilization of 18-electron 5-coordinate intermediate state thereby reducing the reactivity.

The second-order rate constants in Table 4.3 shows that replacing one of the 2-pyridinylmethyl group of the bpma ligand in **Pd1** with 8-quinolylinyl moiety increases π-conjugation of the ligand of **Pd2** but reduces its reactivity by factors of between 5-7 relative to **Pd1** depending on

the steric bulk of the nucleophiles. This is similar to what has been reported[22] in $[Pt(terpy)Cl]^+$ type of complexes when a replacement of one of the *cis*-positioned pyridine ring of terpyridine ligand with an isoquinoline caused an unusual reduction in the rate of substitution by a factor of 4 with the same nucleophiles. The high reactivity of **Pd1** is because of its two but isolated pyridine rings which are strong π-acceptors withdrawing electron density from Pd(II) metal centre through π-backbonding. This makes it more electrophilic as a result of electron density delocalization,[20, 24] than **Pd2** and hence more susceptible to nucleophilic attack.[30, 32, 63] The 8-quinolinyl moiety weakens the π-acceptability of the resultant ligand in **Pd2** through σ-inductive effects as well as donates electrons towards the metal centre. This increases the electron density around the metal, making it less electrophilic and retards the swift attack of the incoming nucleophiles as already reported when quinolinyl or isoquinolinyl group formed part of the *cis*-spectator tridentate ligand.[18, 22, 36, 64] This is supported by the calculated electrophilicity indices in Table 4.2 where **Pd2** (5.696) has lower values than **Pd1**(6.077).

When the reactivity of **Pd2** and **Pd4** is compared with that of **Pd3**, the reactivity of **Pd3** is faster by factors of 1 and 5 for all the nucleophiles in relation to that of **Pd2** and **Pd4**, respectively. The ligand of **Pd2** is bridged by an imine to confer extended π-conjugation and hence electron delocalisation of the ligand in **Pd3** than that in **Pd2**. Indeed, this improves the π-acceptor property of the entire imine bridged ligand, making it more electrophilic than the complexes hence increase in the rate of substitution. But because of the σ-donor properties of the 8-quinolinyl group, the acceleration of the rate is not as would be expected based on its extended π-surface. It is well known that Pt(II) complexes of N^N^N tridentate ligands with π-conjugation molecular orbitals show high rates of substitution. [6, 9, 19, 21, 22, 27, 29] The reactivity of **Pd4** is lower than those of **Pd2** and **Pd3** because of the σ-donor effects of the two 8-quinolinyl groups retarding the reactivity than the complexes.

However, the deceleration of the incoming nucleophiles in the substitution process is further enhanced by factors ranging between 25 – 30 times relative to that of **Pd1** when its bpma ligand is replaced with bis(8-quinolinyl)amine ligand in **Pd4**. This further confirm the fact that the 8-quinolinyl moiety just like its related isoquinolinyl group is a poor-π-acceptor of the electron density from the metal-based orbitals, while it donates towards the metal centre through the lateral bonds. This makes quinoline-based ligand better in stabilizing the complex than the pyridine-based ligand. The electrophilicity of the metal is thus lowered leading to reduced rate of substitution. Interestingly, through the π-resonance at the amido group, the ligand of **Pd4** has the highest π-surface yet it is the most inert towards substitution. Unlike in **Pd3** whose acceleration in reactivity is due to extended π-surface, though not as expected, the reactivity of **Pd4** is contrary to the expectation that it should be the most reactive. It has been observed that the bis(8-quinolinyl)amine ligand in **Pd4** is monoanionic when coordinated to a metal, as opposed to similar donor ligands such as terpy and its derivatives, leading to its complex being more electron-rich than those of terpy complexes.[65] Therefore the low reactivity of the **Pd4** complex than the rest of the complexes, despite its large π-surface, is due to the electron-rich environment caused by the good σ-donation, larger σ-inductive effects as well as poor π-acceptability of the quinolinyl moiety. This results into the repulsion of the incoming nucleophiles thus dampening of the reactivity.[40] This is supported by the smaller NBO charges and electrophilicity index than the other complexes. In addition, the fact that the LUMO energy in **Pd4** is also higher, further confirms that it is the harder complex and a poorer electrophile[66] of the complexes.

From the DFT calculations, the electrophilicity indices of the complexes decreasing from **Pd1** to **Pd4** with exception of **Pd3**, supports the general reactivity trend. The electrophilicity of **Pd3** is out of place because of the change in the nature of the *trans*-effect.[9] For example, in **Pd2** the *trans*-effect is characterized with the donation of electron from the amine into the *trans* axis of

the complex while in **Pd3** the strong π-acceptor character introduced by imine acts by draining electron density from the metal and the *trans*-ligand's chloride orbitals as depicted in Figure 4.5. The interactions between the d_z^2-orbitals of the metal and the ligand's p_z-orbitals is thus increased in **Pd3** leading to shortening of the Pd–Cl bond as well as making Pd, N2 and Cl centres more positive than those of **Pd2** as depicted in their NBO charges in Table 4.2. However, the moderate difference in the reactivity between **Pd3** and **Pd2**, despite the large electrophilicity index difference, is an indication that the net σ-donor effect of the ligand moiety (which is larger in **Pd3** than **Pd2**) is still powerful and prevails upon their reactivity.

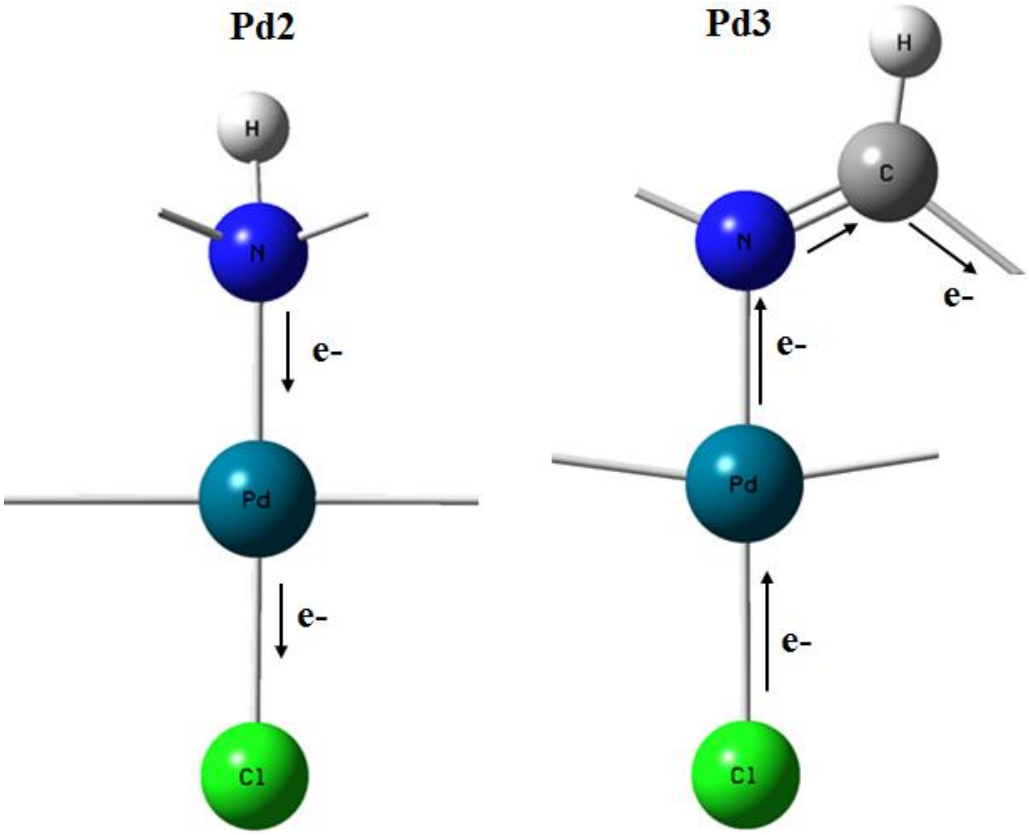

Figure 4. 5 A pictorial illustration of nature of change in the trans-effect indicating flow of electron density in **Pd2** and **Pd3** complexes.

The trend in the HOMO-LUMO energy difference decreasing from **Pd1** going to **Pd4** reflects the increasing trend of π-conjugation as depicted in Table 4.2 indicating that the reactivity should increase in that order.[66] However, this notion is counteracted by the dipole moment and the electrophilicity of the majority of the complexes being in good agreement with the reactivity trend. As already shown 8-quinolinyl moiety plays two roles on the complexes, *viz;* enhances π-extension and σ-donation effects. Based on the results, it is clear that the σ-donation effect is the dominant effect that controls the reactivity of the complexes over the π-back bonding as a result of π-extension. This explains why the resultant reactivity trend of the Pd(II) complexes is opposite to the increasing π-conjugation in the investigated systems.

As depicted from Table 4.3, the reactivity with respect to thiourea nucleophiles decreases in the order **Tu** > **Dmtu** > **Tmtu** across all the complexes. This order agrees with the degrees of their sizes and steric demands. In addition, the substitution of the chloride ligand from the Pd(II) complexes by thiourea nucleophiles follows the two-term rate law in accordance with associatively activated mode of mechanism which is generally common for square planar d^8 complexes.[67-69] This conclusion is in agreement with the values of activation parameters enthalpies ($\Delta H^{\neq}$) being positive and relatively low, while entropies ($\Delta S^{\neq}$) are all negative.

4.5 Conclusions

This study has shown that the reactivity of Pd metal can be controlled using quinoline moiety as part of the complex's ligand framework. The reactivity of the Pd metal reduced by a factor of between 25-30 for the studied nucleophiles when the bis(2-pyridylmethyl)amine ligand of **Pd1** (strong π-acceptors) was replaced by bis(8-quinolinyl)amine in **Pd4** (good σ-donors). It is evident that the σ-donation and inductive effects of 8-quinolinyl moiety weakens the π-back donation effect of the entire ligand framework, making the metal centre less electrophilic and as such less reactive. This means that comparing π-back bonding in systems of this nature, the σ-

effect has more dominant effect in controlling the reactivity, slowing it when not in *trans* and accelerating it when in *trans* as shown in the literature.[21, 25] The mode of mechanism remains associative in nature.

4.6 References

1. J. Bogojeski, R. Jelić, D. Petrović, E. Herdtweck, P. G. Jones, M. Tamm and Ž. D. Bugarčić, *Dalton Transactions*, 2011, **40**, 6515-6523.
2. E. Breet and R. Van Eldik, *Inorganic Chemistry*, 1984, **23**, 1865-1869.
3. Ž. D. Bugarčić, J. Bogojeski, B. Petrović, S. Hochreuther and R. van Eldik, *Dalton Transactions*, 2012, **41**, 12329-12345.
4. Ž. D. Bugarčić, J. Bogojeski and R. van Eldik, *Coordination Chemistry Reviews*, 2015, **292**, 91-106.
5. M. Chipangura, A. Mambanda and D. Jaganyi, *Journal of Coordination Chemistry*, 2014, **67**, 2048-2061.
6. B. Petrović, Ž. D. Bugarčić, A. Dees, I. Ivanović-Burmazović, F. W. Heinemann, R. Puchta, S. N. Steinmann, C. Corminboeuf and R. Van Eldik, *Inorganic Chemistry*, 2012, **51**, 1516-1529.
7. Ž. D. Bugarčić, D. M. Jančić, A. A. Shoukry and M. M. Shoukry, *Monatshefte für Chemie/Chemical Monthly*, 2004, **135**, 151-160.
8. P. Illner, S. Kern, S. Begel and R. van Eldik, *Chemical Communications*, 2007, **0**, 4803-4805.
9. M. Đurović, J. Bogojeski, B. Petrović, D. Petrović, F. W. Heinemann and Ž. D. Bugarčić, *Polyhedron*, 2012, **41**, 70-76.
10. M. Marques, *ISRN Spectroscopy*, 2013, **2013**, 1 - 29.
11. A. S. Abu-Surrah and M. Kettunen, *Current Medicinal Chemistry*, 2006, **13**, 1337-1357.
12. A. Mijatović, J. Bogojeski, B. Petrović and Ž. D. Bugarčić, *Inorganica Chimica Acta*, 2012, **383**, 300-304.
13. B. Rosenberg, L. Vancamp, J. E. Trosko and V. H. Mansour, *Nature*, 1969, **222**, 385.
14. B. Lippert, *Cisplatin: chemistry and biochemistry of a leading anticancer drug*, John Wiley & Sons, 1999.
15. Ž. D. Bugarčič, G. Liehr and R. van Eldik, *Journal of the Chemical Society, Dalton Transactions*, 2002, 2825-2830.
16. M. D. Hall, M. Okabe, D.-W. Shen, X.-J. Liang and M. M. Gottesman, *Annual Review Pharmacology Toxicology*, 2008, **48**, 495-535.
17. A. S. Abu-Surrah, H. H. Al-Sa'doni and M. Y. Abdalla, *Cancer Therapy*, 2008, **6**, 1-10.
18. I. M. Wekesa and D. Jaganyi, *Dalton Transactions*, 2014, **43**, 2549-2558.

19. D. Reddy, K. J. Akerman, M. P. Akerman and D. Jaganyi, *Transition Metal Chemistry*, 2011, **36**, 593-602.
20. D. Jaganyi, A. Hofmann and R. van Eldik, *Angewandte Chemie International Edition*, 2001, **40**, 1680-1683.
21. D. Jaganyi, D. Reddy, J. Gertenbach, A. Hofmann and R. van Eldik, *Dalton Transactions*, 2004, 299-304.
22. P. Ongoma and D. Jaganyi, *Dalton Transactions*, 2012, **41**, 10724-10730.
23. D. Jaganyi, F. Tiba, O. Q. Munro, B. Petrović and Ž. D. Bugarčić, *Dalton Transactions*, 2006, 2943-2949.
24. A. Hofmann, D. Jaganyi, O. Q. Munro, G. Liehr and R. van Eldik, *Inorganic Chemistry*, 2003, **42**, 1688-1700.
25. A. Hofmann, L. Dahlenburg and R. van Eldik, *Inorganic Chemistry*, 2003, **42**, 6528-6538.
26. A. Mambanda and D. Jaganyi, in *Advances in Inorganic Chemistry*, Elsevier, 2017, vol. 70, pp. 243-276.
27. I. M. Wekesa and D. Jaganyi, *Journal of Coordination Chemistry*, 2016, **69**, 389-403.
28. A. Mambanda and D. Jaganyi, *Dalton Transactions*, 2011, **40**, 79-91.
29. D. Jaganyi, K. L. D. Boer, J. Gertenbach and J. Perils, *International Journal of Chemical Kinetics*, 2008, **40**, 808-818.
30. Ž. D. Bugarčić, G. Liehr and R. van Eldik, *Journal of the Chemical Society, Dalton Transactions*, 2002, 951-956.
31. S. Kern, P. Illner, S. Begel and R. van Eldik, *European Journal of Inorganic Chemistry*, 2010, **2010**, 4658-4666.
32. D. Jaganyi and F. Tiba, *Transition Metal Chemistry*, 2003, **28**, 803-807.
33. B. Pitteri, G. Marangoni, L. Cattalini, F. Visentin, V. Bertolasi and P. Gilli, *Polyhedron*, 2001, **20**, 869-880.
34. J. Bogojeski and Ž. D. Bugarčić, *Transition Metal Chemistry*, 2011, **36**, 73-78.
35. A. Shaira, PhD, University of KwaZulu-Natal, South Africa, 2013.
36. B. B. Khusi, A. Mambanda and D. Jaganyi, *Journal of Coordination Chemistry*, 2016, **69**, 2121-2135.
37. H. Zorbas and B. K. Keppler, *ChemBioChem*, 2005, **6**, 1157-1166.
38. S. van Zutphen and J. Reedijk, *Coordination Chemistry Reviews*, 2005, **249**, 2845-2853.

39. N. P. Barry and P. J. Sadler, *Chemical Communications*, 2013, **49**, 5106-5131.
40. G. Kinunda and D. Jaganyi, *Transition Metal Chemistry*, 2014, **39**, 451-459.
41. L. Carlsen, H. Egsgaard and J. R. Andersen, *Analytical Chemistry*, 1979, **51**, 1593-1595.
42. J. Lu, Q. Sun, J.-L. Li, W. Gu, J.-L. Tian, X. Liu and S.-P. Yan, *Journal of Coordination Chemistry*, 2013, **66**, 3280-3290.
43. J. C. Peters, S. B. Harkins, S. D. Brown and M. W. Day, *Inorganic Chemistry*, 2001, **40**, 5083-5091.
44. B. A. Kruis and J. Boersma, *Organometallics*, 1995, **14**, 4213.
45. C. F. Weber and R. van Eldik, *European Journal of Inorganic Chemistry*, 2005, **2005**, 4755-4761.
46. M. Bortoluzzi, G. Paolucci, B. Pitteri, P. Zennaro and V. Bertolasi, *Journal of Organometallic Chemistry*, 2011, **696**, 2565-2575.
47. M. Bortoluzzi, G. Paolucci, B. Pitteri and A. Vavasori, *Inorganic Chemistry Communications*, 2006, **9**, 1301-1303.
48. M. Kosović, Ž. Jaćimović, Ž. D. Bugarčić and B. V. Petrović, *Transition Metal Chemistry*, 2016, **41**, 161-168.
49. S. Jovanović, B. Petrović, D. Čanović and Ž. D. Bugarčić, *International Journal of Chemical Kinetics*, 2011, **43**, 99-106.
50. M. Tobe and J. Burgess, *Inorganic Reaction Mechanisms* Addison Wesley Longman Inc, Essex, 1999.
51. M. Frisch, G. Trucks, H. Schlegel, G. Scuseria, M. Robb, J. Cheeseman, G. Scalmani, V. Barone, B. Mennucci, G. Petersson, Gaussian 09, revision D. 01, Gaussian, Inc., Wallingford CT (2009).
52. P. J. Hay and W. R. Wadt, *The Journal of Chemical Physics*, 1985, **82**, 299-310.
53. V. Barone and M. Cossi, *The Journal of Physical Chemistry A*, 1998, **102**, 1995-2001.
54. M. Cossi, N. Rega, G. Scalmani and V. Barone, *Journal of Computational Chemistry*, 2003, **24**, 669-681.
55. S. B. Harkins and J. C. Peters, *Organometallics*, 2002, **21**, 1753-1755.
56. C. A. Mebi, *Journal of Chemical Sciences*, 2011, **123**, 727-731.
57. R. G. Parr, L. v. Szentpa´ly and L. Shubin, *Journal of American Chemical Society*, 1999, **121**, 1922-1924.

58. OriginPro 9.1. OriginLab Corporation, One Roundhouse Plaza, Suite 303, Northampton, MA 01060, United States. 1800-969-7720.
59. H. Eyring, *The Journal of Chemical Physics*, 1935, **3**, 107-115.
60. P. Bruice, *Organic Chemistry*, Prentice-Hall, Upper Saddle River, New Jersey, 2nd edn., 1998.
61. R. S. Hosmane and J. F. Liebman, *Structural Chemistry*, 2009, **20**, 693-697.
62. J. Gurnos, *The Chemistry of Heterocyclic compounds. In: Quinolines*, Wiley & Sons, London, 2009.
63. Ž. D. Bugarčić, B. Petrović and E. Zangrando, *Inorganica Chimica Acta*, 2004, **357**, 2650-2656.
64. A. Shaira, D. Reddy and D. Jaganyi, *Dalton Transactions*, 2013, **42**, 8426-8436.
65. T. A. Betley, B. A. Qian and J. C. Peters, *Inorganic Chemistry*, 2008, **47**, 11570-11582.
66. R. Singh, K. Suresh and D. Prabhu, *International Journal of ChemTech Research*, 2011, **3**, 1571-1579.
67. F. Basolo and R. G. Pearson, *Mechanisms in Inorganic Reactions*, Wiley, New York, 2nd edn., 1967.
68. J. D. Atwood, *Inorganic and organometallic reaction mechanisms*, Wiley-VCH Publishers, New York, 2nd edn., 1997.
69. R. Van Eldik, T. Asano and W. Le Noble, *Chemical Reviews*, 1989, **89**, 549-688.

4.7 Supporting Information (ESI‡)

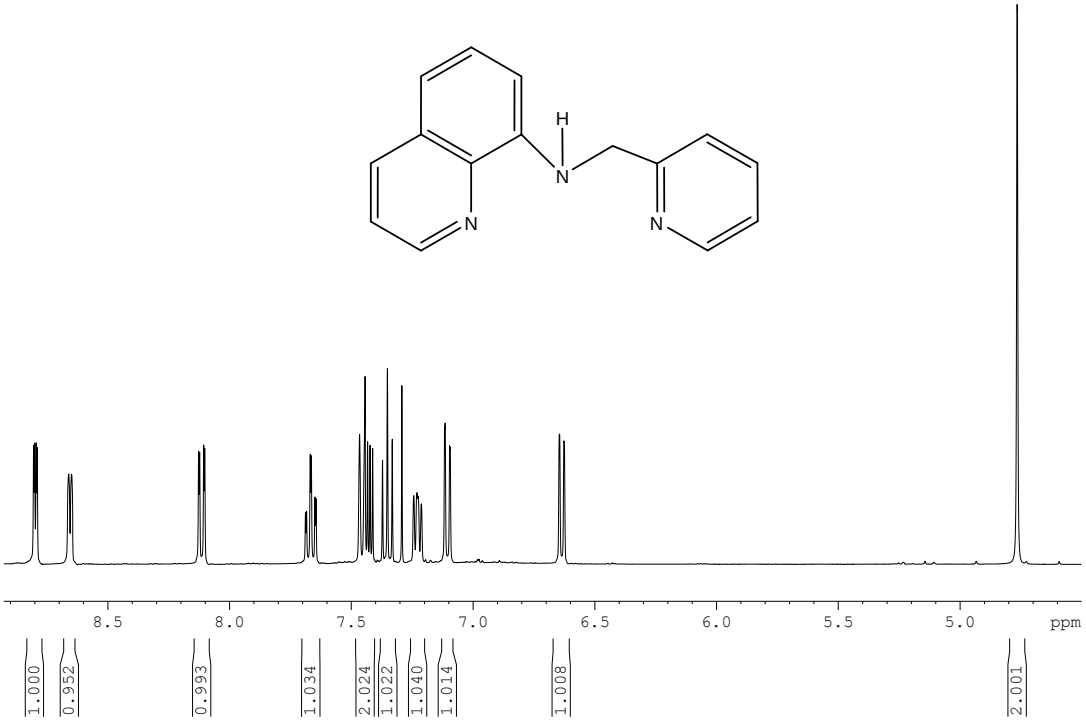

Figure SI 4. 1 ^{1}H-NMR spectrum for 8-[(2-pyridylmethyl)amino]-quinoline ligand

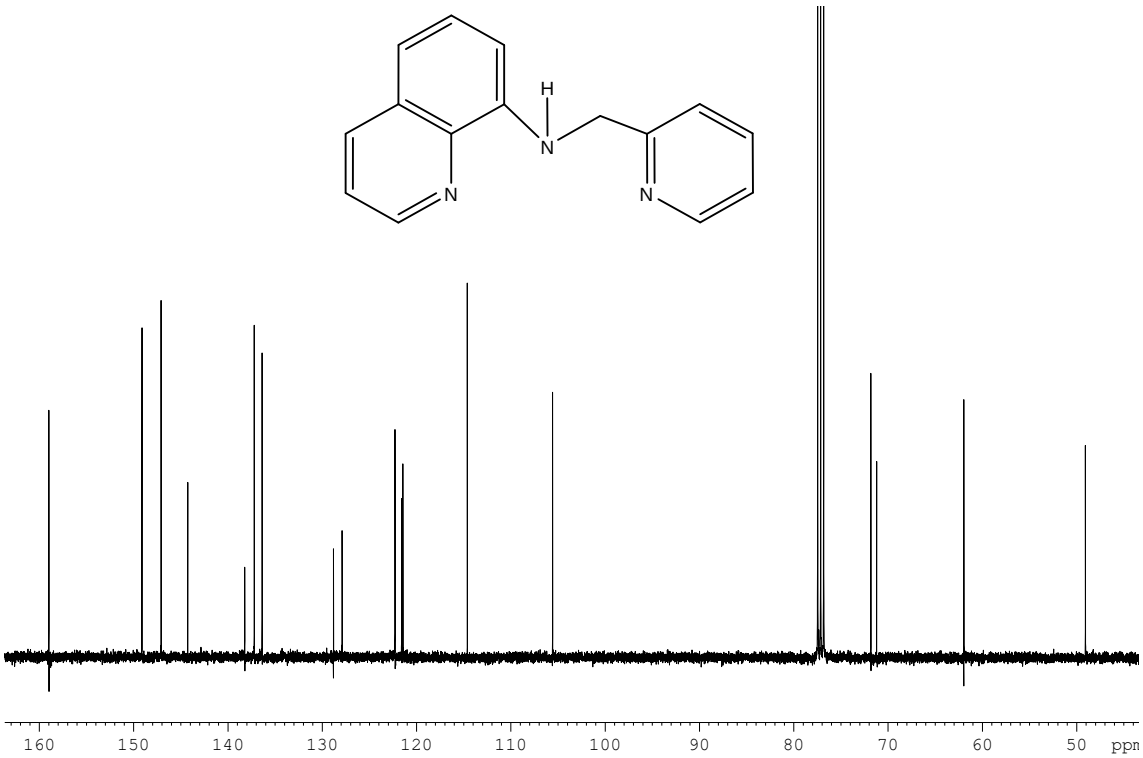

Figure SI 4. 2 ^{13}C-NMR for 8-[(2-pyridylmethyl)amino]-quinoline ligand

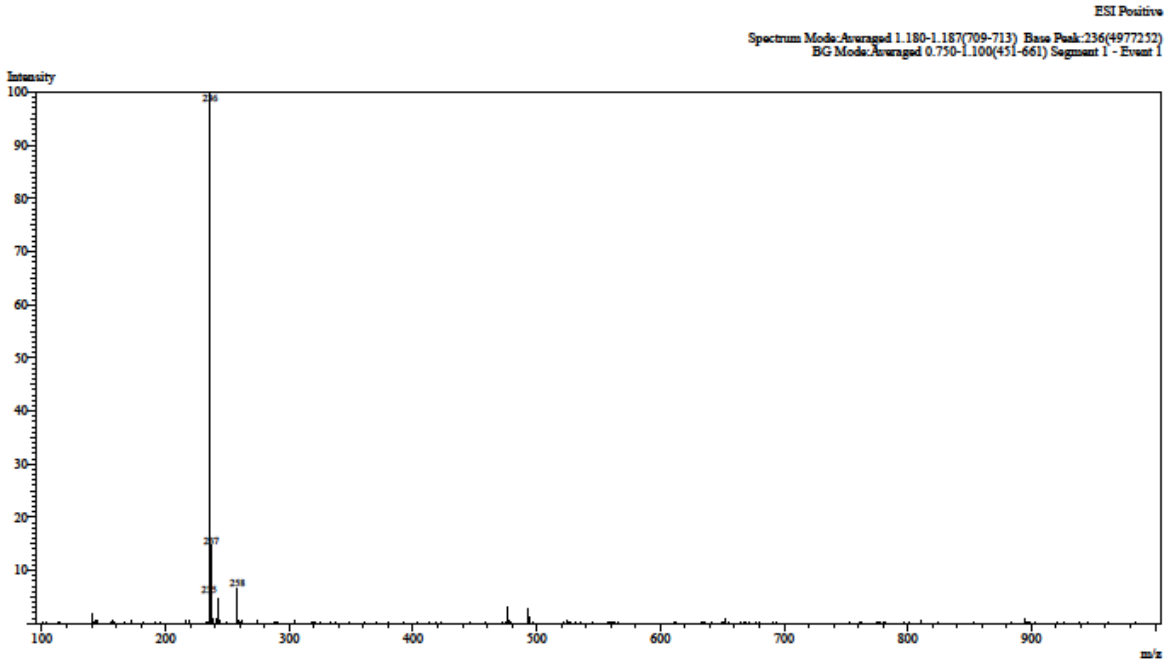

Figure SI 4. 3 LC-MS mass spectrum for 8-[(2-pyridylmethyl)amino]-quinoline ligand

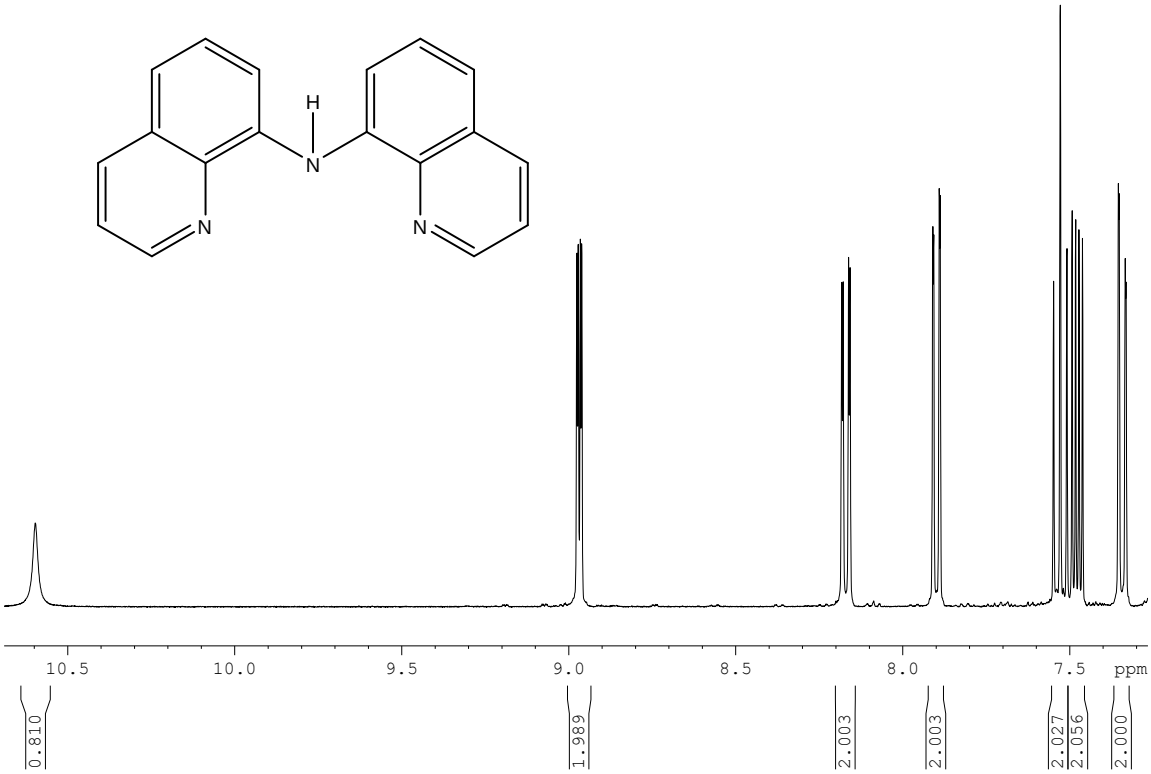

Figure SI 4. 4 ^{1}H-NMR for Bis(8-quinolinyl)amine ligand

Figure SI 4. 5 ^{13}C-NMR for Bis(8-quinolinyl)amine ligand

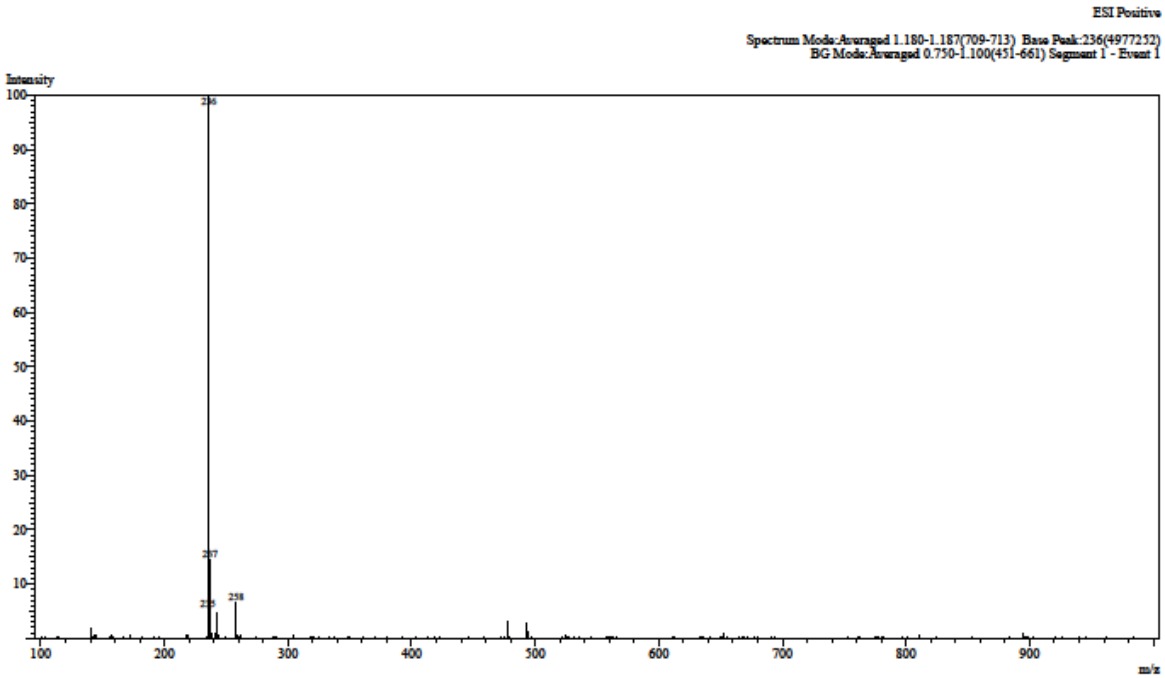

Figure SI 4. 6 LC-MS mass spectrum for 8-[(2-pyridylmethyl)amino]-quinoline ligand

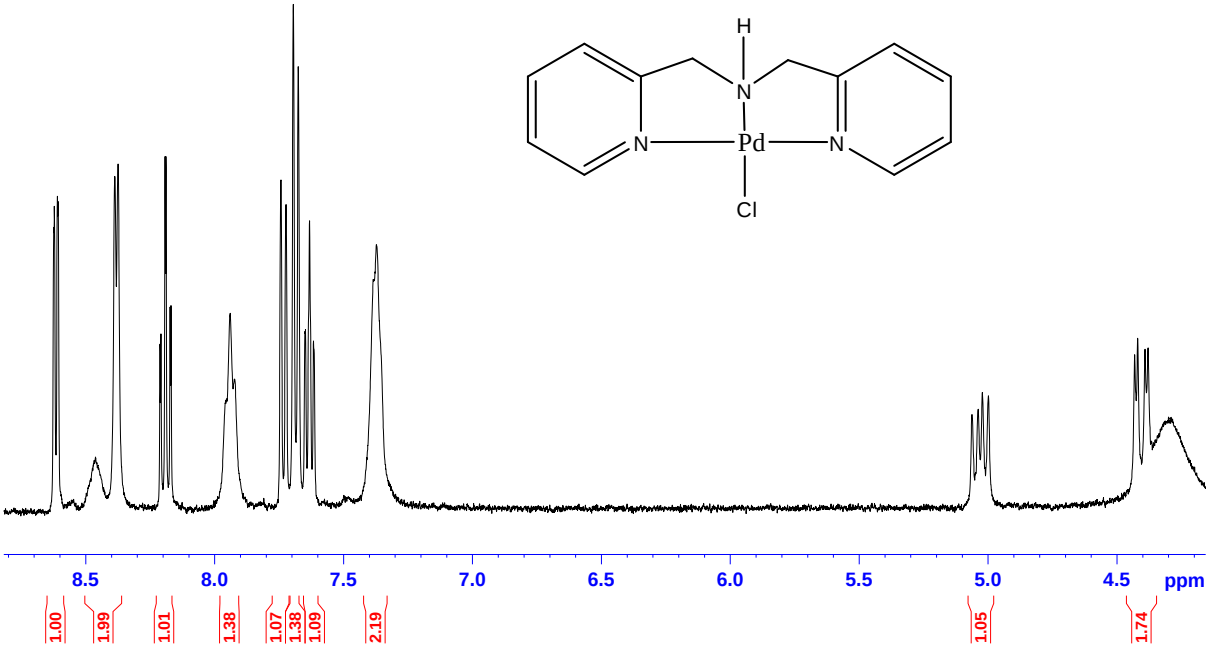

Figure SI 4. 7 ^{1}H-NMR spectrum **Pd1** complex

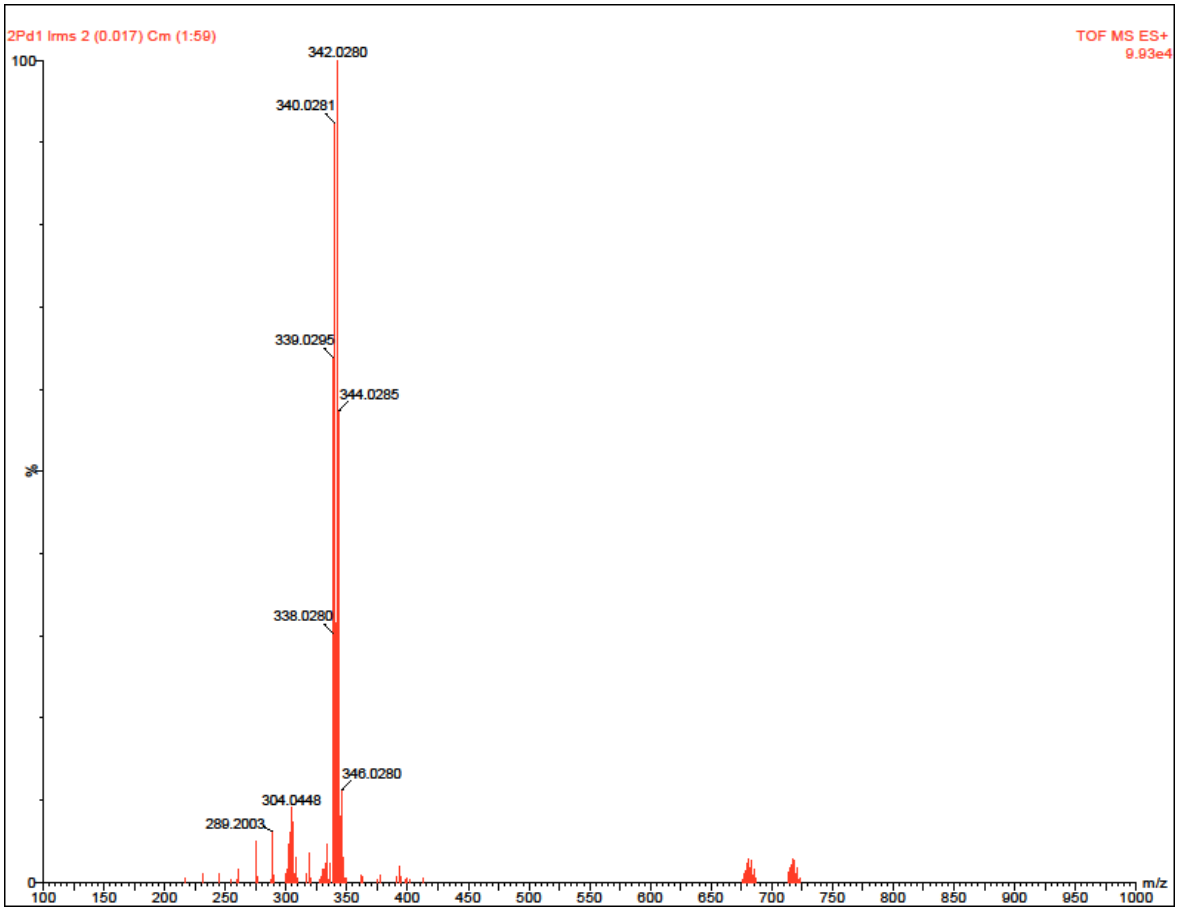

Figure SI 4. 8 TOF-MS mass spectrum for **Pd1** complex

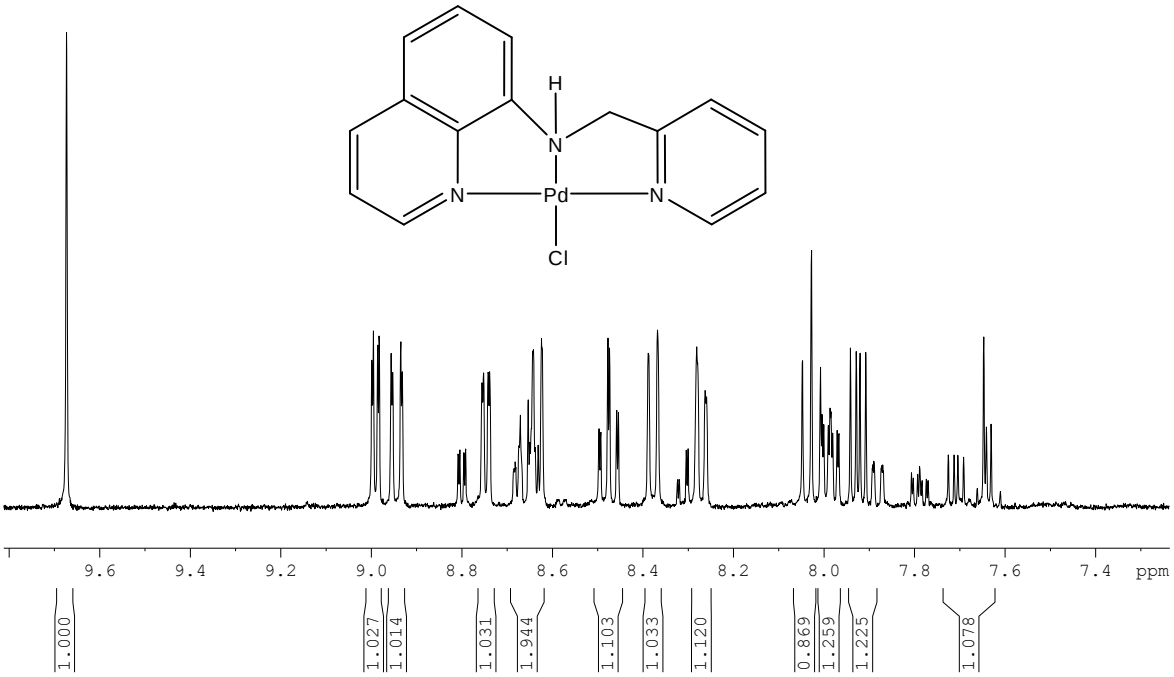

Figure SI 4. 9 ^{1}H-NMR spectrum for **Pd2** complex

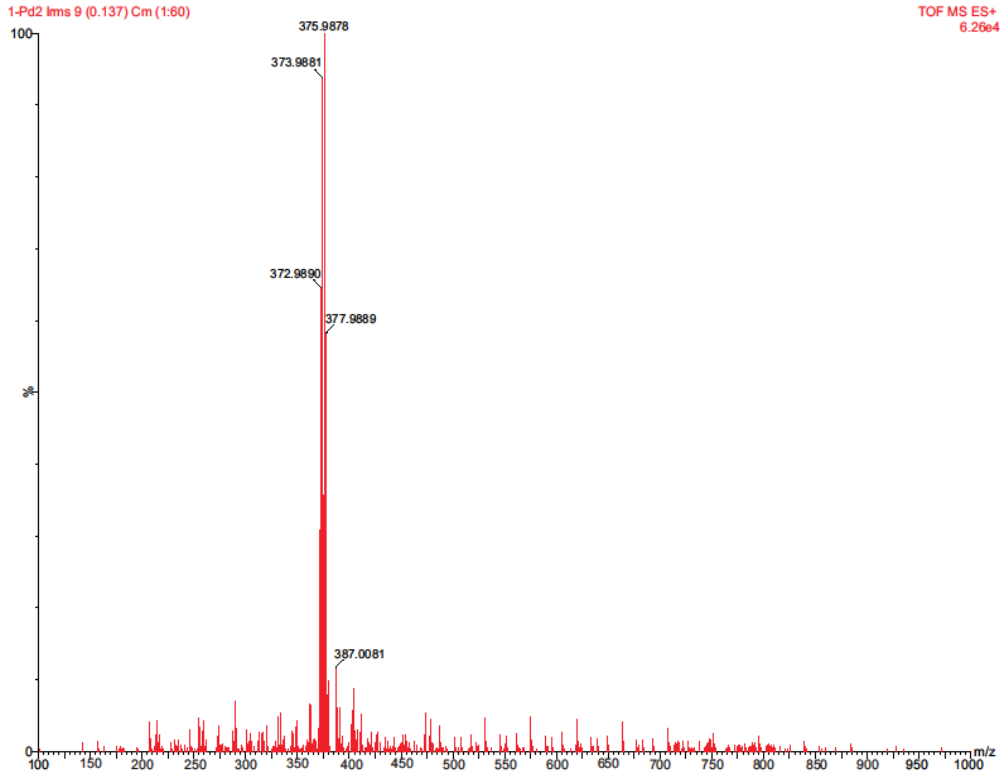

Figure SI 4. 10 TOF-MS mass spectrum of **Pd2** complex

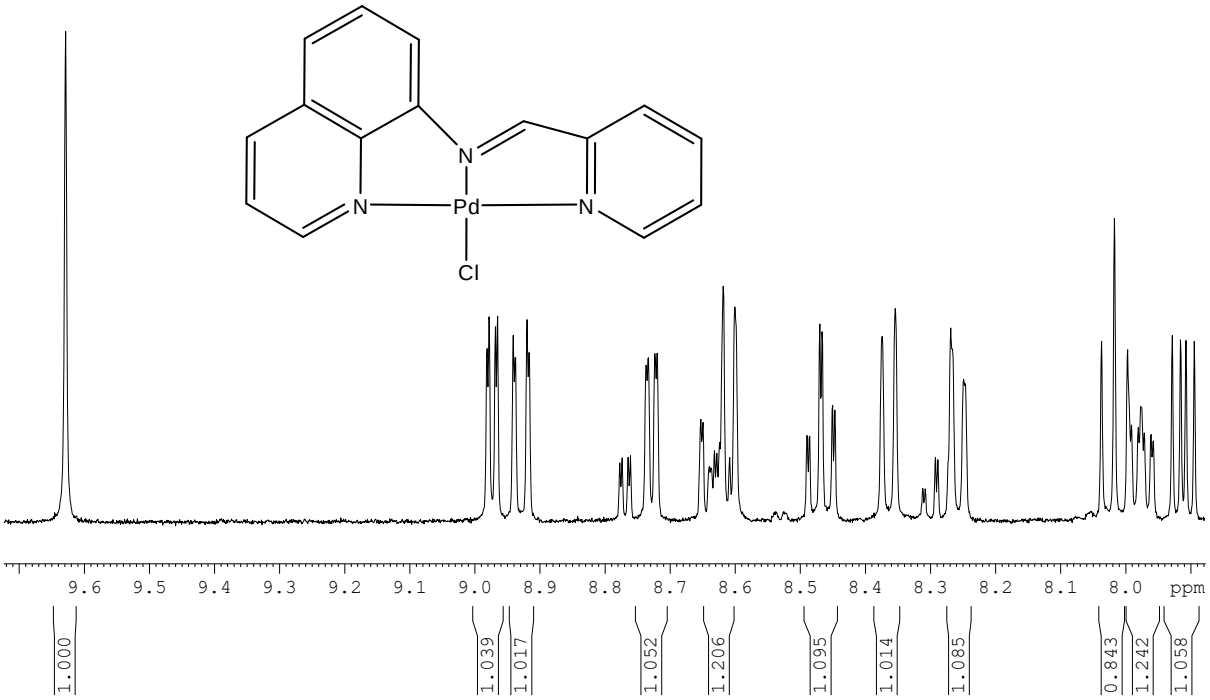

Figure SI 4. 11 ^{1}H-NMR spectrum of **Pd3** complex

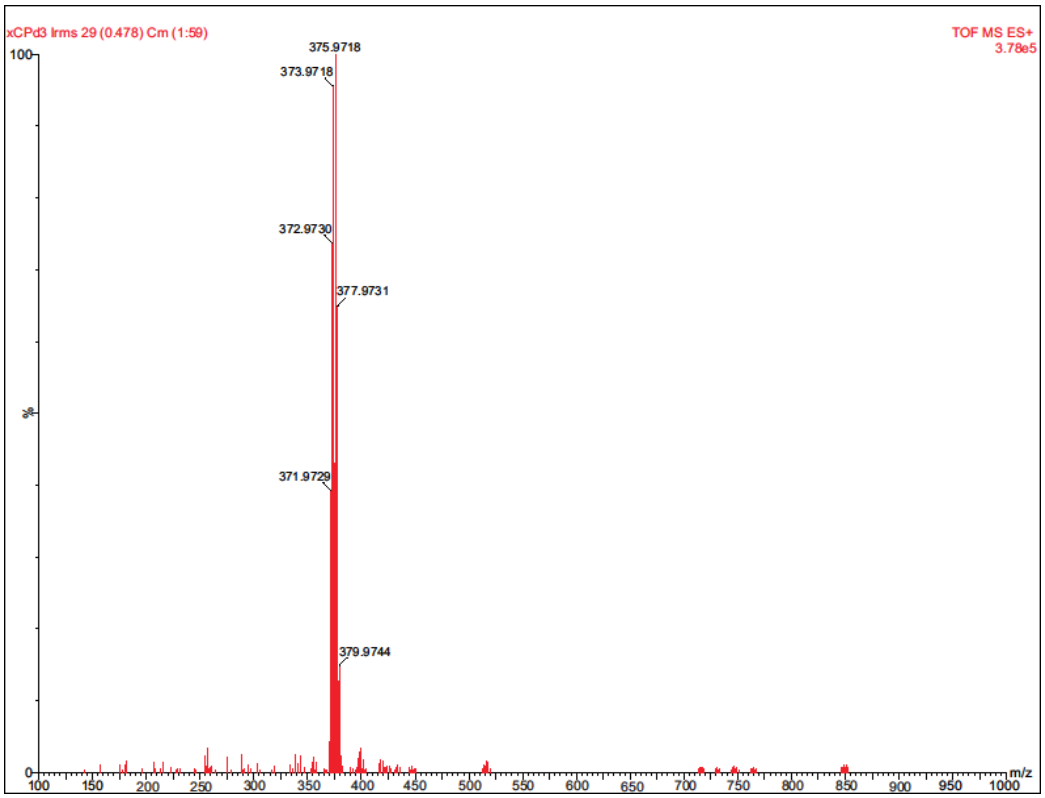

Figure SI 4. 12 TOF-MS mass spectrum for **Pd3** complex

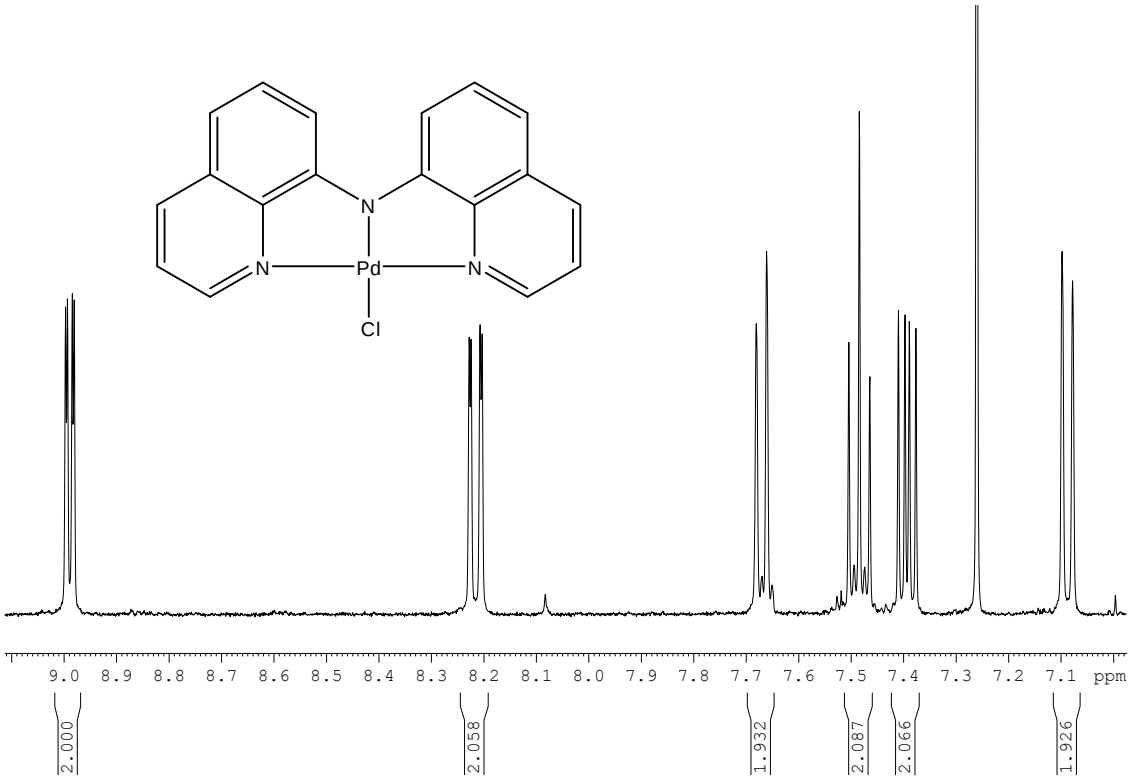

Figure SI 4. 13 ^{1}H-NMR spectrum for **Pd4** complex

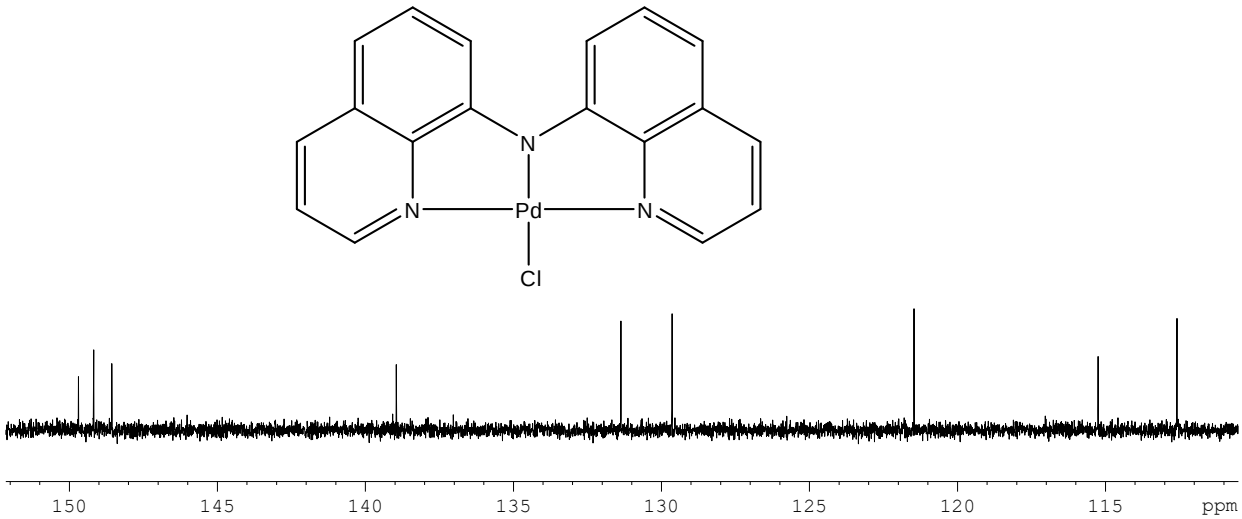

Figure SI 4. 14 ^{13}C-NMR spectrum for **Pd4** complex

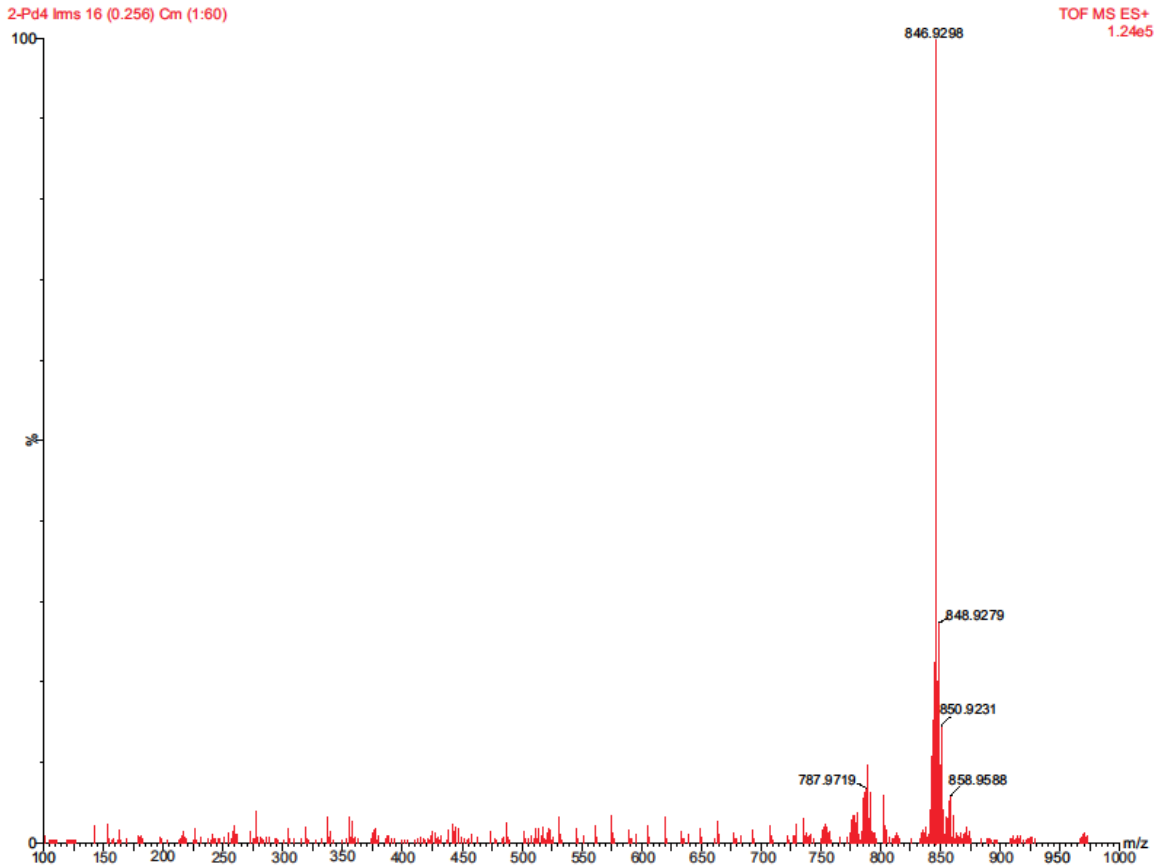

Figure SI 4. 15 TOF-MS mass spectrum for **Pd4** complex

Table S1 4. 1: Wavelengths (nm) use for monitoring the kinetic reactions of Pd(II) complexes with thiourea nucleophiles

Complex	Nucleophiles	Wavelength, λ (nm)
Pd1	Tu	350
	Dmtu	356
	Tmtu	374
Pd2	Tu	320
	Dmtu	385
	Tmtu	320
Pd3	Tu	308
	Dmtu	330
	Tmtu	396
Pd4	Tu	367
	Dmtu	367
	Tmtu	367

Concentration dependent reactions

Table S1 4. 2: A average k_{obs} (s^{-1}) for the reactions of **Pd1** with the nucleophiles in methanol at T = 298 K, I = 20 mM LiCl

Concentration, (M)	k_{obs} (s^{-1})		
	Tu	Dmtu	Tmtu
0.002	10.89328	5.20952	3.83976
0.004	21.72818	10.22477	7.56386
0.006	32.89019	14.82938	10.74003
0.008	43.32697	19.26763	14.2715
0.010	54.13021	24.18669	18.4209

Table S1 4. 3: Average values of k_{obs} (s^{-1}) for the substitution of chloride from **Pd2** by the nucleophiles in methanol at T = 298K, I = 20 mM LiCl

Concentration, (M)	k_{obs} (s^{-1})		
	Tu	Dmtu	Tmtu
0.002	1.64877	1.2373	0.69935
0.004	3.05963	1.92588	1.33357
0.006	4.453	2.89935	2.01659
0.008	5.95207	3.88256	2.60177
0.010	7.06748	4.53761	3.34581

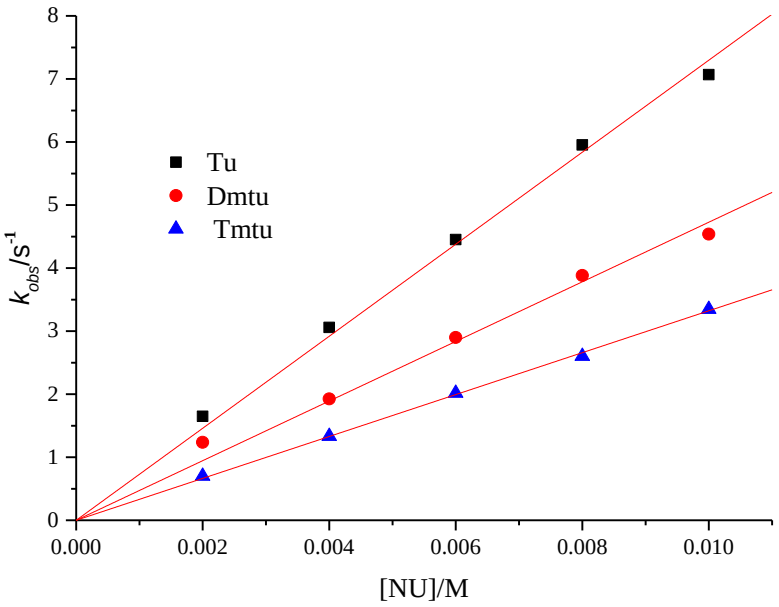

Figure SI 4. 16: The dependence k_{obs} (s^{-1}) on the nucleophile concentrations for the reactions of **Pd2** in methanol, I= 20 mM LiCl, T = 298K

Table S1 4. 4: Average values of k_{obs} (s^{-1}) for the substitution of chloride from **Pd3** by the nucleophiles in methanol at T = 298K, I = 20 mM LiCl.

Concentration, (M)	k_{obs} (s^{-1})		
	Tu	Dmtu	Tmtu
0.002	1.8295	1.19598	0.60001
0.004	3.41985	2.17224	1.37953
0.006	4.9684	3.02208	2.1083
0.008	6.80025	4.16598	2.81112
0.010	8.51825	5.45214	3.53147

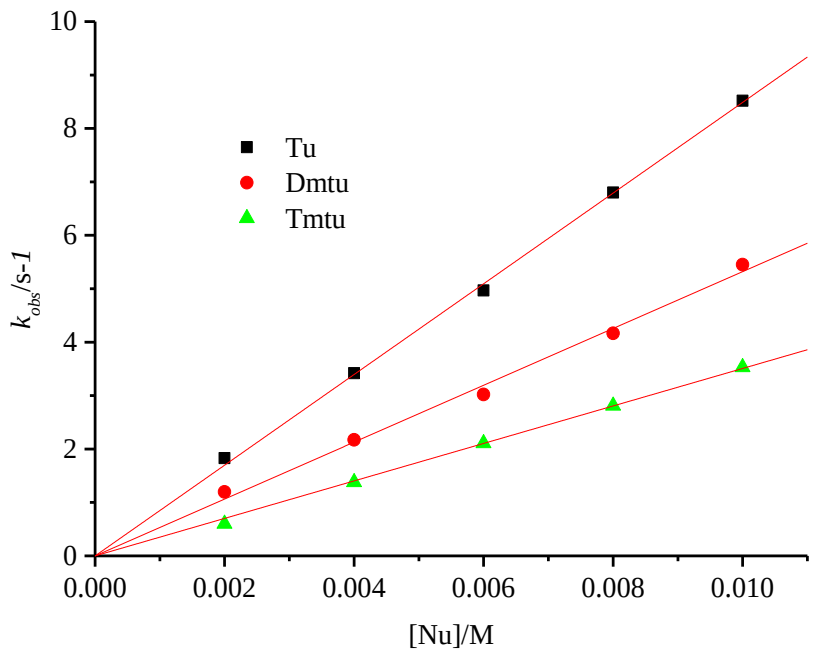

Figure SI 4. 17: The dependence of k_{obs} (s^{-1}) on the nucleophile concentrations for chloride substitution from **Pd3** in methanol, I = 20 mM LiCl, T = 298K.

Table S1 4. 5: Average values of k_{obs} (s^{-1}) for the substitution of chloride from **Pd4** by the nucleophiles in methanol at T = 298K, I = 20 mM LiCl

Concentration, (M)	k_{obs} (s^{-1})		
	Tu	Dmtu	Tmtu
0.002	0.38985	0.19666	0.15498
0.004	0.65341	0.3906	0.3036
0.006	1.10442	0.58523	0.43575
0.008	1.4273	0.83787	0.61994
0.010	1.82998	0.98491	0.72625

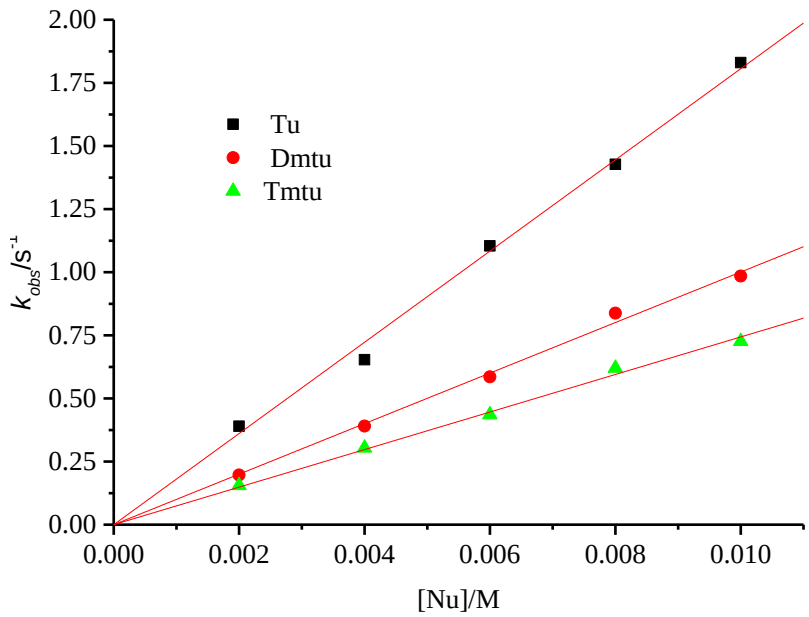

Figure SI 4. 18: The dependence of k_{obs} (s^{-1}) on the nucleophile concentrations for chloride substitution from **Pd4** in methanol, I = 20 mM LiCl, T = 298K.

Temperature dependence reactions

Table S1 4. 6: Temperature dependence of k_2 $M^{-1}s^{-1}$ for the reactions of **Pd1** with the nucleophiles at 30-fold in methanol, I = 20 mM LiCl.

	ln(k_2/T)		
(1/T) K^{-1}	Tu	Dmtu	Tmtu
0.00341	2.73459	1.79266	1.51170
0.00336	2.91208	2.07341	1.79288
0.0033	3.12008	2.35842	2.08103
0.00325	3.31810	2.59998	2.32264
0.00319	3.55123	2.89005	2.55899

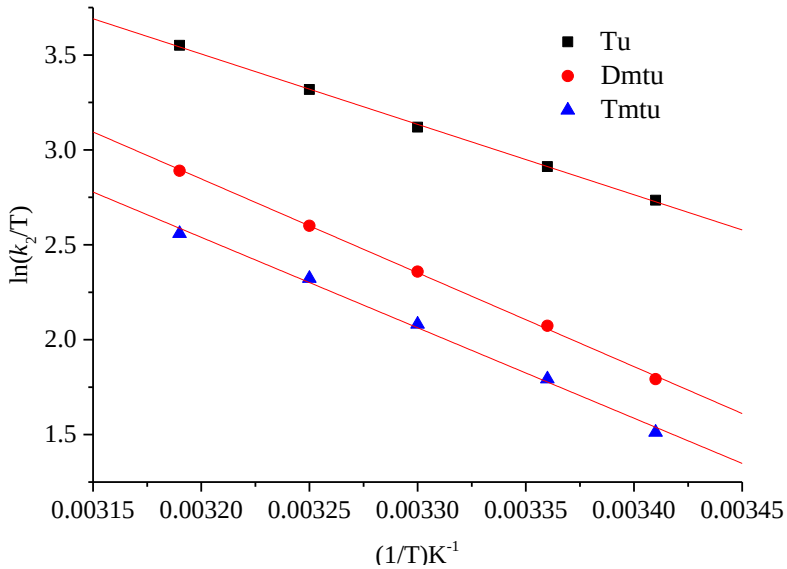

Figure SI 4. 19: Eyring plots for the reactions of **Pd1** with the nucleophiles

Table S1 4. 7: Temperature dependence of k_2 M^{-1} s^{-1} for the reaction of **Pd2** with the nucleophiles at 30-fold in methanol, I = 20 mM LiCl.

	ln(k_2/T)		
(1/T) K^{-1}	Tu	Dmtu	Tmtu
0.00341	0.47887	0.13954	-0.19725
0.00336	0.78042	0.48339	0.12031
0.0033	1.04293	0.784	0.51894
0.00325	1.21354	1.03169	0.82679
0.00319	1.46728	1.2947	1.11789

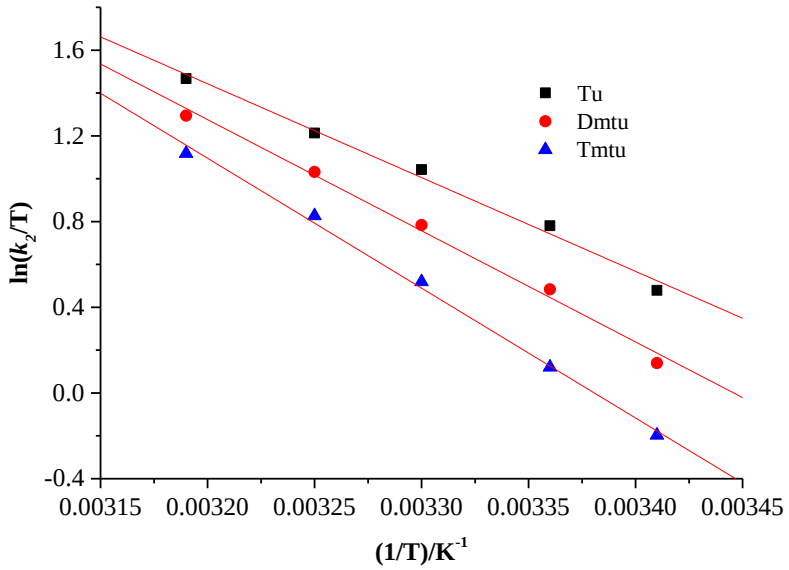

Figure SI 4. 20: Eyring plots for the reactions of **Pd2** with the nucleophiles

Table S1 4. 8: Temperature dependence of k_2 $M^{-1}s^{-1}$ for reactions of **Pd3** with the nucleophiles at 30-fold in methanol, I = 20 mM LiCl.

(1/T) K^{-1}	ln(k_2/T)		
	Tu	Dmtu	Tmtu
0.00341	-0.81358	-1.4254	-3.03919
0.00336	-0.54523	-1.12691	-2.81624
0.00330	-0.28727	-0.72722	-2.49153
0.00325	0.04061	-0.45915	-2.32655
0.00319	0.3778	-0.16806	-2.02382

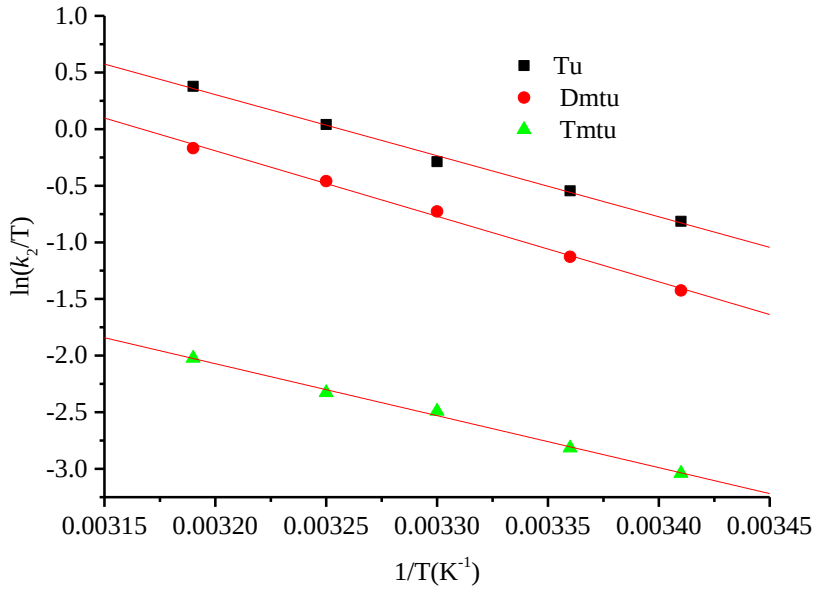

Figure SI 4. 21: Eyring Plots of **Pd3** with thiourea nucleophiles at different temperatures

Table S1 4. 9: Temperature dependence of k_2 $M^{-1}s^{-1}$ for the reactions of **Pd4** with the nucleophiles at 30-fold in methanol, I = 20 mM LiCl.

(1/T) K^{-1}	ln(k_2/T)		
	Tu	Dmtu	Tmtu
0.00341	-0.20687	-0.59484	-0.86658
0.00336	0.01463	-0.37672	-0.62320
0.00330	0.32979	-0.09567	-0.33761
0.00325	0.59713	0.13463	-0.08136
0.00319	0.88169	0.40465	0.11162

CHAPTER 5

Controlling the Reactivity of Pd(II) Complexes of 1,3-Bis(2-pyridylimino)isoindoline Ligands through Alkylation and Benzannulation: X-ray structure, Kinetics, Mechanistic and DFT Study

5.0 Abstract

The kinetics and mechanism of the chloride ligand substitution reactions of a series of 1,3-bis(2-pyridylimino)isoindoline Pd(II) complexes; chlorido(1,3-bis(2-pyridylimino)isoindoline)palladium(II), **Pd(BPI)Cl**, chlorido(1,3-bis(4-methyl-2-pyridylimino)isoindoline)palladium(II), **Pd(4-Me-PBI)Cl**, chlorido(1,3-bis(2-pyridylimino)benz(*f*)isoindoline)palladium(II), **Pd(BBPI)Cl** and chlorido(1,3-bis(1-isoquinolylimino)isoindoline)palladium(II), **Pd(BII)Cl**, with biologically relevant thiourea ligands, thiourea (**Tu**), N,N'-dimethylthiourea (**Dmtu**) and N,N,N',N'-tetramethylthiourea (**Tmtu**) were investigated. The investigations were conducted under *pseudo*-first-order conditions as a function of temperature and nucleophile concentration by stopped-flow and UV-visible spectrophotometry. The rate was first-order with respect to each complex and nucleophile. The substitution reactions proceeded in two-steps complexes for all the complexes except for **Pd(BII)Cl**, for which only the first step was observed. The reaction rate is described by the equation, law $k_{obs(1/2)} = k_{(1/2)}$[Nu], and decreases in the order **Pd(BPI)Cl** > **Pd(4-Me-PBI)Cl** > **Pd(BBPI)Cl > Pd(BII)Cl**. The reactivity of **Pd(BPI)Cl**, **Pd(4-Me-PBI)Cl** and **Pd(BBPI)Cl** is significantly influenced by electron rich density around the metal centre from the ligand moiety, while that of **Pd(BII)Cl** is mainly determined by steric effects. *Trans*-benzannulation increases the electron donor properties of the ligand, while *cis*-benzannulation increases the π-acceptor property of the ligand and at the same time causes steric effect to the incoming nucleophile. The *cis*-methylation increases the electron donor property of the ligand through σ-inductive donation into the pyridine ring while to a small extent causes steric effect as well. The reactivity trend is contrary to the increasing extended π-conjugation. X-ray crystal

structure of **Pd(4-Me-PBI)Cl** is presented. The DFT calculations was performed to give insights into the experimental results and the data shows that alkylation and benzannulation successively destabilizes the HOMO energy which supports the reactivity trend.

Keywords: Pd(II)(N^N^N) complexes, *cis*-effect, alkylation, *pseudo*-first-order, 1,3-bis(2-pyridylimino)isoindoline (BPI)

5.1 Introduction

The ligands of 1,3-bis(2-pyridylimino)isoindoline (BPI) are characteristically monoanionic tridentates (N^N^N) and their coordination chemistry have attracted a lot of interest since their discovery in 1950s.[1-3] This class of ligands are rich chelators, which enables them form stable complexes, of square planar or octahedral geometries, with a wide range of transition metal ions such as cobalt, copper, palladium, manganese, zinc, aluminium, nickel, iron and platinum as well as metalloids such as boron, gallium and indium.[4-13] Their strain free six-membered chelated Pt(II) and Pd(II) complexes have found applications in catalysis[11] electrochemistry and photophysics.[7, 13] A perusal of literature shows that, a structurally closely related free ligands to BPI have shown anticancer activity.[14, 15] Hitherto, Pt(II)/Pd(II) complexes of BPI ligands have not been reported for antitumoral activity. Therefore, the coordination chemistry of BPI with Pt(II)/Pd(II) could be very insightful into providing complexes with improved efficacy as antitumor drugs over widely used known drug , *cisplatin*.

Cisplatin, (*cis*-[$Pt(NH_3)_2Cl_2$]) as well as other Pt(II) metal based antitumor drugs, remains the most widely used drug against testicular, ovarian and non-small lung cancer cells.[16-18] These drugs have been plagued by serious side effects among others, nausea, ototoxicity, neurotoxicity, vomiting and nephrotoxicity. [17, 19-21] These drawbacks provide opportunities for the continuous search for alternative non-platinum drugs with high efficacy, easy administration, and less side effects. Among the non-platinum metal complexes, Pd(II) derivatives are readily chosen because of their structural analogy with those of Pt(II) complexes for cancer treatment studies.[22] However, designing Pd(II) compounds with anticancer activity presents enormous challenges since their ligand exchange studies shows they are 10^2–10^5 times faster than analogous Pt(II) compounds.[23] To develop a good antitumor Pd(II) based drugs, sterically hindered and a strongly coordinated N-donor chelates are required to afford kinetically inert and thermodynamic stabile

Pd(II) complexes. The complex structure would thus be stabilized long enough in biological systems so as to reach its DNA target and perform its therapeutic action.[24, 25] In essence, these ligands are structurally modified so as to slow down the reactivity of Pd(II) metal centre, hence improve its cytotoxicity towards cancer cells.[26-31]

Extensive studies of substitution reactions from tridentate (N^N^N)Pd(II)/Pt(II) complexes (N^N^N = diethylenetriamine (dien), bis(2-pyridylmethyl)amine (bpma) and terpyridine (terpy) ligands) have provided useful information in controlling the reactivity of these complexes.[32-39] For example, when a σ-donor groups are bonded *cis* or attached to the core ligand, a reduction in the rate of substitution is experienced due to σ-inductive donation of electron density to the metal centre.[40-42] Furthermore, extended π-conjugation especially with π-acceptors, *cis* or *trans*, enhances reactivity due to π-backbonding from the dπ-orbitals of the metal into the π*-orbitals of ligands [39, 43] with the *cis*-π acceptor having a stronger influence on the reactivity than the *trans* π-acceptor. However, when π-extension involves quinoline or isoquinoline in the *cis*-position, a reduction in the rate of substitution is witnessed due to good σ-inductive donation effects of the benzopyridines weakening the π-acceptability of the ligand.[44-46] Steric effects of the spectator ligands as a result of bulky groups on the N^N^N ligands, especially at the *cis*-position (steric *cis*-effect) to the leaving group can reduce the rate of substitution from the Pd(II) complexes and is capable of dominating the reactivity over the electronic factors.[47] For instance, van Eldik and his coworkers,[48-52] reported a steric controlled reduction of the rate of substitution of Pd metal up to six orders of magnitude [53] from a series of Pd(II) dien substituted complexes. In some cases, dechelation of the Pt(II) metal centre from the N^N^N ligand of the dinuclear Pt(II) complexes have been reported, during a substitution process, as a result of either strong *trans*-influence or steric influence caused by the coordinated sulfur donor thiourea nucleophiles after successful ligand exchange.[54-56]

Unlike N^N^N tridentate ligands which forms five-membered chelates,[23, 44, 57, 58] ligands which form six-membered chelates especially those with bis(methylene spacer) groups within the N^N^N framework significantly reduces the reactivity of the square planar Pt(II) complexes. [23, 53, 59-61] This is also true for the N^N^N ligands with the *cis*-positioned azaindoles.[62] The reduction in reactivity was due to the incorporation of flexibility in the complexes through methylene spacers conferring aerial steric effects within the plane. [53] In the case of azaindole-based ligands, the effect of pyrollic-N lowered the reactivity of the Pt(II) complex through accumulation of electron density around the metal centre. In addition, ligands forming six-membered chelates encompassing imino spacer groups between the extended π-conjugation rings have been reported to stabilize the Pt metal centre.[63] A careful design of ligands with such properties may be the key to unlocking the anticancer potential of the Pd(II) complexes by taming the high reactivity of the Pd metal which have been blamed for rapid deactivation. However, there remains limited information on the kinetic and thermodynamic behaviour of Pd(II) complexes, in particular, bearing tridentate six-membered chelates with imino spacer chelate ring.

In this contribution, given that six-membered chelates, particularly those encompassing methylene spacer groups decelerate substitution reactivity of Pt(II) complexes,[23, 53, 59-61] this work sought to unravel the role of imino spacer group in slowing the reactivity of Pd(II) complexes bearing BPI ligands. To explore this aspect, Pd(II) complexes coordinated with BPI, shown in Figure 5.1, whose *cis*-pyridyl ring had been alkylated or benzannulated or whose isoindolinyl group's π-surface extended by phenyl ring were synthesized and their labile chloride ligand exchange rate with thiourea nucleophiles measured. A detailed investigation demonstrated a stepwise substitution of the chloride ligand and the detachment of the metal from the ligand in the presence of a strong thiourea nucleophiles. The reactions were studied using stopped-flow

and UV-visible spectrophotometric techniques while the ^{1}H-NMR technique was used to confirm the decomposition mechanism. Density function theory (DFT) calculations was performed to give insights in the discussion of the experimental results.

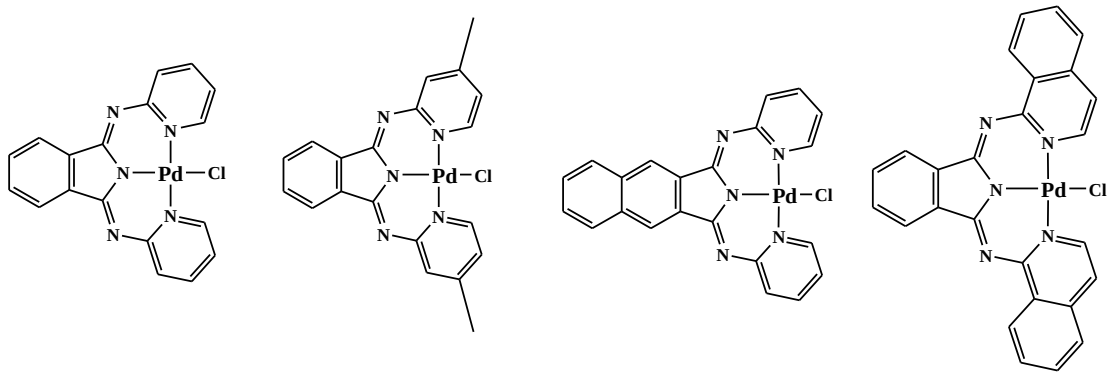

Pd(BPI)Cl **Pd(4-Me-BPI)Cl** **Pd(BBPI)Cl** **Pd(BII)Cl**

Figure 5. 1 Structures of the investigated Pd(II) complexes in this study

5.2 Experimental Section

5.2.1 Materials and Methods

Syntheses were performed under nitrogen atmosphere using standard Schlenk techniques. 1,2-dicyanobenzene, 1-butanol, 1,3-diiminobenz(*f*)isoindoline, triethylene amine (NEt_3), 2-aminopyridine, 2-amino-4-methylpyridine, 1-aminoisoquinoline, thiourea **(Tu)**, N,N'-dimethylthiourea **(Dmtu),** N,N,N',N'-tetramethylthiourea **(Tmtu)**, anhydrous 1-butanol and benzene were purchased from Aldrich. Bis(benzonitrile)dichloropalladium(II), $(C_6H_5CN)_2PdCl_2$, (95%), Anhydrous calcium chloride ($CaCl_2$), and dichloro(1,5-cyclooctadiene)palladium(II), $Pd(COD)Cl_2$, (99%) were also procured from Sigma-Aldrich and used as received without further purification.

5.2.2 Syntheses of Ligands

The ligands 1,3-bis(2-pyridylimino)isoindole **(BPI)** and 1,3-bis(4-methyl-2-pyridylimino)isoindoline **(4-Me-BPI)** [64] 1,3-bis(2-pyridylimino)benz(*f*)isoindoline **(BBPI)**[4] and 1,3-bis(1-isoquinolylimino)isoindole **(BII)**[65] were synthesized according to the standard literature methods.

1,3-Bis(2-pyridylimino)isoindoline(Z) (BPI). A mixture of 1,2-dicyanobenzene (1298.0 mg, 10.0 mmol), 2-aminopyridine (1980.0 mg, 21 mmol), $CaCl_2$ (110.0 mg, 1 mmol) and 1-butanol (20 mL) was added to the reaction flask and refluxed under nitrogen atmosphere for 48 hours. Upon cooling to ambient temperature, a yellow-green precipitate was formed. The precipitate was filtered, washed with water, and purified by recrystallization with equal amounts of ethanol and water. Yield: 952.2 mg (32 %). ^{1}H NMR (400 MHz, $CDCl_3$, ppm) δ = 14.01 (s, N–H broad, 1H), 8.62 (m, 2H), 8.10 (m, 2H), 7.81–7.74 (m, 2H), 7.66 (m, 2H), 7.48 (d, 2H), 7.12 (m, 2H). ^{13}C NMR (100 MHz, $CDCl_3$, ppm) δ = 160.7, 153.7, 148.0, 138.3, 135.9, 131.9, 123.4, 122.9, 120.4. LC-MS ESI$^+$, *m/z* = 300 $(M + H)^+$. *Anal Calc for* $C_{18}H_{13}N_5$: C, 72.23; H, 4.38; N, 23.40 *Found:* C, 71.82; H, 4.30; N, 23.01.

1,3-Bis(4-methyl-2-pyridylimino)isoindoline(Z) (4-Me-BPI). This ligand was prepared using analogous procedure to BPI. A mixture of 1,2-dicyanobenzene (1281.3 mg, 10 mmol), 4-methyl-2-aminopyridine (2216.9 mg, 20.5 mmol), $CaCl_2$ (111.0 mg, 1.0 mmol) and 1-butanol (20 mL) was added to the reaction flask and refluxed under nitrogen atmosphere for 48 hours. Upon cooling to ambient temperature, a yellow-orange solid precipitate formed, which was separated by filtration and washed with water. The residue solid was purified by recrystallization with equal amounts of ethanol and water. Yield: 2028.1 mg, (43.3 %). ^{1}H NMR (400 MHz, $CDCl_3$, ppm) δ = 13.97 (s, N–H broad, 1H), 8.47 (d, 2H), 8.07 (m, 2H), 7.65–7.63 (m, 2H), 7.30 (m, 2H), 6.95 (d, 2H), 2.40 (s, 6H). ^{13}C NMR (100 MHz, $CDCl_3$, ppm) δ = 154.1, 149.6, 147.6,

140.5, 136.1, 131.7, 123.8, 122.7, 121.7, 21.1. LC - MS ESI$^+$, *m/z* = 328 (M + H)$^+$. *Anal Calc for* $C_{20}H_{16}N_5.H_2O$: C, 69.55; H, 5.54; N, 20.28. *Found:* C, 69.50; H, 5.49; N, 20.03.

1,3-Bis(2-pyridylimino)benz(*f*)isoindoline(Z), (BBPI). A dry reaction flask equipped with a magnetic stir bar was filled with 1,3-diiminobenz(*f*)isoindoline (347.5 mg, 1.78 mmol), 2-aminopyridine (339.0 mg, 3.6 mmol), $CaCl_2$ (19.5 mg, 0.178 mmol) and 1-butanol (20 mL). The resulting mixture was refluxed for 24 hours and allowed to cool to room temperature. The volume of the mixture was reduced in vacuo to 5 mL and the resulting green precipitate filtered off and washed with water. The crude product was purified by recrystallization in ethanol/water (1:1) yielding yellow/green needles which was filtered and dried in vacuo. Yield: 206.0 mg (33.2 %). ^{1}H NMR (400 MHz, $CDCl_3$, ppm): δ = 14.37 (s, N–H broad, 1H), 8.64 (m, 2H), 8.61 (s, 2H), 8.07 (q, 2H), 7.79 (m, 2H), 7.63 (m, 2H), 7.51 (d, 2H), 7.14 (m, 2H). ^{13}C NMR (100 MHz, $CDCl_3$, ppm) δ = 160.7, 153.8, 147.9, 138.3, 135.3, 132.1, 129.9, 128.0, 123.3, 120.3, 119.9. LC-MS ESI$^+$, *m/z* = 350 (M + H)$^+$. *Anal Calc for* $C_{22}H_{15}N_5.H_2O$: C, 71.92; H, 4.66; N, 19.06 *Found:* C, 71.52; H, 4.60; N, 18.76.

1,3-Bis(1-isoquinolylimino)isoindoline(Z) (BII). A mixture of 1,2-dicyanobenzene (210.0 mg, 1.64 mmol), 1-aminoisoquinoline (480.0 mg, 3.329 mmol) and $CaCl_2$ (55.0 mg, 0.5 mmol) in 1-butanol (20 mL) was added to a reaction flask and refluxed under N_2 for 5 days. Upon cooling the reaction mixture to ambient temperature, a precipitate was formed. The precipitate was collected by filtration and washed with copious amounts of water under vacuum to give a golden yellow solid. The product was purified by recrystallization in ethanol/water (1:1). Yield: 388.3 mg (59.3 %). ^{1}H NMR (400 MHz, $CDCl_3$, ppm) δ = 9.02 (d, 2H), 8.55 (d, 2H), 8.25 (q, 2H), 7.82 (dd, 2H), 7.75–7.70 (m, 4H), 7.66 (t, 2H), 7.51 (dd, 2H). ^{13}C NMR (125 MHz, CDCl3, ppm) δ = 158.6, 137.9, 136.4, 132.0, 130.7, 127.2, 126.8, 126.4, 123.0, 118.4. LC - MS ESI$^+$, *m/z* = 400

$(M + H)^+$. *Anal. Calc. for* $C_{26}H_{17}N_5$: C, 78.29; H, 4.29; N, 17.53. *Found;* C: 78.18; H, 4.21; N, 17.47.

5.2.3 Syntheses of Complexes

The Pd(II) complexes **Pd(BPI)Cl**, **Pd(4-Me-BPI)Cl**, **Pd(BBPI)Cl** and **Pd(BII)Cl** were prepared according to published procedures.[6, 11, 66]

Chlorido(1,3-bis(2-pyridylimino)isoindoline)palladium(II), **Pd(BPI)Cl**. $Pd(COD)Cl_2$ (142.8 mg, 0.5 mmol) was added into a stirring solution of 1,3-bis(2-pyridylimino)isoindoline (149.5 mg, 0.5 mmol) in methanol (20 mL) and triethylamine, NEt_3 (70 μL, 0.5 mmol) added. The mixture was heated to 50 °C under nitrogen atmosphere for 24 hours. The mixture was left to cool to room temperature and the precipitated solid separated by filtration. The solid was washed three times with water (50 mL) to remove impurities. The washed precipitate was recrystallised from a dichloromethane/n-hexane solution mixture yielding a yellow solid. Yield: 110 mg (50 %). ^{1}H NMR (400 MHz, $CDCl_3$, ppm) δ = 9.88 (m, 2H), 8.06 (m, 2H), 7.86 (m, 2H), 7.63 (m, 4H), 7.09 (m, 2H). ^{13}C NMR (100 MHz, $CDCl_3$, ppm) δ =153.9, 152.3, 139.5, 138.4, 138.0, 126.7, 131.7, 122.6, 120.0. TOF- MS ESI$^+$ *m/z* = 461.9970 $(M + Na)^+$. *Anal. Calc. for* $C_{18}H_{12}N_5PdCl$: C, 49.11; H, 2.75; N, 15.91. *Found:* C, 48.71; H, 2.29; N, 15.92.

Chlorido(1,3-bis(4-methyl-2-pyridylimino)isoindoline)palladium(II), Pd(4-Me-BPI)Cl. To a mixture of $Pd(PhCN)_2Cl_2$ (767.1 mg, 2.0 mmol) and 1,3-bis(4-methyl-2-pyridylimino)-isoindoline (654 mg 2.0 mmol) in benzene (20 mL), NEt_3 (279 μL, 2.0 mmol) was added. The mixture was then stirred at room temperature under nitrogen atmosphere for 2 days. The precipitate solid product observed was separated by filtration. The solid was washed three times with water (50 mL) to remove impurities. The washed precipitate was recrystallised from a dichloromethane/n-hexane solution mixture yielding a yellow-ochre solid. Yield: 150.8 mg (16.1

%). ^{1}H NMR (400 MHz, $CDCl_3$, ppm): δ = 9.70 (d, 2H), 8.02 (m, 2H), 7.61 (m, 2H), 7.42 (s, 2H), 670 (m, 2H), 2.42 (s, 6H). ^{13}C NMR (100 MHz, $CDCl_3$, ppm) δ = 153.1, 152.1, 151.6, 149.4, 138.1, 131.6, 126.9, 122.4, 121.5, 20.9. TOF- MS ESI$^+$ *m/z* = 469.9752 (M + H)$^+$. *Anal. Calc. for* $C_{20}H_{16}N_5PdCl$: C, 51.30; H, 3.44; N, 14.96. *Found:* C, 51.33; H, 3.11; N, 15.29.

Chlorido(1,3-bis(2-pyridylimino)benz(*f*)isoindoline)palladium(II), **Pd(BBPI)Cl**. To a mixture of $Pd(COD)Cl_2$ (142.8 mg, 0.5 mmol) and 1,3-bis(2-pyridylimino)benz(*f*)isoindoline (174.5 mg, 0.5 mmol) in methanol (20 mL), NEt_3 (70 μL, 0.5 mmol) was added. The mixture was then heated to 50 °C under nitrogen atmosphere for 2 days. The mixture was left to cool to room temperature and the precipitated solid separated by filtration. The solid was washed three times with water (50 mL) to remove impurities. The washed precipitate was recrystallised from a dichloromethane/n-hexane solution mixture yielding a yellow solid. Yield: 133.3 mg (54.4 %). ^{1}H NMR (400 MHz, $CDCl_3$, ppm) δ = 9.85 (m, 2H), 8.50 (s, 2H), 8.05 (q, 2H), 7.85 (m, 2H), 7.64-7.59 (m, 4H), 7.06 (m, 2H). ^{13}C NMR (125 MHz, $CDCl_3$, ppm) δ = 153.9, 153.6, 152.3, 139.3, 131.1, 134.0, 130.0, 128.0, 126.5, 123.0, 119.6. TOF-MS ESI$^+$ *m/z* = 954.9501 (2M + Na)$^+$. *Anal. Calc. for* $C_{22}H_{14}N_5PdCl$: C, 53.90; H, 2.88; N, 14.29. *Found:* C, 53.78; H, 2.76; N, 13.99.

Chlorido(1,3-bis(1-isoquinolylimino)isoindoline)palladium(II), **Pd(BII)Cl**. To a mixture of $Pd(COD)Cl_2$ (142.8 mg, 0.5 mmol) and 1,3-bis(1-isoquinolylimino)isoindoline (199.5 mg 0.5 mmol) in methanol (20 mL), NEt_3 (70 μL, 0.5 mmol) was added. The mixture was stirred at 50 °C under nitrogen atmosphere for 2 days. The mixture was left to cool to room temperature and the precipitated solid separated by filtration. The solid was washed three times with water (50 mL) to remove impurities. The washed precipitate was recrystallised from a dichloromethane/n-hexane solution mixture yielding an orange solid. Yield: 98.7 mg (36.5 %). ^{1}H NMR (400 MHz,

$CDCl_3$, ppm) δ = 9.74 (d, 2H), 9.32 (d, 2H), 8.29 (q, 2H), 7.84 (d, 2H), 7. 83 (d, 2H), 7.76 -7.72 (m, 4H), 7.41 (d, 2H). ^{13}C NMR (125 MHz, $CDCl_3$, ppm) δ = 151.0, 145.4, 138.4, 137.1, 132.5, 131.8, 128.4, 128.2, 127.9, 126.9, 122.9, 118.1. TOF-MS ESI^+ *m/z* = 855.3387 $(M + 4DMSO + 3H)^+$. *Anal. Calc. for* $C_{26}H_{16}N_5PdCl$: C, 57.80; H, 2.98; N, 12.96. *Found:* C, 57.51; H, 2.66; N, 12.93.

5.2.4 Physical Measurements and Instrumentation

^1H and ^{13}C NMR spectral data were acquired from either Bruker Avance DPX 500 or DPX 400 NMR with a 5 mm BBOZ probe at 30 ºC. Shimadzu LC-MS 2020 or on a Waters TOF Micro-mass LCT Premier both having ESI ion source analyser spectrophotometers were used for mass analysis. The NMR and mass spectra data of the synthesized ligands and complexes are presented in Figures SI 5.1– 5.21, supporting information (ESI‡). Carlo Erba Elemental Analyzer 1106 was used for elemental analysis of the synthesized compounds. The X-ray data was collected on a Bruker Apex Duo fitted with an Incoatec microsource operating at 30 W power and Oxford Instruments Cryojet operating at 100(2) K. Cary 100 Bio UV–visible spectrophotometer was used for determining suitable wavelengths at which fast substitution reactions would be monitored and for slow kinetic reactions. Applied Photophysics SX 20 stopped-flow reaction analyzer coupled to an online data acquisition system was used for measuring the rate constants for fast reactions. The instrument was thermo-controlled within ± 0.1 °C.

5.2.5 X-ray Crystallography

Single crystals of **Pd(4-Me-BPI)Cl** were recrystallised from slow evaporation of chloroform. A crystal (0.34×0.22×0.14) mm^3 was selected and mounted on a MITIGEN holder in paratone oil on a Bruker APEX-II CCD diffractometer. The crystal was kept at T = 100(2) K during data collection. Using Olex2,[67] the structure was solved with the ShelXS-2013[68] structure solution

program, using the direct solution method. The structure was refined with version 2016/6 of ShelXL[69] using Least Squares minimisation procedures.

The crystal structure was deposited at Cambridge Crystallographic Data Centre (deposition number; CCDC 1829125).

5.2.6 Computational Modelling

Ground state electronic structures of the complexes were optimized using the density functional theory (DFT). The trends in the obtained data were used to explain the trends in the reactivity of the complexes. The DFT calculations were performed with the Gaussian 09 program suite[70] using the B3LYP (Becke 3-Lee-Yang-Parr) functional method, utilizing LANL2DZ (Los Alamos National Laboratory 2 Double ζ)[71] as the basis set. The influence caused by the bulk solvent was evaluated *via* single-point computations using the C-PCM (conductor-like polarizable continuum model) [72, 73] formalism in ethanol solvent. All the complexes were modelled with a formal charge of 0, in accordance to their neutrality, and at singlet state.

5.2.7 Kinetic Solutions

The solutions of Pd(II) complexes (with a concentration of about 1.0 x 10^{-4} M) were prepared by dissolving requisite amounts of the complexes in 4 % THF to enhance solubility. It was then topped up to the final volume with ethanolic solution whose ionic strength had been adjusted to 0.01 M by adding Triflic acid (CF_3SO_3H,). The $CF_3SO_3^-$ was chosen to adjust the reaction media is known to be a weak nucleophile and would not interfere with the substitution process from square planar d^8 complexes.[74, 75] Nucleophile solutions were freshly prepared just before use in a similar manner described for preparation of the complexes. The freshly prepared stock solution of the nucleophiles approximately 50-fold excess of the concentration of the complex was serially diluted with the ethanolic solution to afford 40- 30- 20- and 10-fold in excess of the complex concentrations to maintain *pseudo*-first-order reaction conditions.

5.2.8 Kinetic Analysis

The fast reactions were monitored using stopped a flow spectrophotometer while the conveniently slow reactions were monitored using a UV-visible spectrophotometer. Suitable wavelengths at which the kinetic reactions were monitored were predetermined spectrophotometrically by recording the spectral changes over a range of wavelengths between 800 nm – 200 nm for the reactions between the solutions of the complexes and the nucleophiles. The predetermined wavelengths selected for the stopped flow spectrophotometric and UV-visible kinetic analysis are reported in Table SI 5.1, in the supporting information (ESI‡). All kinetic reactions were initiated by mixing equal volumes of the ligand and complex solutions directly in the stopped-flow and into thermally equilibrated tandem cuvettes used in the UV-visible spectrophotometer for kinetic analysis. The temperature dependence reactions were carried out within a range of 20 °C to 40 °C with 5 °C intervals for all the reactions. All the kinetic traces for concentration and temperature dependence were of excellent fit to a single-exponential decay function. The *pseudo*-first-order rate observed, $k_{obs(1/2)}$, were calculated as the average value of 6-8 independent runs and triplicate measurements for stopped flow and Uv-visible spectrophotometric methods, respectively. The second-order rate constants, $k_{(1/2)}$, for the reaction of each metal complex with a specific nucleophile concentration were obtained from a slope of a linear regression of a plot of $k_{obs(1/2)}$ versus nucleophile concentration using OriginPro 9.1® software.[76]

5.3 Results

5.3.1 X-ray Crystal Structure

The molecular structure of the **Pd(4-Me-PBI)Cl (**$C_{20}H_{16}ClN_5Pd$) complex, was confirmed by X-ray crystal structure determination. The crystal suitable for crystallographic analysis was grown from slow evaporation of chloroform solution. The crystallographic data, data collection and

structural refinement parameters of **Pd(4-Me-BPI)Cl** are summarized in Table 5.1, while the molecular structure is shown in Figure 5.2. In addition, the selected bond lengths and angles are presented in Table 5.2.

Table 5. 1 Crystal data and structure refinement parameters

	Pd(4-Me-BPI)Cl
Molecular formula	$C_{20}H_{16}ClN_5Pd$
M_r	468.23
Crystal size/ mm^3	0.340 x 0.220 x 0.140
T/K	100(2)
λ/ Å	0.71073
Crystal system	Monoclinic
Space group	P21/n
a/Å	8.7230(5)
b/Å	21.0417(12)
c/Å	10.1571(6)
α/º	90
β/º	110.189(2)
γ/º	90
V/ $Å^3$	1749.76(18)
Z	4
D_c /Mg m^{-3}	1.777
μ/ mm^{-1}	1.229
F(000)	936
θ range/º	1.936 - 27.495
Reflections collected (independent)	15931 (3964)
R_{int}	0.0239
No. of parameters (restraints)	246 (1)
R indices (all data)	R_1=0.0218, wR_2=0.0508
Goodness-of-fit on F^2	1.044
Max, Min Δρ/e $Å^{-3}$	0.469, - 0.616

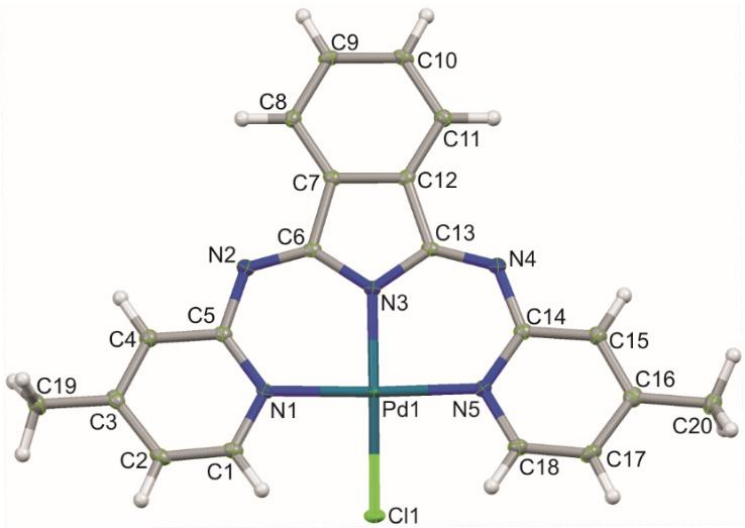

Figure 5. 2 Molecular structure of **Pd(4-Me-PBI)Cl** with atom numbering scheme. The displacement ellipsoids of atoms are shown at the 50% probability level.

Table 5. 2 Selected bond angles and bond lengths for X-ray and DFT for **Pd(4-Me-PBI)Cl**.

	X-ray	DFT
Bond lengths (Å)		
Pd1 – N1	2.057(6)	2.090
Pd1 – N3	1.964(1)	2.004
Pd1– N5	2.061(2)	2.090
Pd1 – Cl1	2.339(1)	2.480
Angles (º)		
N1 – Pd1 – Cl1	91.55(4)	91.75
N3 – Pd1 – Cl1	165.27(5)	164.26
N5 – Pd1 – Cl1	91.47(4)	91.76
N1 – Pd1 – N3	89.27(6)	89.62
N1 – Pd1 – N5	172.17(6)	169.68
N3 – Pd1 – N5	89.64(6)	89.62

In the molecular structure of **Pd(4-Me-PBI)Cl**, the 4-methylated BPI tridentate ligand coordinates palladium(II) metal ion through the three nitrogen atoms N1, N3 and N5 at distances

of 2.057(6), 1.964(1) and 2.061(2) Å, respectively. The fourth coordination site of the near square planar geometry is occupied by the chloride atom which is covalently bonded at a distance of 2.339(1) Å. These bond distances are within the range reported for other related X-ray crystal structures of Pd(II) complexes of 1,3-bis(2-arylimino)isoindolines derivatives. [6, 11, 66, 77] The bond distance of the central Pd–N3 is noticeably shorter than the other two Pd–N bonds, and this is attributed to the increased ionic nature of the bond [11] as a result of largely localised negative charge at the N3 of the isoindoline head.[78]

The complex adopts distorted square planar coordination geometry than a normal uncharged N around the metal (since N3 is indeed a deprotonated negatively charged atom). This is evidenced by the chloropalladium unit slightly displaced from the molecular plane of the three N atoms by an angle of 19.59º. Also, the N1–Pd–N5 makes an of angle 172.17(6)º which slightly deviates from linearity (180º). The deviation is even further pronounced by the N3–Pd–Cl1 angle, 165.27(5)º, attributed to the repulsive interaction between the *ortho*-hydrogen atoms of the pyridyl groups and the coordinated chloride ligand.[11] These bond angles are comparable to the DFT calculated angles of N1–Pd–N5 (169.68º) and N3–Pd–Cl1 (164.26º) as presented in Table 5.2. Unlike the terpy type of ligands, the BPI ligands form two strain free six-membered chelates with the central metal atom which in turn lowers ring strain labilising the labile chloride ligand of the complexes. The angle between the planes of the two six-membered chelates coordinated to the Pd metal is 0.90º assuring that the coordinated portion of the ligand is almost flat. The crystal packing shows an inversion dimer with no metal-metal interactions as the Pd–Pd distance being 6.3601(6) Å is larger than 4 Å.[79] Also, within the crystal packing, the molecules is characterised by non-conventional contacts C20–H···Cl1 and C17–H···C9, which may indicate weak van der Waals intermolecular interactions as shown in Figure S1 5.22 in the supporting information (ESI‡). In addition, **Pd(4-Me-PBI)Cl** packs into stacked arrangement coaxial to crystallographic

axis as illustrated in Figure S1 5.23 in the supporting information (ESI‡). This type of packing is comparable to that reported for the X-ray structure of a structurally related Pd(II) complex.[66]

5.3.2 DFT-Calculated Optimized Structures

The HOMO, LUMO geometry optimized structures and selected calculated data are presented in Tables 5.3 and 5.4 respectively. Frontier orbital mappings in Table 5.3 shows that the LUMOs are distributed all over the atoms of the complexes, while the HOMOs predominantly by the orbitals derived from the pyridylimino-3,4-pyrrolate moieties of the complexes which appears to dictate their HOMO energies. These frontier orbital mappings compare well with those of Pt(II) complexes.[7, 13] The HOMOs are contributed by the 3p-orbitals of chlorine and 4d-orbitals of Pd atoms together with the π-system of the pyridyl and imino-pyrrolate subunits of the ligand. The HOMO energy increases across the series of Pd(II) complexes (Table 5.4) as the BPI is alkylated and benzannulated at the cis-positioned pyridyl ring and its isoindoline's head is extended by an additional phenyl ring. The HOMO energy is raised through alkylation from **Pd(BPI)Cl** (-6.209 eV) to **Pd(4-Me-PBI)Cl** (-6.133 eV). Similarly, the HOMO energy is raised with each successive increase in benzannulation from **Pd(BPI)Cl** (-6.209 eV) to **Pd(BBPI)Cl** (-6.197 eV) and **Pd(BII)Cl** (-6.104 eV)**.** Thus, alkylation and benzannulation of the core BPI ligand destabilizes the HOMO energy through σ-inductive donation of electron density into the chelate rings.

Table 5. 3 The DFT optimized HOMO, LUMO frontier molecular orbitals and planarity for the complexes at B3LYP/LANL2DZ theory level (Iso value = 0.02).

Complex structure	HOMO maps	LUMO maps	Planarity
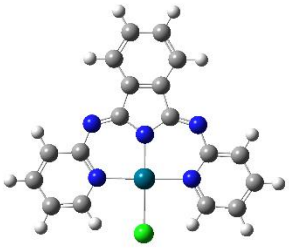 **Pd(BPI)Cl**	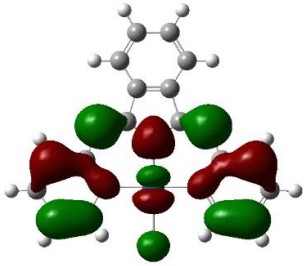	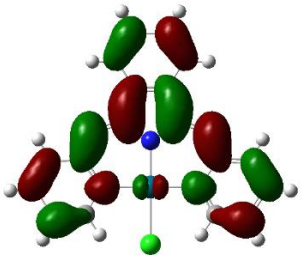	
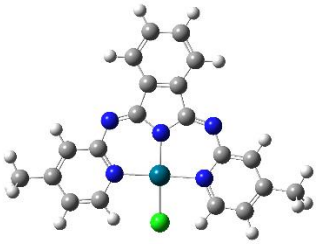 **Pd(4-Me-PBI)Cl**	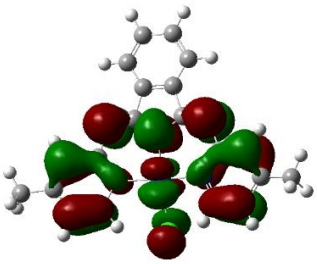	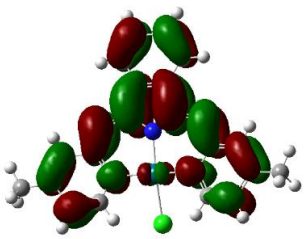	
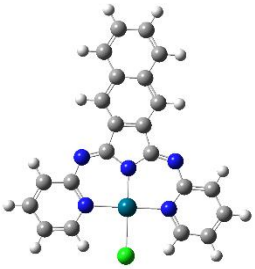 **Pd(BBPI)Cl**	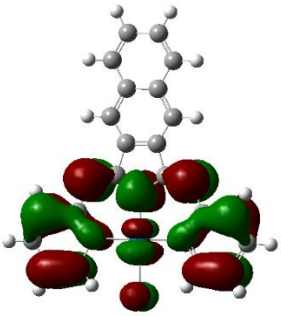	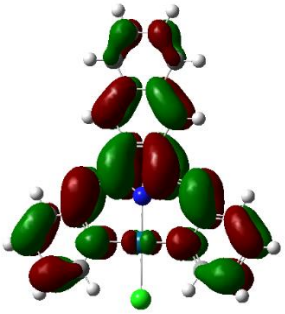	
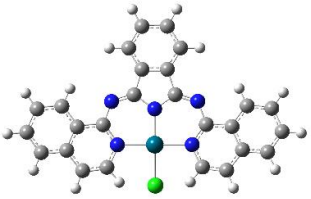 **Pd(BII)Cl**	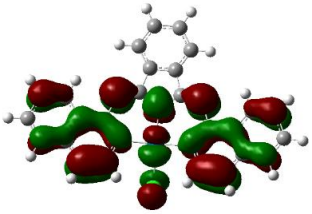	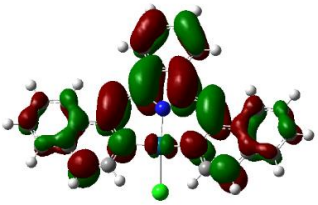	

Table 5. 4 Summary of the calculated parameters for complexes studied

Property	**Pd(BPI)Cl**	**Pd(4-Me-PBI)Cl**	**Pd(BBPI)Cl**	**Pd(BII)Cl**
NBO Charges				
Pd^{2+}	0.573	0.557	0.573	0.566
Cl^{-}	-0.545	-0.560	-0.544	-0.562
Electrophilicity index (ω)	6.544	6.366	6.245	7.400
Bond lengths (Å)				
Trans- N3–Pd	2.009	2.004	2.011	1.997
Cis- N–Pd	2.137	2.090	2.138	2.090
Pd–Cl	2.479	2.479	2.478	2.484
H⋯Cl	2.24	2.41	2.24	2.43
Energy gap (eV)				
LUMO (eV)	-2.982	-2.917	-2. 891	-3.180
HOMO (eV)	-6.209	-6.133	-6.197	-6.104
$\Delta E_{LUMO-HOMO}$	3.227	3.216	3.306	2.912
Bond angles (º)				
Trans N3 – Pd – Cl	179.998	164.264	179.989	162.572
Cis N1 – Pd – N5	178.764	169.677	178.999	169.027
Deviation of Pd – Cl from the main axis	0	13.13	0	34.56
Dipole moment (Debye)	3.445	4.765	4.677	6.687

The LUMOs, have orbital contributions from an admixture of π* molecular orbitals of the pure carbon moieties (phenylene for **Pd(BPI)Cl, Pd(4-Me-PBI)Cl** and **Pd(BII)Cl** or naphthalene for **Pd(BBPI)Cl**) and the N-containing moiety[13] with only a small contribution from the 4d-orbitals of the Pd atom. The orbital interactions raises the LUMO energy going from **Pd(BPI)Cl** (-2.982 eV) to **Pd(4-Me-PBI)Cl** (-2.917 eV) to **Pd(BBPI)Cl** (-2.891 eV) while it significantly lowers

that of **Pd(BII)Cl** (-3.180 eV) so as to give a lower LUMO energy leading smaller HOMO-LUMO gap for **Pd(BII)Cl** in comparison to the rest of the complexes.

The HOMO-LUMO energy gap increases in the order **Pd(BII)Cl < Pd(4-Me-PBI)Cl < Pd(BPI)Cl < Pd(BBPI)Cl** as can be seen in the calculated values in Table 5.4 which in effect have minimal influence in determining their reactivity trend. Therefore it can be noted that alkylation destabilizes the LUMOs of **Pd(4-Me-PBI)Cl** while benzannulation destabilizes that of **Pd(BBPI)Cl,** but stabilizes that of **Pd(BPI)Cl** and **Pd(BII)Cl**.

The calculated geometrical angles around the Pd(II) centres of **Pd(BPI)Cl** and **Pd(BBPI)Cl** show near perfect square planar geometry, while those of **Pd(BII)Cl** and **Pd(4-Me-PBI)Cl** deviates significantly due to steric repulsions between the *ortho*-hydrogen atoms at the pyridyl rings and chloride atom.[7, 11]

5.3.3 Kinetic Analysis

The rate of substitution reactions of the labile chloride ligand by the thiourea nucleophiles proceeded *via* two consecutive steps for all the complexes except **Pd(BII)Cl** which proceeded in a single step. The second order rate constant, k_1 (first step) was monitored using the stopped flow, while UV-visible spectroscopy was used to monitor k_2 (second step). The wavelength at which the kinetic measurements would be monitored were predetermined spectrophotometrically by recording the spectral changes over a range of wavelengths between 800 nm – 200 nm of a reaction between the solutions of the complex and the nucleophile. Wavelengths ranging between 525 nm – 355 nm and 426 nm – 350 nm were picked and used for kinetic measurements in the stopped flow (fast reaction) and UV-visible (slow reaction) respectively, depending on the specific complex and the nucleophile. The wavelengths used for kinetic measurements are tabulated in Table S1, supporting information (ESI‡).

A representative stopped-flow kinetic trace for the first step and the UV-visible spectral changes together with the kinetic trace in the inset for the second step reaction between **Pd(BPI)Cl** and **Tu** are shown in Figures 5.3 and 5.4, respectively.

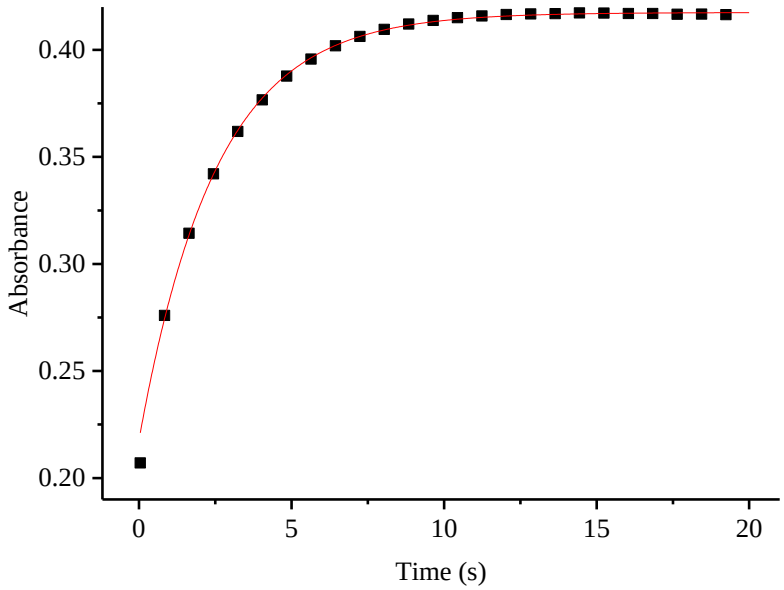

Figure 5. 3 Stopped flow kinetic trace at 360 nm for the first step reaction of **Pd(BPI)Cl** (1.0×10^{-4} M) with **Tu** (3.0×10^{-3} M) at 308 K.

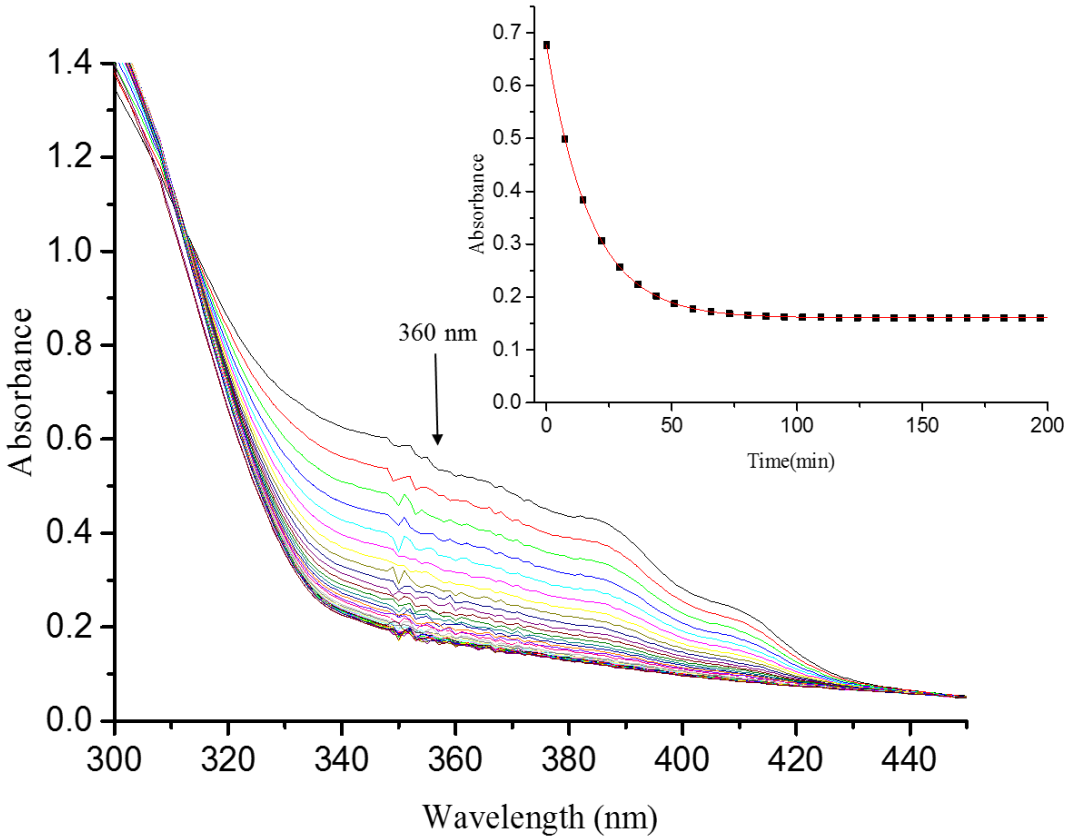

Figure 5. 4 UV-visible spectra for the second step reaction of **Pd(BPI)Cl** (1.0×10^{-4} M) with Tu (3.0×10^{-3} M). Inset; single exponential kinetic trace at 360 nm at 298 K.

The average observed rate constants, $k_{obs(1/2)}$, plotted against the concentration of the entering nucleophiles gave straight line plots with zero intercepts which indicated that the reverse or solvolytic pathway was absent or insignificant. Representative plots of $k_{obs(1/2)}$ versus concentration of the nucleophiles is shown in Figure 5.5 for the reactions of **Pd(BBPI)Cl,** similar plots for the other complexes are shown in Figures SI 5.24 – 5.28 while the values of k_{obs} with their respective nucleophile concentrations are tabulated in Tables SI 5.2 – 5.8 in the supporting information, ESI‡). Thus, the dependency on *pseudo*-first-order rate constant for substitution reactions can be stated as in *Equation 5.1*.

$$k_{obs(1/2)} = k_{(1/2)}\,[Nu] \qquad Nu = \mathbf{Tu}, \mathbf{Dmtu}, \mathbf{Tmtu} \qquad (5.1)$$

The values of the second order rate constants, $k_{(1/2)}$, are summarized in Table 5.5.

a

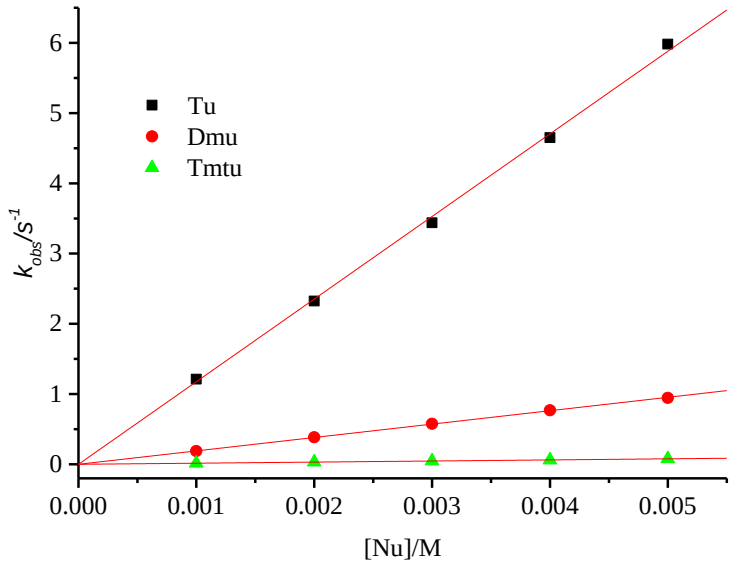

b

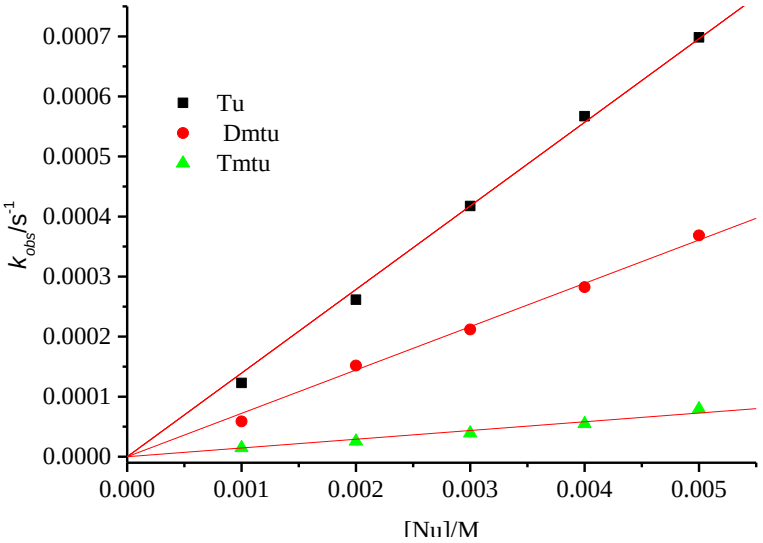

Figure 5. 5 Dependence of $k_{obs(1\ or\ 2)}$ on the nucleophile concentrations reactions with **Pd(BBPI)Cl** in ethanol solvent, I = 0.01 M CF_3SO_3H, T = 298 K (**a**) First step (chloride substitution) (**b**) Second step (dechelation).

Table 5. 5 k_1 and k_2 data for the reactions of the Pd(II) complexes with the nucleophiles in ethanol, I = 0.01M CF_3SO_3H, T = 298 K.

Complexes	Nucleophiles	k_1($M^{-1}s^{-1}$)	k_2($\times 10^{-2}$ $M^{-1}s^{-1}$)
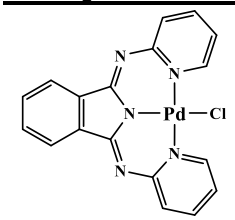 **Pd(BPI)Cl**	**Tu**	2046 ± 23	53 ± 0.6
	Dmtu	848 ± 7	40 ± 0.4
	Tmtu	319 ± 2	26 ± 0.3
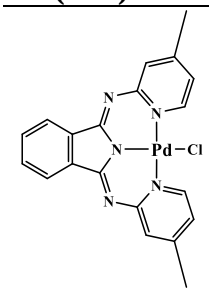 **Pd(4-Me-BPI)Cl**	**Tu**	1322 ± 4	16 ± 0.3
	Dmtu	288 ± 2	12 ± 0.2
	Tmtu	69 ± 1	5 ± 0.2
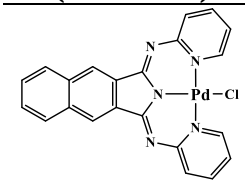 **Pd(BBPI)Cl**	**Tu**	1176 ± 10	14 ± 0.2
	Dmtu	191 ± 1	7 ± 0.1
	Tmtu	16 ± 0.1	1.5 ± 0.1
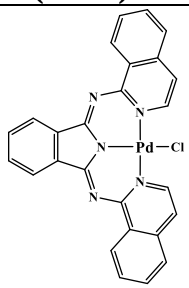 **Pd(BII)Cl**	**Tu**	4.22 ± 0.03	-
	Dmtu	1.01 ± 0.01	-
	Tmtu	0.35 ± 0.004	-

- No second step observed

The temperature dependence of $k_{1/2}$ was studied within a range of temperatures between 20 – 40º C at 5º C intervals and Eyring *Equation 5.2* [80] was used to calculate activation parameters, enthalpy **(**$\Delta H^{\neq}$) and entropy ($\Delta S^{\neq}$) from the slopes and intercepts from the graphs of ln $\left(\frac{k_{1/2}}{T}\right)$ versus $\frac{1}{T}$, respectively.

$$\ln\left(\frac{k_{1/2}}{T}\right) = -\frac{\Delta H^{\neq}{}_{\frac{1}{2}}}{RT} + \left(23.8 + \frac{\Delta H^{\neq}{}_{\frac{1}{2}}}{R}\right) \tag{5.2}$$

where T and R represent temperature and gas constant, respectively. A representative Eyring plot for **Pd(BII)Cl** is presented in Figure 5.6; similar plots are also shown in Figures SI 5.29 – SI 5.34 and the values $\frac{1}{\mathrm{T}}$ and their respective $ln\left(\frac{k_2}{T}\right)$ are tabulated in Tables SI 5.9 – 5.15 in the supporting information (ESI‡), while the calculated activation parameter data are summarized in Table 5.6.

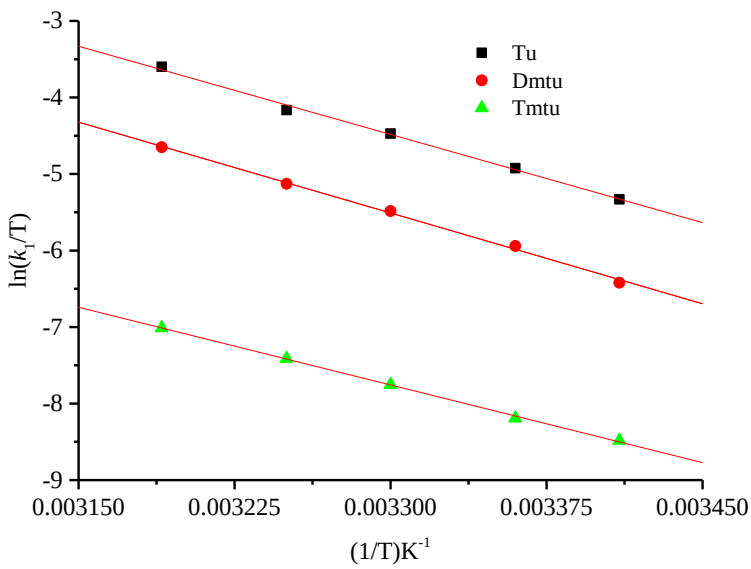

Figure 5. 6 Eyring plots of the reactions of **Pd(BII)Cl** with the nucleophiles

Table 5. 6 Thermodynamic parameters

Complexes	Nucleophiles	Enthalpy (kJ mol^{-1})		Entropy (JK^{-1} mol^{-1})	
		$\Delta H_1^{\neq}$	$\Delta H_2^{\neq}$	$\Delta S_1^{\neq}$	$\Delta S_2^{\neq}$
Pd(BPI)Cl	**Tu**	33 ± 2	70 ± 1	-72 ± 7	- 49 ± 3
	Dmtu	50 ± 2	41 ± 1	-21 ± 8	- 132 ± 3
	Tmtu	41 ± 1	54 ± 1	-104 ± 5	- 71 ± 4
Pd(4-Me-BPI)Cl	**Tu**	56 ± 3	65 ± 3	- 25 ± 10	- 59 ± 9
	Dmtu	49 ± 1	60 ± 1	- 41 ± 3	- 80 ± 4
	Tmtu	51 ± 2	65 ± 1	- 50 ± 5	- 52 ± 3
Pd(BBPI)Cl	**Tu**	53 ± 2	59 ± 1	-20 ± 7	- 76 ± 2
	Dmtu	53 ± 1	57 ± 3	-19 ± 5	- 79 ± 8
	Tmtu	47 ± 1	61 ± 2	-65 ± 3	- 57 ± 6
Pd(BII)Cl	**Tu**	64 ± 2	-	-24 ± 7	-
	Dmtu	66 ± 2	-	-27 ± 6	-
	Tmtu	56 ± 1	-	-77 ± 3	-

Data in Table 5.5 shows that the second-order rate constants, k_1 is 3-4 orders of magnitude larger than those of k_2 for all the reactions. The first step represents the nucleophilic substitution of the coordinated chloride ligand of the Pd(II) complexes. The second step has been postulated to be the dechelation of the ligands off the Pd metal centres of the first three Pd(II) complexes of BPI. The coordinated thiourea nucleophiles induces dechelation of the BPI ligand possibly through the *trans-effect* or steric influence to form $[Pd(Nu)_2BPI]^{1+}$ at the rate of k_2. This phenomenon have been reported in a structurally related dinuclear Pt(II) complexes coordinated to tridentate N^N^N ligands [54, 81-83] and dinuclear Pt(II) complexes coordinated to N^N bidentate ligands.[84-87] The third and fourth Nu species acts in a rapid concert and further substitute the remaining

coordinated BPI ligand resulting into complete release of the free tridentate BPI ligand and formation of $[Pd(Nu)_4]^{2+}$ species.

To confirm the dechelation process, the coordination shift of 6-pyridyl protons of the complex from the reaction of 6 equivalents of **Tu** with **Pd(4-Me-BPI)Cl** in tetrahydrofuran-d_8 solvent was monitored by ^{1}H NMR spectroscopy. It has been observed that the coordination shift of the 6-pyridyl protons of the coordinated BPI ligand to Pd(II) metal resonates approximately at 9.5 ppm while that of the free ligand resonates approximately at 8.4 ppm alongside the N–H resonance of the isoindole unit.[11] The array of spectra recorded during the reaction and the spectrum of the free **4-Me-BPI** ligand are presented in Figure 5.7.

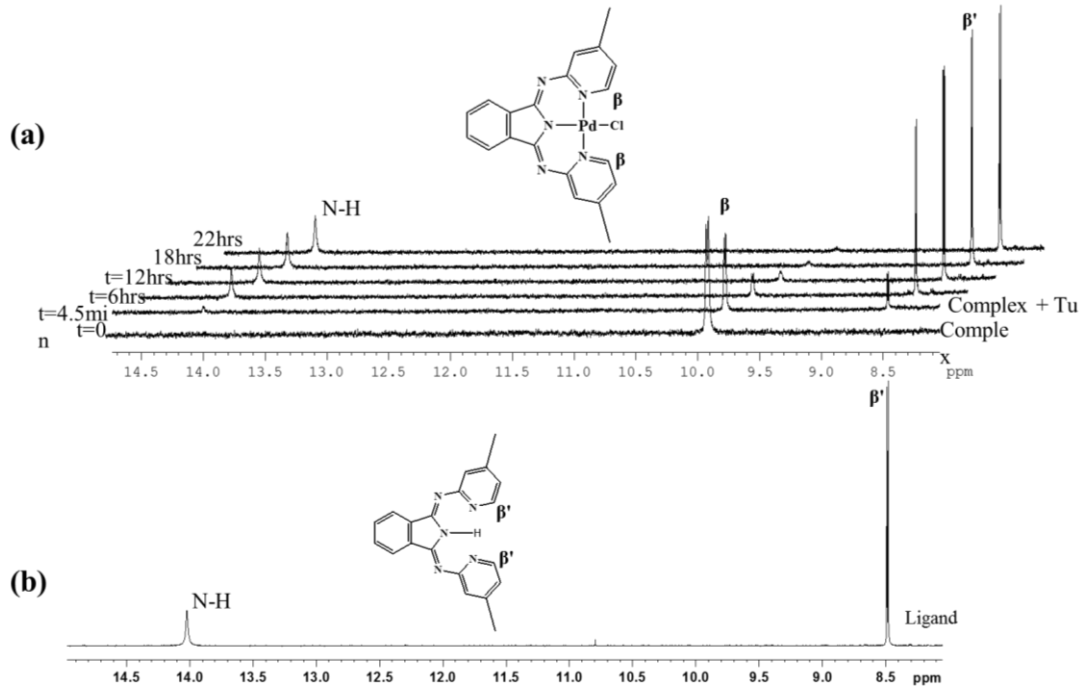

Figure 5. 7 **(a)** Time-dependent changes in the ^{1}H NMR chemical shifts of the $H_\beta/H_{\beta'}$ and N–H protons for the reaction between **Pd(4-Me-BPI)Cl** and **Tu** (6 equivalents) in tetrahydrofuran-d_8. (**b**) ^{1}H NMR of the free ligand showing only the $H_{\beta'}$ proton and N-H chemical shifts.

Figure 5.7 (a) shows the resonance of the $H_{\beta}/H_{\beta'}$ protons of the coordinated ligand in **Pd(4-Me-BPI)Cl**. At time, t = 0, a signal due to the H_{β} starting complex **Pd(4-Me-BPI)Cl** before mixing with the **Tu** resonates at 9.78 ppm (doublet). Within 4.5 min after the onset of the reaction two other more signals emerge at 8.49 ppm (doublet) and at 14.02 ppm (broad-singlet) for the $H_{\beta'}$ and the N-H respectively, belonging to the free ligand (Figure 5.7(b)), forming in the mixture. The intensity of the signal H_{β} (9.78 ppm) protons in the coordinated ligand decreases gradually and completely disappears after 22 hours, while the $H_{\beta'}$ (8.49 ppm) protons of the free **4-Me-BPI** emerged with increasing intensity over the same duration. A new peak signal resonating at 14.02 ppm due to the proton at the isoindoline unit (N–H) appeared and its intensity increased in equal proportion to those of the $H_{\beta'}$ of the pyridyl rings of the free ligand. These observations suggest complete decoordination (dechelation of the tridentate ligand) induced by the *trans-effect* or steric effect of the coordinated sulfur containing thiourea nucleophile as will be discussed later. This effect decreases the chelate stability of the complex leading to complete decoordination. Thus, the mechanism of the substitution is as proposed in scheme 5.1.

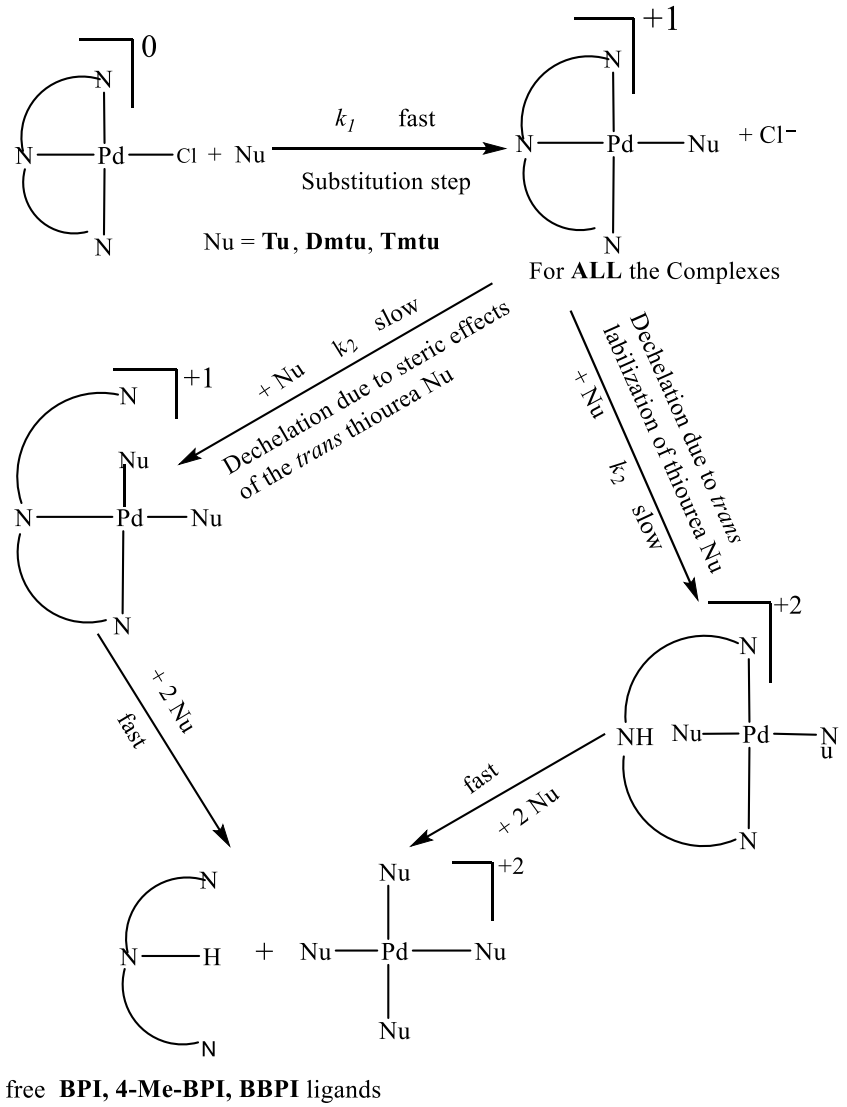

free **BPI, 4-Me-BPI, BBPI** ligands

Scheme 5. 1 Possible proposed mechanism for the reaction between Pd(II) complexes with thiourea nucleophiles in ethanol, I = 0.01M CF_3SO_3H.

5.4 Discussion

In this study, the effect of alkylation and varying degrees of extended π-conjugation through benzannulation at various sites to the core ligand on the reactivity of Pd(II) complexes was investigated. The objective was to determine if these effects on the ligand framework would stabilize the reactive Pd metal thereby controlling its reactivity. Starting from **Pd(BPI)Cl**, the complexes were varied by attaching methyl substituent group in the *cis*-ligand at the 4-pyridyl position for **Pd(4-Me-PBI)Cl** and benzannulation at the *trans*-isoindoline unit for **Pd(BBPI)Cl**

and *cis*-pyridyl unit for **Pd(BII)Cl**. The results from this investigation show that the reactivity of Pd metal can be tuned and controlled. Its stability after substitution is only controllable if the rate of the reaction is slowed to a single digit.

The data in Table 5.5 shows that the second order rate constant, k_1, (first step) for the substitution of the chloride ligand from the Pd(II) complexes by **Tu** decreased in the order **Pd(BPI)Cl > Pd(4-Me-PBI)Cl > Pd(BBPI)Cl > Pd(BII)Cl.** A Similar trend was also noted in the k_2 values (for the second step) for all the complexes except for **Pd(BII)Cl.** Quite surprising was the reactivity of **Pd(BII)Cl** given that its N^N^N ligand is the most conjugated.[39, 43] One would have expected it to have the highest k_1 value since its electrophilicity index is the highest (Table 5.4). The lower rates of substitution in **Pd(BII)Cl** is due to the *cis*-benzannulation effect on the ligand of the complex as will be discussed later. The observed reactivity of the modelled Pd(II) complexes can be accounted for in terms of their electronic and steric properties.

The reactivity of **Pd(BPI)Cl** was compared with that of **Pd(4-Me-PBI)Cl** in order to understand the role played by alkylation. The structural difference between the complexes is the introduction of methyl substituent in the 4-position of the *cis*-pyridyl ring in **Pd(4-Me-PBI)Cl**. This difference in the ligand framework is responsible for decreasing the reactivity of the metal in **Pd(4-Me-PBI)Cl** by factors in the range of 2–5 for all the nucleophiles in comparison to **Pd(BPI)Cl**. Thus, methylation at the 4-position of the *cis*-pyridyl rings of the BPI decreases the reactivity of **Pd(4-Me-PBI)Cl** by increasing the electron density around the metal centre through σ-donation as well as inductive effects [41] into the aromatic pyridyl ring, reducing the π-acceptor property of the ligand and the positive charge at the metal centre. This retards the rate of substitution of the chloride ligand from the complex [40, 75] by repelling the incoming nucleophile.[88]

To pin down the role played by electronic effects in determining the reactivity trend. The reactivity of **Pd(BPI)Cl** was compared with that of **Pd(4-Me-PBI)Cl** and **Pd(BBPI)Cl**. The high lability of **Pd(BPI)Cl** in comparison to the complexes is attributed to its ligand having a stronger π-acceptability property, as a result, electron density is readily back donated from the filled d-orbitals of the Pd metal into the empty nonbonding or antibonding(π*) orbitals of the in-plane expanded π-surface of the ligand. This is supported by the DFT calculated data (Table 5.4) where the electrophilicity of **Pd(BPI)Cl** is higher than that of **Pd(4-Me-PBI)Cl** and **Pd(BBPI)Cl**, thus making the nucleophilic attack facile. Benzannulation (addition of the phenyl ring) on the isoindoline chelate unit of the BPI ligand extends the π-surface in the ligand of **Pd(BBPI)Cl**, but leads to a reduction of the reactivity by factors in the range of 2 - 20 for all the three nucleophiles relative to **Pd(BPI)Cl**. This is contrary to what would be expected (increased reactivity) on the basis of increased π-bonding into the ligand due to its extended π-conjugation [41, 44, 53, 62, 75, 88, 89] as well as *trans*-labilization effect.[42, 90-92] The resultant naphthalene moiety caused by the benzannulation increases the π/σ-donation property of the *trans*-ligand into the chelate ring which reduces the π-acceptability of the entire ligand, leading to lower rates of substitution.

In addition, the low reactivity of **Pd(BBPI)Cl** is caused by the nature of its HOMO-LUMO interactions within the complex due to a contribution from the naphthalene moiety of the ligand, than the contribution from the phenyl moiety in the ligands of **Pd(BPI)Cl** and **Pd(4-Me-PBI)Cl**. Although the naphthalene in **Pd(BBPI)Cl** has a larger π-conjugation system, the energy march between the π* orbitals of the naphthalene and the π* orbitals of the N-containing moiety is worse in this complex than the other two complexes as a result of less significant orbital interaction,[13] thus resulting in higher level of the LUMO and hence a larger HOMO-LUMO gap (Table 5.4).

In understanding the distinctive role played by the *trans*- and *cis*-benzannulation on the BPI ligand of the complexes, the reactivity of **Pd(BPI)Cl** was compared with that of **Pd(BBPI)Cl** and **Pd(BII)Cl**. The *trans*-benzannulation of the BPI reduces the reactivity by factors already mentioned, while the *cis*-benzannulation on the pyridyl rings magically enhances the reduction of the rate of substitution by factors in the range of 500 – 900 for all the nucleophiles. The reactivity of **Pd(BII)Cl** is the slowest despite its higher electrophilicity index (Table 5.4) and its **BII** ligand having more aromatic conjugated properties than the ligand of the other complexes. This trend can be explained in terms of their ligands' properties imposing effects on the complexes.

Absorption studies of **BPI, BBPI** and **BII** ligands from the literature[7] showed energetic metal-to-ligand and intraligand charge transfer (ML-ILCT) following the order **BII < BPI < BBPI**. This was in agreement with the order of their reduction potentials.[13] This means that **BII** ligand is the strongest π-acceptor of the three. Therefore, one would expect that **Pd(BII)Cl** should be the most reactive. Nonetheless, the results show that it is the least reactive. This discrepancy in reactivity can be accounted for by the steric effect of the complex. From the planarity structure of **Pd(BII)Cl** in Table 5.3, the Pd–Cl fragment experiences more out of plane distortion than the other complexes. This deviation causes steric hindrance to the incoming nucleophile which significantly lower rate of the substitution in **Pd(BII)Cl**. Therefore, the reactivity of **Pd(BPI)Cl** is higher because it is more electrophilic than **Pd(BBPI)Cl** while that of **Pd(BII)Cl** is the slowest due to steric effect by the *cis*-benzannulation. It has been reported that the steric effect *cis* (steric *cis*-effect) to the leaving group is usually stronger and is able to dominate over electronic factors[47] which is in agreement with the observed reactivity of **Pd(BII)Cl** in this study.

Alkylation at the 4-position and benzannulation at the 3, 4-position of the *cis*-pyridyl ring for **Pd(4-Me-PBI)Cl** and **Pd(BII)Cl**, respectively introduces steric effects into the complexes in comparison to the other two which affect their reactivities. The Pd–Cl fragment of the complexes deviates from the main axis by 13.13º and 34.56º for **Pd(4-Me-PBI)Cl** and **Pd(BII)Cl**, respectively (Table 5.4). This deviation is caused by the repulsive interactions between the *ortho*-hydrogens atoms of the pyridyl rings [H⋯Cl; **Pd(BII)Cl** (2.43 Å) and **Pd(4-Me-PBI)Cl** (2.41 Å)] and the coordinated chloride ligand due to the steric congestion between the two atoms within the complexes. This interaction introduces steric hinderances to the incoming nucleophiles. **Pd(4-Me-PBI)Cl** is more reactive because it is less sterically hindered than **Pd(BII)Cl**. It can therefore be concluded that the *cis*-benzannulation is stronger in introducing steric hinderance, stabilizes the complex and hence significantly lower reactivity than the alkylation at the *cis*-pyridyl ring of isoindolatopalladium complexes.

The second step, for the substitution reactions of **Pd(BPI)Cl, Pd(4-Me-PBI)Cl** and **Pd(BBPI)Cl** with the nucleophiles is a complete substitution induced dechelation of the bis(2-pyridylimino)isoindoline based ligands. This was representatively confirmed for the reaction of **Pd(4-Me-PBI)Cl** with **Tu** by ^{1}H NMR spectroscopy. The dechelation process was postulated to possibly occur in two ways, given that the thiourea nucleophiles are of different steric demands. First, it could have been initiated by the coordinated thiourea nucleophile *trans* to the amine of the isoindoline unit of the spectator ligand. Because of the strong *trans-effect* of the sulfur atom, the amine of the isoindoline unit is slowly substituted by another molecule of the thiourea nucleophile in the reaction system. Such *trans-effect* of thiourea have been observed in the dechelation of dinuclear Pt(II) complexes where NH_3 *trans* to the coordinated thiourea was substituted by another thiourea molecule before complete detachment of the metal.[84, 93] The increase in the number of sulfur bound molecules in the Pd(II) atom weakens the Pd–N bonds

with the pyridyl units which enhances simultaneous substitution of the pyridyl units of the ligand resulting into the release of the free ligand and formation of $[Pd(Nu)_4]^+$ species.

The second possible way could have been due to the steric hinderance caused by the already coordinated thiourea nucleophile, from the first step, leading to the substitution of one of the pyridyl unit of the ligand as was observed in a related N^N^N dinuclear Pt(II) complexes.[55, 56, 81, 82] The number of sulfur bound atoms to the Pd(II) is thus increased to two which are *cis* to each other but are *trans* to the amine of the pyridyl and the isoindoline units, respectively. The strong *trans-effect* of the two sulfur atoms *trans* to the amine of the pyridyl unit and isoindoline unit, synergistically enhances rapid simultaneous substitution of the remaining pyridine and the isoindoline units leading to the release of the free ligand and formation of $[Pd(Nu)_4]^+$ as the products of the dechelation process. However, it is noted that the rate at which the substitution induced dechelation of the BPI ligands proceed in the same order as that of the substitution of the chloride leaving group. This is because the rate of the nucleophilic attack is still affected by the BPI ligands in the intermediate species formed from the substitution of the chloride.

No evidence of a similar dechelation of the **BII** ligand was observed for the reactions of **Pd(BII)Cl** with the thiourea nucleophiles possibly because the complex is more thermodynamically and kinetically stabilized by the steric effect than the rest of the complexes. Another reason is because the **BII** ligand therein is a strong π-acceptor hence it withdraws electron density from the metal orbitals. This enhances the interaction between the d-orbitals of the metal and the p-orbitals of the ligands leading to shortening of the Pd–N3 bond (Table 5.4) than the rest of the complexes making the detachment of Pd metal from the ligand very difficult. In addition, the dechelation may have been prevented by the shielding effect of the ligand towards induced decoordination of itself by the nucleophile.

The activation entropies ($\Delta S^{\#}_{1/2}$) are negatively large while those of enthalpies ($\Delta H^{\#}_{1/2}$) are positive for all the reactions in this study (Table 5.6). Thus, both the chlorido substitution and nucleophilic induced dechelation proceed by an associative substitution mechanism. This is quite common in the reactions of square-planar d^8 complexes.[94 95, 96]

5.5 Conclusions

Alkylation at the *cis*-positioned pyridyl rings of BPI ligand decelerates the reactivity of the **Pd(BPI)Cl** through electronic and steric effects by factors between 2 – 5. Benzannulation at the *trans*-isoindoline head further weakens the reactivity of **Pd(BBPI)Cl** by factors of 2 – 20. The *cis*-benzannulation magically lowers the reactivity of palladium metal in **Pd(BII)Cl** by upto approximately 2 – 3 orders of magnitude relative to **Pd(BPI)Cl** through steric effects. Whereas, benzannulation on the *trans*-position maintains the planarity, that on the *cis*-position distorts the planarity through steric repulsion which dominates in determining the reactivity over electronic factors in **Pd(BII)Cl**. Therefore, extended π-conjugation through benzannulation on the *cis*-position is more powerful in controlling the reactivity of Pd(II) metal centre than that on the *trans*-position. The reactivity trend is opposite to the increasing π-surface which is linked to the destabilization of the HOMOs as illustrated by the DFT calculations. Nucleophilic-induced dechelation of the BPI ligands of all the complexes except that of **Pd(BII)Cl** occurs upon successful substitution of the chloride ligand indicating that these type of Pd(II) complexes may be unstable in biological systems. The stability of **Pd(BII)Cl** makes it a suitable candidate for such biological applications. The thermodynamic parameters confirm that the reaction mechanism is associative in nature.

5.6 References

1. J. Elvidge and R. Linstead, *Journal of the Chemical Society (Resumed)*, 1952, 5000-5007.
2. J. Elvidge and R. Linstead, *Journal of the Chemical Society (Resumed)*, 1952, 5008-5012.
3. P. Clark, J. Elvidge and R. Linstead, *Journal of the Chemical Society (Resumed)*, 1953, 3593-3601.
4. D. M. Baird, W. Maehlmann, R. D. Bereman and P. Singh, *Journal of Coordination Chemistry*, 1997, **42**, 107-126.
5. J. D. Dang and T. P. Bender, *Inorganic Chemistry Communications*, 2013, **30**, 147-151.
6. B. L. Dietrich, J. Egbert, A. M. Morris, M. Wicholas, O. P. Anderson and S. M. Miller, *Inorganic Chemistry*, 2005, **44**, 6476-6481.
7. K. Hanson, L. Roskop, P. I. Djurovich, F. Zahariev, M. S. Gordon and M. E. Thompson, *Journal of the American Chemical Society*, 2010, **132**, 16247-16255.
8. B. K. Langlotz, J. Lloret Fillol, J. H. Gross, H. Wadepohl and L. H. Gade, *Chemistry-A European Journal*, 2008, **14**, 10267-10279.
9. M. B. Meder and L. H. Gade, *European Journal of Inorganic Chemistry*, 2004, **2004**, 2716-2722.
10. A. Scheja, D. Baabe, D. Menzel, C. Pietzonka, P. Schweyen and M. Bröring, *Chemistry-A European Journal*, 2015, **21**, 14196-14204.
11. B. Siggelkow, M. B. Meder, C. H. Galka and L. H. Gade, *European Journal of Inorganic Chemistry*, 2004, **2004**, 3424-3435.
12. K.-N. T. Tseng, J. W. Kampf and N. K. Szymczak, *ACS Catalysis*, 2015, **5**, 5468-5485.
13. H.-M. Wen, Y.-H. Wu, Y. Fan, L.-Y. Zhang, C.-N. Chen and Z.-N. Chen, *Inorganic Chemistry*, 2010, **49**, 2210-2221.
14. I. Sović, S. K. Pavelić, E. Markova-Car, N. Ilić, R. Nhili, S. Depauw, M.-H. David-Cordonnier and G. Karminski-Zamola, *European Journal of Medicinal Chemistry*, 2014, **87**, 372-385.
15. I. Sović, V. Stilinović, B. Kaitner, S. Kraljević-Pavelić, M. Bujak, K. Čuljak, P. Novak and G. Karminski-Zamola, *Journal of Molecular Structure*, 2011, **1006**, 259-265.
16. E. Pantoja, A. Gallipoli, S. van Zutphen, S. Komeda, D. Reddy, D. Jaganyi, M. Lutz, D. M. Tooke, A. L. Spek and C. Navarro-Ranninger, *Journal of Inorganic Biochemistry*, 2006, **100**, 1955-1964.
17. J. Reedijk, *Chemical Reviews*, 1999, **99**, 2499-2510.

18. T. Storr, K. H. Thompson and C. Orvig, *Chemical Society Reviews*, 2006, **35**, 534-544.
19. E. Wong and C. M. Giandomenico, *Chemical Reviews*, 1999, **99**, 2451-2466.
20. J. Lokich, *Cancer Investigation*, 2001, **19**, 756-760.
21. S. Shibata, *Neurologia Medico-Chirurgica*, 1990, **30**, 242-245.
22. E. Z. Jahromi, A. Divsalar, A. A. Saboury, S. Khaleghizadeh, H. Mansouri-Torshizi and I. Kostova, *Journal of the Iranian Chemical Society*, 2016, **13**, 967-989.
23. Ž. D. Bugarčić, J. Bogojeski and R. van Eldik, *Coordination Chemistry Reviews*, 2015, **292**, 91-106.
24. A. S. Abu-Surrah and M. Kettunen, *Current Medicinal Chemistry*, 2006, **13**, 1337-1357.
25. M. Marques, *ISRN Spectroscopy*, 2013, **2013**, 1 - 29.
26. J. Bogojeski, J. Volbeda, M. Freytag, M. Tamm and Ž. D. Bugarčić, *Dalton Transactions*, 2015, **44**, 17346-17359.
27. N. P. Barry and P. J. Sadler, *Chemical Communications*, 2013, **49**, 5106-5131.
28. B. Lippert, *Cisplatin: chemistry and biochemistry of a leading anticancer drug*, John Wiley & Sons, 1999.
29. S. van Zutphen and J. Reedijk, *Coordination Chemistry Reviews*, 2005, **249**, 2845-2853.
30. H. Zorbas and B. K. Keppler, *ChemBioChem*, 2005, **6**, 1157-1166.
31. D. Wang and S. J. Lippard, *Nature Reviews Drug Discovery*, 2005, **4**, 307-320.
32. Ž. D. Bugarčić, G. Liehr and R. van Eldik, *Journal of the Chemical Society, Dalton Transactions*, 2002, 951-956.
33. D. Jaganyi, F. Tiba, O. Q. Munro, B. Petrović and Ž. D. Bugarčić, *Dalton Transactions*, 2006, 2943-2949.
34. S. Kern, P. Illner, S. Begel and R. van Eldik, *European Journal of Inorganic Chemistry*, 2010, **2010**, 4658-4666.
35. P. Illner, S. Kern, S. Begel and R. van Eldik, *Chemical Communications*, 2007, **0**, 4803-4805.
36. D. Jaganyi and F. Tiba, *Transition Metal Chemistry*, 2003, **28**, 803-807.
37. B. Pitteri, G. Marangoni, L. Cattalini, F. Visentin, V. Bertolasi and P. Gilli, *Polyhedron*, 2001, **20**, 869-880.
38. J. Bogojeski and Ž. D. Bugarčić, *Transition Metal Chemistry*, 2011, **36**, 73-78.
39. D. Jaganyi, A. Hofmann and R. van Eldik, *Angewandte Chemie International Edition*, 2001, **40**, 1680-1683.

40. D. Reddy and D. Jaganyi, *Dalton Transactions*, 2008, 6724-6731.
41. D. Jaganyi, K. L. D. Boer, J. Gertenbach and J. Perils, *International Journal of Chemical Kinetics*, 2008, **40**, 808-818.
42. A. Hofmann, L. Dahlenburg and R. van Eldik, *Inorganic Chemistry*, 2003, **42**, 6528-6538.
43. A. Hofmann, D. Jaganyi, O. Q. Munro, G. Liehr and R. van Eldik, *Inorganic Chemistry*, 2003, **42**, 1688-1700.
44. P. Ongoma and D. Jaganyi, *Dalton Transactions*, 2012, **41**, 10724-10730.
45. G. Kinunda and D. Jaganyi, *Transition Metal Chemistry*, 2014, **39**, 451-459.
46. B. B. Khusi, A. Mambanda and D. Jaganyi, *Journal of Coordination Chemistry*, 2016, **69**, 2121-2135.
47. M. L. Tobe and J. Burgess, *Inorganic reaction mechanisms*, Longman, London, 1999.
48. E. Breet and R. Van Eldik, *Inorganic Chemistry*, 1984, **23**, 1865-1869.
49. M. Kotowski and R. Van Eldik, *Inorganic Chemistry*, 1984, **23**, 3310-3312.
50. M. Kotowski and R. Van Eldik, *Inorganic Chemistry*, 1986, **25**, 3896-3899.
51. J. Pienaar, M. Kotowski and R. Van Eldik, *Inorganic Chemistry*, 1989, **28**, 373-375.
52. J. Berger, M. Kotowski, R. Van Eldik, U. Frey, L. Helm and A. Merbach, *Inorganic Chemistry*, 1989, **28**, 3759-3765.
53. B. Petrović, Ž. D. Bugarčić, A. Dees, I. Ivanović-Burmazović, F. W. Heinemann, R. Puchta, S. N. Steinmann, C. Corminboeuf and R. Van Eldik, *Inorganic Chemistry*, 2012, **51**, 1516-1529.
54. A. Shaira, PhD, University of KwaZulu-Natal, South Africa, 2013.
55. A. Mambanda and D. Jaganyi, *Dalton Transactions*, 2011, **40**, 79-91.
56. H. Ertürk, R. Puchta and R. van Eldik, *European Journal of Inorganic Chemistry*, 2009, **2009**, 1331-1338.
57. Ž. D. Bugarčić, B. Petrović and E. Zangrando, *Inorganica Chimica Acta*, 2004, **357**, 2650-2656.
58. Ž. D. Bugarčič, G. Liehr and R. van Eldik, *Journal of the Chemical Society, Dalton Transactions*, 2002, 2825-2830.
59. A. Mijatović, J. Bogojeski, B. Petrović and Ž. D. Bugarčić, *Inorganica Chimica Acta*, 2012, **383**, 300-304.

60. R. Romeo, M. R. Plutino, L. Monsù Scolaro, S. Stoccoro and G. Minghetti, *Inorganic Chemistry*, 2000, **39**, 4749-4755.
61. A. Mambanda and D. Jaganyi, in *Advances in Inorganic Chemistry*, Elsevier, 2017, vol. 70, pp. 243-276.
62. I. M. Wekesa and D. Jaganyi, *Journal of Coordination Chemistry*, 2016, **69**, 389-403.
63. I. M. Wekesa and D. Jaganyi, *Dalton Transactions*, 2014, **43**, 2549-2558.
64. W. O. Siegl, *The Journal of Organic Chemistry*, 1977, **42**, 1872-1878.
65. *United states Pat.*, 2008.
66. M. Meder, C. H. Galka and L. H. Gade, *Monatshefte für Chemie/Chemical Monthly*, 2005, **136**, 1693-1706.
67. O. V. Dolomanov, L. J. Bourhis, R. J. Gildea, J. A. Howard and H. Puschmann, *Journal of Applied Crystallography*, 2009, **42**, 339-341.
68. G. M. Sheldrick, *Acta Crystallographica Section A: Foundations of Crystallography*, 2008, **64**, 112-122.
69. G. M. Sheldrick, *Acta Crystallographica Section C: Structural Chemistry*, 2015, **71**, 3-8.
70. M. Frisch, G. Trucks, H. Schlegel, G. Scuseria, M. Robb, J. Cheeseman, G. Scalmani, V. Barone, B. Mennucci, G. Petersson, Gaussian 09, revision D. 01, Gaussian, Inc., Wallingford CT (2009).
71. P. J. Hay and W. R. Wadt, *The Journal of Chemical Physics*, 1985, **82**, 299-310.
72. V. Barone and M. Cossi, *The Journal of Physical Chemistry A*, 1998, **102**, 1995-2001.
73. M. Cossi, N. Rega, G. Scalmani and V. Barone, *Journal of Computational Chemistry*, 2003, **24**, 669-681.
74. T. Appleton, J. Hall, S. Ralph and C. Thompson, *Inorganic Chemistry*, 1984, **23**, 3521-3525.
75. D. Reddy, K. J. Akerman, M. P. Akerman and D. Jaganyi, *Transition Metal Chemistry*, 2011, **36**, 593-602.
76. OriginPro 9.1. OriginLab Corporation, One Roundhouse Plaza, Suite 303, Northampton, MA 01060, United States. 1800-969-7720.
77. M. Bröring and C. Kleeberg, *Inorganica Chimica Acta*, 2009, **362**, 1065-1070.
78. M. Bröring, C. Kleeberg and E. Cónsul Tejero, *European Journal of Inorganic Chemistry*, 2007, **2007**, 3208-3216.

79. S. A. Willison, H. Jude, R. M. Antonelli, J. M. Rennekamp, N. A. Eckert, J. A. Krause Bauer and W. B. Connick, *Inorganic Chemistry*, 2004, **43**, 2548-2555.
80. H. Eyring, *The Journal of Chemical Physics*, 1935, **3**, 107-115.
81. H. Ertürk, J. Maigut, R. Puchta and R. van Eldik, *Dalton Transactions*, 2008, 2759-2766.
82. A. Mambanda, D. Jaganyi, S. Hochreuther and R. van Eldik, *Dalton Transactions*, 2010, **39**, 3595-3608.
83. P. A. Wangoli and G. Kinunda, *New Journal of Chemistry*, 2018, **42**, 214-227.
84. P. O. Ongoma and D. Jaganyi, *Dalton Transactions*, 2013, **42**, 2724-2734.
85. P. W. Asman, *Inorganica Chimica Acta*, 2018, **469**, 341-352.
86. W. P. Asman and D. Jaganyi, *International Journal of Chemical Kinetics*, 2017, **49**, 545-561.
87. P. W. Asman, *Journal of Coordination Chemistry*, 2017, 1-20.
88. D. Jaganyi, D. Reddy, J. Gertenbach, A. Hofmann and R. van Eldik, *Dalton Transactions*, 2004, 299-304.
89. M. Đurović, J. Bogojeski, B. Petrović, D. Petrović, F. W. Heinemann and Ž. D. Bugarčić, *Polyhedron*, 2012, **41**, 70-76.
90. S. Otto and L. I. Elding, *Journal of the Chemical Society, Dalton Transactions*, 2002, 2354-2360.
91. O. F. Wendt and L. I. Elding, *Inorganic Chemistry*, 1997, **36**, 6028-6032.
92. O. F. Wendt and L. I. Elding, *Journal of the Chemical Society, Dalton Transactions*, 1997, **0**, 4725-4732.
93. M. E. Oehlsen, A. Hegmans, Y. Qu and N. Farrell, *JBIC Journal of Biological Inorganic Chemistry*, 2005, **10**, 433-442.
94. F. Basolo and R. G. Pearson, *Mechanisms in Inorganic Reactions*, Wiley, New York, 2nd edn., 1967.
95. J. D. Atwood, *Inorganic and organometallic reaction mechanisms*, Wiley-VCH Publishers, New York, 2nd edn., 1997.
96. R. Van Eldik, T. Asano and W. Le Noble, *Chemical Reviews*, 1989, **89**, 549-688.

5.7 Supporting Information (ESI‡)

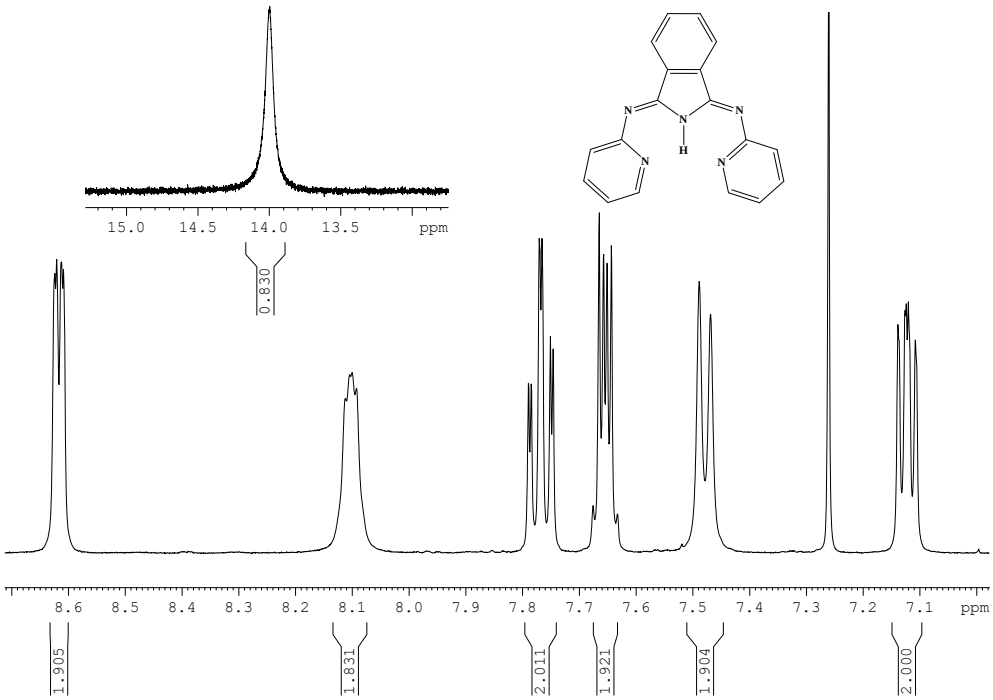

Figure SI 5.1 ^{1}H NMR spectrum for **BPI** ligand

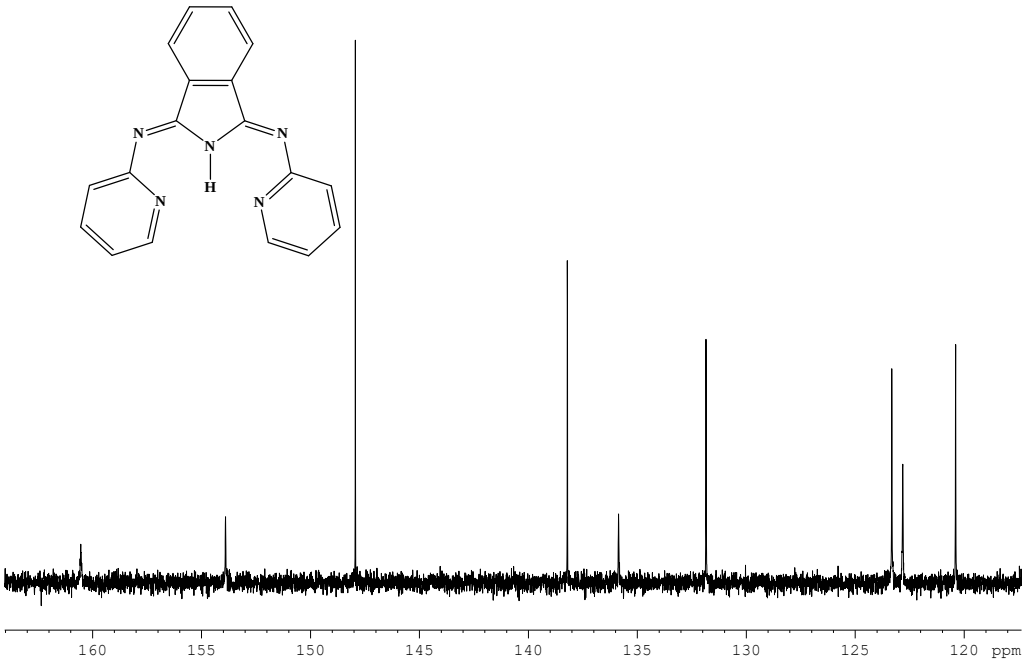

Figure SI 5.2 ^{13}C NMR spectrum for **BPI** ligand

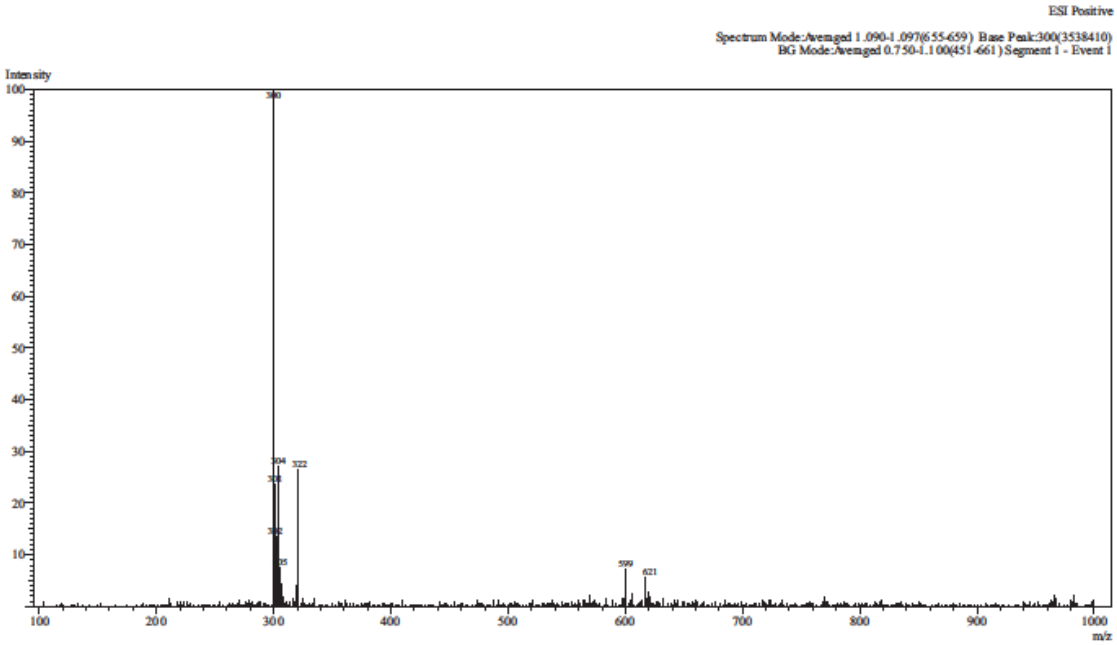

Figure SI 5.3 LC-MS mass spectrum **BPI** ligand

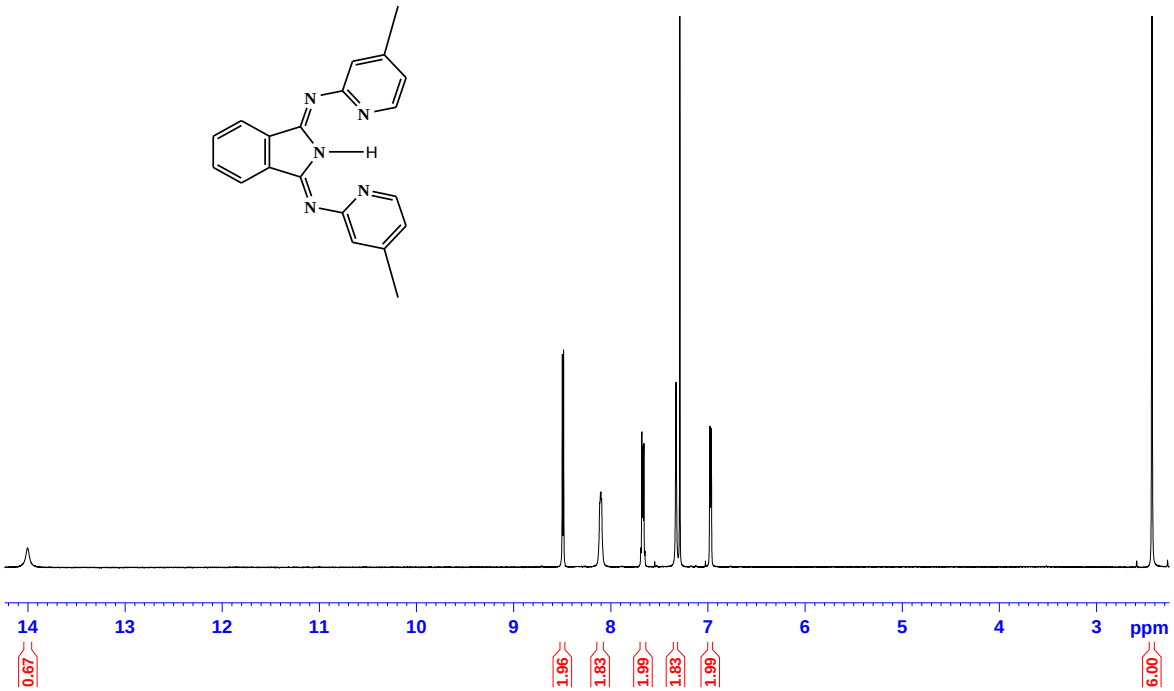

Figure SI 5.4 ^{1}H NMR spectrum of **4-Me-BPI** Ligand

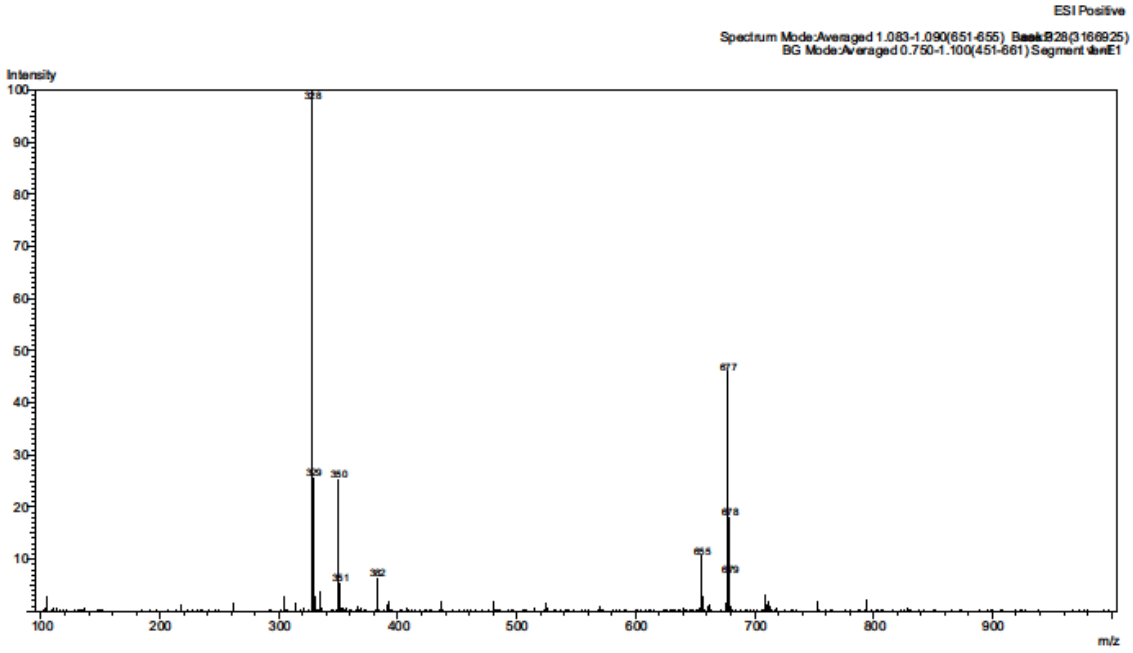

Figure SI 5.5 LC-MS mass spectrum **4-Me-BPI** Ligand

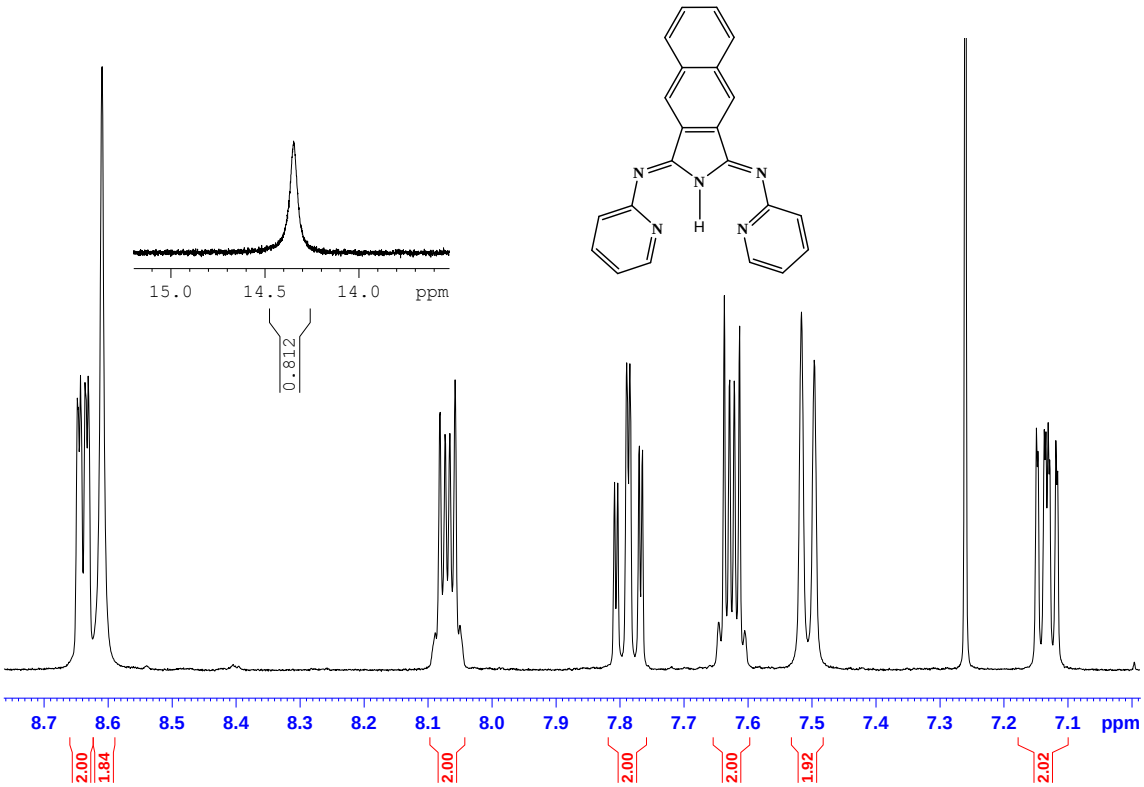

Figure SI 5.6 ^{1}H NMR spectrum for **BBPI** ligand

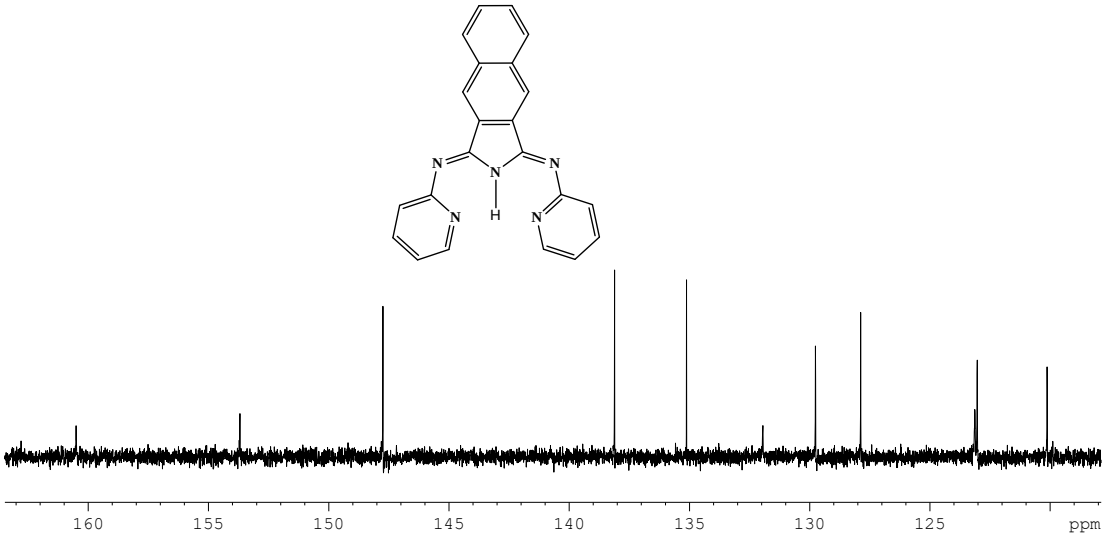

Figure SI 5.7 ^{13}C NMR spectrum for **BBPI** ligand

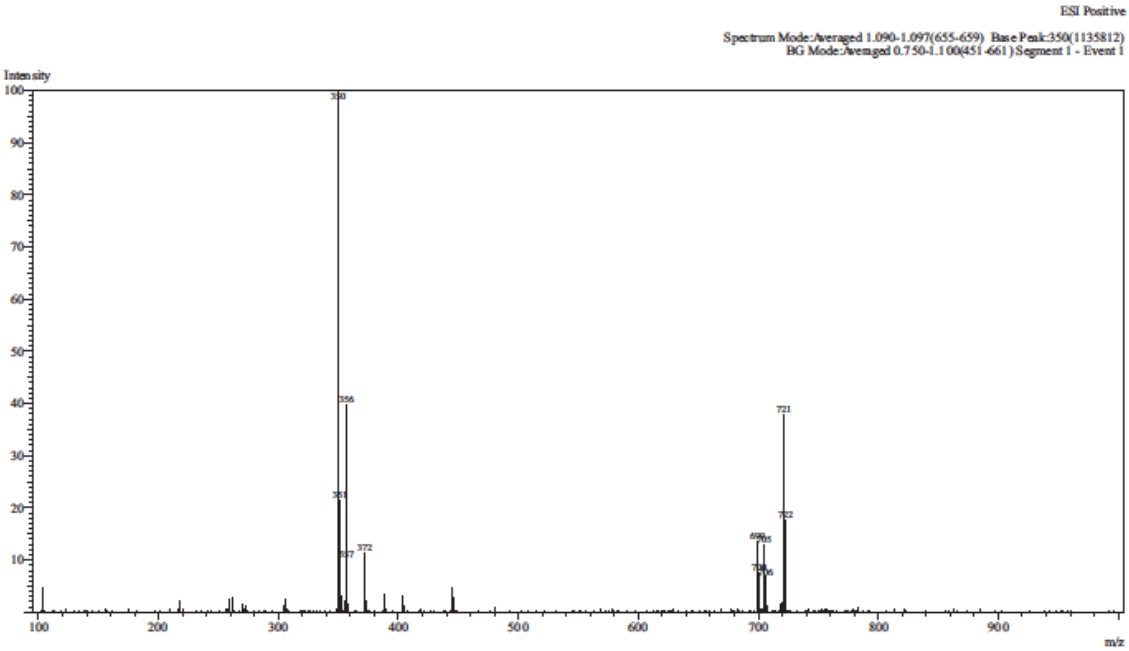

Figure SI 5.8 LC-MS mass spectrum of **BBPI** ligand

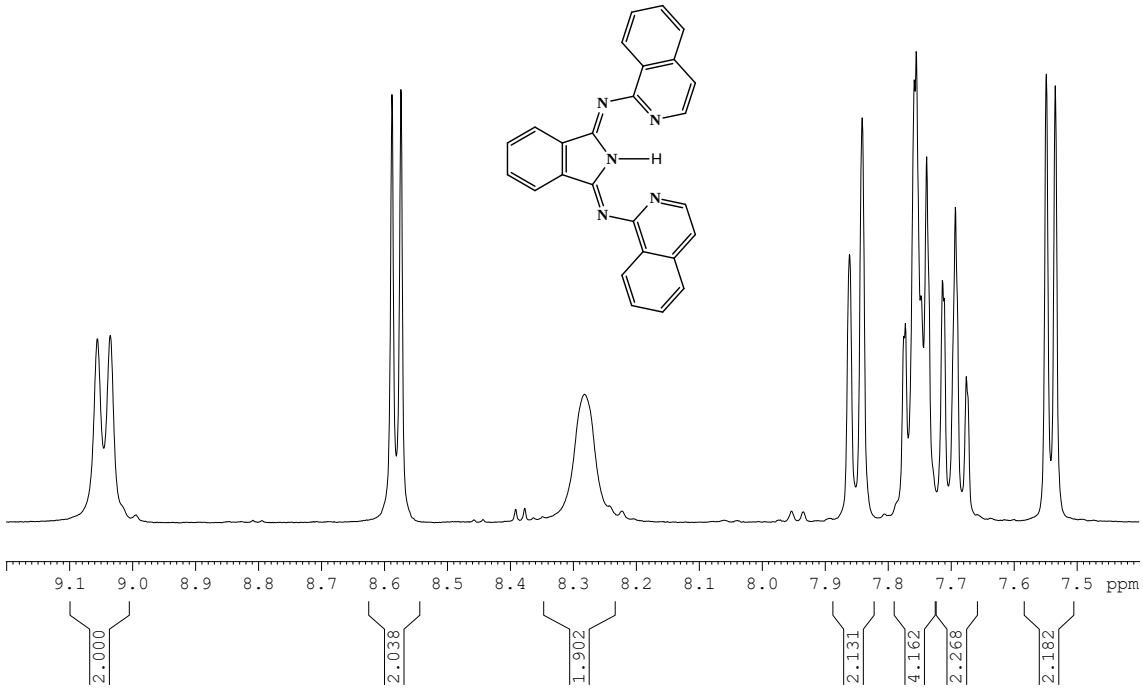

Figure SI 5.9 ^{1}H NMR spectrum of **BII** ligand

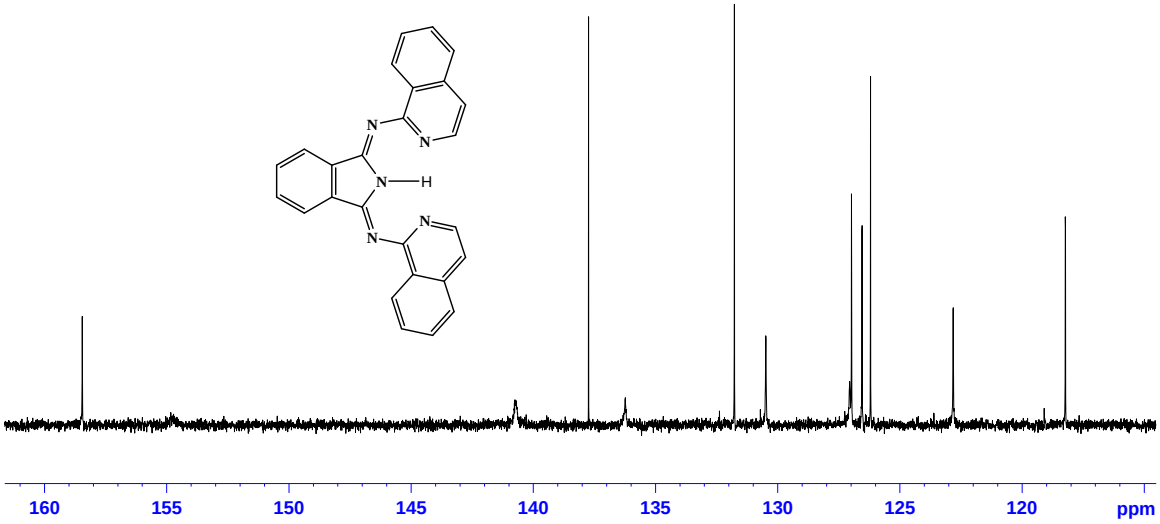

Figure SI 5.10 ^{13}C NMR spectrum of **BII** ligand

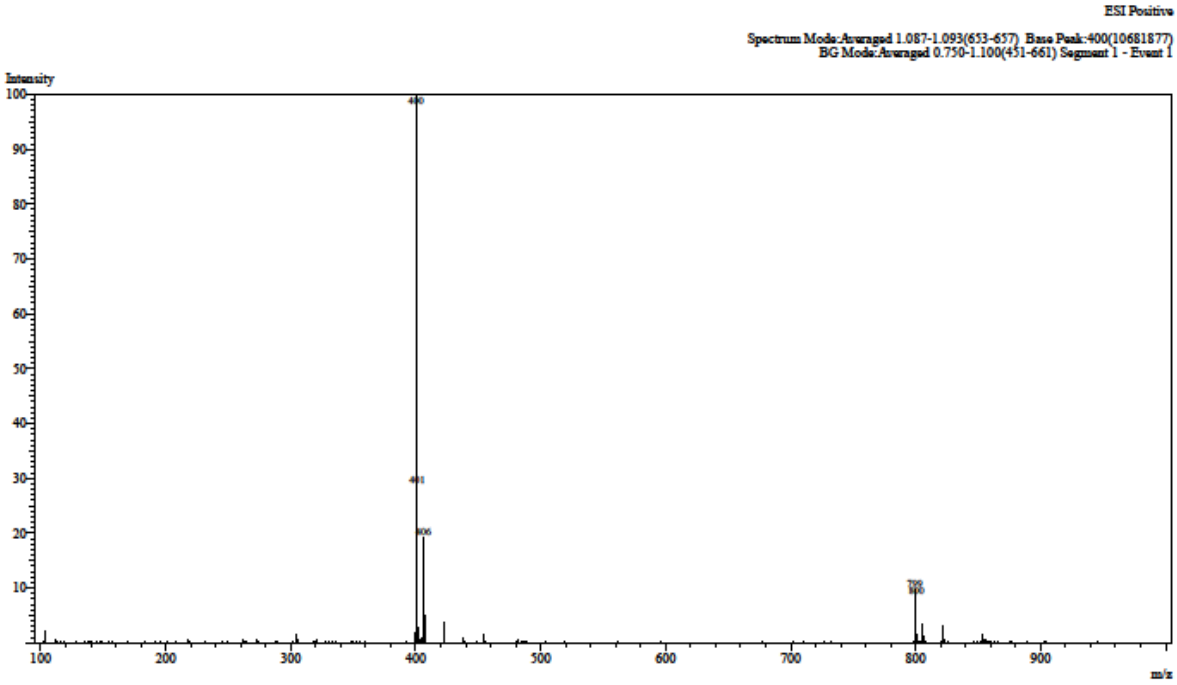

Figure SI 5.11 LC-MS mass spectra of **BII** ligand

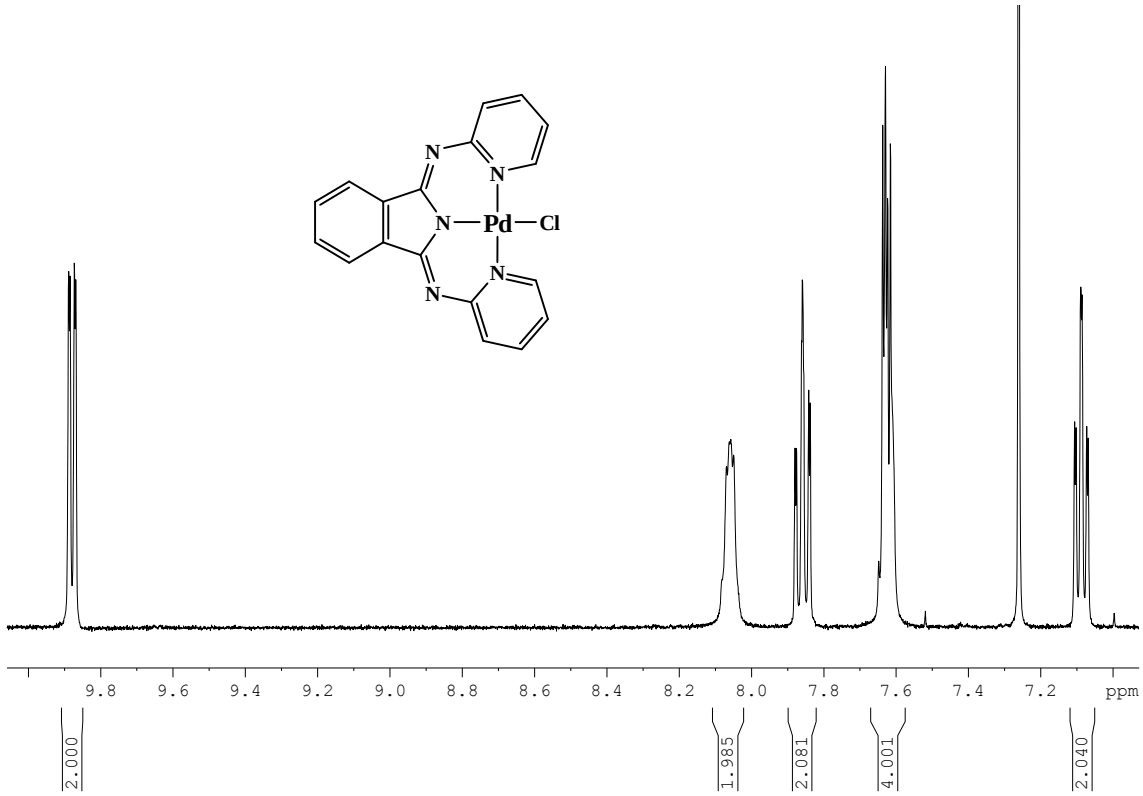

Figure SI 5.12 ^{1}H NMR spectrum for **Pd(BPI)Cl** complex

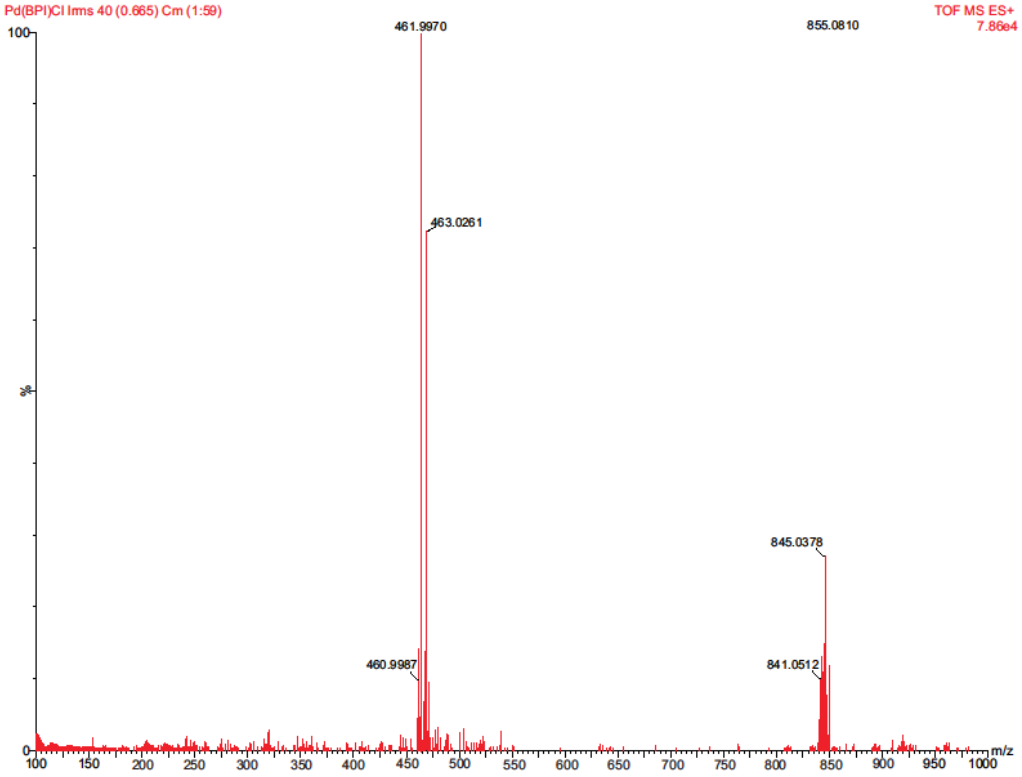

Figure SI 5.13 TOF-MS mass spectrum for **Pd(BPI)Cl** complex

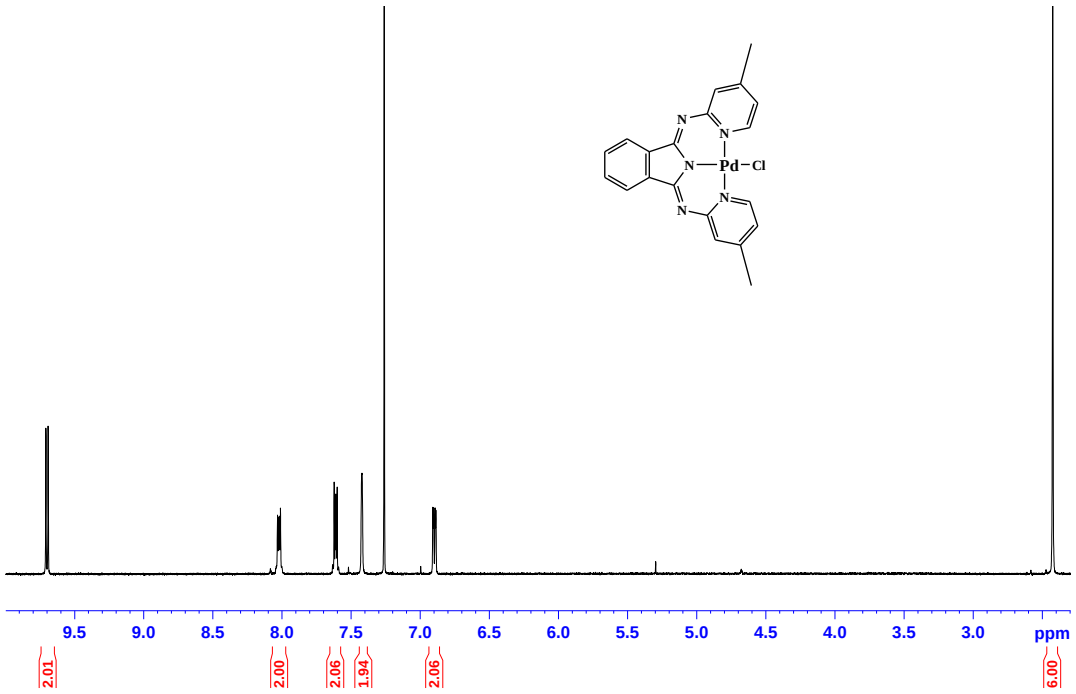

Figure SI 5.14 ^{1}H NMR spectrum **Pd(4-Me-BPI)Cl** complex

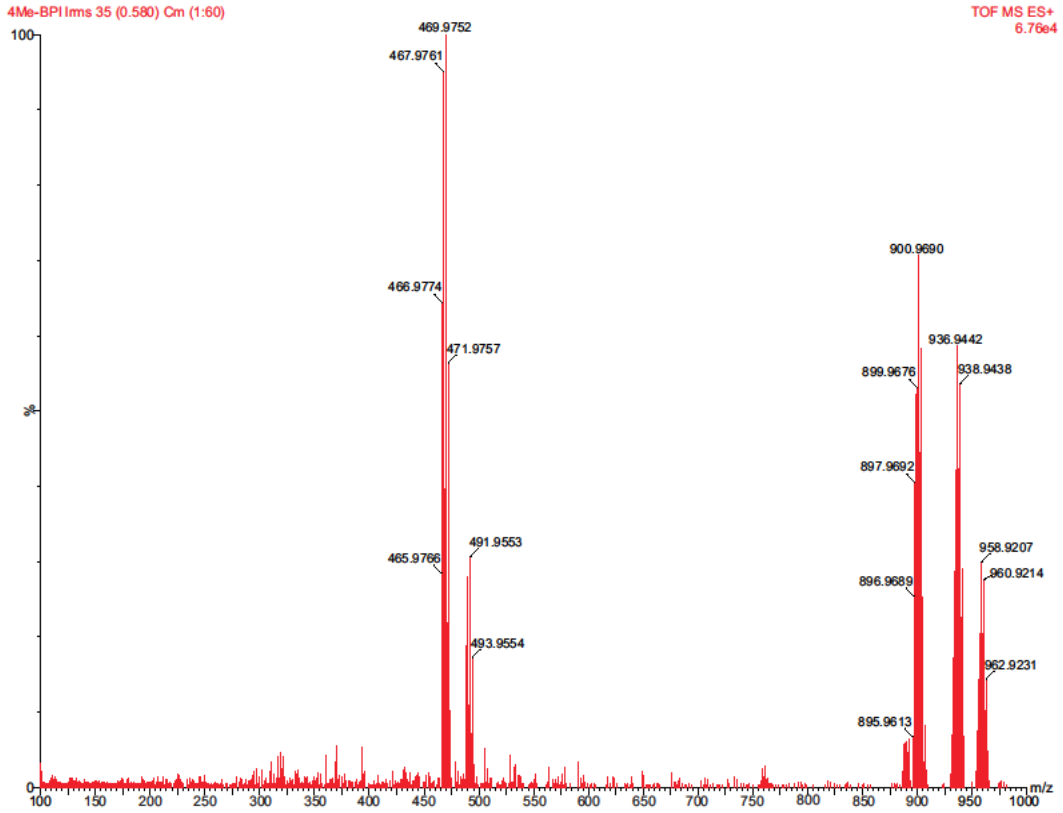

Figure SI 5.15 TOF-MS mass spectra **Pd(4-Me-BPI)Cl** complex

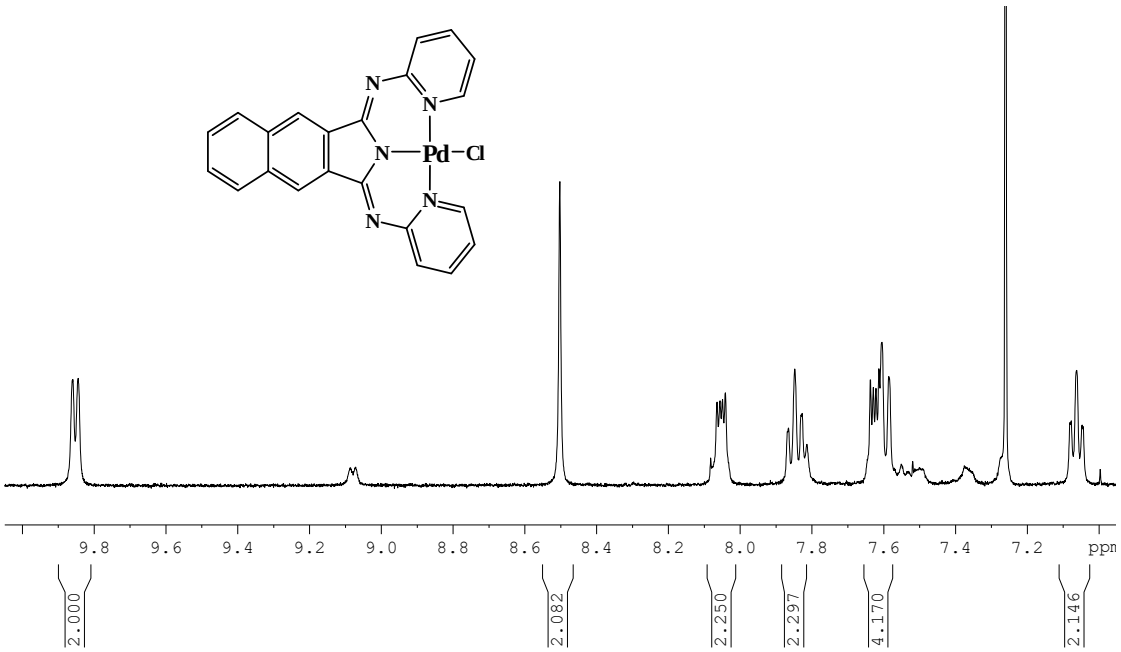

Figure SI 5.16 ^{1}H NMR spectrum for **Pd(BBPI)Cl** complex

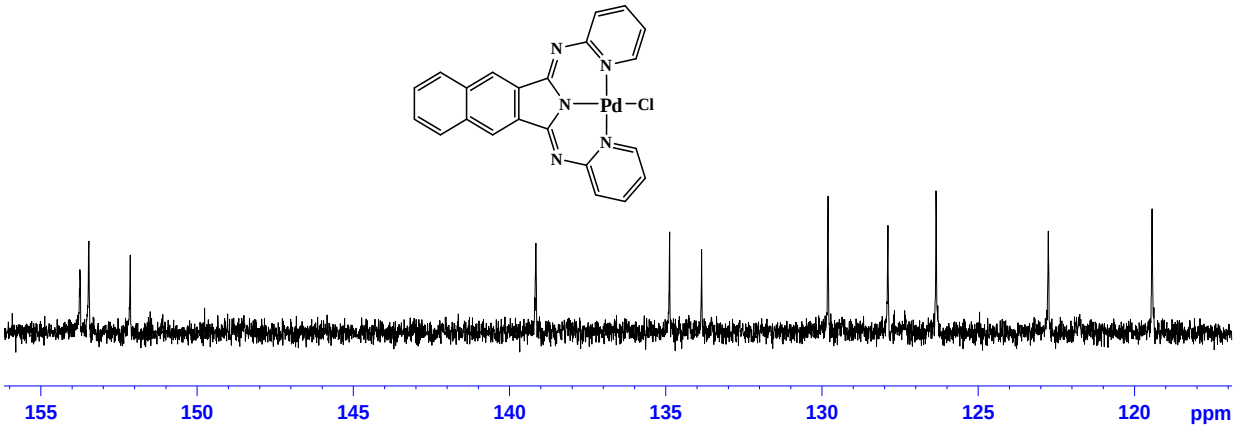

Figure SI 5.17 ^{13}C NMR spectrum for **Pd(BBPI)Cl** complex

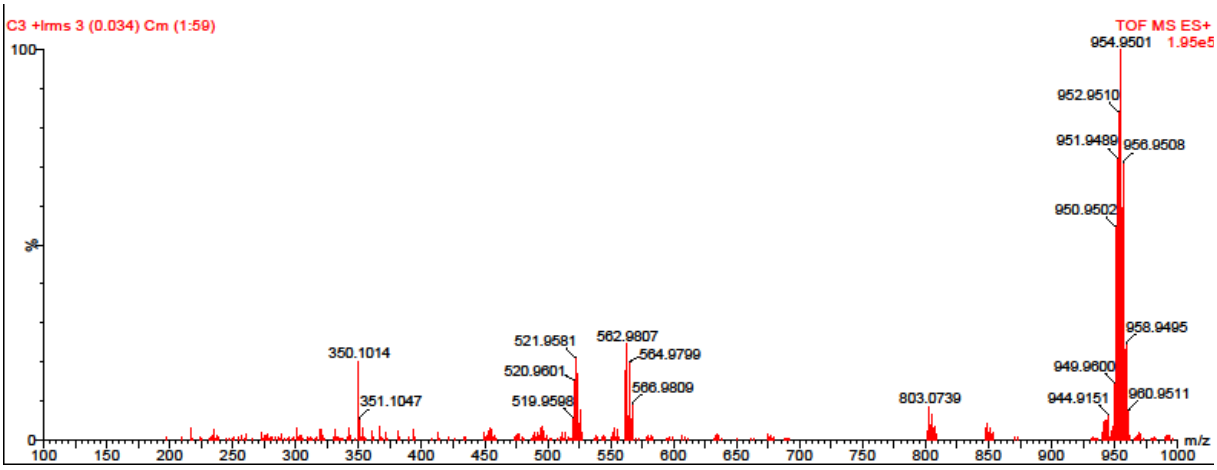

Figure SI 5.18 TOF-MS mass spectra for **Pd(BBPI)Cl** complex

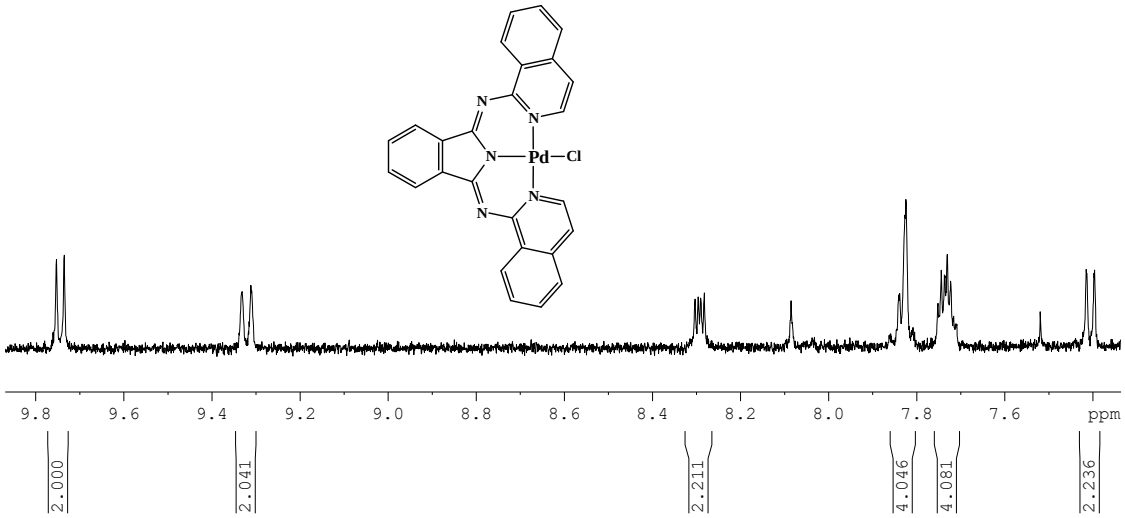

Figure SI 5.19 ^{1}H NMR spectrum of **Pd(BII)Cl** complex

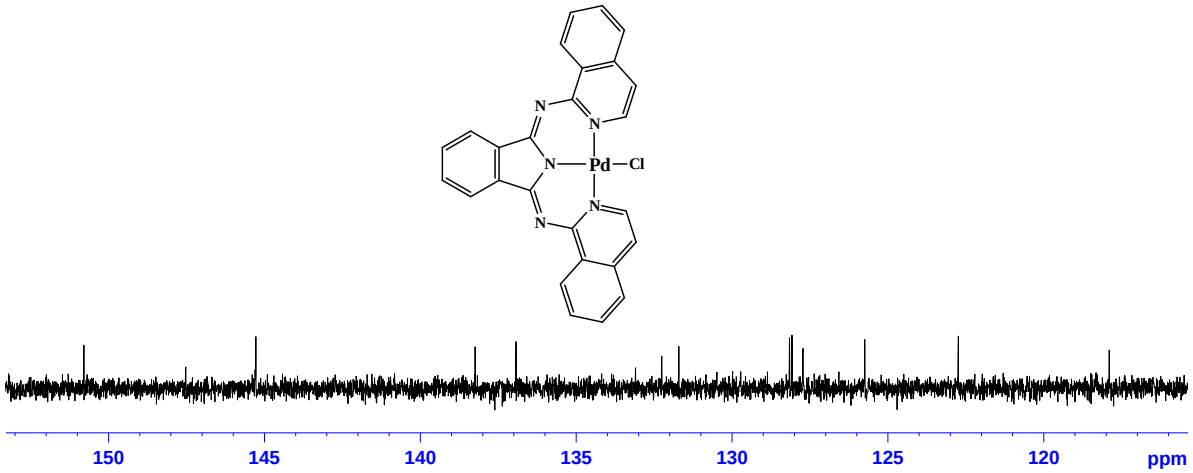

Figure SI 5.20 ^{13}C NMR spectrum of **Pd(BII)Cl** complex

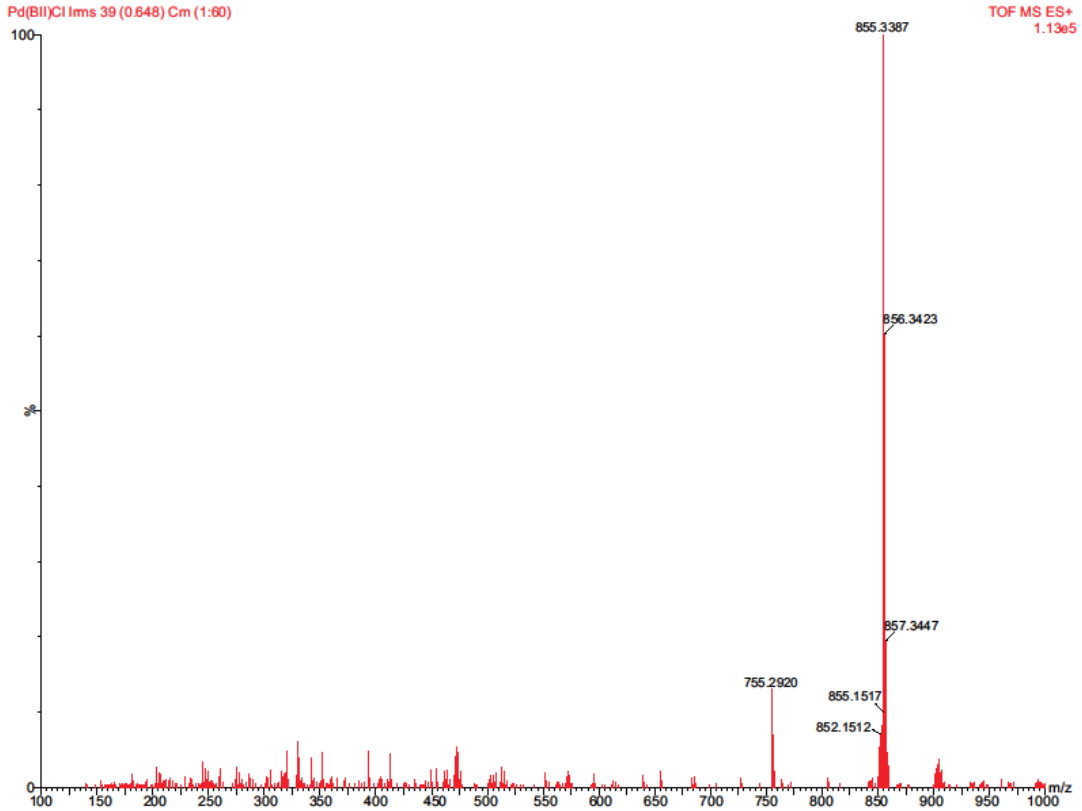

Figure SI 5.21 TOF-MS mass spectrum of **Pd(BII)Cl** complex

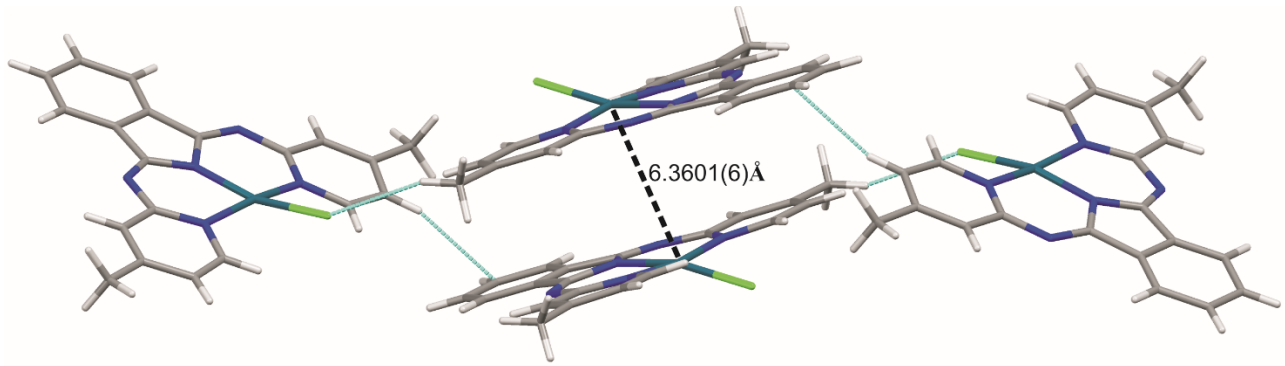

Figure SI 5.22: Crystal packing of **Pd(4-Me-PBI)Cl** compound showing an inversion dimer with no Pd–Pd interactions alongside C20 - H···Cl1 and C17 - H···C9 interactions between the molecules (shown in blue dashed lines).

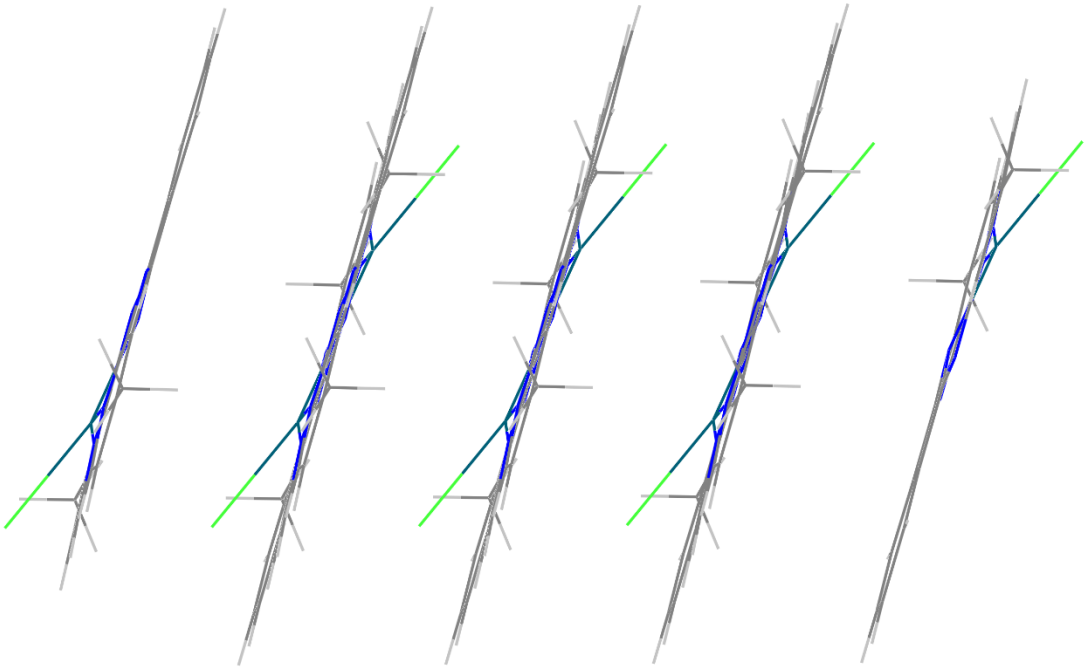

Figure SI 5.23: Stacked arrangement of the crystal packing of **Pd(4-Me-PBI)Cl**

Table S1 5.1: Wavelengths(nm) used for kinetic reactions of Pd(II) complexes with the nucleophiles

Complex	Nucleophiles	Wavelength, λ (nm)	
		Stopped flow	**Uv/visible**
Pd(BPI)Cl	Tu	360	360
	Dmtu	360	360
	Tmtu	360	360
Pd(4-MeBPI)Cl	Tu	420	350
	Dmtu	420	350
	Tmtu	360	426
Pd(BBPI)Cl	Tu	360	365
	Dmtu	355	370
	Tmtu	375	400
Pd(BII)Cl	Tu	505	-
	Dmtu	503	-
	Tmtu	525	-

Table S1 5.2: A summary of average $k_{obs(1)}$ (s^{-1}) for the chloride substitution from **Pd(BPI)Cl** by the nucleophiles in ethanol at T = 298 K. and I = 0.01M CF_3SO_3H,

Concentration, (M)	$k_{obs(1)}$ (s^{-1})		
	Tu	Dmtu	Tmtu
0.001	1.95459	0.78151	0.31745
0.002	4.02283	1.77215	0.67129
0.003	6.10042	2.54927	0.95235
0.004	7.96857	3.34976	1.26789
0.005	10.4750	4.25068	1.58725

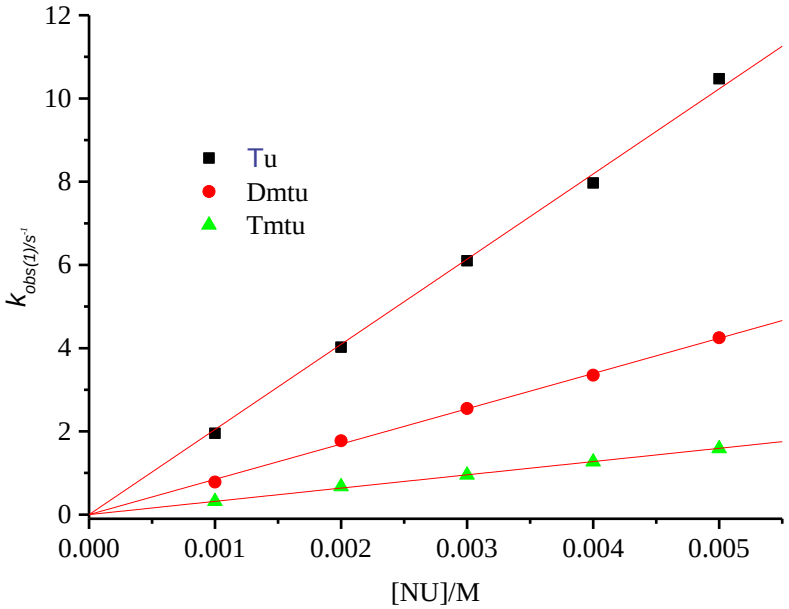

Figure SI 5.24: Dependence of the *pseudo*-first-order rate constants ($k_{obs(1)}$) on the concentration of thiourea nucleophiles for chloride substitution on **Pd(BPI)Cl** in ethanol, I = 0.01M CF_3SO_3H, T = 298K.

Table S1 5.3: A summary of average $k_{obs(1)}$ (s^{-1}) for the chloride substitution from **Pd(4-Me-BPI)Cl** by the nucleophiles in ethanol at T = 298 K. and I = 0.01M CF_3SO_3H,

Concentration, (M)	$k_{obs(1)}$ (s^{-1})		
	Tu	Dmtu	Tmtu
0.001	1.35288	0.28603	0.06645
0.002	2.67692	0.55718	0.13875
0.003	3.96471	0.85732	0.20019
0.004	5.31250	1.14310	0.27751
0.005	6.57324	1.46289	0.34443

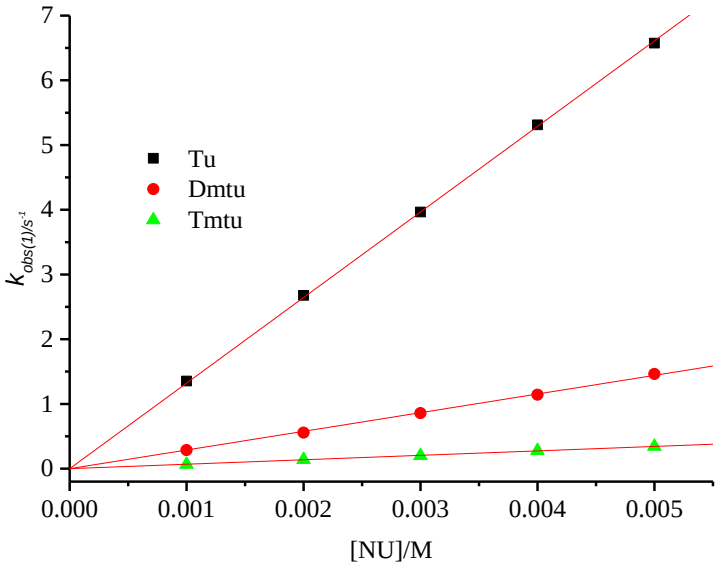

Figure SI 5.25: Dependence of $k_{obs(1)}$ on the nucleophile concentration reactions with **Pd(4-Me-BPI)Cl** in ethanol, I = 0.01M CF_3SO_3H, T = 298 K.

Table S1 5.4: Average $k_{obs(1)}$ (s^{-1}) for the chloride substitution from **Pd(BBPI)Cl** with the thiourea nucleophiles in ethanol at T = 298 K, I = 0.01M CF_3SO_3H.

Concentration, (M)	$k_{obs(1)}$ (s^{-1})		
	Tu	Dmtu	Tmtu
0.001	1.21246	0.18914	0.01567
0.002	2.32493	0.38511	0.03146
0.003	3.43740	0.57623	0.04750
0.004	4.64986	0.76871	0.06077
0.005	5.98215	0.94571	0.07835

Table S1 5.5: Average $k_{obs(1)}$ (s^{-1}) for the chloride substitution of **Pd(BII)Cl** by the nucleophiles in ethanol at T = 298 K and I = 0.01M CF_3SO_3H.

Concentration, (M)	$k_{obs(1)}$ (s^{-1})		
	Tu	Dmtu	Tmtu
0.001	0.00417	0.00106	0.00034494
0.002	0.00849	0.00206	0.0007298
0.003	0.01267	0.00293	0.00102
0.004	0.01725	0.00413	0.00135
0.005	0.02083	0.00502	0.00174

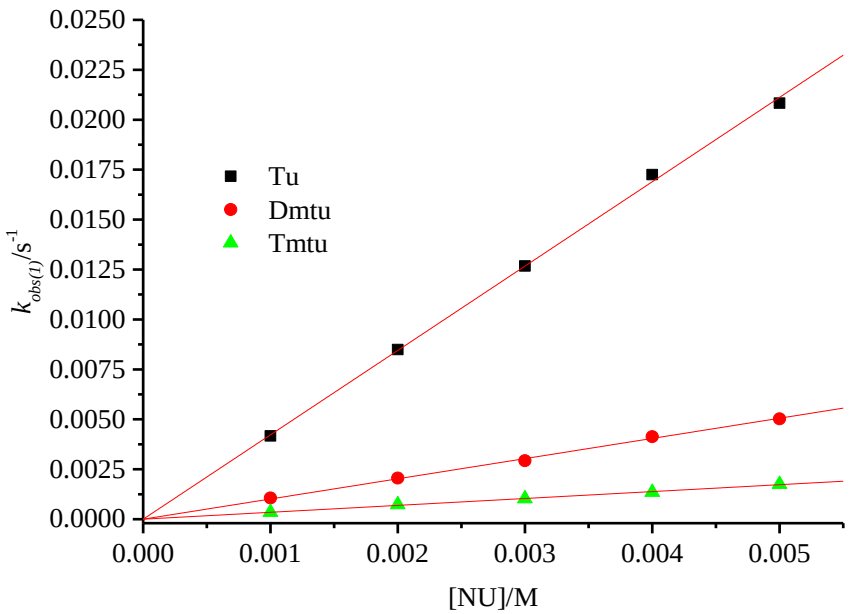

Figure SI 5.26: Dependence of $k_{obs(1)}$ on the concentration of nucleophiles for chloride substitution of **Pd(BII)Cl** in ethanol, I = 0.01M CF_3SO_3H, T = 298 K

Table S1 5.6: Average $k_{obs(2)}$ (s^{-1}) for the dechelation reaction of **Pd(BPI)Cl** with the nucleophiles in ethanol at T = 298 K and I = 0.01M CF_3SO_3H.

Concentration, (M)	$k_{obs(2)}$ (s^{-1})		
	Tu	Dmtu	Tmtu
0.001	0.0006057	0.000396	0.000296
0.002	0.00109	0.00080217	0.000549857
0.003	0.0016	0.00121	0.000792719
0.004	0.00212	0.00153	0.00105
0.005	0.00263	0.00201	0.00129

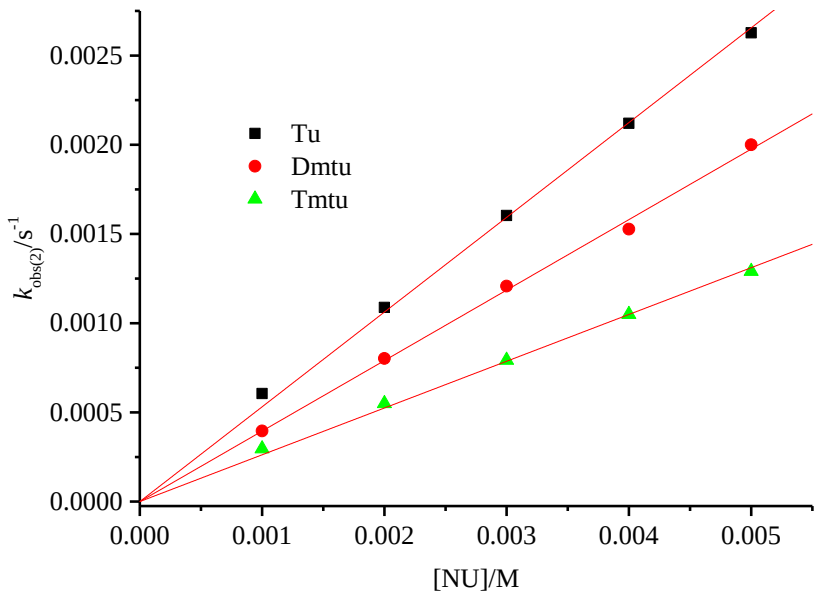

Figure SI 5.27: Dependence of $k_{obs(2)}$ on the nucleophile concentration for the chloride substitution of **Pd(BPI)Cl** in ethanol, I = 0.01M CF_3SO_3H, T = 298 K.

Table S1 5.7: Average $k_{obs(2)}$ (s^{-1}) for the dechelation reaction of **Pd(4-Me-BPI)Cl** with the nucleophiles in ethanol, I = 0.01M CF_3SO_3H, T = 298 K.

Concentration, (M)	$k_{obs(2)}$ (s^{-1})		
	Tu	Dmtu	Tmtu
0.001	1.95833E-4	1.38119E-4	6.9854E-5
0.002	3.3759E-4	2.53603E-4	1.15209E-4
0.003	4.78433E-4	3.73271E-4	1.68177E-4
0.004	6.17509E-4	4.81981E-4	2.08498E-4
0.005	7.67938E-4	5.96979E-4	2.59234E-4

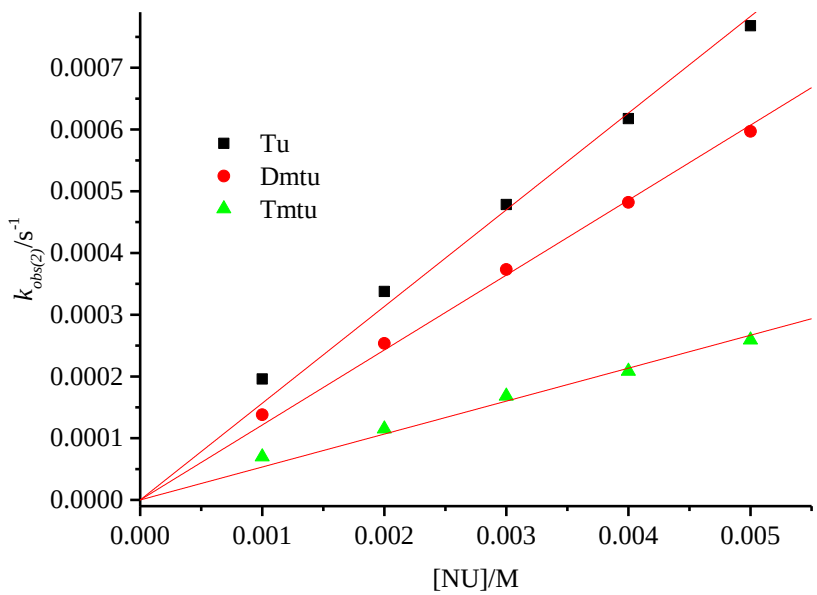

Figure SI 5.28: Dependence of $k_{obs(2)}$ on the nucleophile concentrations for the chloride substitution of **Pd(4-Me-BPI)Cl** in ethanol, I = 0.01M CF_3SO_3H, T = 298K.

Table S1 5.8: Average $k_{obs(2)}$ (s^{-1}) for the dechelation reaction of **Pd(BBPI)Cl** with the nucleophiles in ethanol, I = 0.01M CF_3SO_3H, T = 298 K.

Concentration, (M)	$k_{obs(2)}$ (s^{-1})		
	Tu	Dmtu	Tmtu
0.001	1.22884E-4	5.88375E-5	1.48E-5
0.002	2.61547E-4	1.51804E-4	2.55956E-5
0.003	4.17433E-4	2.11905E-4	3.92563E-5
0.004	5.67013E-4	2.82538E-4	5.47754E-5
0.005	6.98352E-4	3.68485E-4	7.95499E-5

Table S1 5.9: Temperature dependence of k_1 $M^{-1}s^{-1}$ for the chloride substitution reaction of **Pd(BPI)Cl** by the nucleophiles at 30-fold in ethanol, I = 0.01M CF_3SO_3H.

(1/T) K^{-1}	ln(k_1/T)		
	Tu	Dmtu	Tmtu
0.00341	1.8426	0.95205	-5.56638
0.00336	1.97939	1.25822	-5.33504
0.00330	2.17597	1.69386	-5.06694
0.00325	2.44325	1.95117	-4.81393
0.00319	2.69120	2.24184	-4.46554

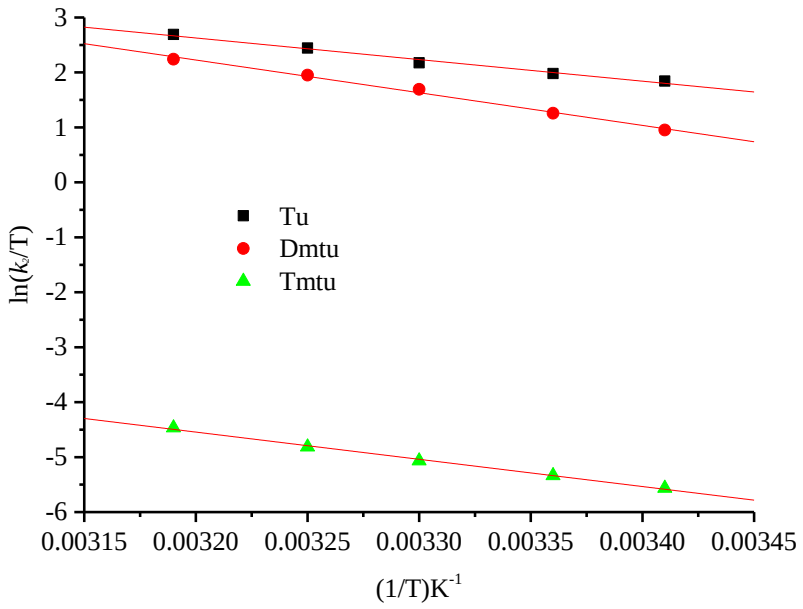

Figure SI 5.29: Eyring plots of **Pd(BPI)Cl** with thiourea nucleophiles at different temperatures

Table S1 5.10: Temperature dependence of k_1 $M^{-1}s^{-1}$ for the chloride substitution reactions of **Pd(4-Me-BPI)Cl** by the thiourea nucleophiles at 30-fold in ethanol, I = 0.01M CF_3SO_3H

(1/T) K^{-1}	ln(k_1/T)		
	Tu	Dmtu	Tmtu
0.00341	-2.09265	-1.29328	-3.09211
0.00336	-1.77097	-1.00925	-2.75425
0.00330	-1.38147	-0.63613	-2.41623
0.00325	-0.92886	-0.37365	-2.05482
0.00319	-0.66851	0.0182	-1.75683

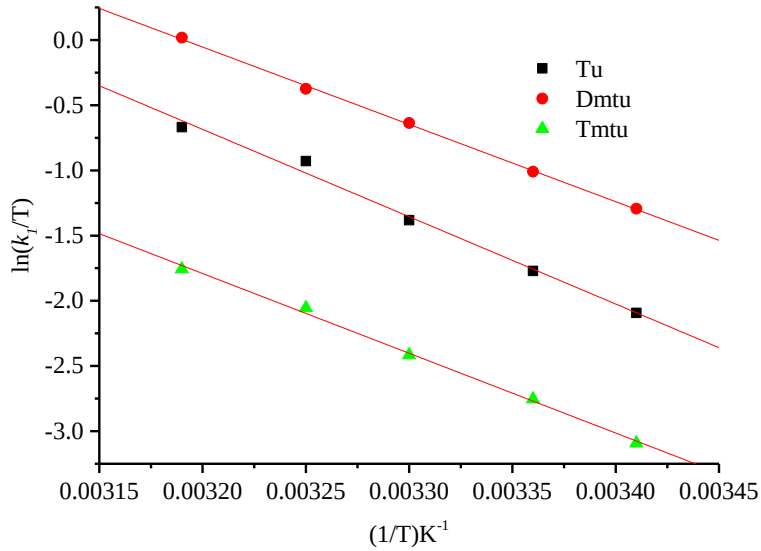

Figure SI 5.30: Eyring plots of **Pd(4-Me-BPI)Cl** with nucleophiles at different temperatures

Table S1 5.11: Temperature dependence of k_1 $M^{-1}s^{-1}$ for the reaction of **Pd(BBPI)Cl** with nucleophiles at 30-fold in ethanol, I = 0.01M CF_3SO_3H

	ln(k_1/T)		
(1/T) K^{-1}	Tu	Dmtu	Tmtu
0.00341	-0.20196	-0.04486	-3.23479
0.00336	0.12354	0.27284	-2.93481
0.0033	0.45064	0.65931	-2.59709
0.00325	0.75453	1.01432	-2.34797
0.00319	1.22211	1.32155	-1.97621

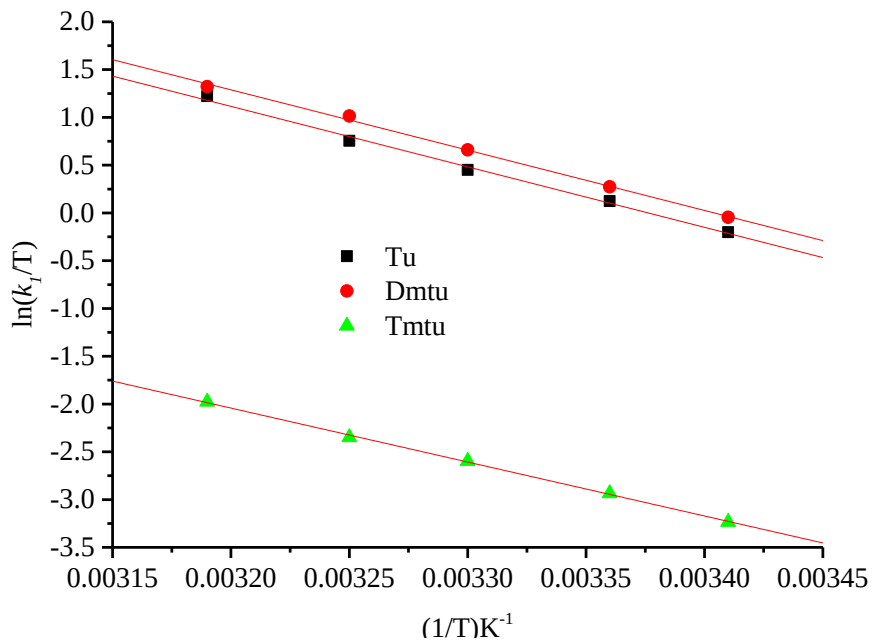

Figure SI 5.31: Eyring plots of **Pd(BBPI)Cl** with the nucleophiles at different temperatures

Table S1 5.12: Temperature dependence of k_1 $M^{-1}s^{-1}$ for the reactions of **Pd(BII)Cl** by the nucleophiles at 30-fold in ethanol, I = 0.01M CF_3SO_3H

	ln(k_1/T)		
(1/T) K^{-1}	Tu	Dmtu	Tmtu
0.00341	-5.33067	-6.42138	-8.48214
0.00336	-4.92354	-5.94146	-8.19216
0.00330	-4.47204	-5.48431	-7.75223
0.00325	-4.16507	-5.12829	-7.41216
0.00319	-3.59984	-4.65058	-7.01229

Table S1 5.13: Temperature dependence of k_2 $M^{-1}s^{-1}$ for reactions of **Pd(BPI)Cl** by the nucleophiles at 30-fold in ethanol, I = 0.01M CF_3SO_3H

(1/T) K^{-1}	ln(k_2/T)		
	Tu	Dmtu	Tmtu
0.00341	-10.42357	-8.85013	-7.02569
0.00336	-10.00593	-8.6061	-6.65892
0.0033	-9.50214	-8.32366	-6.25872
0.00325	-9.08766	-8.07008	-5.96826
0.00319	-8.5695	-7.76874	-5.57569

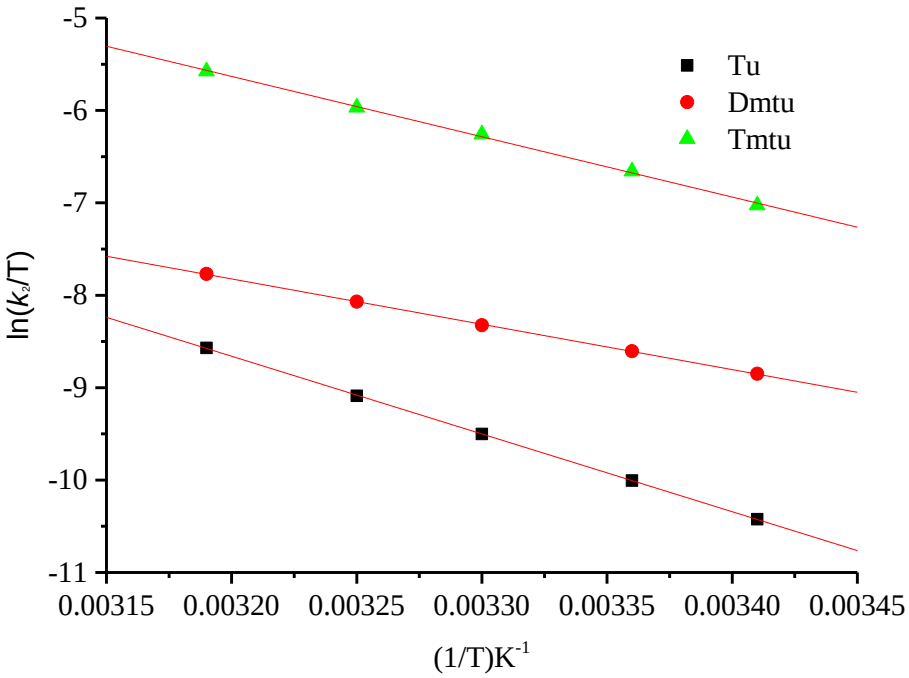

Figure SI 5.32: Eyring plots for the Second step of **Pd(BPI)Cl** with the nucleophiles at different temperatures.

Table S1 5.14: Temperature dependence of k_2 $M^{-1}s^{-1}$ for reactions of **Pd(4-Me-BPI)Cl** with the nucleophiles at 30-fold in ethanol, I = 0.01M CF_3SO_3H

(1/T) K^{-1}	ln(k_2/T)		
	Tu	Dmtu	Tmtu
0.00341	-10.05876	-10.48569	-9.25987
0.00336	-9.73658	-10.13993	-8.88884
0.0033	-9.25842	-9.65694	-8.43689
0.00325	-8.89781	-9.35875	-8.00497
0.00319	-8.32007	-8.8911	-7.53987

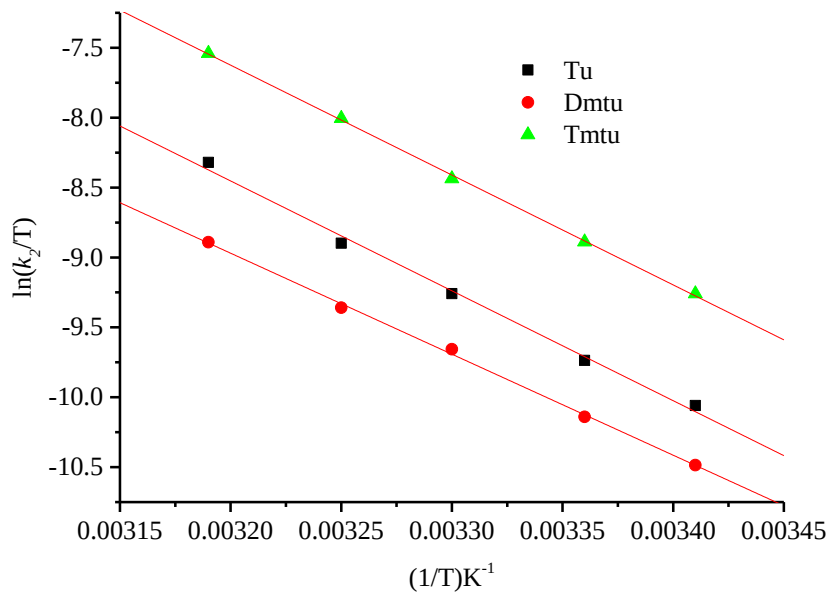

Figure SI 5.33: Eyring plots for the Second step of **Pd(4-Me-BPI)Cl** with the nucleophiles at different temperatures

Table S1 5.15: Temperature dependence of k_2 $M^{-1}s^{-1}$ for the reactions of **Pd(BBPI)Cl** the nucleophiles at 30-fold in ethanol, I = 0.01M CF_3SO_3H

(1/T) K^{-1}	ln(k_2/T)		
	Tu	Dmtu	Tmtu
0.00341	-9.58159	-9.3100	-8.15026
0.00336	-9.25004	-8.98425	-7.75777
0.00330	-8.81698	-8.50102	-7.28986
0.00325	-8.46871	-8.1379	-7.00492
0.00319	-8.01442	-7.83062	-6.51005

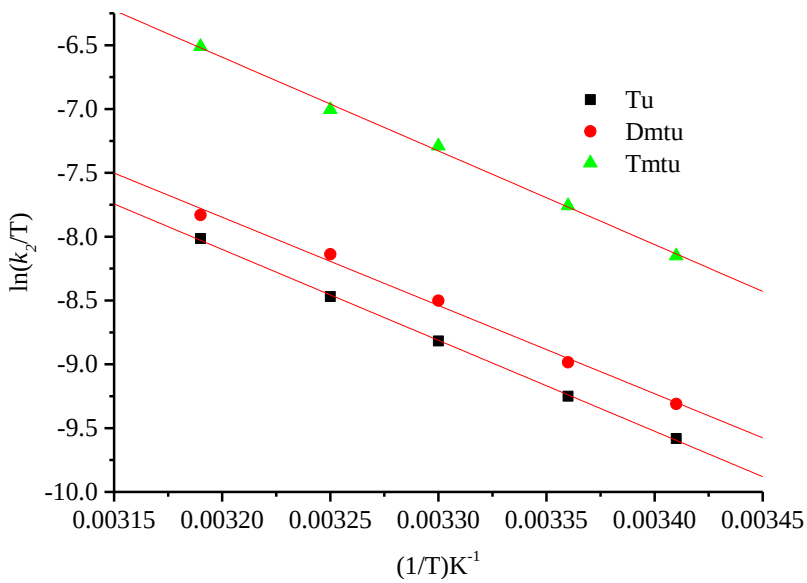

Figure SI 5.34: Eyring plots for the second step of **Pd(BBPI)Cl** with the nucleophiles at different temperatures.

CHAPTER 6

The Reactivity of Pd(II) Complexes with C^N^N Cyclometalated Polypyridylphenyl Ligands: Crystal Structures, Kinetics and Computational studies

6.0 Abstract

The rate and mechanism of substitution of the labile chloride ligand from cyclometalated Pd(II) complexes coordinated to C^N^N polypyridylphenyl ligands; chloro-4-(3,5-di-tert-butylphenyl)-6-phenyl-2,2'-bipyridine)palladium(II), **PdL^1**, chloro-3-(4-(3,5-di-tert-butylphenyl)-6-phenylpyridin-2-ylisoquinoline)palladium(II), **PdL^2**, chloro-(4-(3,5-di-tert-butylphenyl)-6-(naphthalen-2-yl)-2,2'-bipyridine)palladium(II), **PdL^3** and chloro-3-(4-(3,5-di-tert-butylphenyl)-6-(naphthalen-2-yl)pyridin-2-ylisoquinoline)palladium(II), **PdL^4** is reported. The reactions were performed under *pseudo*-first-order conditions with thiourea nucleophiles *viz* thiourea (**Tu**), N,N'-dimethylthiourea (**Dmtu**) and N,N,N',N'-tetramethylthiourea (**Tmtu**) in dichloromethane as a function of concentration and temperature using the stopped-flow spectrophotometric technique. The observed rate of substitution can be expressed as $k_{obs} = k_2$[Nu] and the values of k_2 the rate constant for the nucleophilic attack decrease in the order: **PdL^1** > **PdL^2** > **PdL^3** > **PdL^4**. The strong σ-donation of the *cis*-ligand moiety controls the reactivity of the complexes. The *cis*-coordinated naphthyl group behaves in anomalous way in **PdL^3** and **PdL^4** and reduces the reactivity of the Pd metal centre more than the *cis*-isoquinolyl group in **PdL^2** in a similar coordination position. **PdL^4** is the least reactive due to a combination of both naphthyl and isoquinolyl moieties in its ligand structure. The solid-state crystal structures of **PdL^2** and **PdL^3** belonging to *P-1* and *Pbca* space groups respectively, are reported. The DFT descriptor electronic chemical potential (μ) supports the reactivity trend of the complexes.

Keywords: Pd(II) C^N^N complexes, *cis*-π-extension, isoquinolyl, naphthyl, *pseudo*-first-order

6.1 Introduction

Cyclometalated Pd/Pt(II) complexes of C-deprotonated extended π-conjugation, bearing C^N^N polypyridylphenyl ligands have attracted great research interests because of their applications in photophysics, luminescent bioprobes, cell imaging, electrochemistry and antitumor drugs.[1-7] The anticancer activities of Pd(II) complexes coordinated to these types of ligands have been reported. [5, 6] This have lifted hope that a more effective drug based on other metals such as Pd is possible given the side effects and resistance[8-10] of the currently used Pt(II)-based anticancer drugs.[11] However, the knowledge about their kinetics and thermodynamic properties still remains largely unexplored. The kinetic data forms the basis for predicting their interactions with DNA and designing new anticancer drugs. The development of Pd(II) antitumor drugs benefitted from the same strategies used to design potential Pt(II) antitumor drugs[12] because of the similarity in their structural and mechanism of ligand exchange.[13] Moreover, the design of Pd(II) drugs with better therapeutic indices still remains a challenge because of their fast ligand exchange kinetics. They react 10^2 - 10^5 times faster than the Pt(II) complexes. [13-16] In addition, their strong affinity towards N and S donor ligands lowers their selectivity hence limiting their antitumor activity.[17] The cyclometalated ligands with π-extension having N- and C-donor atoms are good chelates with deprotonated carbon atom having a strong σ-donation[4] towards the metal centre. Such good chelators with varied σ-donor and π-acceptor properties can play a role in controlling the reactivity of Pd(II) complexes.[18]

The data on the influence of a single carbon-metal bond on the rate of substitution reactions from cyclometalated Pt(II) complexes is readily available.[19-25] However, the data for analogous Pd(II) complexes are rare and remains scanty.[26] In all these studies the metal-carbon bond was located in the *trans*-position to the leaving group resulting in high rate of substitution due to strong σ-*trans*-effect of the deprotonated carbon.[27, 28] High increase in the rate of substitution of upto six

orders of magnitude reported [21, 29] was attributed to destabilization of the ground state due to σ-electron donation along the *trans* axis hence stabilizing the transition state.[30] However, a reduction in the reactivity by 2 orders of magnitude was observed moving from Pt(II) complexes having N^C^N ligand system (*trans*-metal–carbon bond) to that of N^N^C framework (*cis*-metal–carbon bond).[28] The result indicated that the σ-*cis*-effect presents an opposite trend to *trans*-effect.[31, 32] In addition, the rate of substitution was systematically reduced upto 40 times in a series of complexes coordinated to N^N^C ligand systems.[33] Furthermore, a retardation in the rate of substitution of labile chloride of Pt(II) complexes by a factor of 15 – 16 was observed when the *cis*-pyridyl group was replaced with a phenyl group in a terpy system.[28, 34] This was explained in terms of accumulation of electron density around the metal centre which stabilizes the transition state and destabilizes the ground state, thus making the complex less electrophilic and hence repels the incoming nucleophiles.[28, 33, 34]

The electron donating substituents at the 4'-position of the central pyridine of a terpyridyl complex [35, 36] are known to lower the lability by diminishing the π-back bonding ability of the terpy framework.[37, 38] In all these studies the substitution mode of mechanism remained associative. Therefore, it can be envisaged that Pd(II) complexes with C^N^N ligands having both a strong deprotonated-C σ-donor at the *cis*-position and a strong σ-donor substituents on the phenyl group at the 4'-position of tridentate could potentially reduce the rate of substitution from the complexes thereby controlling the reactivity of the Pd metal. This may provide kinetically inert Pd(II) complexes that survives deactivation by biological nucleophiles, thus raising hopes for alternative type of anticancer metallodrugs.

Except for Pt(II) complexes [28, 33, 34] having cyclometalated N^N^C ligands without *π*-extension, particularly on the *cis*-position, the effect these type of ligands with extended π-conjugation

could pose on the rate of substitution of their Pd(II) complexes remains largely unknown. Indeed, the effects of the extended π-conjugation of the *cis*-pyridyl and *cis*-phenyl of N^N^C ligands through benzannulation (addition of phenyl rings) on the rate of substitution on the square-planar d^8 complexes remains rare in literature. Therefore, this study sought to investigate if the π-extension and the σ-donation effects from both the *cis*-ligand fragments and the *trans*-ancillary ligand subunits of the cyclometalated polypyridylphenyl, C^N^N ligands could play a significant role in controlling the reactivity of the Pd metal centre. In this regard, the rate of substitution of the chloride ligand of the Pd(II) complexes shown in Figure 6.1 was studied using thiourea nucleophiles of varied steric influences. The crystal structures of **PdL^2** and **PdL^3** were isolated and the density function theory (DFT) calculations were performed on the complexes to give insights to the experimental kinetic data results obtained in this investigation.

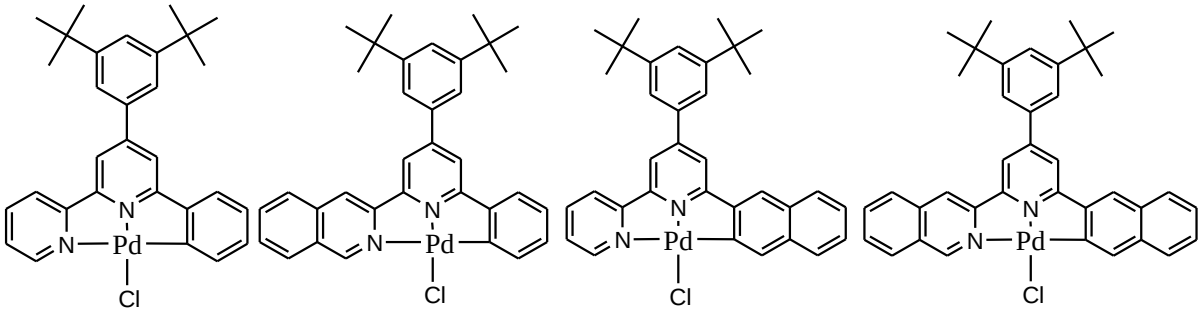

PdL^1 **PdL^2** **PdL^3** **PdL^4**

Figure 6. 1 Structures of the investigated Pd(II) complexes

6.2 Experimental Section

6.2.1 Materials and Methods

Pyridine, acetophenone, 3,5-di-*tert*-butylbenzaldehyde, ammonium acetate, 2-acetylpyridine, anhydrous ethyl acetate, anhydrous benzene, methyl-3-isoquinolinecarboxylate, 2-acetonaphthone, sodium ethoxide, hydrochloric acid, sodium hydroxide, thiourea **(Tu)**, N,N'-dimethylthiourea **(Dmtu),** N,N,N',N'-tetramethylthiourea **(Tmtu)** were purchased from Aldrich

and used directly as acquired. Bis(benzonitrile)dichloropalladium(II), $(C_6H_5CN)_2PdCl_2$, 95% and ligand precursor 1-(2-pyridylacetyl)pyridinium iodide were also procured from Sigma-Aldrich and used as supplied. 3-acetylisoquinoline was prepared from methyl-3-isoquinoline carboxylate according the method of Field and co-workers.[39] All syntheses were performed under nitrogen atmosphere using standard Schlenk techniques.

6.2.2 Syntheses of Precursors and C^N^N Ligands

3-Acetylisoquinoline

A mixture of anhydrous ethylacetate (3.42 mL, 14 mmol) and methyl-3-isoquinolinecarboxylate (2201.2 mg, 11.8 mmol) in dry benzene (35.0 mL) was added to a stirring solution of sodium ethoxide (803 mg, 11.8 mmol) in dry benzene (35 mL). The resulting mixture was refluxed for 36 hours. The mixture was cooled to room temperature and poured into a solution of sodium hydroxide (472 mg, 11.8 mmol) in water (15 mL). The light-yellow solid was filtered off, and water (40 mL) added to the filtrate. After the phases separated, the benzene layer was washed with water, and the combined aqueous layers extracted with diethyl ether (3 × 30 mL). The combined diethyl ether extracts were evaporated, added to the light-yellow solid and then refluxed for 2 hours in hydrochloric acid (32 mL, 4 M). The mixture was cooled to room temperature, made basic by addition of sodium carbonate, then extracted with diethyl ether (3 × 30 mL) and dried over sodium sulfate. Removal of the solvent and drying gave the 3-acetylisoquinoline as a pale-yellow solid. Yield: (1200 mg, 60 %). ^{1}H NMR (400 MHz, $CDCl_3$): δ = 9.30 (s, 1H), 8.49 (s, 1H), 8.06 (d, 1H), 8.00 (d, 1H), 7.72 – 7.80 (m, 2H), 2.84 (s, 3H). ^{13}C NMR (100 MHz, $CDCl_3$): δ = 200.34, 152.02, 147.74, 135.74, 131.27, 130.32, 129.66, 128.83, 127.82, 120.50, 26.72. LC-MS ESI$^+$, *m/z* = 172 $(M + H)^+$

The precursors for the synthesizing the C^N^N ligands namely; 3,5-di-*tert*-butylbenzylidene-2-acetophenone[3], 3,5-di-*tert*-butylbenzylidene-2-acetonaphthone[40] and 1-(2-(isoquinolin-3-yl)-2-oxoethyl)pyridinium iodide[3] were prepared according to published procedures.

3,5-di-*tert*-butylbenzylidene-2-acetophenone

To a stirring solution of a mixture of acetophenone (660.8 mg, 642 µL, 5.5 mmol) and 3,5-di-*tert*-butylbenzaldehyde (1200.8 mg, 5.5 mmol) in methanol (20 mL), a solution of NaOH (267 mg, 6.6 mmol) in methanol (5 mL) was added dropwise. The reaction mixture was refluxed for 12 hours and the solvent was removed under reduced pressure to give a crude brownish yellow oil. The crude oil was purified by column chromatography on a silica gel column using *n*-hexane: ethyl acetate (9:1) as eluent, giving the product as an off-white/yellow solid after removal of solvent. Yield: (1340 mg, 76%). ^{1}H NMR (400 MHz, $CDCl_3$): δ = 8.02 (m, 2H), 7.82 (d, 1H), 7.59 (t, 1H), 7.50 – 7.53 (m, 3H), 7.46 – 7.50 (m, 3H), 1.37 (s, 18H). ^{13}C NMR (100 MHz, $CDCl_3$): δ = 191.3, 152.2, 146.5, 139.0, 134.9, 133.3, 128.7, 128.6, 125.4, 122.9, 121.9, 35.0, 31.5. LC-MS ESI$^+$, *m/z* = 321 $[M + H]^+$

3,5-di-*tert*-butylbenzylidene-2-acetonaphthone

Acetonaphthone (936.2 mg, 5.5 mmol), 3,5-di-*tert*-butylbenzaldehyde (1200.8 mg, 5.5 mmol) and NaOH (s) (220 mg, 5.5 mmol) were crushed and mixed using a mortar and pestle, and the yellow medium was aggregated until a pale-yellow powder formed. The aldol product was isolated by washing with water–ethanol, and 10% HCl, yielding a pure product as an off-white powder. Yield: (1300.0 mg, 63.9%). ^{1}H NMR (400 MHz, $CDCl_3$): δ = 8.54 (s, 1H), 8.07 (q, 1H), 8.03 (m, 1H), 7.96 (q, 1H), 7.92 (m, 1H), 7.90 (m, 1H), 7.86 (m, 1H), 7.63 (m, 1H), 7.60 (m, 1H), 7.56 (d, 1H), 7.52 (s, 3H), 1.38 (s, 18H). ^{13}C NMR (100 MHz, $CDCl_3$): δ = 191.04, 151.61, 146.44, 135.90, 135.43, 134.27, 132.64, 129.85, 129.58, 128.49, 128.29, 127.75, 126.73, 125.16, 124.75, 122.85, 121.90, 35.01, 31.41. LC-MS ESI$^+$, *m/z* = 371 $[M + H]^+$

1-(2-(isoquinolin-3-yl)-2-oxoethyl)pyridinium iodide.

To a solution of 3-acetylisoquinoline (766.5.0 mg, 4.5 mmol) in pyridine (10 mL) was added iodine (1235.8 mg, 4.87 mmol). The mixture was heated at 90 ºC for 5 hours and the resultant mixture was cooled to room temperature and ethanol (10.0 mL) was added to enhance precipitation. The brownish yellow solids which formed were filtered and washed with ethanol until the filtrate became colourless. Yield: (1499.5 mg, 88.7%). ^{1}H NMR (400 MHz, $CDCl_3$): δ = 6.63 (s, 2H), 7.93 – 7.99 (m, 2H), 8.28 – 8.37 (m, 4H), 8.69 (s, 1H), 8.75 (t, 2H), 9.06 (d, 2H), 9.59 (s, H). ^{13}C NMR (100 MHz, $CDCl_3$): δ = 191.80, 152.63, 146.35, 146.23, 144.63, 134.85, 131.98, 130.68, 130.34, 128.83, 127.97, 127.70, 120.97, 67.22. LC-MS ESI$^+$, *m/z* = 249 [M – I]$^+$

6.2.3 Syntheses of Ligands

All C^N^N ligands were synthesized following literature procedures.[3, 41]

4-(3,5-di-tert-butylphenyl)-6-phenyl-2,2'-bipyridine, HL^1.

A mixture of 1-(2-pyridylacetyl)pyridinium iodide (326.1 mg, 1.0 mmol), 3,5-di-*tert*-butylbenzylidene-2-acetophenone (320.5mg, 1 mmol) and ammonium acetate (1541.6 mg, 20 mmol) in methanol (20 mL) was refluxed for 24 hours. The solvent was removed under reduced pressure yielding a dark brown liquid as the crude product. Purification of the crude product was done by column chromatography on a silica gel using *n*-hexane: ethyl acetate (8:2) as eluent, giving the product as a pale-yellow solid. Yield: (184.3 mg, 43.8%). ^{1}H NMR (400 MHz, $CDCl_3$): δ = 8.73 (d, 1H), 8.69 (dd, 1H), 8.61 (d, 1H), 8.21 (q, 2H), 7.95 (d, 1H), 7.88 (m, 1H), 7.59 (d, 2H), 7.56-7.54 (m, 2H), 7.52 (d, 1H), 7.48-7.46 (m, 1H), 7.36-7.33 (t, 1H), 1.42 (s, 18). ^{13}C NMR (100 MHz, $CDCl_3$): δ = 129.0, 127.6, 124.1, 123.2, 122.0, 119.3, 118.1, 35.4, 31.7. LC-MS ESI$^+$, *m/z* = 421 [M + H]$^+$. *Anal. Calc. for* $C_{30}H_{32}N_2$: C, 85.67; H, 7.67; N, 6.66 *Found*: C, 85.32; H, 7.45; N, 6.29%.

3-(4-(3,5-di-tert-butylphenyl)-6-phenylpyridin-2-yl)isoquinoline, HL^2.

A mixture of 1-(2-(isoquinolin-3-yl)-2-oxoethyl)pyridinium iodide (376.2 mg, 1.0 mmol), 3,5-di-*tert*-butylbenzylidene-2-acetophenone (320.5 mg, 1 mmol) and ammonium acetate (4206.7 mg, 55 mmol) in methanol (20 mL) was refluxed for 24 hours resulting in the formation of a precipitate. The mixture was cooled to room temperature and the precipitate filtered and washed with methanol to give an off-white crystalline solid. Yield: (217.5 mg 46.2%). ^{1}H NMR (400 MHz, $CDCl_3$): δ = 9.43 (s, 1H), 9.10 (s, 1H), 8.79 (s, 1H), 8.29 (dd, 2H), 8.085 (d, 2H), 7.98 (d, 1H), 7.79 (t, 1H), 7.69 (d, 1H), 7.66 (d, 2H), 7.63-7.59 (m, 3H), 7.52 (t, 1H), 1.47 (s, 18). LC-MS ESI$^+$, *m/z* = 471 [M + H]$^+$. *Anal. Calc. for* $C_{34}H_{34}N_2$: C, 86.77; H, 7.28; N, 5.95 *Found*: C, 86.65; H, 7.24; N, 6.61%.

4-(3,5-di-tert-butylphenyl)-6-(naphthalen-2-yl)-2,2'-bipyridine, HL^3.

A mixture of 1-(2-pyridylacetyl)pyridinium iodide (326.1, 1.0 mmol) and 3,5-di-*tert*-butylbenzylidene-2-acetonaphthone (370.5, 1.0 mmol) and ammonium acetate (4659.7 mg, 60.5 mmol) in methanol (30 mL) was refluxed for 24 hours. The solvent was removed under reduced pressure, giving a crude dark brown liquid product. The product was purified by a column chromatography on a silica gel using *n*-hexane: ethyl acetate (9:1) as the eluent, giving the product as a pale-yellow solid. Yield: (291.6 mg, 62.0%). ^{1}H NMR (400 MHz, $CDCl_3$): δ = 1.43 (s, 18H), 7.35 – 7.38 (m, 1H), 7.53 – 7.55 (m, 2H), 7.57 (t, 1H), 7.62 (d, 2H), 7.89 – 7.93 (m, 2H), 7.99 – 8.02 (m, 2H), 8.09 (s, 1H), 8.38 (dd, 1H), 8.63 (s, 1H), 8.66 (s, 1H), 8.74 - 8.76 (m, 2H). LC-MS ESI$^+$, *m/z* = 471 [M+H]$^+$. *Anal. Calc. for* $C_{34}H_{34}N_2.0.5H_2O$: C, 85.14; H, 7.35; N, 5.84 *Found*: C, 85.51; H, 7.36; N, 5.83%.

3-(4-(3,5-di-tert-butylphenyl)-6-(naphthalen-2-yl)pyridin-2-yl)isoquinoline, HL^4.

A mixture of 1-(2-(isoquinolin-3-yl)-2-oxoethyl)pyridinium iodide (741.0 mg, 1.97 mmol), 3,5-di-*tert*-butylbenzylidene-2-acetonaphthone (730.0 mg, 1 mmol) and ammonium acetate (9652.8

mg, 125.23 mmol) in methanol (20 mL) was refluxed for 36 hours forming a precipitate. After cooling the mixture to room temperature, the precipitate collected by filtration and washed with methanol gave an off-white crystalline solid. Yield: (360.3 mg, 35.1%). ^{1}H NMR (400 MHz, $CDCl_3$): δ = 9.41 (s, 1H), 9.12 (s, 1H), 8.77 (s, 1H), 8.69 (s, 1H), 8.42 (td, 1H), 8.08 (m, 1H), 8.05 (m, 1H), 8.01-8.03 (m, 3H), 7.92 (q, 1H), 7.77 (t, 1H), 7.65 (d, 2H), 7.59 (s, 1H), 7.57 (t, 1H), 7.55-7.53 (m, 2H) 1.45 (s, 18). LC-MS ESI$^+$, *m/z* = 521 [M+H]$^+$. *Anal. Calc. for* $C_{38}H_{36}N_2.H_2O$: C, 86.16; H, 7.04; N, 5.29 *Found*: C, 86.42; H, 6.89; N, 5.62%.

6.2.4 Syntheses of Cyclometalated Pd(II) Complexes

The complexes were synthesized according to published literature procedures.[1-4]

Chloro-4-(3,5-di-tert-butylphenyl)-6-phenyl-2,2'-bipyridine)palladium(II), PdL^1.

$Pd(PhCN)_2Cl_2$ (105.5 mg, 0.275 mmol) was added to a solution of **HL^1** (104.3 mg, 0.25 mmol) in acetone (30 mL). The mixture was refluxed for 24 hours and the solvent evaporated to dryness under reduced pressure. The resulting solid was washed with n-hexane, methanol, deionized water, and diethyl ether consecutively to yield a yellow microcrystalline solid. Yield: (92.6 mg, 66%). ^{1}H NMR (400 MHz, $CDCl_3$): δ = 1.44 (s, 18H), 7.11 (m, 2H), 7.42 – 7.44 (m, 1H), 7.49 – 7.52 (m, 3H), 7.63 (t, 1H), 7.66 (d, 1H), 7.76 (d, 1H), 7.79 – 7.81 (m, 1H), 7.98 (ddd, 1H), 8.03 (d, 1H), 8.89 (d, 1H). LC-MS ESI$^+$, *m/z* = 568 [M$^+$ + MeCN]. *Anal. Calc. for* $C_{30}H_{31}N_2PdCl$: C, 64.18; H, 5.57; N, 4.99 *Found*: C, 64.12; H, 5.46; N, 5.28%.

Chloro-3-(4-(3,5-di-tert-butylphenyl)-6-phenylpyridin-2-ylisoquinoline)palladium(II), PdL^2.

$Pd(PhCN)_2Cl_2$ (232.1 mg, 0.605 mmol) was added to a solution of **HL^2** (257.1 mg, 0.55 mmol) in acetone (30 mL). The mixture was refluxed for 24 hours and the resulting yellow suspension was filtered and washed with n-hexane, methanol, deionized water, and diethyl ether consecutively to yield a yellow solid. Yield: (224.3 mg, 54.5%). ^{1}H NMR (400 MHz, $CDCl_3$): δ

= 1.49 (s, 18H), 6.90 (t, 1H), 6.99 (t, 1H), 7.23 (d, 1H), 7.35 (s, 1H), 7.59 (t, 1H), 7.61 – 7.63 (m, 2H), 7.65 (s, 2H), 7.71 – 7.75 (m, 2H), 7.88 (s, 1H), 7.92 (d, 1H), 8.39 (s, 1H), 9.15 (s, 1H). LC-MS ESI$^+$, *m/z* = 616 [M$^+$ + MeCN]. *Anal. Calc. for* $C_{34}H_{33}N_2PdCl$: C, 66.78; H, 5.44; N, 4.58 *Found*: C, 67.06; H, 5.02; N, 4.72%.

Chloro-(4-(3,5-di-tert-butylphenyl)-6-(naphthalen-2-yl)-2,2'-bipyridine)palladium(II), PdL^3.

$Pd(PhCN)_2Cl_2$ (126.6 mg, 0.33 mmol) was added to a solution of **HL^3** (111.2 mg, 0.3 mmol) in acetone (30 mL). The mixture was refluxed for 24 hours and the resulting yellow suspension was filtered and washed with n-hexane, methanol, deionized water, and diethyl ether consecutively. The desired product was then extracted with dichloromethane. Pure product was obtained by slow diffusion of diethyl ether into dichloromethane yielding a yellow microcrystalline solid. Yield: (26.6 mg, 8.20%). ^{1}H NMR (400 MHz, $CDCl_3$): δ = 1.49 (s, 18H), 7.29 (dd, 2H), 7.32 (t, 1H), 7.44 (m, 1H), 7.61 (d, 2H), 7.62 (d, 1H), 7.66 (d, 1H), 7.71 (t, 1H), 7.73 (d, 1H), 7.78 (d, 1H), 7.79 (td, 1H), 7.91(s, 1H), 7.97 (d, 1H), 8.71 (dd, 1H). LC-MS ESI$^+$, *m/z* = 616 [M$^+$ + MeCN]. *Anal. Calc. for* $C_{34}H_{33}N_2PdCl$: C, 66.78; H, 5.44; N, 4.58 *Found*: C, 66.87; H, 5.42; N, 4.25%.

Chloro-3-(4-(3,5-di-tert-butylphenyl)-6-(naphthalen-2-yl)pyridin-2-ylisoquinoline)palladium(II), PdL^4.

$Pd(PhCN)_2Cl_2$ (168.9 mg, 0.44 mmol) was added to a solution of **HL^4** (208.2 mg, 0.40 mmol) in acetone (30 mL). The mixture was refluxed for 24 hours and the resulting yellow suspension was filtered and washed with n-hexane, methanol, deionized water, and diethyl ether consecutively to give a yellow solid. Yield: (244.6 mg, 92.4%). ^{1}H NMR (400 MHz, CD_2Cl_2): δ = 1.51 (s, 18H), 7.34-7.36 (m, 2H), 7.49 (t, 1H), 7.64 (s, 1H), 7.65 (t, 1H), 7.71 (s, 3H), 7.74-7.77 (m, 1H), 7.80-7.82 (m, 2H), 7.85 (s, 1H), 7.88 (s, 1H), 7.94 (s, 1H), 7.98 (d, 1H), 8.40 (s, 1H), 8.71 (s, 1H).

LC-MS ESI$^+$, *m/z* = 666 [M$^+$ + MeCN]. *Anal. Calc. for* $C_{38}H_{35}N_2PdCl$: C, 68.99; H, 5.33; N, 4.23 *Found*: C, 68.91; H, 5.29; N, 4.42%.

6.2.5 Physical Measurements and Instrumentation

^{1}H-NMR and ^{13}C-NMR spectral data were obtained from either Bruker Avance DPX 400 NMR or DPX 500 with a 5 mm BBOZ probe at 30° C to characterize the complexes and ligands. A Shimadzu LC-MS 2020 spectrometer with an ESI source was used for mass spectral characterization while a Thermo Scientific Flash 2000 and a Carlo Erba Elemental Analyzer 1106 was used to determine the elemental composition of the ligands and complexes. The NMR and mass spectra data for the synthesized ligands and complexes are sampled in Figures SI 6.1–6.25, supporting information (ESI‡). The X-ray data was collected on a Bruker Apex Duo fitted with an Incoatec microsource operating at 30 W power and an Oxford Instruments Cryojet operating at 100(2) K. Cary 100 Bio UV–visible spectrophotometer having a cell compartment thermostated by a Varian Pelter temperature controller with accuracy of ± 0.05º C was used to determine suitable wavelengths for monitoring the substitution reactions. The rates of the substitution reactions were monitored using Applied Photophysics SX 20 stopped-flow reaction analyzer coupled to an online data acquisition system. The instrument temperature was thermo-controlled within ± 0.1 °C.

6.2.6 X-ray Crystallography

Single X-ray quality crystals of **PdL^2**, which were orange and block-shaped, were grown from slow evaporation of chloroform solution, while orange and plate-shaped crystals of **PdL^3** were obtained from slow diffusion of diethyl ether into dichloromethane solution. A suitable crystal was selected and mounted on a MITIGEN holder in paratone oil on a Bruker APEX-II CCD diffractometer. The crystal was kept at T = 100(2) K during data collection. Using Olex2,[42] the

structure was solved with the ShelXS-2013 [43] structure solution program using intrinsic phasing and refined with a 2016/6 of ShelXL program[44] using least squares minimisation method.

6.2.7 Computational Modelling

To understand the steric and electronic factors of the complexes in relation to how they affect observed trend, ground state electronic structures of the complexes were optimized using the density functional theory (DFT) calculations. The DFT calculations were performed with the Gaussian 09 program suite [45] using the B3LYP (Becke 3-Lee-Yang-Parr) functional method using the LANL2DZ (Los Alamos National Laboratory 2 Double ζ)[46] as the basis set. All the complexes were treated as neutral species and in the singlet spin. Global electrophilicity index (ω) and electronic chemical potential (μ) of the complexes were calculated from the optimized data using literature methods.[47-51]

6.2.8 Preparation of Kinetic Solutions and Measurements

The solutions of the Pd(II) complexes were prepared by dissolving appropriate amounts in 90% dichloromethane in methanol. Similarly, the stock solution of each nucleophile was freshly prepared by dissolving appropriate weighed amounts in 90% dichloromethane in methanol. The stock solution of the nucleophiles approximately 50-fold excess of the complex concentration was serially diluted with a 90% dichloromethane in methanol to afford 40- 30- 20- and 10-fold to maintain the *pseudo*-first-order conditions. The concentration dependent reactions were performed at 298 K. The temperature dependence of the rate of substitution were monitored within a range of temperatures between 10 °C to 30 °C at 5 °C intervals using a nucleophile solution whose concentration was 30-fold excess of the complexes. All reactions were initiated by mixing equal volumes of ligand and complex solutions directly into the drive syringes of stopped-flow spectrophotometer.

6.3 Results

6.3.1 X-ray Crystal Structures

The molecular structures of **PdL^2** (**$C_{143}H_{139}Cl_{25}N_8Pd_4$**) and **PdL^3** (**$C_{34}H_{33}ClN_2Pd$**) complexes were confirmed by single crystal X-ray diffraction analysis. The data of the crystal structures have been deposited (deposition numbers; CCDC 1872831 and 1872832 for **PdL^2** and **PdL^3**, respectively) at Cambridge Crystallographic Data Centre. The ellipsoid diagram of the complexes is depicted in Figure 6.2, while the crystallographic data, selected bond lengths and angles are presented in Tables 6.1 and 6.2.

PdL^2 crystallized out in the triclinic space group P-1 with Z = 1 as an inversion dimer with chloroform solvent molecules, while **PdL^3** crystallized in the orthorhombic space group Pbca with Z = 8 as a simple monomer. The geometry around the metal centre of the complexes displays a tridentate coordination fashion in which Pd metal ion is coordinated to two nitrogen atoms N1, N2 and a deprotonated one carbon atom C1 of the ligand and the respective bond lengths are 1.960(5), 2.124 (5) and 1.971(6), for **PdL^2** and 1.964(3), 2.128(3), and 1.978(3)Å for **PdL^3**, respectively.

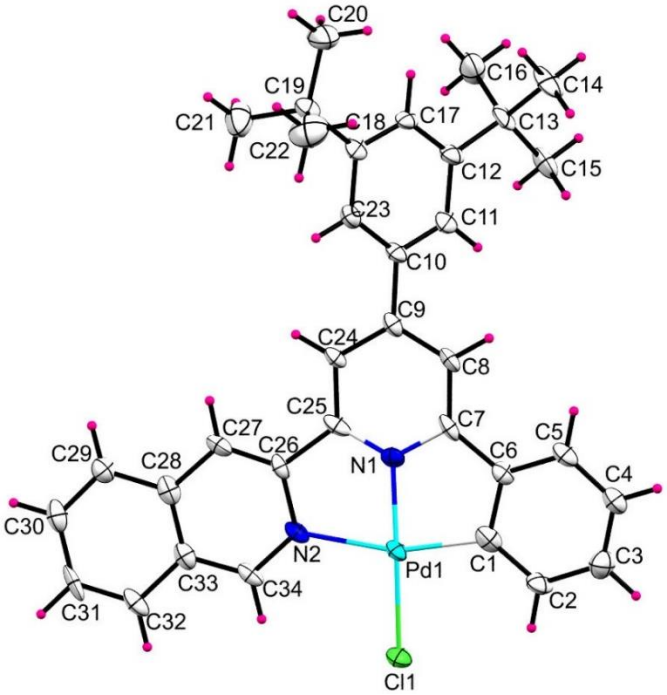

[a]

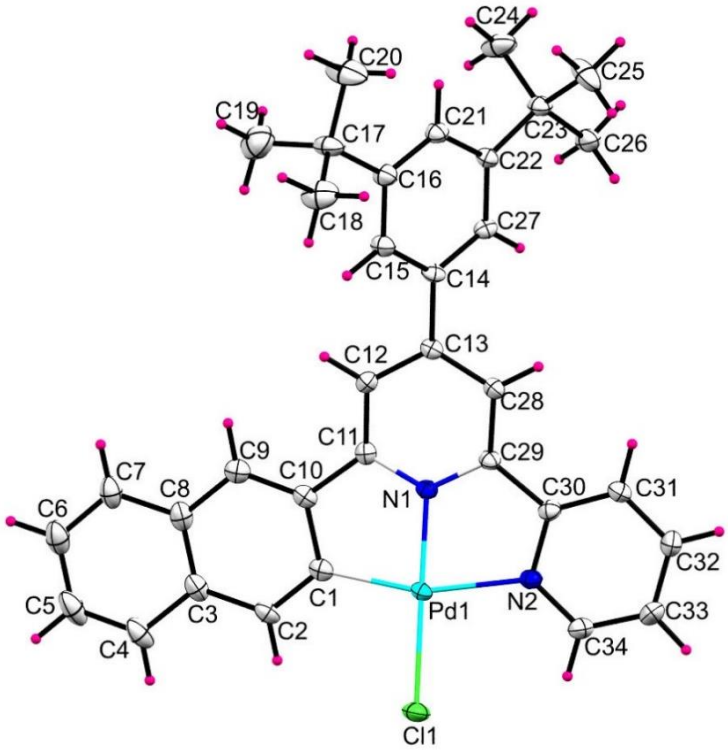

[b]

Figure 6. 2 Molecular structure of [**a**] **PdL²** and [**b**] **PdL³** with atom numbering scheme. The displacement ellipsoids of atoms are shown at 50% probability. Solvent of crystallization is omitted for clarity in the case of **PdL²**.

Table 6. 1 Crystal data and structure refinement parameters for **PdL²** and **PdL³**

	PdL²	**PdL³**
Molecular formula	$C_{143}H_{139}Cl_{25}N_8Pd_4$	$C_{34}H_{33}ClN_2Pd$
Mr	3281.46	611.47
Crystal size/ mm^3	0.32×0.14×0.09	0.28×0.20×0.08
T/K	99.98	100(2)
λ/ Å	0.71073	0.71073
Crystal system	Triclinic	Orthorhombic
Space group	*P-1*	*Pbca*
a/Å	14.099(3)	12.3997(18)
b/Å	14.609(4)	20.182(3)
c/Å	18.758(5)	23.110(3)
α/º	110.724(4)	90
β/º	91.482(5)	90
γ/º	101.391(4)	90
V/ $Å^3$	3523.1(15)	5783.3(14)
Z	1	8
Dc /Mg m^{-3}	1.547	1.405
μ/ mm^{-1}	1.030	0.759
θ range/º	2.334-52	1.762-28.302
Reflections collected (independent)	25781(12922)	32491(7059)
R_{int}	0.0331	0.0384
No. of parameters (restraints)	841(42)	349(0)
R indices (all data)	R1=0.0538, wR2=0.1442	R_1=0.0473, wR_2= 0.1066
Goodness-of-fit on F^2	1.056	1.137
Max, Min Δρ/e $Å^{-3}$	1.60, -1.36	2.417, -0.940

Similarly, the fourth coordination site is covalently bonded by the chloride atom at Pd–Cl1 bond distances of 2.315(1) and 2.308(1) Å for **PdL²** and **PdL³**, respectively. These bond distances around the metal centre are within the ranges observed for X-ray crystal structures of related complexes of Pt(II) and Pd(II).[3, 4, 28, 52] The Pd1–N1 and Pd1–C1 bond lengths are comparable and shorter than those of Pd1–Cl1 and Pd1–N2 possibly due to strong interactions between the Pd(II) metal centre, the *trans*-N-pyridyl ring and the deprotonated *cis*-carbon of phenyl and naphthalene moiety for **PdL²** and **PdL³**, respectively.

Table 6. 2 Selected bond lengths and bond angles

	PdL^2	**PdL^3**
Bond Lengths (Å)		
N1–Pd1	1.960(5)	1.964(3)
N2–Pd1	2.124(5)	2.128(3)
C1–Pd1	1.971(6)	1.978(3)
Cl1–Pd1	2.315(1)	2.308(1)
Bond angles (^{0})		
N1–Pd1–Cl1	173.95(1)	176.58(8)
N1–Pd–C1	82.71(2)	82.41(1)
N1–Pd–N2	79.15(2)	79.37(1)
N2–Pd–C1	161.81(2)	161.70(1)
N2–Pd–Cl1	98.85(1)	99.68(8)
C1–Pd–Cl1	99.34(2)	98.61(1)

The complex structures assume distorted square planar coordination geometry as shown by the slight displacement of the chloropalladium unit from the molecular plane containing C1, N1, N2 and N1, Pd, Cl1 atoms make angles of 173.9(1)º for **PdL^2** and 176.5(8)º for **PdL^3** showing some slight deviating from linearity (180º). Moreover, the angles N1–Pd–N2 and N2–Pd–C1 are 79.1(1) and 161.8(2) for **PdL^2**, while those of **PdL^3** are 79.4(1)º and 161.7(1)º. This type of distortion has been reported for square planar d^8 complexes coordinated to tridentate ligands forming two fused five-membered chelate rings.[1, 53-56] The bond angles are comparable to the DFT calculated values shown in Table 6.4. In addition, the geometry structure of the complexes shows that the plane of the 4-(3,5-di-*tert*-butyl)phenyl group, ancillary ligand, twists away from the plane of the central pyridyl ring coordinated to the metal centre leading to the complexes having two major planes. The plane of the ligand portion defined by Pd, N, C and Pd, N, N atoms coordinated to the metal centre is almost flat, having a dihedral angle for **PdL^3**, 2.81º between the planes of the two five-membered chelate rings higher than that of a related X-ray crystal structure[52] while that of **PdL^2** (1.0 º) is comparable. This could be attributed to the steric imposed demands on the formed chelate ring in the case of **PdL^3** compared to **PdL^2**. The

ancillary ligand substituted phenyl ring is non-coplanar with the central pyridyl ring and the rest of the aromatic system leading to a tilted angle of 46.45º and 42.86º between their mean planes for **PdL²** and **PdL³**, respectively. This means that extension of π-backbonding cannot be up to the 4' attached (3,5-di-*tert*-butyl)phenyl ring. Hence the σ-donation towards the cyclometalated is prominent. This weakens the π-acceptor property of the C^N^N ligands to some extent.

The crystal packing in **PdL²** shows tetrameric molecules arranged in an inversion head-to-tail manner without metal-metal interactions. Intermolecular interactions between the molecules *via* the C34–H···Cl1 is noted in the molecules. The solvent-molecule interactions are evident particularly through the bonding linkages between the chloride atom of the solvent and the H attached at the C19/C23 as well as the H of the solvent and Cl1. There is intermolecular π···π stacking interactions as evidenced by the Cg ... Cg (center of gravity of the aromatic ring) interplanar distances ranging between 3.583 Å – 4.056 Å. In addition, there is C···C linkages [C16···C47 (3.355 Å), C15···C47 (3.306 Å) and C16···C48 (3.369 Å)] ranging between 3.306 Å – 3.369 Å. The C···C linkages and the π···π interactions are shown in Figure 6.3.

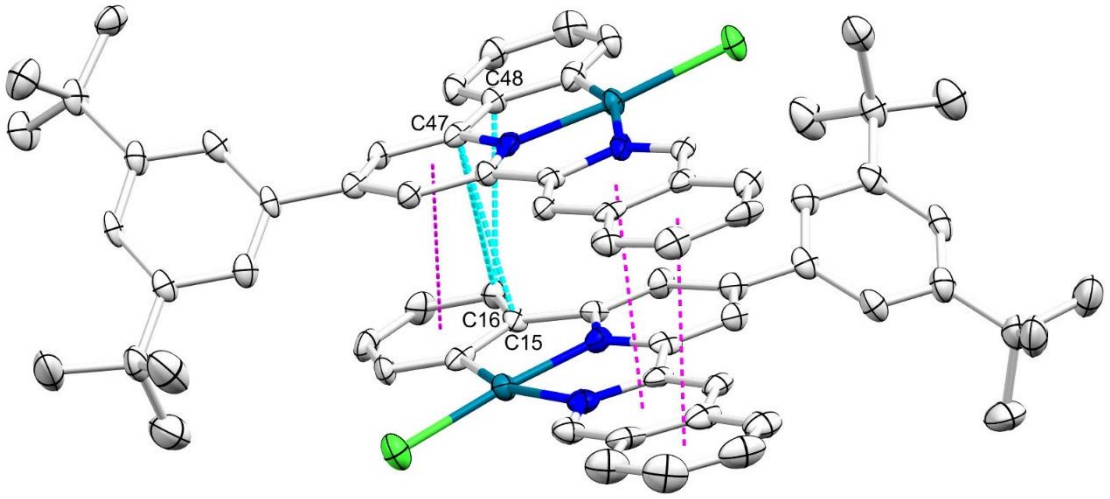

Figure 6. 3 Part of the crystal packing of **PdL²** showing asymmetric unit of inversion dimer with C···C interactions (shown in blue dashed lines) and π···π interactions (shown in purple lines) between the aromatic rings of the molecules.

However, The **PdL³** crystal packing shows an inversion dimer with no metal-metal interactions as the Pd–Pd distance being 6.286(1) Å is much larger than 4 Å.[57] The dimeric molecules are arranged in a head-to-tail fashion. The interplanar distances of 3.615 Å between the rings within the dimeric molecules allows for π···π interactions between the molecues [4, 41, 58] as well as C···C linkages of C24···C2 (2.774 Å) and C24···C1 (3.861 Å) as depicted in Figure 6.4. Further extensive intermolecular attractions characterised by bonding linkages C–H···Cl and [C23–H···Cl1 (2.751 Å), C34–H···Cl1 (2.939 Å)] are observed in the crystal structure.

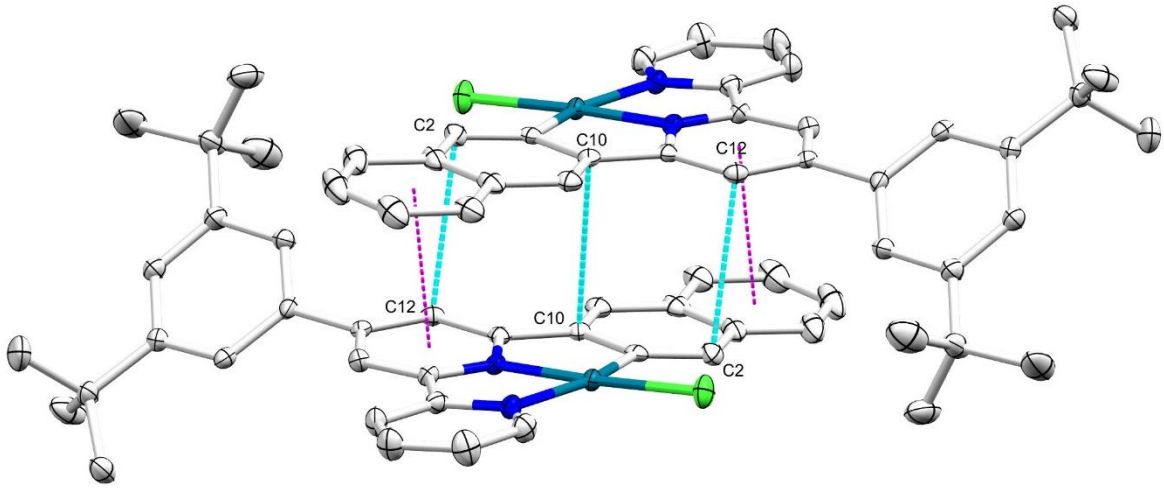

Figure 6. 4 A section of the crystal packing diagram of **PdL³** showing an inversion dimer with C···C interactions (shown in blue dashed lines) and π···π interactions (shown in purple lines) between the aromatic rings of the molecules.

6.3.2 Computational Details

To gain more insight into how the steric and electronic factors of the Pd(II) complexes influences their reactivity, ground state optimized structures were computed using the DFT. The geometry optimized molecular frontier orbitals, the planarity of the structures for the complexes, and excerpts of calculated data are presented in Tables 6.3 and 6.4, respectively. Also included in Table 6.4 for comparison purposes are the calculated values of **[Pd(terpy)Cl]⁺**.

Table 6. 3 DFT optimized HOMO and LUMO frontier molecular orbitals and the planarity for the complexes at B3LYP/LANL2DZ theory level (Iso value = 0.02).

Complex structure	HOMO maps	LUMO maps	Planarity
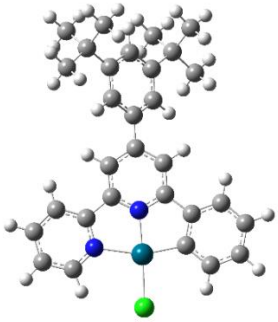 **PdL^1**	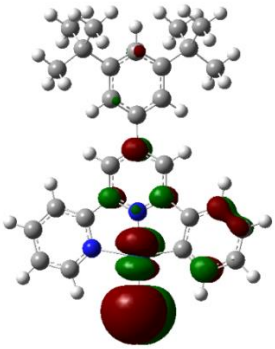	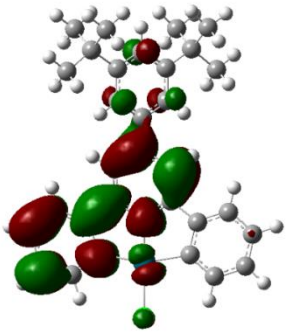	
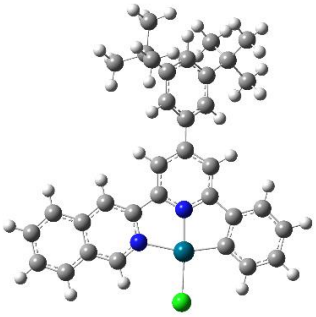 **PdL^2**	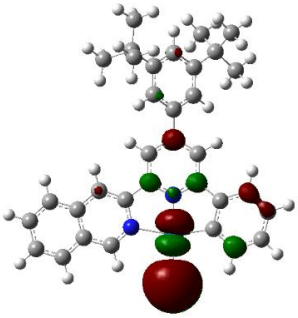	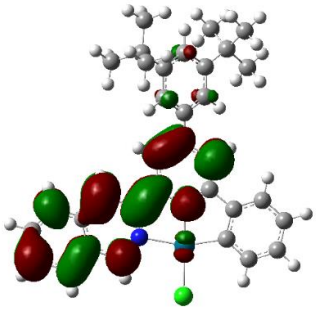	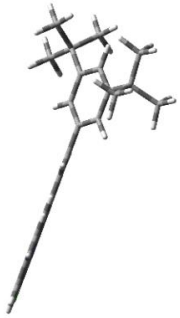
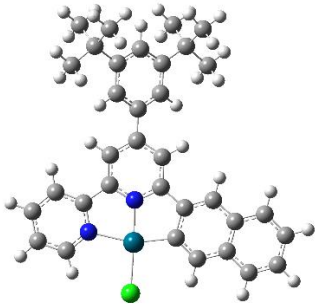 **PdL^3**	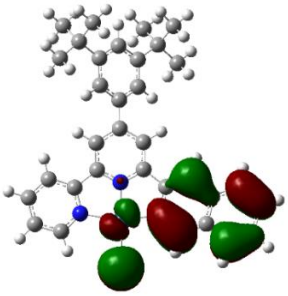	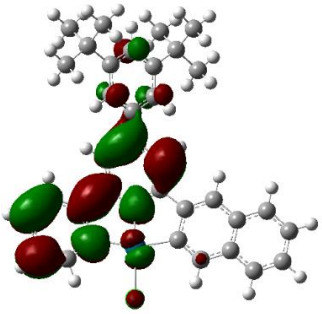	
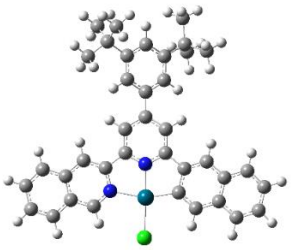 **PdL^4**	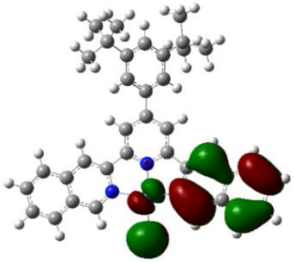	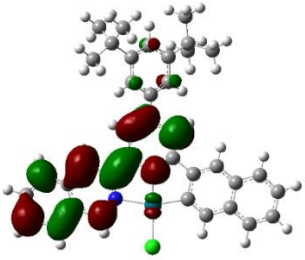	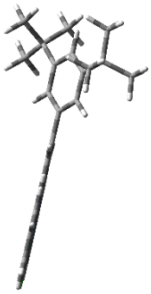

Table 6. 4 Calculated parameters of the Pd(II) complexes

Property	**PdL[1]**	**PdL[2]**	**PdL[3]**	**PdL[4]**	[a]**[Pd(terpy)Cl]$^+$**
NBO Charges					
Pd^{2+}	0.372	0.372	0.372	0.372	0.582
Cl^-	-0.479	-0.485	-0.480	-0.486	-0.522
Trans- N1	-0.466	-0.468	-0.466	-0.467	-0.422
Cis- N2	-0.504	-0.506	-0.503	-0.505	-0.483
Cis- C	-0.108	-0.109	-0.122	-0.123	-
Electrophilicity index (ω)	5.659	5.353	5.815	5.516	7.046
Electronic Chemical Potential (μ) (eV)	-4.415	-4.058	-4.055	-3.976	-5.302
Bond lengths (Å)					
Trans- N1 – Pd	1.992	1.992	1.992	1.991	1.970
Cis- N2 – Pd	2.174	2.167	2.172	2.164	2.063
Cis- C1 –Pd	2.004	2.003	2.002	2.003	-
Pd – Cl	2.387	2.390	2.388	2.391	2.415
HOMO – LUMO Energy (eV)					
LUMO (eV)	-2.627	-2.520	-2. 641	-2.543	-3.307
HOMO (eV)	-5.663	-5.596	-5.468	-5.408	-7.296
$\Delta E_{LUMO-HOMO}$	3.036	3.076	2.827	2.865	3.989
Bond angles (º)					
N1 – Pd – Cl1	177.697	177.599	177.739	177.428	179.998
N1 – Pd – C1	82.096	82.157	82.353	82.410	-
N1 – Pd – N2	78.335	78.683	78.427	78.794	80.670
N2 – Pd – C1	160.431	160.839	160.780	161.204	-
N2 – Pd – Cl1	99.362	98.916	99.334	98.634	99.339
C – Pd – Cl1	100.207	100.244	99.905	100.161	-
Dipole moment (Debye)	12.577	12.608	12.765	12.848	13.163

From the frontier orbital mappings in Table 6.3, the HOMOs are mainly from the contributions from the 3p-orbitals of the chlorine atom, 4d-orbitals of the palladium atom and π*-orbitals of the carbon ligand moiety (phenyl or naphthalene). This implies that the phenyl moiety in **PdL[1]/PdL[2]** and naphthalene moiety in **PdL[3]** are electron rich, respectively. The naphthalene group in **PdL[3]** has a larger contribution to the HOMOs in comparison to the phenyl group. The LUMO electrons are mainly distributed on the N- containing moiety, *trans*- and/or *cis*- pyridyl and the isoquinoline moieties. All complexes have near planar geometry with slight distortions as

witnessed in Table 6.4. The NBO charges representing the point charge on Pd atom remain unchanged across the complexes possibly due to the strong *cis*-σ-donation from the carbon, while the electrophilicity indices of the complexes [**PdL^1** (5.659), **PdL^2** (5.353), **PdL^3** (5.815) and **PdL^4** (5.516)] changes. It is observed that on stepwise extension of the π-conjugation, moving from **PdL^1** to **PdL^4**, the energy levels of the HOMO orbitals are successively raised. This suggests that the σ-donation of electron density towards the Pd(II) metal centres [59] subsequently increases in the same order. This therefore means that the electron acceptability reduces going from **PdL^1** to **PdL^4**, (Table 6.4) which is reflected in the reactivity trend.

In addition, the electronic chemical potential (μ) descriptor, which is defined as the negative of electronegativity of a complex,[47, 60] and physically describes the escaping tendency of electrons from an equilibrium system[47, 61] shows a clear trend. As the magnitude of the negative value of μ increases, the electron acceptability of the system increases.[50, 51] This further confirms that the π-acceptability of the ligands in the complexes decreases in the order [**Pd(terpy)Cl**]$^+$ < **PdL1** < **PdL2** < **PdL3** < **PdL^4** which is in support of the reactivity trend.

6.3.3 Kinetic Analysis

Substitution reactions of the labile chloride of the modelled Pd(II) complexes with thiourea nucleophiles as the incoming nucleophiles was investigated as a function of concentration and temperature under *pseudo*-first-order conditions. The rate of substitution was studied using the stopped-flow methods at predetermined wavelength for which the spectral changes between the reactions of the complex and the nucleophiles were accompanied by large spectral changes. The wavelengths at which the kinetics of the reaction were monitored are reported in Table SI 6.1 in the supporting information (ESI‡). A representative kinetic trace recorded on the stopped-flow spectrophotometer for the substitution of the chloride ligand from **PdL^4** by **Dmtu** is depicted in

Figure 6.5. The *pseudo*-first-order rate constant, k_{obs}, was obtained by fitting the data to a standard single exponential function as shown in Figure 6.5.

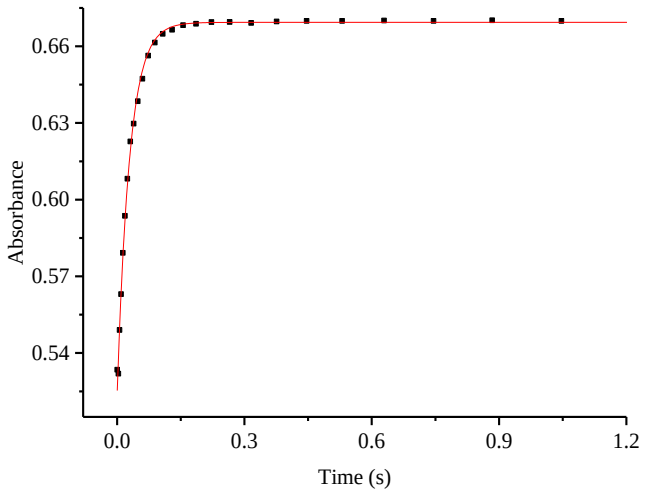

Figure 6. 5 Stopped-flow kinetic trace at 388 nm of **PdL^4** (1.0 x 10^{-4} M) and **Dmtu** (4.0 x 10^{-3} M) at 298 K.

This was an indication that the rate of substitution reactions were first-order in both the Pd(II) complexes and the thiourea nucleophiles. The second-order rate constants, k_2, was obtained from the gradient of the plots of average k_{obs} against the nucleophile concentration using OriginPro 9.1® [62] Straight line plots with zero intercepts were obtained indicating that the reverse or solvotic pathway was absent or insignificant. A representative plot of k_{obs} versus the concentration of the nucleophiles for the chloride substitution from **PdL^2** by the nucleophiles is shown in Figure 6.6; similar plots for the other complexes are presented in Figures SI 6.26 – 6.28, whereas the values of k_{obs} with their respective nucleophile concentrations are shown in Tables SI 6.2 – 6.5 in the supporting information (ESI‡). Thus, the *pseudo*-first-order rate constant is related to the nucleophile concentration [Nu] by *Equation 6.1*. This means that the incoming thiourea nucleophiles displace the leaving chloride ligand from the metal complexes in an irreversible manner.

$$k_{obs} = k_2 [Nu] \tag{6.1}$$

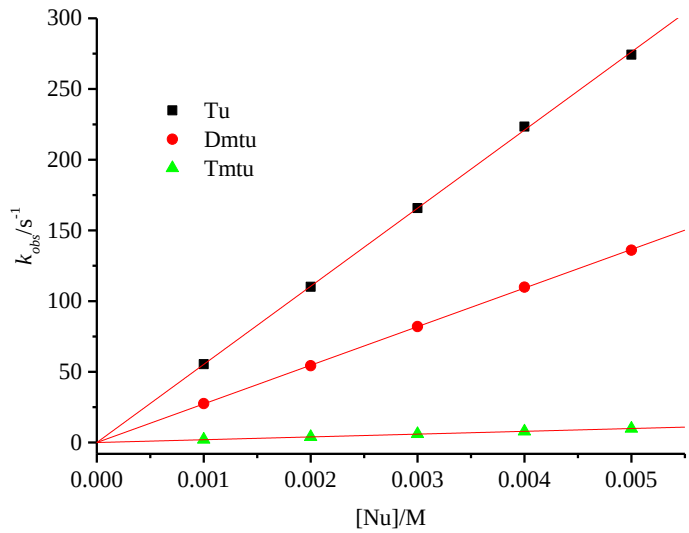

Figure 6. 6 Dependence of k_{obs} on the concentration of the nucleophiles for the reactions with from **PdL²** at T = 298 K.

The values of the second-order rate constants, k_2, obtained from the substitution reactions of the complexes and the nucleophiles are presented in Table 6.5. Data on the temperature dependence of k_2 was plotted according to the Eyring *Equation 6.2*. [63] From the plots of ln $\left(\frac{k_2}{T}\right)$ versus $\frac{1}{T}$, the activation enthalpy **(**$\Delta H^{\neq}$) change and the activation entropy ($\Delta S^{\neq}$) change were calculated from the slopes and y-intercepts of the plots, respectively.

$$\ln\left(\frac{k_2}{T}\right) = -\frac{\Delta H^{\neq}}{RT} + \left(23.8 + \frac{\Delta S^{\neq}}{R}\right) \tag{6.2}$$

where T and R represent temperature and gas constant, respectively. Representative Eyring plots for the reactions of **PdL³** is presented in Figure 6.7; similar plots for the reactions of the other

Table 6. 5 Values k_2 at 298 K, $\Delta H^{\#}$ and $\Delta S^{\#}$ for the reactions of Pd(II) complexes with the nucleophiles.

Complexes	Nu	k_2 ($M^{-1}s^{-1}$)	$\Delta H^{\neq}$ (kJ mol^{-1})	$\Delta S^{\neq}$ ($JK^{-1}mol^{-1}$)
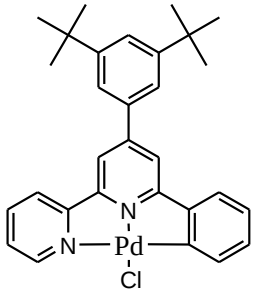 **PdL^1**	Tu	81690 ± 800	15 ± 1	- 101 ± 3
	Dmtu	43850 ± 400	16 ± 1	- 105 ± 3
	Tmtu	3035 ± 40	23 ± 1	- 103 ± 3
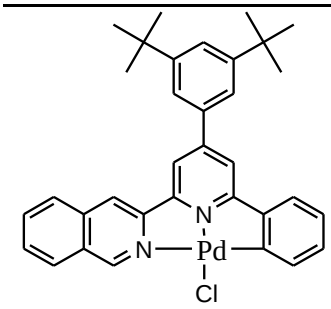 **PdL^2**	Tu	55246 ± 200	22 ± 1	- 77 ± 3
	Dmtu	27310 ± 60	25 ± 1	- 75 ± 3
	Tmtu	1980 ± 10	39 ± 1	- 54 ± 4
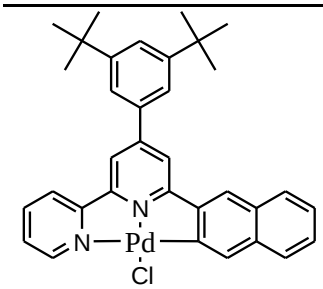 **PdL^3**	Tu	36451 ± 180	32 ± 1	- 86 ± 2
	Dmtu	17047 ± 170	31 ± 1	- 60 ± 2
	Tmtu	1886 ± 20	45 ± 1	- 32 ± 5
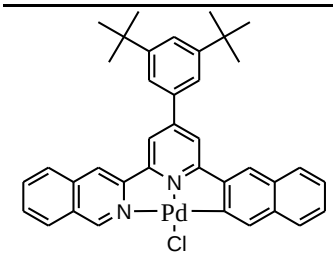 **PdL^4**	Tu	20432 ± 220	33 ± 1	- 52 ± 4
	Dmtu	9412 ± 30	33 ± 1	- 58± 3
	Tmtu	1030 ± 10	48 ± 2	- 29 ± 6

complexes are shown in Figures SI 6.29 – 6.31 and the values $\frac{1}{T}$ and their respective $ln\left(\frac{k_2}{T}\right)$ are depicted in Tables SI 6.6 – 6.9 in the supporting information (ESI‡). The calculated activation parameter data are summarized in Table 6.5.

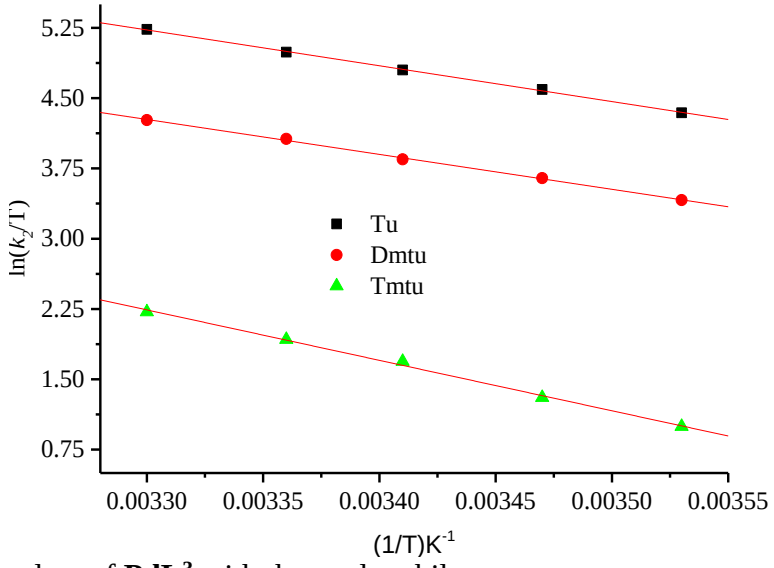

Figure 6. 7 Eyring plots of **PdL³** with the nucleophiles

6.4 Discussion

In this study, mononuclear Pd(II) complexes with π-extended cyclometalated C^N^N polypyridyl phenyl ligands were synthesized and their rate of chloride substitution behaviour by thiourea nucleophiles measured. Since these reactions mimics possible interactions of the Pd(II) complexes in biological systems to provide data which will form part of the protracted search for alternative palladium anticancer drugs, the interesting feature of the designed complexes is that they offer three in one function namely; (1) a constant 4'–(3,5-di-*tert*-butyl)phenyl ring offers possible favourable van-der-waal's stabilizing interactions at specific hydrophobic DNA pockets,[64] (2) a planar cyclometallation coordination sphere would facilitate insertion of the complex between the DNA base-pairs through covalent binding[65, 66] since precovalent interactions increases going from **PdL¹** to **PdL⁴**, and (3) a labile chloride group facilitates hydrolysis and formation of reactive species that interact with DNA to form monofunctional adducts that are stabilised in two other forms.[67-69] Theoretically, for all the Pd(II) complexes, a constant amount of electron density flows into the central pyridyl ring through σ-donation (from 4'-(3,5-di-*tert*-butyl)phenyl ring) which will weaken its π-acceptability. The 4'–phenyl ring is

twisted off the cyclometalated plane as shown in the X-ray crystal structures of **PdL^2** and **PdL^3** as well as the planarity of the DFT calculated geometry structures (Table 6.3).

From the DFT calculated data, all the complexes are slightly distorted square planar with N2–Pd–C angles ranging between 160° – 161° deviating from planarity (Table 6.4). The (3,5-di-*tert*-butyl)phenyl group lies out-of-plane with the plane of the central pyridyl moiety. This interannular bond of the complexes twists in such a way that the plane of the (3,5-di-*tert*-butyl)phenyl ring is at an angle of 36.77° with respect to the plane of the central pyridyl ring for **PdL^1**. The phenomenon is similar for **PdL^2**, **PdL^3** and **PdL^4** having angles 36.84°, 36.52° and 35.16°, respectively. This out-of-plane distortion in the structures observed rules out any possibility of π-electronic communication (π-back bonding) and π-extension beyond the bipyridyl phenyl subunits coordinated to the Pd metal centre. Only the *trans* σ-donation of the (3,5-di-*tert*-butyl)phenyl fragment would play a role in weakening the π-acceptor ability of the ligands, which is constant and equal in the complexes given that the differences in their structural orientation is marginal. In addition, the proximity of the (3,5-di-*tert*-butyl)phenyl fragment to the coordinated Pd metal centre rules out any possibility of steric hinderance to the incoming nucleophiles by the ancillary ligand of the complexes.[34, 70] Therefore, the differences in the reactivity of the Pd(II) complexes under present study is mainly due to the electronic effects caused by the *cis*-ligand moieties.

The high lability of the chloride ligand in these complexes enables us to compare the reactivity of **PdL^1** with [**Pd(terpy)Cl]$^+$** complex from a previous study (in **chapter 3** in Table 3.5). The structural difference in the complexes is that [**Pd(terpy)Cl]$^+$** has a tridentate N^N^N ligand system as opposed to N^N^C ligand system in **PdL^1**. This structural difference would be helpful in clarifying the role played by the carbon *cis* effect in the presence of a strong π-acceptor ligand

backbone. The reactivity of [**Pd(terpy)Cl]**$^{+}$ (118,000 $M^{-1}s^{-1}$) is higher than that of **PdL**^{1} by a factor of 1.4. The low reactivity of **PdL**^{1} in comparison to [**Pd(terpy)Cl**]$^{+}$ is thus due to the role played by carbon in the *cis*-position to the leaving group and the *trans*-(3,5-di-tert-butyl)phenyl, ancillary ligand. The *trans*-(3,5-di-*tert*-butyl)phenyl group and Pd–C bond introduced in **PdL**^{1} both causes a strong σ electron donation towards the Pd-metal centre through the *trans*-pyridyl ring and the *cis*-carbon, respectively. This leads to accumulation of electron density at the Pd-metal centre which reduces its electrophilicity and repels the incoming nucleophiles than in [**Pd(terpy)Cl**]$^{+}$. The increase of electron density around the Pd metal centre destabilises the transition state while ground state is stabilised and hence the resulting net effect is the retardation of the substitution reaction of **PdL**^{1} in comparison to [**Pd(terpy)Cl**]$^{+}$. This is supported by DFT data which shows that the total electrophilicity as well as the NBO charges of [**Pd(terpy)Cl**]$^{+}$ is more positive than that of **PdL**^{1} (Table 6.4). This phenomenon has been reported in literature for platinum complexes.[28, 33, 34]

Comparing the reactivities of the Pd(II) complexes under this study with **Tu** as a reference, the trend decreases in the order **PdL**^{1} **>** **PdL**^{2} **>** **PdL**^{3} **>** **PdL**^{4} as shown in the presented k_2 values in Table 6.5. A similar trend is noted with the other nucleophiles, **Dmtu** and **Tmtu**. When the k_2 values for the reactions of **PdL**^{1} is compared with those of **PdL**^{2}, **PdL**^{3} and **PdL**^{4}, the reactivity of **PdL**^{1} is higher by factors of 1.5, 2.2 and 4, respectively. **PdL**^{2} is slower than **PdL**^{1} due to the weaker π-acceptability of the isoquinoline as well as the net σ-donation effect through the Pd–N bond than pyridine in the later.[39, 71] This leads to accumulation of electron density around the Pd metal centre, making it less electrophilic and repels the incoming nucleophiles resulting in lower reactivity.[36, 72] This is supported by their electrophilicity indices as well as the *cis*-N–Pd bond lengths (Table 6.4). A similar trend in the reduction of substitution rates have been reported in

Pt(II) complexes when the *cis*-pyridine moiety was substituted with isoquinoline or quinoline moiety.[36, 48, 72, 73]

Similarly, the rate of substitution of **PdL^3** is lower than that of **PdL^2** and **PdL^1**, indicating that the *cis*-positioned naphthalene donates strongly towards the metal centre through a deprotonated carbon. The reactivity of **PdL^4** is the slowest. Although it has the largest π-surface, the spectator ligand is coordinated at the lateral position to the Pd with the two intrinsically weak π-acceptor moieties (i.e. the isoquinoline and naphthalene) but better σ/π-donors towards the metal centre. This basically results into low electrophilicity at the Pd metal, thus retarding the approach of the nucleophiles.

The electrophilicity indices of **PdL^3** and **PdL^4** shows that their ligands are better π-acceptors than that of **PdL^2** (Table 6.4). However, their experimental reactivity results, as supported by their electronic chemical potentials, clearly demonstrates that they are poor π-acceptors and better electron donors to the metal centre as compared to the latter. This can be attributed to the anomalous behaviour of the naphthalene moiety in **PdL^3** and **PdL^4**. The theoretical characteristic behaviour of the **HL^3** ligand being a stronger π-acceptor ligand than **HL^2** have been observed in DFT/TDDFT studies of their Pt(II) complexes.[3] Therefore, it can be noted that the *cis*-coordinated naphthyl group reduces the reactivity of the Pd metal more than the *cis*-isoquinolyl group coordinated in a similar position.

The reactivity of the Pd(II) complexes decreases with the increasing π-conjugation contrary to the generally known observation that the increase in π-surfaces results into increased reactivity.[74, 75] This is supported by the trend of the calculated electronic chemical potential (μ) of the complexes (Table 6.4) indicating that the electron donor character at the metal increases [50, 51] with increasing incorporation of the weak π-acceptor moieties in the *cis*-position of the C^N^N

spectator ligands. In addition, the dipole moment which is a parameter that correlates to inductive negative charge in the complex,[76] shows an increase as the σ-donation is increased or as the π-backbonding effect of the terpy moiety is decreasing. This is consistent with the observed reactivity trend.[48] However, the unchanging NBO charge (which depicts a charge on Pd atom) is due to the presence of strong *cis*-σ-donation in the complexes shielding the Pd atom from electronic influence around its sphere.

The reactivity of the nucleophiles decreases following the order **Tu** > **Dmtu** > **Tmtu** (Table 6.5). The observed trend is in accordance with their steric hinderances, where the less sterically hindered **Tu** reacts faster while the most sterically hindered **Tmtu** is significantly slower. Also, the substitution reactions of the chloride ligand from the Pd(II) complexes by the thiourea nucleophiles in this study follows the two-term rate law in accordance with associatively activated mode of mechanism which is generally reported for square planar d^8 complexes.[77-79] The associative mode of mechanism is supported by the values of activation parameters enthalpies ($\Delta H^{\neq}$) being positive and relatively low, while entropies ($\Delta S^{\neq}$) are all negative and large (Table 6.5).

6.5 Conclusions

This study has demonstrated that the lability of Pd(II) complexes coordinated to C^N^N cyclometalated ligands is electronically controlled. The *cis*-naphthalene behaves anomalously as a stronger π/σ -donor ligand than the *cis*-isoquinoline. The weak π-acceptors, naphthalene and isoquinoline acts in a concerted way, weakening the π-acceptability of the ligand which lowers the rate of substitution from **PdL^4** by factors ranging 3 – 5 times when compared to **PdL^1** for all the nucleophiles depending on their steric bulk. The activation mode remains associative in nature throughout the studied systems.

6.6 References

1. F. Neve, A. Crispini and S. Campagna, *Inorganic Chemistry*, 1997, **36**, 6150-6156.
2. S.-W. Lai, T.-C. Cheung, M. C. Chan, K.-K. Cheung, S.-M. Peng and C.-M. Che, *Inorganic Chemistry*, 2000, **39**, 255-262.
3. P. K. Chow, G. Cheng, G. S. M. Tong, W. P. To, W. L. Kwong, K. H. Low, C. C. Kwok, C. Ma and C. M. Che, *Angewandte Chemie International Edition*, 2015, **54**, 2084-2089.
4. P. K. Chow, W. P. To, K. H. Low and C. M. Che, *Chemistry–An Asian Journal*, 2014, **9**, 534-545.
5. T. T. H. Fong, C. N. Lok, C. Y. S. Chung, Y. M. E. Fung, P. K. Chow, P. K. Wan and C. M. Che, *Angewandte Chemie International Edition*, 2016, **55**, 11935-11939.
6. R. W.-Y. Sun, A. L.-F. Chow, X.-H. Li, J. J. Yan, S. S.-Y. Chui and C.-M. Che, *Chemical Science*, 2011, **2**, 728-736.
7. S. C. Kui, I. H. Sham, C. C. Cheung, C. W. Ma, B. Yan, N. Zhu, C. M. Che and W. F. Fu, *Chemistry-A European Journal*, 2007, **13**, 417-435.
8. J. Reedijk, *Chemical Reviews*, 1999, **99**, 2499-2510.
9. E. Wong and C. M. Giandomenico, *Chemical Reviews*, 1999, **99**, 2451-2466.
10. S. Shibata, *Neurologia Medico-Chirurgica*, 1990, **30**, 242-245.
11. E. Pantoja, A. Gallipoli, S. van Zutphen, S. Komeda, D. Reddy, D. Jaganyi, M. Lutz, D. M. Tooke, A. L. Spek and C. Navarro-Ranninger, *Journal of Inorganic Biochemistry*, 2006, **100**, 1955-1964.
12. A. S. Abu-Surrah, H. H. Al-Sa'doni and M. Y. Abdalla, *Cancer Therapy*, 2008, **6**, 1-10.
13. B. Petrović, Ž. D. Bugarčić, A. Dees, I. Ivanović-Burmazović, F. W. Heinemann, R. Puchta, S. N. Steinmann, C. Corminboeuf and R. Van Eldik, *Inorganic Chemistry*, 2012, **51**, 1516-1529.
14. Ž. D. Bugarčić, J. Bogojeski, B. Petrović, S. Hochreuther and R. van Eldik, *Dalton Transactions*, 2012, **41**, 12329-12345.
15. Ž. D. Bugarčić, D. M. Jančić, A. A. Shoukry and M. M. Shoukry, *Monatshefte für Chemie/Chemical Monthly*, 2004, **135**, 151-160.
16. P. Illner, S. Kern, S. Begel and R. van Eldik, *Chemical Communications*, 2007, **0**, 4803-4805.
17. J. Bogojeski, R. Jelić, D. Petrović, E. Herdtweck, P. G. Jones, M. Tamm and Ž. D. Bugarčić, *Dalton Transactions*, 2011, **40**, 6515-6523.

18. Ž. D. Bugarčić, G. Liehr and R. van Eldik, *Journal of the Chemical Society, Dalton Transactions*, 2002, 951-956.
19. G. v. Koten, M. Schmülling, D. Grove, R. v. Eldik, N. Veldman and A. Spek, *Organometallics*, 1996, **15**, 1384-1391.
20. R. Eldik, *Journal of the Chemical Society, Dalton Transactions*, 1994, 1257-1263.
21. L. I. Elding, R. Romeo, M. Schmulling, A. Ryabov and R. Van Eldik, *Journal of the Chemical Society. Dalton transactions*, 1996, 1471-1473.
22. O. F. Wendt and L. I. Elding, *Inorganic Chemistry*, 1997, **36**, 6028-6032.
23. O. F. Wendt, Å. Oskarsson, J. G. Leipoldt and L. I. Elding, *Inorganic Chemistry*, 1997, **36**, 4514-4519.
24. U. Frey, D. M. Grove and G. van Koten, *Inorganica Chimica Acta*, 1998, **269**, 322-325.
25. I. M. Wekesa and D. Jaganyi, *Journal of Coordination Chemistry*, 2016, **69**, 389-403.
26. A. D. Ryabov, L. G. Kuz'mina, V. A. Polyakov, G. M. Kazankov, E. S. Ryabova, M. Pfeffer and R. van Eldik, *Journal of the Chemical Society, Dalton Transactions*, 1995, 999-1006.
27. M. L. Tobe and J. Burgess, *Inorganic reaction mechanisms*, Longman, London, 1999.
28. A. Hofmann, L. Dahlenburg and R. van Eldik, *Inorganic Chemistry*, 2003, **42**, 6528-6538.
29. M. Schmülling, D. M. Grove, G. van Koten, R. van Eldik, N. Veldman and A. Spek, *Organometallics*, 1996, **15**, 1384-1391.
30. A. F. Cotton, G. Wilkinson, M. Bochmann and C. A. Murillo, *Advanced inorganic chemistry*, Wiley, 1999.
31. J. K. Burdett, *Inorganic Chemistry*, 1977, **16**, 3013-3025.
32. S. Okeya, K. Wakamatsu, T. Shibahara, H. Yamakado and K. Nishimoto, *Journal of Computer Chemistry, Japan*, 2002, **1**, 97-102.
33. R. Romeo, M. R. Plutino, L. Monsù Scolaro, S. Stoccoro and G. Minghetti, *Inorganic Chemistry*, 2000, **39**, 4749-4755.
34. D. Jaganyi, D. Reddy, J. Gertenbach, A. Hofmann and R. van Eldik, *Dalton Transactions*, 2004, 299-304.
35. A. Shaira, D. Reddy and D. Jaganyi, *Dalton Transactions*, 2013, **42**, 8426-8436.
36. P. Ongoma and D. Jaganyi, *Dalton Transactions*, 2012, **41**, 10724-10730.
37. D. Reddy and D. Jaganyi, *Dalton Transactions*, 2008, 6724–6731.

38. D. Reddy, K. J. Akerman, M. P. Akerman and D. Jaganyi, *Transition Metal Chemistry*, 2011, **36**, 593-602.
39. J. S. Field, J.-A. Gertenbach, D. Jaganyi, D. R. McMillin, A. Shaira and D. J. Stewart, *Zeitschrift für Naturforschung B*, 2010, **65**, 1318-1326.
40. G. W. Cave and C. L. Raston, *Journal of the Chemical Society, Perkin Transactions 1*, 2001, 3258-3264.
41. F. Neve, A. Crispini, C. Di Pietro and S. Campagna, *Organometallics*, 2002, **21**, 3511-3518.
42. O. V. Dolomanov, L. J. Bourhis, R. J. Gildea, J. A. Howard and H. Puschmann, *Journal of Applied Crystallography*, 2009, **42**, 339-341.
43. G. M. Sheldrick, *Acta Crystallographica Section A: Foundations of Crystallography*, 2008, **64**, 112-122.
44. G. M. Sheldrick, *Acta Crystallographica Section C: Structural Chemistry*, 2015, **71**, 3-8.
45. M. Frisch, G. Trucks, H. Schlegel, G. Scuseria, M. Robb, J. Cheeseman, G. Scalmani, V. Barone, B. Mennucci, G. Petersson, Gaussian 09, revision D. 01, Gaussian, Inc., Wallingford CT (2009).
46. P. J. Hay and W. R. Wadt, *The Journal of Chemical Physics*, 1985, **82**, 299-310.
47. C. A. Mebi, *Journal of Chemical Sciences*, 2011, **123**, 727-731.
48. I. M. Wekesa and D. Jaganyi, *Dalton Transactions*, 2014, **43**, 2549-2558.
49. R. G. Parr, L. v. Szentpa´ly and L. Shubin, *Journal of American Chemical Society*, 1999, **121**, 1922-1924.
50. R. G. Pearson, *Inorganica Chimica Acta*, 1992, **198**, 781-786.
51. R. G. Pearson, *Journal of Molecular Structure: THEOCHEM*, 1992, **255**, 261-270.
52. F. Neve, M. Ghedini and A. Crispini, *Chemical Communications*, 1996, 2463-2464.
53. C. W. Chan, T. F. Lai, C. M. Che and S. M. Peng, *Journal of the American Chemical Society*, 1993, **115**, 11245-11253.
54. H.-K. Yip, L.-K. Cheng, K.-K. Cheung and C.-M. Che, *Journal of the Chemical Society, Dalton Transactions*, 1993, 2933-2938.
55. M. AgostinaáCinellu, *Journal of the Chemical Society, Dalton Transactions*, 1995, 777-781.
56. T.-C. Cheung, K.-K. Cheung, S.-M. Peng and C.-M. Che, *Journal of the Chemical Society, Dalton Transactions*, 1996, 1645-1651.

57. S. A. Willison, H. Jude, R. M. Antonelli, J. M. Rennekamp, N. A. Eckert, J. A. Krause Bauer and W. B. Connick, *Inorganic Chemistry*, 2004, **43**, 2548-2555.
58. V. M. Miskowski and V. H. Houlding, *Inorganic Chemistry*, 1989, **28**, 1529-1533.
59. A. Mambanda and D. Jaganyi, *Dalton Transactions*, 2011, **40**, 79-91.
60. R. G. Parr and R. G. Pearson, *Journal of the American Chemical Society*, 1983, **105**, 7512-7516.
61. P. K. Chattaraj and B. Maiti, *Journal of the American Chemical Society*, 2003, **125**, 2705-2710.
62. OriginPro 9.1. OriginLab Corporation, One Roundhouse Plaza, Suite 303, Northampton, MA 01060, United States. 1800-969-7720.
63. H. Eyring, *The Journal of Chemical Physics*, 1935, **3**, 107-115.
64. P. O. Ongoma, PhD Thesis, University of KwaZulu-Natal, 2012.
65. C. Icsel and V. T. Yilmaz, *DNA and Cell Biology*, 2013, **32**, 165-172.
66. F. Ari, B. Cevatemre, E. I. I. Armutak, N. Aztopal, V. T. Yilmaz and E. Ulukaya, *Bioorganic & Medicinal Chemistry*, 2014, **22**, 4948-4954.
67. T. Lazarević, A. Rilak and Ž. D. Bugarčić, *European Journal of Medicinal Chemistry*, 2017, **142**, 8-31.
68. D. Wang and S. J. Lippard, *Nature Reviews Drug Discovery*, 2005, **4**, 307-320.
69. D. P. Bancroft, C. A. Lepre and S. J. Lippard, *Journal of the American Chemical Society*, 1990, **112**, 6860-6871.
70. D. Jaganyi, K. L. D. Boer, J. Gertenbach and J. Perils, *International Journal of Chemical Kinetics*, 2008, **40**, 808-818.
71. A. Juris, F. Barigelletti, V. Balzani, P. Belser and A. Von Zelewsky, *Inorganic Chemistry*, 1985, **24**, 202-206.
72. G. Kinunda and D. Jaganyi, *Transition Metal Chemistry*, 2014, **39**, 451-459.
73. B. B. Khusi, A. Mambanda and D. Jaganyi, *Journal of Coordination Chemistry*, 2016, **69**, 2121-2135.
74. D. Jaganyi, A. Hofmann and R. van Eldik, *Angewandte Chemie International Edition*, 2001, **40**, 1680-1683.
75. A. Hofmann, D. Jaganyi, O. Q. Munro, G. Liehr and R. van Eldik, *Inorganic Chemistry*, 2003, **42**, 1688-1700.
76. M. Das and E. L. Stanley, *Dalton Transactions*, 1975, 452-455.

77. F. Basolo and R. G. Pearson, *Mechanisms in Inorganic Reactions*, Wiley, New York, 2nd edn., 1967.

78. J. D. Atwood, *Inorganic and organometallic reaction mechanisms*, Wiley-VCH Publishers, New York, 2nd edn., 1997.

79. R. Van Eldik, T. Asano and W. Le Noble, *Chemical Reviews*, 1989, **89**, 549-688.

6.7 Supporting Information (ESI‡)

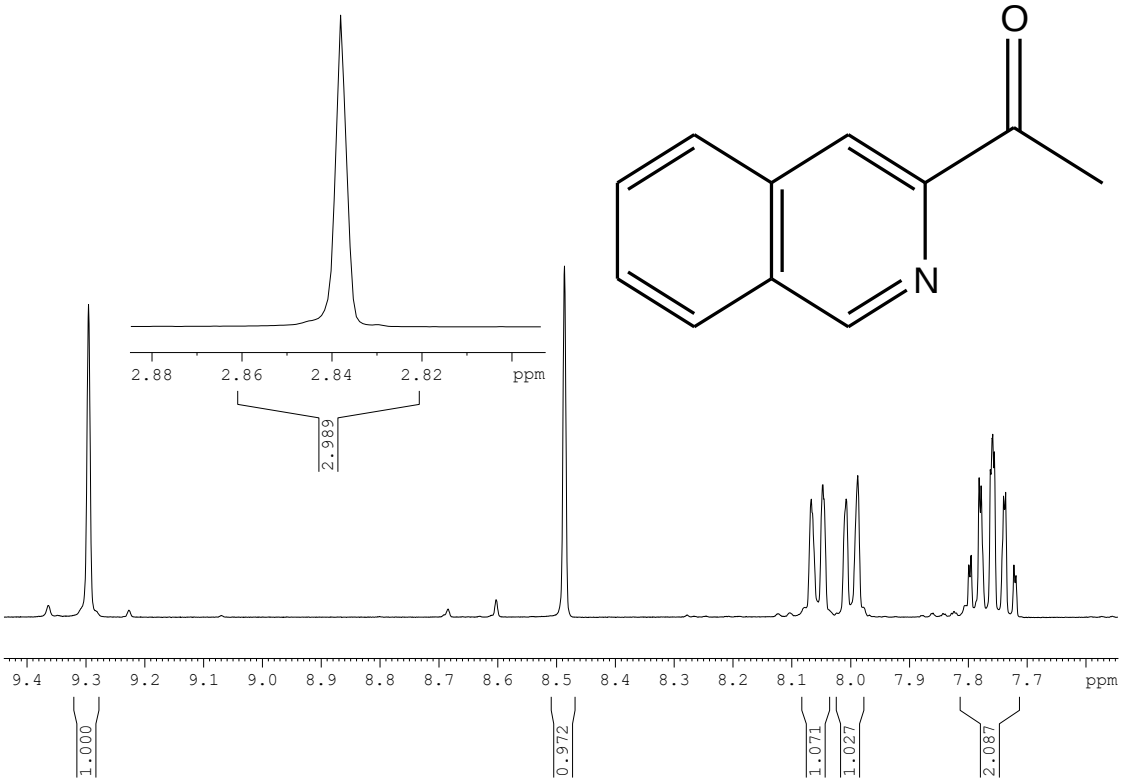

Figure SI 6.1 ^{1}H NMR spectrum of 3-Acetylisoquinoline

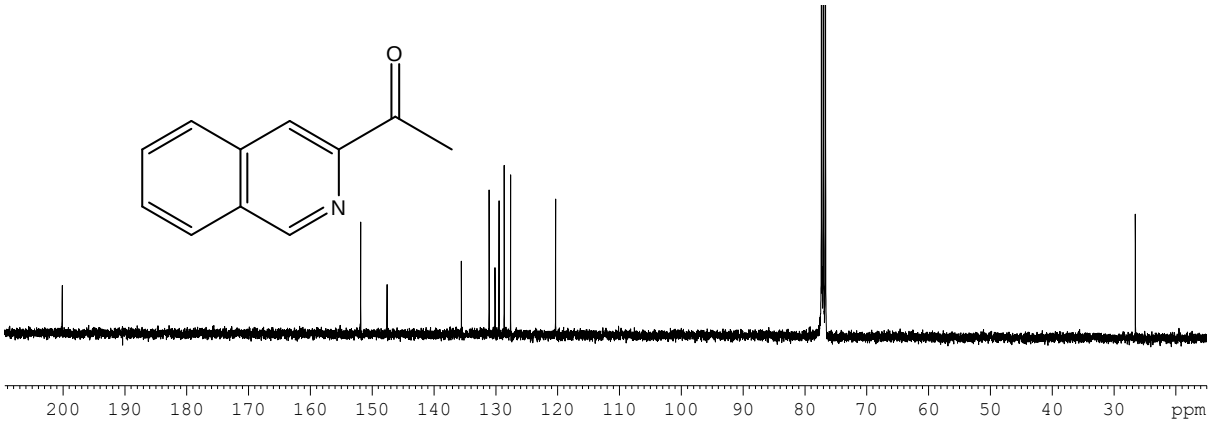

Figure SI 6.2 ^{13}C NMR spectrum of 3-Acetylisoquinoline

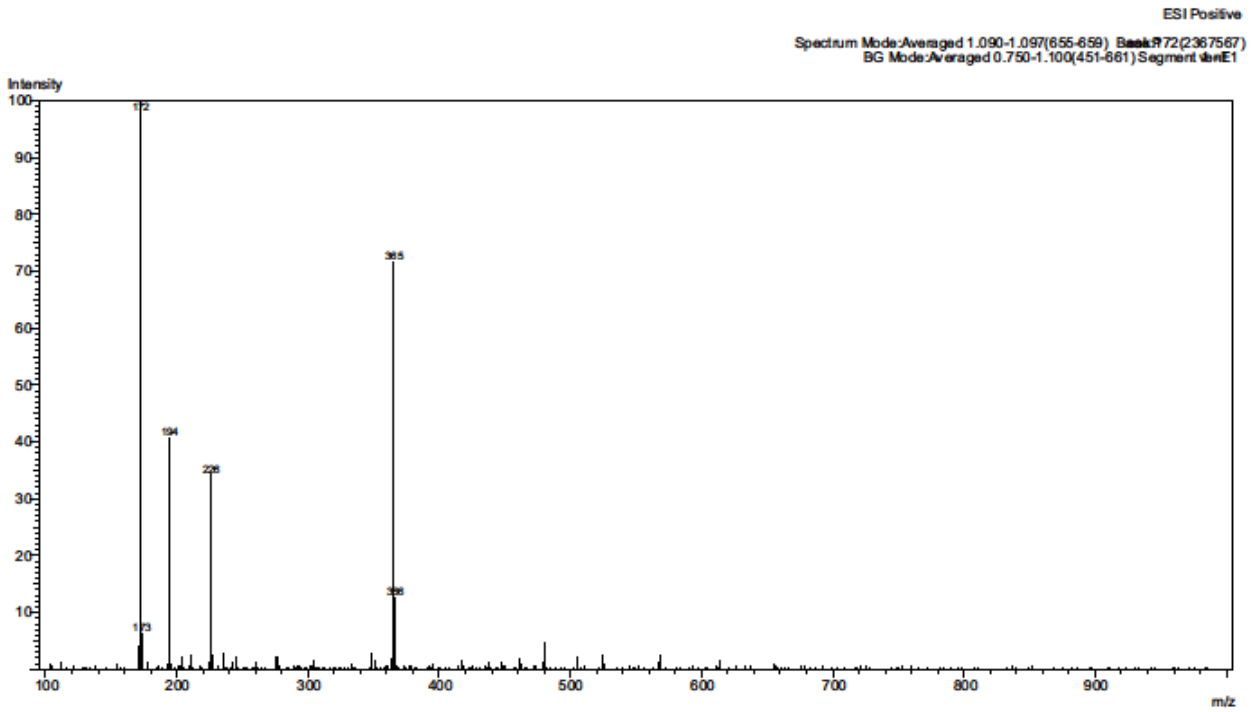

Figure SI 6.3 LC-MS mass spectrum of 3-Acetylisoquinoline

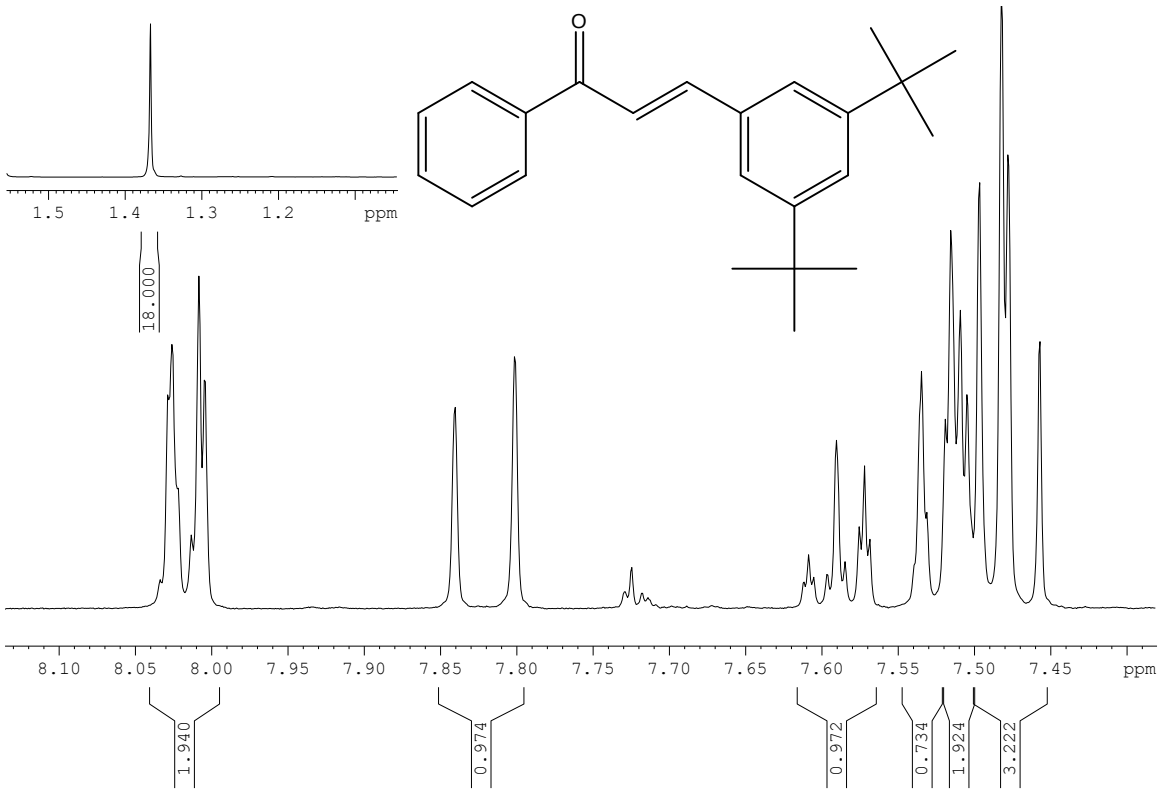

Figure SI 6.4 ^{1}H NMR spectrum of 3,5-di-*tert*-butylbenzylidene-2-acetophenone

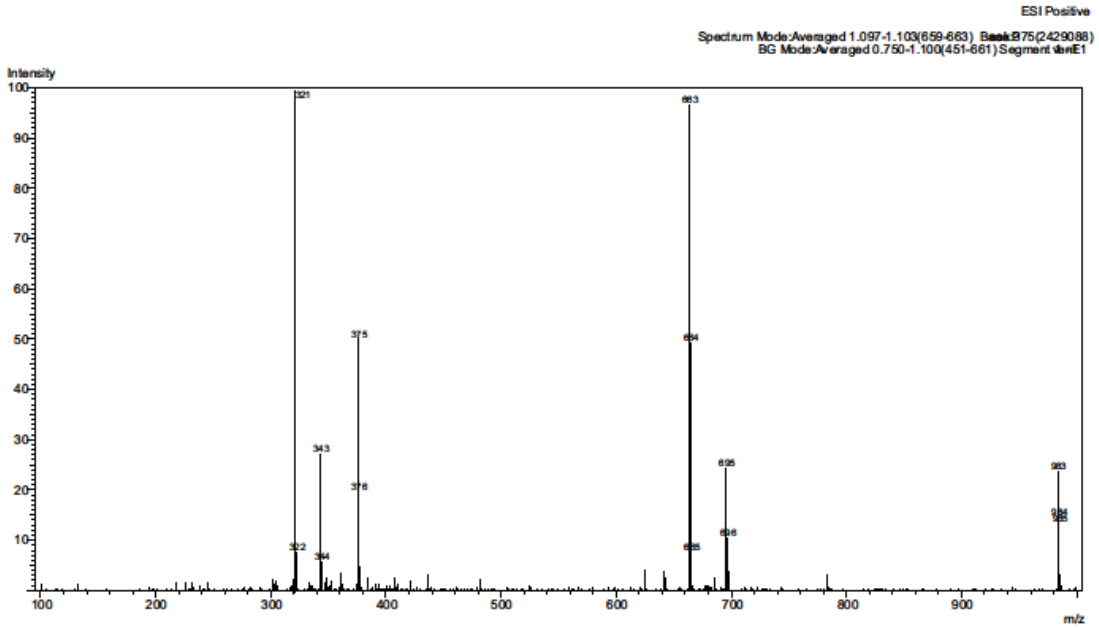

Figure SI 6.5 LC-MS mass spectrum of 3,5-di-*tert*-butylbenzylidene-2-acetophenone

Figure SI 6.6 ^{1}H NMR spectrum of 3,5-di-*tert*-butylbenzylidene-2-acetonaphthone

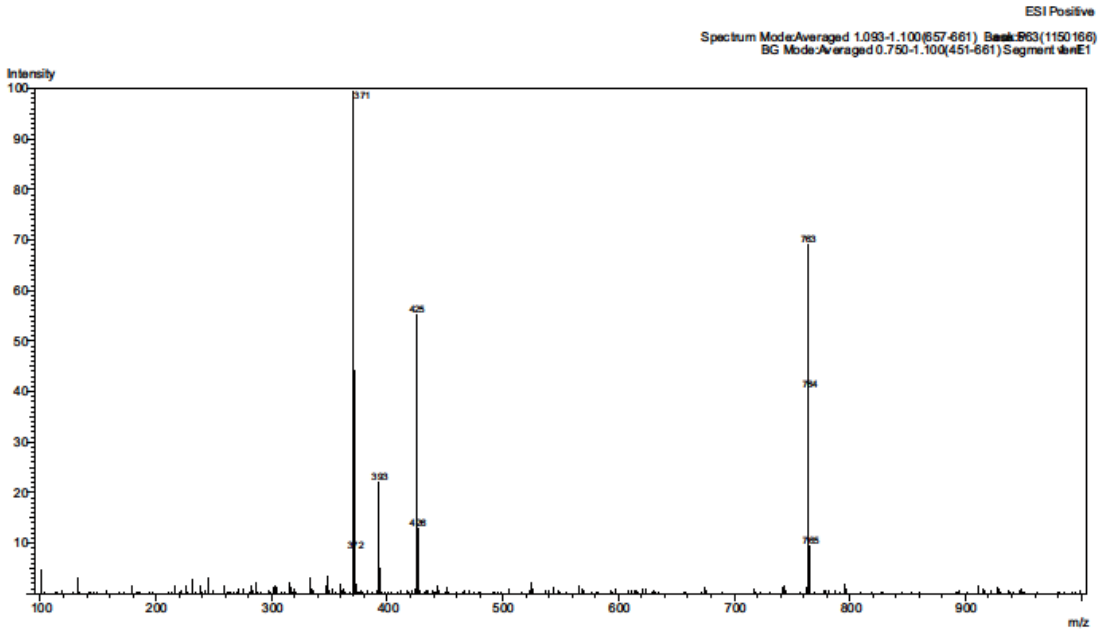

Figure SI 6.7 LC-MS mass spectrum of 3,5-di-*tert*-butylbenzylidene-2-acetonaphthone

Figure SI 6.8 ^{1}H NMR spectrum of 1-(2-(isoquinolin-3-yl)-2-oxoethyl)pyridinium iodide

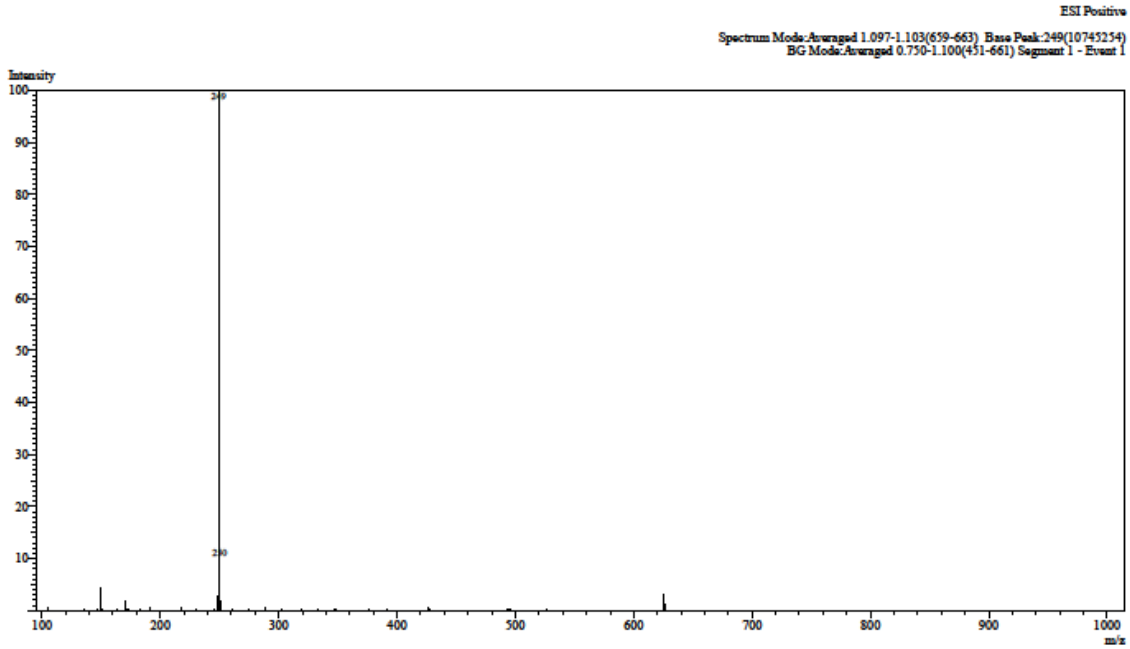

Figure SI 6.9 LC-MS mass spectrum of 1-(2-(isoquinolin-3-yl)-2-oxoethyl)pyridinium iodide

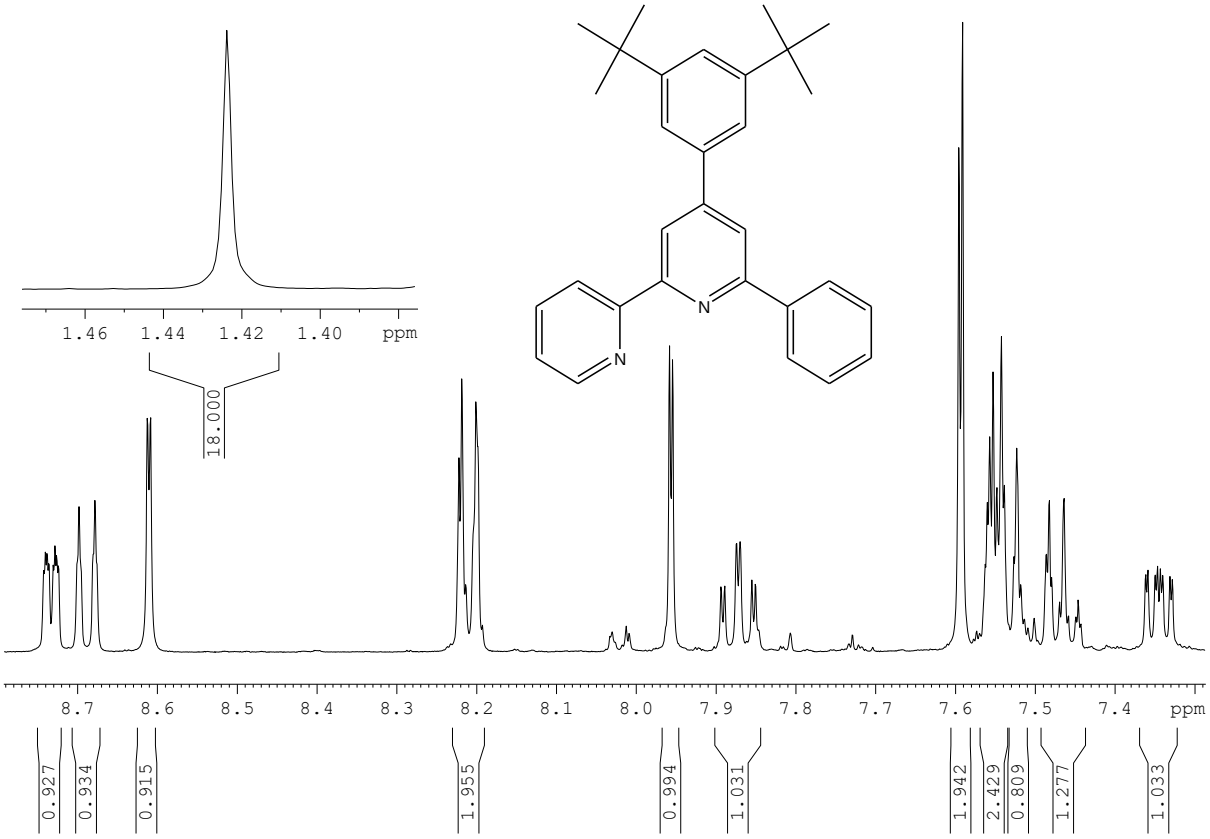

Figure SI 6.10 ^{1}H NMR spectrum of **HL^{1}** ligand

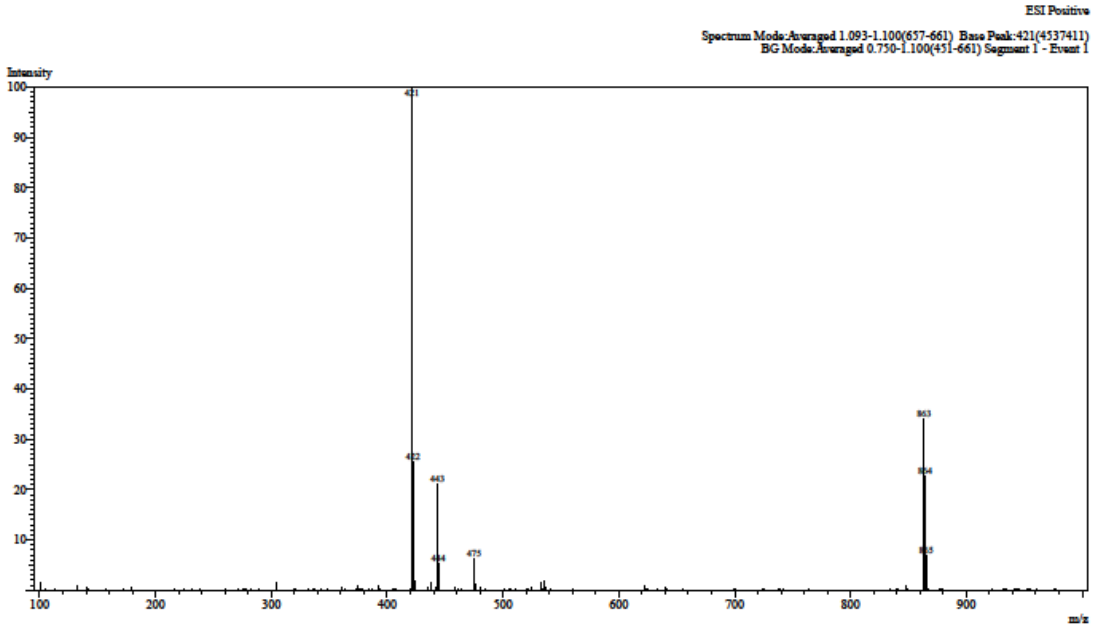

Figure SI 6.11 LC-MS mass spectrum of **HL[1]** ligand

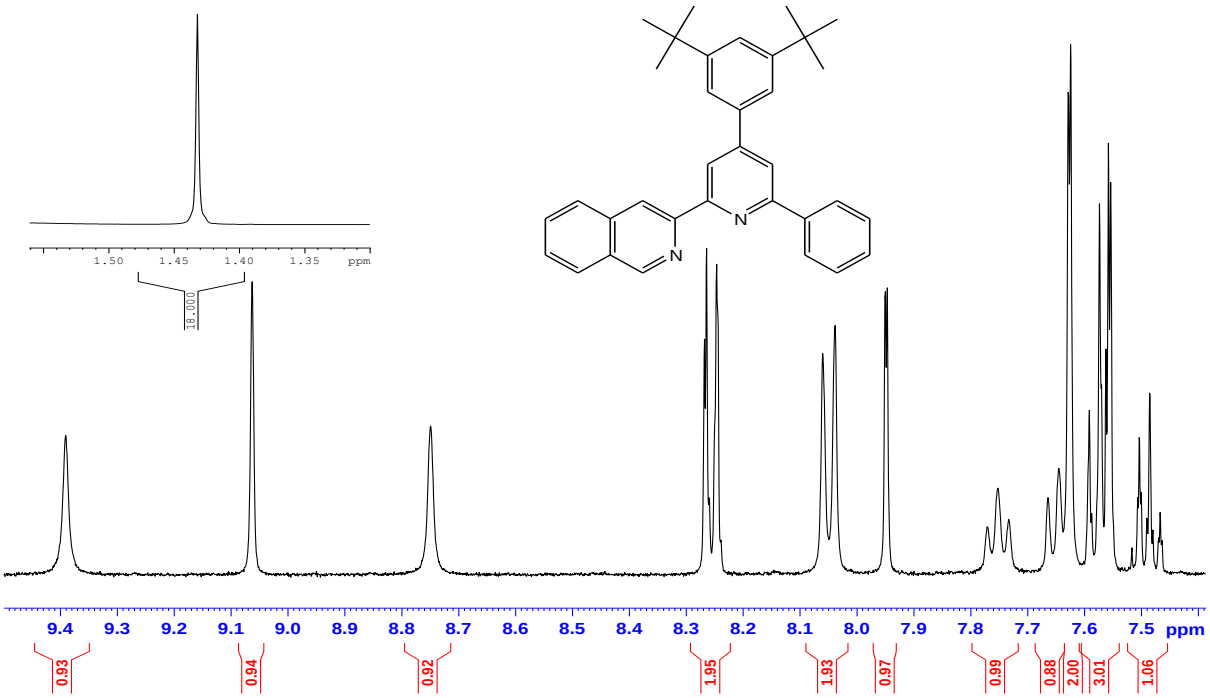

Figure SI 6.12 ^{1}H NMR spectrum of **HL[2]** ligand

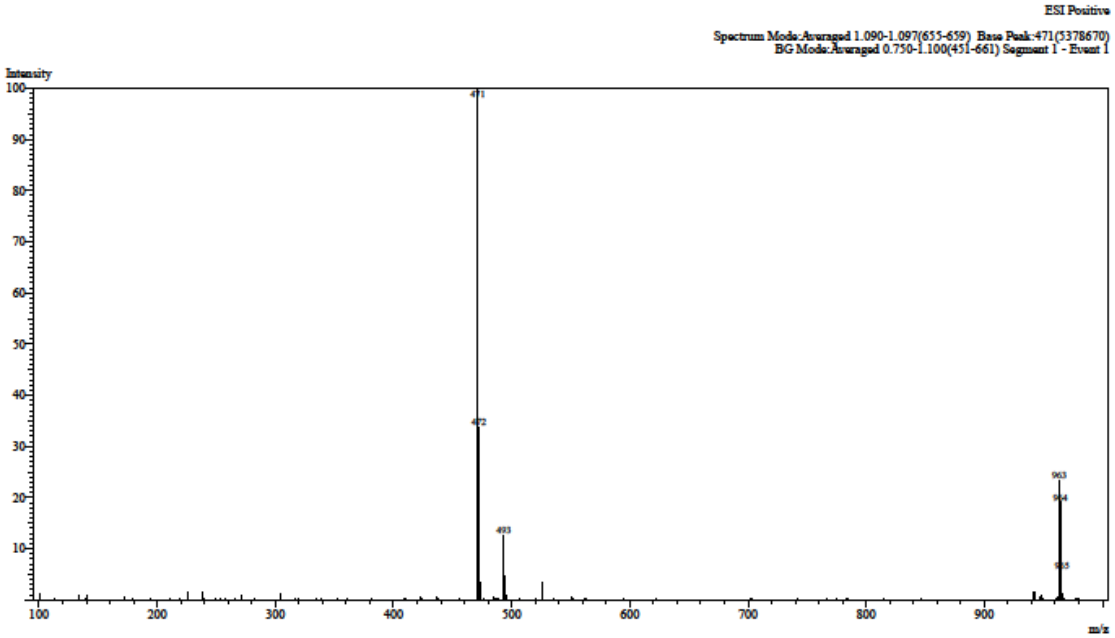

Figure SI 6.13 LC-MS mass spectrum of **HL²** ligand

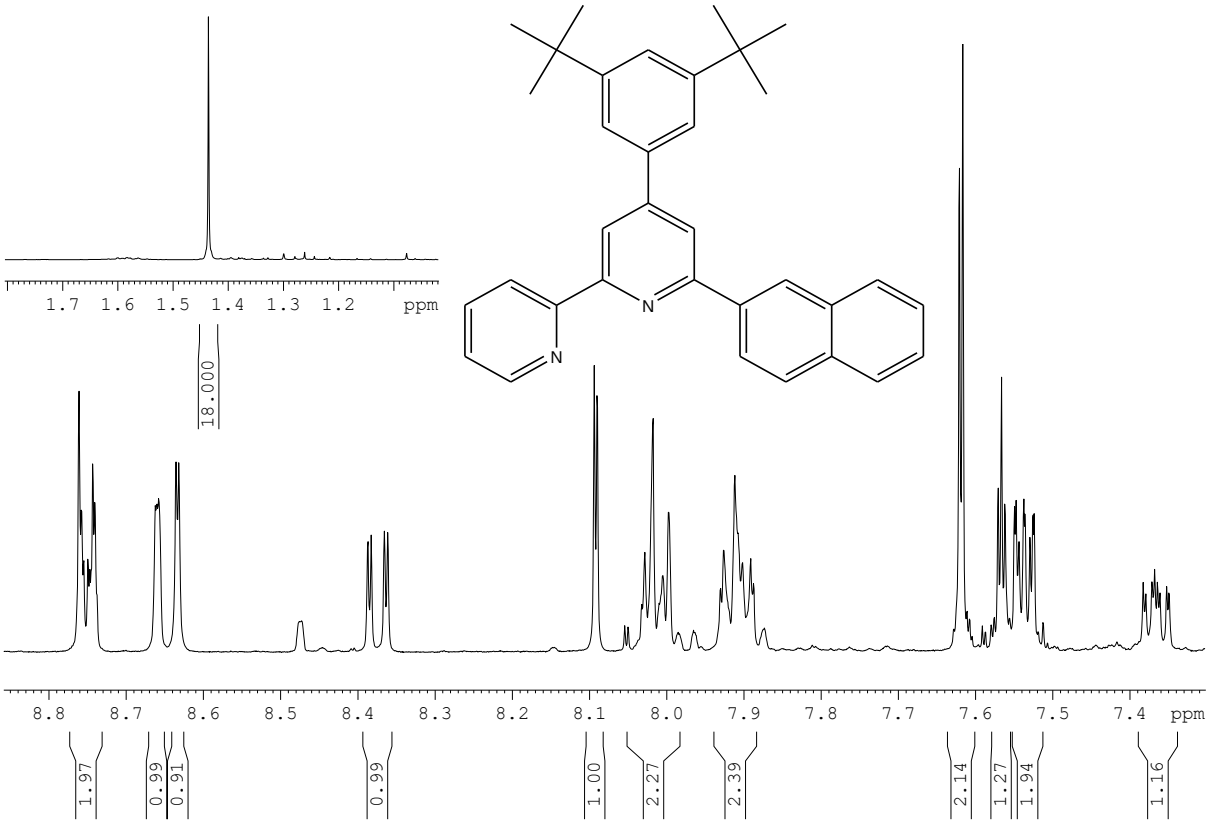

Figure SI 6.14 ^{1}H NMR spectrum of **HL³** ligand

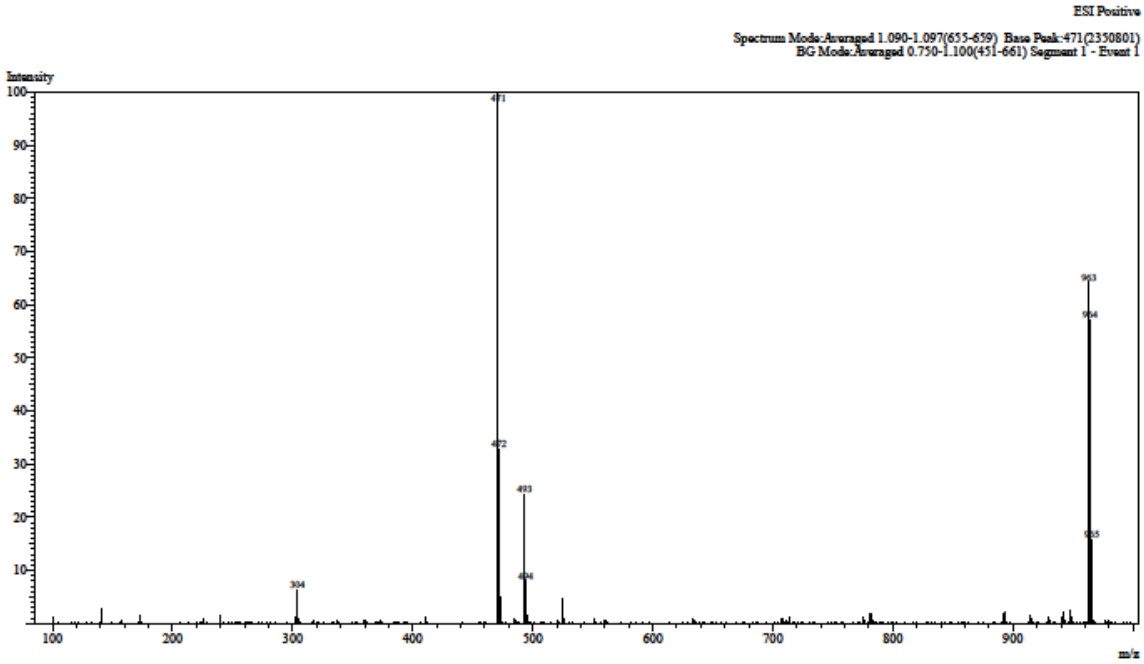

Figure SI 6.15 LC-MS mass spectrum of **HL³** ligand

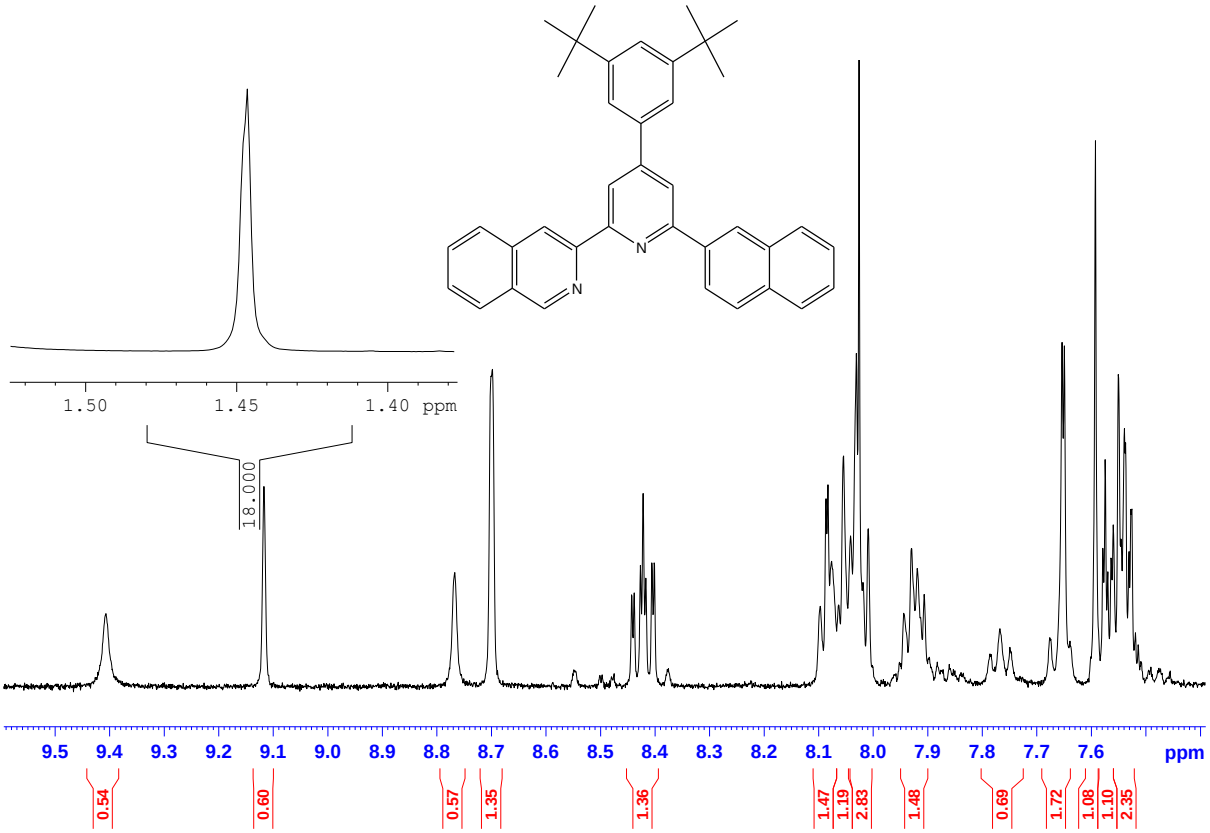

Figure SI 6.16 ^{1}H NMR spectrum of **HL⁴** ligand

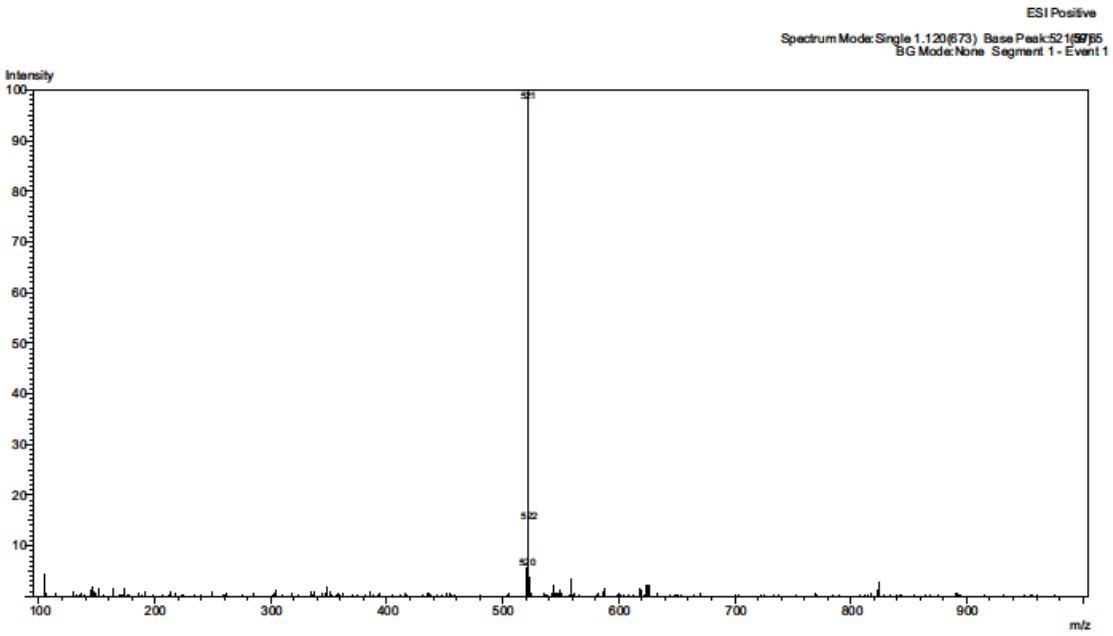

Figure SI 6.17 LC-MS mass spectrum of **HL[4]** ligand

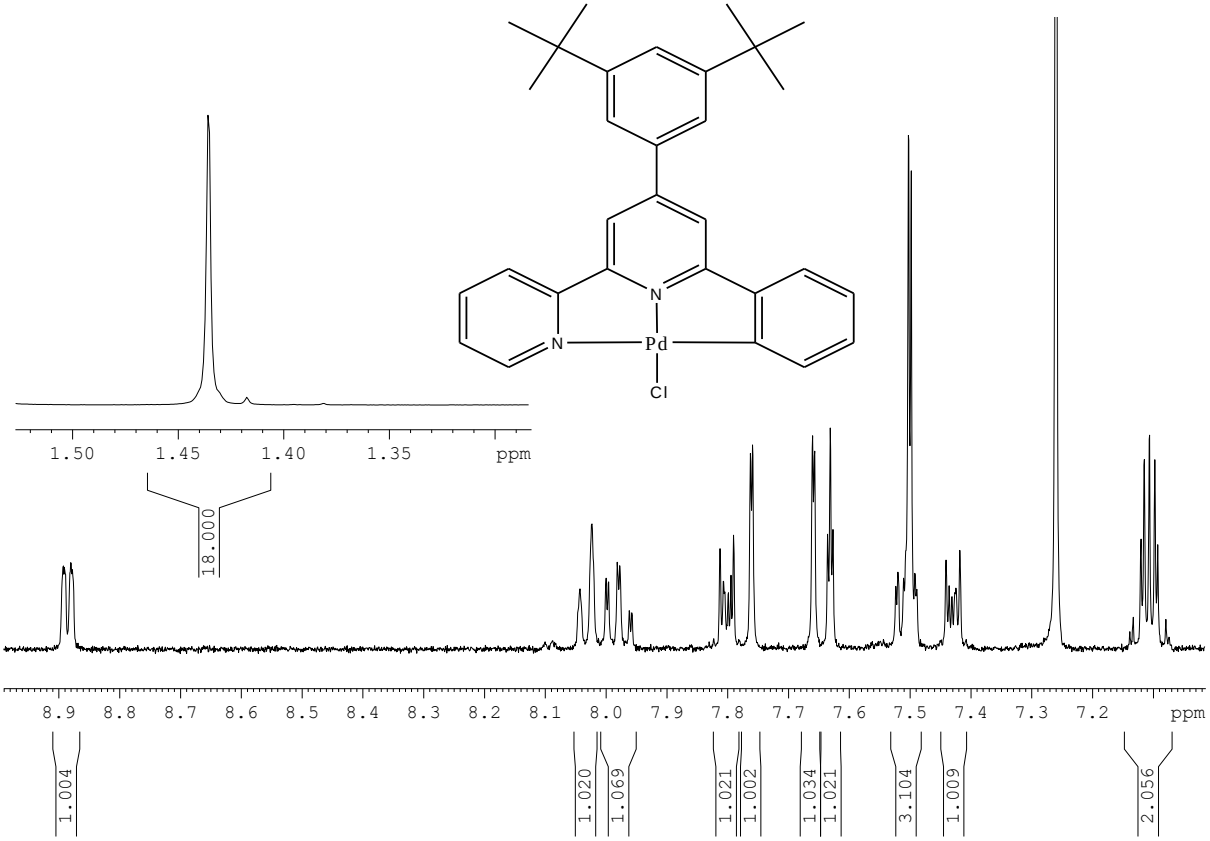

Figure SI 6.18 ^{1}H NMR spectrum of **PdL[1]** complex

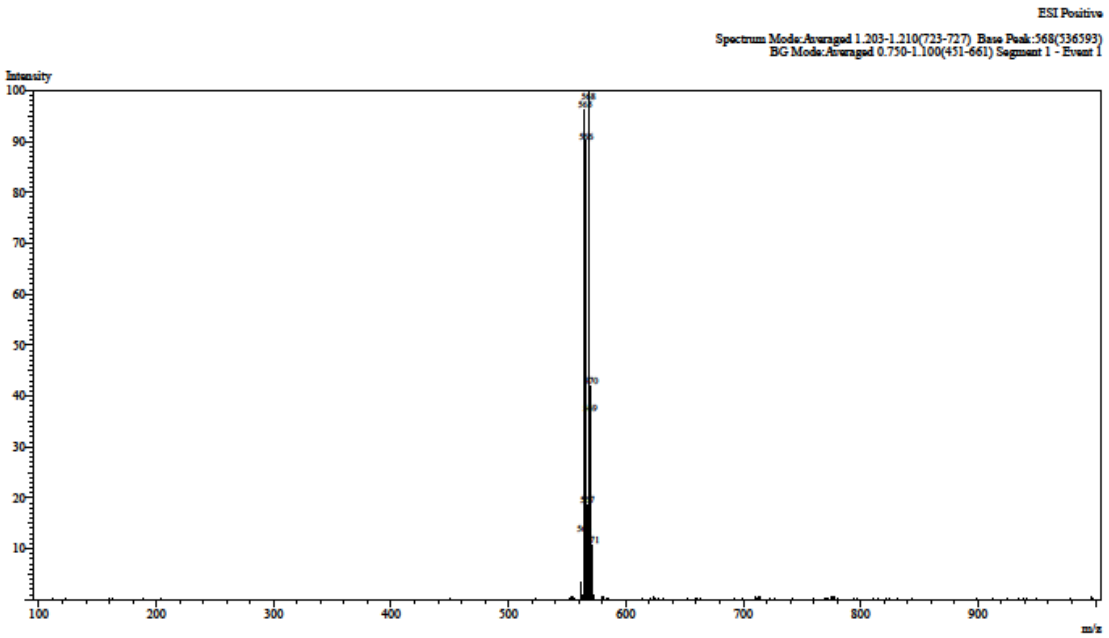

Figure SI 6.19 LC-MS mass spectrum of **PdL[1]** complex

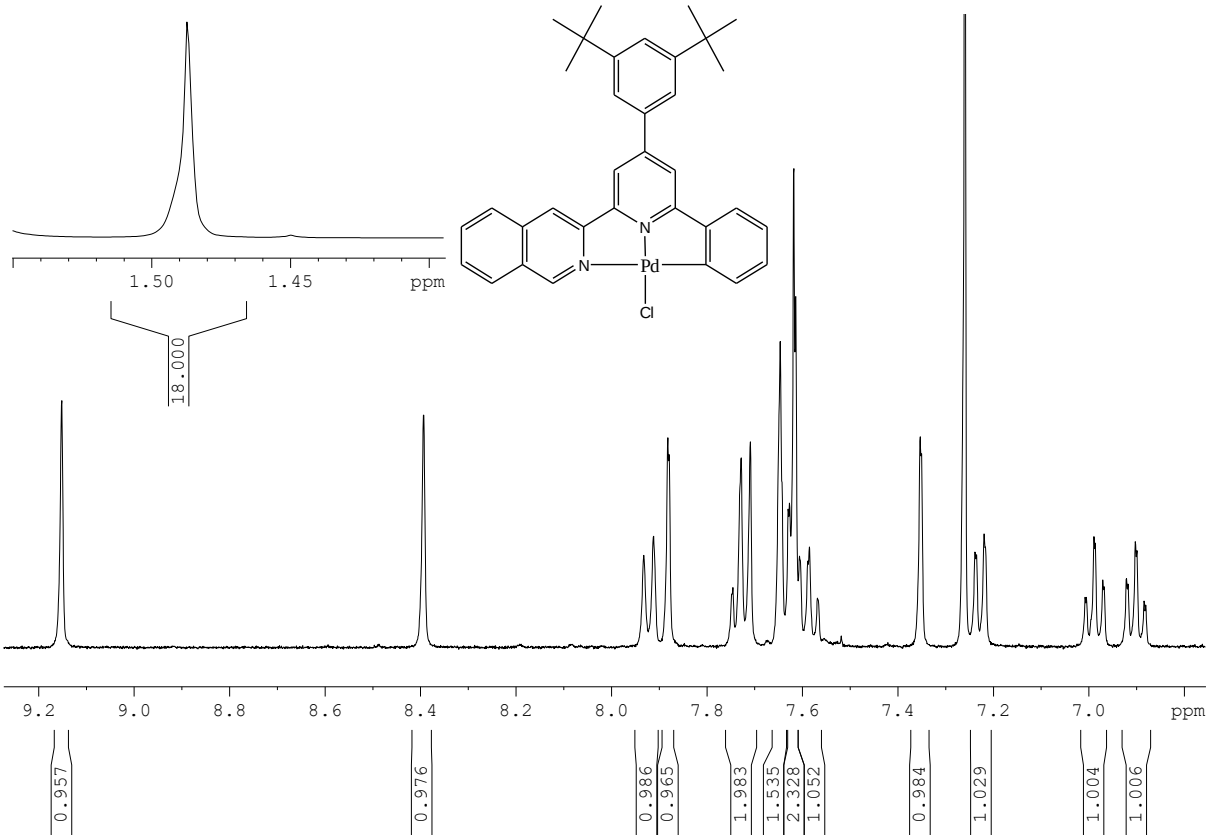

Figure SI 6.20 ^{1}H NMR spectrum of **PdL[2]** complex

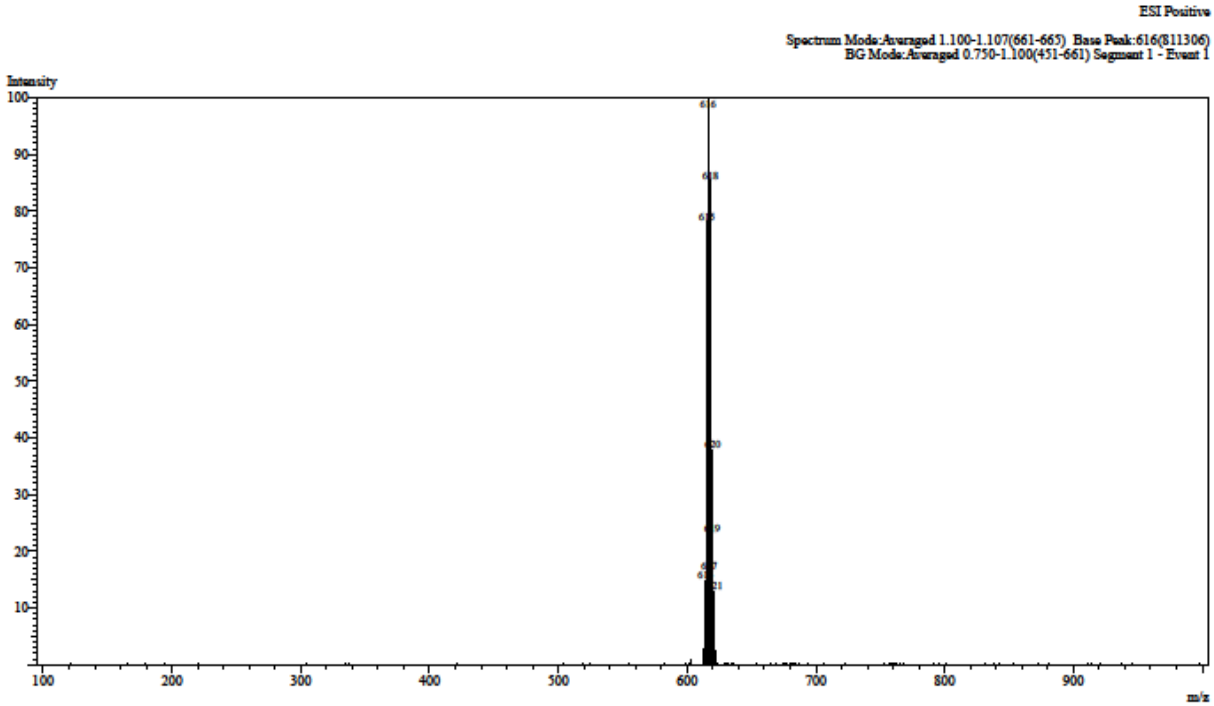

Figure SI 6.21 LC-MS mass spectrum of **PdL^2** complex

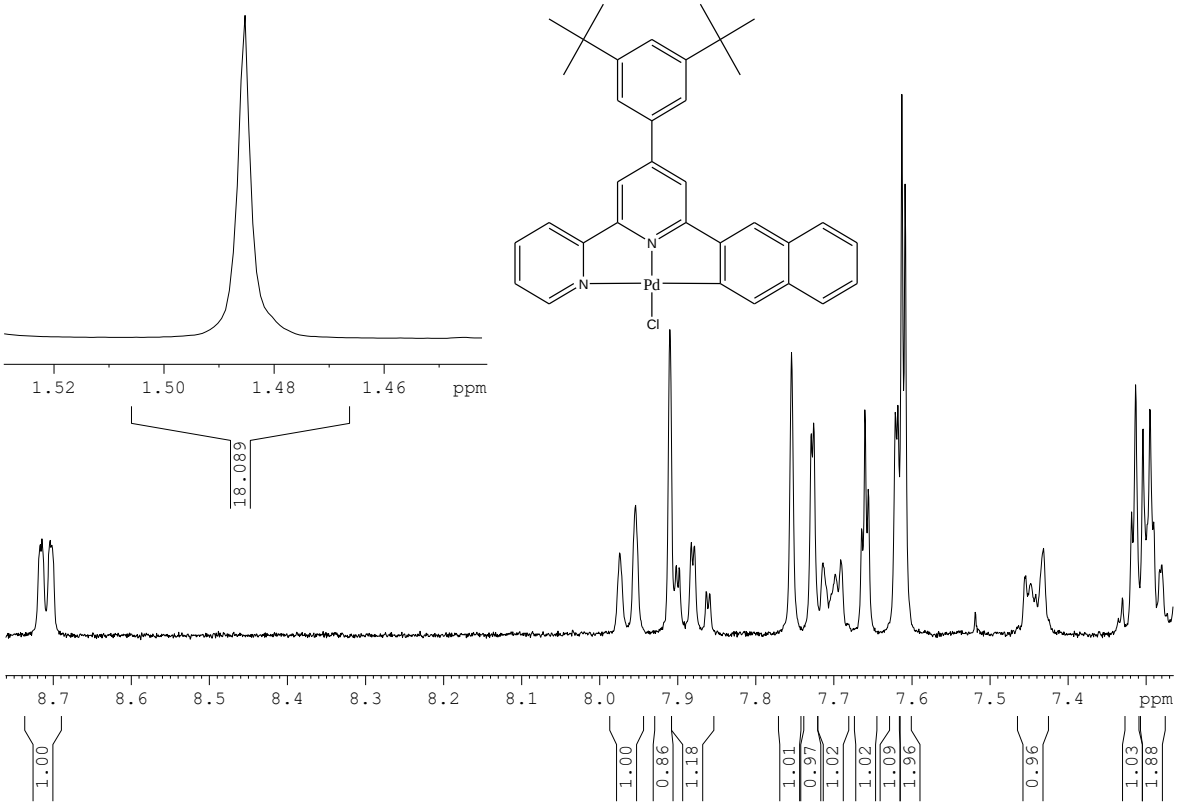

Figure SI 6.22 ^{1}H NMR spectrum of **PdL^3** complex

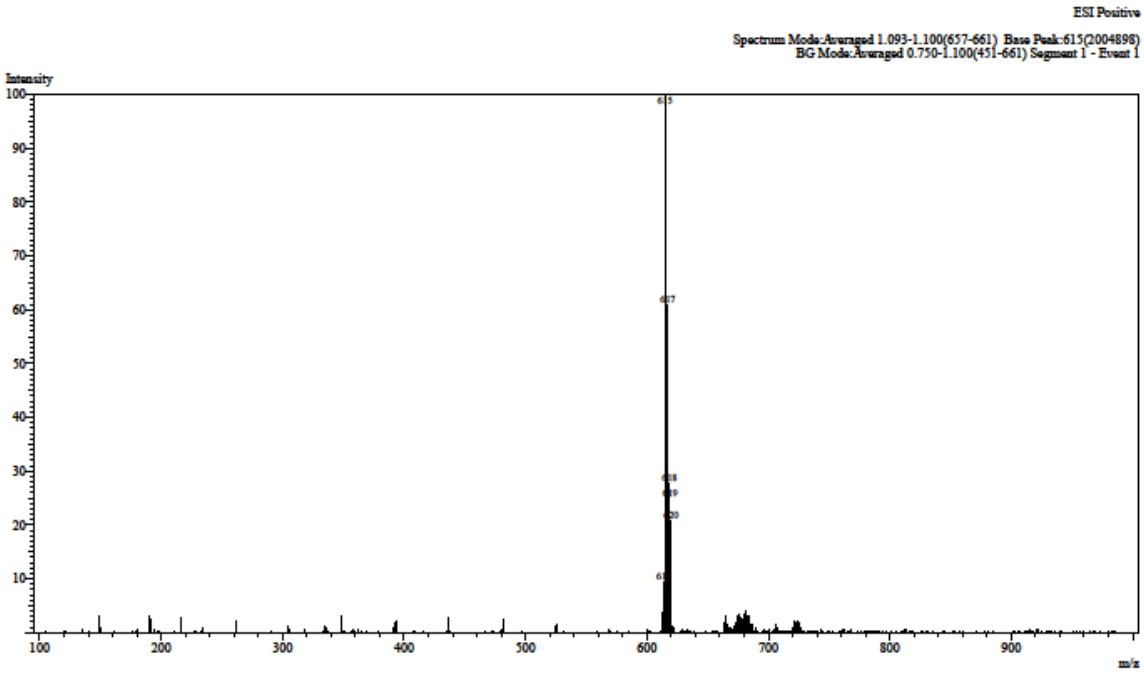

Figure SI 6.23 LC-MS mass spectrum of **PdL^3** complex

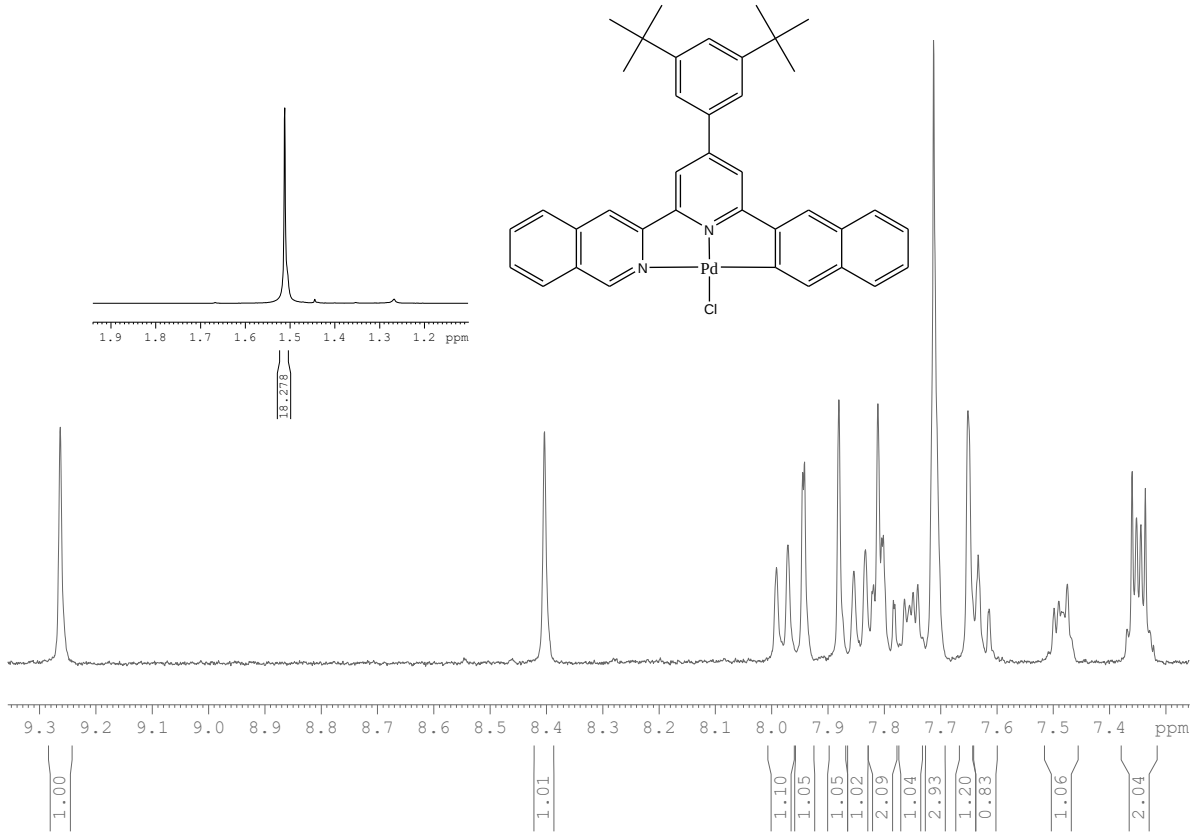

Figure SI 6.24 ^{1}H NMR spectrum of **PdL^4** complex

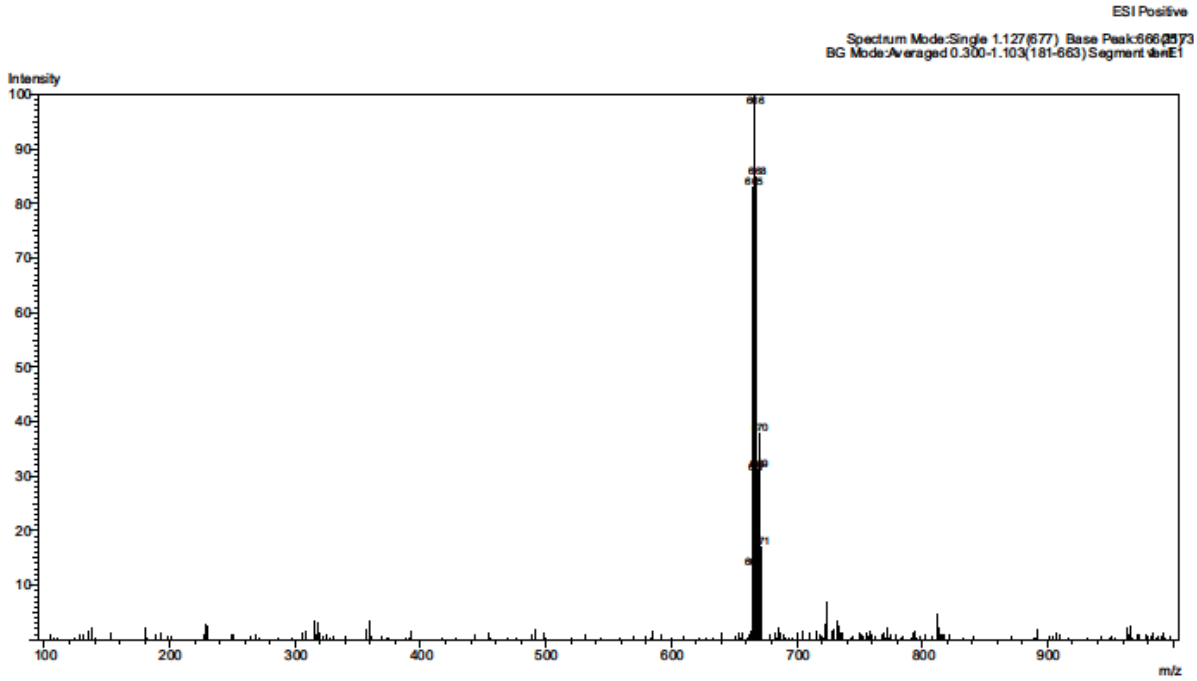

Figure SI 6.25 LC-MS mass spectrum of **PdL^4** complex

Table S1 6.1: The wavelengths(nm) used for studying kinetic reactions of Pd(II) complexes with the nucleophiles

Complex	Nucleophiles	Wavelength, λ (nm)
PdL^1	Tu	319
	Dmtu	319
	Tmtu	380
PdL^2	Tu	380
	Tmtu	380
	Dmtu	375
PdL^3	Tu	318
	Dmtu	318
	Tmtu	309
PdL^4	Tu	388
	Dmtu	388
	Tmtu	386

Table S1 6.2: Average k_{obs} (s^{-1}) for the reactions of **PdL^1** with the nucleophiles at T = 298 K.

Concentration, (M)	k_{obs} (s^{-1})		
	Tu	Dmtu	Tmtu
0.001	85.43899	49.3498	3.31885
0.002	172.2617	85.25905	5.86089
0.003	238.1713	130.1867	8.65774
0.004	324.7974	174.1934	12.23116
0.005	409.8597	220.9137	15.39312

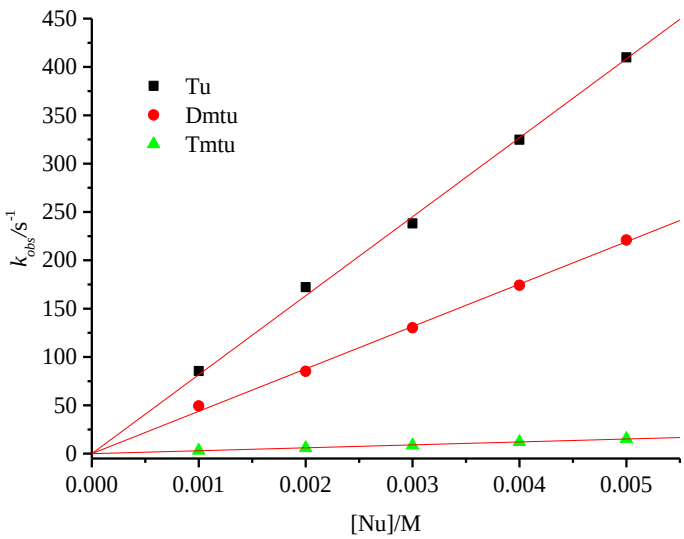

Figure SI 6.26: Dependence of k_{obs} on the concentration of the nucleophiles for reactions with **PdL^1** at T = 298 K.

Table S1 6.3: Average k_{obs} (s^{-1}) for the reactions of **PdL^2** with the nucleophiles at T = 298 K.

Concentration, (M)	k_{obs} (s^{-1})		
	Tu	Dmtu	Tmtu
0.001	55.37984	27.55513	2.08294
0.002	110.1208	54.36084	3.96561
0.003	165.8409	82.00799	6.04314
0.004	223.4603	109.9097	7.90125
0.005	274.3044	136.0261	9.83168

Table S1 6.4: Average k_{obs} (s^{-1}) for reactions of **PdL³** with the nucleophiles at T = 298 K.

Concentration, (M)	k_{obs} (s^{-1})		
	Tu	Dmtu	Tmtu
0.0005	17.63539	8.30587	0.97237
0.0010	37.48280	16.47703	1.95392
0.0015	54.5873	25.44058	2.89022
0.0020	73.22850	35.06498	3.72058
0.0025	90.62328	42.18979	4.68781

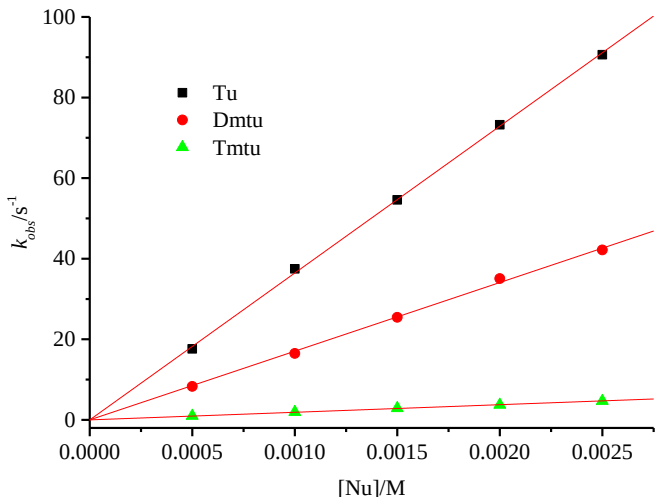

Figure SI 6.27: Dependence of the k_{obs} on the concentration of the nucleophiles for the reactions with **PdL³** at T = 298 K.

Table S1 6.5: Average k_{obs} (s^{-1}) for the reactions of **PdL⁴** with the nucleophiles at T = 298 K.

Concentration, (M)	k_{obs} (s^{-1})		
	Tu	Dmtu	Tmtu
0.001	19.66878	9.25954	1.16596
0.002	40.02389	18.6170	2.02617
0.003	58.77396	28.07542	3.08172
0.004	83.36661	37.84187	4.12818
0.005	102.8528	47.11043	5.12981

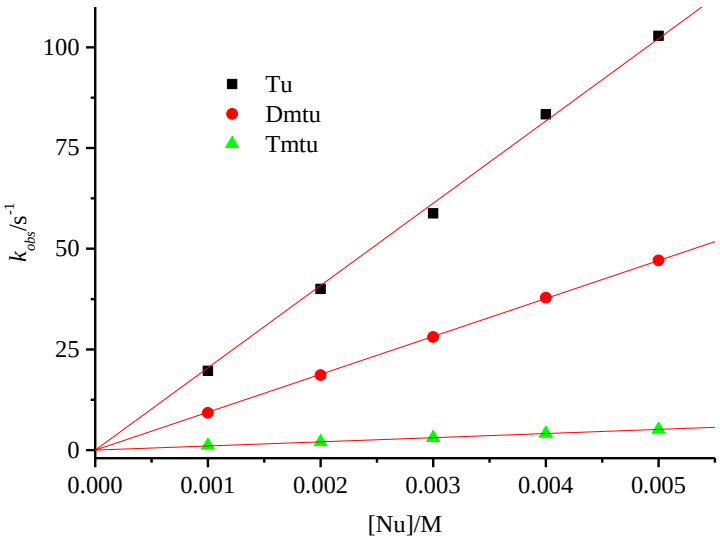

Figure SI 6.28: Dependence of k_{obs} on the concentration of the nucleophiles for the reactions with **PdL^4** at T = 298 K.

Table S1 6.6: Temperature dependence of k_2 $M^{-1}s^{-1}$ for the reactions of **PdL^1** with nucleophiles at 30-fold in dichloromethane.

(1/T) K^{-1}	ln(k_2/T)		
	Tu	Dmtu	Tmtu
0.00353	5.21237	4.5946	1.65126
0.00347	5.31301	4.71951	1.83029
0.00341	5.42662	4.84213	1.99202
0.00336	5.53638	4.9363	2.13300
0.00330	5.61894	5.01867	2.29212

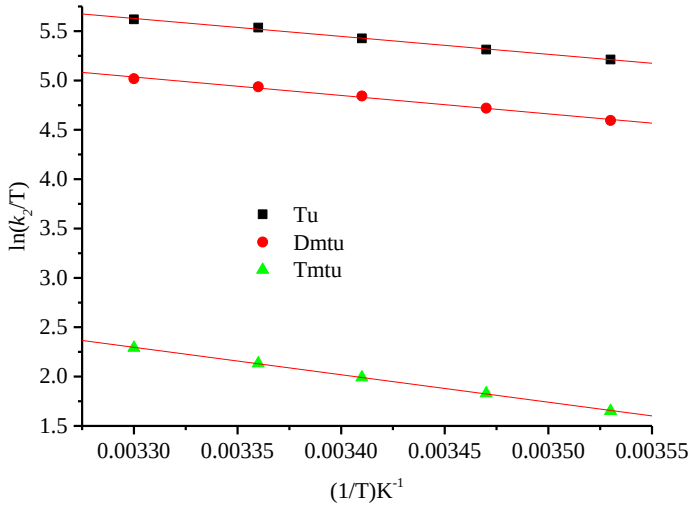

Figure SI 6.29: Eyring plots of **PdL^1** with the nucleophiles at different temperatures

Table S1 6.7: Temperature dependence of k_2 $M^{-1}s^{-1}$ for reactions of **PdL²** with the nucleophiles at 30-fold in dichloromethane.

(1/T) K^{-1}	ln(k_2/T)		
	Tu	Dmtu	Tmtu
0.00353	4.89254	4.06326	0.75644
0.00347	5.05167	4.24437	1.08897
0.00341	5.22673	4.42017	1.35407
0.00336	5.34818	4.60273	1.61045
0.00330	5.51457	4.75093	1.84810

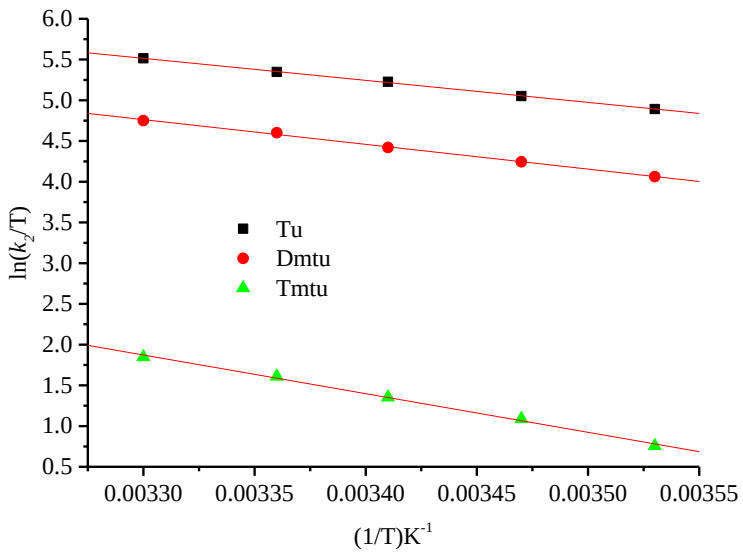

Figure SI 6.30: Eyring Plots of **PdL²** with the nucleophiles at different temperatures

Table S1 6.8: Temperature dependence of k_2 $M^{-1}s^{-1}$ for the reaction of **PdL³** with the nucleophiles at 30-fold in dichloromethane.

(1/T) K^{-1}	ln(k_2/T)		
	Tu	Dmtu	Tmtu
0.00353	4.34338	3.41232	0.99566
0.00347	4.59203	3.64679	1.30542
0.00341	4.80051	3.84724	1.69059
0.00336	4.98998	4.06563	1.92433
0.00330	5.23367	4.26584	2.21874

Table S1 6.9: Temperature dependence of k_2 $M^{-1}s^{-1}$ for the reactions of **PdL^4** with the nucleophiles at 30-fold in dichloromethane.

(1/T) K^{-1}	ln(k_2/T)		
	Tu	Dmtu	Tmtu
0.00353	3.67682	2.83524	0.14455
0.00347	3.87605	3.07215	0.55335
0.00341	4.13548	3.32619	0.84827
0.00336	4.36921	3.50429	1.1875
0.00330	4.55616	3.74511	1.45715

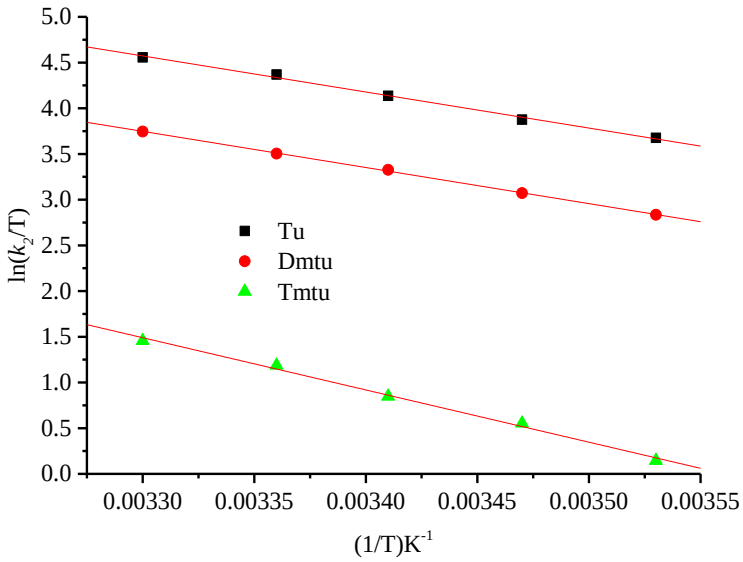

Figure SI 6.31: Eyring plots of **PdL^4** with the nucleophiles at different temperatures

CHAPTER 7

Controlling the Reactivity of Palladium(II) Complexes Using 2,6-Bis-N-heterocyclic Carbene Ligands: Kinetic and Computational Study

7.0 Abstract

In this study, the kinetic and mechanistic studies of the substitution of chloride ligand in a series of modelled Pd(II) complexes coordinated to bis(NHC) carbene spectator ligands:- 2,6-bis(3-methylimidazolium-1-yl)pyridine chloropalladium(II) tetrafluoroborate, **(NHC)Pd1**, 2,6-bis[(3-methylimidazolium-1-yl)methyl]pyridine chloropalladium(II) tetrafluoroborate, **(NHC)Pd2**, 2,6-bis[(3-butylimidazolium-1-yl)methyl]pyridine chloropalladium(II) tetrafluoroborate, **(NHC)Pd3**, and 2,6-bis[(3-methylbenzimidazol-1-yl)methyl]pyridine chloropalladium(II) tetrafluoroborate, **(NHC)Pd4** by thiourea nucleophiles *viz*; thiourea (**Tu**), N,N'-dimethylthiourea (**Dmtu**) and N,N,N',N-tetramethylthio-urea (**Tmtu**) was investigated. The reactions were monitored in aqueous media containing 20 mM LiCl using stopped flow spectrophotometry as a function of concentration and temperature under *pseudo*-first-order conditions. The reactivity of the complexes followed the order **(NHC)Pd1** > **(NHC)Pd2** > **(NHC)Pd4** > **(NHC)Pd3** obeying the rate law $k_{obs} = k_2$[Nu]. It is found that the reactivity of these complexes is controlled by steric and electronic effects. The reactivity of **(NHC)Pd1** is higher than that of the rest of the complexes due to π-backbonding of the in-plane aromatic rings. While the reactivity of the rest of the complexes are controlled by both electronic and steric factors with **(NHC)Pd3** being the least reactive as a result of a strong donation by the N-butyl substituent into the coordination centre. The introduction of methylene spacer groups in the chelate ring of the complexes introduces six-membered ring chelate causing steric influence in the complexes which significantly leads to lower rates of substitution. In addition, the net σ-donation of the ligands to the metal centre plays a role in determining the reactivity trend of the complexes. This is seen in the successive increase

in HOMO energy level going from **(NHC)Pd1** (most reactive) to **(NHC)Pd3** (least reactive) from the DFT calculations supporting the reactivity trend.

Keywords: bis(NHC) carbenes, σ-donation, thiourea, kinetics, *pseudo*-first-order

7.1 Introduction

Since the discovery of free stable N-heterocyclic carbenes (NHCs) by Arduengo et al.[1] in 1991, their chemistry have attracted immense interest. The renaissance in NHCs have seen their adoption as π-donor, poor (weak or even negligible) π-acceptors and strong σ-donor ligands[2-8] towards several transition metals. [9-13] A wide range of NHC–metal complexes have found use in catalysis[14, 15] and biomedical applications such as antibacterial, antiparasitical, and anticancer agents.[16-21] Much interest have been focussed on the donor-functionalized carbene ligands with pyridine- and lutidine-bridged, pincer-type, bis-(carbene) ligands (C^N^C ligands).[9, 22, 23] The coordination chemistry of Pd(II) complexes with these type of ligands have extensively been explored mainly for their catalytic applications.[24-29] However, reports on their anticancer activity and including substitution kinetic properties remains limited.

It is well known that among the widely used antitumor drugs such as *cisplatin*, (*cis*-$[Pt(NH_3)_2Cl_2]$) and other Pt(II) metal based drugs for treatment of ovarian, testicular and small lung cancer among others.[30-32] However, Pt(II)-based drugs have shown elaborate serious side effects,[31, 33-35] which have led to Pd(II) derivatives [18, 36-38] to be readily chosen as alternatives to mitigate these side effects. This is because of their structural analogy with those of Pt(II) complexes for cancer treatment studies.[39] However, the Pd(II) design remains a challenge since their ligand exchange studies show that they are 10^2–10^5 times faster than analogous Pt(II) compounds.[40] To develop a good antitumor Pd(II) based drugs, sterically hindered and a strongly coordinated terdentate chelates with good π/σ-donation are required to afford kinetically inert and thermodynamic stabile Pd(II) complexes. This would stabilize the complex so as to maintain its structure long enough in biological systems to reach its DNA target and perform the required therapeutic action[41, 42] thereby improving its antitumor activity.[43-48] Bis(NHC) ligand system, having terdentate C^N^C system, could be helpful in stabilizing Pd(II) complexes

because as mentioned: 1) they are poor π-acceptors and strong σ-donors;[2-7] 2) their coordination results into a robust and thermal stable complexes;[26] and lastly, 3) they are adaptable family of ligands whose electronic and steric features can be controlled and tuned almost at wish.[4, 49] Based on these favourable qualities, it is envisaged that bis-(NHC) ligands may play a crucial role in making the highly reactive Pd metal kinetically inert and thermodynamically stabilizes it, leading to providing new Pd(II) complex candidates with improved antitumor activity. Therefore, to design such drugs, with good kinetic inertness and thermodynamic stable qualities, investigating the factors that influences the reactivity of the bis-(NHC) Pd(II) complexes is very important.[50] Once these factors are resolved and well understood, it would principally be easy to design Pd(II) complexes with known thermodynamic and kinetic properties having a desirable biological activity.

Substitution kinetic studies of square planar d^8 complexes involving metal-carbon bond in the *cis*-position have been studied in an attempt to isolate the distinctive role of strong σ-donation from carbon to the metal centre in determining the mechanistic mode and the rate of substitution reactions.[51-53] For instance, in controlling the reactivity of Pt(II) complexes, the rate of substitution was systematically reduced upto 40 times in a series of complexes coordinated to N^N^C ligand systems[52] attributed to the *cis*-effect. Such electronic tuning of the reactivity of Pt(II) complexes of this type makes it easy to study the reactivity of the analogous Pd(II) complexes.[54] However, an increase in the rate of substitution of upto six orders of magnitude was reported [55, 56] when the metal-carbon bond was located *trans* to the leaving group due to kinetic *trans*- labilization effect.[51, 57-59] This effect was attributed to destabilization of the ground state due to σ-electron donation along the *trans* axis hence stabilizing the transition state.[60] Therefore, the *cis*-effect shows an opposite behaviour to the *trans*-effect[61, 62] on the rate of

substitution. In almost all these studies the investigations were on the single metal-carbon bond and the substitution reactions mechanisms remained associative in nature.

However, a dissociative pathway was witnessed when the reactivity of mononuclear and dinuclear Pt(II) complexes having two carbon donors both in the *cis*-position.[53, 63-65] This was evident in the complexes of the type *cis*-[PtR_2L_2] where R = alkyl or Aryl and L= DMSO, thioethers (neutral ligands). The phenomenon was explained in terms of the stabilization of the 14-valence electron (three-coordinate) intermediate influenced by the two strong *cis*-σ-donor carbon atoms. On the contrary, when one of the neutral ligands was replaced with a carbonyl group as a spectator ligand, the mechanism sharply changed to associative.[64] The reason invoked to explain this mechanistic changeover is that the π-acceptability of carbonyl is very strong and therefore withdraws the excess electron density from the metal centre thereby favouring the 18 valence electron (five-coordinate) intermediate known for associative mechanism. The extent of electron density around the metal centre therefore plays a very important role in determining the nature of the substitution mechanism.

Several studies have illustrated that six membered chelates having methylene spacer groups leads to the reduction in the reactivity of Pt(II)/Pd(II) complexes.[40, 52, 59, 66, 67] The observed reactivity was due to their flexibility which stabilizes the complexes through steric effects [40, 66, 67] However, there remains limited information on the kinetic and thermodynamic behaviour of Pd(II) complexes bearing tridentate five- and six-membered chelates with bis(NHC) carbenes.

In this study, the role of the donor-functionalised carbene, bis(NHC) ligand, in stabilising the highly reactive Pd metal is explored. The objective was to try to understand how the σ-donating abilities of bis(NHC) carbene ligands, having 2,6-bis(benz/imidazolin-2-ylidene)pyridine ligand framework, would control the reactivity of the Pd metal. Therefore, the rate of substitution of the

chloride ligand from the Pd(II) complexes, shown in Figure 7.1, by bio-relevant thiourea-based nucleophiles of varied steric demands was investigated. The density function theory (DFT) calculations were performed to provide an insight to the understanding of the experimental kinetic results gotten from this investigation.

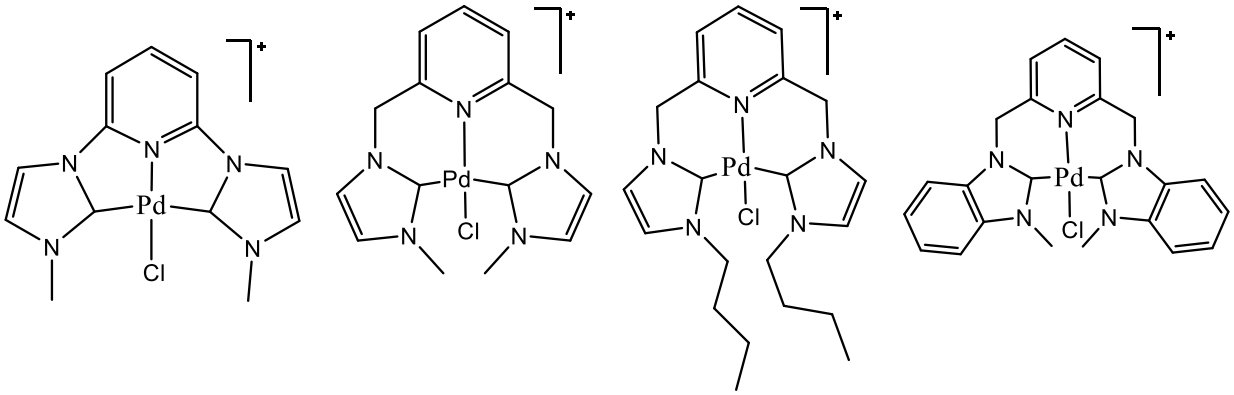

(NHC)Pd1 **(NHC)Pd2** **(NHC)Pd3** **(NHC)Pd4**

Figure 7. 1 Structures of the investigated complexes (counter ion tetrafluoroborate omitted for clarity)

7.2 Experimental Section

7.2.1 Materials and Methods

All syntheses were conducted under dry atmosphere of nitrogen using Schlenk-line techniques. The chemicals; Anhydrous tetrahydrofuran (THF), 2,6-bis(bromomethyl)pyridine (98%), 2,6-dibromopyridine, difluoropyridine, benzimidazole, bromomethane, 1-methylimidazole (99%) 1-methylbenzimidazole (99%), silver (I) oxide (Ag_2O), silver tetrafluoroborate, bis(acetonitrile)dichloropalladium(II), $(CH_3CN)_2PdCl_2$ (99.99%) and dichloro(1,5-cyclooctadiene)palladium(II), $Pd(COD)Cl_2$, 99%. The nucleophiles; Thiourea (**Tu**), N,N'-dimethylthiourea (**Dmtu**), and N,N,N',N'-tetramethylthiourea (**Tmtu**) were purchased from Aldrich and used as received without further purification.

7.2.2 Syntheses of Azolium Ligand Salts

The azolium ligands salts; 2,6-bis(3-methylimidazolium-1-yl)pyridine dibromide,[23, 68] 2,6-bis[(3-methylimidazolium-1-yl)methyl]pyridine dibromide, 2,6-bis[(3-butylimidazolium-1-yl)-methyl]-pyridine dibromide[69] and 2,6-bis[(3-methylbenzimidazol-1-yl)methyl]pyridine dibromide[26] were synthesized according to published procedures.

2,6-Bis(3-methylimidazolium-1-yl)pyridine dibromide. A mixture of 2,6-dibromopyridine (3200 mg, 13.5 mmol) and 1-methylimidazole (2216.7 mg, 27 mmol) was heated under N_2 in a Schlenk tube at 150 °C in the absence of solvent for 20 hours to give an off-white solid. The solid was cooled to room temperature, washed with CH_2Cl_2, and filtered. Yield (3484.6 mg 64.3%). ^{1}H NMR (400 MHz, DMSO-d_6): δ = 10.57 (d, 2H), 8.80(d, 2H), 8.61(m, 1H), 8.24 (d, 2H), 8.08 (d, 2H), 4.05 (s, 6H). ^{13}C NMR (100 MHz, DMSO-d_6): δ = 145.92, 145.46, 136.92, 125.58, 119.68, 114.62, 37.05. TOF MS/ESI$^+$, *m/z* = 320.0518 [M – Br$^-$]$^+$. *Anal. Calc. for* $C_{13}H_{15}Br_2N_5$: C, 38.93; H, 3.77; N, 17.46 %. *Found:* C, 38.70; H, 3.91; N, 17.37 %.

2,6-Bis[(3-methylimidazolium-1-yl)methyl]pyridine dibromide. To a stirring solution of 2,6-Bis(bromomethyl)-pyridine (953.0 mg, 3.59 mmol) in anhydrous THF (25 mL), 1-methylimidazole (660 mg, 0.64 mL, 8.0 mmol) was added. A white solid began precipitating within 30 minutes and after stirring for 5 days at room temperature, diethyl ether (25 mL) was added and the product filtered on a glass sinter and washed with diethyl ether. The desired product was obtained as a white powder after drying under vacuum. Yield (1412 mg, 91.6%). ^{1}H NMR (400 MHz, DMSO-d_6): δ = 9.23(s, 2H), 7.97 (t, 1H), 7.76 (m, 2H), 7.71 (m, 2H), 7.50 (d, 2H), 5.57 (s, 4H), 3.92 (s, 6H). ^{13}C NMR (100 MHz, DMSO-d_6): δ = 154.20, 139.28, 137.71, 123.96, 123.71, 122.59, 53.07, 36.46. TOF MS/ESI$^+$, *m/z* = 348.0832 [M – Br$^-$]$^+$. *Anal. Calc. for* $C_{15}H_{19}Br_2N_5.H_2O$: C, 40.29; H, 4.73; N, 15.66 %. *Found:* C, 40.33; H, 4.70; N, 15.67 %.

2, 6-Bis[(3-butylimidazolium-1-yl)methyl]pyridine dibromide. To a stirring solution of 2,6-Bis(bromomethyl)pyridine (1192.3 mg, 4.5 mmol) in anhydrous THF (25 ml), 1-butylimidazole (1179.7 mg, 1.25 mL, 9.5 mmol) was added. An off-white solid began precipitating after 1 hour and after stirring for 5 days at 35 ºC, the mixture was then allowed to cool to room temperature. Diethyl ether (25 ml) was then added, the product filtered and washed with diethyl ether to obtain an off-white solid product. Yield (2449.3 mg, 91.6%). ^{1}H NMR (400 MHz, DMSO-d_6): δ = 8.28 (s, 2H) 7.56 (t, 1H) 7.19 (d, 2H) 7.16 (sxt, 2H) 7.12(d, 2H), 5.41 (d, 4H), 4.03 (t, 4H), 1.89 (quin, 4H), 1.34 (m, 4H), 0.93 (t, 6H). ^{13}C NMR (100 MHz, DMSO-d_6): δ = 153.9, 138.7, 136.9, 123.3, 122.1, 52.7, 48.7, 31.3, 18.8, 13.4. LC MS/ESI$^+$, *m/z* = 432 [M – Br$^-$]$^+$. *Anal. Calc. for* $C_{15}H_{19}Br_2N_5.H_2O$: C, 40.29; H, 4.73; N, 15.66 %. *Found:* C, 40.33; H, 4.70; N, 15.67 %.

2,6-Bis[(3-methylbenzimidazol-1-yl)methyl]pyridine dibromide. This compound was synthesized using a modified procedure of Haque et al.[26] Briefly, 1-methylbenzimidazole (561.7 mg, 4.25 mmol) in acetonitrile (10 mL) was added dropwise to a stirring solution of 2,6-bis-(bromomethyl)pyridine (560 mg, 2.13 mmol) in acetonitrile (20 mL) for over a period of 1 hour under N_2. The mixture was then heated at reflux under N_2 and a white precipitate started forming after 5 hours. After 24 hours the precipitate was cooled to room temperature, filtered and washed sequentially with acetonitrile and diethyl ether. Yield (1088 mg, 96.5%). ^{1}H NMR (400 MHz, DMSO-d_6): δ = 9.69 (s, 2H), 8.01 (t, 1H), 7.96 (d, 2H), 7.66-7.62 (m, 4H), 7.57 (d, 2H), 7.44 (dt, 2H), 5.82 (s, 4H), 4.04 (s, 6H). ^{13}C NMR (100 MHz, DMSO-d_6): δ = 153.12, 143.04, 138.78, 131.37, 130.84, 126.29, 122.40, 113.52, 113.30, 50.35, 33.37. TOF MS/ESI$^+$, *m/z* = 448.1145 [M – Br$^-$]$^+$. *Anal. Calc. for* $C_{23}H_{23}Br_2N_5$: C, 52.19; H, 4.38; N, 13.23 %. *Found:* C, 52.06; H, 4.50; N, 13.26 %.

7.2.3 Syntheses of Palladium Carbene Complexes

The Pd(II) complexes were synthesized using standard published literature procedures[3, 24, 26, 69, 70] with slight modifications.

2,6-Bis(3-methylimidazolium-1-yl)pyridine chloropalladium (II) tetrafluoroborate, (NHC)Pd1

2,6-Bis(3-methylimidazolium-1-yl)pyridine dibromide (501.4 mg, 1.250 mmol) was suspended in dichloromethane (50 mL) and methanol (6 mL) added to effect dissolution. Ag_2O (289.9 mg, 1.251 mmol) was added and the resulting black suspension was protected from light and stirred at room temperature for 3 days. The product was filtered and washed with methanol. The residue was suspended in acetonitrile (70 mL) and $AgBF_4$ (243.3 mg, 1.250 mmol) added, followed by $PdCl_2$ (cod) (354.0 mg, 1.240 mmol). The resulting mixture was protected from light and stirred at 50 ºC under N_2 for 2 days and filtered. The solvent was removed in vacuo and the yellow residue washed with dichloromethane and diethyl ether to give a brown-yellow solid. Yield (421.7 mg, 72.4%). ^{1}H NMR (400 MHz, DMSO-d_6): δ = 8.54 (t, 1H), 8.39 (d, 2H), 7.97 (d, 2H), 7.63 (d, 2H), 3.98 (S, 6H). ^{13}C NMR (100 MHz, DMSO-d_6): δ = 166.8, 150.5, 146.7, 125.6, 118.3, 108.9, 36.5. TOF MS/ESI$^+$, *m/z* = 381.9808 (M – BF_4) $^+$. *Anal. Calc. for* $C_{13}H_{15}N_5ClPdBF_4$: C, 33.22; H, 3.22; N, 14.90 %. Found: C, 33.42; H, 3.35; N, 15.15 %

2,6-Bis[(3-methylimidazolium-1-yl)methyl]pyridine chloropalladium(II) tetrafluoroborate, (NHC)Pd2

2,6-Bis[(3-methylimidazolium-1-yl)methyl]pyridine dibromide (536.4 mg, 1.250 mmol) was suspended in acetonitrile (30 mL) and methanol (3 mL) added to effect dissolution. Ag_2O (289.9 mg, 1.251 mmol) was added and the resulting black suspension was protected from light and stirred at 50 – 60 ºC for 24 hours. To the reaction mixture, $AgBF_4$ (244.7 mg, 1.257 mmol) was added, followed by $PdCl_2(MeCN)_2$ (324.5 mg, 1.251 mmol). The reaction mixture was protected from light and stirred at 50 ºC under N_2 for 24 hours. The mixture was then allowed to cool to

room temperature. After filtration, the solvent was removed in vacuo and the yellow residue washed with dichloromethane and diethyl ether to give a yellow solid. Yield (555.6 mg, 89.2%). ^{1}H NMR (400 MHz, DMSO-d_6): δ = 8.20 (t, 1H), 7.85 (d, 2H), 7.56 (d, 2H), 7.36 (d, 2H), 5.74(d 2H), 5.66(m, 4H), 3.94 (s, 6H). ^{13}C NMR (100 MHz, DMSO-d_6): δ = 164.37, 155.46, 141.71, 125.53, 123.54, 121.53, 54.86, 36.9. TOF MS/ESI^{+}, *m/z* = 410.0377 (M – BF_4)$^{+}$. *Anal. Calc. for* $C_{15}H_{19}N_5ClPdBF_4$: C, 43.81; H, 4.66; N, 17.03%. Found: C, 43.62; H, 4.89; N, 16.98 %.

2,6-Bis[(3-butylimidazolium-1-yl)methyl]pyridine chloropalladium(II) tetrafluoroborate, (NHC)Pd3

To a solution of 2,6-Bis[(3-butylimidazolium-1-yl)methyl]pyridine dibromide (614.6 mg, 1.250 mmol) in acetonitrile (30 mL), Ag_2O (289.9 mg, 1.251 mmol) was added and the resulting black suspension protected from light and stirred at 50 – 60 ºC for 24 hours. To the reaction mixture, $AgBF_4$ (244.7 mg, 1.257 mmol) was added, followed by $PdCl_2(MeCN)_2$ (324.5 mg, 1.251 mmol). The reaction mixture was protected from light and stirred at 50 ºC under N_2 for 24 hours. The mixture was then allowed to cool to room temperature. After filtration, the solvent was removed in vacuo and the yellow residue washed with diethyl ether. The product was dissolved in small amount of dichloromethane, precipitated with diethyl ether and filtered to give an off-white/yellow solid. Yield (526.4 mg, 72.3%). ^{1}H NMR (400 MHz, DMSO-d_6): δ = 8.20 (t, 1H), 7.84 (d, 2H), 7.58 (d, 2H), 7.43 (d, 2H), 5.63 (d, 2H), 4.48 (m, 2H), 4.24 (m, 2H), 1.75 (q, 4H), 1.26 (q, 4H), 1.09 (t, 4H), 0.89 (m, 6H). ^{13}C NMR (100 MHz, DMSO-d_6): δ = 164.5, 155.7, 141.9, 125.7, 121.9 54.6, 48.7, 32.9, 19.3, 13.8. LC-MS/ESI^{+}, *m/z* = 494 (M – BF_4) $^{+}$. *Anal. Calc. for* $C_{21}H_{31}N_5ClPdBF_4$: C, 43.32; H, 5.37; N, 12.03 %. Found: C, 43.54; H, 5.25; N, 11.91%.

2,6-Bis[(3-methylbenzimidazol-1-yl)methyl]pyridine chloropalladium(II) tetrafluoroborate, (NHC)Pd4

2,6-Bis(3-methybenzimidazolium-1-yl)pyridine dibromide (381.0 mg, 0.750 mmol) was suspended in dichloromethane (50 mL) and methanol (6 mL) added to effect dissolution. Ag_2O (167.0 mg, 0.751 mmol) was added and the resulting black suspension protected from light and stirred at room temperature for 3 days. The product was filtered and washed with methanol. The residue was suspended in acetonitrile (50 mL) and $AgBF_4$ (116.8 mg, 0.600 mmol) added, followed by $Pd(COD)Cl_2$ (199.9 mg, 0.700 mmol). The resulting mixture was protected from light and stirred at 50 ºC under N_2 for 2 days. The mixture was left to cool to room temperature, filtered. The solvent was reduced in vacuo to about 3 mL, then precipitated with diethyl ether. The yellow precipitate was filtered and washed sequentially with dichloromethane and diethyl ether. Yield (193.5 mg, 46.2 %). ^{1}H NMR (400 MHz, DMSO-d_6): δ = 8.24 (t, 1H), 8.07 (m, 4H), 7.79 (d, 2H), 7.51 (m, 5H), 6.25 (d, 2H), 5.94 (d, 2H), 4.23 (S, 6H). ^{13}C NMR (100 MHz, DMSO-d_6): δ = 175.5, 155.8, 142.1, 134.7, 132.4, 125.4, 124.3, 111.3, 51.2, 34.6. TOF MS/ES$^+$, *m/z* = 510.0770 (M – BF_4) $^+$. *Anal. Calc. for* $C_{23}H_{23}N_5ClPdBF_4$: C, 46.18; H, 3.88; N, 11.71 %. Found: C, 46.39; H, 4.15; N, 11.52 %.

7.2.4 Physical Measurements and Instrumentation

NMR spectroscopic characterization was performed using either Bruker Avance DPX 400 NMR or DPX 500 with a 5 mm BBOZ probe at 30 ºC. Shimadzu LC-MS 2020 or a Waters TOF Micro-mass TOF Micro-mass LCT Premier spectrophotometer fitted with a positive ion mode and Carlo Erba Elemental Analyzer 1106 was used for mass spectroscopic and elemental analysis, respectively for the characterization of ligands and complexes. A selection of NMR and mass spectra data for the synthesized precursors, ligands and complexes are presented in Figures SI 7.1– 7.24, Supporting Information (ESI‡). Cary 100 Bio UV–visible spectrophotometer was used to determine a suitable wavelength for monitoring the substitution reactions. Applied

Photophysics SX 20 stopped-flow reaction analyzer coupled to an online data acquisition system was used for kinetic and thermodynamic studies of the reactions. The instrument was thermo-controlled within ± 0.1 °C.

7.2.5 Preparations of the Kinetic Solutions

The solutions of Pd(II) complexes (4.0 x 10^{-4} M) were prepared by weighing appropriate amounts and dissolving in water solvent system containing 20 mM LiCl.[71] Nucleophiles solutions were freshly prepared just before use by dissolving a measured quantity in aqueous solution containing 20 mM LiCl. LiCl was used to suppress possibility of any solvolysis.[72, 73] The stock solution of the nucleophiles approximately 50-fold excess of the concentration of the complex was serially diluted with the aqua solution (20 mM LiCl) to afford 40- 30- 20- and 10-fold in excess of the complex concentrations to maintain *pseudo*-first-order conditions.

7.2.6 Kinetic Analysis

The wavelengths at which kinetic measurements were monitored was spectrophotometrically established by recording the spectral changes over a range of wavelengths between 800 nm – 200 nm for the reactions of each complex and the respective nucleophile solutions. All reactions were initiated by mixing equal volumes of ligand and complex solutions directly in the stopped-flow instrument. Concentration dependence on the rate of substitution of the entering nucleophiles were monitored at 298 K. On the other hand, the temperature dependence reactions were carried out within a range of 15 °C to 35 °C with 5 °C intervals for all the substitution reactions to determine activation parameters $\Delta H^{\neq}$ and $\Delta S^{\neq}$. All the *pseudo*-first-order rate observed, k_{obs}, were average values computed from 3 – 6 independent runs.

7.2.7 Computational Modelling

The ground state electronic structures of the complexes were optimized using the density functional theory (DFT). This was performed to gain more insights into structural, steric and

electronic factors influencing the kinetics and thermodynamics of the substitution reactions. The DFT calculations were performed using the Gaussian 09 program suite.[74] The B3LYP (Becke 3-Lee-Yang-Parr) functional method, utilizing LANL2DZ (Los Alamos National Laboratory 2 Double ζ)[75-78] were used as the basis set. The influence caused by the bulk solvent was evaluated *via* single-point computations using the C-PCM (conductor-like polarizable continuum model) [79, 80] formalism in water solvent. All the complexes were modelled at a charge of +1 in a singlet state due to the low electronic spin of the Pd(II). Global electrophilicity index (ω) and electronic chemical potential (μ) of the complexes were calculated using literature methods.[50, 81, 82]

7.3 Results

7.3.1 Computational Analysis

The geometry of the optimized molecular frontier orbitals and the planarity structures for the complexes are presented in Table 7.1, while the geometric data extracted from the DFT calculations are presented in Table 7.2.

The frontier orbital mappings in Table 7.1 show that the HOMOs are mainly contributed from 4d-orbitals of the Pd atom, 3p-orbitals of the chlorine atom as well as from the *cis*-ligand moiety (imidazolin-2-ylidene and benzimidazolin-2-ylidene) of all the complexes except in **(NHC)Pd1**. In **(NHC)Pd1** they are contributed from the 4d-orbital of the Pd atom and the entire ligand. The HOMO electron density distribution mainly on the imidazole and benzimidazole fragments of the complexes is an indication that these moieties are electron rich. The introduction of methylene spacer group between the pyridine and the imidazole or benzimidazole significantly raises the HOMO energy levels of the complexes compared to the pyridine bridged **(NHC)Pd1** (Table 7.2). This means that the methylene spacer group destabilizes the HOMO energy thus making the ligand a poor π-acceptor. Additionally, the energy levels of the HOMO orbitals are successively raised from **(NHC)Pd1** to **(NHC)Pd2** to

Table 7. 1 DFT optimized HOMO, LUMO molecular orbitals and planarity of Pd(II) complexes at B3LYP/LANL2DZ theory level (Iso value = 0.02).

Complex structure	HOMO	LUMO	Planarity
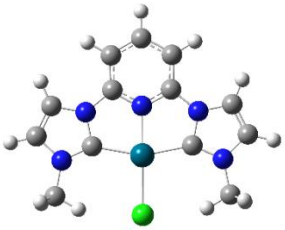 **(NHC)Pd1**	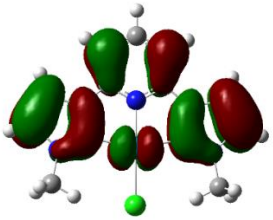	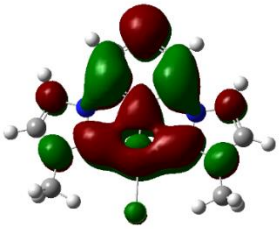	
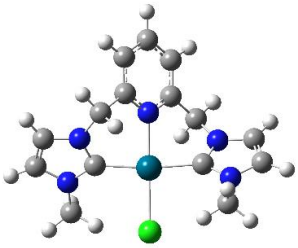 **(NHC)Pd2**	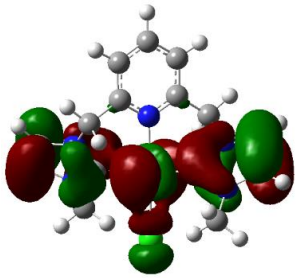	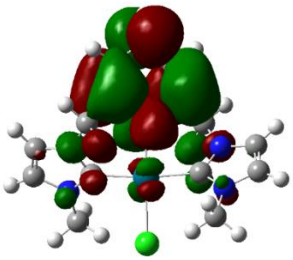	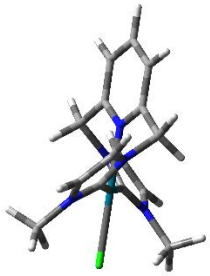
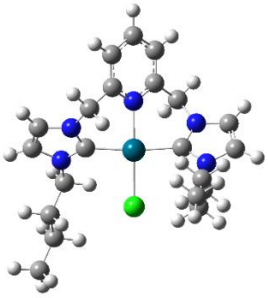 **(NHC)Pd3**	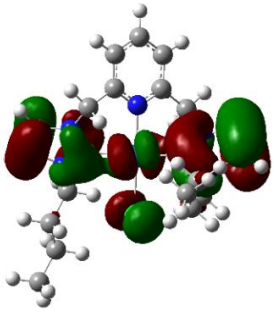	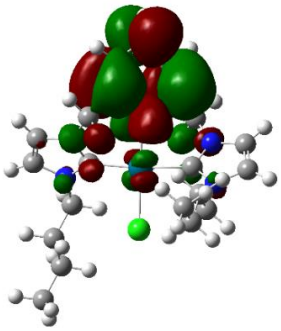	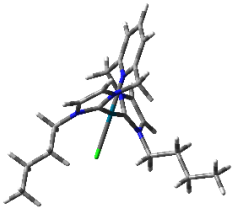
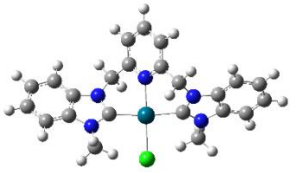 **(NHC)Pd4**	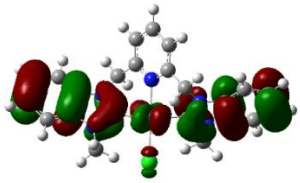	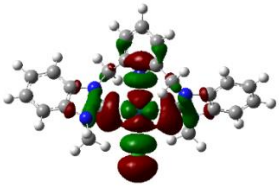	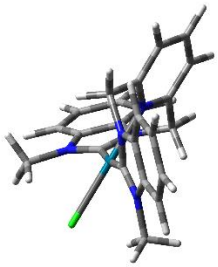

Table 7. 2 Summary of calculated parameters for complexes studied

Property	**(NHC)Pd1**	**(NHC)Pd2**	**(NHC)Pd3**	**(NHC)Pd4**
NBO Charges				
Pd^{2+}	0.300	0.259	0.262	0.272
Cl^{-}	-0.490	-0.486	-0.484	-0.482
Global descriptors				
Electrophilicity index (ω)	5.600	4.525	4.509	4.610
Electronic Chemical Potential (μ)/ eV	-4.915	-4.601	-4.577	-4.619
Bond lengths (Å)				
Pd –N	2.007	2.100	2.101	2.094
Pd – C	2.065	2.059	2.060	2.059
Pd – Cl	2.414	2.425	2.423	2.423
H···Cl	2.610	2.662	2.684	2.685
Energy gap (eV)				
LUMO (eV)	-2.758	-2.262	-2.254	-2. 305
HOMO (eV)	-7.071	-6.939	-6.900	-6.932
$\Delta E_{LUMO-HOMO}$	4.313	4.677	4.646	4.627
Bond angles (º)				
N – Pd – Cl	179.642	179.971	179.561	179.961
C – Pd – C	158.505	174.047	173.916	174.166
N – Pd – C	79.252	87.021	86.958	87.080
C – Pd – Cl	100.747	92.987	93.042	92.927
Deviation of *cis*-ligand from the main axis plane	0	58.540	59.160	59.390
Dipole moment (Debye)	12.353	12.571	15.271	12.275

(NHC)Pd4 and finally to **(NHC)Pd3**. This suggests that the σ-donation of electron density towards the Pd(II) metal centres [58] subsequently increases in the same order.

The LUMOs are mainly contributions from the ligand framework as well as from the 4d-orbitals for **(NHC)Pd1**, **(NHC)Pd2** and **(NHC)Pd3** while in **(NHC)Pd4** the electrons are distributed entirely on the chloride ligand, *cis*-imidazolyl fragment, *trans*-pyridine and the Pd metal centre. As was observed in the HOMOs, the LUMO energy of the complexes are similarly raised in **(NHC)Pd2**, **(NHC)Pd3** and **(NHC)Pd4** in relation to **(NHC)Pd1** leading to destabilization of the LUMO energy.

From the planarity structures, the complexes adopt slightly distorted square planar geometry as the C–Pd–C angle deviates from the ideal expected 180º ranging from 158.505º to 174.916º. The complexes with methylene spacer group **(NHC)Pd2**, **(NHC)Pd3** and **(NHC)Pd4** have a significant twisting of their *cis*-ligand moieties at 58.54º, 59.16º and 59.39º respectively, away from the N–Pd–Cl main axis and the *trans*-pyridyl plane. The twisting of the C^N^C ligands in the complexes causes an inclination of the *cis*-ligand subunit and the pyridyl planes and the Pd coordination plane. It appears that the extent of twisting is influenced by the nature of the steric bulk of the N-substituent [70] and the extended conjugation in the case of benzimidazolin-2-ylidene. However, it is noticed through the C–Pd–C angle that the twisted complexes deviate slightly (173.916º – 174.166º) from the ideal square planar geometry than the non-twisted rigid planar **(NHC)Pd1** (158.505º). A typical example of such twisting is shown for **(NHC)Pd4** in Figure 7.2. In addition, the bond distances of Pd–C and Pd–N are significantly shorter than that of Pd–Cl due to the formation of the chelates with pincer-type ligands.[26]

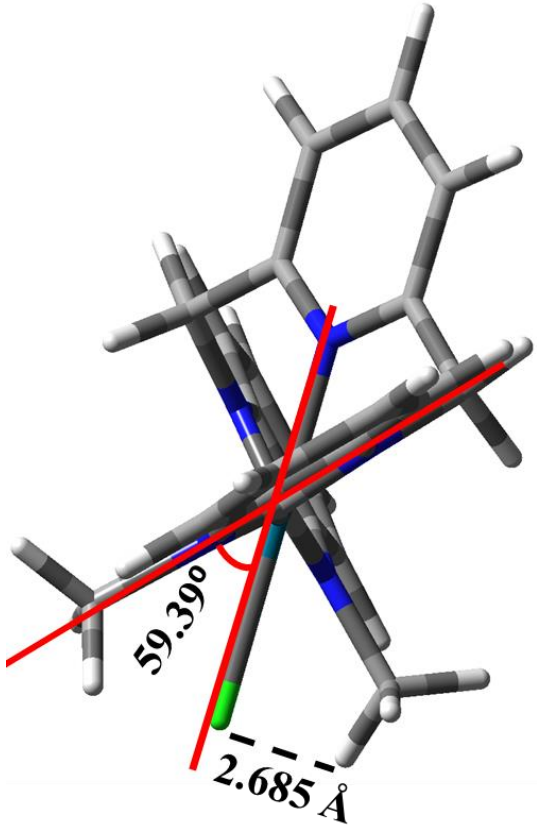

Figure 7. 2 DFT optimized structure of **(NHC)Pd4** showing the deviation of the twisted angle between the *cis*-fragment plane and the main plane and the H···Cl length

7.3.2 Kinetic and Mechanistic Studies

The chloride substitution reactions of the Pd(II) complexes with the nucleophiles was investigated as a function of nucleophile concentration and temperature. The reactions were monitored using stopped flow techniques with a specified wavelength that was predetermined from the Uv-Visible spectrophotometer from the complex and nucleophile reaction. The wavelengths used for the substitution reactions ranged between 315 nm to 350 nm depending on the respective complexes and the nucleophiles are presented in Table SI 7.1, supporting information (ESI‡). The kinetic traces were of excellent fit to a single-exponential decay function which generated observed *pseudo*-first-order rate constant (k_{obs}) using *Equation 7.1*,[83] suggesting that the substitution reactions are first-order in both the thiourea nucleophiles and Pd(II) complexes.

$$A_t = A_0 + (A_0 - A_\infty)\exp(-k_{obs}t) \qquad 7.1$$

where A_t , A_0 and A_∞ represent the absorbance of initial reaction mixture, at time t, and at the end of the reaction respectively. A typical example of stopped-flow kinetic trace at 320 nm recorded by mixing the aqua solutions of **(NHC)Pd3** and **Dmtu** at 298 K is shown in Figure 7.3.

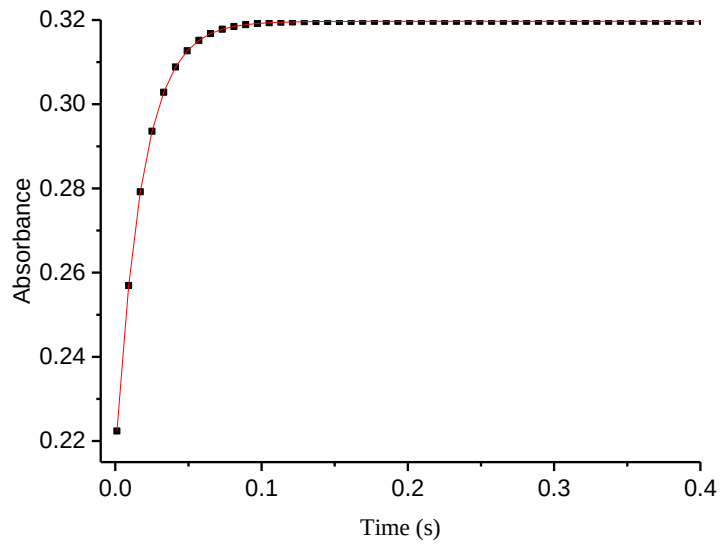

Figure 7. 3 Stopped-flow kinetic trace at 320 nm of **(NHC)Pd3** (4.0 x 10^{-4} M) and **Dmtu** (1.6 x 10^{-2} M) at 298 K.

The second-order rate constants, k_2, for the reactions was obtained from the gradient of a plot of k_{obs} versus nucleophile concentration using OriginPro 9.1® software.[84] Straight line plots with zero intercepts were obtained which indicated that the reverse or solvotic pathway was absent or insignificant. A representative plot of k_{obs} versus concentration of the nucleophiles of **(NHC)Pd2** is shown in Figure 7.4, other similar plots for the other complexes are shown in Figures SI 7.25 – 7.27, while the nucleophile concentrations with their respective k_{obs} values are shown in Tables SI 7.2 – 7.5 in the supporting information (ESI‡). Based on these results, the *pseudo*-first-order dependence on rate constant is related to the nucleophile concentration [Nu] by *Equation 7.2*. The values of the second order rate constants, k_2, are presented in Table 7.3.

$$k_{obs} = k_2[Nu] \qquad 7.2$$

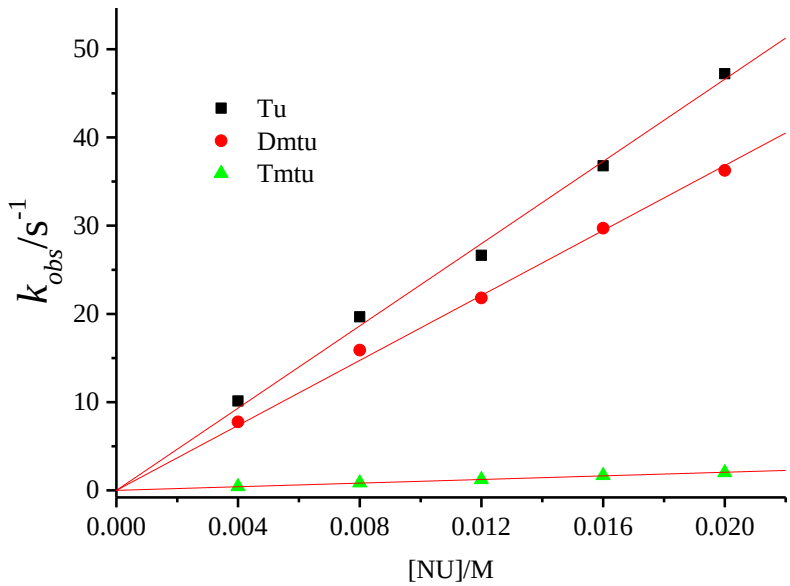

Figure 7. 4 Dependence of k_{obs} (s^{-1}) on the concentration of nucleophiles for the reactions with **(NHC)Pd2** in water I = 20 mM LiCl, T = 298 K.

Data from the temperature dependence of k_2 was plotted according to the Eyring *Equation 7.3*. The values of activation parameters,[85] enthalpy **(**$\Delta H^{\neq}$) and entropy ($\Delta S^{\neq}$) were computed from the slopes and y-intercepts respectively, from the plots of ln $\left(\frac{k_2}{T}\right)$ versus $\frac{1}{T}$

$$\ln\left(\frac{k_2}{T}\right) = -\frac{\Delta H^{\neq}}{RT} + \left(23.8 + \frac{\Delta S^{\neq}}{R}\right) \qquad (7.3)$$

where T and R represent temperature and gas constant, respectively. A representative Eyring plot for **(NHC)Pd4** is presented in Figure 7.5; similar Eyring plots for other complexes are shown in Figures SI 7.28 – 7.30, while the values of $\frac{1}{T}$ with their respective ln $\left(\frac{k_2}{T}\right)$ are depicted in Tables SI 7.6 –7.9 in the supporting information (ESI‡). The calculated activation parameter data are reported in Table 7.3.

Table 7. 3 The values of k_2 and thermodynamic parameter data of the reactions Pd(II) complexes with thiourea ligands in water, I = 20 mM LiCl.

Complexes	Nu	k_2 ($M^{-1}s^{-1}$)	$\Delta H^{\neq}$ (kJ mol^{-1})	$\Delta S^{\neq}$ ($JK^{-1}mol^{-1}$)
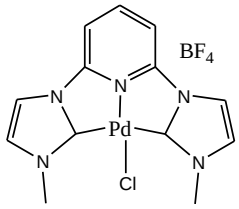 **(NHC)Pd1**	**Tu**	2678 ± 12	23 ± 1	- 103 ± 3
	Dmtu	2303 ± 29	39 ± 1	- 52 ± 3
	Tmtu	228 ± 4	42 ± 1	- 59 ±2
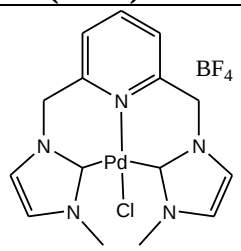 **(NHC)Pd2**	**Tu**	2330 ± 34	25 ± 1	- 95 ± 5
	Dmtu	1841 ± 24	39 ± 1	- 52 ± 2
	Tmtu	103 ± 1	42 ± 1	- 69 ± 3
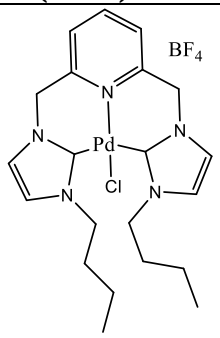 **(NHC)Pd3**	**Tu**	217 ± 2	51 ± 3	- 32 ± 9
	Dmtu	159 ± 2	55 ± 3	- 22 ± 9
	Tmtu	19 ± 0.1	57 ± 2	- 33 ± 5
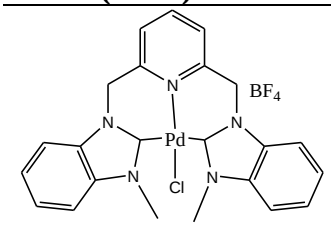 **(NHC)Pd4**	**Tu**	1822 ± 19	40 ± 1	- 50 ± 3
	Dmtu	1681 ± 22	38 ± 2	- 54 ± 5
	Tmtu	98 ± 1	37 ± 3	- 85 ± 10

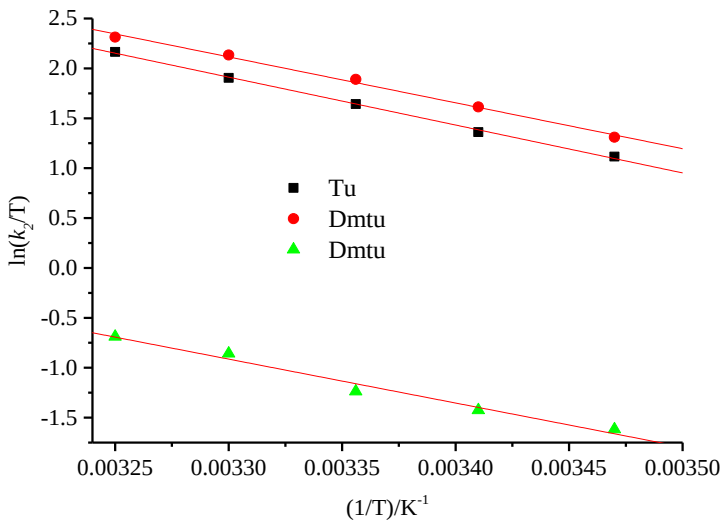

Figure 7. 5 Eyring plots for the reactions of **(NHC)Pd4** with the nucleophiles

7.4 Discussion

In this study, a series of 2,6-bis(NHC) Pd(II) complexes were synthesized and the rate of substitution of their chloro ligand with thiourea nucleophiles investigated. Starting from pyridine-bridged bis(imidazolylidene), **(NHC)Pd1** to lutidine-bridged pincer complexes; bis(imidazolin-2-ylidene) with varied size of N-substituents, **(NHC)Pd2** and **(NHC)Pd3**, to bis(benzimidazolin-2-ylidene) **(NHC)Pd4**. These complexes have strong σ-donor properties caused by the two *cis*-carbon of the bis(NHC) carbene ligand as well as steric properties forced on their coordinated Pd metal centre. The two effects acts in a concerted way in most of the complexes under this investigation to stabilize the Pd metal thereby controlling its reactivity. The reactivity trend of the complexes with respect to the thiourea nucleophiles decreases in the order **(NHC)Pd1** > **(NHC)Pd2** > **(NHC)Pd4** > **(NHC)Pd3** as shown in their second-order rate constant, k_2, values tabulated in Table 7.3.

When the reactivity of **(NHC)Pd1** is compared with that of **(NHC)Pd2**, the reactivity of **(NHC)Pd1** is slightly faster than that of **(NHC)Pd2**. The structural difference between the complexes is in the introduction of methylene spacer group between the *trans*-pyridyl ring and

the *cis*-imidazol-2-ylidene derivative in **(NHC)Pd2** which accounts for the reactivity difference. The methylene spacer group in **(NHC)Pd2** introduces a six-membered ring into the coordination sphere of the Pd metal centre destroying the aromaticity of the ligand. The π-acceptability of the ligand is thus decreased as supported by the less positive NBO charges and electrophilicity index (Table 7.2) indicating that **(NHC)Pd2** has a poor interaction between the orbitals of d_{xz} and d_{yz} with the empty anti-bonding or non-bonding orbitals of the ligand in relation to **(NHC)Pd1**.

In addition, **(NHC)Pd2** is more flexible due to six-membered chelate system than the five-membered chelate system, **(NHC)Pd1**, as observed in the planarity of the DFT optimized structures in Table 7.1 where **(NHC)Pd2** shows a twisted planar as compared to the rigid planar structure of **(NHC)Pd1**. The tetrahedral arrangement of the methylene spacer groups causes the imidazol-2-ylidene derivative ligands to be forced out of plane with the metal centre forming a two boat-shaped palladacycle.[69] This significantly introduces steric effects and eventually retards the rate of chloride substitution in **(NHC)Pd2**.[66, 67] The effect is further enhanced in **(NHC)Pd4** and **(NHC)Pd3** whose reactivities are lowered in that order.

In the Pd(II) complexes having methylene spacer groups, the *cis*-benz/imidazole-2-ylidene fragments are twisted out of plane with the *trans*-pyridine rings to the Pd coordination plane by 58.54º, 59.16º and 59.39º for **(NHC)Pd2**, **(NHC)Pd3** and **(NHC)Pd4**, respectively (Table 7.2). The higher reactivity of **(NHC)Pd2** is due to it being less sterically hindered than the other complexes. While **(NHC)Pd3** is slower because of the concerted effects of the steric and the higher positive σ-inductive effects into the chelate ring[58, 86] caused by the N-butyl substituents than the N-methyl substituents in **(NHC)Pd2** and **(NHC)Pd4**. The σ-donation of N-butyl substituents' leads to more accumulation of electron density around the Pd metal centre[87, 88] in

(NHC)Pd3 than in the other complexes leading to lower electrophilicity and thereby retarding the incoming nucleophile through electron repulsion.[89]

The trend in electronic chemical potential (μ) (Table 7.2), which measures the tendency of a system to gain or lose an electron,[90, 91] supports the reactivity trend of all the complexes except that of **(NHC)Pd4**. The apparent discrepancy in **(NHC)Pd4** with the reactivity trend is due to the improper behaviour of the electronic chemical potential.[81] In general, the reactivity of pyridine-bridged complex, **(NHC)Pd1** is faster than the rest of the lutidine-bridged complexes in this study.

The higher reactivity of **(NHC)Pd1** than the rest of the complexes is also because of π-backbonding from the filled metal's d_{xz} and d_{yz} orbitals into the empty nonbonding or antibonding *cis*-carbon p_{π} orbitals [4, 92, 93] and *trans*-pyridyl p_z orbitals of the bis(NHC) carbene ligand. This means that the ligand in **(NHC)Pd1** is a stronger π-acceptor than the rest of the ligands of the other complexes. The withdrawal of electron density from the metal centre of **(NHC)Pd1** by the ligand leads to increased electrophilicity at the metal centre making it more attractive to the incoming nucleophile. However, it is noted that the reactivity of **(NHC)Pd1** is slower than that of $[Pd(terpy)Cl]^+$ complex in literature[94] by 2 orders of magnitude when compared given that their ligand systems are both aromatic having π-backbonding character. This is attributable to the stronger σ-donation from the *cis*-carbons [3, 93] together with further stabilization by the pπ-donation from the adjacent *cis*-N-atoms into the empty p_{π} orbitals of the carbene carbon atoms.[4, 5, 95] The resultant effect is the weaker π-backbonding of bis(NHC) carbene ligand from the metal centre than that of the terpy ligand.

As tabulated in Table 7.3, the reactivity with respect to the nucleophiles decreases following the order **Tu** > **Dmtu** > **Tmtu** in accordance with their steric hinderances since the least sterically

hindered **Tu** reacts faster while the most sterically hindered **Tmtu** is significantly slower. On the other hand, the thermodynamic parameters illustrate that the activation values of entropies ($\Delta S^{\neq}$) are negative, whereas the enthalpies ($\Delta H^{\neq}$) are positive and small. The trend in these parameters is a clear indication that the substitution mechanism is associative, which is commonly observed for square-planar d^8 metal complexes.[73, 96] The values of the thermodynamic parameter suggests that the activation process is highly dominated by bond-making process leading to formation of trigonal bipyramidal intermediate structure. Therefore, the modelled bis(NHC) ligands' coordination in this study is unable to induce mechanistic change over as have been observed in Pt(II) complexes having two carbon σ-donors bounded to the metal centre in the *cis*-position to the leaving group in literature.[53, 63-65] This can be attributed to the nature of the leaving group since in all the Pt(II) complexes that experienced the mechanistic change over, sulfur atom formed part of the leaving group, while in this study chloride is the leaving group. It can therefore be concluded that the leaving group plays a role in determining the mechanistic change over.

7.5 Conclusions

This study has demonstrated that the reactivity of Pd(II) complexes can be controlled by a series of bis(NHCs) ligands having differing steric and electronic properties. These factors promoted the reduction in the reactivity of the Pd metal in **(NHC)Pd3** (lowest reactive) by factors ranging 12 – 15 times relative to that of **(NHC)Pd1** (highest reactive) with the thiourea nucleophiles. The reactivity of **(NHC)Pd1** is majorly controlled by electronic factors while that of the other complexes are determined by both steric and electronic factors. The introduction of methylene spacer groups in the chelate ring introduces steric influence in the complexes which significantly lowers the rates of substitution. It is clear that the length of the alkyl chain of the N-substituent of the bis(NHC) ligand significantly slows down the reactivity as in the case of **(NHC)Pd3**. In

addition, **(NHC)Pd4** and **(NHC)Pd3** showing slightly higher electron donating capabilities, linked to the destabilization of their HOMO energy, indicates that the modifications on the *cis*-ligand, imidazolin-2-ylidene subunit, permits effective tuning of steric and electronic properties. The substitution mechanism is associative as the two *cis*-σ-bound carbon donors of the complexes is unable to induce dissociative substitution mechanism. This study presents a preliminary findings that forms a basis for further research on tuning the reactivity of Pd metal using bis(NHC) type of ligands which could lead to complexes useful in biological applications as metallodrugs.

7.6 References

1. A. J. Arduengo III, R. L. Harlow and M. Kline, *Journal of the American Chemical Society*, 1991, **113**, 361-363.
2. A. A. Danopoulos, N. Tsoureas, S. A. Macgregor and C. Smith, *Organometallics*, 2007, **26**, 253-263.
3. T. Nakamura, S. Ogushi, Y. Arikawa and K. Umakoshi, *Journal of Organometallic Chemistry*, 2016, **803**, 67-72.
4. H. Jacobsen, A. Correa, A. Poater, C. Costabile and L. Cavallo, *Coordination Chemistry Reviews*, 2009, **253**, 687-703.
5. E. F. Penka, C. W. Schläpfer, M. Atanasov, M. Albrecht and C. Daul, *Journal of Organometallic Chemistry*, 2007, **692**, 5709-5716.
6. H. Jacobsen, A. Correa, C. Costabile and L. Cavallo, *Journal of Organometallic Chemistry*, 2006, **691**, 4350-4358.
7. T. Tu, J. Malineni and K. H. Doetz, *Advanced Synthesis & Catalysis*, 2008, **350**, 1791-1795.
8. M. Nonnenmacher, D. M. Buck and D. Kunz, *Beilstein Journal of Organic Chemistry*, 2016, **12**, 1884.
9. C. Gunanathan and D. Milstein, *Chemical Reviews*, 2014, **114**, 12024-12087.
10. J. A. Loch, M. Albrecht, E. Peris, J. Mata, J. W. Faller and R. H. Crabtree, *Organometallics*, 2002, **21**, 700-706.
11. D. H. Brown and B. W. Skelton, *Dalton Transactions*, 2011, **40**, 8849-8858.
12. A. A. Danopoulos, J. A. Wright and W. B. Motherwell, *Chemical Communications*, 2005, 784-786.
13. F. E. Hahn and M. C. Jahnke, *Angewandte Chemie International Edition*, 2008, **47**, 3122-3172.
14. E. A. B. Kantchev, C. J. O'Brien and M. G. Organ, *Angewandte Chemie International Edition*, 2007, **46**, 2768-2813.
15. S. Diez-Gonzalez, N. Marion and S. P. Nolan, *Chemical Reviews*, 2009, **109**, 3612-3676.
16. P. Zhang and P. J. Sadler, *Journal of Organometallic Chemistry*, 2017, **839**, 5-14.
17. M. Porchia, M. Pellei, M. Marinelli, F. Tisato, F. Del Bello and C. Santini, *European Journal of Medicinal Chemistry*, 2018.
18. A. R. Kapdi and I. J. Fairlamb, *Chemical Society Reviews*, 2014, **43**, 4751-4777.

19. L. Oehninger, R. Rubbiani and I. Ott, *Dalton Transactions*, 2013, **42**, 3269-3284.
20. P. V. Simpson, C. Schmidt, I. Ott, H. Bruhn and U. Schatzschneider, *European Journal of Inorganic Chemistry*, 2013, **2013**, 5547-5554.
21. T. Bernardi, S. Badel, P. Mayer, J. Groelly, P. de Frémont, B. Jacques, P. Braunstein, M. L. Teyssot, C. Gaulier and F. Cisnetti, *ChemMedChem*, 2014, **9**, 1140-1144.
22. J. Dupont, C. Consorti, J. Spencer, D. Morales-Morales and C. Jensen, *Journal*, 2007.
23. J. C. Chen and I. J. Lin, *Journal of the Chemical Society, Dalton Transactions*, 2000, 839-840.
24. J. Vaughan, D. J. Carter, A. L. Rohl, M. I. Ogden, B. W. Skelton, P. V. Simpson and D. H. Brown, *Dalton Transactions*, 2016, **45**, 1484-1495.
25. D. H. Brown, G. L. Nealon, P. V. Simpson, B. W. Skelton and Z. Wang, *Organometallics*, 2009, **28**, 1965-1968.
26. R. A. Haque, P. O. Asekunowo, S. Budagumpi and L. Shao, *European Journal of Inorganic Chemistry*, 2015, **2015**, 3169-3181.
27. F. E. Hahn, M. C. Jahnke, V. Gomez-Benitez, D. Morales-Morales and T. Pape, *Organometallics*, 2005, **24**, 6458-6463.
28. A. A. Danopoulos, A. A. Tulloch, S. Winston, G. Eastham and M. B. Hursthouse, *Dalton Transactions*, 2003, 1009-1015.
29. F. E. Hahn, M. C. Jahnke and T. Pape, *Organometallics*, 2007, **26**, 150-154.
30. E. Pantoja, A. Gallipoli, S. van Zutphen, S. Komeda, D. Reddy, D. Jaganyi, M. Lutz, D. M. Tooke, A. L. Spek and C. Navarro-Ranninger, *Journal of Inorganic Biochemistry*, 2006, **100**, 1955-1964.
31. J. Reedijk, *Chemical Reviews*, 1999, **99**, 2499-2510.
32. T. Storr, K. H. Thompson and C. Orvig, *Chemical Society Reviews*, 2006, **35**, 534-544.
33. E. Wong and C. M. Giandomenico, *Chemical Reviews*, 1999, **99**, 2451-2466.
34. J. Lokich, *Cancer Investigation*, 2001, **19**, 756-760.
35. S. Shibata, *Neurologia Medico-Chirurgica*, 1990, **30**, 242-245.
36. M. Tanaka, H. Kataoka, S. Yano, H. Ohi, K. Kawamoto, T. Shibahara, T. Mizoshita, Y. Mori, S. Tanida and T. Kamiya, *BMC Cancer*, 2013, **13**, 237
37. A. S. Abu-Surrah, M. Kettunen, K. Lappalainen, U. Piironen, M. Klinga and M. Leskelä, *Polyhedron*, 2002, **21**, 27-31.

38. M. Al-Noaimi, A. S. Abu-Surrah and L. Tahtamouni, *Arabian Journal of Chemistry*, 2012, **9**, S1503-S1509.
39. E. Z. Jahromi, A. Divsalar, A. A. Saboury, S. Khaleghizadeh, H. Mansouri-Torshizi and I. Kostova, *Journal of the Iranian Chemical Society*, 2016, **13**, 967-989.
40. Ž. D. Bugarčić, J. Bogojeski and R. van Eldik, *Coordination Chemistry Reviews*, 2015, **292**, 91-106.
41. A. S. Abu-Surrah and M. Kettunen, *Current Medicinal Chemistry*, 2006, **13**, 1337-1357.
42. M. Marques, *ISRN Spectroscopy*, 2013, **2013**, 1 - 29.
43. J. Bogojeski, J. Volbeda, M. Freytag, M. Tamm and Ž. D. Bugarčić, *Dalton Transactions*, 2015, **44**, 17346-17359.
44. N. P. Barry and P. J. Sadler, *Chemical Communications*, 2013, **49**, 5106-5131.
45. B. Lippert, *Cisplatin: chemistry and biochemistry of a leading anticancer drug*, John Wiley & Sons, 1999.
46. S. van Zutphen and J. Reedijk, *Coordination Chemistry Reviews*, 2005, **249**, 2845-2853.
47. H. Zorbas and B. K. Keppler, *ChemBioChem*, 2005, **6**, 1157-1166.
48. D. Wang and S. J. Lippard, *Nature Reviews Drug Discovery*, 2005, **4**, 307-320.
49. R. A. Haque, P. O. Asekunowo and S. Budagumpi, *Inorganic Chemistry Communications*, 2014, **47**, 56-59.
50. I. M. Wekesa and D. Jaganyi, *Dalton Transactions*, 2014, **43**, 2549-2558.
51. A. Hofmann, L. Dahlenburg and R. van Eldik, *Inorganic Chemistry*, 2003, **42**, 6528-6538.
52. R. Romeo, M. R. Plutino, L. Monsù Scolaro, S. Stoccoro and G. Minghetti, *Inorganic Chemistry*, 2000, **39**, 4749-4755.
53. M. Rashidi, S. M. Nabavizadeh, A. Zare, S. Jamali and R. J. Puddephatt, *Inorganic Chemistry*, 2010, **49**, 8435-8443.
54. A. D. Ryabov, L. G. Kuz'mina, V. A. Polyakov, G. M. Kazankov, E. S. Ryabova, M. Pfeffer and R. van Eldik, *Journal of the Chemical Society, Dalton Transactions*, 1995, 999-1006.
55. L. I. Elding, R. Romeo, M. Schmulling, A. Ryabov and R. Van Eldik, *Journal of the Chemical Society. Dalton transactions*, 1996, 1471-1473.
56. M. Schmülling, D. M. Grove, G. van Koten, R. van Eldik, N. Veldman and A. Spek, *Organometallics*, 1996, **15**, 1384-1391.

57. M. L. Tobe and J. Burgess, *Inorganic reaction mechanisms*, Longman, London, 1999.
58. A. Mambanda and D. Jaganyi, *Dalton Transactions*, 2011, **40**, 79-91.
59. A. Mambanda and D. Jaganyi, in *Advances in Inorganic Chemistry*, Elsevier, 2017, vol. 70, pp. 243-276.
60. A. F. Cotton, G. Wilkinson, M. Bochmann and C. A. Murillo, *Advanced inorganic chemistry*, Wiley, 1999.
61. J. K. Burdett, *Inorganic Chemistry*, 1977, **16**, 3013-3025.
62. S. Okeya, K. Wakamatsu, T. Shibahara, H. Yamakado and K. Nishimoto, *Journal of Computer Chemistry, Japan*, 2002, **1**, 97-102.
63. M. R. Plutino, L. Monsù Scolaro, R. Romeo and A. Grassi, *Inorganic Chemistry*, 2000, **39**, 2712-2720.
64. R. Romeo, A. Grassi and L. Monsu Scolaro, *Inorganic Chemistry*, 1992, **31**, 4383-4390.
65. M. Schmüling and R. van Eldik, *Chemische Berichte*, 1997, **130**, 1791-1799.
66. B. Petrović, Ž. D. Bugarčić, A. Dees, I. Ivanović-Burmazović, F. W. Heinemann, R. Puchta, S. N. Steinmann, C. Corminboeuf and R. Van Eldik, *Inorganic Chemistry*, 2012, **51**, 1516-1529.
67. A. Mijatović, J. Bogojeski, B. Petrović and Ž. D. Bugarčić, *Inorganica Chimica Acta*, 2012, **383**, 300-304.
68. E. Peris, J. A. Loch, J. Mata and R. H. Crabtree, *Chemical Communications*, 2001, 201-202.
69. D. J. Nielsen, K. J. Cavell, B. W. Skelton and A. H. White, *Inorganica Chimica Acta*, 2002, **327**, 116-125.
70. D. J. Nielsen, K. J. Cavell, B. W. Skelton and A. H. White, *Inorganica Chimica Acta*, 2006, **359**, 1855-1869.
71. M. Kosović, Ž. Jaćimović, Ž. D. Bugarčić and B. V. Petrović, *Transition Metal Chemistry*, 2016, **41**, 161-168.
72. S. Jovanović, B. Petrović, D. Čanović and Ž. D. Bugarčić, *International Journal of Chemical Kinetics*, 2011, **43**, 99-106.
73. M. Tobe and J. Burgess, *Inorganic Reaction Mechanisms* Addison Wesley Longman Inc, Essex, 1999.

74. M. Frisch, G. Trucks, H. Schlegel, G. Scuseria, M. Robb, J. Cheeseman, G. Scalmani, V. Barone, B. Mennucci, G. Petersson, Gaussian 09, revision D. 01, Gaussian, Inc., Wallingford CT (2009).
75. P. J. Hay and W. R. Wadt, *The Journal of Chemical Physics*, 1985, **82**, 299-310.
76. A. D. Becke, *Journal of Chemical Physics*, 1993, **98**, 5648-5652.
77. C. Lee, W. Yang and R. G. Parr, *Physical Review B*, 1988, **37**, 785.
78. P. J. Hay and W. R. Wadt, *The Journal of Chemical Physics*, 1985, **82**, 270-283.
79. V. Barone and M. Cossi, *The Journal of Physical Chemistry A*, 1998, **102**, 1995-2001.
80. M. Cossi, N. Rega, G. Scalmani and V. Barone, *Journal of Computational Chemistry*, 2003, **24**, 669-681.
81. C. A. Mebi, *Journal of Chemical Sciences*, 2011, **123**, 727-731.
82. R. G. Parr, L. s. v. Szentpa´ly and L. Shubin, *Journal of American Chemical Society*, 1999, **121**, 1922-1924.
83. J. D. Atwood, *Inorganic and organometallic reaction mechanisms*, Wiley-VCH Publishers, New York, 2nd edn., 1997.
84. OriginPro 9.1. OriginLab Corporation, One Roundhouse Plaza, Suite 303, Northampton, MA 01060, United States. 1800-969-7720.
85. H. Eyring, *The Journal of Chemical Physics*, 1935, **3**, 107-115.
86. P. O. Ongoma and D. Jaganyi, *Dalton Transactions*, 2013, **42**, 2724-2734.
87. D. Jaganyi, D. Reddy, J. Gertenbach, A. Hofmann and R. van Eldik, *Dalton Transactions*, 2004, 299-304.
88. I. M. Wekesa and D. Jaganyi, *Journal of Coordination Chemistry*, 2016, **69**, 389-403.
89. G. Kinunda and D. Jaganyi, *Transition Metal Chemistry*, 2014, **39**, 451-459.
90. R. G. Pearson, *Inorganica Chimica Acta*, 1992, **198**, 781-786.
91. R. G. Pearson, *Journal of Molecular Structure: THEOCHEM*, 1992, **255**, 261-270.
92. J. C. Green, R. G. Scurr, P. L. Arnold and F. G. N. Cloke, *Chemical Communications*, 1997, 1963-1964.
93. M. C. Perry and K. Burgess, *Tetrahedron: Asymmetry*, 2003, **14**, 951-961.
94. S. Kern, P. Illner, S. Begel and R. van Eldik, *European Journal of Inorganic Chemistry*, 2010, **2010**, 4658-4666.
95. D. Bourissou, O. Guerret, F. P. Gabbai and G. Bertrand, *Chemical Reviews*, 2000, **100**, 39-92.

96. R. Van Eldik, T. Asano and W. Le Noble, *Chemical Reviews*, 1989, **89**, 549-688.

7.7 Supporting Information (ESI‡)

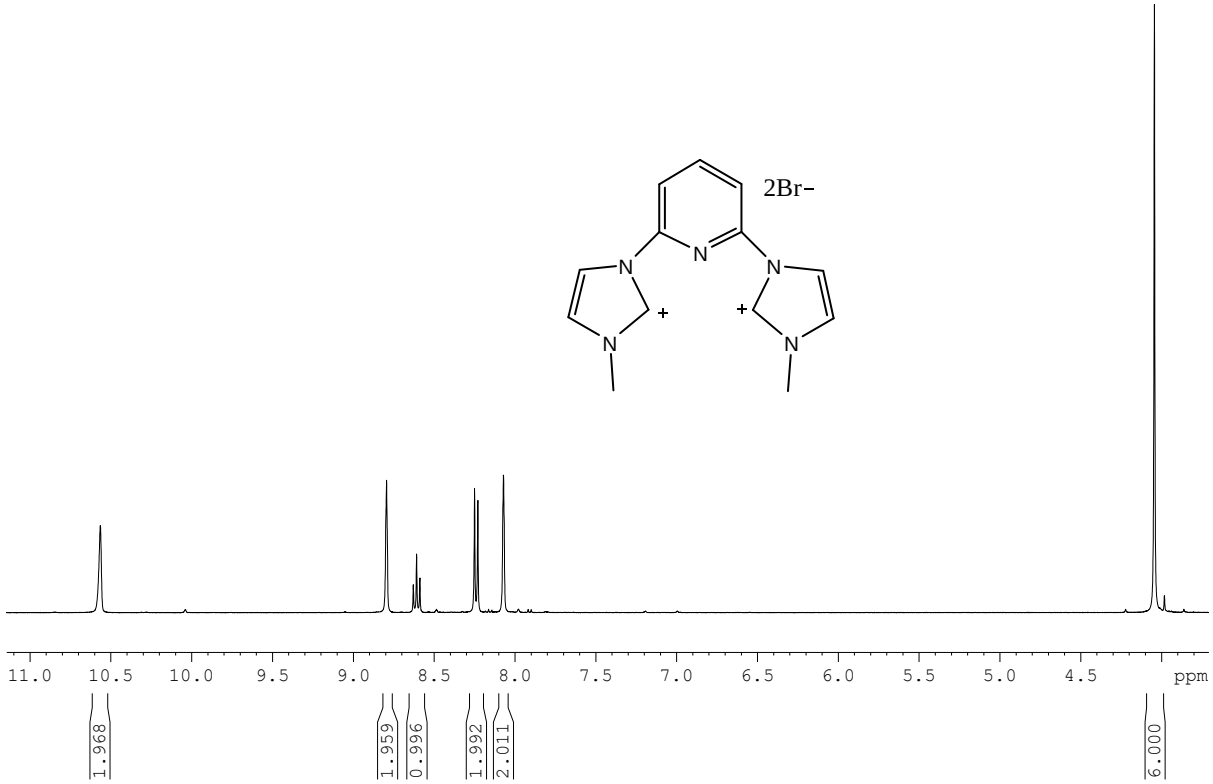

Figure SI 7.1 ^{1}HNMR spectrum of 2,6-Bis(3-methylimidazolium-1-yl)pyridine dibromide

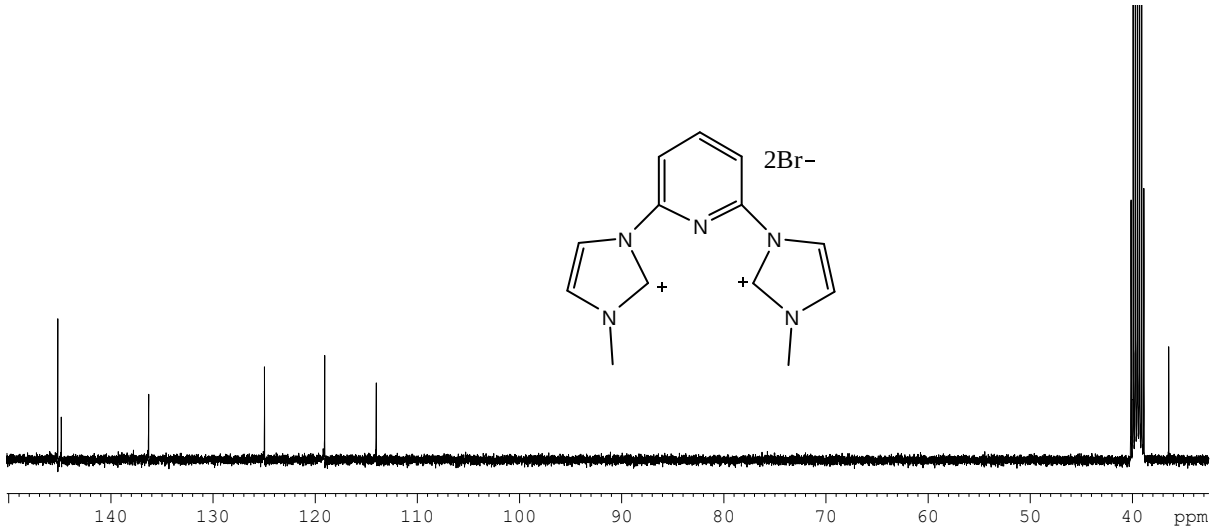

Figure SI 7.2 ^{13}CNMR spectrum of 2,6-Bis(3-methylimidazolium-1-yl)pyridine dibromide

Elemental Composition Report **Page 1**

Single Mass Analysis
Tolerance = 50.0 PPM / DBE: min = -1.5, max = 500.0
Element prediction: Off
Number of isotope peaks used for i-FIT = 2

Monoisotopic Mass, Even Electron Ions
10 formula(e) evaluated with 1 results within limits (up to 20 closest results for each mass)
Elements Used:
C: 10-15 H: 15-20 N: 0-5 Br: 0-1

1-S4L1 29 (0.945) Cm (1:61)
TOF MS ES+

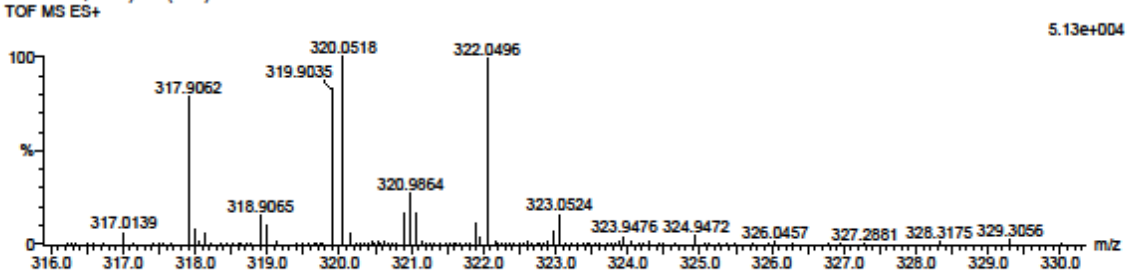

Minimum:				-1.5			
Maximum:		5.0	50.0	500.0			
Mass	Calc. Mass	mDa	PPM	DBE	i-FIT	i-FIT (Norm)	Formula
320.0518	320.0511	0.7	2.2	8.5	278.8	0.0	C13 H15 N5 Br

Figure SI 7.3 TOF-MS mass spectrum of 2,6-Bis(3-methylimidazolium-1-yl)pyridine dibromide

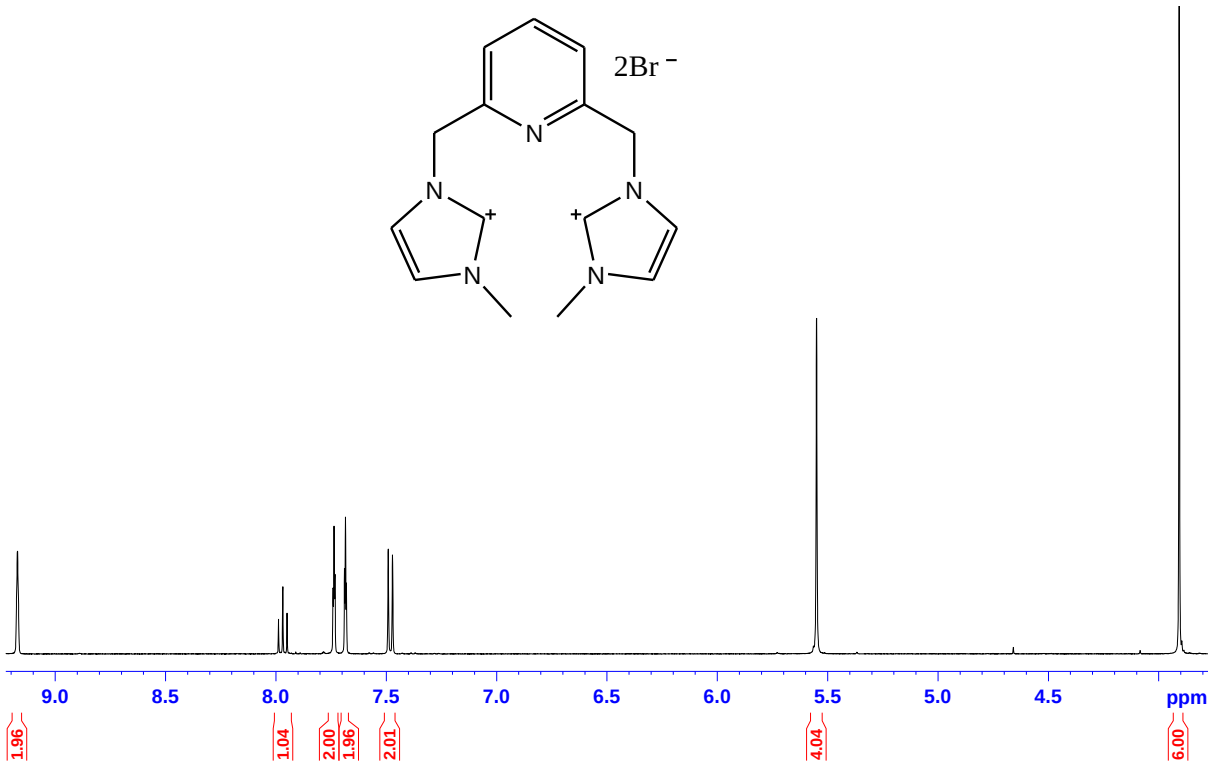

Figure SI 7.4 ^{1}HNMR spectrum of 2,6-bis[(3-methylimidazolium-1-yl)methyl]pyridine dibromide

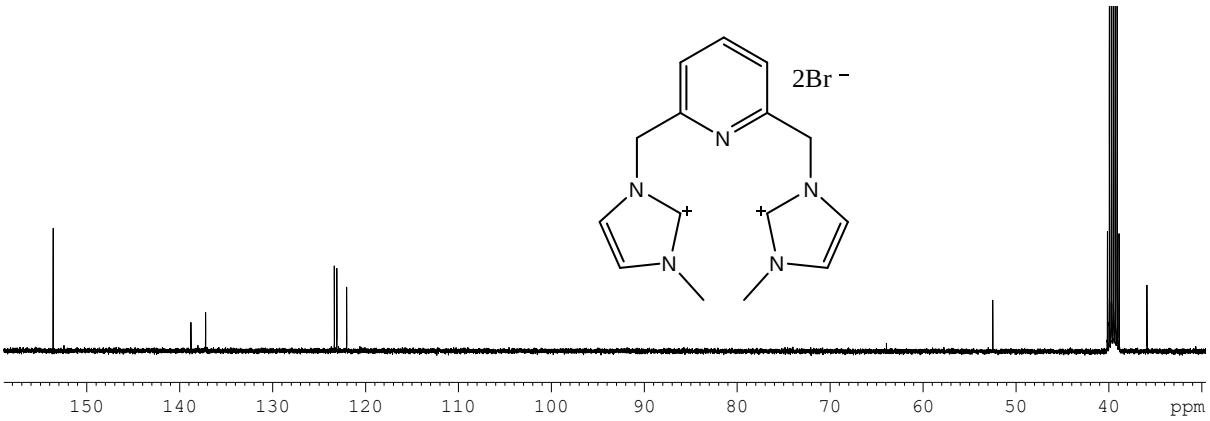

Figure SI 7.5 ^{13}CNMR spectrum of 2,6-bis[(3-methylimidazolium-1-yl)methyl]pyridine dibromide

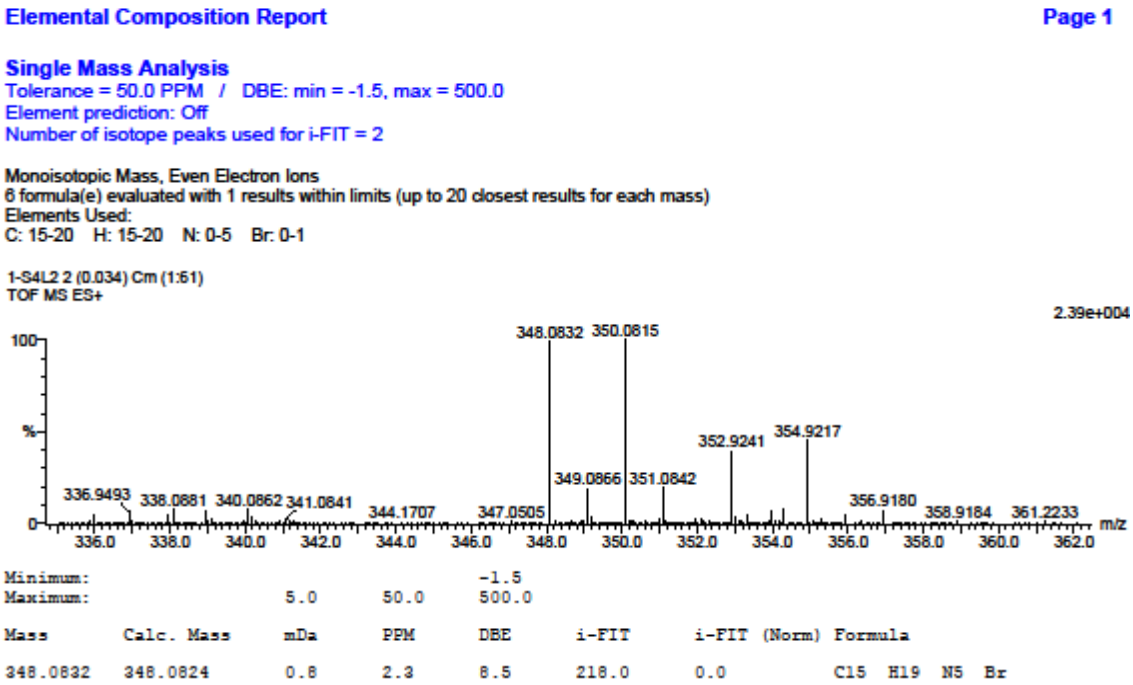

Elemental Composition Report Page 1

Single Mass Analysis
Tolerance = 50.0 PPM / DBE: min = -1.5, max = 500.0
Element prediction: Off
Number of isotope peaks used for i-FIT = 2

Monoisotopic Mass, Even Electron Ions
6 formula(e) evaluated with 1 results within limits (up to 20 closest results for each mass)
Elements Used:
C: 15-20 H: 15-20 N: 0-5 Br: 0-1

1-S4L2 2 (0.034) Cm (1:61)
TOF MS ES+

Minimum:				-1.5			
Maximum:		5.0	50.0	500.0			
Mass	Calc. Mass	mDa	PPM	DBE	i-FIT	i-FIT (Norm)	Formula
348.0832	348.0824	0.8	2.3	8.5	218.0	0.0	C15 H19 N5 Br

Figure SI 7.6 TOF-MS mass spectrum of 2,6-bis[(3-methylimidazolium-1-yl)methyl]pyri-dine dibromide

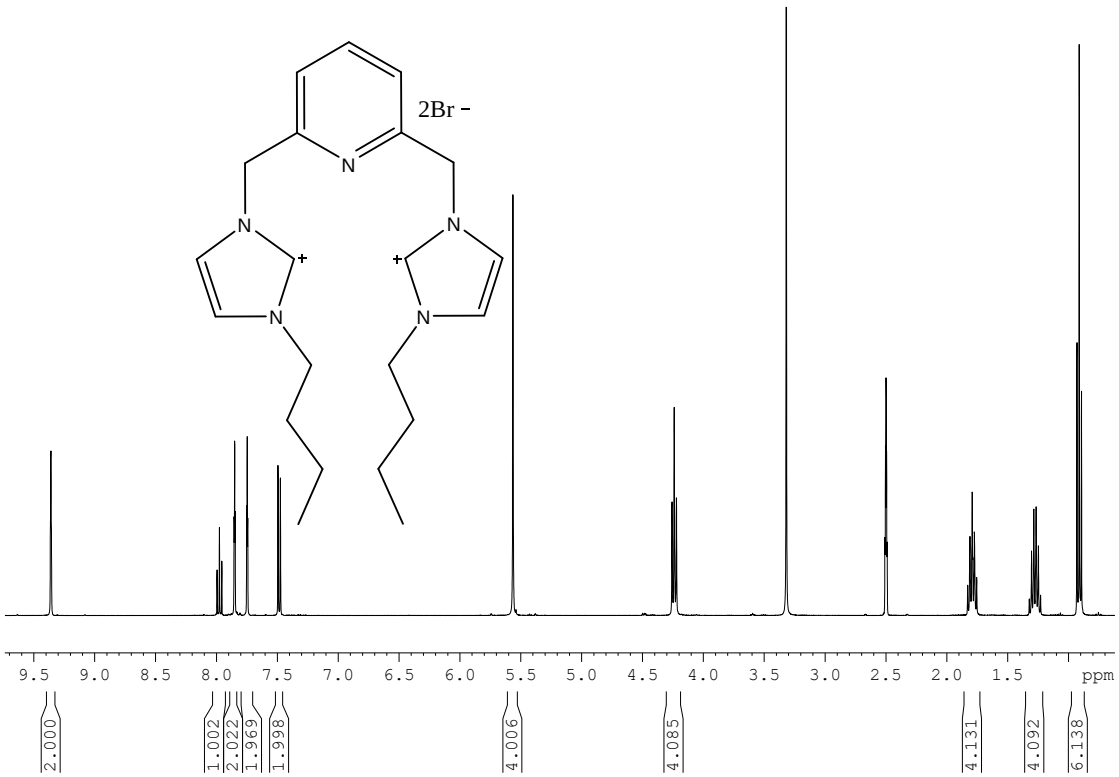

Figure SI 7.7 ^{1}HNMR spectrum of 2,6-Bis[(3-butylimidazolium-1-yl)methyl]pyridine dibromide

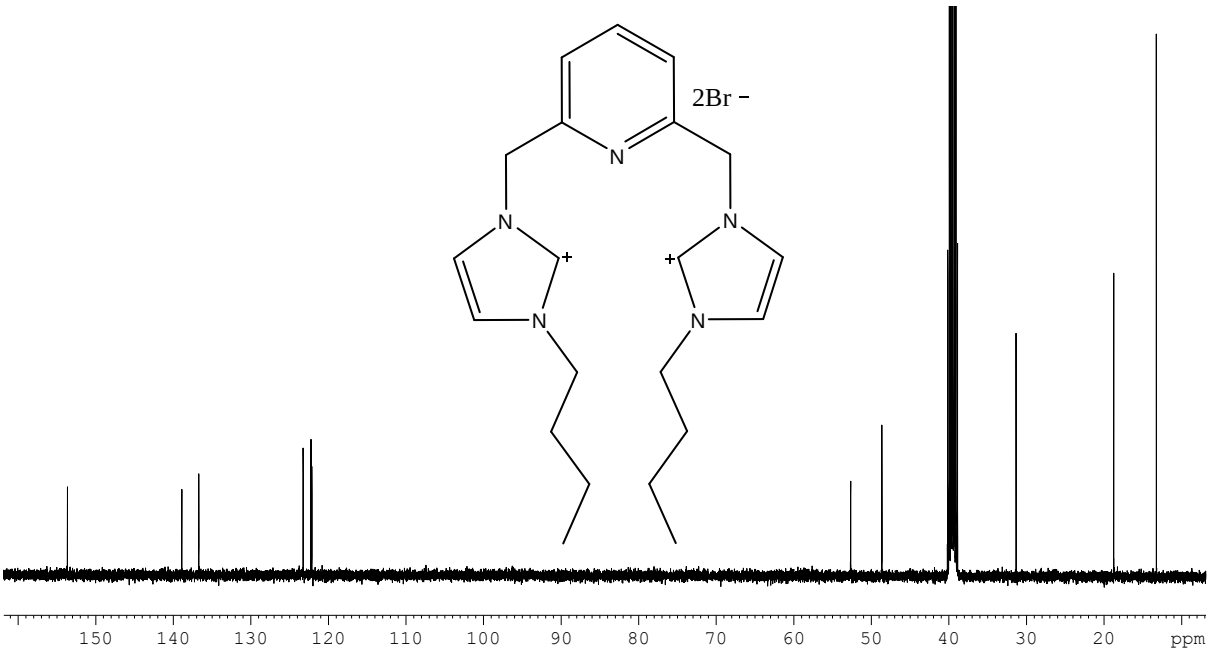

Figure SI 7.8 ^{13}CNMR spectrum of 2,6-Bis[(3-butylimidazolium-1-yl)methyl]pyridine dibromide

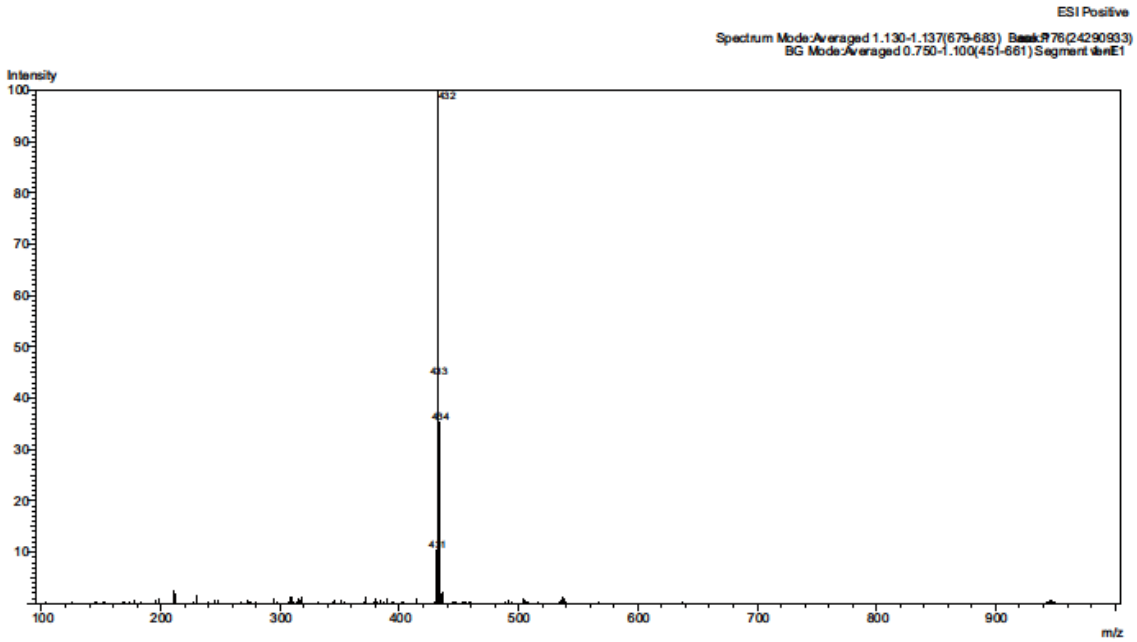

Figure SI 7.9 LC-MS mass spectrum of 2,6-Bis[(3-butylimidazolium-1-yl)methyl]pyridine dibromide

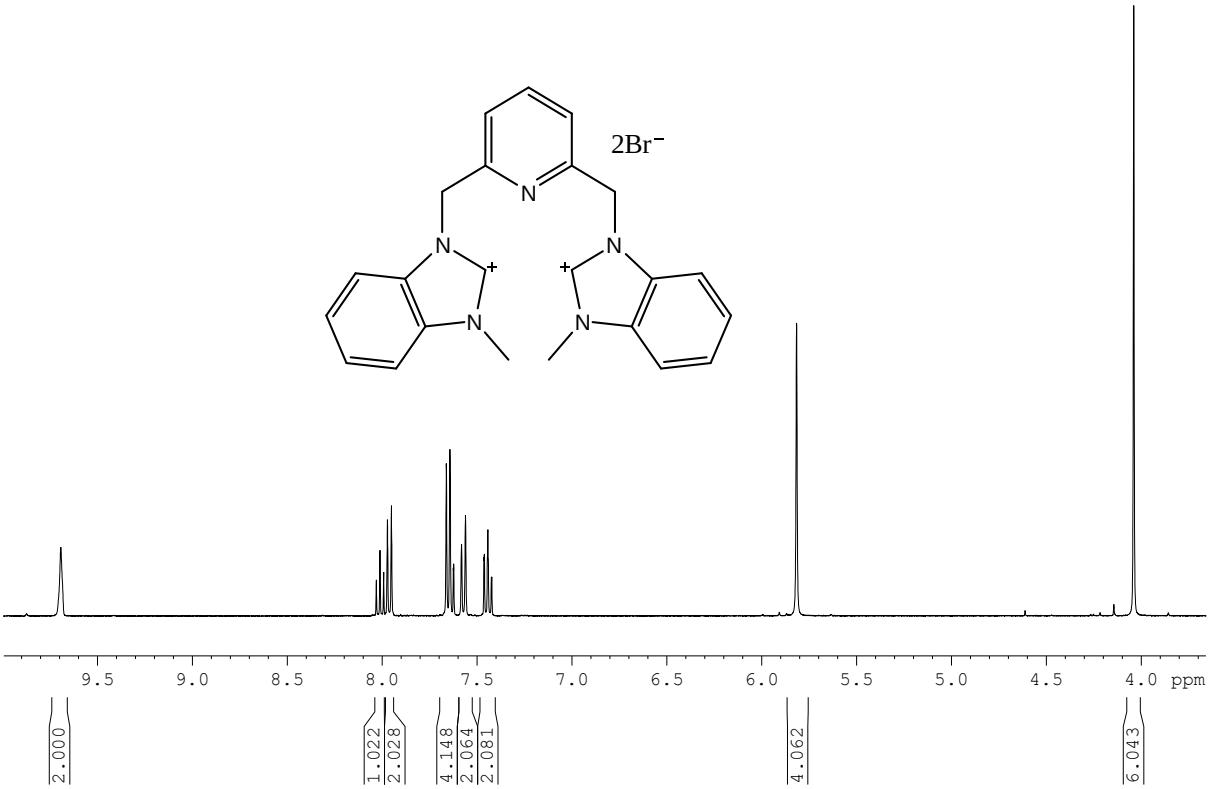

Figure SI 7.10 ^{1}HNMR spectrum of 2,6-Bis[(3-methylbenzimidazol-1-yl)methyl]pyridine dibromide

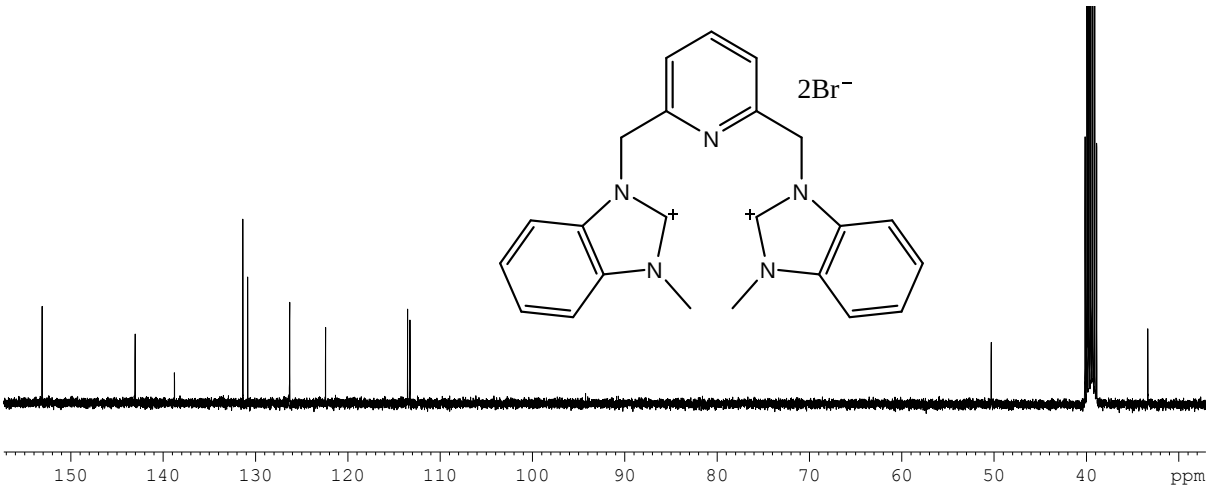

Figure SI 7.11 ^{13}CNMR spectrum of 2,6-Bis[(3-methylbenzimidazol-1-yl)methyl]pyridine dibromide

Elemental Composition Report **Page 1**

Single Mass Analysis
Tolerance = 50.0 PPM / DBE: min = -1.5, max = 500.0
Element prediction: Off
Number of isotope peaks used for i-FIT = 2

Monoisotopic Mass, Even Electron Ions
8 formula(e) evaluated with 1 results within limits (up to 20 closest results for each mass)
Elements Used:
C: 20-25 H: 20-25 N: 0-5 Br: 0-1

1-S4L3 49 (1.619) Cm (1:61)
TOF MS ES+

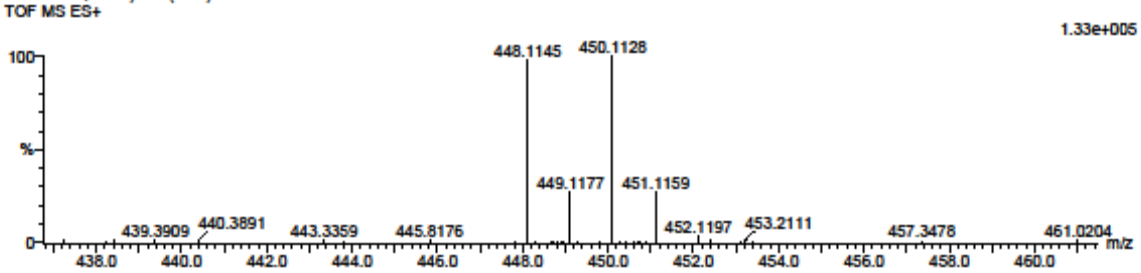

Minimum:				-1.5			
Maximum:		5.0	50.0	500.0			
Mass	Calc. Mass	mDa	PPM	DBE	i-FIT	i-FIT (Norm)	Formula
448.1145	448.1137	0.8	1.8	14.5	94.5	0.0	C23 H23 N5 Br

Figure SI 7.12 TOF-MS mass spectrum of 2,6-Bis[(3-methylbenzimidazol-1-yl)methyl]pyridine dibromide

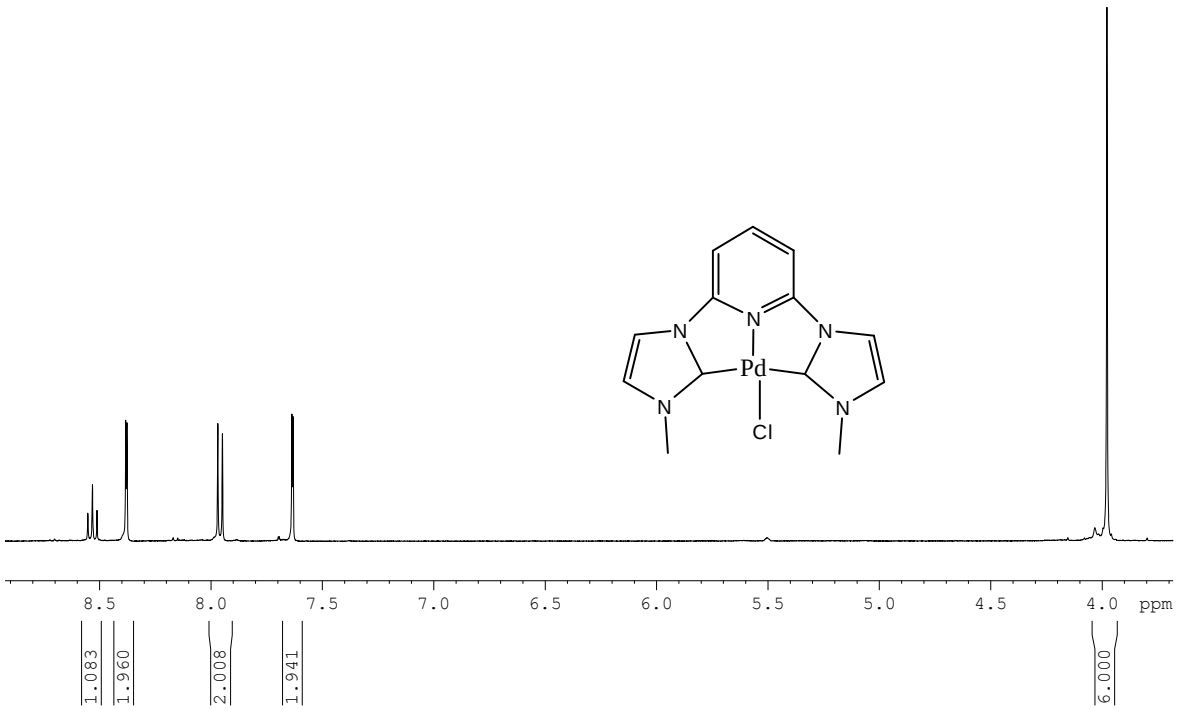

Figure SI 7.13 ^{1}HNMR spectrum for **(NHC)Pd1** complex

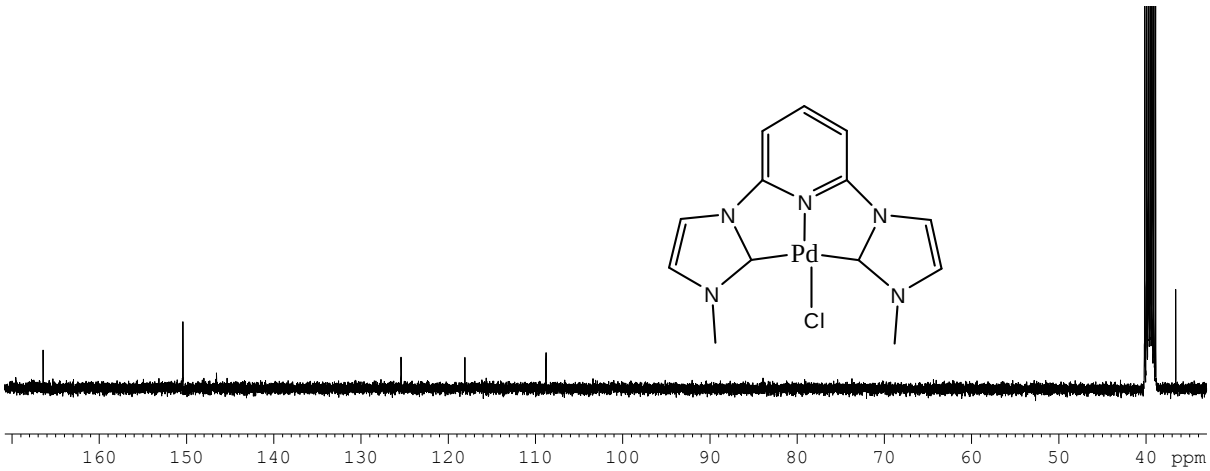

Figure SI 7.14 ^{13}CNMR spectrum for **(NHC)Pd1** complex

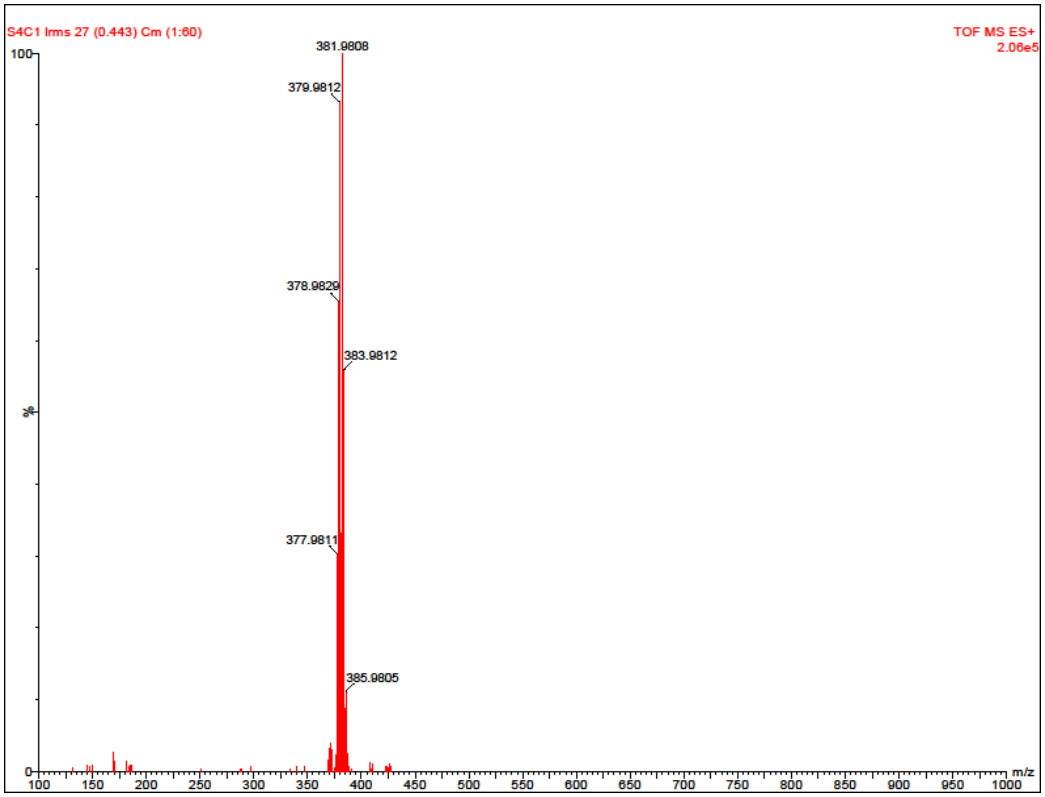

Figure SI 7.15 TOF-MS mass spectrum of **(NHC)Pd1**

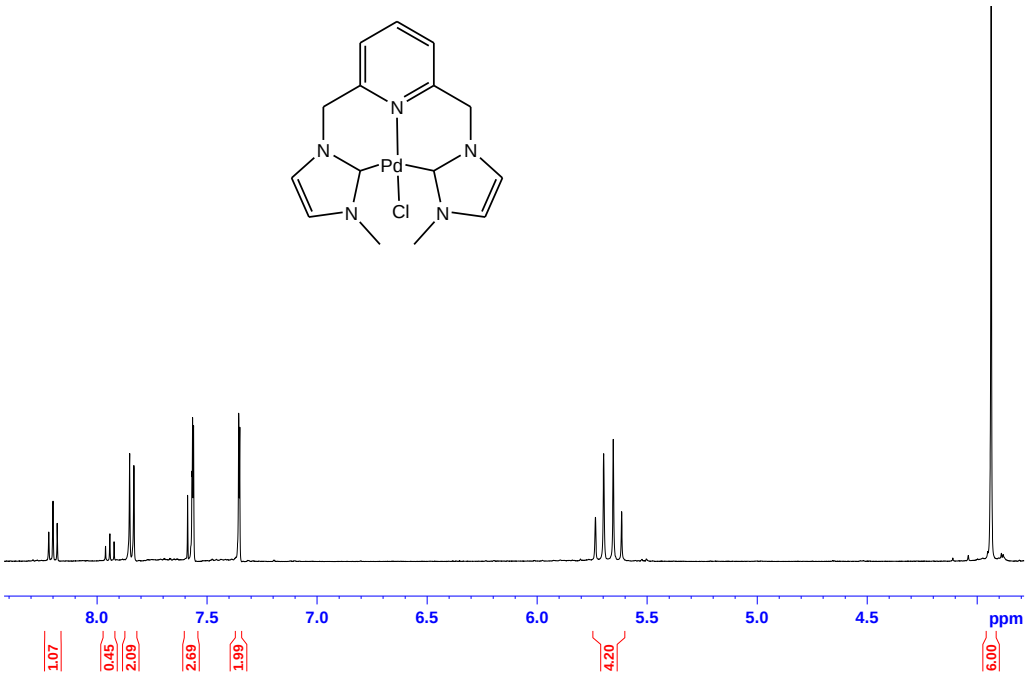

Figure SI 7.16 ^{1}HNMR spectrum for **(NHC)Pd2** complex

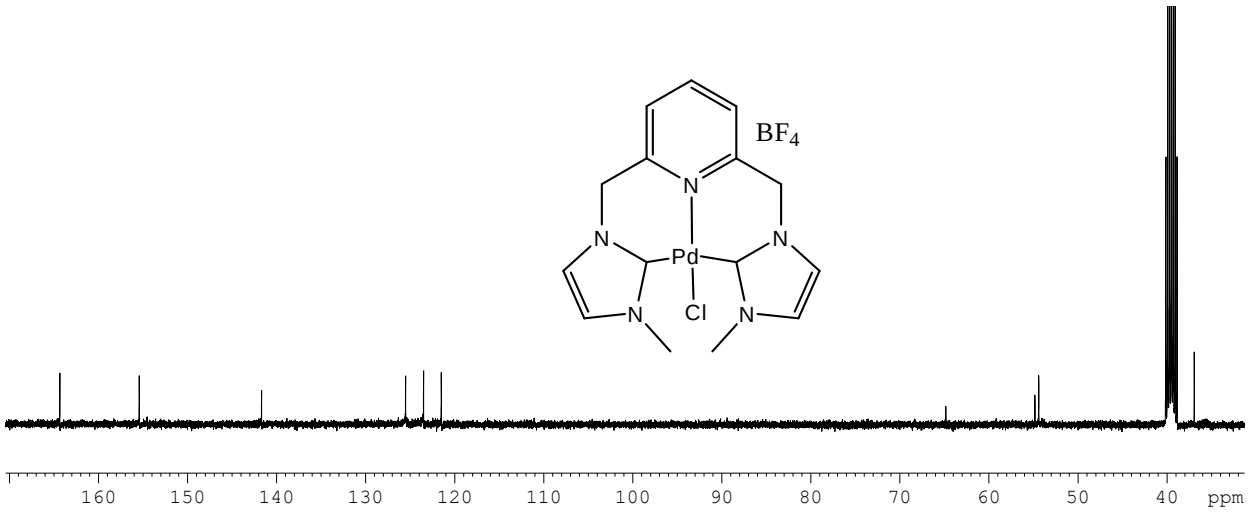

Figure SI 7.17 ^{13}CNMR spectrum for **(NHC)Pd2** complex

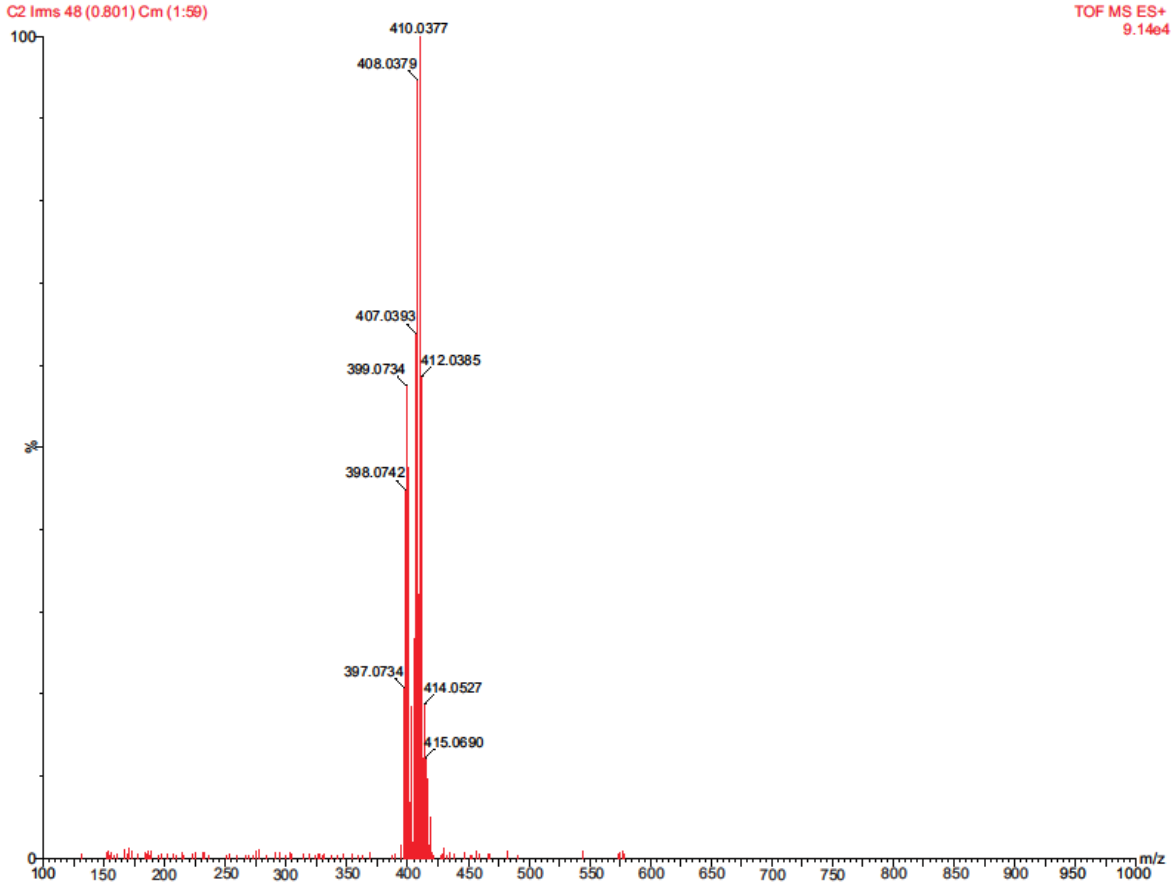

Figure SI 7.18 TOF-MS mass spectrum for **(NHC)Pd2** complex

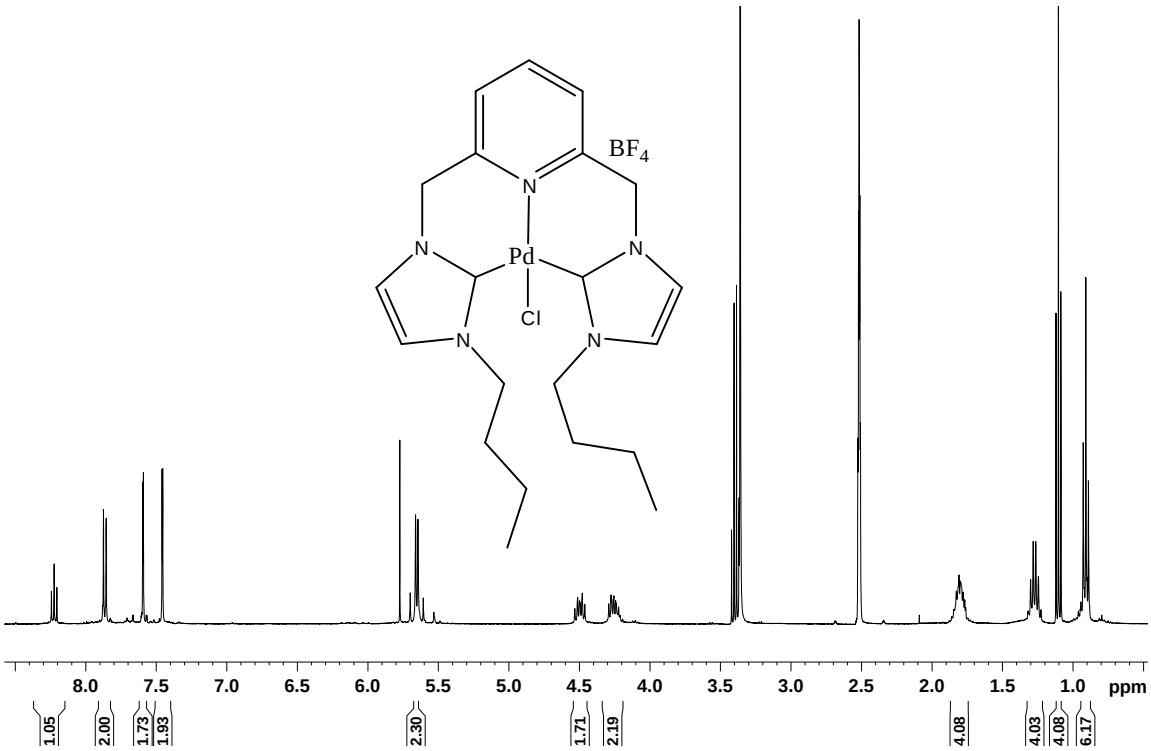

Figure SI 7.19 ^{1}HNMR spectrum for **(NHC)Pd3** complex

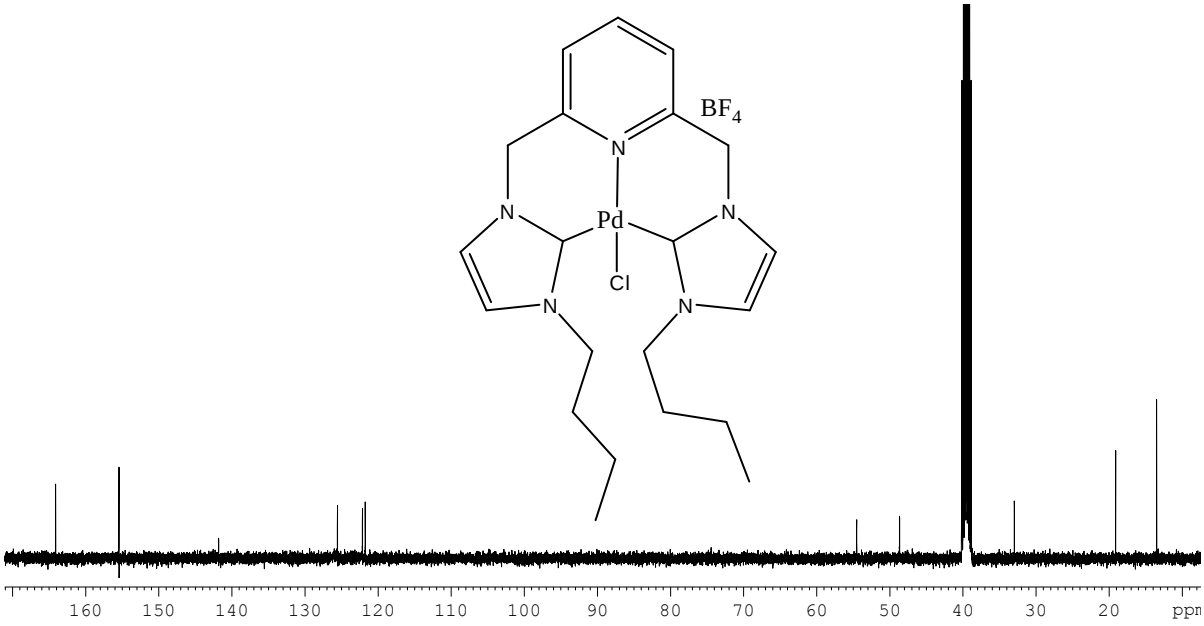

Figure SI 7.20 ^{13}CNMR spectrum for **(NHC)Pd3** complex

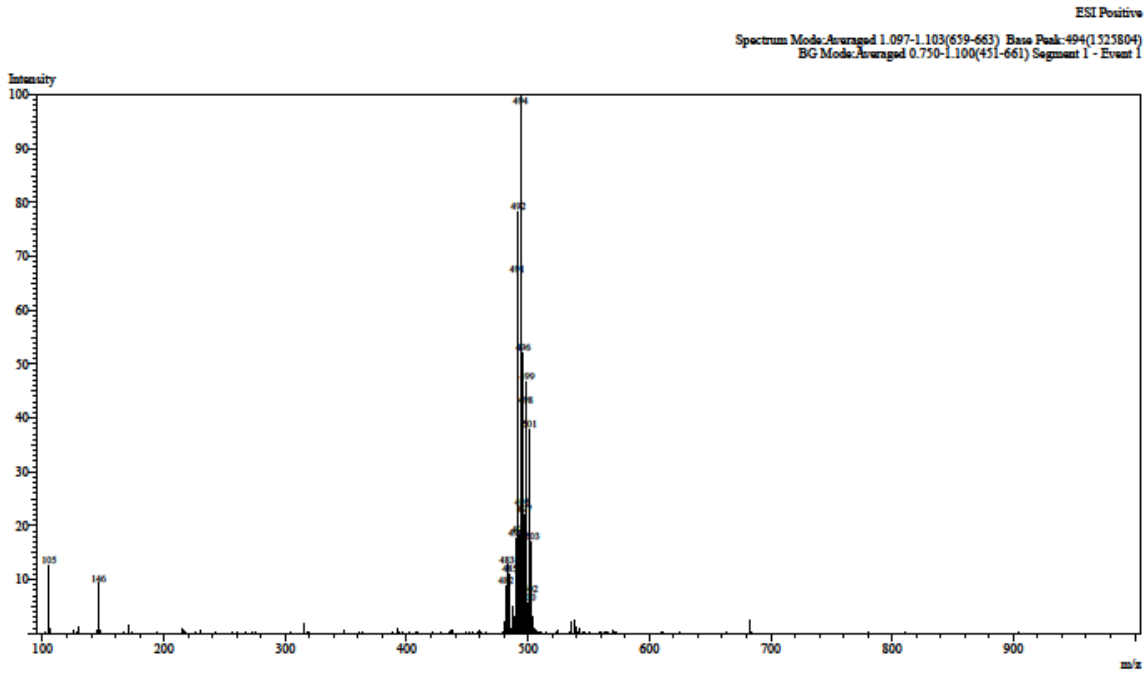

Figure SI 7.21 LC-MS mass spectrum for **(NHC)Pd3** complex

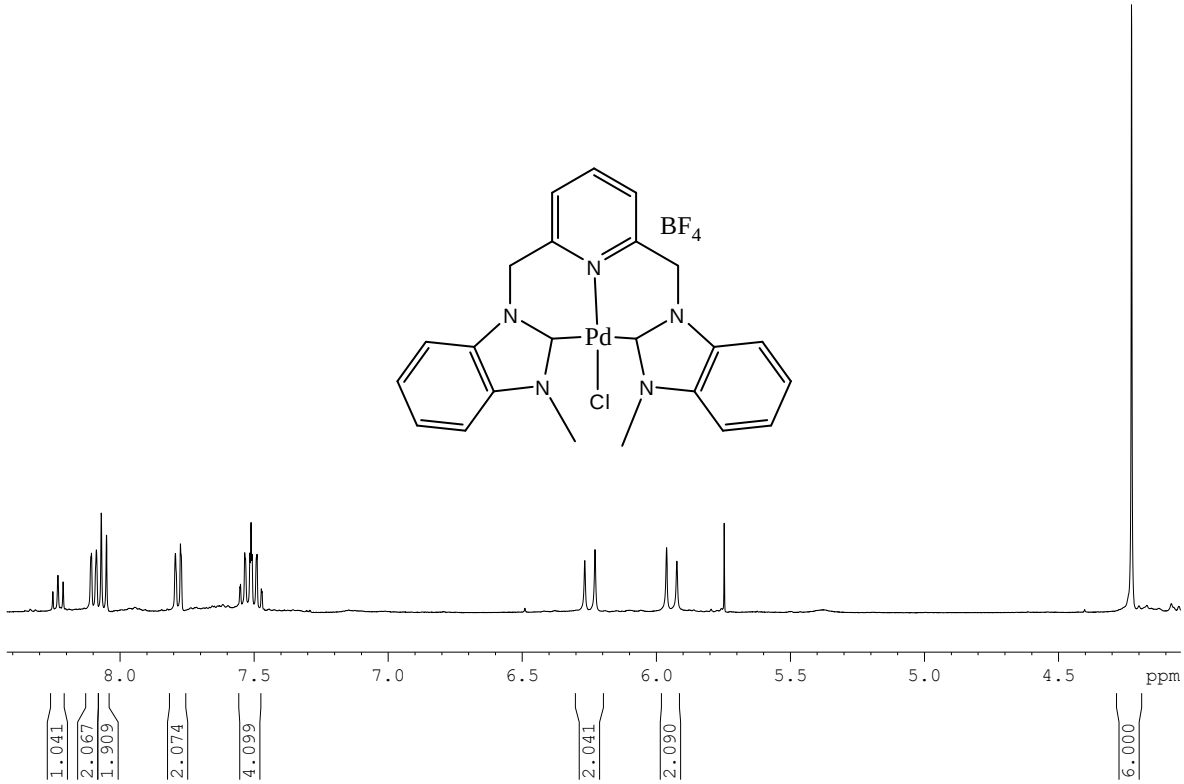

Figure SI 7.22 ^{1}HNMR spectrum for **(NHC)Pd4** complex

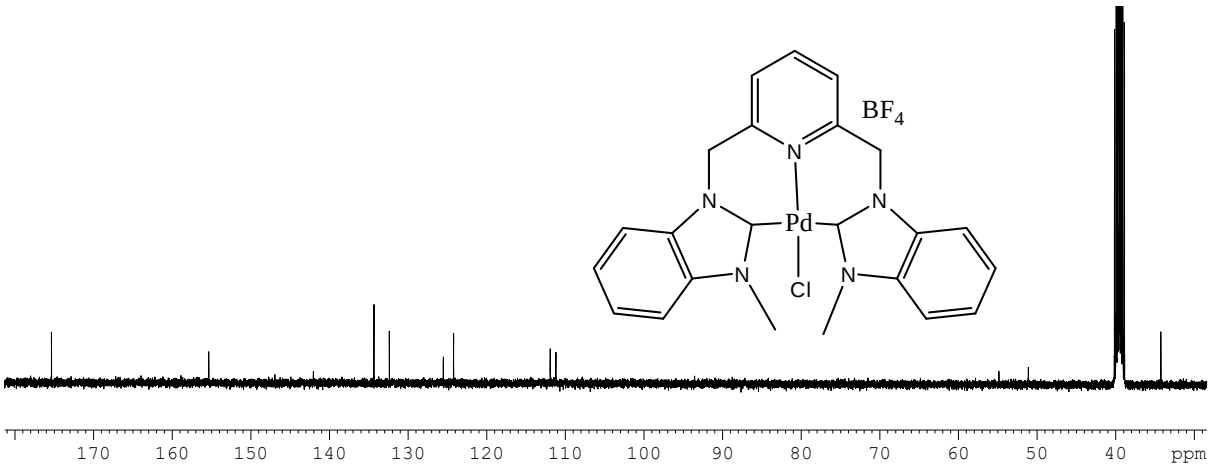

Figure SI 7.23 ^{13}CNMR spectrum for **(NHC)Pd4** complex

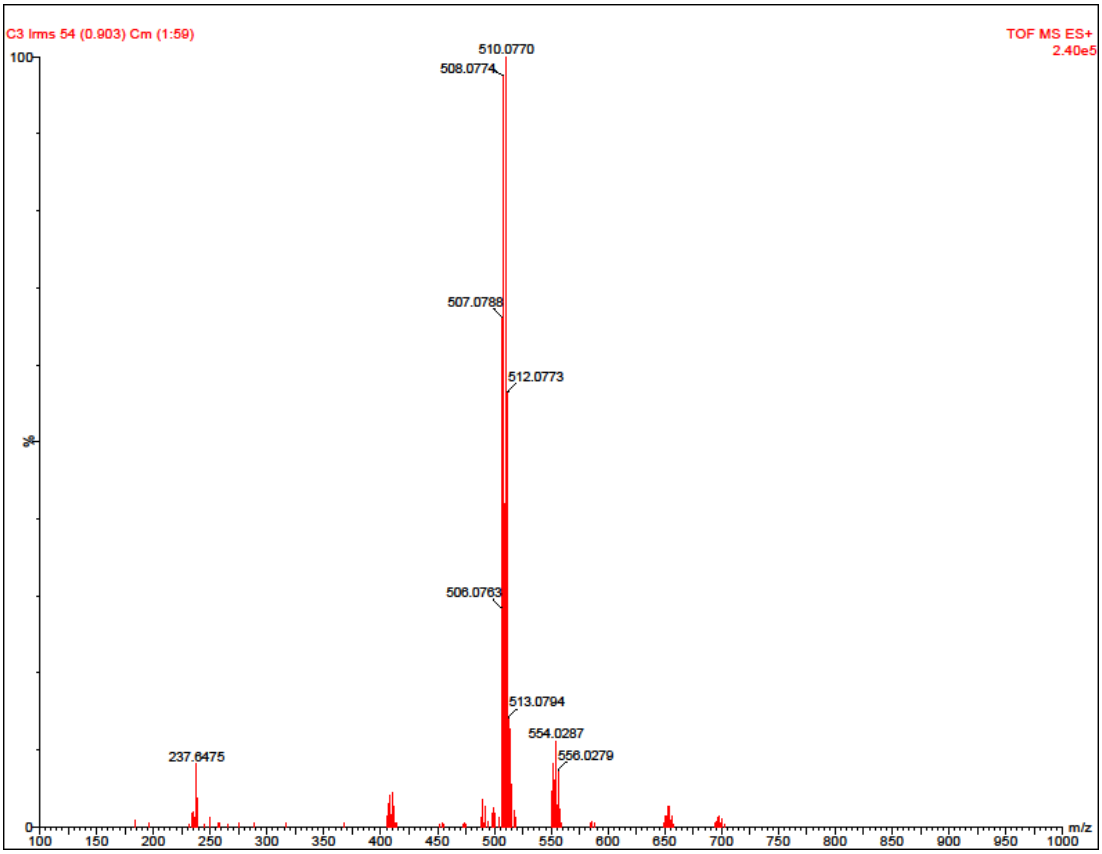

Figure SI 7.24 TOF-MS mass spectrum for **(NHC)Pd4** complex

Table S1 7.1: A summary of a table of wavelengths (nm) use for monitoring the kinetic reactions of Pd(II) complexes with thiourea nucleophiles

Complex	Nucleophiles	Wavelength, λ (nm)
(NHC)Pd1	Tu	330
	Dmtu	315
	Tmtu	335
(NHC)Pd2	Tu	320
	Dmtu	300
	Tmtu	330
(NHC)Pd3	Tu	320
	Dmtu	320
	Tmtu	340
(NHC)Pd4	Tu	315
	Dmtu	320
	Tmtu	350

Concentration dependent reactions

Table S1 7.2: A summary of average rate constants, k_{obs} (s^{-1}) for the chloride substitution reaction of **(NHC)Pd1** and thiourea nucleophiles in water at T = 298 K, I = 20 mM LiCl

Concentration, (M)	k_{obs} (s^{-1})		
	Tu	Dmtu	Tmtu
0.004	11.07598	9.4332	0.95313
0.008	21.52508	17.94004	1.99586
0.012	31.80864	29.13468	2.83908
0.016	42.53658	36.3922	3.59179
0.02	53.9047	45.68631	4.45276

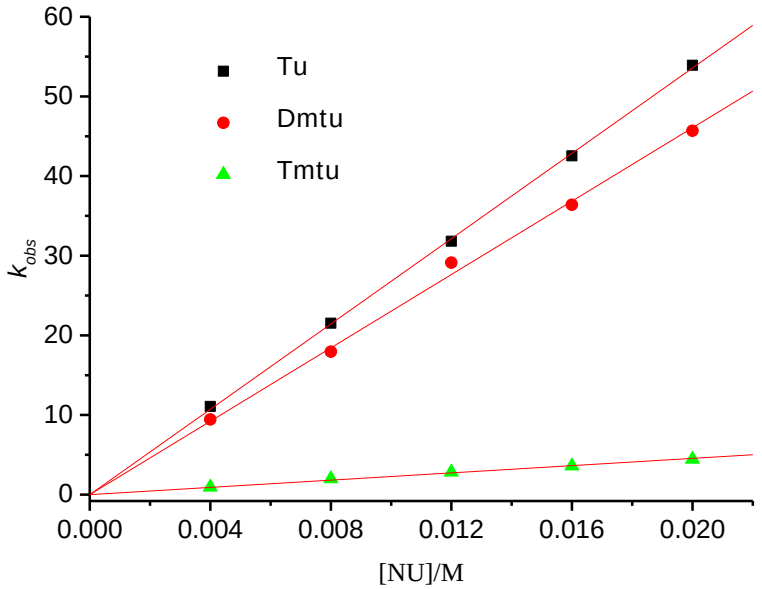

Figure SI 7.25: Dependence of the *pseudo*-first-order rate constants, k_{obs} (s^{-1}) on the concentration of thiourea nucleophiles for chloride substitution on **(NHC)Pd1** in water, I = 20 mM LiCl, T = 298 K.

Table S1 7.3: A summary of average rate constants, k_{obs} (s^{-1}) for the chloride substitution reaction of **(NHC)Pd2** and thiourea nucleophiles in water at T = 298 K, I = 20 mM LiCl.

Concentration, (M)	k_{obs} (s^{-1})		
	Tu	Dmtu	Tmtu
0.004	10.13475	7.75785	0.42472
0.008	19.67154	15.89433	0.85794
0.012	26.63593	21.80072	1.22072
0.016	36.7819	29.70666	1.6792
0.02	47.23196	36.25984	2.01509

Table S1 7.4: A summary of average rate constants, k_{obs} (s^{-1}) for the chloride substitution reaction of **(NHC)Pd3** and thiourea nucleophiles in water at T = 298 K, I = 20 mM LiCl.

Concentration, (M)	k_{obs} (s^{-1})		
	Tu	Dmtu	Tmtu
0.004	0.83156	0.66778	0.07505
0.008	1.78161	1.32975	0.15214
0.012	2.53551	1.95886	0.22494
0.016	3.41645	2.52543	0.30328
0.02	4.39364	3.1257	0.38025

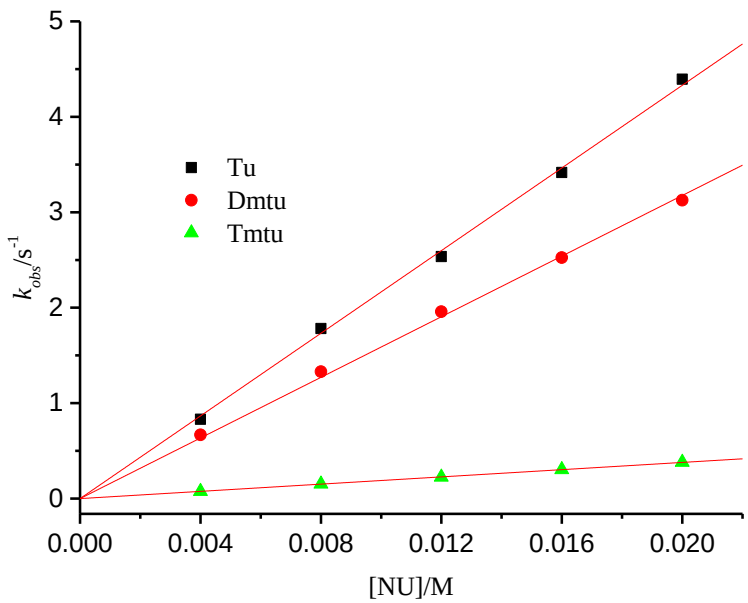

Figure SI 7.26: Dependence of the *pseudo*-first-order rate constants, k_{obs} (s^{-1}) on the concentration of thiourea nucleophiles for chloride substitution on **(NHC)Pd3** in water, I = 20 mM LiCl, T = 298 K.

Table S1 7.5: A summary of average rate constants, k_{obs} (s^{-1}) for the chloride substitution reaction of **(NHC)Pd4** and thiourea nucleophiles in water at T = 298 K, I = 20 mM LiCl.

Concentration, (M)	k_{obs} (s^{-1})		
	Tu	Dmtu	Tmtu
0.004	7.44378	7.15888	0.40154
0.008	13.70058	14.36546	0.76408
0.012	22.27366	20.66515	1.14259
0.016	29.56793	26.24328	1.58626
0.02	36.1768	33.40486	1.95366

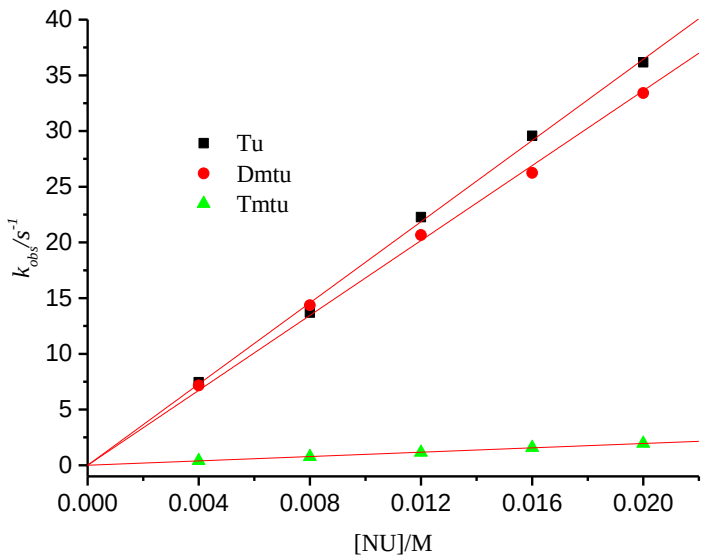

Figure SI 7.27: Dependence of the *pseudo*-first-order rate constants, k_{obs} (s^{-1}) on the concentration of thiourea nucleophiles for chloride substitution on **(NHC)Pd4** in water, I = 20 mM LiCl, T = 298 K.

Table S1 7.6: Temperature dependence of k_2 $M^{-1}s^{-1}$ for the chloride ligand substitution reaction of **(NHC)Pd1** by the thiourea nucleophiles at 30-fold in water, I = 20 mM LiCl.

(1/T) K^{-1}	ln(k_2/T)		
	Tu	Dmtu	Tmtu
0.00347	1.79564	1.26061	-0.90311
0.00341	1.96672	1.58931	-0.60431
0.00336	2.12842	1.81072	-0.32263
0.0033	2.25506	2.08898	-0.02412
0.00325	2.40675	2.30265	0.20264

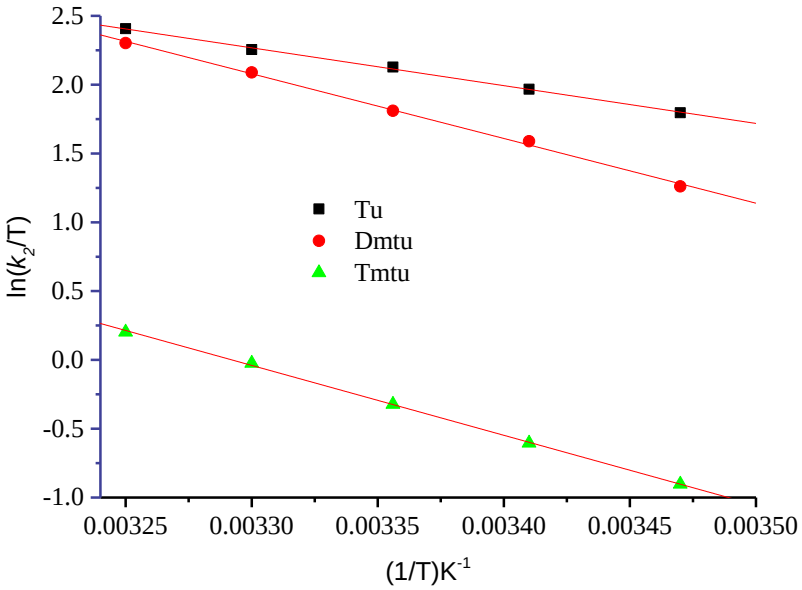

Figure SI 7.28: Eyring plots of **(NHC)Pd1** with thiourea nucleophiles at different temperatures

Table S1 7.7: Temperature dependence of k_2 $M^{-1}s^{-1}$ for the chloride ligand substitution reaction of **(NHC)Pd2** by the thiourea nucleophiles at 30-fold in water, I = 20 mM LiCl.

(1/T) K^{-1}	ln(k_2/T)		
	Tu	Dmtu	Tmtu
0.00347	1.75164	1.25584	-2.04751
0.00341	1.95672	1.52873	-1.70554
0.00336	2.15842	1.8077	-1.44665
0.0033	2.30006	2.05777	-1.19057
0.00325	2.41675	2.28254	-0.91548

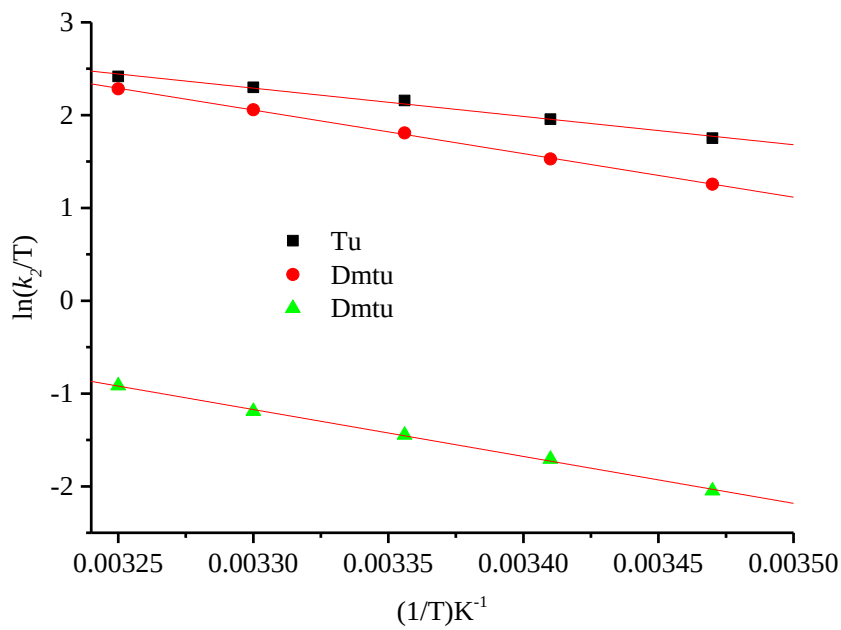

Figure SI 7.29: Eyring Plots of **(NHC)Pd2** with thiourea nucleophiles at different temperatures

Table S1 7.8: Temperature dependence of k_2 $M^{-1}s^{-1}$ for the chloride ligand substitution reaction of **(NHC)Pd3** by the thiourea nucleophiles at 30-fold in water, I = 20 mM LiCl.

(1/T) K^{-1}	ln(k_2/T)		
	Tu	Dmtu	Tmtu
0.00347	-1.53775	-1.64218	-3.75787
0.00341	-1.08599	-1.15389	-3.37496
0.00336	-0.79875	-0.83257	-2.96264
0.0033	-0.39367	-0.43001	-2.56724
0.00325	-0.18661	-0.20179	-2.29398

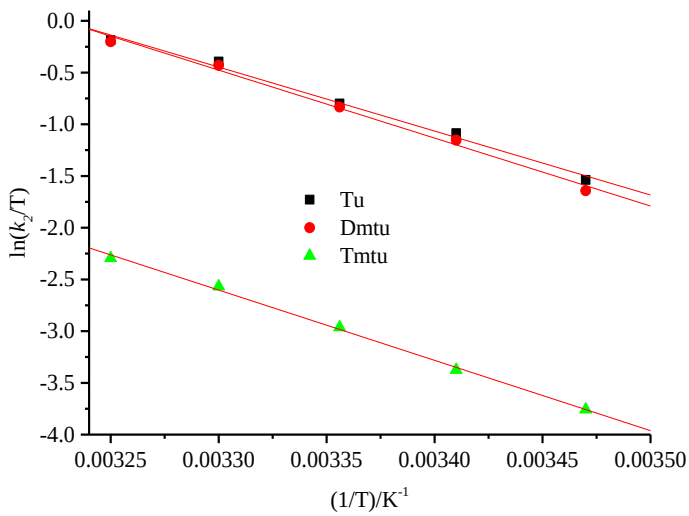

Figure SI 7.30: Eyring Plots of **(NHC)Pd3** with thiourea nucleophiles at different temperatures

Table S1 7.9: Temperature dependence of k_2 $M^{-1}s^{-1}$ for the chloride ligand substitution reaction of **(NHC)Pd4** by the thiourea nucleophiles at 30-fold in water, I = 20 mM LiCl.

(1/T) K^{-1}	ln(k_2/T)		
	Tu	Dmtu	Tmtu
0.00347	1.11597	1.3098	-1.6173
0.00341	1.36068	1.61366	-1.42469
0.00336	1.64229	1.89045	-1.23782
0.0033	1.90487	2.13378	-0.85808
0.00325	2.16536	2.31274	-0.68831

CHAPTER 8

Summary and Future Prospects

8.1 Introduction

The main aim of this study focussed on tuning the reactivity of mononuclear Pd(II) complexes coordinated to a variety of tridentate ligand systems *viz* NNN, NNC and CNC with different structural motifs and to try to understand how the electronic and steric properties of the ligands would influence or control the reactivity of palladium metal. Such influences was reflected in the rates of substitution of their labile chloride ligand from the complexes by thiourea nucleophiles as a function of concentration and temperature under *pseudo* first-order conditions. The palladium metal was coordinated to the ligands in a mononuclear fashion. This was inspired by the hope that such tuning could provide kinetically inert and thermodynamically stable Pd(II) complexes which exhibits antitumor activity that can be presented as an alternative candidate drug to the widely used Pt(II)-based drugs. All the modelled Pd(II) complexes were subjected to DFT calculations to provide insight into the trends of experimental results. This section summarizes the experimental findings in the trends of the reactivity of the Pd(II) complexes in **chapters 3** to **7**.

8.2 Summary

In **chapter 3**, a series of mononuclear Pd(II) complexes of terpyridyl pyrazolyl-based ligands is introduced. In this first set, the structure of the complexes was varied by replacing the *cis*-pyridyl ring of the well-known labilising terpyridine ligand in chlorido(2,2′:6′,2″-terpyridine)palladium(II) chloride (**PdL1**) with pyrazole in chlorido(2,6-bis(N-pyrazolyl)pyridine)palladium(II) chloride (**PdL2**) and its methyl substituted derivative in chlorido(2,6-bis(3,5-dimethyl-N-pyrazoly-l)pyridine)palladium(II) chloride (**PdL3**) as well as introducing methylene spacer group between the *trans*-pyridyl ring and the substituted pyrazole in chlorido(2,6-bis(3,5-dimethyl-N-pyrazolylmethyl)pyridine)palladium(II) tetrafluoroborate (**PdL4**). The main

characteristic feature about these complexes is that they all have delocalised π-system allowing facile electron transfer between the metal and ligand except in **PdL4** whose aromaticity is destroyed. The aim was to investigate the role of the electron rich pyrazole in tuning the thermodynamic stability as well as facilitating kinetic inertness at the Pd(II) complexes. The reactivity of the complexes under this study is controlled by both electronic and steric factors. **PdL1**, **PdL2** and **PdL3** are controlled by the electronic factors, while that of **PdL4** is dominated by steric factors in addition to the electronic effects. The interesting part of this study is that the reactivity of Pd(II) metal can be tuned and controlled using pyrollic-N-π-donor which decreases the ability of π-back bonding and accumulating the electron density around the metal centre. In addition, the removal of the aromatic property around the metal centre through the introduction of a six-membered ring using methylene spacer group in **PdL4** introduces steric hinderance, destroys the electronic communication through π-back bonding and renders the complex inert. The nature of the ligand in **PdL4** renders the complex inert and reduces its reactivity by 4 – 6 orders of magnitude compared to the most labile **PdL1** for all the nucleophiles depending on their steric bulk. This makes the reactivity of Pd(II) in **PdL4** be comparable to those of Pt(II) metal in their complexes. This is an important finding since ligands that can control the reactivity of Pd(II) metal centre to the level comparable to those of Pt(II) complexes, could present Pd(II) complexes as a candidate alternative antitumor drug with improved antitumor potential and less side effects that might possibly be useful for biological application.

In **Chapter 4** the role of π-conjugation and the σ-donicity of quinoline moiety in N^N^N ligands coordinated to Pd(II) complexes was investigated. In this set, π-conjugation was progressively increased by replacing the 2-pyridylmethyl in the bis(2-pyridylmethyl)amine with 8-quinolinyl and imine bond with the amine. This study revealed that the reactivity of Pd metal can be controlled using quinoline moiety as part of the complex's ligand system which increases the π-

conjugation but weakens the π-acceptability of the entire ligand. The reactivity of the Pd metal reduced by a factor of between 25-30 for the studied nucleophiles when the bis(2-pyridylmethyl)amine ligand of chlorobis-(2-pyridylmethyl)aminepalladium(II), **Pd1**, (strong π-acceptors) was replaced by bis(8-quinolinyl)amine in chlorobis(8-quinolinyl)amine-palladium(II), **Pd4**, (good σ-donors). It is evident that the σ-donation and inductive effects of 8-quinolinyl moiety weakens the π-back donation effect of the entire ligand framework, making the metal centre less electrophilic and as such less reactive. This means that comparing π-back bonding in systems of this nature, the σ-effect has more dominant effect in controlling the reactivity slowing it when not in *trans* and accelerating it when in *trans* as shown in the literature.[1, 2] The mode of mechanism remains associative in nature.

In **chapter 5**, rate of substitution and mechanism of a set of Pd(II) complexes coordinated with tridentate N^N^N ligands of 1,3-bis(2-pyridylimino)isoindoline was investigated. The variation in these complexes involved alkylation using methyl substituents in the *cis*-pyridyl ring and extending the π-conjugation in the ligand of 1,3-bis(2-pyridylimino)isoindoline in the complexes through *cis* and *trans* benzannulation. The results showed that the substitution reactions occurred in two steps namely; substitution of the chloride ligand from the complexes (at a rate k_1) and the detachment of the metal from the ligand (at a rate k_2) in the presence of a strong thiourea nucleophiles in which k_1 was 3 – 4 orders of magnitude higher than k_2 for the reactions. The Alkylation at the *cis*-positioned pyridyl rings of BPI ligand decelerates the reactivity in the chlorido(1,3-bis(4-methyl-2-pyridylimino)isoindoline)palladium(II), **Pd(4-Me-PBI)Cl**, through electronic and steric effects by factors between 2 – 5 compared to chlorido(1,3-bis(2-pyridylimino)isoindoline)palladium(II), **Pd(BPI)Cl**. Benzannulation at the *trans*-isoindoline head further weakens the reactivity of chlorido(1,3-bis(2-pyridylimino)benz(*f*)isoindoline)palladium(II), **Pd(BBPI)Cl** by factors of 2 – 20. The *cis*-benzannulation lowers the reactivity of

palladium metal in chlorido(1,3-bis(1-isoquinolylimino)isoindoline)palladium(II), **Pd(BII)Cl** by upto approximately 2 – 3 orders of magnitude relative to **Pd(BPI)Cl** through steric effects. The study revealed that the *trans*-benzannulation at the isoindoline head maintains the planarity, while that on the *cis*-position distorts the planarity through steric repulsion which dominates in determining the reactivity over electronic factors in **Pd(BII)Cl**. Therefore, extended π-conjugation through benzannulation on the *cis*-positioned pyridyl rings is more powerful in controlling the reactivity of Pd(II) metal centre than that on the *trans*-positioned isoindoline head. The reactivity trend is opposite to the increasing π-surface linked to the destabilization of the HOMOs as illustrated by the DFT calculations. The second step was as a result of dechelation of the BPI ligands off the Pd(II) metal centres for all the complexes except that of **Pd(BII)Cl.** The dechelation was induced by the strong *trans* effect of the already coordinated nucleophiles. The values of the thermodynamic parameters revealed that in both the chlorido substitution and nucleophilic induced dechelation proceed by an associative substitution mechanism.

Chapter 6 attempted to introduce deprotonated carbon in one of the *cis*-position in the N^N^N ligand framework. This involved measuring the rate of substitution of the chloride ligand from a cyclometalated tridentate C^N^N ligands coordinated to the Pd(II) complexes in which the deprotonated *cis*-positioned phenyl and pyridyl rings are changed to naphthyl and isoquinolyl groups respectively, with a common phenyl ring with 3,5-di-*tert*-butyl substituents in the 4'-postion of the *trans*-pyridyl ring. The findings of the study demonstrated that the lability of the modelled Pd(II) complexes could electronically be controlled by the coordinated cyclometalated C^N^N ligands leading to a reduction of the rate of substitution by factors of upto 4. The *cis*-naphthalene behaves anomalously as a stronger π/σ-donor ligand than the *cis*-isoquinoline. The weak π-acceptors, naphthalene and isoquinoline acts in a concerted way to lower the reactivity of

chloro-3-(4-(3,5-di-tert-butylphenyl)-6-(naphthalen-2-yl)pyridin-2-ylisoquinoline)palladium(II), **PdL^4** making it become the least reactive of the rest of the complexes. The activation mode remains associative in nature throughout the studied systems.

The Pd(II) (C^N^C) complexes in **chapter 7** involved the variation of the steric and electronic effects through lutidinyl and pyridyl bridged as well as the size of the N-substituent on the tridentate C^N^C, bis(NHCs) carbene ligands. In these set of complexes, the reactivity of the Pd(II) metal can be controlled by a series of bis(NHCs) ligands differing in steric and electronic properties. This was seen when the rate of substitution was reduced by factors of 10 – 15 in the 2,6-Bis[(3-butylimidazolium-1-yl)methyl]pyridine chloropalladium(II) tetrafluoroborate, **(NHC)Pd3** (the slowest) relative to the reference complex, 2,6-Bis(3-methylimidazolium-1-yl)pyridine chloropalladium(II) tetrafluoroborate, **(NHC)Pd1** (highest reactive). The reactivity of **(NHC)Pd1** is majorly controlled by electronic factors while that of the other complexes are determined by both steric and electronic factors. The length of the alkyl chain of the N-substituent of the bis(NHC) ligand significantly slows down the reactivity as in the case of **(NHC)Pd3**. The ligands in 2,6-Bis[(3-methylbenzimidazol-1-yl)methyl]pyridine chloropalladium(II) tetrafluoroborate, **(NHC)Pd4** and **(NHC)Pd3** have slightly higher electron density donating abilities, linked to the destabilization of the HOMO energy of the complexes. The modifications on the *cis*-ligand moieties allows for effective tuning of steric and electronic properties. The substitution mechanism is associative as the two *cis*-σ-bound carbon donors of the complexes is unable induce dissociative substitution mechanism. The obtained kinetic data presents a preliminary findings that forms a basis for further research on tuning the reactivity of Pd metal using bis(NHC) type of ligands which could lead to complexes useful in biological applications as metallodrugs.

Throughout the sets of the mononuclear Pd(II) complexes investigated, there is a clear indication that with a careful choice of ligand with good π/σ-donor abilities with appropriate steric orientations, thermodynamically stabile and kinetically inert coordinated Pd(II) complexes can afforded. This in effect can control the reactivity of the highly reactive Pd metal to levels comparable to those of Pt(II) complexes. The thermodynamic and the kinetic data obtained forms part of the important aspect for the design of alternative and efficient, less toxic as well as improved anticancer Pd(II) drugs.

8.3 Future Prospects

From the results, the reactivity of Pd(II) can be tuned and controlled. This information is intended to contribute to the design and development of an alternative antitumour Pd-based drugs with broad spectrum of activity towards several cancerous cells,[3] less side effects,[4-6] higher cancer cell selectivity and better aqueous solubility[7-10] relative to the well-known conventional Pt-drugs currently in clinical use. It would therefore be interesting to evaluate and compare the cytotoxicity of the studied Pd(II) complexes towards several human cancer cell lines as well as their DNA binding studies.

Moreover, further studies should involve converting the chlorido Pd(II) complexes into their corresponding aqua Pd(II) complexes since in the physiological systems, the aqua complex is the intermediate complex responsible for binding with the DNA. [9, 11] The rates and the mechanism of substitution from the aqua Pd(II) complexes with nucleophiles of DNA fragments such as guanosine-5'-monophosphate (5'-GMP), L-histidine (L-His), L-methionine (L-Met) and glutathione (GSH) shown in Figure 8.1 can then be measured. Studying kinetics and mechanism of substitution reactions from the Pd(II) aqua complexes with these nucleophiles would present favourable advantages for several reasons. For example, reactions with 5'-GMP are used as models for binding to DNA, while sulfur-containing biomolecules such as GSH and L-Met play

a crucial role in toxic side effects in the antitumour action of the complexes.[12] The investigations using these DNA substrates would mimic the interactions of Pd(II) complexes with DNA which will bring the reactions much closer to the physiological conditions aiding potential pharmaceutical applications.

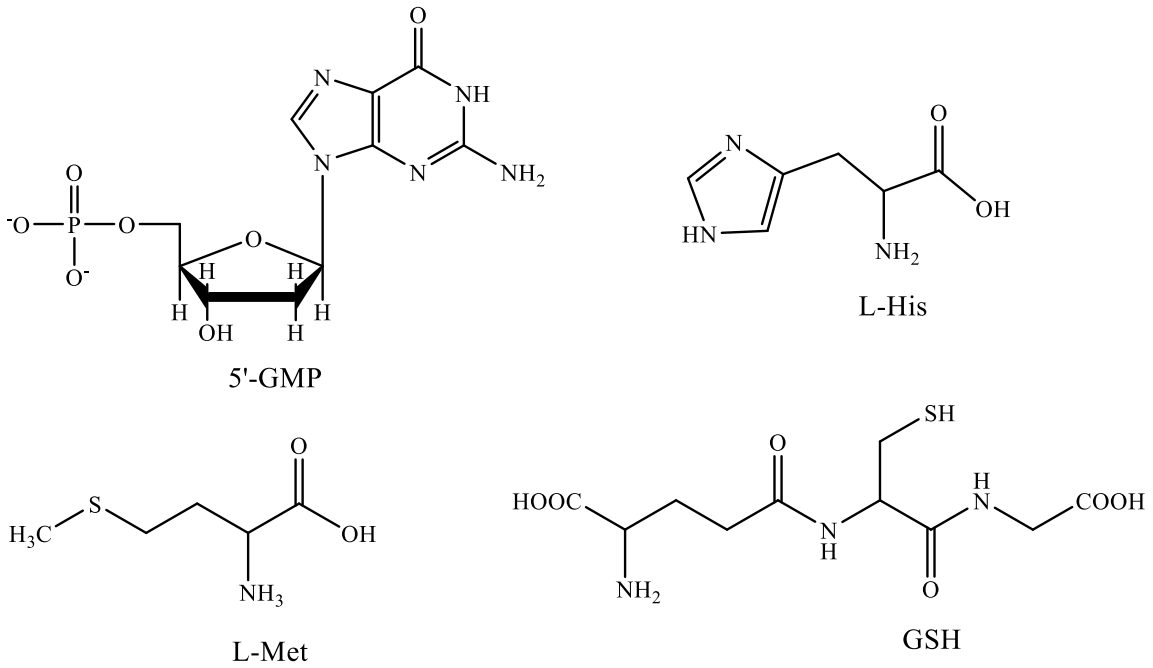

Figure 8. 1 Structures of the nucleophiles suggested for the substitution from the Pd(II) aqua complexes

Another approach in extending this work is to use other bioactive metal centres such as Ir(III),[13-16] Ru(II),[17] Rh(I),[18] gold(III), [19, 20] silver,[21] iron(II) and Iron(III)[22-24] in place of the Pd(II) metal centre. In addition, in **chapters 3**, **4** and **6** of the Pd(II) complexes of N^N^N and N^N^C, it would be quite interesting to investigate complexes with terpyridine-like ligand involving five- and six-membered chelate ring [25] depicted in Figure 8.2. The role of both six- and five-membered chelate in a Pd(II) complex on the rate of substitution as well as the distinctive role of

quinoline and naphthalene forming part of the six-membered chelate. The stability of the final products would be evaluated including the factors responsible for their reactivity trend.

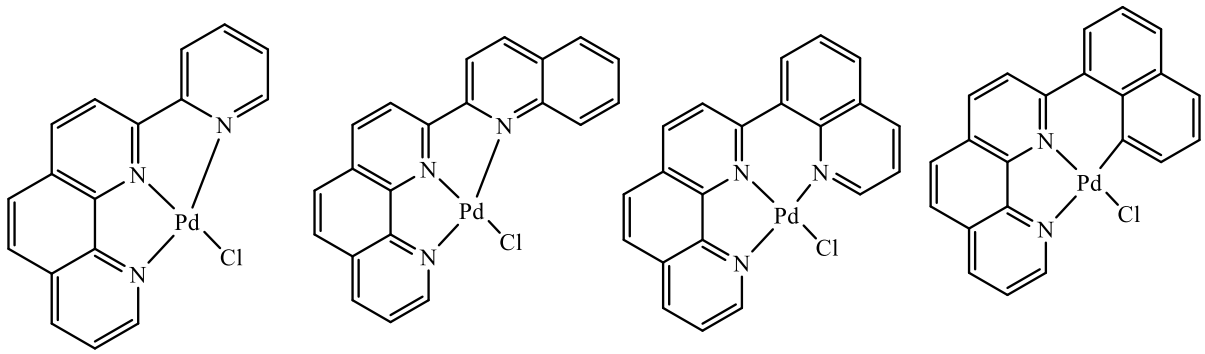

Figure 8. 2 Proposed polypyridyl Pd(II) complexes to further the work in this study.

8.4 References

1. D. Jaganyi, D. Reddy, J. Gertenbach, A. Hofmann and R. van Eldik, *Dalton Transactions*, 2004, 299-304.
2. A. Hofmann, L. Dahlenburg and R. van Eldik, *Inorganic Chemistry*, 2003, **42**, 6528-6538.
3. N. Sharma, R. Ameta and M. Singh, *Journal of Cancer Science and Research*, 2016, **1**, 1-7.
4. E. Gao, C. Liu, M. Zhu, H. Lin, Q. Wu and L. Liu, *Anti-Cancer Agents in Medicinal Chemistry (Formerly Current Medicinal Chemistry-Anti-Cancer Agents)*, 2009, **9**, 356-368.
5. K. S. Prasad, L. S. Kumar, S. Chandan, R. N. Kumar and H. D. Revanasiddappa, *Spectrochimica Acta Part A: Molecular and Biomolecular Spectroscopy*, 2013, **107**, 108-116.
6. A. Divsalar, A. A. Saboury, H. Mansoori-Torshizi and F. Ahmad, *The Journal of Physical Chemistry B*, 2010, **114**, 3639-3647.
7. L. Tušek-Božić, A. Furlani, V. Scarcia, E. De Clercq and J. Balzarini, *Journal of Inorganic Biochemistry*, 1998, **72**, 201-210.
8. N. A. Al-Masoudi, B. H. Abdullah, A. H. Essa, R. Loddo and P. LaColla, *Archiv der Pharmazie: An International Journal Pharmaceutical and Medicinal Chemistry*, 2010, **343**, 222-227.
9. T. Lazarević, A. Rilak and Ž. D. Bugarčić, *European Journal of Medicinal Chemistry*, 2017, **142**, 8-31.
10. A. S. Abu-Surrah, K. A. A. Safieh, I. M. Ahmad, M. Y. Abdalla, M. T. Ayoub, A. K. Qaroush and A. M. Abu-Mahtheieh, *European Journal of Medicinal Chemistry*, 2010, **45**, 471-475.
11. D. P. Bancroft, C. A. Lepre and S. J. Lippard, *Journal of the American Chemical Society*, 1990, **112**, 6860-6871.
12. B. Petrović, Ž. D. Bugarčić, A. Dees, I. Ivanović-Burmazović, F. W. Heinemann, R. Puchta, S. N. Steinmann, C. Corminboeuf and R. Van Eldik, *Inorganic Chemistry*, 2012, **51**, 1516-1529.
13. V. Novohradsky, L. Zerzankova, J. Stepankova, A. Kisova, H. Kostrhunova, Z. Liu, P. J. Sadler, J. Kasparkova and V. Brabec, *Metallomics*, 2014, **6**, 1491-1501.

14. J. M. Hearn, G. M. Hughes, I. Romero-Canelón, A. F. Munro, B. Rubio-Ruiz, Z. Liu, N. O. Carragher and P. J. Sadler, *Metallomics*, 2018, **10**, 93-107.
15. R. P. Paitandi, S. Mukhopadhyay, R. S. Singh, V. Sharma, S. M. Mobin and D. S. Pandey, *Inorganic Chemistry*, 2017, **56**, 12232-12247.
16. K. Xiong, Y. Chen, C. Ouyang, R.-L. Guan, L.-N. Ji and H. Chao, *Biochimie*, 2016, **125**, 186-194.
17. M. H. V. Huynh, J. M. Lasker, M. Wetzler, B. Mort, L. F. Szczepura, L. M. Witham, J. M. Cintron, A. C. Marschilok, L. J. Ackerman and R. K. Castellano, *Journal of the American Chemical Society*, 2001, **123**, 8780-8784.
18. Y. Geldmacher, M. Oleszak and W. S. Sheldrick, *Inorganica Chimica Acta*, 2012, **393**, 84-102.
19. S. M. Janković, A. Djeković, Ž. Bugarčić, S. V. Janković, G. Lukić, M. Folić and D. Čanović, *BioMetals*, 2012, **25**, 919-925.
20. L. Giovagnini, L. Ronconi, D. Aldinucci, D. Lorenzon, S. Sitran and D. Fregona, *Journal of medicinal chemistry*, 2005, **48**, 1588-1595.
21. K. Potgieter, Z. Engelbrecht, G. Naganagowda, M. J. Cronjé and R. Meijboom, *Journal of Coordination Chemistry*, 2017, **70**, 2644-2658.
22. W. A. Wani, U. Baig, S. Shreaz, R. A. Shiekh, P. F. Iqbal, E. Jameel, A. Ahmad, S. H. Mohd-Setapar, M. Mushtaque and L. T. Hun, *New Journal of Chemistry*, 2016, **40**, 1063-1090.
23. G. Mojžišová, J. Mojžiš and J. Vašková, *Acta Biochimica Polonica*, 2014, **61**.
24. J. Chen, Z. Luo, Z. Zhao, L. Xie, W. Zheng and T. Chen, *Biomaterials*, 2015, **71**, 168-177.
25. Y.-Z. Hu, M. H. Wilson, R. Zong, C. Bonnefous, D. R. McMillin and R. P. Thummel, *Dalton Transactions*, 2005, 354-358.